OPTIMISATION OF ULTRA-VIOLET AND VISIBLE LIGHT BASED TECHNOLOGIES FOR DISINFECTION APPLICATIONS IN CLINICAL AND OTHER ENVIRONMENTS

ENDARKO

Thesis submitted in accordance with the requirements of the University of Strathclyde for the degree of

Doctor of Philosophy

2011

Department of Electronic and Electrical Engineering

University of Strathclyde

Glasgow, UK

D E C L A R A T I O N

This thesis is the result of the author's original research. It has been composed by the author and has not been previously submitted for examination which has led to the award of a degree.

A B S T R A C T

Despite enormous worldwide research efforts and resource commitments, infectious disease problems associated with medical care and with food and water supplies remain as serious public health problems in both developed and developing countries. New infection control technologies are required and this study investigated ultraviolet and visible light-based technologies for microbial inactivation. A major aspect of the work was the modelling optimisation of the High-Intensity Narrow-Spectrum light Environmental Decontamination System (HINS-light EDS), a ceiling-mounted light source developed at the Robertson Trust Laboratory for Electronic Sterilisation Technologies (ROLEST), which provides continuous decontamination of air and surfaces within illuminated environments. This study involved the design and development of a fully integrated and controllable HINS-light EDS.

Initial investigations in the study involved the use of pulsed ultraviolet (PUV)-light for microbial inactivation, and results demonstrated the effectiveness of PUV-light for inactivation of the bacterial species *Staphylococcus epidermidis* and *Staphylococcus aureus* and the yeast species *Saccharomyces cerevisiae* in liquid suspension using both a broadband spectrum and 260 (± 10) nm light pulses.

To determine the visible-light wavelength sensitivity of a number of significant bacterial species, this study utilized a continuous xenon white-light source in combination with a range of narrow-band optical filters (10 nm FWHM) to expose *L. monocytogenes*, *S. aureus* and methicillin-resistant *Staphylococcus aureus* (MRSA) in liquid suspension. Results demonstrated that the bacteria showed sensitivity to wavelengths of light within the visible region, with the peak wavelength for inactivation being 405 (± 5) nm. The study also investigated the use of 405 nm High Intensity Narrow Spectrum (HINS) light, generated from light-emitting diodes (LEDs). When comparing the inactivation kinetics of MRSA, *S. aureus*, *S. epidermidis* and *L. monocytogenes* using the 405 nm HINS-light with those from the 405 nm filtered light, at an irradiance of 8.6 $mWcm^{-2}$, similar results are found, indicating that the applied dose is the important factor regardless of the source.

The most significant area of this study was the development, testing and modelling of a fully-integrated HINS-light Environmental Decontamination System (EDS). Previous work within ROLEST saw the development of an initial prototype model which has been successfully trialled within an NHS hospital, with results showing significant reductions of environmental contamination levels in isolation rooms. This initial prototype had a number of design and operational limitations which required improving. In this study, a new topology for the HINS-light EDS has been developed and its light distribution has been studied. Optimal parameters for the uniform light distribution have been established including: the Lambertian mode number (*m*), configuration of the Fresnel lens and diffuser, space distance between light source (LEDs), Fresnel lens and diffusers, and the optimum LED-to-LED array spacing. A mathematical model which allows analysis of the light distribution from different topologies has been successfully developed, with results proving that intensity distribution of the system is in good agreement with experimental data. In addition the system has improved thermal management with integrated power supplies providing a light-weight compact design suitable for ceiling mounting.

Analytical study of safety calculations and risk assessment of the new HINS-light EDS prototype have been evaluated and calculated. The results confirm that the HINS-light EDS, at an irradiance level of 0.08 $mWcm^{-2}$ for each individual 405 nm LED engine, and with a total irradiance level of 0.32 $mWcm^{-2}$ at a distance of 200 cm below the system, is safe in relation to UV, UV-A and thermal interaction with unprotected skin and eyes and blue light retinal hazard.

Bacterial inactivation data using this new prototype HINS-light EDS has been shown to achieve reductions in bacterial levels on agar surfaces of up to 73% for *S. aureus*, 57% for *E. coli* and 55% for *L. monocytogenes*, after 6 hours exposure at a distance of 200 cm below the system. The results demonstrate that the improved prototype system is effective for inactivation of pathogenic bacteria in exposed environments.

TABLE OF CONTENTS

LIST OF ABBREVIATIONS

Acronym	Corresponding Phrase
ACGIH	American Conference of Governmental Industrial Hygienists
BP	Bandpass Filter
CFU	Colony forming unit
EDS	Environmental decontamination system
FAO	Food and Agriculture Organization
FWHM	Full width half maximum
HINS	High intensity narrow spectrum
HPA	Health Protection Agency
ICNIRP	The International Commission on Non-ionizing Radiation Protection
IESNA	The Illuminating Engineering Society of North America
LWP	Long-wave pass filter
NHS	National Health Service
PDI	Photodynamic Inactivation
PDT	Photodynamic Therapy
PS	Photosensitiser
PUV	Pulsed ultraviolet
SWP	Short-wave pass filter
WHO	World Health Organization

LIST OF SYMBOLS

Symbol	Definition
η	Germicidal efficiency
m	The Lambertian mode number
Ω	Solid angle
E	Irradiance
E_v	Illuminance
r	Radius
L	Radiance
L_v	Luminance
$A(\lambda)$	Aphakic function
$B(\lambda)$	Blue-light hazard function
$R(\lambda)$	Retinal thermal function
$S(\lambda)$	Relative spectra effectiveness

LIST OF FIGURES

LIST OF TABLES

CHAPTER 1

INTRODUCTION

Despite the progress and the advancement of microbial inactivation technologies, the problem of medical, food and waterborne diseases is still growing, and is becoming a serious public health problem in both developed and developing countries. Various types of bacteria, yeast, fungi, virus and protozoa are responsible for causing these diseases, and numerous decontamination methods and technologies have been investigated for reduction and eliminate of these pathogens. Light-based technologies are one such method that have been of interest for decontamination applications.

Light interacts with microorganisms in different ways, with these processes depending critically on wavelength. Microbial inactivation using ultraviolet (UV) light is well known and has been utilized to eliminate air, water and surface contamination in hospital environments, food products, public buildings, water plants and agricultural products.

Due to the safety issues associated with UV light damage to skin and eyes, visible-light technologies for microbial inactivation are becoming useful alternative for general applications. Visible light in combination with a wide range of exogenous photosensitizing molecules (such as methylene blue, the cationic thiazine dye toluidine blue, cationic porphyrins, phthalocyanines and chlorins) is well-established as being an effective antimicrobial treatment and it has been successfully demonstrated to inactivate bacteria, yeast, fungi, protozoan parasites and viruses.

The initial aim of this study was to determine the efficacy of pulsed ultraviolet (PUV)-light for inactivation of the bacterial species *Staphylococcus epidermidis* and *Staphylococcus aureus*, and the yeast *Saccharomyces cerevisiae*, whilst in liquid suspension, and to also demonstrate that agitation of the sample during PUV

exposure significantly enhances the inactivation rate of densely populated microbial suspensions.

With the focus of the study on light-based technologies for microbial inactivation, the study then investigated the inactivation spectrum for *Listeria monocytogenes*, an important food-borne pathogen. This inactivation spectrum assessed the sensitivity of *L. monocytogenes* to UV and visible-light wavelengths and was performed using a continuous Xenon white-light source in combination with a range of broadband longwave and shortwave optical filters. Further studies using a range of narrowband (10 nm FWHM) filters investigated the wavelength sensitivity of *L. monocytogenes, S. aureus* and methicillin-resistant *Staphylococcus aureus (*MRSA), and found that bacterial inactivation using visible-light wavelengths was maximum with 405 (± 5) nm light.

Following identification of 405 (± 5) nm as the most bactericidal wavelength band, the study then investigated the use of high-intensity narrow-spectrum (HINS) 405 nm light, generated from light-emitting diodes (LEDs) for inactivation of a selection of significant foodborne pathogens including *Listeria monocytogenes, Salmonella enteritidis*, *Shigella sonnei* and *Escherichia coli* 0157:H7.

Research within the Robertson Trust Laboratory for Electronic Sterilisation Technologies (ROLEST) used the 405 nm HINS-light inactivation technology to develop the *HINS-light Environmental Decontamination System* (HINS-light EDS), which is a ceiling-mounted light source for continuous decontamination of the air and exposed surfaces. A recent publication demonstrated the successful application of this novel decontamination system within hospital isolation rooms for reducing environmental bacterial contamination [1].

The HINS-light EDS used in this previous study [1] was a prototype system with many features requiring optimising and improving (e.g. size/weight, high cost, non-integrated). The main objectives of this research project were to improve on the initial HINS-light EDS prototype design by creating a fully-integrated system, and to focus on the modelling optimisation of this new prototype system. This novel decontamination system will disinfect air and surfaces, therefore can have

applications in, not only clinical environments, but a variety of environments where disinfection and clean environments are required, e.g. food industry, public areas, schools, offices.

Overall, this study into light technologies for inactivation of pathogenic bacteria can be divided into two main parts;

1. Investigation into the effects of pulsed ultraviolet light and visible-light for microbial inactivation (Chapters 4 – 6).
2. Modelling, development and testing of a fully integrated and controllable HINS-light Environmental Decontamination System (Chapters 7 – 10).

The following is an overview of the breakdown of the chapters and brief description of the content of each.

Chapter 2 (Background and Literature review) discusses light as a decontamination technology including the electromagnetic spectrum (UV-light and visible light), light properties and the basics of light measurement, comparison of experimental data and mathematical models, light-based technologies for microbial inactivation and optical radiation safety. A review of microbial infections including hospital-acquired infections (HAI) and food and waterborne infections, as well as the problem of antimicrobial resistance is detailed.

Chapter 3 (Microbiological Techniques) provides information on the microorganisms, media, methods of microbial enumeration and statistical analysis, equipment and microbiological tests used during this study.

Chapter 4 (Investigation into the use of Pulsed UV-light for Microbial Inactivation) investigates the effectiveness of PUV light treatment for inactivation of the bacterial species *Staphylococcus epidermidis* and the yeast species *Saccharomyces cerevisiae* whilst in liquid suspension. PUV-light inactivation of *S. aureus* using both broadband spectrum light and 260 (± 10) nm light is also investigated.

Chapter 5 (Investigation into the Visible Light Wavelength Sensitivity of Pathogenic Bacteria) investigates the wavelength sensitivity of *Listeria monocytogenes, Staphylococcus aureus* including MRSA strains, to visible light, using both

broadband and narrowband wavelength ranges, in order to identify the optimal bactericidal wavelengths.

Chapter 6 (Investigation into the use of 405 nm High-Intensity Narrow-Spectrum light (HINS-light) for Bacterial Inactivation) reports on the inactivation of *Staphylococcus aureus*, MRSA, *Staphylococcus epidermidis* and *Listeria monocytogenes* using different sources of 405 nm HINS-light (an LED array and filtered light from a xenon lamp). To expand on the data for *L. monocytogenes*, dose dependence experiments were also carried out in order to determine the critical dose for bacterial inactivation. Inactivation of other *Listeria* species was also investigated. This chapter also investigates the inactivation of other foodborne pathogens using HINS-light from a 405 nm LED array. The foodborne pathogens used were *Listeria monocytogenes*, *Salmonella enteritidis*, *Shigella sonnei* and *Escherichia coli* 0157:H7.

Chapter 7 (Investigation into irradiance distribution of light from an LED light engine) describes experimental work that focuses on analysis of the irradiance distribution from a single LED array with regard to both angular and linear distribution. The Lambertian mode number is also investigated.

Chapter 8 (Optimisation of the High-Intensity Narrow-Spectrum-light Environmental Decontamination System (HINS-light EDS)) describes the development, testing and modelling of a fully integrated HINS-light EDS unit. This includes generation of a mathematical model for analysis of the light intensity distribution, and studies of thermal management options. A new topology for the HINS-light EDS has been developed and its light distribution has been studied. Optimal parameters for the uniform light distribution have been established including: the Lambertian mode number, space distance between light engines, Fresnel lens and diffuser, and light engine topology.

Chapter 9 (Design of the HINS-light Environmental Decontamination System) builds upon the EDS design in Chapter 8 and focuses on the mechanical and electrical design features and system controllability. A detailed study of light distribution for the new prototype HINS-light EDS is also presented. A comparison of components

and light distribution for this new prototype HINS-light EDS design versus the initial prototype is also reported. Analytical studies involving safety calculations and optical risk assessments are also completed.

Chapter 10 (Application of the New Prototype HINS-light Environmental Decontamination System for Inactivation of Pathogenic Bacteria) initially investigates the bactericidal effectiveness of an individual 405 nm LED light engine, (four of which were used in the final design of the new prototype HINS-light). The study then focuses on the use of the complete four light engine prototype HINS-light EDS for inactivation of *Staphylococcus aureus, Escherichia coli* and *Listeria monocytogenes* on agar surfaces. The results presented demonstrate that the improved prototype system is effective for inactivation of pathogenic bacteria.

Chapter 11 (General Conclusions and Recommendations for Future Work) discusses the results obtained throughout the study, and proposes potential applications for the new prototype HINS-light EDS. Areas of future work are discussed including recommendations for further developmental work that could be carried out on this novel light-based disinfection technology.

CHAPTER 2

BACKGROUND AND LITERATURE REVIEW

2.1 General

This literature review focuses on the properties of light, the basic principles of light measurement, irradiance distribution of light, the accuracy of reconstructions for comparison of experimental data and mathematical models, and optical radiation safety. Also reviewed is the application of light as a decontamination technology and the problem of hospital-acquired infections (HAI) and food and waterborne infections.

2.2 Electromagnetic spectrum

Electromagnetic radiation is generally divided into 7 regions which consist of radio wave, microwave, infrared, visible light, ultraviolet, X rays and gamma rays [2]. Ultraviolet (UV) and visible light radiation are a small part of the electromagnetic spectrum ranging from 100 – 700 nm, lying between X rays and infrared radiation (Fig. 2.1). Infrared light is electromagnetic radiation with wavelength regions in the range of 1 mm to 770 nm, and can be divided into two parts: far-infrared (1.4 – 1000 μm) and near-infrared (770 – 1400 nm) [2, 3]. In the literature review, only UV light and visible-light sources will be discussed.

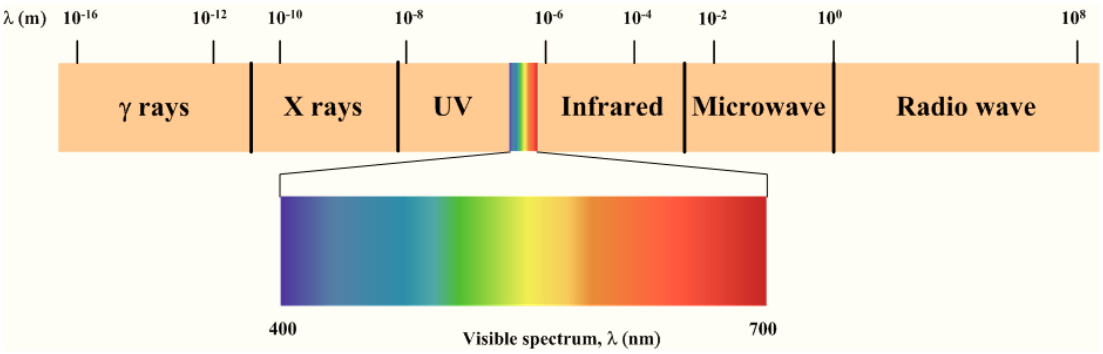

Fig. 2.1. *Electromagnetic wave spectrum (Adapted from [2]).*

2.2.1 Ultraviolet light

Ultraviolet light is electromagnetic radiation with a spectrum which is in the range of electromagnetic waves between X-rays and visible light with a wavelength of 100 nm to 400 nm. Ultraviolet radiation is typically divided into four categories according to its biological effects [4]:

- Vacuum UV (VUV) (100 – 200 nm), can only be transmitted through vacuum and is absorbed by almost all substances, and is strongly absorbed by air.
- UV-C (200 – 280 nm), is also known as the germicidal wavelengths because UV-C is effective for inactivation of microorganisms.
- UV-B (280 – 315 nm), is associated with skin burning which leads to skin cancer.
- UV-A (315 – 400 nm), is normally associated with tanning in human skin.

Ultraviolet radiation can also be arbitrarily divided into three bands: UV-A, UV-B and UV-C, and common ultraviolet band designations is shown in Fig. 2.2 [3].

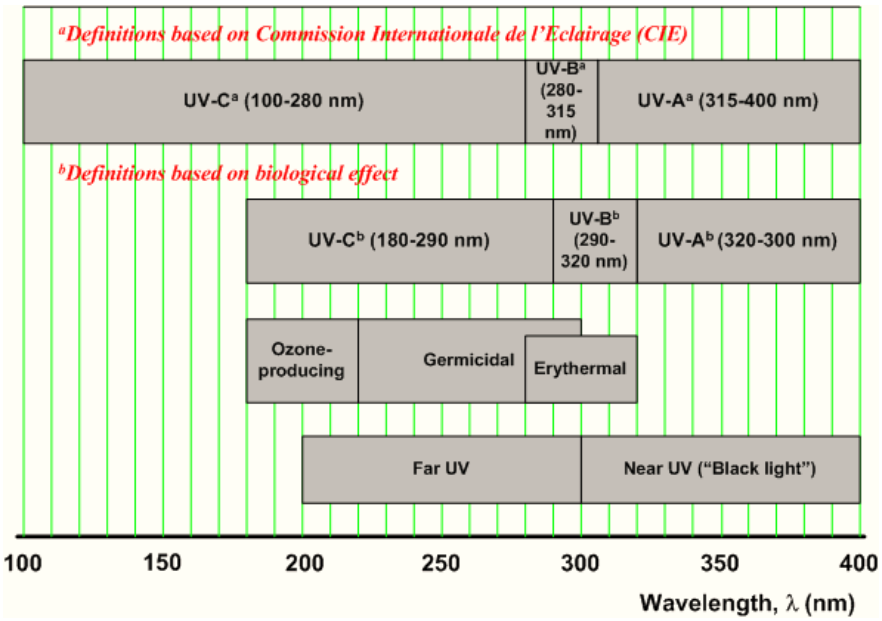

Fig. 2.2. *Ultraviolet band designations (Adapted from [3]).*

2.2.2 Sources of Ultraviolet Radiation

Different types of UV sources have been used for many application including disinfection, preservation and sterilization. Generally, UV light sources can be divided into two major types: (i) natural UV light sources, and (ii) artificial UV light sources. The characteristics and description for each light source will be detailed in this section.

2.2.2.1 Natural UV light

The Sun emits electromagnetic radiation with a spectrum covering the range from X-rays to radio waves, and the solar radiation spectrum at high altitude (extraterrestrial) is similar to the radiation emitted from a black body source at 6000 K [3, 5]. A small part of UV radiation is received at the surface of the earth and this component is important in various biological processes. Solar radiation is mostly absorbed by the stratospheric ozone layer, around 97 – 99%, and the minimum wavelength ever recorded at sea level was at 284 nm [5, 6]. The radiation energy of UV-A and UV-B reaching the earth's surface is less than 3% of global radiation, and varies with altitude (extraterrestrial), position and weather conditions, and has no industrial disinfection applications [5]. Although UV-C exists in the extraterrestrial solar spectrum, these wavelengths are totally screened out by the stratospheric ozone layer [7]. Meanwhile, infrared reaches the earth's surface, around 55% of the solar radiation, and warms the earth [7].

2.2.2.2 Artificial UV light Sources

Although ultraviolet radiation can cause lethal effects in all living organisms, ranging from prokaryotic bacteria to eukaryotic, plants, animal and humans, ultraviolet radiation technology can also be used in processes of disinfection, sterilization and preservation to help people obtain a better quality of life. Three types of artificial UV light source are reviewed in this section: mercury lamps, excimer lamps and flashlamps.

Mercury Lamps

The mercury arc lamp is an artificial UV light source which has been commonly used in UV disinfection technologies for drinking water and wastewater. Light is

produced by an electrical arc discharge between two electrodes that contains a small quantity of elemental mercury and an inert gas (e.g. argon), which is enclosed by a quartz tube. Mercury lamps can be divided into 2 types: (i) low-pressure mercury arc lamps and (ii) medium-pressure mercury arc lamps [8].

Low-pressure mercury lamps operate at low-pressure, less than 10 torr with a total vapour pressure of around 2 mbar, low external temperature (50 – 100 °C) and produce a sharp emission line with wavelength of 254 nm, which is nearly monochromatic emission [8, 9]. Medium-pressure mercury arc lamps produce polychromatic wavelengths ranging from far UV to infrared (185 nm to 1367 nm) and operate at pressures around 1000 torr [9].

Excimer Lamps

The excimer lamp is a non-coherent source of ultraviolet radiation; it is a spontaneous emission source which is based on excimer formation and it has the ability to produce quasi-monochromatic radiation from ranging the vacuum UV (126 nm) to the near UV (354 nm) [10]. The basic principle of excimer lamps is based on the radiative decomposition of excimers, examples include Ar_2 with output emission at 126 nm, Kr_2 (146 nm), Xe_2 (172 nm), KrCl (222 nm) and XeCl (308 nm) [10]. The main advantage of excimer lamps is a low surface temperature that permits use with heat-sensitive substrates [11].

Flash Lamps

The xenon flashlamp, is an alternative UV radiation source that produces pulses of broad spectrum light with wavelengths ranging from UV to near-infrared (180 – 1100 nm) and has a high output in the UV region [12]. The lamp operates with an internal xenon pressure of typically 50 – 100 kPa, and the pulse width ranges from a few milliseconds to a few microseconds [13]. The high peak power dissipation of the flashlamp can reach around 10^7 – 10^8 W and it emits pulses of high intensity polychromatic light 20,000 times more intense than sunlight at the earth's surface [12, 14].

2.2.3 Visible light

Light or visible light, according to the Illuminating Engineering Society of North America (IESNA) is defined as "radiant energy that is capable of exciting the human retina and creating a visual sensation", and as a physical quantity, "light is defined in terms of its relative efficiency throughout the electromagnetic spectrum lying between approximately 380 nm and 780 nm" [2]. Typically, visible-light has wavelengths in the range 400 to 700 nm, as shown in Fig. 2.1, but some people have the ability to see light wavelengths down to 380 nm or up to 770 nm (Fig. 2.3) [3].

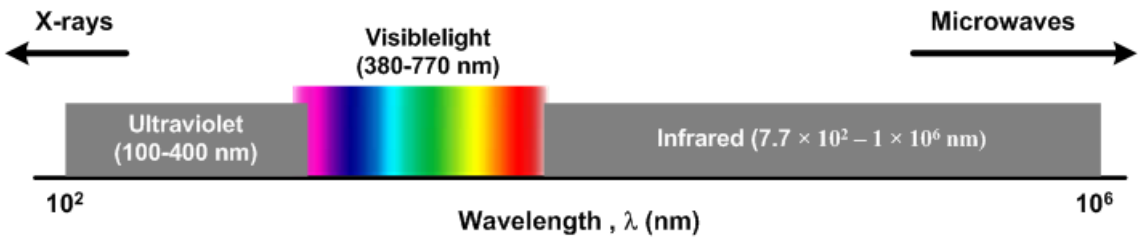

Fig. 2.3. *Electromagnetic spectrum in the range of UV to Infrared (Adapted from [3]).*

2.2.4 Sources of Visible Light

This section focuses on the two major types of visible light source, namely, non-coherent source, such as lamps and light emitting diodes (LEDs) and coherent sources (e.g. lasers) [15]. A brief review of these sources is given in the section.

2.2.4.1 Non-coherent

This light source can be divided into two types: light sources with a continuous spectrum, such as incandescent lamps and xenon arc lamps, and light sources with their spectrum located in bands, such as gas discharge lamps and xenon lamps [15].

Tungsten Lamp and Tungsten halogen Lamp

The tungsten lamp is a light source which generates light by passing electrical current through a filament which causes the filament to heat up to a high temperature until it glows. Typically, this lamp has a colour temperature in the range 2,200 – 3,000 K and produces a continuous emission spectrum with peak wavelength in the visible light and near infrared wavelengths [15]. Tungsten halogen lamps typically have halogen gas, such as iodine or bromine, filled in a small quartz balloon that encloses a wolfram filament. The basic principle of this lamp is based on the regenerative cycle of the halogen gas [15].

Gaseous-discharge Lamp

The basic principle of this lamp is the use of electrical discharge between two electrodes in a gas atmosphere. Commonly, the lamp uses volatile metal such as cadmium, zinc, mercury and gallium to generate light based on radiation of the bands of each metal [2, 15].

Xenon Lamp

Xenon lamps consist of an anode and cathode with a distance ranging from 1 – 10 mm sealed in a spherical quartz balloon and filled with xenon. This lamp produces high luminosity with continuous spectrum ranging from UV to infrared and working at high pressure (1000 – 5000 kPa) and temperature around 900 °C [2, 15].

Light emitting diode (LED)

A light-emitting diode (LED) is a semiconductor light source. Compared to an incandescent light source or a traditional light source, LEDs have more advantages such as lower energy consumption, longer lifetime, faster response, environmentally friendly, greater durability and reliability, efficiency and vivid colour [16].

2.2.4.2 Coherent

An example of a coherent light source is a laser. Laser stands for light amplification by the stimulated emission of radiation, and it is monochromatic, directional and coherent (spatially and temporally). Lasers emit light within a very tight wavelength, or with the exact wavelength, which can be targeted accurately with very high

intensity, and is suitable for photodynamic inactivation of bacteria, due to its properties [15].

2.3 Light measurement

This part of the literature review focuses on light properties and basic principles of light measurement. Also reviewed are the irradiance distribution of light, the accuracy of reconstruction and optical radiation safety.

2.3.1 Light properties

When light falls on a surface, it might be possibly reflected, transmitted, refracted or absorbed by the surface. The characteristics and description for each light property will be reviewed in this section.

2.3.1.1 Reflection

The three main types of reflection when light falls on a surface are specular, spread and diffuse reflection [2]. Fig. 2.4 shows an illustration of the three types of reflection. A specular reflection (Fig. 2.4a) allows demonstration of the general reflection law, as shown in Fig. 2.5. Light falling onto the surface with angle θ_i from the normal which is perpendicular to the surface (incident angle) is equal to the light reflected away from the surface with angle θ_r from normal (reflected angle) [3, 17].

Spread reflection occurs when the light encounters a rough surface, such as corrugated, etched, or hammered surfaces [2]. The light may spread parallel rays into a cone pattern of reflected rays [2], as shown in Fig. 2.4b.

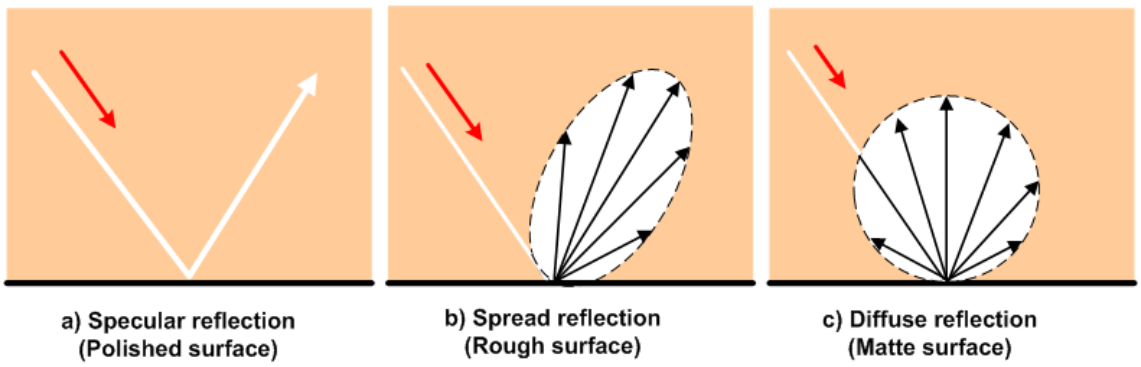

Fig. 2.4. *Types of reflection from surface: a) specular reflection, b) spread reflection, c) diffuse reflection (Adapted from [2]).*

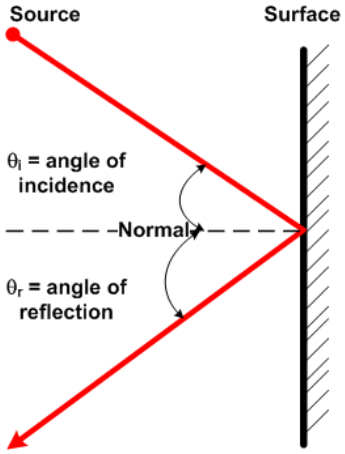

Fig. 2.5. *Law of reflection(Adapted from [2]).*

Diffuse reflection occurs when the light falls onto a matte surface, and the rays will appear uniformly bright from every direction [3]. Diffuse reflection (Fig. 2.4c) is also known as Lambertian scattering or diffusion [17].

2.3.1.2 Transmission and Absorption

When light passes through a filter glass, light transmission varies with wavelength and filter glass thickness [3]. According to IESNA, Bouguer's or Lambert's Law is defined as "absorption in a clear transmitting medium is an exponential function of the thickness of the medium traversed" [2] and can be expressed as follows:

$$I = I_0 e^{-\alpha d}, \tag{2.1}$$

$$I = I_0 \tau^d, \tag{2.2}$$

where,

I = intensity of transmitted light (Wm^{-2}),

I_0 = intensity of light entering the medium after surface reflection (Wm^{-2}),

α = absorption coefficient (m^{-1}),

τ = transmittance of unit thickness, d = 1 m, (τ is the ratio of the total emitted light to the total incident light; $\alpha = -\ln(\tau)$),

d = thickness of the medium traversed (m).

2.3.1.3 Refraction

Refraction occurs when light passes through different materials, where the light may bend and change its velocity [3]. The incident angle (θ) and the refractive index (n) of the material are two factors which cause refraction to occur [3]. The relationship between θ and n of the material is known as Snell's law of refraction [2, 3, 17], as shown in Fig. 2.6.

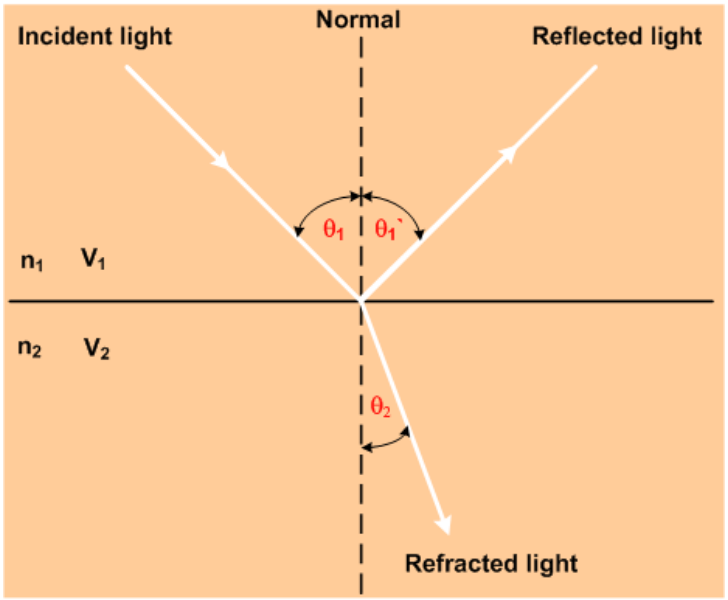

Fig. 2.6. *Snell's Law of refraction (Adapted from [17]).*

Snell's law of refraction can be expressed as follows [2]:

$$\frac{\sin\theta_1}{\sin\theta_2} = \frac{v_1}{v_2} = \frac{n_1}{n_2}, \tag{2.3}$$

where,

θ_1= angle of incidence,

θ_2 = angle of refraction,

n_1 = refractive index of the material 1,

n_2 = refractive index of the material 2,

v_1 = velocity in the material (ms^{-1}) 1,

v_2 = velocity in the material (ms^{-1}) 2.

2.3.2 Basic principles of light measurement

According to IESNA, all radiation from visible light, ultraviolet (UV) and infrared (IR) that can be quantified by specific techniques and equipment such as filters, diffraction gratings, lenses, prisms and mirrors, is called optical radiation [2]. The study of the measurement of optical radiation is also known as radiometry [2]. IESNA has defined radiometry as "the science of measuring radiant quantities without regard for the visual effects of the radiation" [2]. Meanwhile, photometry focuses on the measurement of radiation within the human visual response range of 380 nm to 780 nm [2]. Quantities, units and symbol used in radiometric and photometric quantities are presented in Table 2.1.

Table 2.1 *Radiometric and photometric quantities, symbol and units*

Quantity	Radiometric Symbol & Units		Quantity	Photometric Symbol & Units	
Radiant flux	Φ	Watt (W)	Luminous Flux	Φ_v	lumen (lm)
Radiant intensity	I	Wsr^{-1}	Luminous intensity	I_v	candela (cd), $lm\ sr^{-1}$
Radiance	L	$Wm^{-2}sr^{-1}$	Luminance	L_v	$lm\ m^{-2}sr^{-1}$, $cd\ m^{-2}$
Irradiance	E	Wm^{-2}	Illuminance	E_v	lux (lx), $lm\ m^{-2}$
Spectral radiance	E_λ	$Wm^{-2}\ nm^{-1}$	Spectral illuminance		$lm\ m^{-2}\ nm^{-1}$ or $lx\ nm^{-1}$

The study and measurement of light is complicated because it involves units of both radiometric and photometric quantities. Solid angle and quantities of radiometric and photometric are further reviewed and discussed in this section.

2.3.2.1 Solid angle

According to IESNA, solid angle is defined as "the ratio of intercepted surface area of a sphere centered on that point to the square of the sphere's radius", and is expressed in steradians [2]. Solid angle is illustrated in Fig. 2.7a. IESNA defines steradian as "the solid angle subtending an area on the surface of a sphere equal to the square of the sphere's radius" [2]. Fig. 2.7b shows the solid angle value that measures 1 steradian ($A = r^2$). Solid angle (Ω), in steradians, is the same as surface area (A) divided by the square of the radius (r^2) [3]:

$$\Omega = \frac{A}{r^2}. \tag{2.4}$$

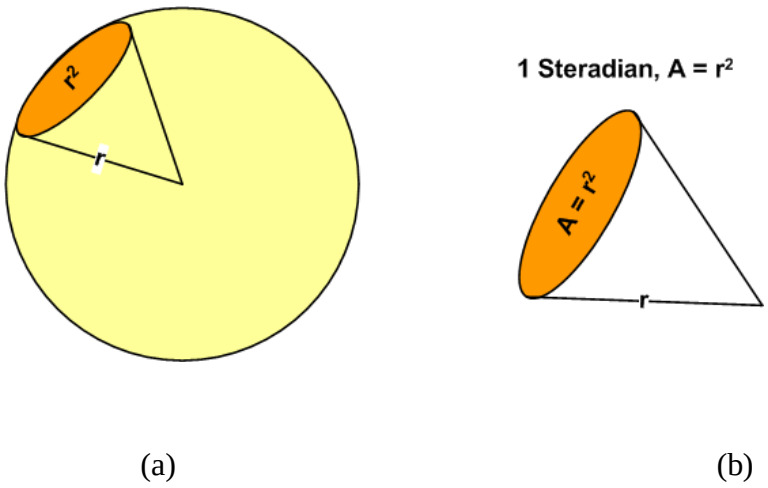

(a) (b)

Fig. 2.7. *Illustration of solid angle: a) 1 steradian illustration b) solid angle with value of 1 steradian ($A = r^2$)(Adapted from [3]).*

2.3.2.2 Radiant and Luminous flux

Radiant flux (Φ) or power is defined as the flow rate of radiant energy [17], and in standard international (SI) units is commonly expressed in Joules per second or Watts (Js^{-1} or W) [3, 17]. In the region of visible light, the power measured in lumens (lm), is called luminous flux.

2.3.2.3 Irradiance and illuminance

The irradiance is a measure of the light power (or radiant flux) per unit area received by a surface [3], and in SI units is commonly expressed in Wm^{-2}. The photometric flux per unit area or visible flux density - in SI units is typically expressed in lm m^{-2} or lux – is called illuminance [3].

2.3.2.4 Radiance and luminance

Radiance is defined as irradiance per unit solid angle, while luminance is illuminance per unit solid angle [3]. Radiance and luminance are commonly expressed in $Wm^{-2}sr^{-1}$ and cd m^{-2} or lm $m^{-2}sr^{-1}$, respectively [3]. Radiance indicates the amount of power emitted by an optical radiation received by an optical system from a certain angle of view, while luminance is correlated well with human perception, i.e. how bright the surface will look.

2.3.2.5 Radiant and luminous intensity

Radiant intensity is defined as the total flow rate of radiant energy (power) per unit solid angle, typically expressed in Wsr^{-1} [3]. Luminous intensity is photometric power per unit solid angle, commonly expressed in lm sr^{-1} or cd [3].

2.3.2.6 Inverse square law

IESNA defines the inverse square law as "a law stating that the illuminance *E* at a point on a surface varies directly with the intensity *I* of a point source and inversely as the square of the distance *d* (m) between the source and the point" [2]. The relationship between intensity of a point source and illuminance can be expressed as follows [3]:

$$E_v = \frac{I_v}{d^2}. \tag{2.5}$$

If the illuminance of a 20 lm m^{-2} is measured at 100 cm from a light source, the illuminance of a 5 lm m^{-2} will be achieved at a distance of 200 cm from the light source, as illustrated in Fig. 2.8. Henceforth, Eq. (2.5) could be written as follows [3]:

$$E_{v1}d_1^2 = E_{v2}d_1^2, \tag{2.6}$$

where,

E_{v1} = illuminance at position 1 (lm m^{-2}),

E_{v2} = illuminance at position 2 (lm m^{-2}),

d_1= distance 1 from light source (m),

d_2= distance 2 from light source (m).

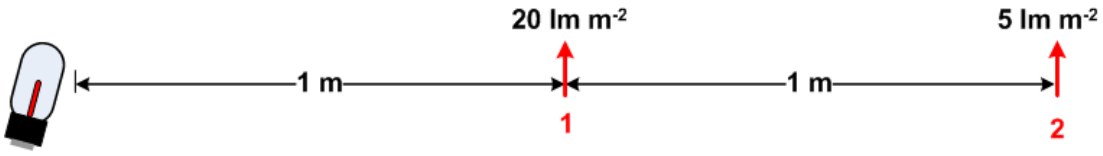

Fig. 2.8. *Illustration of inverse square law.*

2.3.2.7 Lambert's cosine law

IESNA defines Lambert's cosine law as "the law stating that the luminous intensity in any direction from an element of a perfectly diffusing surface varies as the cosine of the angle between that direction and the perpendicular to the surface element" [2] and it can be expressed through Eq. (2.7). From Eq. (2.7), it can be analysed that the maximum irradiance or illuminance on an illuminated area is achieved when the angle of incidence light is perpendicular to the illuminated area ($\theta = 0°$) and the minimum will be achieved at an angle of 90°.

$$E(\theta) = E\cos\theta, \tag{2.7}$$

where,

E = the irradiance (Wm^{-2}) at the viewing angle $\theta = 0°$,

$E(\theta)$ = the irradiance (Wm^{-2}) at the viewing angle $\theta > 0°$.

2.4 Irradiance distribution

As described in Section 2.3.2.7, the Lambert's cosine law is the irradiance falling on illuminated area varies as the cosine of the angle between that direction and the perpendicular to the illuminated area [2].

Ideally, an LED source that is used in practical applications is a Lambertian emitter, and has an irradiance distribution of light represented by a cosine function (see Eq. (2.7)). In fact, this depends on a power law due to the encapsulant and semiconductor region shapes of a LED source [18]. A practical approximation of the irradiance distribution for an LED source is given by [18-21]

$$E(r,\theta) = E(r)\cos^{m}(\theta), \tag{2.8}$$

where *E(r)* is the irradiance (Wm^{-2}) at distance *r* between the normal irradiance E_0 and the viewing angle $\theta > 0^{\circ}$ and *m* is the Lambertian mode number, $m > 0$ (Fig. 2.9). The mode number (*m*) is given by the angle $\theta_{1/2}$ (It's related to the angle at which the irradiance has fallen to half power or is defined as "the view angle when irradiance is half of the value at 0°") [18]

$$m = \frac{-\ln 2}{\ln(\cos\theta_{1/2})}. \tag{2.9}$$

Fig. 2.9 shows the irradiance distribution across a horizontal flat surface at position *A*, where *p* is the distance between a LED source and an irradiance measured, which is the projection from the vertical distance (*h*) of the LED with angle θ, and *r* is the distance between *O* (centre) and *A*.

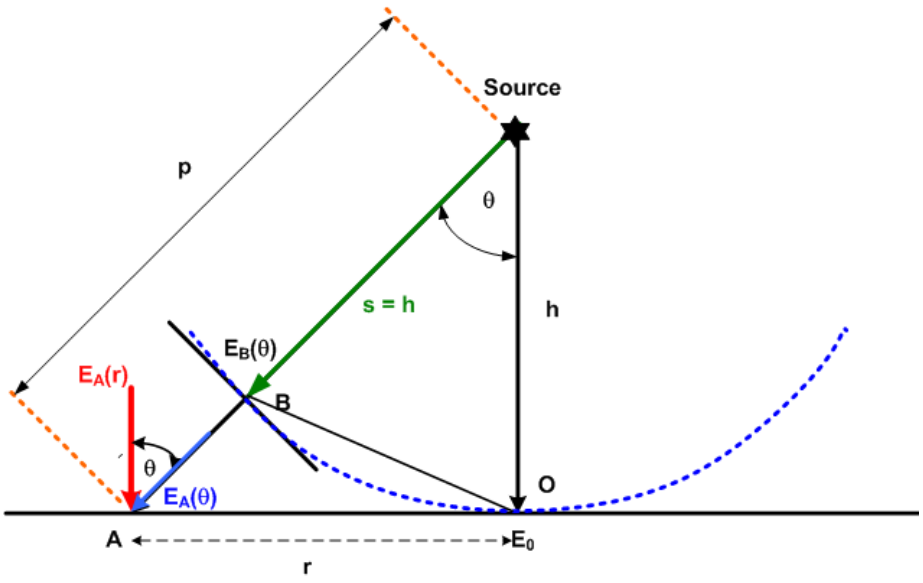

Fig. 2.9. *Path of the irradiance distribution across a horizontal surface.*

It can be observed from Fig. 2.9 that $p^2 = r^2 + h^2$ and $\cos\theta = \frac{h}{p} = \frac{h}{(h^2 + r^2)^{1/2}}$. Since, from Eq. (2.8), the angular distribution of the irradiance is of the form:

$$E(\theta) = E_0 \cos^m \theta, \text{ then } \frac{E}{E_0} = \left(\frac{h}{\left[h^2 + r^2 \right]^{1/2}} \right)^m = \left(1 + \frac{r^2}{h^2} \right)^{-\frac{m}{2}}, \qquad (2.10)$$

where E_0 is the irradiance (Wm^{-2}) at the viewing angle $\theta = 0°$ which has vertical distance between the LED and the perpendicular to the illuminated area (the horizontal plane) with length h and E is the angular distribution of the irradiance at any point.

Hence, $E = E_0 \left(1 + \frac{r^2}{h^2} \right)^{-\frac{m}{2}}$. (2.11)

Eq. (2.12) is the angular distribution of the irradiance at the point B,

$$E_B = E_0 \left(1 + \frac{r^2}{h^2} \right)^{-\frac{m}{2}}. \qquad (2.12)$$

As described in Section 2.3.2.6, according to the inverse square law the angular distribution of the irradiance at point *A* can be expressed in the form:

$$\frac{E_A}{E_B} = \frac{s^2}{p^2} = \frac{h^2}{h^2 + r^2}. \tag{2.13}$$

At the point *A*, the vertical component of the irradiance distribution is $E_A(r)$. This value represents the irradiance at any point on the horizontal surface. From Fig. 2.9, $E_A(r)$ can be expressed in form:

$$E_A(r) = E_A \cos(\theta) = E_A \frac{h}{\left(h^2 + r^2\right)^{1/2}}. \tag{2.14}$$

Hence, by substitution, Eq. (2.13) and then Eq. (2.14) can be expressed in form:

$$E_A(r) = E_B \frac{h^2}{h^2 + r^2} \times \frac{h}{\left(h^2 + r^2\right)^{1/2}} = E_B \left(1 + \frac{r^2}{h^2}\right)^{-\frac{3}{2}}. \tag{2.15}$$

Combining Eq. (2.12) and Eq. (2.15):

$$E_A(r) = E_0 \left(1 + \frac{r^2}{h^2}\right)^{-\frac{(3+m)}{2}}. \tag{2.16}$$

Eq. (2.16) is the generalized Lambert's cosine law at any point on the horizontal surface as a function of *r*.

The irradiance given by Eq. (2.16) for a LED can be written in terms of Cartesian coordinates (x, y, z) (Fig. 2.10) as follows,

$$E(x, y, z) = E(x_0, y_0, z_0) \left(1 + \frac{\left[x - x_0\right]^2 + \left[y - y_0\right]^2}{\left[z - z_0\right]^2}\right)^{-\frac{(3+m)}{2}}, \tag{2.17}$$

or,

$$E(x, y, z) = \left(z - z_0\right)^{(3+m)} E(x_0, y_0, z_0) \left(\left[x - x_0\right]^2 + \left[y - y_0\right]^2 + \left[z - z_0\right]^2\right)^{-\frac{(3+m)}{2}}, \tag{2.18}$$

where $E(x_0, y_0, z_0)$ is the irradiance (Wm^{-2}) at the viewing angle $\theta = 0°$. Eq. (2.18) is the irradiance over every point (x, y) on the horizontal surface at distance of z from the LED, and this equation will be used to predict, estimate and analyse the light distribution pattern from LED array. A study of the LED irradiance distribution pattern for single LED array will be further discussed in Chapter 7.

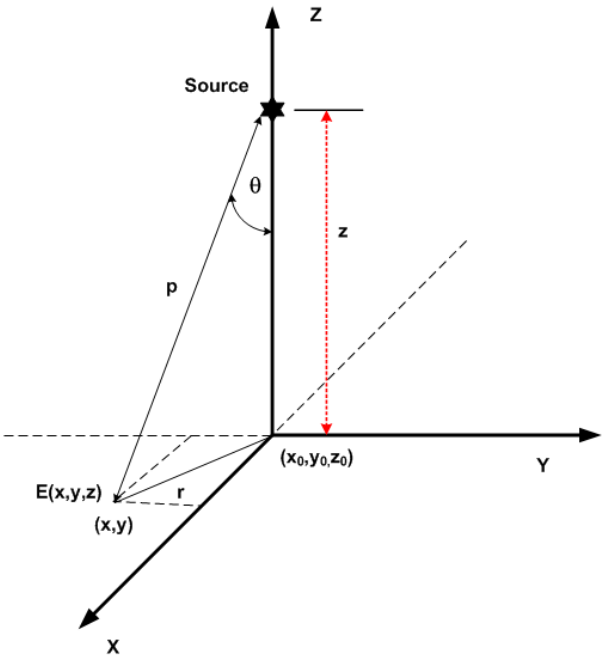

Fig. 2.10. *The irradiance distribution across a horizontal surface in terms of Cartesian coordinates (x, y, z).*

2.5 The accuracy of reconstruction

In order to show the accuracy of reconstruction for comparison between experimental data and mathematical models, the difference between both of them must be compared by calculating the normalized cross correlation (NCC) and root mean square (RMS) error [19].

To examine the similarity between the pattern of experimental data and mathematical model, the normalized cross correlation (NCC) can be applied using Eq. (2.19) [16, 19, 22, 23].

$$NCC = \frac{\sum_n \left[P(\theta_n)_e - \overline{P_e} \right] \left[P(\theta_n)_m - \overline{P_m} \right]}{\sqrt{\sum_n \left[P(\theta_n)_e - \overline{P_e} \right]^2 \sum_n \left[P(\theta_n)_m - \overline{P_m} \right]^2}}, \tag{2.19}$$

where P_e and P_m are the relative intensity of the experimental data and mathematical model, respectively. θ_n is the *n*-th angular displacement, and the mean values of the experimental data and mathematical model across the angular range, labeled $\overline{P_e}$ and $\overline{P_m}$, respectively. If the NCC is higher than 99% [19], the NCC gives guarantee that similarity between the experimental data and mathematical model can be achieved.

To ensure the accuracy of the difference between the experimental data and mathematical model, not only the NCC but also the root mean square (RMS) error has been calculated to give guarantee the accuracy of the Lambertian mode number (*m*) resulted from the calculation of curve fit method. The RMS error can be evaluated on a range of M points over the domain as follows [19]:

$$RMS\ error = \sqrt{\frac{\sum_{n=1}^{M} \left(P(\theta_n)_m - P(\theta_n)_e \right)^2}{M}}, \tag{2.20}$$

where again P_e and P_m are the relative intensity of the experimental data and mathematical model, respectively and θ_n is the *n*-th angular displacement. The difference between the experimental data and mathematical model is accurate if the RMS error is less than the standard limit of 5% [19]. The RMS demonstrates that if the two data sets are compared, the pairwise differences of them can assist as a measure how far on average the error is from 0.

2.6 Optical radiation safety

Optical radiation sources can have detrimental effects on skin and eyes in several different ways. Nine types of hazard to the eye and skin caused by an intense optical radiation source have been reported by Sliney [24] as follows:

1. *Ultraviolet photokeratoconjuctivitis (also known as "welder's flash" or simply "photokeratitis", one aspect of "snow-blindness")*, occurs in the wavelength region 180 – 400 nm.

2. *Ultraviolet cataract* occurs in the wavelength region 295 – 325 nm and perhaps to 400 nm.

3. *Ultraviolet erythema ("sunburn" or reddening of the skin),* occurs in the wavelength region 200 – 400 nm.

4. *Skin cancers,* mostly within UV-B region in the range 280 – 315 nm but also revealed for UV-A in the wavelength region 315 – 400 nm.

5. *Thermal injury to the retina* commonly arises within wavelengths ranging from 400 nm to 1400 nm.

6. *Blue-light photochemical injury to the retina*, principally occurs in the blue light region ranging from 400 nm to 550 nm.

7. *Near-infrared thermal hazard to the lens*, (with potential detrimental effect of industrial heat cataract) can occur within the near-infrared region ranging from 800 nm to 3000 nm.

8. *Thermal injury of the cornea and conjunctiva* can occur in the wavelength around 1400 nm to 1 mm.

9. *Thermal injury of the skin* can occur in the wavelength around 400 nm to 1 mm.

Other factors that can become potential hazards of a light source are also reported by Sliney [24] and include lamp envelope and filtration, source size and distance, source uniformity, source stability, aging characteristic, temperature and environmental sensitivities, and radiant efficiency.

2.6.1 Exposure limit guidelines

The American Conference of Governmental Hygienists (ACGIH) is one group that have recommended occupational or public exposure limits (ELs) for optical radiation

(i.e., ultraviolet (UV), visible light and infrared (IR) radiant energy). Exposure limits (ELs) are also known as 'Threshold Limit Values' or TLVs [24].

The International Commission on Non-ionizing Radiation Protection (ICNIRP) has published guidelines on limits of exposure to broadband incoherent optical radiation in the wavelength region 0.38 to 3μm. Its main goal was to determine the principles of protection against visible and infrared radiation emitted by broadband, conventional, non-laser sources (including LEDs) [25].

As described in Section 2.10, wavelengths within 180 – 400 nm (UV region) can cause hazards to the eye and skin, such as photokeratitis, ultraviolet cataract, ultraviolet erythema and skin cancers. To prevent detrimental effects caused by UV radiation, ICNIRP has published guidelines on limits of exposure to UV radiation (180 – 400 nm) for incoherent optical radiation [26]. Both ACGIH and ICNIRP collaborate with the World Health Organization (WHO) to develop guidelines on limits of human exposure to establish the safety criteria for optical radiation [24].

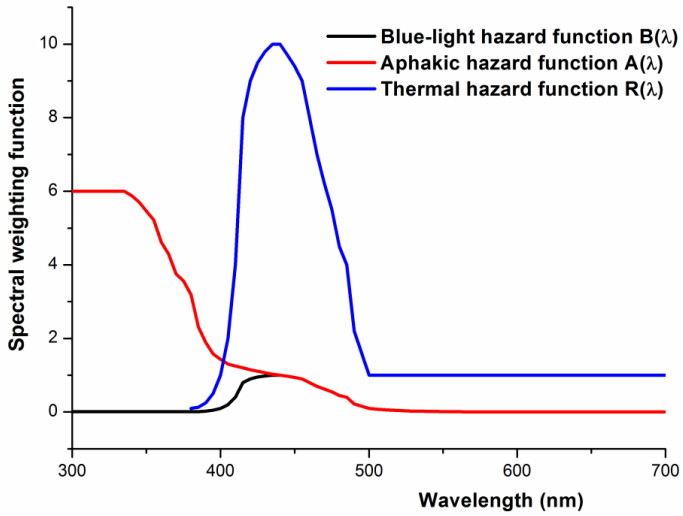

Fig. 2.11. *Retinal hazard spectral weighting functions in the wavelength region 300 – 700 nm (Adapted from [24, 25]).*

Fig. 2.11 demonstrates retinal hazard spectral weighting as a function of wavelength between 300 nm and 700 nm. The graph shows that the peak wavelengths for the blue-light hazard function $B(\lambda)$ and retinal thermal hazard function $R(\lambda)$ are between

435 nm and 440 nm, and for the aphakic hazard function $A(\lambda)$ within the wavelength region 300 – 335 nm. Miller *et al.* have described that the difference between the blue light hazard function and the aphakic function are that these functions are used for eyes with an intact natural lens and with the normal lens removed, respectively [27].

According to ICNIRP the exposure limits (ELs) for retinal thermal hazards in the wavelength region 380 – 1400 nm are defined as follows [25]:

$$L_{HAZ} = \frac{50}{\left(\alpha t^{0.5}\right)}\left(\text{in kWm}^{-2}\text{sr}^{-1}\right) \text{ or } L_{HAZ} = \frac{5}{\left(\alpha t^{0.5}\right)}\left(\text{in Wcm}^{-2}\text{sr}^{-1}\right), \qquad (2.21)$$

where,

L_{HAZ} = the exposure limit for hazardous radiance,

α = function of angular subtense of the source (the mean light source dimension D_L divided by the viewing distance r, as shown in Fig. 2.12) in radians,

t = exposure duration (in seconds) for the condition 10 μs ≤ t ≤ 10 s.

According to ICNIRP, the exposure limit for hazardous radiance is termed L_{HAZ} and is defined as "a function of the angular subtense of the source (α) in radians (the mean light-source dimension D_L (Fig. 2.12) divided by the viewing distance *r*) and the exposure duration (*t*) in seconds for the condition 10μs ≤ t ≤ 10 s: $L_{HAZ} = 50/\alpha t^{0.25}$ ($\text{Wcm}^{-2}\text{sr}^{-1}$)" [25].

ICNIRP has also mentioned that the exposure limit for retinal thermal hazard in the wavelength region 380 – 1400 nm can be calculated as follows [25]:

$$\sum_{380}^{1400} L_\lambda R(\lambda)\, \Delta\lambda < L_{HAZ}\,, \qquad (2.22)$$

where L_λ is the weighted spectral radiance of the light source ($\text{Wm}^{-2}\text{sr}^{-1}\text{nm}^{-1}$), $R(\lambda)$ is the retinal thermal hazard function and $\Delta\lambda$ is the measurement interval (nm) [25].

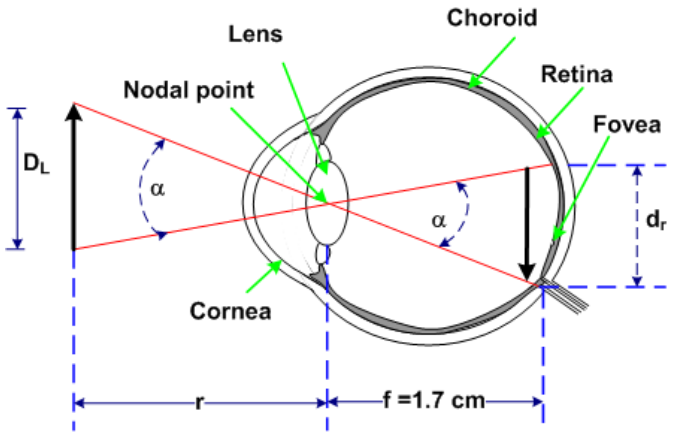

Fig. 2.12. *The retinal image size (d_r) can be calculated based upon $d_r = D_L(f/r)$, where f is the effective focal length of the eye in air and r is the viewing distance from the light source (Adapted from [24, 25]).*

For protection of the retina against photoretinitis, ICNIRP has stipulated that the exposure limit for blue-light photochemical retinal hazard in the wavelength region 300 – 700 nm can be calculated as follows [25]:

$$L_B t = \sum_{300}^{700} L_\lambda B(\lambda) t \Delta\lambda \le 100\,\mathrm{Jcm^{-2}sr^{-1}}\ (\text{effective}), \tag{2.23}$$

or

$$L_B = \sum_{300}^{700} L_\lambda B(\lambda) \Delta\lambda \le 100\,\mathrm{Jcm^{-2}sr^{-1}}\ (\text{effective}), \tag{2.24}$$

where,

L_B = the effective blue light radiance, $\mathrm{mWcm^{-2}sr^{-1}}$ or $\mathrm{Wm^{-2}\ sr^{-1}}$,

L_λ = spectral radiance from measurement, $\mathrm{mWcm^{-2}sr^{-1}nm^{-1}}$ or $\mathrm{Wm^{-2}\ sr^{-1}nm^{-1}}$,

$B(\lambda)$ = blue-light hazard function (unitless),

$\Delta\lambda$ = measurement intervals (nm),

t = exposure time (s).

The effective blue light irradiance must not exceed 10 $mWcm^{-2}sr^{-1}$ ($L_B \leq 10$ $mWcm^{-2}sr^{-1}$ (effective)) and the exposure time maximum for protection of the retina against photoretinitis can be calculated as follows [25]:

$$t_{\max} = \frac{100\ \mathrm{Jcm^{-2}sr^{-1}}}{L_B} \quad (\text{effective}). \tag{2.25}$$

Eq. (2.24) is used for normal healthy eyes, for the eye with the normal lens which has been removed by cataract operation – referenced as aphakic eye, Eq. (2.24) can be rewritten as follows [25]:

$$L_A = \sum_{300}^{700} L_\lambda A(\lambda)\Delta\lambda \leq 100\ \mathrm{Jcm^{-2}sr^{-1}}\ (\text{effective}), \tag{2.26}$$

where L_λ is the weighted spectral radiance of the light source (Wm^{-2} $sr^{-1}nm^{-1}$), $A(\lambda)$ is the aphakic hazard function and $\Delta\lambda$ is measurement intervals (nm). For protection of the skin or eye against ultraviolet radiation (UVR) in the wavelength region 180 – 400 nm, ICNIRP has indicated that radiant exposure of UV to the unprotected eye(s) or skin should not exceed 3 $mJcm^{-2}$ (at 270 nm) effective spectrally weighted factors based on Fig. 2.13 [26].

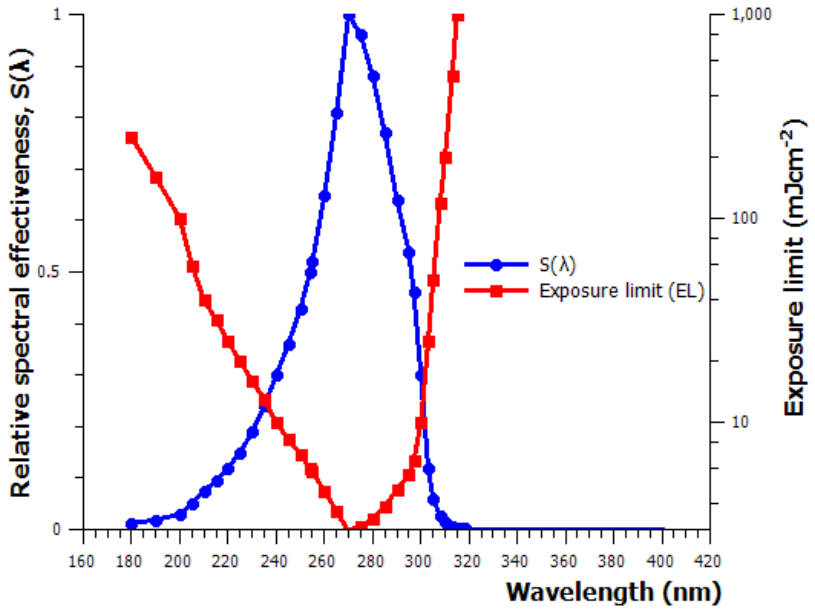

Fig. 2.13. *Relative spectral effectiveness, S(λ) and UV exposure limits (ELs) (Adapted from [26]).*

To determine the effective irradiance (E_{eff}) of a broadband source, ICNIRP has defined the equation that should be used to calculate E_{eff} as follows [26]:

$$E_{eff} = \sum_{180}^{400} E_{\lambda} S(\lambda) \Delta\lambda \,, \tag{2.27}$$

where,

E_{eff} = effective irradiance in $mWcm^{-2}$ or Wm^{-2}, normalised to a monochromatic source at 270 nm,

E_{λ} = spectral irradiance from measurements in $mWcm^{-2}nm^{-1}$ or $Wm^{-2}nm^{-1}$,

$S(\lambda)$ = relative spectral effectiveness (unitless) (Fig. 2.13),

$\Delta\lambda$ = measurement intervals (nm).

Guidelines on limits of exposure to ultraviolet radiation for unprotected eye(s) or skin should be calculated using the relation Eq. (2.26), and example calculations of exposure time maximum for safety reasons are summarised in Table 2.2.

Table 2.2 *Guidelines on limits of exposure to ultraviolet radiation (Adapted from [26])*

Permissible exposure time per day	**E_{eff} (Wm^{-2})**
8 hours	0.001
4 hours	0.002
2 hours	0.004
1 hours	0.008
30 min	0.017
15 min	0.033
10 min	0.05
5 min	0.1
1 min	0.5
30 s	1.0
10 s	3.0
1 s	30
0.5 s	60
0.1 s	300

2.6.2 Photopic curve

As described in Section 2.3.2, photometric quantities correlate with the measurement of radiation from human visual response in the range 380 nm to 780 nm [2]. The sensitivity of the eye depends on wavelength as shown in the photopic curve of Fig. 2.14.

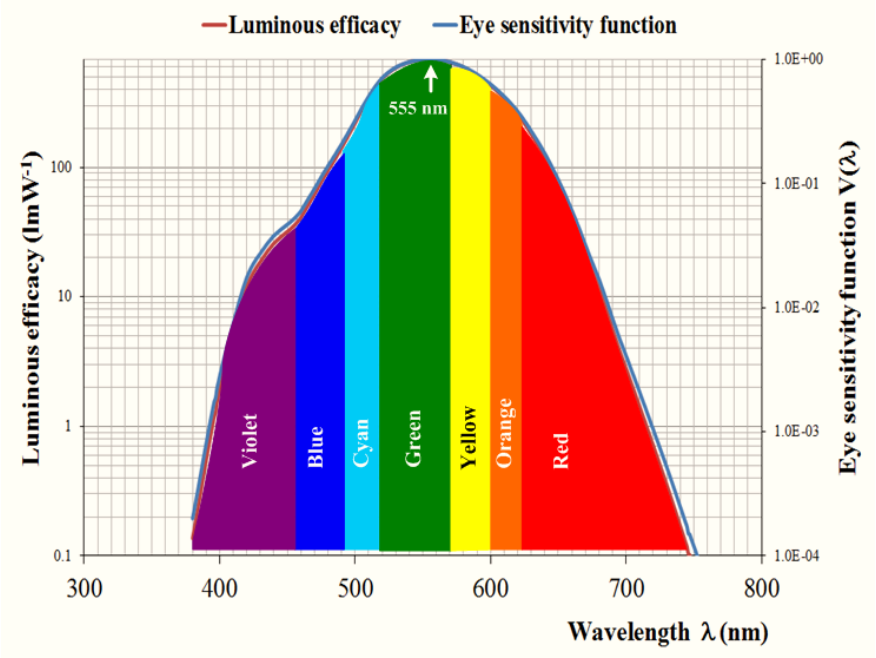

Fig. 2.14. *Eye sensitivity function, V(λ) and luminous efficacy based on Commission Internationale de l'Eclarage (CIE) 1988 (Adapted from [28-30]).*

According to ICNIRP, illuminance (E_v) can be calculated from irradiance measurement using Eq. (2.28).

$$E_v = 683\sum_{380}^{780} V(\lambda)E_\lambda \Delta\lambda, \qquad (2.28)$$

where $V(\lambda)$ is the CIE photopic luminous efficiency function (CIE 1988) (Fig. 2.14), E_λ is spectral irradiance from measurements in $mWcm^{-2}nm^{-1}$ or $Wm^{-2}nm^{-1}$, $\Delta\lambda$ is the measurement interval (nm) [25], and luminance (L_v) is defined as illuminance (E_v) divided by solid angle of the source , Ω [25]:

$$L_v = \frac{E_v}{\Omega}. \tag{2.29}$$

2.7 The problem of microbial infections

Microbial infection, and the illnesses which can result, are an increasingly important global health issue and such illness can be acquired by ingesting contaminated foodstuff/water, or by transmission from infected sources in the clinical environment. As such, a review of the problem of hospital-acquired and food and waterborne infections are given in this section, along with a discussion about the antimicrobial properties of light and how light-based technologies can be utilised for decontamination applications to help reduce the incidence of microbial infections.

2.7.1 Hospital-acquired infections (HAI)

Hospital-acquired infections (HAI), also termed nosocomial infections, "are infections transmitted to patients (and healthcare workers) as a result of healthcare procedures, in hospitals and other healthcare settings" [31], the World Health Organization (WHO) defines these as "infections acquired during hospital care which are not present or incubating at admission" [32]. The World alliance for patient safety has mentioned that over 1.4 million people worldwide are suffering from HAI, and around 5% to 10% of patients admitted to modern hospitals in the developed world acquire one or more infections [33]. The comparative risk of HAI in developing countries compared to developed countries is 2 to 20 times more; with the percentage rising to more than 25% in some developing countries [33]. In the United States, it is estimated that around two million cases, and about 80,000 deaths a year, are caused by an infection in hospital [33]. In the UK, the Parliamentary Office of Science and Technology (POST) reported that there are an estimated 300,000 cases and over 15,000 deaths per year caused by HAI [31].

In the UK the estimated cost of HAI is around £1 billion per year [31, 34, 35] and in the United States, the estimate is between US$ 4.5 billion and US$ 5.7 billion per year [33].

Nosocomial infections can be caused by a variety of microorganisms. The most common nosocomial pathogens are listed in Table 2.3.

Table 2.3 *Common nosocomial pathogens (Adapted from [32])*

Gram (+) Bacteria	**Gram (-) Bacteria**	**Viruses**	**Parasites and Fungi**
Clostridium	*Escherichia coli*	*Hepatitis B*	*Giardia lamblia*
Staphylococcus aureus	*Proteus*	*Hepatitis C*	*Candida albicans*
beta-haemolytic streptococci	*Klebsiella*	*Respiratory Syncytial Virus (RSV)*	*Aspergillus spp*
	Enterobacter	*Rotavirus*	*Cryptococcus neoformans*
	Serratia marcescens	*Enteroviruses*	*Crypto sporidium*
	Pseudomonos spp	*Cytomegalovirus*	*Sarcoples scabies*
	Legionella	*HIV*	
		Ebola	
		Influenza virus	
		Herpes simplex virus	
		Varicella-zoster	

Antimicrobial resistance is a significant factor associated with the rise in hospital-acquired infections. Antimicrobial agents are synthetic or natural substances used to kill bacteria, viruses and other microorganisms or to stop them growing and multiplying [31, 36, 37]. These substances are generally used to improve public health by reducing the number of infectious diseases in human and veterinary medicine for instance in the form of antibiotics [38].

Microbial resistance to antibiotics is a natural biological phenomenon that has proven to be problematic in the treatment of patients. The main factors increasing microbial resistance to antibiotics can be divided into four categories: (i) over prescription of antibiotics, (ii) pattern of antibiotic use – patients do not complete their course of

prescribed antibiotic, (iii) using leftover antibiotics to self-medicate against a fresh infection, and (iv) the indiscriminate use of antibiotics in livestock [31].

The most notable example of an antibiotic-resistant microorganisms is meticillin-resistant *Staphylococcus aureus* (MRSA). This organism is often resistant to several antibiotics in addition to the penicillinase-resistant penicillins and cephalosporins, and another form of antibiotic-resistant *S. aureus*, vacomycin-resistant *S. aureus* (VRSA), is resistant to vancomycin and teicoplanin [31, 32], making infections caused by these organisms increasingly difficult to treat.

2.7.2 Food and waterborne infections

Food and waterborne infections are caused by consumption of food and water contaminated with bacteria, viruses and parasites. Rapid globalization of food production and trade causes the increasing problem of foodborne diseases. Many outbreaks of foodborne diseases have been reported worldwide, and the US Centre for Disease Control and Prevention (CDC) reported that around 76 million cases of foodborne diseases, resulting in 325,000 hospitalizations and 5,000 deaths, are estimated to occur each year in the US [39]. The World Health Organization (WHO) has also declared that food-borne disease is growing and becoming a serious public health problem in both developed and developing countries [40].

One example of a significant food-borne illness is Listeriosis. Listeriosis is caused by *Listeria monocytogenes*, a bacterium commonly found in soil and water. Foodborne listeriosis is a relatively uncommon infection but has a high case fatality rate, in the range 20 to 30% [39]. The WHO and the Food and Agriculture Organization of the United Nations (FAO) reported that there are two main categories of listeriosis: invasive listeriosis and non-invasive listeriosis [41]. Serious problems of invasive listeriosis that occur in adults are septicema, meningitis, enceplalitis, abortion, or stillbirth [42]. Non-invasive foodborne listeriosis causes diarrhoea, fever, headache and myalgia [41].

The main cases of human listeriosis occur among pregnant, elderly, and immunosuppressed individuals [43]. McLauchlin *et al.* reported that 91 cases of

pregnancy associated listeriosis in England and Wales during 1995-1999, had a death rate of 28.24%, including miscarriages, stillbirths, and neonatal deaths [44].

Major outbreaks of listeriosis are associated with ready-to-eat (RTE) foods, and one example was in the United States where around 101 cases of illness and 21 deaths occurred after consumption of contaminated hot dogs [45]. Outbreaks of listeriosis associated with RTE foods, reported in several locations during 1980-1999, are summarised in Table 2.4 [46].

Table 2.4 *Summary of listeriosis outbreak associated with RTE during 1980-1999 (Adapted from [46])*

Place	Total cases	Perinatal (%)	Fatality rate (%)	Food source
Maritime Provinces of Canada	41	83	34	Coleslaw
New England	49	14	29	Pasteurised milk
Switzerland	57	9	32	Soft cheese
Western United States	142	65	34	Mexican-style cheese
Pennsylvania	36	11	44	Unknown
Connecticut	10	20	10	Shrimp
Italy	39			Rice salad
France	38	82	32	Rillettes (pork)
Illinois	45			Chocolate milk
Italy	1566			Corn salad
United States	101	12	21	Hot dogs, deli meats
France	32	28	31	Pork tongue

Waterborne diseases are also a significant global problem. Most waterborne diseases cause diarrhoea, and around 88% of cases of diarrhoea worldwide are related to unsafe water, inadequate sanitation or insufficient hygiene, and these cases result in 1.5 million deaths each year, commonly children [47]. During the period 1992 – 2003 in England and Wales, around 4300 people were affected by waterborne infectious intestinal disease with 89 outbreaks being involved: 24 outbreaks (27%) associated with public water supplies, 25 outbreaks (28%) associated with private water supplies, 35 outbreaks (39%) associated with swimming pools, and other sources were implicated in the five other outbreaks (6%). The microorganisms

associated with these outbreaks were *Cryptosporidium* (69%), *Campylobacter sp.* (14%), *Giardia* (2%), *E. coli* O157 (3%) and *Astrovirus* (1%) [48].

In the United States over the period 1999 – 2000, 39 outbreaks associated with drinking water were reported by 25 states, with one of these outbreaks affecting 10 states. These were estimated to have caused around 2,000 illness cases and two deaths [49]. A study by Yoder *et al.* reported 78 cases of waterborne-disease outbreaks associated with recreational water in 31 states during 2005 – 2006, affecting approximately 4,500 individuals, and resulting in 116 hospitalizations and five deaths [50].

Three common waterborne diseases in the United States are Legionnaires' disease, cryptosporidiosis and giardiasis, as reported by the Center for Disease Control and Prevention in 2010 [51]. The total estimated costs for these diseases were $154 – 539 million, containing around $44 – 147 million in direct government payment for Medicare and Medicaid. Estimated annual costs for giardiasis are about $16 – 63 million, cryptosporidiosis is $37 – 145 million and Legionnaires' disease is around $101 – 321 million [51]. Some common sources of food and waterborne diseases or illness are listed in Table 2.5.

2.8 Bactericidal properties of light

Decontamination is a process that removes or destroys hazardous substances from contaminated objects or materials, in order to prevent adverse effects on health or the environment. Ultraviolet (UV) and visible light radiation can react with microorganisms directly to provide the effect of decontamination. The use of light technologies for decontamination applications within areas such as the hospital environment, the food industry, public buildings, water and agricultural plants is not new. However, renewed interest in the development of light-based technologies for the inactivation of microorganisms is growing. This is due to the need for complementary and/or alternative solutions to enhance the decontamination procedures already in use in clinical and industrial applications in order to reduce the incidence of microbial infection. UV light and visible-light for microbial inactivation will be discussed in this section.

Table 2.5 *Microorganisms commonly associated with food and waterborne illness*

Foodborne illness		**Waterborne illness**	
Bacteria	**Virus**	**Bacteria**	**Virus**
Campylobacter jejuni	*Enterovirus*	*Clostridium botulinum*	*Adenovirus*
	Hepatitis A	*Campylobacter jejuni*	*Astrovirus*
Salmonella spp	*Hepatitis E*	*Vibrio cholerae*	*Calicivirus*
Escherichia coli	*Norovirus*	*Escherichia coli*	*Enteric Adenovirus*
Bacillus cereus	*Rotavirus*	*Mycobacterium marinum*	*Parvovirus*
Listeria monocytogenes	**Fungi/Yeast**	*Shigella*	*Coronavirus*
Shigella spp	*Fusarium* spp	*Salmonella*	*Hepatitis A*
Staphylococcus aureus	*Rhodotorula* spp	*Legionella pneumophila*	*Poliovirus*
Clostridium perfringens	*Botrytis* spp	*Vibrio cholerae*	*Polyomavirus*
	Aspergillus spp		**Fungi/Yeast**
Vibrio parahaemolyticus	*Brettanomyces* spp		*Aspergillus*
	Candida spp	*Vibrio parahaemolyticus* *Yersinia enterocolitica* *Yersinia pseudotuberculosis*	*Alternaria*
Yersinia enterocolitica	*Zygosaccharomyces* spp	**Parasites**	*Cladosporium*
Yersinia pseudotuberculosis	*Rhizopus stolonifer*	*Schistosoma*	*Epicoccum*
Brucella spp.	*Saccharomyces bailii*	*Dracunculus medinensis*	*Philaphora*
Clostridium botulinum	*Debaryomyces* spp	*Taenia*	*Phoma*
Parasites	*Peniciillium* spp	*Fasciolopsis buski*	*Ulocladium*
Diphyllobothrium sp.	*Byssochlamys* spp	*Hymenolepis nana*	*Actinomycetes*
Nanophyetus sp.		*Echinococcus granulosus*	*Cyanobacteria*
Taenia saginata		*Ascaris lumbricoides*	*Candida albicans*
Taenia solium		*Enterobius vermicularis*	*Geotrichum candidum*
Fasciola hepatica		*Entamoeba histolytica*	
Anisakis sp.		*Cryptosporidium parvum*	
Ascaris lumbricoides		*Cyclospora cayetanensis*	
Eustrongylides spp		*Giardia lamblia*	
Trichinella spiralis		*Microsporidia*	
Trichuris trichiura			
Acanthamoeba			
Cryptosporidium parvum			
Cyclospora cayetanensis			
Entamoeba histolytica			
Giardia lamblia			

2.8.1 UV light for microbial inactivation

UV energy radiation can be used for inactivation of microorganisms, and it depends on the exposure time and amount of energy radiation. The UV radiant exposure (UV dosage) has been defined as follows [11, 52]:

$$UV\ Dose = I\,t, \tag{2.30}$$

where I is the irradiance of UV light in Wcm^{-2}, t is exposure duration in seconds and the radiant exposure (UV dose) in Jcm^{-2}.

The effect of UV light on microbial inactivation varies. A study by Guerrero-Beltrán *et al.* mentioned that wavelengths of UV radiation ranging between 220 nm and 300 nm is also germicidal against microorganisms, where the highest germicidal effect is obtained in the range 250 nm and 270 nm [53]. In these ranges, the wavelengths are effective to inactivate microorganisms such as bacteria, viruses, protozoa, moulds and yeasts and algae [53]. Meanwhile, a study by Chang *et al.*, which used UV radiation at wavelength of 254 nm, reported that most of the vegetative bacteria tested, including *Escherichia coli*, *Staphylococcus aureus*, *Shigella sonnei*, and *Salmonella typhi*, demonstrated similar resistance to UV irradiation, with a 3-$\log_{10}$ reduction (99.9%) at around a dose of 7 $mJcm^{-2}$. They also compared the response of poliovirus and rotavirus to UV irradiation, and they exhibited three to four times more resistance than the vegetative bacteria [54].

It is difficult to directly compare the doses of UV light required for inactivation of microorganisms due to issues such as the difficulties in measuring UV dose accurately, and also because microorganisms vary in their response to UV irradiation depending on the type of microorganism, the growth medium, the culture period and influences of the plating methods [54].

Table 2.6 gives examples of the response of microorganisms to UV irradiation, with differences in inactivation rates (i.e. the same microbial species resulting in different log reductions with the same UV dose, or vice versa) likely to be associated with the above reasoning.

Table 2.6 *Examples of microbial inactivation using continuous UV sources*

Microorganisms	UV source lamp	Dose ($mJcm^{-2}$)	Log_{10} Reduction	Reference
Escherichia coli	low-pressure	10	5	[9]
	medium-pressure	10	5.2	[9]
	Not stated	8	3	[54]
	low-pressure	8	3.5	[55]
Staphylococcus aureus	Not stated	8	3	[54]
Shigella sonnei	Not stated	8	3	[54]
Streptococcus faecalis	Not stated	11	3	[54]
Salmonella typhi	Not stated	9	5	[54]
Encephalitozoon intestinalis spores	low and medium pressure	6	> 3.6	[56]
	low and medium pressure	3	1.6-2	[56]
Cryptosporidium parvum oocyst	low and medium pressure	3	2-2.9	[56]
	low and medium pressure	>25	3	[57]
Acanthamoeba cysts	Not stated	70	2	[54]
Bachillus subtilis	low-pressure	60	4	[58]
	low-pressure	50	3	[55]
	low-pressure	40	4	[59]
	Xel* excilamp	20-25	4	[59]
	Not stated	78	4	[54]
Bachiluus anthracis	low-pressure	60	3.5	[58]
S. aureus phage	low-pressure	30	3.5	[55]
Adenoviruses	low-pressure	123 - 182	4	[60]
	medium-pressure	65 - 90	4	[60]
Poliovirus	Not stated	20	3	[54]
Rotavirus	Not stated	25	3	[54]

Microbial inactivation using Pulsed-UV (PUV) has been used for decontamination applications, and is a potential alternative to continuous UV-light decontamination technologies as continuous UV-light has disadvantages due to low penetration and low emission power.

The high peak power dissipation of PUV can reach around 35 MW, while the emission power of continuous UV-light sources is in the range of 100 to 1,000 W [14, 52, 54]. PUV is a non-thermal technology which uses short duration high-energy pulses of broad-spectrum white light. It has been applied for food processing applications with a dose of around 0.01 to 50 Jcm^{-2} per 1 pulse at the surface of the material to be sterilized, and pulse duration ranging from 1 μs to 0.1 s, typically 1 to 20 pulses per second [14, 61].

The effectiveness of PUV-light for inactivation of bacteria, viruses, fungi, protozoa, fungi and yeasts is well documented [13, 14, 61-65]. A study by Wekhof *et al.* demonstrated *Aspergillus niger* spore inactivation resulting in 4.8-log_{10} reduction, with UV dose at 1 Jcm^{-2} (equivalent to 5 pulses) [66]. Lamont *et al.* reported that poliovirus and andenovirus can be inactivated by around 4-log_{10} reduction and 1-log_{10} reduction with 10 pulses at a dose of 12 $mJcm^{-2}$, respectively [13]. McDonald *et al.* also reported that about 5.5-log_{10} reduction in aqueous suspension and 3-log_{10} reduction on surfaces of *Bacillus subtilis* can be achieved by a UV dose of 44 $mJcm^{-2}$ and 8 $mJcm^{-2}$, respectively [67]. Gomez-Lopez *et al.* has also reported the effect of PUV-light technology for microbial inactivation and detailed data for this report are summarised in Table 2.7 [68].

2.8.2 Mechanism of UV Inactivation

The UV light radiation which is most effective for inactivation of microorganisms is UV-C [69], and UV-C is also known as ultraviolet germicidal irradiation (UVGI). It has the ability to alter the deoxyribonucleic acid (DNA) molecules and, consequently, prevent cell replication which ultimately causes cell death. The wavelengths in the range between 250 nm and 270 nm have the highest germicidal effect on microorganisms [53, 69], and this is the reason for the frequent use of low-pressure

mercury lamps (which have a peak at 254 nm) for the surface decontamination of foods, liquid food products and water [53, 70-72].

Table 2.7 *Summary of the effect of PUV-light technology for microbial inactivation (Adapted from[68])*

Microorganism	No. of Pulses	Pulse Intensity (J)	Log_{10} reduction
Gram-positive bacteria			
Alicyclobacillus acidoterrestris	50	7	>5.2
Bacillus circulans	50	7	>4.1
Brochotrix thermosphacta	50	7	3.1
Lactobacillus sake	50	7	2.5
Leuconostoc mesenteroides	50	7	4
Bacillus cereus	50	7	>3.0
Clostridium perfringens	50	7	>2.9
Listeria monocytogenes	50	7	2.8
Staphylococcus aureus	50	7	>5.1
Gram-negative bacteria			
Photobacterium phosphoreum	50	7	>4.4
Pseudomonas fluorescens	50	7	4.2
Shewanella putretaciens	50	7	3.9
Aeromonas hydrophila	50	7	2.3
Escherichia coli	50	7	4.7
Salmonella typhimurium	50	7	3.2
Shigella flexnii	50	7	3.8
Yersinia enterocolitica	50	7	3.9
Enterobacter aerogenes	50	7	2.4
Klebsiella oxytoca	50	7	4.2
Yeasts			
Candida lambica	50	7	2.8
Rhodotorula mucilaginosa	50	7	>2.8
Fungi			
Aspergillus flavus	50	7	2.2
Botrytis cinerea	50	7	1.2

The absorbed ultraviolet light can cause two major types of DNA lesions, cyclobutane–pyrimidine dimers (CPD) and 6–4 photoproducts (6–4PP), and these make up around 75% and 25% of DNA damage products, respectively [73]. CPD and 6–4PP induce distortion in the DNA helix, and consequently cause bends or kinks in the DNA of 7 – 9° and 44°, respectively [74, 75]. If DNA lesions are unrepaired they can disrupt DNA transcription and replication, resulting in the misreading of genetic code, causing mutations and cell death [74].

2.8.3 Mechanisms of UV Repair

Microorganisms have the ability to repair UV-induced DNA damage from exposure to UV radiation from natural sunlight. Two main types of repair mechanisms used to compensate for the damaging effects of UV radiation are light-independent (dark-repair) and light-dependent (photoreactivation) [9, 74].

2.8.3.1 Dark-repair Mechanisms

In light-independent, or dark-repair, mechanisms the process may not directly reverse DNA damage caused by UV radiation but it involves numerous proteins and enzymes replacing the damaged DNA with new, undamaged nucleotides [9, 74]. Two major types of dark-repair mechanisms are base excision repair (BER) and nucleotide excision repair (NER) [74].

BER repairs the oxidative DNA damage that occurs in both the cell nucleus and mitochondria [76]. NER has an important role in the repair of DNA damage and involves a complex pathway which removes a wide variation of DNA distorting lesions, including CPD thymine dimers and 6-4PP [74, 75, 77]. NER utilises around 30 gene products to remove damage- from cellular DNA [74, 78].

2.8.3.2 Photoreactivation

In contrast to dark-repair mechanisms, photoreactivation is a light-dependent process that requires the energy of light to reverse the DNA damage caused by UV radiation [9]. The specific wavelengths of light required for the photorepair process are near UV-visible light in the range 300 – 500 nm [9, 79]. Photolyase is the enzyme responsible for removing DNA lesions caused by UV radiation. Many microorganisms use CPD photolyase or 6–4 photolyase to repair DNA damage [75].

CPD photolyases can be found in bacteria, fungi, plants, invertebrates and many vertebrates, while 6-4 photolyases can be identified in *Drosophila*, silkworm, *Xenopus laevis* and rattlesnakes, but not in *E. coli* or yeast [75]. Photolyases are absent in humans [80, 81].

Photoreactivation and dark-repair mechanisms can be used to reverse the formation of a dimer. Formation of PRE-dimer complex, and the subsequent release of PRE (Photoreactivating Enzyme) and the repaired DNA molecule has been suggested as a two-step reaction for photoreactivation, and is summarised in Fig. 2.15 [82].

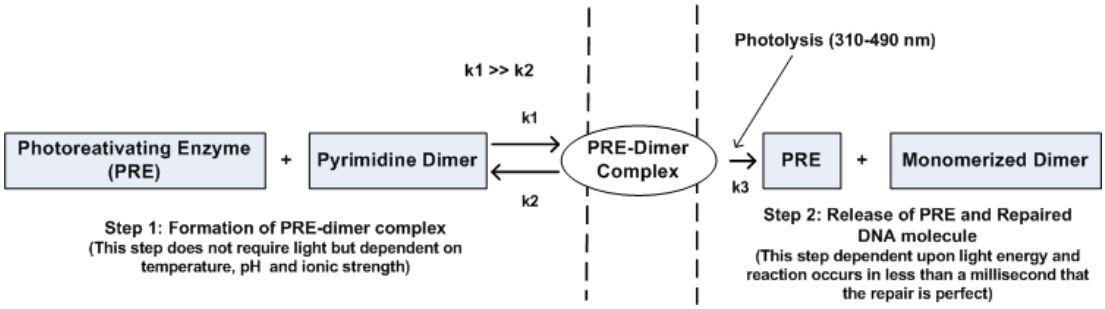

Fig. 2.15. *Two-step reaction scheme for photoreactivation (Adapted from [82]).*

UV-A wavelengths can be involved in a phenomenon called *concomitant photoreactivation*. This mean that these wavelengths have both the potential to cause oxidative damage to microbial cells, but also have the potential to photorepair UV-induced lesions in the DNA [83].

2.8.4 Visible light for microbial inactivation: Photodynamic inactivation

As with UV-light radiation, visible light can also be used for inactivation of microorganisms. Photodynamic inactivation (PDI), also known as photodynamic therapy (PDT), is a process involving the use of a non-toxic dye or photosensitizer in combination with particular wavelengths of light (usually visible) in order to induce a phototoxic reaction, typically via the production of singlet oxygen ($^1O_2$), which causes microbial cell death [15, 84-86].

Photodynamic activity of chemical compounds towards microorganisms has been known for over 100 years. Nevertheless, since antibiotics were discovered by

Alexander Fleming in 1928 and mass produced (penicillin) by H. Florey and E. Chain in the 1940s, antimicrobial photodynamic therapy began to be forgotten [87]. The rapidly increasing emergence of antibiotic resistant microorganisms has driven research into the development of new antimicrobial strategies, such as the use of PDI, as alternative antimicrobial treatments. Both Gram-positive and Gram-negative bacteria are killed with this process [85, 87].

In general, PDI uses the combination of a photosensitizing substance and light (either visible or UV) to produce singlet oxygen and other oxidising products, which results in cell death [87].]. An advantage of PDI for medical antimicrobial therapy, is that the photosensitizer and the light irradiation can be directed straight into the target tissue or lesion [85].

Even though UV-light tends to be more bactericidal than visible light, visible light (with or without photosensitisers) has safety advantages which means that it can be used for applications that might not be suitable for UV-light.

2.8.5 Porphyrins

Porphyrins are natural molecules that have a broad use in biological processes such as oxygen transport, photosynthesis, catalysis and pigmentation [88]. Porphyrins can also act as photosensitising molecules. The basic structure of porphyrins is a porphine macrocycle that has the configuration of a 16-atoms ring containing 4 nitrogen atoms, obtained from 4 tetrapyrrolic (C_4H_5N) subunits linked by 4 methine bridges (=CH-) [88], as shown in Fig. 2.16.

Porphyrins can absorb light within the UV and visible spectrum [88] and act as photosensitising molecules. Light wavelengths of approximately 400 nm are absorbed well by porphyrin molecules, and this absorption peak is known as the Soret band. Porphyrins also have several smaller absorption peaks at longer wavelengths, known as Q bands, although these are much weaker [88]. The high absorption peak at 400 nm indicates that porphyrin molecules are very suitable for photodynamic inactivation using light sources with light emission in the region of 400 nm .

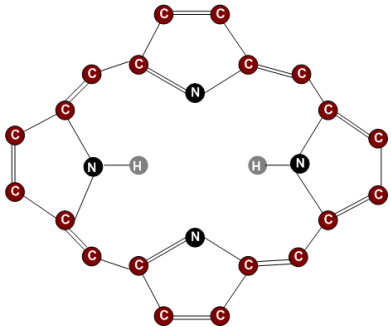

Fig. 2.16. *Basic structure of porphyrins, porphine macrocycle (Adapted from [88])*

Many porphyrin molecules within biological systems have metal atoms or ions (iron, nickel, zinc, copper, cobalt) inserted in the centre of the macrocycle forming metalloporphyrins. Metalloporphyrins are not suitable for photodynamic inactivation reactions as the metal rapidly quenches any singlet oxygen that is produced.

2.8.6 Mechanisms of Photodynamic Inactivation

Three main factors required for photodynamic inactivation reactions are the photosensitiser, light of an appropriate wavelength, and molecular oxygen [89]. An illustration summarising photodynamic inactivation reactions is shown in Fig. 2.17. The process involves absorption of light energy by the photosensitizer. This excited photosensitizer then reacts with molecular oxygen to form the highly reactive singlet oxygen ($^1O_2$), which then causes oxidisation within the cell, and consequently, cell damage or death [89].

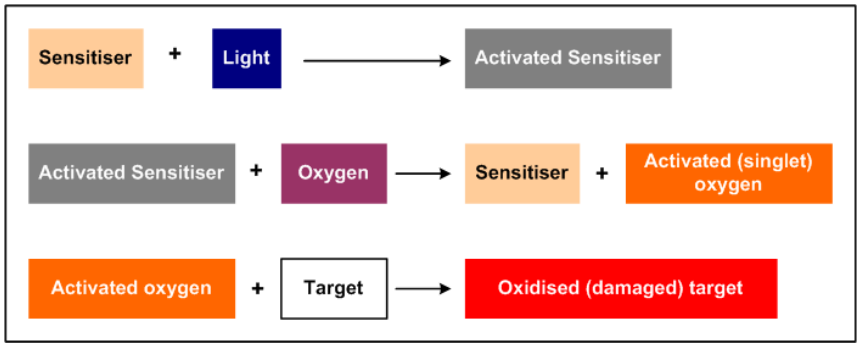

Fig. 2.17. *An illustration of photodynamic inactivation processes (Adapted from [89]).*

Absorption of light energy of the appropriate wavelength excites the photosensitizer molecule to the triplet state. The triplet state photosensitizer can then follow one of two pathways for photodynamic inactivation to occur: these are known as Type I and

Type II reactions, and both require the presence of oxygen [85]. Fig. 2.18 shows the photosensitization mechanisms involved in Type I and Type II photodynamic inactivation reactions. It can be seen that when the photosensitizer molecule absorbs the light and is excited from its initial ground state (S_0) into an exited state (S_1) there are three potential things that can occur : (i) release of energy generating heat, (ii) release of fluorescence or (iii) intersystem crossing of the excited singlet state photosensitizer molecule (S_1) to a triplet state (T_1) [84].

Type I photosensitization involves charge transfer from the triplet state (T_1) photosensitizer molecule to the substrate (e.g. bacterial cell components), and results in the production of radical ions that can react with oxygen to generate cytotoxic species, such as hydroxyl, superoxide and lipid-derived radical. Type II photosensitization involves energy transfer from the triplet state (T_1) photosensitizer molecule to ground state molecular oxygen ($^3O_2$), producing the highly reactive singlet oxygen ($^1O_2$) [85, 86]. Singlet oxygen is highly-oxidizing and capable of damaging the bacterial cell wall, lipids, enzymes, nucleic acids and proteins, and plays the major role in photodynamic inactivation of pathogens [84-86].

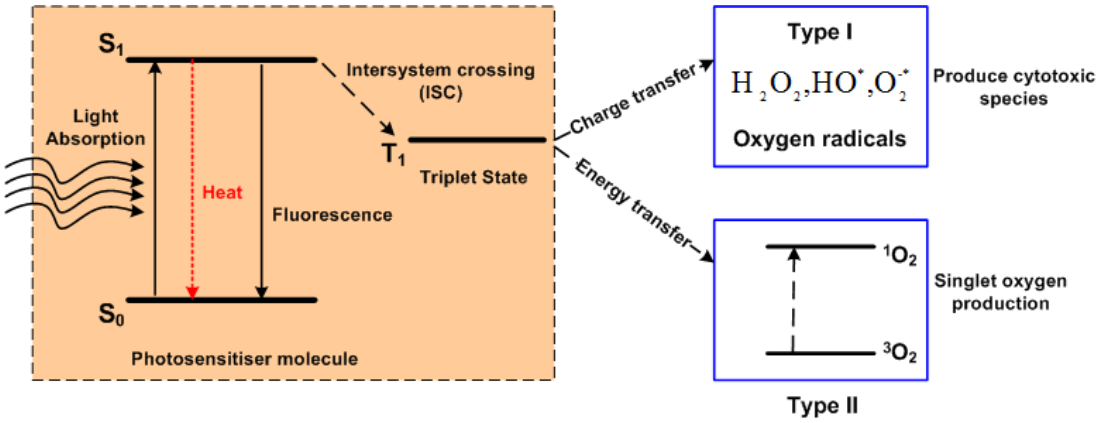

Fig. 2.18. *Schematic diagram of photosensitization mechanisms to produce Type I and Type II photodynamic inactivation reaction (Adapted from [84, 85, 90]).*

There are two main types of photosensitiser molecule which can be utilised in photodynamic inactivation mechanisms:

- exogenous photosensitisers: These are chemicals, dyes or porphyrins which are added into the system either during light exposure or for pre-treatment prior to light exposure.

- endogenous photosensitisers: These are naturally-occurring photosensitisers (i.e. porphyrins) within the cell. In this case, microbial photodynamic inactivation relies on the presence of endogenous porphyrins and does not require the addition of other photosensitiser molecules.

Photodynamic inactivation using exogenous and endogenous photosensitizer molecules will be discussed in the following sections (Sections 2.12.6.1, and 2.12.6.2, respectively).

2.8.6.1 Microbial Photodynamic Inactivation involving Exogenous Photosensitisers

Microorganisms can be inactivated by administration of a non-toxic dye or photosensitiser and light *in vitro* [85]. The concept of photosensitization-based inactivation of microorganisms relies on the photosensitiser molecule being taken up by the cell and accumulating in significant amounts in the target area (e.g. cytoplasmic membrane) leading to irreversible damage in bacteria when exposed to the appropriate wavelength of light [85].

Gram-positive bacteria are more susceptibility than Gram-negative bacteria to photosensitization mechanisms. Gram-positive bacteria can easily take up photosensitiser molecules because they have a cytoplasmic membrane which is surrounded by a relatively porous layer of peptidoglycan and lipoteichoic acid [85]. Gram-positive bacteria have a $40 - 80$ nm peptidoglycan wall with very small number of lipids and proteins [87]. Meanwhile, Gram-negative bacteria not only have a peptidoglycan wall but also have an outer membrane layer that contains negatively charged lipopolysaccharides (LPS), lipo-proteins and proteins with porin function. Porins are trans-membrane proteins which allow diffusion of hydrophilic solute across outer membranes of gram negative bacteria. This outer membrane

causes Gram-negative bacteria to show a significant resistance to antimicrobial PDT [87]. In order to enhance photodynamic inactivation of Gram-negative bacteria, some chemical molecules such as nona-petide polymyxin or Tris-EDTA, which are membrane disorganising substances, are commonly used [87].

Another method of enhancing inactivation is the use of 5-aminolevulinic acid (ALA), and is known as ALA based photodynamic therapy (ALA-PDT) [91]. According to Karrer *et al.,* 5-ALA is defined as "a precursor of endogenous porphyrins in the biosynthetic pathway for haem which induces the biosynthesis of photosensitising concentrations of protoporphyrin IX and other porphyrin metabolites within the cells" [92]. This means that photosensitising concentrations of protoporphyrin IX can be modulated by administration of the haem precursor δ-aminolevulinic acid (ALA) [91]. Previous work has shown that pre-incubation of some Gram-positive and Gram-negative bacteria with exogenous 5-ALA supplemented into the culture medium has the capability to enhance porphyrin biosynthesis, mostly enhancing coproporphyrin levels [92, 93]. For example, *Escherichia coli* pre-incubated with 5-ALA demonstrated a significant reduction in viability after light treatment with wavelengths of near-UV light [94].

Many reports have been published about the use of photosensitisers and light for microbial inactivation of viruses, fungi, yeasts and parasites *in vitro*. Some reports regarding the PDI of viruses have concluded that enveloped viruses are more sensitive to the photosensitising action than non-enveloped strains. In the same way, PDI is able to inactivate yeasts, parasites and fungi *in vitro* [85]. Some examples of microbial photodynamic inactivation with added photosensitizer molecules are listed in Table 2.8.

Table 2.8 *Examples of microbial inactivation using exogenous photosensitisers*

Microorganism	Light Source	Photosensitiser	Log_{10} Reduction / (Dose in Jcm^{-2})	Ref
Bacteria				
Staphylococcus aureus	Tungsten lamp	Protochlorophyllide	7.1 / (1.1)	[95]
	Tungsten lamp (λ = 546-660 nm)	Fenothiazine	4 – 5 / (2 – 4)	[96]
	LED (λ = 663 nm)	Methylene blue	4 / (6)	[97]
	He-Ne laser (λ= 632.8 nm)	Tin (IV) chlorine e6 (SnCe6)	2.5 / (8.4)	[98]
Listeria monocytogenes	Tungsten lamp	Protochlorophyllide	3.4 / (1.1)	[95]
Bacillus subtilis	Tungsten lamp	Protochlorophyllide	5.1 / (1.1)	[95]
	Xenon lamp	Rose Bengal	<< 1 / (100)	[99]
Escherichia coli	Tungsten lamp (λ= 546-660 nm)	Fenothiazine	2 / (5)	[96]
	Tungsten lamp (λ =350-800 nm)	Porphyrins	4.5 / (108)	[100]
	Xenon lamp	Rose Bengal	2 / (43)	[99]
	LED (λ= 663 nm)	Methylene blue	4 / (6)	[97]
Pseudomonas aeruginosa	Tungsten lamp (λ= 546-660 nm)	Fenothiazine	5 / (20)	[96]
	Halogen	5-Aminolevulinic Acid and 5-Aminolevulinic Acid Derivatives	1.9×10^{-3} (survival fraction) / (120)	[101]
MRSA	Halogen	5-Aminolevulinic Acid and 5-Aminolevulinic Acid Derivatives	5×10^{-6} (survival fraction) / (120)	[101]
Porphyromonas gingivalis	Xenon lamp	Toluidine blue O	5 / (10)	[102]
	LED (λ= 671 nm)	poly-L-lysine (pL)–chlorin *e6* (c_{e6})	8.1 (% survival organisms) / (15)	[103]
	Diode laser (λ =665 nm)	Methylene blue	99 – 100% / (21.2)	[104]
Deinococcus radiodurans	Xenon lamp	Rose Bengal	5 / (0.5)	[99]
Actinomyces viscosus	LED (λ= 671 nm)	poly-L-lysine (pL)–chlorin *e6* (c_{e6})	2 (% survival organisms) / (15)	[103]
Fungi & Yeasts				
Candida albicans	LED (λ = 663 nm)	Methylene blue	4 / (66)	[97]
	LED (λ = 455 nm)	The Photogem$^{(R)}$	7 / (18)	[105]
Aspergillus Fumigatus	Visible light	Green 2W	2.7×10^{6} $CFUml^{-1}$ / (385)	[106]
Parasites				
Culex sp., *Chaoborus* sp. Larvae, *Daphnia* sp.	Mercury lamp	Chlorophyllin and pheophorbid	50% of mortality in the tested organisms / (162)	[107]
Cutaneous leishmaniasis	Broad band light (λ= 665 ± 15 nm)	Phenothiazine	5.2 / (50)	[108]
Viruses				
Herpes simplex virus	Red light	Methyl aminolevulinate (Metvix$^{(R)}$)	Completely healed / (2 weeks)	[109]
HIV-1	Visible light	Methylene blue	~100% / ($10^{6.32}$ TCID 50/ml within 10 minutes)	[110]

2.8.6.2 Microbial Photodynamic Inactivation using Endogenous Photosensitisers

A number of studies have published that visible light exposure can be used for the inactivation of bacteria without the requirement for additional photosensitizer molecules. Ashkenazi *et al.* reported that the Gram-positive bacterium *Propionibacterium acnes*, naturally produces high quantities of intracellualar porphyrins, mostly coproporphyrins and protoporphyrin IX (PpIX) (with a minor contribution from uroporphyrin) [85], without the requirement for any trigger molecules such as ALA [117]. They utilised high intensity narrow band blue light with wavelengths ranging from 407 – 420 nm for inactivation of *P. acnes*, and results showed that *P. acnes* could be inactivated by seven orders of magnitude after exposure to a dose of 75 Jcm^{-2} [111]. Phototherapy for the skin disorder acne, (caused by *P. acnes*) with mixed blue-red light (peaks at 415 and 660 nm) has also been utilised for *P. acnes* inactivation, and the study demonstrated that the combination of blue and red light was significantly superior to blue light (peaks at 415 nm) alone for treatment of inflammatory lesions [112]. This is likely due to the red light wavelengths having anti-inflammatory properties.

A study by Feuerstein *et al.* demonstrated that blue light (400 – 500 nm) had the ability to inactivate Gram-negative periodontal pathogens such as *Porphyromonas gingivalis, Fusobacteriurn nucleatun* after light-exposed to a dose of 16 – 62 Jcm^{-2}. Meanwhile, Gram-positive bacteria such as *Streptococcus mutans* and *Streptococcus faecalis* can also be inactivated with a dose of 159 – 21 Jcm^{-2} [113]. The use of 405 nm light to eradicate *Helicobacter pylori* has been successfully demonstrated by Ganz *et al.* [114]. They reported that *H. pylori in vitro* can be inactivated by blue light (405 nm), with around a 5-log_{10} reduction after application of a dose of 40 Jcm^{-2}. Inactivation of *Staphylococcus aureus* and *Pseudomonas aeruginosa* using 405 nm light has also been successfully demonstrated by Guffey *et al.* [115].

Work within ROLEST has termed the use of 405 nm high-intensity narrow-spectrum light for microbial inactivation *HINS-light*. Maclean *et al*. utilized a continuous xenon broadband white-light source in conjunction with bandpass filters in the range 400 – 500 nm for inactivation of *S. aureus*. They found that the optimal wavelength for inactivation was 405 (± 5) nm [116]. Another study by Maclean *et al.*

demonstrated the effectiveness of a 405 nm HINS-light LED array for inactivation of a variety of medically important bacteria without the application of exogenous photosensitizer molecules [117]. The results of this study are summarised in Table 2.9.

Table 2.9 *Summary of the effect of 405 nm LED array for bacterial inactivation (Adapted from [117])*

Microorganism	**Dose (Jcm^{-2})**	**Log_{10} reduction**
Staphylococcus aureus	36	5
methicillin-resistant *S. aureus* (MRSA)	45	5
Staphylococcus epidermidis	42	4.6
Clostridium perfringens	45	4.4
Streptococcus pyogenes	54	5
Acinectobacter baumannii	108	4.2
Proteus vulgaris	144	4.7
Pseudomonas aeruginosa	180	4.2
Klebsiella pneumaniae	180	3.9
Escherichia coli	180	3.1
Enterococcus faecalis	216	2.6

A study by Murdoch *et al.* reported that *Campylobacter jejuni* could be inactivated by using a 405 nm HINS-light LED without application of exogenous photosensitiser molecules, with around a 5-log_{10} reduction achieved after exposure to a dose of 18 Jcm^{-2} [118]. They also found that suspensions of *Salmonella enteritidis* and *Escherichia coli* 0157:H7 could be reduced by 2.96 and 5.3-log_{10}, respectively, after exposure to a dose of 288 Jcm^{-2} [118].

2.8.7 High-Intensity Narrow-Spectrum (HINS) light for environmental decontamination

Previous work within ROLEST has used the bactericidal 405 nm HINS-light technology to develop a HINS-light Environmental Decontamination System (HINS-light EDS). The HINS-light EDS is a ceiling-mounted light source which

continuously decontaminates the air and exposed surfaces within illuminated areas. Initial studies within the clinical environment have successfully demonstrated the use of the HINS-light EDS for significantly reducing levels of environmental contamination within hospital isolation rooms [1]. The HINS-light EDS is a novel disinfection technology and consists of one or more ceiling-mounted light sources and the main active components are 405 nm LED arrays blended with white light and covered by a Fresnel lens and diffuser [119]. Although the emitted light is bactericidal, it is harmless to patients and staff thereby permitting continuous environmental disinfection throughout the day [1]. This HINS-light EDS technology has many potential applications, for instance; disinfection of air and contact surfaces in clinical environments, food processing environments, clean rooms, and public buildings. Essentially, the HINS-light EDS could be deployed in any area where enhanced decontamination would be beneficial.

The system has been used in hospital isolation rooms used to treat burns patients, and its efficacy was assessed by comparing the levels of bacterial contamination in the isolation rooms during periods when the HINS-light EDS was in use against periods when the system was turned off. Bacterial contamination was assessed using contact agar plates. In order to evaluate the level of decontamination achieved with the HINS-light EDS, contact agar plates were used to sample a variety of frequently-touched surfaces (such as door handles, light switches, table tops, bed rails). They reported that approximately a 90% reduction of surface bacterial levels was achieved when the system was used for treatment of an unoccupied isolation room, and reductions in the range of between 56% and 86% were achieved in isolation rooms when occupied by an MRSA-infected burns patient [1].

Studies by Nerandzic *et al.* [120] and Rutala *et al.* [121] have demonstrated that UV-light radiation can be used for decontamination of rooms. They utilized UV-C radiation to reduce clinically important nosocomial pathogens in a contaminated hospital room. In contrast with the HINS-light EDS, due to safety reasons this system can only be used to kill pathogens in unoccupied rooms. During use of the UV system, the device was placed inside the room and the door was then closed and a wireless remote control was used to activate it. In contrast to this, the HINS-light

EDS can be used for room decontamination of occupied rooms as it is harmless to patient and staff.

Another type of system for whole room decontamination is detailed in a study by Boyce *et al.* They utilised Hydrogen Peroxide Vapor (HPV) to eliminate *Clostridium difficile* in the environment [122]. This system has similar safety issues as the UV systems described by Nerandzic *et al.* [120] and Rutala *et al.* [121], in that HPV can only be used in areas that are unoccupied and sealed for the period of the disinfection process.

Therefore, the current study was conducted to improve on the original (initial) HINS-light EDS prototype due to an initial prototype system has limitations and many features requiring optimising and improving: non-integrated power supplies, thermal management issues, light emission more dominant in violet/blue than desirable, safety characteristics and decontamination efficacy.

The literature review gave background theory for this study, two main area of research were carried out during the study as follows:

1. Microbiological investigation into the bactericidal properties of light (PUV and visible sensitivity of bacterial),

2. Engineering design, build and test of new improved prototype HINS-light EDS.

Microbiological techniques for the investigation into the bactericidal properties of light will be discussed in Chapter 3.

CHAPTER 3

MICROBIOLOGICAL TECHNIQUES

3.1 General

This chapter provides information for the microbiological investigation into the bactericidal properties of light, and the aim of this chapter was to give descriptions regarding a procedure and protocol for microbial inactivation. A brief description of the microorganisms, culture media, techniques and equipment used during the study is given in this chapter.

3.2 Microorganisms

The microorganisms and culture techniques used in the experimental work are detailed in this section.

3.2.1 Microbial Strains

The microbial strains used are listed in Table 3.1. Cultures were obtained from the National Collection of Type Culture (NCTC), (Colindale, UK), the Laboratorium voor Microbiologie, Universiteit Gent (LMG), and Mycotheque de l'Universite catholique de Louvain (MUCL) (both LMG and MUCL are a section of The Belgian Co-ordinated Collection of Microorganisms (BCCM)). Methicillin-resistant *Staphylococcus aureus* (MRSA) 16a is a clinical isolate and was obtained from Glasgow Royal Infirmary (Scotland, UK).

A brief description of each organism used during this study as mentioned in Table 3.1 will be reviewed in this section as follows:

- *Staphylococcus epidermidis* is a Gram-positive bacterium and is frequently found in the skin and mucous membranes of the human body [123]. It is an opportunistic pathogen, and Centers for Disease Control and Prevention (CDC) has reported that *S. epidermidis* is the most frequent cause of hospital-acquired infections (HAI), such as infections of the bloodstream, the urinary

tract, the cardiovascular system, pneumonia, and infections of the eye, ear, nose and throat [124].

- *Staphylococcus aureus* is a Gram-positive bacterium commonly found in the human nose and on skin, and is commonly associated with HAI [125, 126]. *S. aureus* can cause minor skin infections and life-threatening diseases such as impetigo, endocarditis, pneumonia, food poisoning, toxic shock syndrome and bacteremia [127]. Also, the CDC reported that food contaminated with *S. aureus* causes around 185,060 illnesses, 1,753 hospitalizations, and 2 deaths annually [128].

- Methicillin-resistant *Staphylococcus aureus* (MRSA) is also known as multidrug-resistant *Staphylococcus aureus* [129]. The National Audit Office (NAO) mentioned that around 9,000 deaths caused by MRSA bloodstream infections in the UK in 2007 [130], while a study by Cooper *et al.* reported that in the UK, there was a significant increase of *S. aureus* bacteraemia caused by MRSA from 2% in 1991 to 42% in 2000 [131].

- Listeria is a Gram-positive and significant foodborne pathogen, commonly found in soil, water, silage, sewage slaughterhouse waste, milk, and human and animal feces [132]. An important factor is that Listeria can grow at refrigerator temperature (~4 °C) when given sufficient time and pH (in the range of 4.5 to 9.6) [133, 134].

- *Listeria ivanovii* is generally pathogenics in ruminants fed on silage and is associated with gastroenteritis and bacteremia in man [135, 136]. Guillet *et al.* reported that human listeriosis caused by *L. ivanovii* is associated with immunodeficiency, underlying debilitating conditions, or advanced age [136]. *Listeria ivanovii* is one of six species of the genus listeria, and rarely cases of infections are found in humans but is responsible for 8% of all animal listeriosis [137, 138]. The commonest cases of infections in ruminants such as sheep and cattle, are associated with conditions such as abortions, stillbirths, and neonatal septicemias [138].

- *Listeria seeligeri* is part of the genus listeria and considered non-pathogenic. It is a Gram-positive, nonsporeforming, facultatively anaerobic rod, motile and contains a low guanine-cytosine content [138, 139]. Although considered non-pathogenic, the first case has been reported by Rocourt *et al.* regarding human infection caused by *L. seeligeri*. They reported human infection in a previously healthy adult and it was associated with acute purulent meningitis caused by *L. seeligeri* [140].

- *Salmonella enteritidis* is a Gram-negative, non-spore-forming rod shaped bacterium and a member of the family Enterobacteriaceae [141]. In the United States, approximately over 1,500 deaths and 14 million illnesses are caused by Salmonella every year [128]. It is estimated that around $464 million is the total costs for medical care and that the impact on the labor market was $2.3 billion in 1989 [142]. Salmonella infections are bacteria generally associated with foods such as eggs, poultry, raw meat and dairy products and theses infections cause significant food related deaths in the United States every year [143].

- *Shigella sonnei* is Gram-negative, facultatively anaerobic, non-sporeforming, non-motile rod-shaped bacterium. It is categorised as serogroup D serotype 1 and is the causative agent of shigellosis or "bacillary dysentery," [141, 144-146]. It has been reported that foodborne shigellosis is responsible for 448,240 cases, resulting in 6,231 hospitalizations and 70 deaths in the United States every year [128]. Niyogi reported that around 5% to 15% cases of *Shigella* are associated with diarrhoea and 30% to 50% with cases of dysentery [147]. The symptoms of shigellosis are commonly caused by the invasion of Shigellae into the local epithelium of the colon (large intestine) [144]. The invasion of Shigellae is controlled by a 180 to 220-kDa virulence plasmid and involves four stages: entry into epithelial cells, intracellular multiplication, intra- and intercellular spreading, and killing of the host cell [144].

- *Escherichia coli* are Gram-negative rod-shaped bacterium and is most commonly harmless. It can cause serious infections in hospitalised patients

and only serotype O157:H7 can cause serious food poisoning in humans [146, 148]. Infection of *E. coli* O157:H7 in individuals commonly causes bloody diarrhea and abdominal cramps with little or no fever. It may also cause hemolytic uremic syndrome (HUS), hemolysis, thrombocytopenia, renal failure and rarely infection by *E. coli* O157:H7 can cause death [149]. A study by Mead *et al.* reported that foodborne infections by *E. coli* O157:H7 in the Unites States has estimated around 73,480 illnesses, 2,168 hospitalisation and 61 deaths annually [128].

- *Saccharomyces cerevisiae* is a yeast, also known as baker's yeast or brewer's yeast. It is commonly used in baking, brewing, wine making, and biotechnology, and is typically regarded to be an occasional digestive commensal [150, 151]. A study by Aucott *et al.* reported three cases of life-threatening invasive infection caused by *S. cerevisiae* [152], and Enache-Angoulvant *et al*. suggested that *Saccharomyces* organisms should be added to the list of emerging fungal pathogens [150].

3.2.2 Culture and Maintenance of Microorganisms

Microorganisms are stored on Microbank™ beads (proLab Diagnostics) at -70 °C. For regular use of a microbial strain, the organism was cultured by taking out an inoculated Microbank bead, and streaking this bead onto an agar plate (agar type dependant on the organism) and incubated at the appropriate temperature and time. After the incubation period, the microorganism was then sub-cultured and incubated on an agar slope then kept refrigerated at 4 °C. This slope was used as a regular source of inoculum for experimental work, and was re-streaked at least every 4 weeks onto fresh agar to ensure the slope contained a pure culture and was not contaminated.

To culture microorganisms for experimental work, all microorganisms were cultivated overnight in 100 ml of broth growth medium at 37 °C and under rotary conditions (120 rpm). The media, temperature, and incubation time used for each microorganism are summarised in Table 3.1.

Table 3.1 *Microbial strains and their associated growth requirements*

Microorganism	Strain	Growth Medium	Incubation Period	Temperature (°C)
Staphylococcus aureus	NCTC 4135	Nutrient Broth/Agar	18-24 Hours	37
Shigella sonnei	LMG 10473	Nutrient Broth/Agar	18-24 Hours	37
Listeria monocytogenes	NCTC 11994	Tryptone Soya Broth / Agar	18-24 Hours	37
Listeria ivanovii	NCTC 11846	Tryptone Soya Broth / Agar	18-24 Hours	37
Listeria seeligeri	NCTC 11856	Tryptone Soya Broth / Agar	18-24 Hours	37
Salmonella enteritidis	NCTC 4444	Nutrient Broth/Agar	18-24 Hours	37
Escherichia coli 0157:H7	NCTC 12900	Nutrient Broth/Agar	18-24 Hours	37
Escherichia coli	NCTC 9001	Nutrient Broth/Agar	18-24 Hours	37
Saccharomyces cerevisiae	MUCL 28749	Malt Extract Broth/Agar	18-24 Hours	37
Staphylococcus epidermidis	NCTC 11964	Tryptone Soya Broth / Agar	18-24 Hours	37
Methicillin Resistant *Staphyloccocus aureus*(MRSA)	16a (Glasgow Royal Infirmary)	Nutrient Broth/Agar	18-24 Hours	37

3.3 Media

Culture media were prepared as required by dissolving the appropriate weights in distilled water according to the quantity stated by the manufacturer. For sterilisation of the media, all media was autoclaved at 121 °C for 15 minutes at 100 kPa, unless stated otherwise. For preparation of agar plates and agar slopes, sterilised molten agar was held in a water bath set at 48 °C until cool enough to pour into sterile Petri dishes or tubes, respectively.

3.3.1 Broths and Agars

Broths

- NUTRIENT BROTH (Oxoid Ltd, UK) [CM0001] 13 g/L
- MALT EXTRACT BROTH (Oxoid Ltd, UK) [CM0067] 20 g/L
- TRYPTONE SOYA BROTH (Oxoid Ltd, UK) [CM0129] 30 g/L

Agars

- NUTRIENT AGAR (Oxoid Ltd, UK) [CM0003] 28 g/L
- MALT EXTRACT AGAR (Oxoid Ltd, UK) [CM0059] 50 g/L
- TRYPTONE SOYA AGAR (Oxoid Ltd, UK) [CM0131] 40 g/L

3.3.2 Diluent

- Phosphate Buffered Saline (PBS) (Oxiod Ltd, UK) [BR0014G]: 1 tablet per 100ml distilled water

For experimental use, 100 ml and 9 ml volumes of PBS were prepared for resuspension of the centrifuged cell pellet, and preparation of serial dilutions, respectively (see Section 3.4.1). The 9 ml volumes of PBS were prepared using a bottletop-dispenser (VITLAB, Germany). The PBS was sterilised by autoclaving at 115 °C for 10 minutes at 67 kPa, and had a final pH of 7.3 ± 0.2 at 25 °C.

3.4 Microbial Enumeration Methods

Accurate methods for enumeration of microbial samples before and after inactivation treatment are very important in order to achieve the exact decrease in population size. To enumerate microorganisms, samples were plated onto agar and incubated at their optimal conditions as stated in Table 3.1. After sample incubation, plates were enumerated and results recorded as colony-forming units per millilitre ($CFUml^{-1}$).

The dilution and plating methods used for enumeration of microorganisms in this study are detailed in the following sections.

3.4.1 Serial Dilutions

After incubation, cultures were centrifuged for 10 min at 4300 rpm and the cell pellet re-suspended in 100 ml PBS, giving a suspension with a population of approximately 10^9 $CFUml^{-1}$. This microbial suspension was then serially diluted in PBS to provide the appropriate population densities for experimental use.

To prepare serial dilutions, 1ml of the undiluted 100ml bacterial suspension was added into 9 ml PBS to give a 10^{-1} dilution. This was then mixed using a Whirly mixer (FisherBrand, UK) to ensure a uniform suspension. One millilitre of this 10^{-1} dilution was then added into another 9 ml volume of PBS to get 10^{-2} dilution. This procedure was followed until the desired dilution factor was achieved.

3.4.2 Plating and Enumeration Techniques

After microbial samples were exposed to light treatment, samples were immediately plated onto agar using either spiral plate, spread plate and/or pour plate methods. The method chosen was dependant on the expected number of CFU's.

3.4.2.1 Spiral Plate Method

Spiral plating is a technique used for the enumeration of bacteria in a liquid sample, and involves dispensing the sample onto the surface of a rotating agar plate in the shape of a logarithmic Archimedes spiral [153, 154].

In this study, a WASP 2 spiral plater (Don Whitley Scientific Ltd, UK), shown in Fig. 3.1, was used to dispense a 50 µl sample volume onto the surface of an agar plate. After the sample was spiral plated, agar plates were incubated and the colonies were enumerated either manually using a colony counter (Stuart Scientific, UK) or on a PC using the aCOLyte colony counter (Don Whitley Scientific Ltd, UK), shown in Fig. 3.2a and 3.2b, respectively. Both methods use a counting grid which is centered over the plate. Each grid segment corresponds to a constant volume of sample, and the number of $CFUml^{-1}$ in the sample can be calculated using either reference charts (when using the manual counter) or the aCOLyte software.

Fig. 3.1. *WASP 2 Spiral Plater*.

(a) (b)

Fig. 3.2. *Colony counting methods: a) manual counting using the colony counter, and b) automatic counting using aCOLyte software.*

3.4.2.2 Spread Plate Method

Spread plates of samples were prepared by pipetting 50, 100, 200 or 500 µl of microbial sample onto an agar plate, and spreading evenly over the agar surface using a sterile L-shaped spreader. After incubation, a colony count of the whole agar plate was taken and this was then multiplied by the appropriate factor (dependant on the sample volume deposited on the plate) to obtain a count of the number of $CFUml^{-1}$ in the sample. Spread plates can also be prepared using the WASP 2 spiral plater. In this case, 100 µl of sample was deposited onto the agar plate using the

linear distribution mode. Enumeration involved counting the whole plate and multiplying the count by ten to get the number of $CFUml^{-1}$ in the sample.

3.4.2.3 Pour Plate Method

If the number of microorganisms in the sample was expected to be less than 250 $CFUml^{-1}$, the pour plate method was used. 1 ml of microbial sample was pipetted into a sterile Petri dish, and then approximately 20 ml of molten agar was poured into the Petri dish. To ensure a uniform mixture between the microbial sample and the molten agar, the Petri dish was gently rotated clockwise (×10) and then anticlockwise (×10). The plate was then left to solidify before incubation. For enumeration, the whole plate was counted, and this represents the number of $CFUml^{-1}$ sample.

3.5 Statistical Analysis

In this study, all data represents a minimum of three replicates for each independent experiment, and the results are documented as mean values with standard deviation (SDs) being included. Significant differences in experiments were calculated using ANOVA (one way) analysis, with 95% confidence interval and p value ≤ 0.05 using MINITAB Release 16.

3.6 Other Equipment

The general descriptions of other equipment used for microbial analysis are detailed in Table 3.2.

Table 3.2 *Equipment used during the study*

Equipment	Function	Manufacturer
Kestrel automatic autoclave	Sterilisation of media and equipment used in experimental work, and contaminated waste prior to disposal	LTE Scientific Ltd, UK
Bench-top autoclave	Sterilisation of all media and equipment used in the experimental work	Dixon Surgical Instruments Ltd, UK

Merit W400 Distil	Distillation of water to provide water free of impurities	Grosseron, France
OHAUS Navigator & OHAUS Adventurer digital balances	Measurement of solid media and reagents	Precision Weighing Balances, USA
Rotary shaker incubator	Rotary incubation of microbial broth cultures	New Brunswick Scientific, USA
Fan-assisted incubator	Incubation of microorganisms on agar plates	LTE Scientific Ltd, UK
Grant Water-Bath	Maintained at 48°C for cooling molten agar prior to pouring	Scientific Laboratory Supplies Ltd, UK
Heraeus Labofuge 400R	To spin down cultures at 4300 rpm for 10 min. Used in combination with 50 ml volume centrifuge tube from Nunc (Thermo Fisher Scientific Inc, Denmark)	Kendro Laboratory Products, USA
Gilson pipettes; 100 µl, 1 ml, 5 ml and 10 ml	Used in conjunction with sterile pipette tips for the transfer of microbial suspensions	Gilson Inc, USA
Refrigerators	For the storage of microbial cultures on agar slopes and agar plates maintained at 4°C	Lee Medical
Biomate 5 UV-Visible Spectrophotometer	To obtain transmission and absorbance reading of liquid samples using either fixed wavelengths or broadband wavelengths (UV- Visible)	Thermo Spectronic, USA
LUMIX (DMC-FX10)	To take photographs of equipment	Panasonic, Japan
Power Meter	To measure irradiance ($mWcm^{-2}$) levels from light sources	L.O.T.-Oriel Ltd, UK
Digital thermometer (KM340)	To measure temperature (°C) levels	Kane-May, UK
MSH basic magnetic stirrer	In conjunction with 7 × 2 magnetic follower (Thermo Fisher Scientific Inc,	Scientific Laboratory

	Denmark) to allow sample agitation	Supplies Ltd, UK
Nikon Eclipse E400 light microscope	Used for viewing Gram stain slides to check purity of cultures	Nikon Instruments, UK
Ocean Optics HR4000 High-Resolution Spectrometer	Used in conjunction with Ocean Optics SpectraSuite software to measure emission spectrum of light sources	Ocean Optics, Inc., USA

3.7 Gram Stain

Gram staining is an important test for the identification and differentiation of Gram-positive and Gram-negative bacteria. It is commonly used to check the purity of bacterial cultures.

Preparation of smear for staining

Using a sterilized wire loop, 1 – 2 colonies of organism were lifted from an agar plate and emulsified with a drop of water on a clean microscope slide, or, if a liquid culture was used, a loopful of suspension was removed and directly place onto a clean microscope slide. After this film was allowed to air dry, the sample was fixed by passing the microscope slide through a Bunsen flame, typically 3 – 5 times.

Gram Staining Procedure

The fixed film was covered with Crystal violet for about 30 seconds, and then drained and rinsed with Lugol's iodine. It should then be covered with fresh iodine and left for 1 minute. After that, the iodine was drained and it was rinsed with 100% alcohol for approximately 15 seconds until no more violet colour came away. The slide was then washed gently with tap water and covered with Safronin and left for about 30 seconds. Finally, the fixed film was rinsed and blot dried and then viewed under an oil immersion lens on a microscope.

After the staining procedure, Gram-positive cells appear deep purple, due to retention of the purple crystal violet stain in the pores of the thick peptidoglycan layer in their

cell wall after dehydration from the alcohol washing stage. In contrast, Gram-negative cells do not retain the crystal violet stain, but retain the pink secondary stain, Safronin, and appear pink. This is because Gram-negative bacteria have a membrane outside of the peptidoglycan layer which allows passage of the solvent (alcohol wash) to remove the crystal violet stain.

Information on the microbial strains, media and culture and maintenance of microorganisms, methods of microbial enumeration and statistical analysis, equipment and microbiological tests will be used for the experimental arrangement and a sample preparation for the microbiological investigation into the bactericidal properties of light (Chapters 4 – 6 and 10).

CHAPTER 4

INVESTIGATION INTO THE USE OF PULSED UV-LIGHT FOR MICROBIAL INACTIVATION

4.1 Background

Ultraviolet (UV) light is electromagnetic radiation with a spectrum that is in the range of 100 nm to 400 nm. UV light is well-established as being highly antimicrobial, especially the wavelengths between 250 and 270 nm. This wavelength range has the highest germicidal effect, effective against microorganisms such as bacteria, viruses, protozoa, yeasts, fungi and algae [69].

Pulsed ultraviolet (PUV)-light is a novel non-thermal high-peak power technology, which achieves rapid inactivation of pathogenic and spoilage microorganisms. PUV-light technology is growing and becoming attractive for decontamination and sterilization applications due to its rapid energy transfer and inactivation rates [61, 66, 67, 155, 156].

As discussed in Section 2.8.2, microbial inactivation using UV-light exposure is mainly caused by microbial DNA absorbing UV-C photons, consequently leading to DNA-based damage in the form of mutagenic lesions, including cyclobutane pyrimidine dimers (CPD) and pyrimidine-pyrimidone 6-4 photoproducts (6-4PP), which block DNA replication and can ultimately render the microbial cell inactive [74].

The aim of this chapter is to investigate the effect of PUV-light from a broadband xenon lamp for inactivation of the bacterial species *Staphylococcus epidermidis*, *Staphylococcus aureus* and the yeast species *Saccharomyces cerevisiae* in liquid suspension. The effect of sample agitation during broadband PUV-light exposure of *S. cerevisiae* in liquid suspension is also investigated. The study then investigated the efficacy of the pulsed UV-light source for inactivation of *S. aureus* using pulses of 260 nm light compared to broadband light pulses.

4.2 Pulsed UV-light System

A schematic diagram of the pulse generator and flashlamp (Samtech Ltd, Glasgow, UK) used for microbial inactivation is shown in Fig. 4.1. The pulse generator has a dual 15 kHz switch mode power supply (SMPS) which supplies 1.1 kV and 0.4 kV as follows: the SMPS energized to 1.1 kV charges an energy storage capacitor, and the 0.4 kV charges a primary trigger circuit and pulse repetition rate (PRR) control. Once the storage capacitor is fully charged then the voltage control switches off the SMPS. The primary trigger circuit generates a 500 V pulse voltage when the system is switched on, which is stepped up to 25 kV by a pulse transformer inside the flashlamp chamber, subsequently generating light pulses. When operating at 1 kV (based upon a 1 kV capacitive discharge circuit), the energy stored in the capacitor (up to 20 J) to be transferred to the flashlamp, resulting in a peak power in the region of 1MW as shown in Fig. 4.2.

The resulting very short duration pulses of UV-rich light are produced from an exponentially decaying waveform, as shown in Fig. 4.2, with the time to half value being approximately 40 µs. Each pulse has an approximate peak current of 1.2 kA and a 6.8 µs rise time (Fig. 4.2).

The light source used in the system is a low-pressure (450 torr) xenon-filled flashlamp (Heraeus Noblelight XAP series, Germany), constructed from a clear fused quartz tube filled with xenon. The spectral emission of the flashlamp is broad, extending from ultraviolet to infrared, but as shown in Fig. 4.3, the emission is UV-rich, which is ideal for microbial inactivation ranging from 200 to 300 nm.

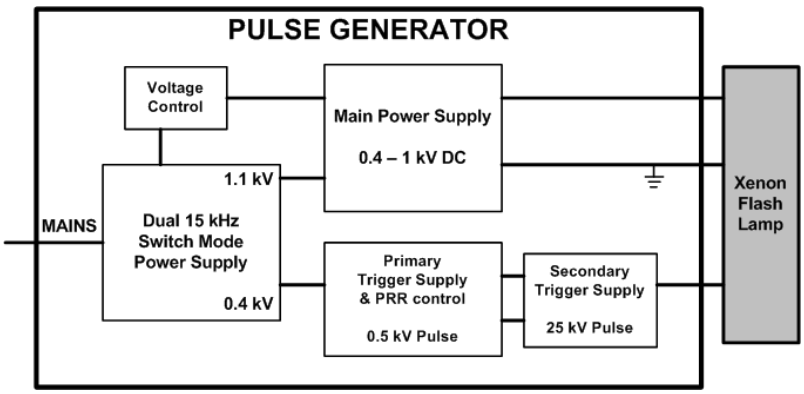

Fig. 4.1. *Schematic diagram of pulsed UV generator and flashlamp.*

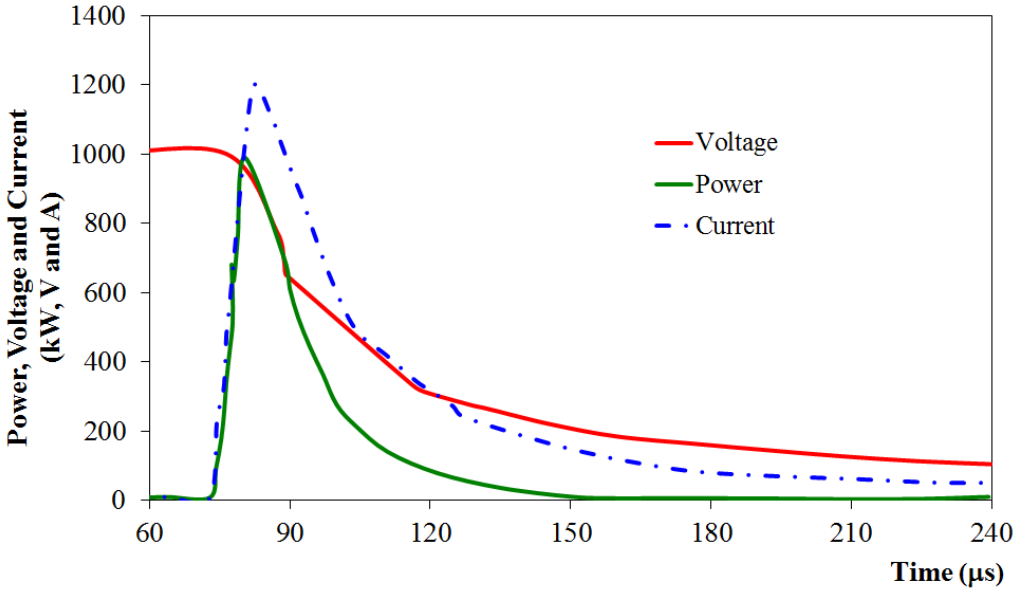

Fig. 4.2. *Waveforms of the Xenon-filled flashlamp (Voltage, Power and Current), recorded at an operating voltage of 1 kV.*

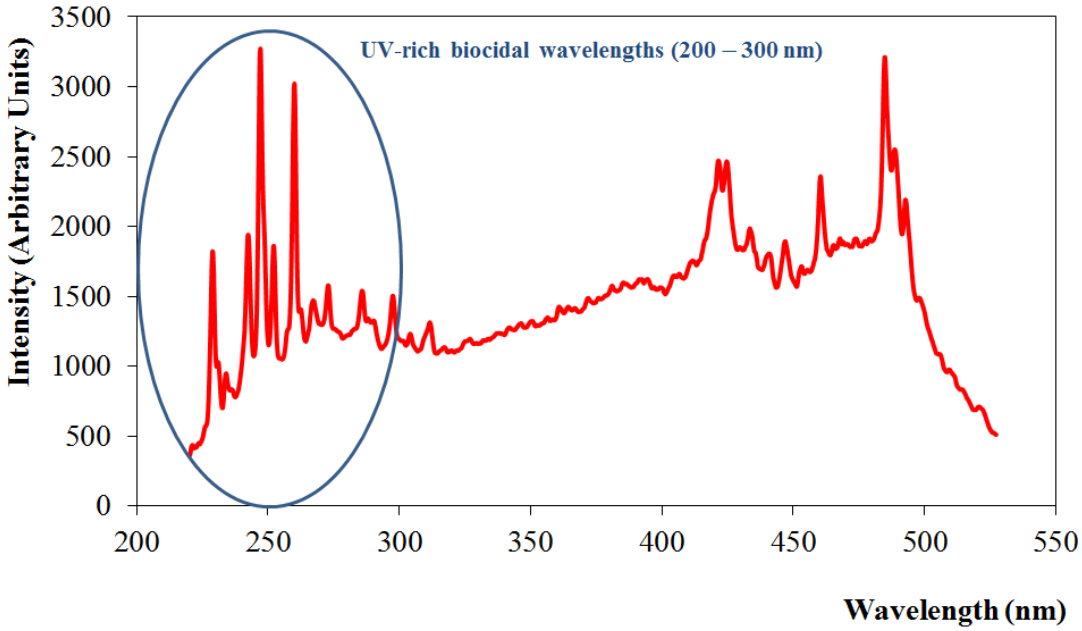

Fig. 4.3. *Emission spectral output of Xenon-filled flashlamp (between 200 – 500 nm), recorded at an operating voltage of 1 kV.*

4.3 Microorganisms and Sample preparation

Microorganisms were cultured as described in Section 3.2.2. As described in Section 3.4.1, after incubation cultures were centrifuged and the cell pellet re-suspended in PBS before serial dilution to provide the appropriate population densities for experimental use. Absorbance and transmission spectra of the microbial population densities were obtained using a Biomate 5 UV-Visible Spectrophotometer (Thermo Spectronic, USA).

4.4 Pulsed Ultraviolet (PUV) Light Exposure Experiments

4.4.1 Inactivation using broad-spectrum PUV light

In the PUV microbial treatment system, as shown in Fig. 4.4, the flashlamp was enclosed within a PVC chamber, with a base platform on which microbial suspensions were held during PUV treatment. The suspensions were positioned directly under the flashlamp at a fixed distance of 8 cm, giving a total average irradiance of 6.4 $mWcm^{-2}$ per pulse [Appendix A].

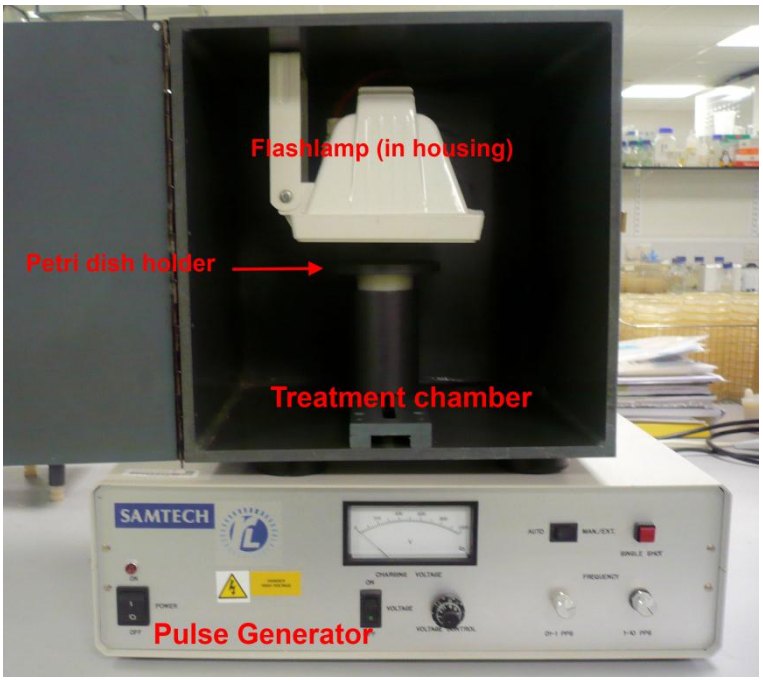

Fig. 4.4. *PUV treatment system for inactivation of microbial suspensions.*

For PUV-light treatment, 20 ml volumes of *S. cerevisiae* with population densities of 10^5 and 10^7 CFUml^{-1}, and *S. epidermidis* with population density of 10^7 CFUml^{-1}, were dispensed into 90 mm Petri dishes. These samples (with the Petri lid off) were then placed into the PVC treatment chamber and exposed to pulses of UV-light.

Suspensions of *S. epidermidis* and *S. cerevisiae*, with population densities of 10^7 and 10^5 CFUml^{-1}, respectively, were exposed to 2, 4, 6, 8 and 10 pulses. Further to this, *S. cerevisiae* suspensions with a population density of 10^7 CFUml^{-1}, were exposed to 25, 50, 75, 100, 125 and 150 pulses.

To investigate the effect of sample agitation during PUV-light exposure of *S. cerevisiae*, suspensions of *S. cerevisiae* with a population density of 10^7 CFUml^{-1}, were exposed to 25, 50, 75, 100, 125 and 150 pulses with the test suspension being manually agitated by rotating the Petri dish 10× clockwise and 10× anticlockwise after every 10 pulses.

4.4.2 A comparison of UV light inactivation using broadband and 260 (± 10) nm light pulses

A photograph of the PUV-light treatment system used for inactivation of *S. aureus* suspensions using both broadband light pulses and 260 (± 10) nm narrowband light pulses is shown in Fig. 4.5a and b. Exposure to wavelengths of 260 (± 10) nm was used as this is the optimum wavelength region for UV inactivation of Gram-positive bacteria [157].

For broadband PUV-light treatment, 2 ml volumes of *S. aureus* bacterial suspensions, with a population density of 10^5 CFUml^{-1}, were dispensed into one well of a 12 well plate (NUNC, Denmark) and placed into the treatment chamber. To expose bacterial suspensions to 260 nm light pulses, the light was passed through a 260 (± 10) nm narrowband optical filter which was placed on top of the well (Fig. 4.5b). The well containing the test bacteria was shielded to prevent stray light entering the well. The distance between the flashlamp and the surface level of the bacterial suspension was fixed at a distance of 5 cm. Liquid test samples were

exposed to increasing pulse numbers using a different 2 ml volume of bacterial suspension each time and repeated in triplicate.

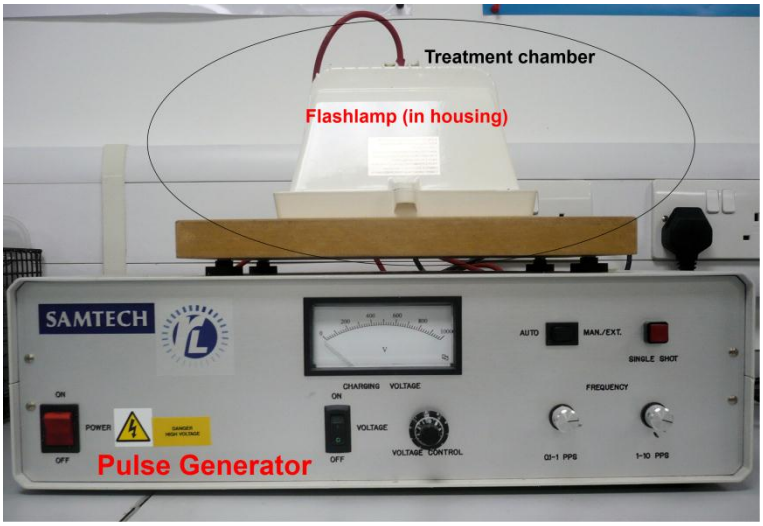

(a)

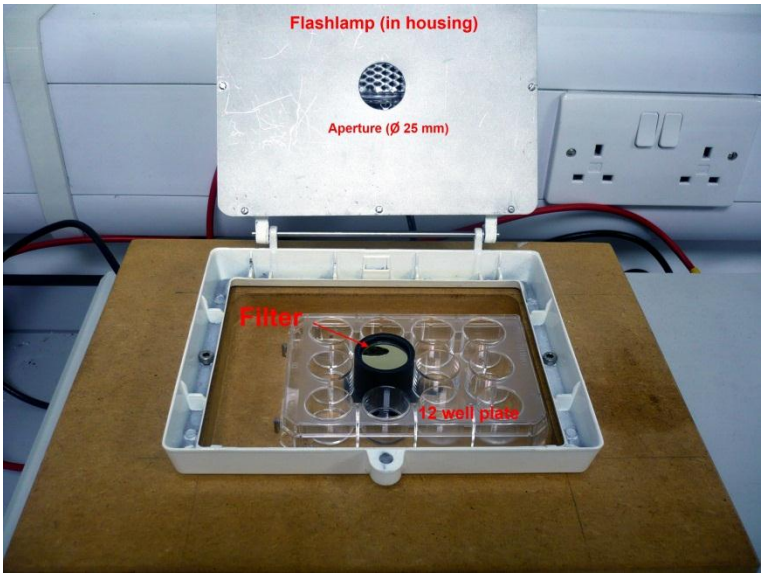

(b)

Fig. 4.5. *PUV-light treatment system for inactivation of S. aureus (a) pulse generator and treatment chamber (b) 12 well plate and optical filter inside the treatment chamber. The filter was removed when bacterial suspensions were exposed to broadband light pulses.*

4.4.3 Plating and Enumeration

After PUV treatment, test samples were immediately plated onto Malt Extract Agar (*S. cerevisiae*), Tryptone Soya Agar (*S. epidermidis*) and Nutrient Agar (*S. aureus*) using standard microbiological plating methods, and incubated at 37 °C for 24 hours before enumeration, as described in Section 3.4.2.

4.5 Experimental Results

The results for microbial inactivation using broad-spectrum PUV light, shown in Fig. 4.6 and Fig. 4.7, demonstrate the effect of PUV-light exposure on liquid suspensions of *S. epidermidis* and *S. cerevisiae*.

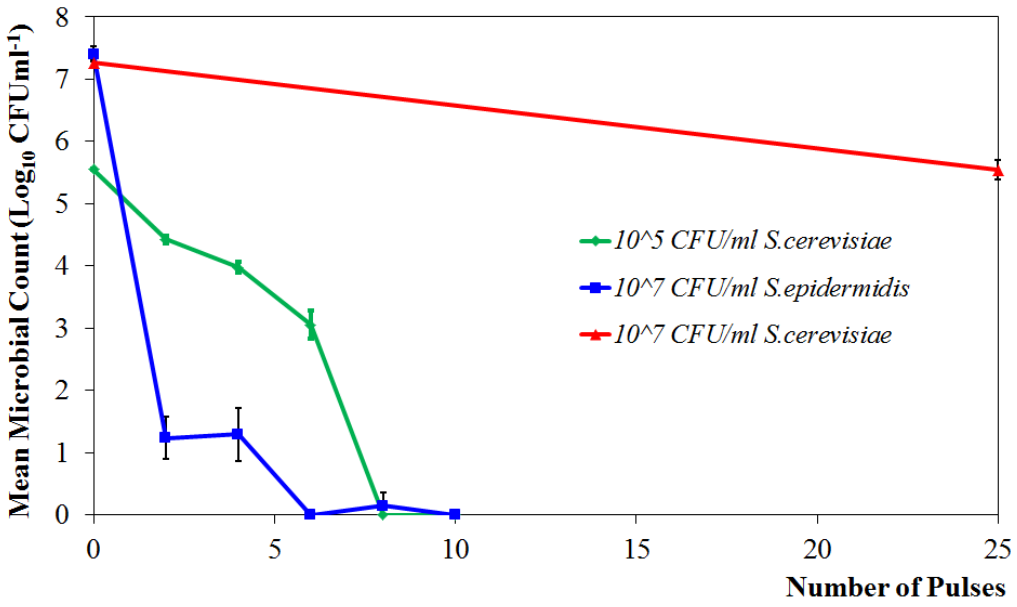

Fig. 4.6. *PUV treatment of S. epidermidis and S. cerevisiae in liquid suspension, with differing population densities.*

Results demonstrate that PUV-light exposure is highly microbicidal, with a 7-$\log_{10}$ reduction of *S. epidermidis* being achieved after application of less than 10 pulses (Fig. 4.6). It can be observed from Fig. 4.6 that a 5-$\log_{10}$ reduction of *S. cerevisiae* was also achieved after exposure to less than 10 pulses, however exposure of 10^7 CFUml^{-1} populations of *S. cerevisiae* were found to require a much higher

number of pulses before the population started to decrease, with approximately 1.5 $\log_{10}$ reduction after exposure to 25 pulses.

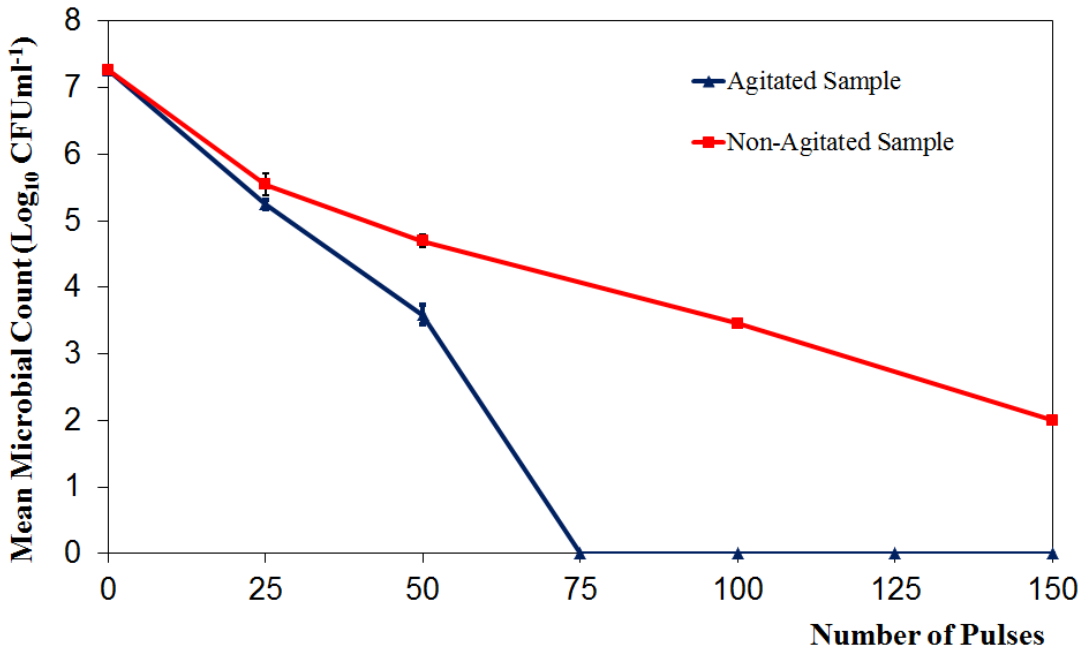

Fig. 4.7. *PUV treatment of S. cerevisiae in liquid suspension, with and without agitation.*

From Fig. 4.7 it can be seen that upon application of higher pulse numbers, further inactivation of the 10^7 CFUml-1 population of *S. cerevisiae* could be achieved, with approximately a 5-$\log_{10}$ reduction being achieved after application of 150 pulses. Agitation of the sample resulted in a significant increase in the inactivation efficiency, with complete inactivation of the 10^7 $CFUml^{-1}$ population after exposure to 75 pulses.

For PUV-light inactivation of *S. aureus* using broadband and 260 (± 10) nm narrowband light pulses, results are shown in Fig. 4.8 and Fig. 4.9, respectively.

The results, shown in Fig. 4.8, demonstrate that a 5-$\log_{10}$ reduction of *S. aureus* was achieved after exposure to 15 pulses of broadband light. When pulses of 260 (± 10) nm narrowband light were used, it can be seen that exposure of a 10^5 $CFUml^{-1}$ bacterial suspension resulted in complete inactivation after exposure to 150 pulses

(Fig. 4.9), ten times the number of pulses required to achieve the equivalent 5-$\log_{10}$ reduction with broadband light pulses.

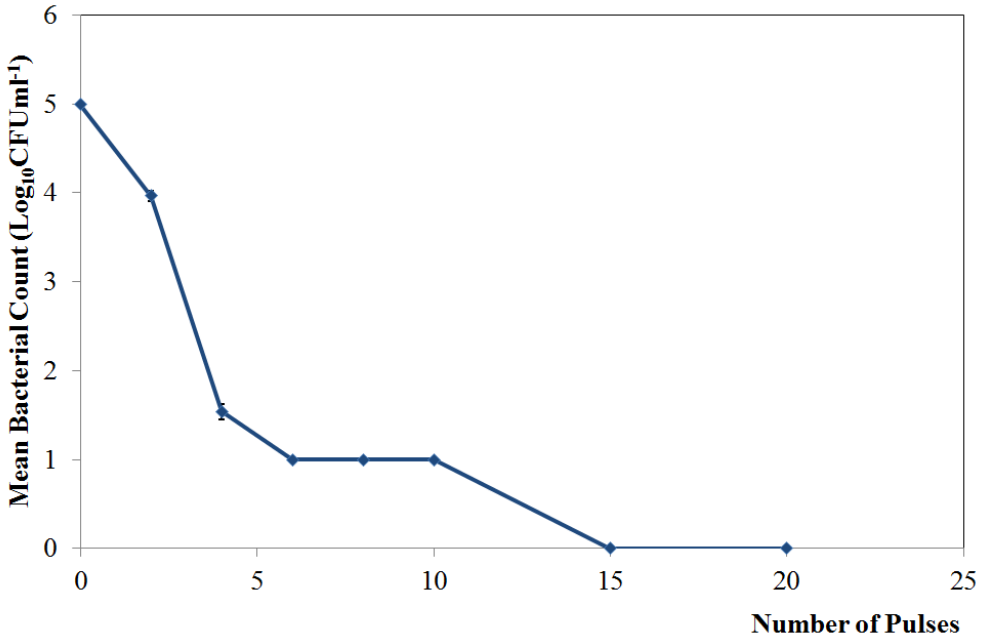

Fig. 4.8. *PUV-light treatment of S. aureus in liquid suspension using broadband light pulses.*

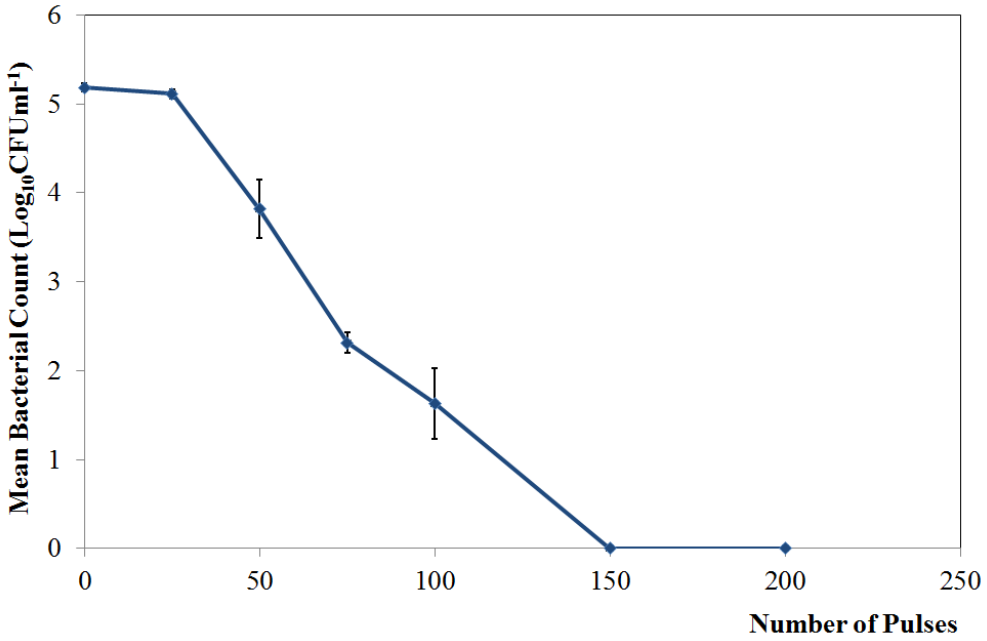

Fig. 4.9. *PUV-light treatment of S. aureus in liquid suspension using 260 (± 10) nm light pulses.*

4.6 Discussion and Conclusions

4.6.1 Inactivation using broad-spectrum PUV light

The transmission and absorbance spectra of the three different microbial population densities used in this study are shown in Fig. 4.10. In order to cover the UV region, the wavelength scan of suspensions of the different microbial population densities utilised was from 200 nm to 400 nm.

Visual assessment of the population densities used in this study indicated that the 10^7 CFUml^{-1} *S. epidermidis* suspension and the 10^5 CFUml^{-1} *S. cerevisiae* suspension were visibly clear, whereas the 10^7 CFUml^{-1} *S. cerevisiae* suspension is opaque, with a cloudy white colour. Spectroscopic analysis of the microbial suspensions showed that both the 10^7 CFUml^{-1} *S. epidermidis* and the 10^5 CFUml^{-1} *S. cerevisiae* suspensions have low absorbance and high transmission of germicidal UV wavelengths, as shown in Fig. 4.10.

The 10^7 CFUml^{-1} liquid suspension of *S. cerevisiae* only permits low transmission of around less than 5% and consequently a high absorbance of germicidal UV wavelengths. This result is readily clarified when the cell size of the two test microorganisms are compared. The bacterium *S. epidermidis* has a cell diameter of 0.5 – 1.5µm whereas the yeast *S. cerevisiae* has a much larger cell diameter of 5 – 10µm. Consequently 10^7 CFUml^{-1} *S. cerevisiae* will appear as a more opaque suspension than 10^7 CFUml^{-1} *S. epidermidis*.

In the present study, the complete inactivation of 10^7 CFUml^{-1} populations of *S. epidermidis* and 10^5 CFUml^{-1} populations of *S. cerevisiae* was achieved within 10 pulses as shown in Fig. 4.6. A study by Maclean *et al.* utilised a similar treatment system for inactivation of *S. aureus* and *Listeria monocytogenes* and demonstrated that both bacterial species could be inactivated with 7-$\log_{10}$ reduction after exposure to 10 pulses of UV-light [158]. The results for the inactivation rates for 10^7 CFUml^{-1} *S. epidermidis* in the current study correlate well with data from this study by Maclean *et al.*.

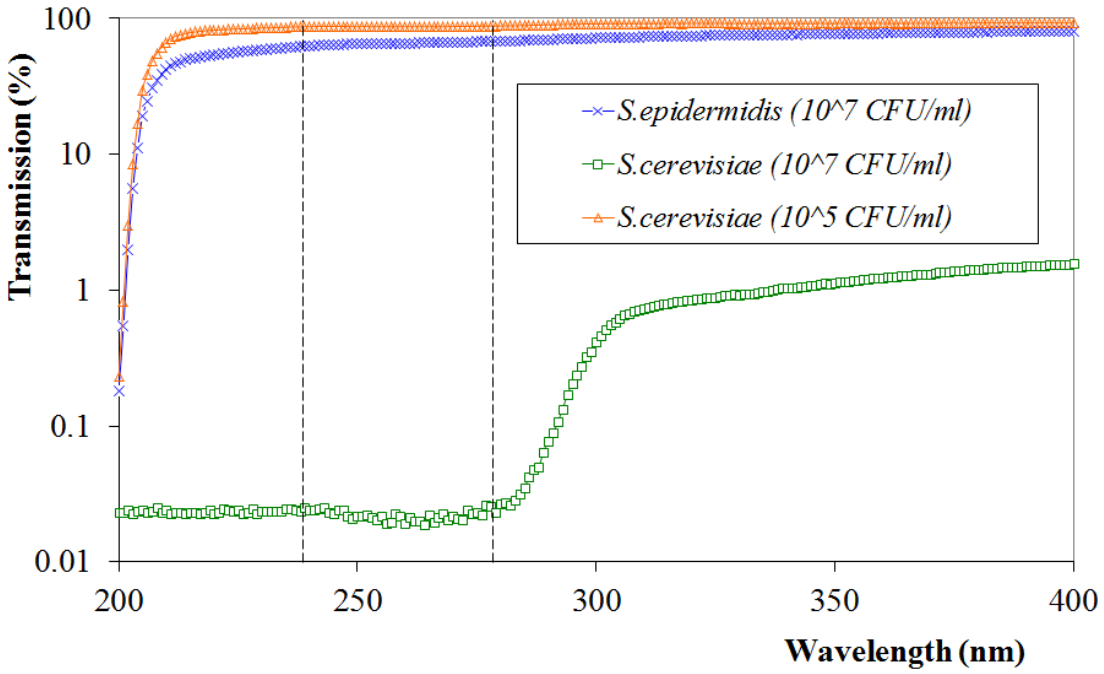

(a)

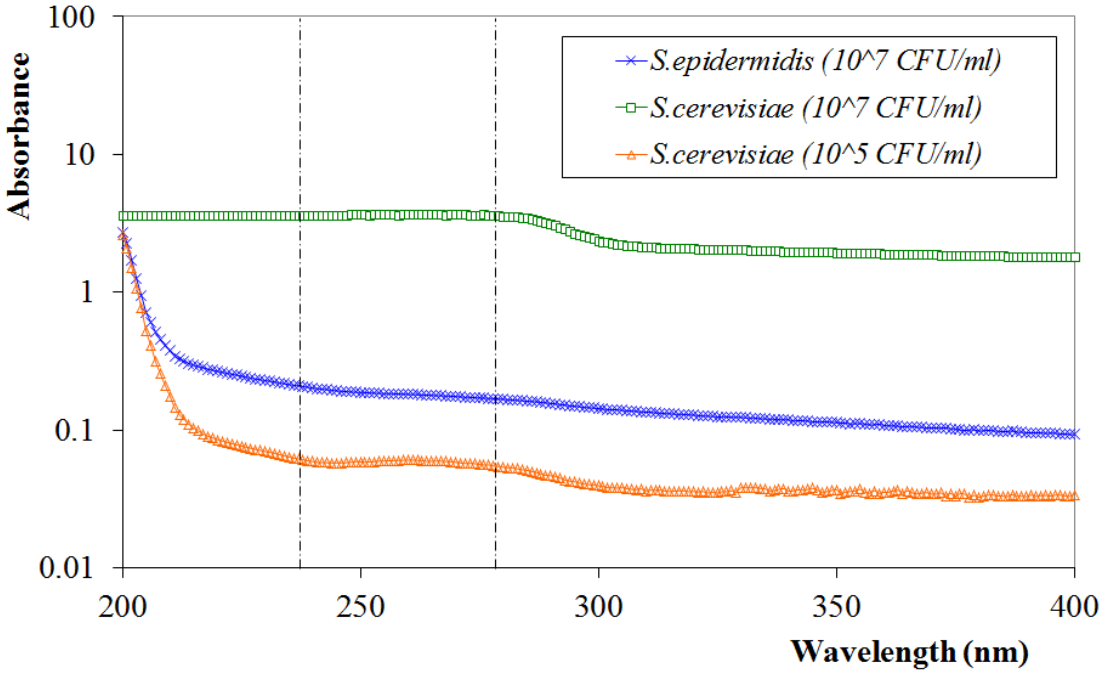

(b)

Fig. 4.10. *Transmission (a) and absorbance (b) spectra of the microbial population densities used in the PUV-light exposure experiments. The area between the dotted lines indicates the highly germicidal wavelength region of 240 - 280 nm.*

In contrast with *S. cerevisiae* inactivation, this result provides reasoning to the low inactivation rate of the 10^7 CFUml^{-1} population of *S. cerevisiae* observed after exposure to 25 pulses, with only around 1-log$_{10}$ reduction, as shown in Fig. 4.6. The low transmissibility of the suspension meant that the UV wavelengths were not capable to completely penetrate through the suspension and affect the total yeast population. Instead, the observed inactivation was likely to have been a result of inactivation of the yeast cells towards the top of the suspension. Some degree of cells beneath this top layer would have been shaded from the UV-wavelengths, and therefore a sufficient UV dose could not be applied to achieve complete inactivation.

Agitation of the liquid suspension significantly improved the inactivation rate of the 10^7 CFUml^{-1} *S. cerevisiae* population. This is likely due to the manual agitation permitting circulation of the yeast cells within the suspension, and consequently enabling shaded cells to reach the surface of the suspension and become intermittently exposed to the pulses of UV-rich light.

In Fig. 4.10 the area between the dotted lines indicates the most efficient wavelengths for germicidal efficiency and these are within the UV-C region of approximately 240 – 280 nm. In this region, nucleotide base components of DNA have peak absorbancy. A study by Wang *et al.* reported that a value of germicidal efficiency for *Escherichia coli* population reduction measured at a wavelength of 270 nm achieved 0.43 log$_{10}$(N/N0) per mJcm^{-2} and no inactivation was observed above 300 nm at the doses applied in this study [157]. UV-light irradiance of longer wavelength in the range 280 nm to 390 nm, can also cause microbial damage indirectly through the generation of reactive oxygen species which can cause protein cross-linking [11]. Overall, this study has demonstrated the effectiveness of PUV-light technology for microbial inactivation.

4.6.2 PUV-light inactivation of *S. aureus* using broadband and 260 (± 10) nm light pulses

The inactivation rate observed for 10^5 CFUml^{-1} *S. aureus* using broadband light pulses and 260 (± 10 nm) light pulses correlates well with data from a study by

Murdoch [159]. This study, which utilized a similar treatment system, showed that the inactivation rate achieved for *S. aureus* when exposed to 260 (± 10) nm pulses is less than PUV-light treatment with broadband pulses. The results in the present study demonstrated that a 10^5 $CFUml^{-1}$ populations of *S. aureus* can be completely inactivated after exposure to 150 pulses of 260 (± 10) nm light. In contrast, when the *S. aureus* population was exposed to broadband PUV-light treatment, results demonstrated a 5-$\log_{10}$ reduction after application of 15 pulses.

This difference is due to the total energy received by the bacterial suspension. When exposing suspension to pulses of 260 (± 10) nm light using the optical filter, only a small fraction of the total energy is transmitted to the bacterial suspension due to the filter having a peak transmission minimum of around 12%. This can be compared to the total energy from the pulse being transmitted to the suspension treatment without optical filter (broadband light pulse), even though the wavelength of 260 nm is highly germicidal against microorganisms.

In a previous study by Lani (2007) that used a similar treatment system with a 260 nm optical filter, the total energy per pulse through the filter was measured to be 6×10^{-2} $mJcm^{-2}$ [160]. In order to calculate the value of the germicidal efficiency (η), defined as $\log_{10}(N/N_0)$ per $mJcm^{-2}$ of UV light at this wavelength, it is necessary to convert pulse number to dose ($mJcm^{-2}$) and mean bacterial count ($\log_{10}CFUml^{-1}$) to a $\log_{10}(N/N_0)$ reduction, as shown in Fig. 4.11. It can be observed from Fig. 4.11 that there is a fourth-degree polynomial relationship between log reduction and the dose of 260 (± 10) nm.

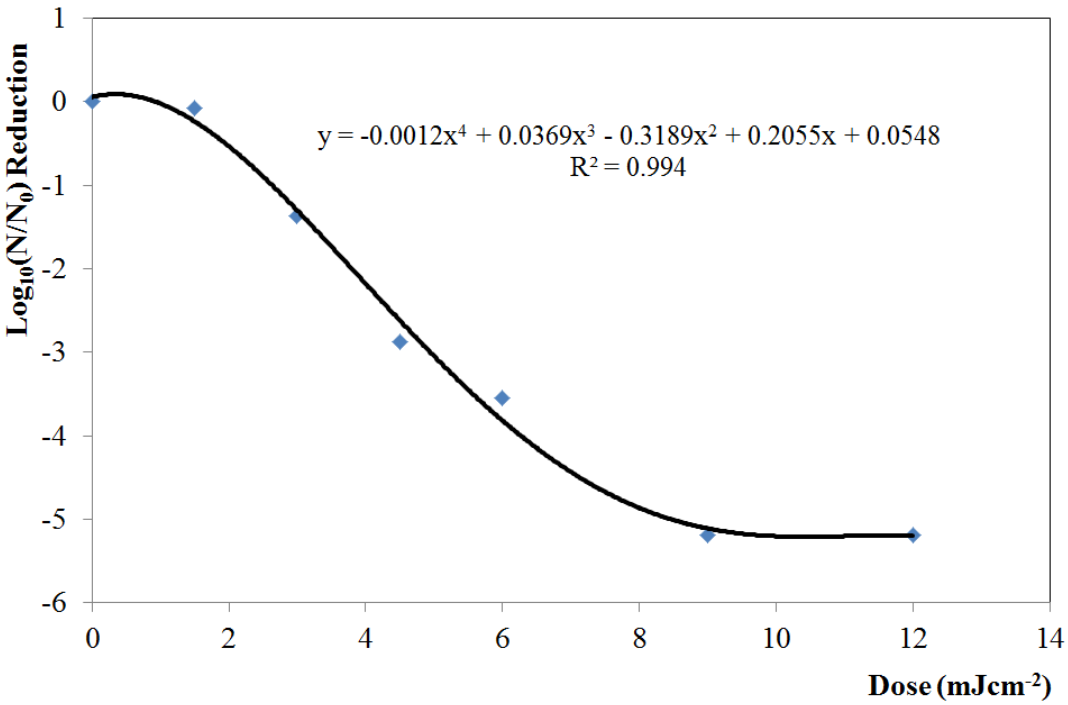

Fig. 4.11. *Log_{10} (N/N_0) reduction as a function of dose for PUV treatment of S. aureus in liquid suspension using pulses of 260 (± 10) nm light.*

The average germicidal efficiency for inactivation of *S. aureus* at 260 (±10) nm has been calculated from the inactivation curve (Fig. 4.11), and corresponds to 0.54 ± 0.09 $\log_{10}(N/N_0)$ per $mJcm^{-2}$. Using an identical experimental setup as in the present study, Murdoch (2010) reported that the germicidal efficiency for *S. aureus* at 260 (±10) nm was 0.45 ± 0.0263 $\log_{10}(N/N_0)$ per $mJcm^{-2}$ [159], which correlates well to the present study.

Meanwhile, a study by Lani (2007) measured the germicidal efficiency for *Listeria monocytogenes* and *Escherichia coli*, and obtained values of 0.26 $\log_{10}(N/N_0)$ per $mJcm^{-2}$ and 0.38 $\log_{10}(N/N_0)$ per $mJcm^{-2}$, respectively [160]. These results demonstrated that the germicidal efficiency for *L. monocytogenes* is less than *E. coli* and *S. aureus*, indicating that *L. monocytogenes* is more resistant than *E. coli* and *S. aureus* to inactivation at wavelengths of 260 (±10) nm.

Overall, the study has demonstrated the effectiveness of pulsed UV-light for microbial inactivation using both broadband spectrum and 260 (± 10) nm light pulses in liquid suspension. When exposing densely populated suspensions used in the study, agitation samples showed that the efficacy of the inactivation of the yeast *Saccharomyces cerevisiae* could significantly be increased.

Due to the safety issues for environmental decontamination system in occupied environments, the study then focused to investigate the visible-light sensitivity for microbial inactivation, and will be further discussed in Chapter 5.

CHAPTER 5

INVESTIGATION INTO THE VISIBLE LIGHT WAVELENGTH SENSITIVITY OF PATHOGENIC BACTERIA

5.1 Background

As described in Chapter 4, ultraviolet (UV) light is well-established as being highly antimicrobial, and pulsed UV-light is capable of achieving rapid inactivation of *Listeria monocytogenes* in UV and visible-light wavelengths. This study, investigates the wavelength sensitivity of important bacterial pathogen: *Listeria monocytogenes,* a common foodborne pathogen that can cause non-invasive and invasive listeriosis (as described in Section 3.2.1). In order to establish the bactericidal effect of the different wavelength regions on *L. monocytogenes*, the study was carried out using a continuous xenon white-light source in conjunction with a range of short-wave pass (SWP), long-wave pass (LWP) and narrow band pass (BP) filters. The wavelength sensitivity of *Staphylococcus aureus* and meticillin-resistant *Staphylococcus aureus* (MRSA), a strain of *S. aureus* that is resistant to antibiotics and is a common cause of HAI [131] is also investigated.

5.2 Experimental Materials

5.2.1 Light source

The light source used in the experimental system was a 150W continuous xenon broadband (185 – 2000 nm) white-light source (Lightningcure LC5, Hamamatsu Photonics UK, Ltd). The emission spectrum from 200 – 900 nm is shown in Fig. 5.1.

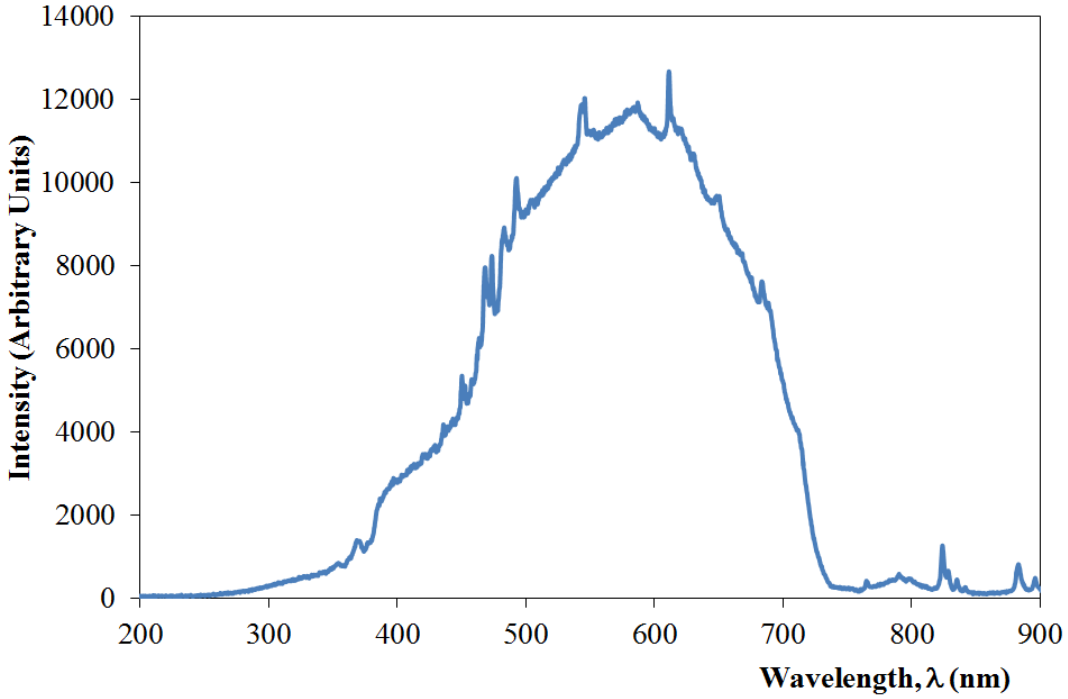

Fig. 5.1. *Emission spectrum of Xenon lamp from 200 to 900 nm.*

5.2.2 Optical Filters

Three types of optical filters used in the study were short-wave pass (SWP), long-wave pass (LWP) and bandpass (BP) filters. Optical short-wave pass filters permit transmission of shorter wavelengths and reflect longer wavelengths, while long-wave pass filters permit transmission of longer wavelengths and reflect shorter wavelengths [161]. Both SWP and LWP permit transmission of wavelengths corresponding to their specified cut-off wavelength, at which transmission is reduced to 50% of its peak value [162]. Bandpass filters permit transmission of a bandwidth of light according to specified wavelength and reject all other undesirable radiation [163]. The range of optical filters used in the experiment are listed in Table 5.1. All filters were round in shape with a diameter of 25 mm, except the 400 nm long-wave pass filter, which was square shaped with an area of 50 mm^2 [162, 163].

Table 5.1 *Optical filters and their specifications*

Filter Type	Wavelength (nm)	CW (nm)	FWHM (nm)	Peak Transmission (%)	Manufacturer
Long-wave pass	400	NA	NA	~93.00	NA
Long-wave pass	450	NA	NA	93.38	L.O.T.-Oriel Ltd
Short-wave pass	500	NA	NA	93.66	L.O.T.-Oriel Ltd
Bandpass	400	402.86	10 ± 2	50.34	L.O.T.-Oriel Ltd
Bandpass	405	405.2	10.2	45.10	Ealing Catalog Inc
Bandpass	410	411.93	10 ± 2	50.02	L.O.T.-Oriel Ltd
Bandpass	415	416.61	10 ± 2	51.40	L.O.T.-Oriel Ltd
Bandpass	420	420.17	10 ± 2	52.77	L.O.T.-Oriel Ltd
Bandpass	430	430.87	10 ± 2	47.28	L.O.T.-Oriel Ltd
Bandpass	440	441.27	10 ± 2	58.23	L.O.T.-Oriel Ltd
Bandpass	450	451.5	10 ± 2	54.97	L.O.T.-Oriel Ltd

NA = not available, CW = Centre wavelength , FWHM = full width half maximum

The emission spectra of the Xenon lamp through the LWP and SWP optical filters (>400 nm, >450 nm and <500 nm) used in the study are shown in Fig. 5.2. The 400 nm LWP and 500 nm SWP filter were used in combination to allow transmission of a 400-500nm wavelength range. It can be observed that all emission spectra of optical filters are in the visible light region, with the exception of the 500 nm SWP filter which allowed transmission of a small amount of UV light.

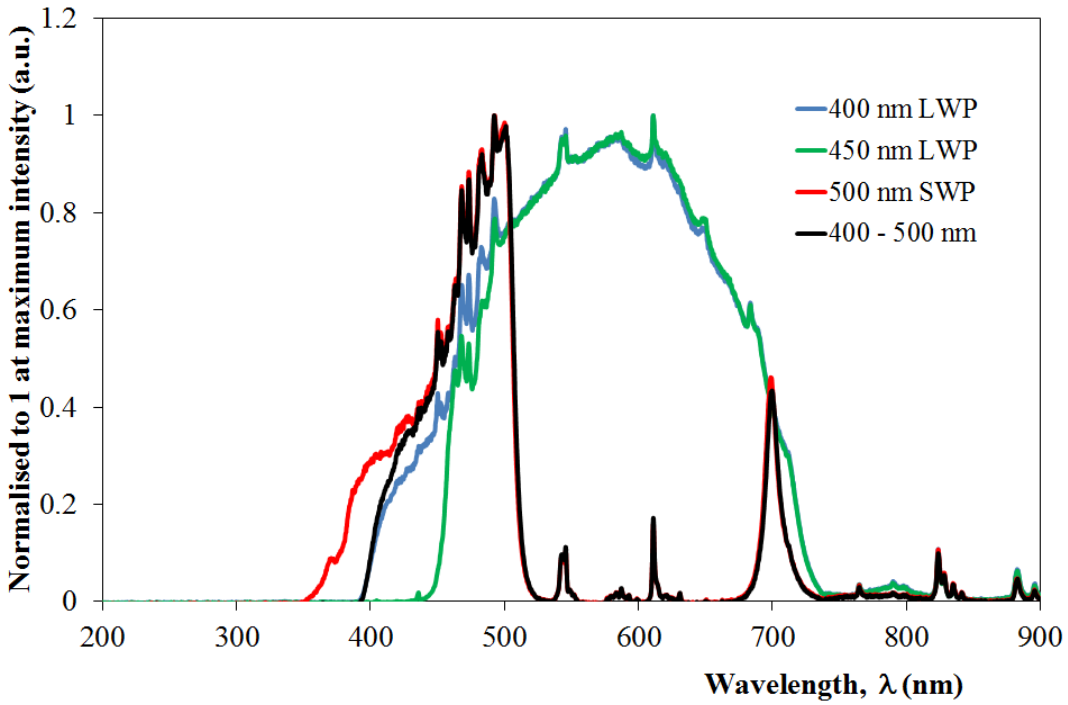

Fig. 5.2. *Emission spectrum of Xenon lamp from 200 to 900 nm when passed through the long-wave and short-wave optical filters used in the study.*

5.2.3 Microorganism and Sample Preparation

The microorganisms used in the study were *Listeria monocytogenes*, *Staphylococcus aureus*, and MRSA. The test microorganisms were cultivated and prepared for experimental use as described in Section 3.2.2 and 3.4.

5.3 Wavelength Sensitivity Experiments

5.3.1 Exposure to broad bandwidths of light

This experiment was carried out using *L. monocytogenes*. For light-treatment of bacterial samples, 2 ml volumes of bacterial suspension with population density of 10^5 CFUml^{-1} were held in one well of a 12-well plate (Nunc, Denmark). Also contained in the well was a 7 mm × 2 mm magnetic follower, which when placed on a magnetic stirrer, allowed continuous sample agitation. A light shield (black PVC cylinder of height 16 mm and diameter 25 mm) was placed around the sample well to ensure samples were not exposed to any stray, unfiltered light. Light treatment was

carried out using the continuous xenon broadband white-light source, in conjunction with the SWP and LWP filters (>400 nm, >450 nm, <500 nm and 400-500 nm). Filters were placed on top of the sample well and bacterial suspensions were exposed to light treatment through each of the filters.

The exposure distance was maintained at 5 cm throughout the experiment, however the output intensity of the Xenon lamp was adjusted to achieved an irradiance 126 $mWcm^{-2}$ throughout the inactivation experiments (Table 5.2). The irradiance has been selected due to avoid a possible temperature effect generated by a light exposure at the longest exposure time of 180 minutes. A photograph of the wavelength sensitivity experimental set-up is presented in Fig. 5.3.

Control samples were also set-up; 2 ml volumes of bacterial suspension with magnetic agitation not exposed to the xenon broadband white-light source but left in laboratory lighting conditions.

Table 5.2 *Output intensity values of the Xenon lamp through the selected optical filters to achieve an irradiance of 126 $mWcm^{-2}$ at the sample surface.*

Filter(s)	Transmitted Wavelengths (nm)	Required Output Intensity (%)
400 nm long-wave pass	>400	29
450 nm long-wave pass	>450	30
500 nm short-wave pass	<500	68
400 nm long-wave pass + 500 nm Short-wave pass	400 - 500	75

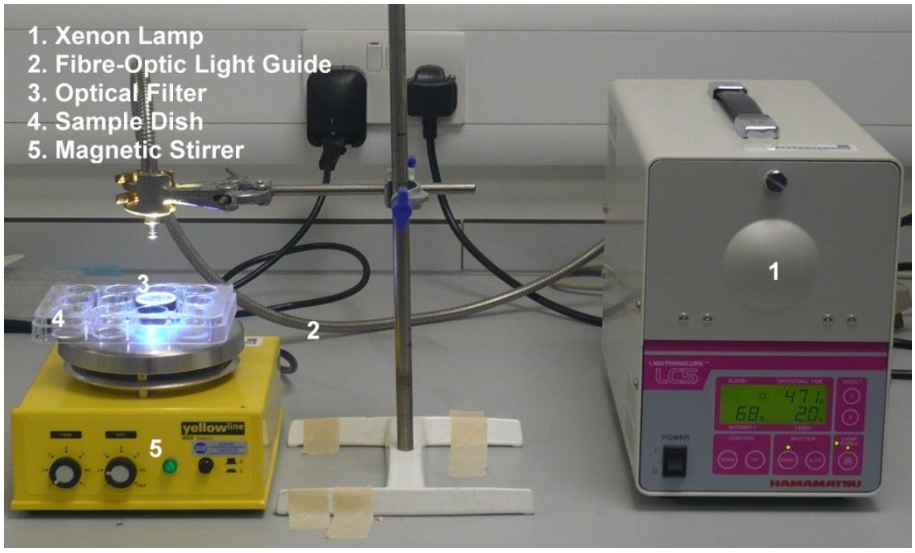

Fig. 5.3. *Photograph of the experimental set-up for investigation of the visible-light wavelength sensitivity experiments.*

5.3.2 Exposure to narrow bandwidths of visible-light between 400 – 450 nm

To investigate the causative bandwidth for inactivation of the selected bacteria, the same procedure as described in Section 5.3.1 was used with the SWP and LWP filters being substituted for bandpass filters ranging from 400 nm to 450 nm with bandwidths of 10 nm FWHM (see Table 5.1). The emission spectrum for each individual bandpass filter can be found in Appendix B. Two ml volumes of bacterial suspension with a population density of 10^5 CFUml^{-1} were used in the experiments.

The exposure distance (5 cm) and output intensity (100%) of the lamp were maintained constant throughout the experiments. As the light transmission through each filter was different, to ensure that, for each bacterium, suspensions were exposed to the same dose through each filter, the exposure time was adjusted for each filter to ensure that suspensions of *S. aureus* received a dose of 77 Jcm^{-2} through each filter, *L. monocytogenes* received 123.3 Jcm^{-2}, and MRSA received 92.5 Jcm^{-2}, as shown in Table 5.3. The reason for using three different doses for each bacterium was to achieve similar $\log_{10}$ reduction values for the bacteria at 405 nm.

Table 5.3 *Exposure time values for investigation of bacterial inactivation using narrow bandwidths of visible-light between 400 and 450 nm*

Bandpass Filter (nm)	Irradiance ($mWcm^{-2}$)	Exposure Time (min)		
		S. aureus **(77.0 Jcm^{-2})**	**MRSA (92.5 Jcm^{-2})**	***L. monocytogenes*** **(123.3 Jcm^{-2})**
400	7.5	172	206	275
405	8.6	150	180	240
410	7.2	180	215	287
415	7.5	171	205	273
420	7.7	166	200	266
430	7.3	175	210	280
440	8.3	154	185	247
450	8.3	154	185	247

5.4 Plating and Enumeration

After light treatment, test samples were immediately plated onto agar plates and incubated at 37 °C for 24 hours before enumeration. Sample plates were enumerated as described in Section 3.4.2.

5.5 Experimental Results

5.5.1 Wavelength Sensitivity Experiment: Exposure to broad bandwidths of light

SWP and LWP filters were selected to identify the wavelength sensitivity of *L. monocytogenes* inactivation. Fig. 5.4 shows the effect of different ranges of light wavelengths on suspensions of *L. monocytogenes*.

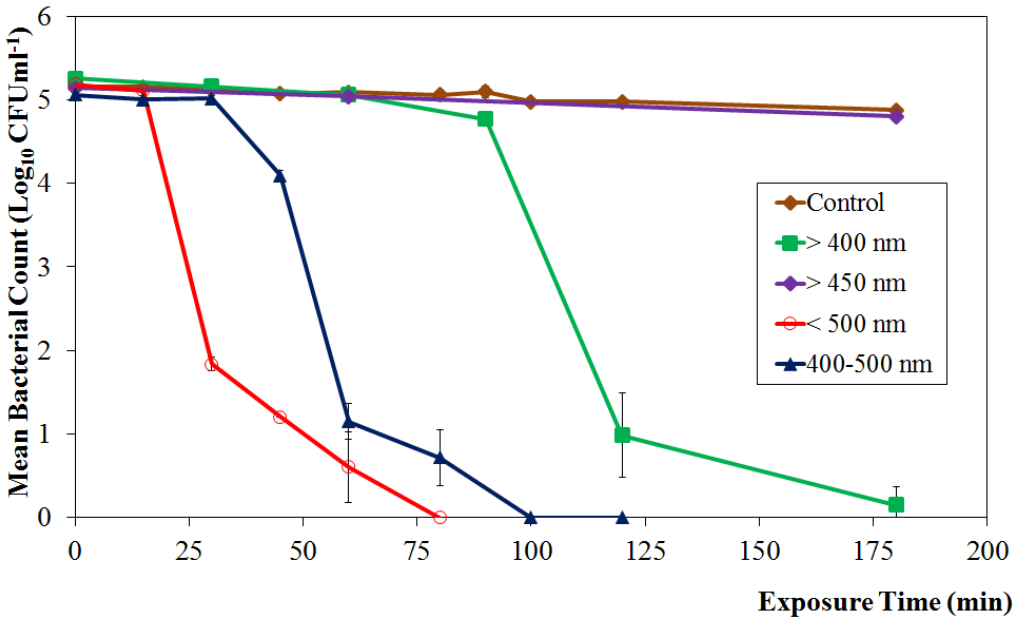

Fig. 5.4. *The effect of different regions of light on L. monocytogenes insuspension. This was carried out using SWP and LWP filters in conjunction with the Xenon lamp light source.*

It can be seen that, for the same applied dose level, the most rapid inactivation rate was found upon exposure to wavelengths of 500 nm and less, with a 5.1-$\log_{10}$ reduction in bacterial population after exposure to a dose of 604.8 J cm^{-2} and this is likely due to the inclusion of some UV-A wavelengths in the exposing light spectrum (see Fig. 5.2). Within the visible-wavelength region tested, *L. monocytogenes* was most susceptible to light of wavelength 400–500 nm, with an approximately 50% faster inactivation rate, at the same applied dose level, than that found when exposed to all wavelengths of 400 nm and above. The reason is that when the total dose applied falls, within the narrow bandwidths of 400–500 nm this causes much greater inactivation than when *L. monocytogenes* is exposed to the same dose in the range of 400 nm and above. It can be observed from Fig. 5.4 that the applied dose of 1360.8 Jcm^{-2} for >450nm light had almost no effect on the 10^5 CFU ml^{-1} population of *L. monocytogenes*, with only an approximate ~0.1-$\log_{10}$ reduction in bacteria cell population being achieved (Table 5.4). This confirms that the visible wavelengths inducing *L. monocytogenes* inactivation are within visible wavelength regions ranging from 400 nm to 450 nm.

Table 5.4 *Summary of inactivation results for visible-light treatment of 10^5 CFUml^{-1} L. monocytogenes suspension using different wavelength ranges*

Wavelength range (nm)	Exposure Time (min)	Dose (Jcm^{-2})	Log_{10} Reduction	Jcm^{-2}/Log_{10} Reduction
>400 nm	180	1360.8	4.7	290
>450 nm	180	1360.8	0.1	22680
<500 nm	80	605	5.1	119
400-500 nm	120	907	5.1	178

5.5.2 Wavelength Sensitivity Experiment: Exposure to narrow bandwidths of light between 400 and 450 nm

5.5.2.1 Wavelength sensitivity of *Listeria monocytogenes*

The log_{10} reduction values of *L. monocytogenes* as a function of wavelength are shown in Fig. 5.5. Significant log_{10} reductions were achieved through exposure to 400 – 440 nm bandwidths, with the peak log_{10} reduction resulting from exposure to 405 (± 5) nm, as detailed in Table 5.5. When *L. monocytogenes* was exposed to 405 nm light at an energy density of 123.3 Jcm^{-2}, 1.45-log_{10} reduction was achieved.

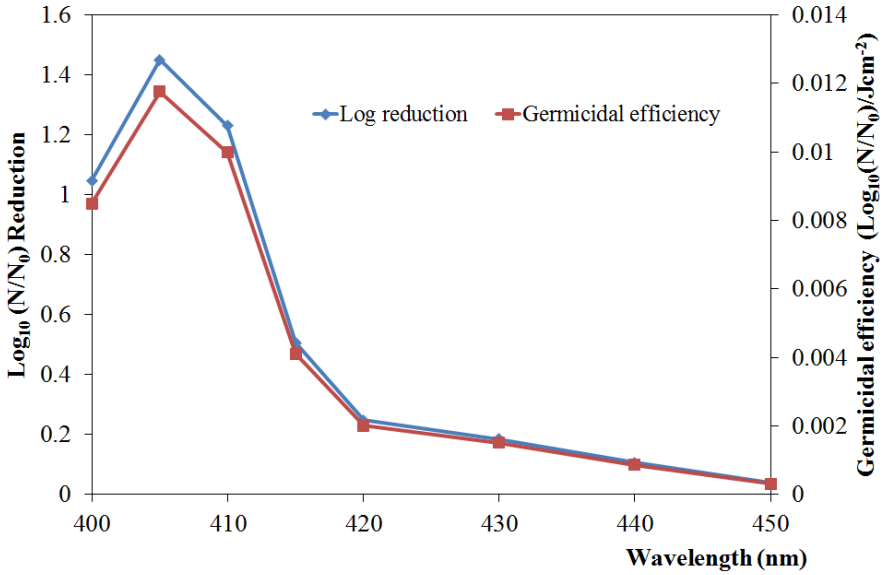

Fig. 5.5. *$Log_{10}(N/N_0)$ reduction and germicidal efficiency of L. monocytogenes as a function of wavelength (in the range 400 – 450 nm) when exposed to a dose of 123.3 Jcm^{-2}.*

The inactivation capability at each wavelength can be quantified as the germicidal efficiency (η), defined as the $\log_{10}$ reduction of a bacterial population by inactivation per unit dose in joules per square centimetre [157] as in Eq. (5.1):

$$\eta = \log_{10}(N/N_0)/\mathrm{Jcm}^{-2}, \tag{5.1}$$

where N_0 is the bacterial starting population and N is the final bacterial population after exposure. The $\log_{10}$ (N/N_0) reduction values can be re-plotted to show germicidal efficiency (η), as shown in Fig. 5.5. The germicidal efficiency peak was achieved at 405 (±5) nm. However, 400 nm and 410 nm light also showed good germicidal activity against *L. monocytogenes,* with a value of 0.009 $\log_{10}$ per Jcm^{-2} and 0.010 $\log_{10}$ per Jcm^{-2}, respectively.

Numerical data for the log reduction, the germicidal efficiency and statistical significance values that have been achieved through light exposure to bandpass filters ranging from 400 nm to 450 nm are summarised in Table 5.5.

Table 5.5 *Summary values for inactivation of a 10^5 CFUml^{-1} L. monocytogenes suspension following exposure to bandpass filters in the range 400 – 450 nm, each with a dose of 123.3 Jcm^{-2}*

Bandwidth (nm)	Irradiance (mWcm^{-2})	Exposure Time (min)	Initial Population, N_0 (Log_{10}CFUml^{-1})	Final Population, N (Log_{10}CFUml^{-1})	$Log_{10}(N/N_0)$ Reduction	η,($Log_{10}(N/N_0)$/Jcm^{-2})	Statistical significance
400 ± 5	7.5	275	4.98 (± 0.01)	3.93 (± 0.01)	1.05*	0.009	0.000
405 ± 5	8.6	240	4.95 (± 0.10)	3.50 (± 0.24)	1.45*	0.012	0.000
410 ± 5	7.2	287	4.90 (± 0.14)	3.67 (± 0.63)	1.23*	0.010	0.001
415 ± 5	7.5	273	4.89 (± 0.03)	4.38 (± 0.61)	0.51*	0.004	0.003
420 ± 5	7.7	266	4.98 (± 0.07)	4.74 (± 0.01)	0.25*	0.002	0.005
430 ± 5	7.3	281	5.01 (± 0.07)	4.82 (± 0.15)	0.19*	0.002	0.031
440 ± 5	8.3	247	5.02 (± 0.01)	4.91 (± 0.07)	0.11*	0.001	0.034
450 ± 5	8.3	247	5.04 (± 0.01)	5.01 (± 0.01)	0.04	0.000	0.410

*Significant bacterial log_{10} reductions, calculated at a 95% confidence interval (p value < 0.05). (Light-exposed sample value was significantly different from control value).

5.5.2.2 Wavelength sensitivity of *Staphylococcus aureus*

The graph shown in Fig. 5.6, demonstrates the log_{10} reduction and germicidal efficiency of *S. aureus* as a function of wavelength. As described in Section 5.5.2.1, this graph also shows that the most effective bactericidal wavelength was 405 (± 5) nm, with 1.6-log_{10} reduction being achieved after exposure to 150 min at 8.6 $mWcm^{-2}$. Significant log_{10} reductions were also achieved through exposure to 400 – 430 nm bandwidths, with values of log_{10} reduction in the range 0.38 – 1.6-log_{10} reduction in bacterial population, as listed in Table 5.6. It can be observed from Fig. 5.6 that the peak germicidal efficiency of 0.021 was at 405 (± 5) nm.

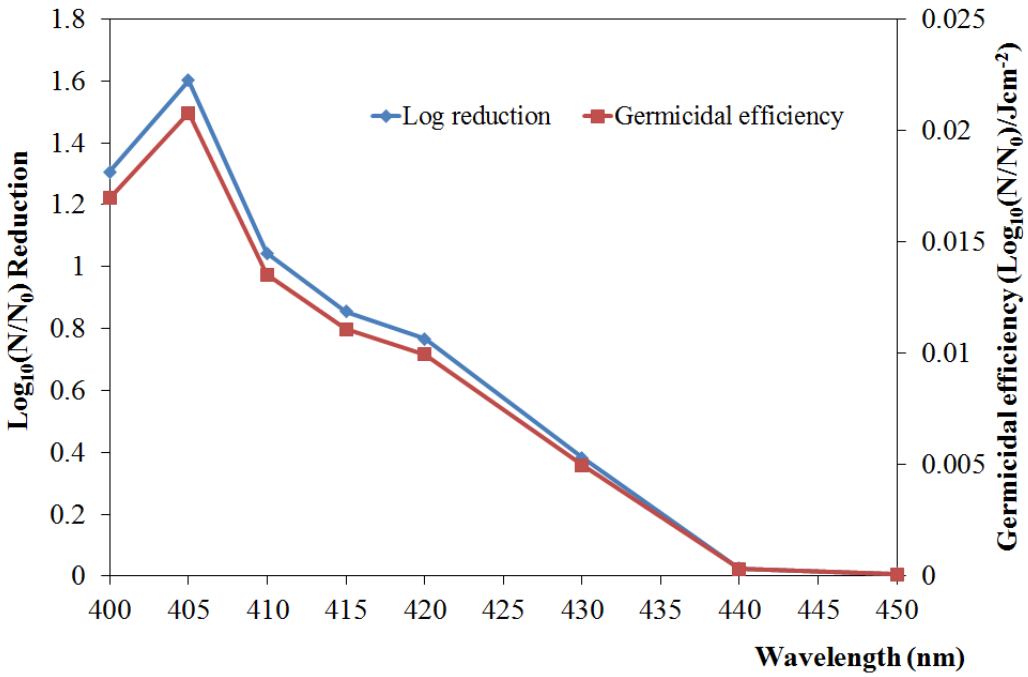

Fig. 5.6. *Log_{10} (N/N_0) reduction and germicidal efficiency of S. aureus as a function of wavelengths (in the range 400 – 450 nm) when exposed to a dose of 77 Jcm^{-2}.*

Table 5.6 *Summary values for inactivation of a 10^5 CFUml^{-1} S. aureus suspension following exposure to bandpass filters in the range 400 – 450 nm, each with a dose of 77 Jcm^{-2}*

Bandwidth (nm)	Irradiance (mWcm^{-2})	Exposure Time (min)	Initial Population, N_0 (Log_{10}CFUml^{-1})	Final Population, N (Log_{10}CFUml^{-1})	$Log_{10}(N/N_0)$ Reduction	η, ($Log_{10}(N/N_0)$/Jcm^{-2})	Statistical significance
400 ± 5	7.5	172	5.02 (± 0.04)	3.71 (± 0.84)	1.31*	0.017	0.000
405 ± 5	8.6	150	5.02 (± 0.07)	3.42 (± 0.43)	1.60*	0.021	0.000
410 ± 5	7.2	180	5.06 (± 0.08)	4.02 (± 0.50)	1.04*	0.014	0.000
415 ± 5	7.5	171	4.93 (± 0.18)	4.08 (± 0.71)	0.85*	0.011	0.000
420 ± 5	7.7	166	5.02 (± 0.02)	4.25 (± 0.41)	0.77*	0.010	0.000
430 ± 5	7.3	175	5.05 (± 0.07)	4.67 (± 0.13)	0.38*	0.005	0.002
440 ± 5	8.3	154	5.08 (± 0.03)	5.05 (± 0.05)	0.02	0.000	0.435
450 ± 5	8.3	154	5.09 (± 0.03)	5.09 (± 0.06)	0.01	0.000	0.852

*Significant bacterial log_{10} reductions, calculated at a 95% confidence interval (p value < 0.05). (Light-exposed sample value was significantly different from control value).

5.5.2.3 Wavelength sensitivity of MRSA

Fig. 5.7 shows the log_{10} reduction and germicidal efficiency for MRSA in suspension. The peak significant log_{10} reduction (1.73-log_{10}) was again achieved through exposure to 405 (± 5) nm with significant log_{10} reductions resulting with exposure to 400 – 430 nm bandwidths.

Good germicidal activity against MRSA was observed using wavelengths of 400 nm and 405 nm, with the germicidal efficiency peak at 405 (± 5) nm, as shown in Fig. 5.7. Summary values for inactivation of MRSA suspension through bandpass filters (400 – 450 nm) at dose of 92.5 Jcm^{-2} are listed in Table 5.7.

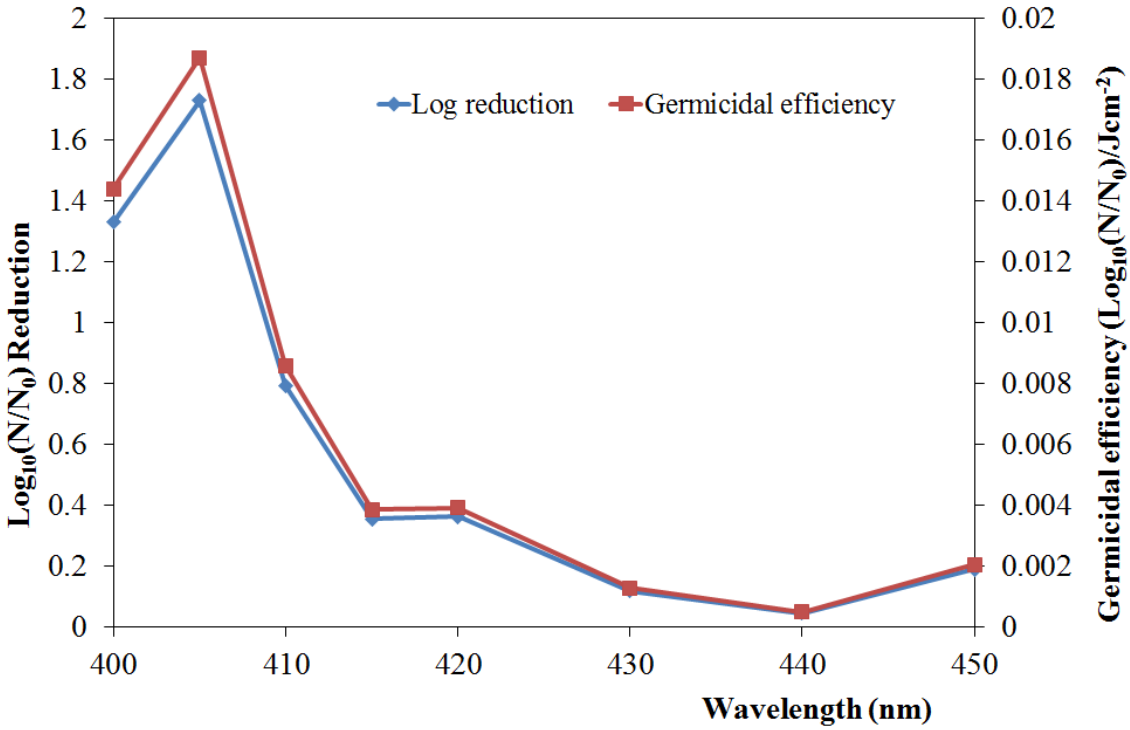

Fig. 5.7. *Log_{10} (N/N_0) reduction and germicidal efficiency of* MRSA *as a function of wavelengths (in the range 400 – 450 nm) when exposed to a dose of 92.5 Jcm^{-2}.*

Table 5.7 *Summary values for inactivation of a 10^5 CFUml^{-1}* MRSA *suspension following exposure to bandpass filters in the range 400 – 450 nm, each with a dose of 92.5 Jcm^{-2}*

Bandwidth (nm)	**Irradiance (mWcm^{-2})**	**Exposure Time (min)**	**Initial Population, N_0 (Log_{10}CFUml^{-1})**	**Final Population, N (Log_{10}CFUml^{-1})**	**$Log_{10}(N/N_0)$ Reduction**	**η, ($Log_{10}(N/N_0)$/Jcm^{-2})**	**Statistical significance**
400 ± 5	7.5	206	4.78 (± 0.24)	3.35 (± 0.34)	1.33*	0.014	0.000
405 ± 5	8.6	180	4.71 (± 0.04)	2.98 (± 0.30)	1.73*	0.019	0.000
410 ± 5	7.2	215	4.83 (± 0.15)	4.03 (± 0.08)	0.79*	0.009	0.000
415 ± 5	7.5	205	5.02 (± 0.08)	4.66 (± 0.10)	0.36*	0.004	0.002
420 ± 5	7.7	200	4.97 (± 0.02)	4.61 (± 0.01)	0.36*	0.004	0.000
430 ± 5	7.3	210	4.87 (± 0.05)	4.75 (± 0.01)	0.12*	0.001	0.026
440 ± 5	8.3	185	5.03 (± 0.07)	4.99 (± 0.08)	0.05	0.001	0.453
450 ± 5	8.3	185	4.90 (± 0.21)	4.71 (± 0.24)	0.19	0.002	0.198

*Significant bacterial log_{10} reductions, calculated at a 95% confidence interval (p value < 0.05). (Light-exposed sample value was significantly different from control value).

5.6 Discussion and Conclusions

Results from this study have demonstrated that visible light treatment using wavelengths of >400 nm, <500 nm and 400-500 nm are effective for inactivation of *L. monocytogenes* in suspension, with up to a 5-$\log_{10}$ reduction being achieved using the doses applied in this study. Approximately 5-$\log_{10}$ reduction of *L. monocytogenes* was achieved after exposure to wavelengths of <500 nm for 80 min, 400-500 nm wavelengths for 100 min and wavelengths of >400 nm for 180 min. The most rapid inactivation rate was found using <500 nm light and this is readily explained as some UV-A light will have been present, which is known to have considerable bactericidal effects. When wavelengths within the visible region were investigated, the best rate of inactivation was found with 400-500 nm. No inactivation was found above 450nm at the dose levels used in this study, therefore the bacteria were most sensitive to visible light wavelengths in the region of 400-450 nm.

During this study, sample temperatures were monitored before and after each exposure using a thermocouple (Digital Thermometer - KAM340, Kane-may, UK) with an accuracy of ± 1°C and, no significant temperature effects were observed to occur, with the maximum sample temperature recorded as 32°C after the longest exposure time of 180 minutes. This means that inactivation of *L. monocytogenes* suspension was a result of visible light exposure alone and not due to any thermal effects.

Many reports have been published on the use of visible light for inactivation of microorganisms using light sources with wavelengths of 400 nm and above. A study by Lipovsky *et al.* utilized broadband visible light in the range between 400 nm and 800 nm to examine the phototoxic effect on the survival of two *Staphylococcus aureus* strains (MRSA and MSSA). The results showed around 99.8% reduction of MSSA and 55.8% reduction of MRSA was achieved after exposure to a dose of 180 Jcm^{-2} [164]. Enwemeka *et al.* have also demonstrated the effectiveness of blue light at wavelengths >400 nm against MRSA. They found that an effective dose for inactivation was around 60 Jcm^{-2} [165].

The use of a similar treatment system for inactivation of *S. aureus* suspensions by Maclean *et al.* reported that 5-$\log_{10}$ reduction of *S. aureus* was achieved after exposure to a dose of 630 Jcm^{-2} using >400 nm light [116]. In the present study, *L. monocytogenes* suspensions can also be inactivated with 4.7-$\log_{10}$ reduction with approximately double the dose (1361 Jcm^{-2}). The data shows that *L. monocytogenes* is more resistant than *S. aureus* to inactivation at wavelengths of >400 nm.

Results from Table 5.5, Table 5.6 and Table 5.7 have highlighted the causative wavelengths as being 400 nm to 420 nm, with the most effective bactericidal activity at 405 (± 5) nm in the case of all three bacterial species. The calculation of germicidal efficiencies associated with the treatment of *L. monocytogenes, S. aureus* and MRSA resulted in values of 0.012 $\log_{10}(N/N_0)$ per Jcm^{-2}, 0.021 $\log_{10}(N/N_0)$ per Jcm^{-2} and 0.019 $\log_{10}(N/N_0)$ per Jcm^{-2}, respectively. The results showed that the germicidal efficiency value for *L. monocytogenes* is lower than MRSA and *S. aureus*, which means that *L. monocytogenes* is more resistant than MRSA and *S. aureus* to inactivation at wavelength of 405 (± 5) nm.

Previous work on the visible-light inactivation of *S. aureus* [115-117, 166, 167] has found 405 nm light to be an effective wavelength for photodynamic inactivation without the use of exogenous photosensitizers. These results correlate well with the new results in the present study using the organisms, *L. monocytogenes* and MRSA, with the peak $\log_{10}$ reductions in all cases, resulting from exposure to 405 (± 5) nm. Experimental work in the present study shows similar results to previous published [116] on visible-light inactivation of *S. aureus* which demonstrates that 405 (± 5) nm is the most effective visible-light wavelength for inactivation.

The effectiveness of visible light for inactivation of *Bacillus thuringiensis* spores has been reported by Griego *et al.*, which showed the most effective wavelength for killing the spores was 400 nm. They mentioned that the absorbance peak occurred in the range between 400 nm and 420 nm [168]. Visible-light inactivation through exposure to 400 – 420 nm is thought to be the result of the photo-stimulation of intracellular porphyrins, which produces singlet oxygen ($^1O_2$) which reacts with intracellular components, and causes bacterial cell death [111, 114, 169]. The mechanism of inactivation is likely to be the same as that in the present study and

this has been discussed in depth in Section 2.8.6.2 This correlates well with the results in the present study, which show that *L. monocytogenes*, *S. aureus* and MRSA are susceptible to light of wavelength 400 – 410 nm.

The significant result obtained from this part of the study was the identification of 405 (± 5) nm as the most effective wavelength for inactivation of *L. monocytogenes*, *S. aureus* and MRSA. This will enable the use of alternative light sources, which are more suitable than the broad-spectrum Xenon lamps for future work.

CHAPTER 6

INVESTIGATION INTO THE USE OF 405 nm HIGH-INTENSITY NARROW-SPECTRUM LIGHT (HINS-LIGHT) FOR BACTERIAL INACTIVATION

6.1 General

The previous chapter has demonstrated that *Listeria monocytogenes, Staphylococcus aureus* and meticillin-resistant *Staphylococcus aureus* (MRSA) could be inactivated using visible light. Through observation of the inactivation results for all the bacteria, the most effective wavelength for inactivation of *L. monocytogenes, S. aureus* and MRSA in liquid suspension is at a wavelength of 405 (± 5) nm. Use of 405 nm for bacterial inactivation has been documented in numerous recent publications [115-118, 166, 167] and this technology has been termed high-intensity narrow-spectrum light or 'HINS-light' by researchers in ROLEST, who have a granted UK patent, and filed international patents.

This chapter examines and discusses the use of 405 nm HINS-light for inactivation of a range of bacterial species commonly associated with healthcare and foodborne infections. The work has been split into three parts:

- In Part I, the study examines the use of different 405 nm light sources for bacterial inactivation. The sources used were (i) a continuous xenon broadband white-light in conjunction with a 405 (± 5) nm optical filter (hereinafter referred to as 405 nm filtered light), and (ii) 405 nm light generated from light-emitting diodes (LEDs) (hereinafter referred to as 405 nm high-intensity LED array). It is important to note that the use of "405 nm", with regard to the optical filter and LED arrays employed in the study, refers to the manufacture's description of these products. Analysis of the emission spectrum (see Fig. 6.1) showed that the measured peaks at this

stage in the study were closer to 400 nm. This variability was particularly associated with the LED sources which, because of technical manufacturing difficulties, could not be guaranteed to have peak values at precisely 405 nm and some of the purchased arrays had peaks slightly above and below this value. Nevertheless, with this limitation stated, the sources used in the following studies will be referred to as 405 nm sources.

- In Part II, the study focuses on the use of 405 nm light generated from light-emitting diodes (LEDs) for inactivation of foodborne pathogens including *Listeria monocytogenes*, *Salmonella enteritidis*, *Shigella sonnei* and *Escherichia coli* 0157:H7.

- In Part III, the dose-dependent nature of bacterial inactivation using 405 nm high-intensity light is investigated.

6.2 The effect of using different 405 nm light sources for bacterial inactivation

6.2.1 405 nm Filtered Light

As described in Section 5.2.1 and Section 5.3.2, light treatment using 405nm filtered light was achieved using a continuous xenon broadband white-light source in conjunction with a 405 (± 5) nm bandpass filter. The emission spectra of the 405 nm filtered light is shown in Fig. 6.1. It can be seen that the peak wavelength for the 405 nm filtered light was measured to be 401.51 nm.

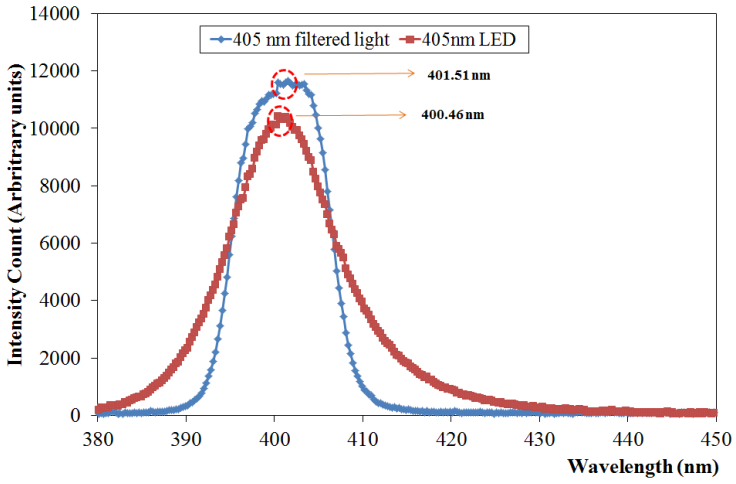

Fig. 6.1. *Emission spectra of 405 nm light sources.*

6.2.2 405 high-intensity LED array

The 405 nm light source used was a light emitting diode in the form of a close-packed rectangular array with 99 individual LEDs in an 11 by 9 matrix (0D-405-99-070, OptoDiode Corp, USA), and had a manufacture's stated output emission bandwidth of 405 nm (14 nm FWHM). The power output and radiation beam angle were 1.3 W and 70°, respectively. The LED array was bonded to a heat sink fan. This ensured that during operation the temperature of the LED array was maintained around 30 °C and ensured that any heat produced by the LED array had no effect on the bacterial samples. The LED array is pictured in Fig. 6.2. The emission spectrum of the 405 nm high-intensity LED array, as tested in our laboratory is shown in Fig. 6.1. It can be seen that the peak wavelength for the 405 nm LED array tested at this stage in the work was 400.46 nm.

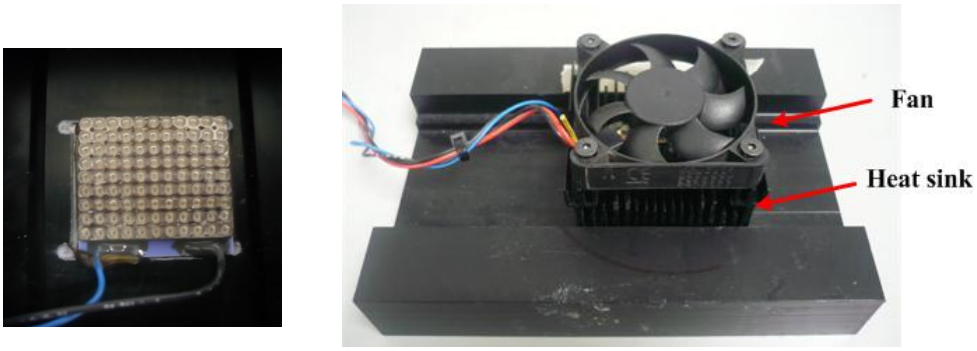

(a) (b)

Fig. 6.2. *(a) 405 nm high-intensity LED array source, and (b) Photograph of the heat sink and fan to which the LED array is bonded (on the underside).*

6.2.3 Experimental Methods

For exposure to 405 nm filtered light, the protocol as described in Section 5.3.1 was followed. The exposure distance (5 cm) and output intensity of the lamp were maintained constant throughout the experiments, providing an irradiance of 8.6 $mWcm^{-2}$ for inactivation of bacteria.

The 405 nm LED array (with heat sink and fan) was mounted in a polyvinyl chloride housing which held the array in position directly above one well of a 12-well plate

(Fig 6.3). For all experiments the voltage was set to 8.9 ± 0.1 V with a current of 0.14 ± 0.01 A, giving an intensity of 8.6 $mWcm^{-2}$ at the surface of the suspension (2 cm distance from the LED array).

For bacterial exposure to both 405 nm filtered light and 405 nm high intensity light from the LED array, 2 ml volumes (with 7 mm depth) of bacterial suspension were held in one well of a 12-well plate. The well also contained a small magnetic follower, which when positioned on a magnetic stirrer, permitted continuous agitation of the sample. Bacterial samples were then exposed to different durations of light. Control samples were set-up using the same procedure but not exposed to 405 nm light sources (Fig 6.3).

The well of a 12-well plate which contained the bacterial sample and a small magnetic follower which was used in the study is shown in Fig. 6.4.

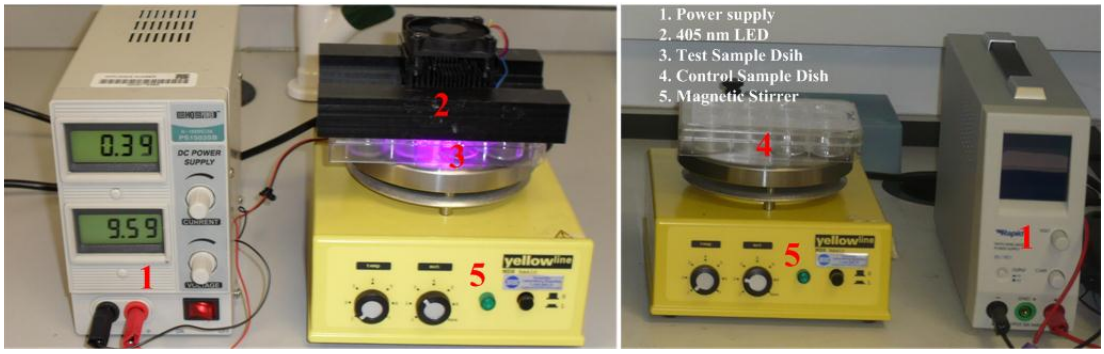

Fig. 6.3. *Experimental set-up for bacterial inactivation using the 405 nm high-intensity LED array.*

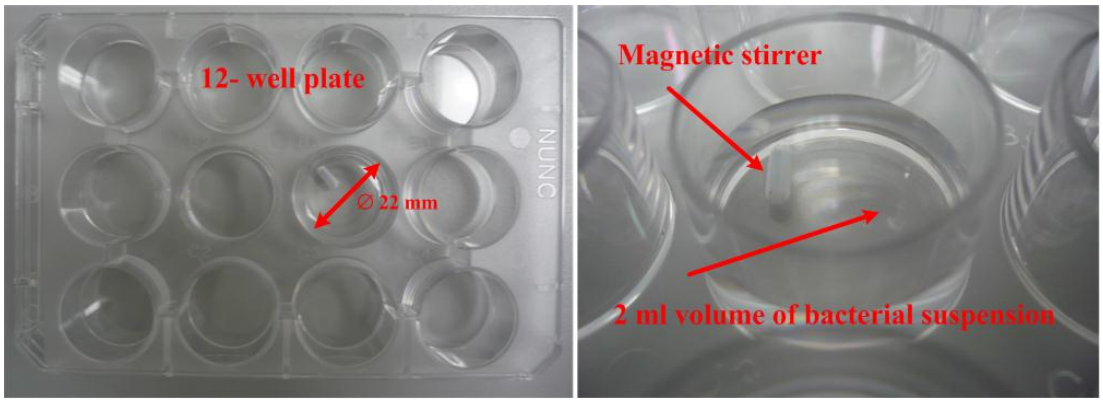

Fig. 6.4. *Sample well used for bacterial exposure.*

6.2.4 Bacterial Preparation and Enumeration

The microorganisms used for this experiment were *Listeria monocytogenes*, *Staphylococcus epidermidis*, *Staphylococcus aureus* and MRSA. Bacteria were cultured and prepared for experimental use as described in Section 3.2.2. Two ml volumes of bacterial suspension with a population density of 10^5 $CFUml^{-1}$ were used in the experiments. After light exposure, bacteria were plated, incubated and enumerated as described in Section 3.4.

6.2.5 Experimental Results: Comparison of inactivation of bacterial suspensions using 405 nm filtered light and a 405 nm LED array

Fig. 6.5, Fig. 6.6, Fig. 6.7 and Fig. 6.8 allows comparison of the results of inactivation of bacterial suspensions using two different 405 nm light sources, each with an irradiance at 8.6 $mWcm^{-2}$. It can be observed from Fig. 6.5 that the log_{10} reduction of *S. aureus* after light exposure to the 405 nm filtered light and the 405 nm LED array followed a similar trend, and all data points demonstrate no significant difference when both light sources are compared. For inactivation of *S. aureus* suspension as shown in Fig. 6.5, it can be seen that 4.7 and 4.6-log_{10} reduction in bacterial population could be achieved with a dose of 154.1 Jcm^{-2} for both a 405 nm filtered light and a 405 nm LED array, respectively.

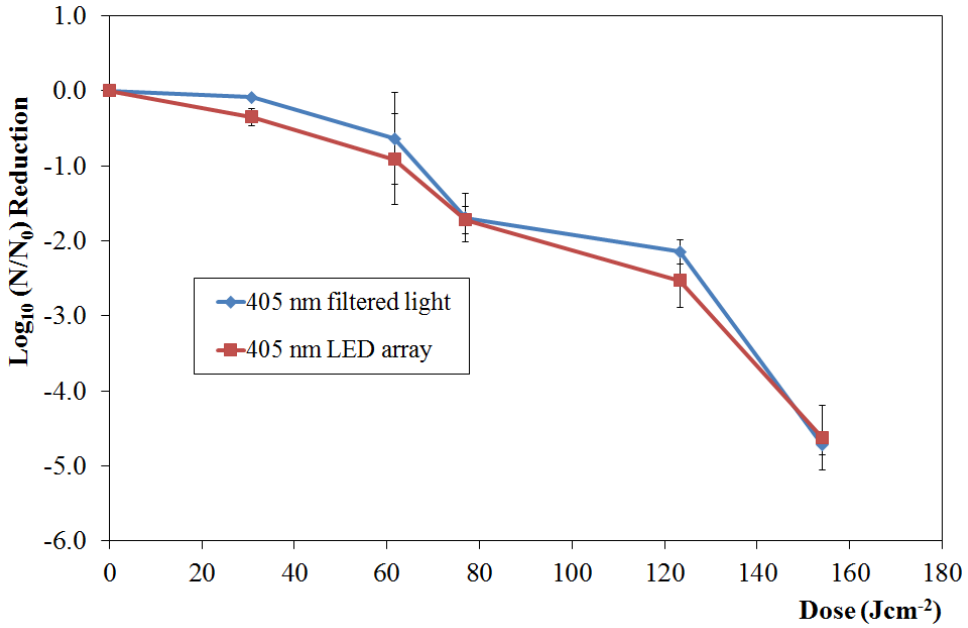

Fig. 6.5. *Log_{10} (N/N_0) reduction as a function of dose for inactivation of 10^5 $CFUml^{-1}$ Staphylococcus aureus suspension.*

Fig. 6.6 shows log_{10} reduction as a function of dose for MRSA. Again both trend lines follow a similar pattern, and all data points demonstrate no significant difference when both light sources are compared, but a slightly more rapid reduction of MRSA occurred with doses between 30.8 Jcm^{-2} and 92.5 Jcm^{-2} when exposed to the 405 nm high intensity LED array. The complete inactivation of MRSA was achieved after exposure to a dose of 123.3 Jcm^{-2}; with exposure to both light sources resulting in a 5-log_{10} reduction.

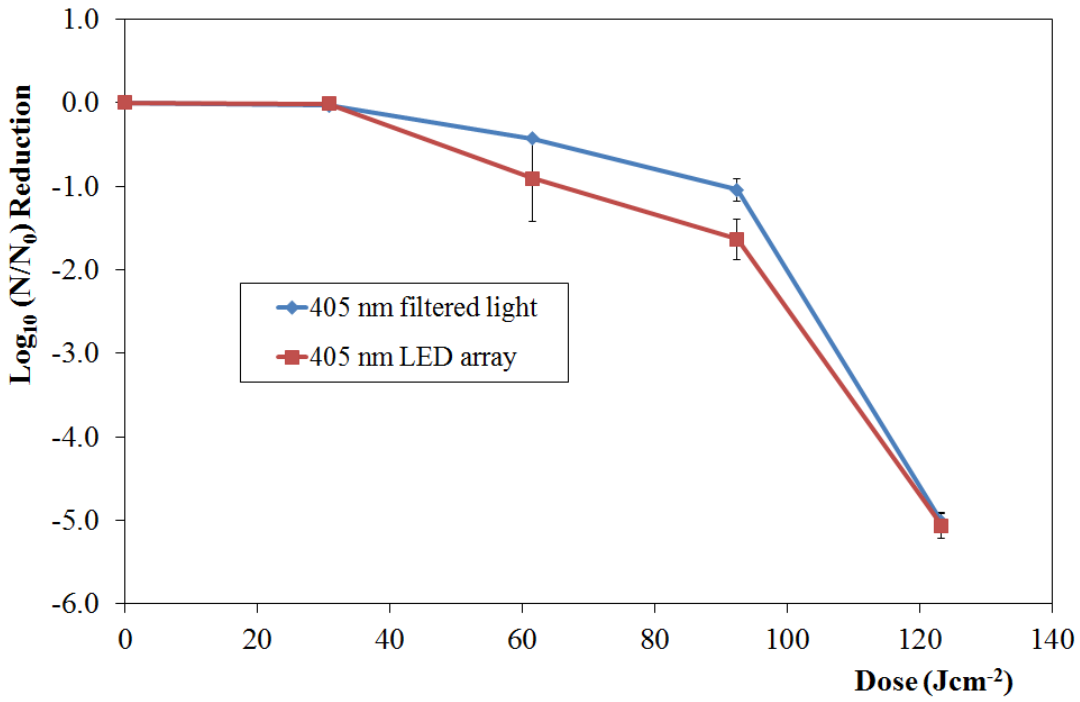

Fig. 6.6. *Log_{10} (N/N_0) reduction as a function of dose for inactivation of 10^5 $CFUml^{-1}$ MRSA 16a suspension.*

For light treatment of *S. epidermidis* (Fig. 6.7) and *L. monocytogenes* (Fig 6.8), again there was no significant difference for all data points and the same pattern of reduction in bacterial population is shown with exposure to both light sources.

For both light-exposed and control samples, temperature was also monitored during treatment for each independent experiment to ensure that bacterial suspensions were not being heat-stressed during light exposure. During experiments, the temperature

only rose to a maximum of around 30 °C after exposure for light exposed samples and around 29 °C for control samples.

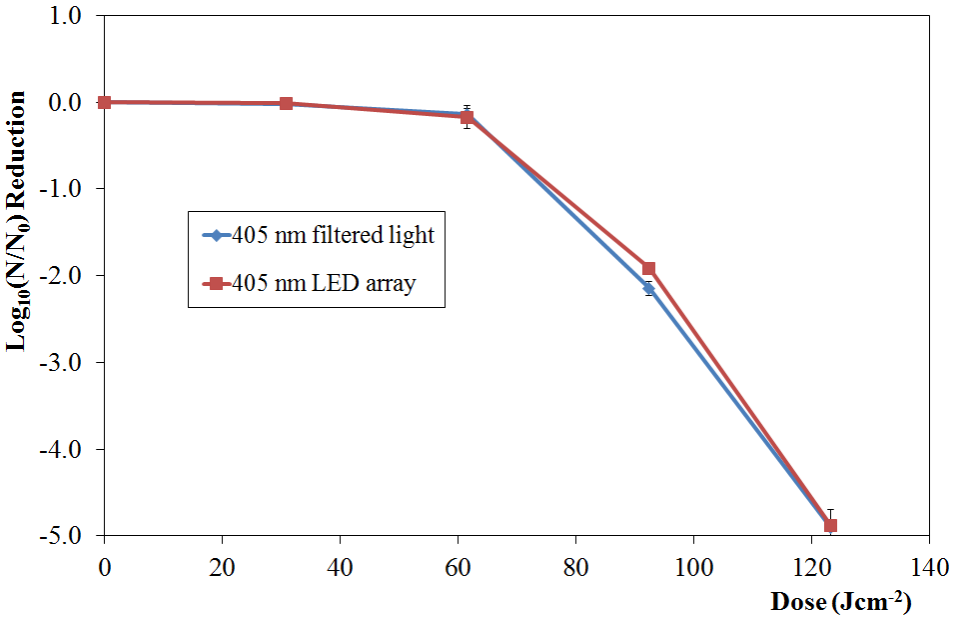

Fig. 6.7. *Log_{10} (N/N_0) reduction as a function of dose for inactivation of 10^5 $CFUml^{-1}$ Staphylococcus epidermidis suspension.*

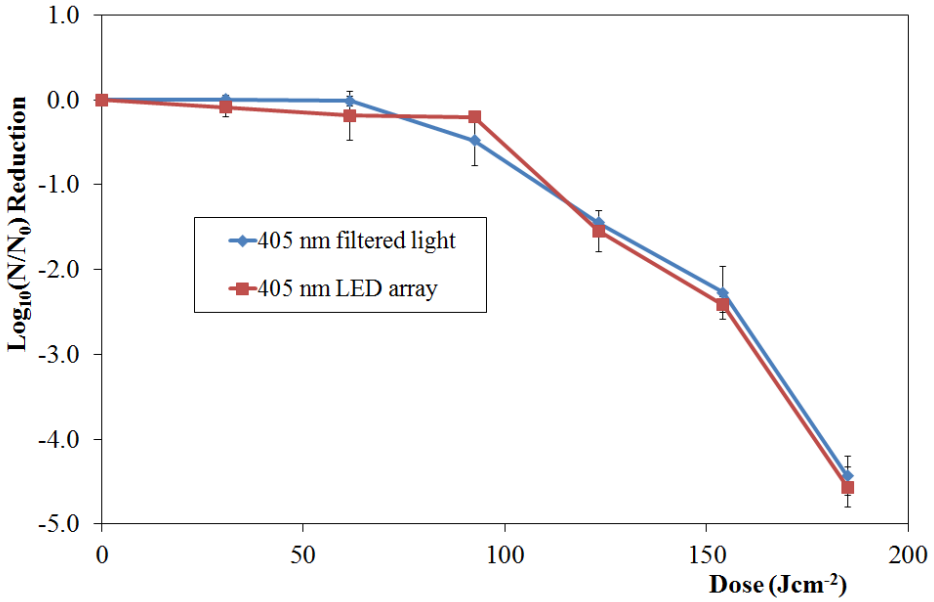

Fig. 6.8. *Log_{10} (N/N_0) reduction as a function of dose for inactivation of 10^5 $CFUml^{-1}$ Listeria monocytogenes suspension.*

6.3 Inactivation of important foodborne pathogen using the 405 nm high-intensity LED array

The use of 405 nm high-intensity light for inactivation of important foodborne bacterial pathogens such as *Listeria monocytogenes, Salmonella enteritidis, Shigella sonnei* and *Escherichia coli* 0157:H7 is investigated in this section. In addition to this, inactivation of other species of *Listeria* is investigated to determine whether similar inactivation kinetics are found within bacteria of the same genera.

6.3.1 Material and Methods

6.3.1.1 Microorganisms

The microorganisms used in this experiement were *L. monocytogenes, L. ivanovii, L. seeligeri, Salmonella enteritidis, Shigella sonnei* and *E.coli* 0157:H7. Microorganisms were cultured and prepared for experimental use as described in Section 3.2.2. Two ml volumes of bacterial suspension with a population density of 10^5 CFUml^{-1} were used in the experiments. After light exposure, bacteria were plated, incubated and enumerated as described in Section 3.4.

6.3.1.2 Exposure to 405 nm high-intensity LED array

The experimental set-up used in these experiments is described in Section 6.2.3 (Fig. 6.3). The irradiance was set at 85.6 mWcm^{-2} at the surface of the suspension throughout the experiments. Two ml volumes of bacterial suspensions were continuously agitated and exposed to increasing durations of 405-nm light before being plated onto agar plates and incubated at 37 °C for 24 hours. Control samples were set-up using the same procedure but exposed to normal laboratory lighting only.

6.3.2 Experimental Results

Fig. 6.9 shows the results of all three species of *Listeria* after exposure to 405 nm high-intensity light from the LED array with an irradiance of 85.6 mWcm^{-2}. When the three species of *Listeria* were exposed to a dose of 185 Jcm^{-2}, approximately 3.78, 3.90 and 3.4-log$_{10}$ reductions in bacterial population were achieved for *L. monocytogenes, L. ivanovii* and *L. seeligeri*, respectively. It can be observed from

Fig. 6.9 that when the three species of *Listeria* were exposed to 405 nm light from the LED array this resulted in similar patterns of inactivation.

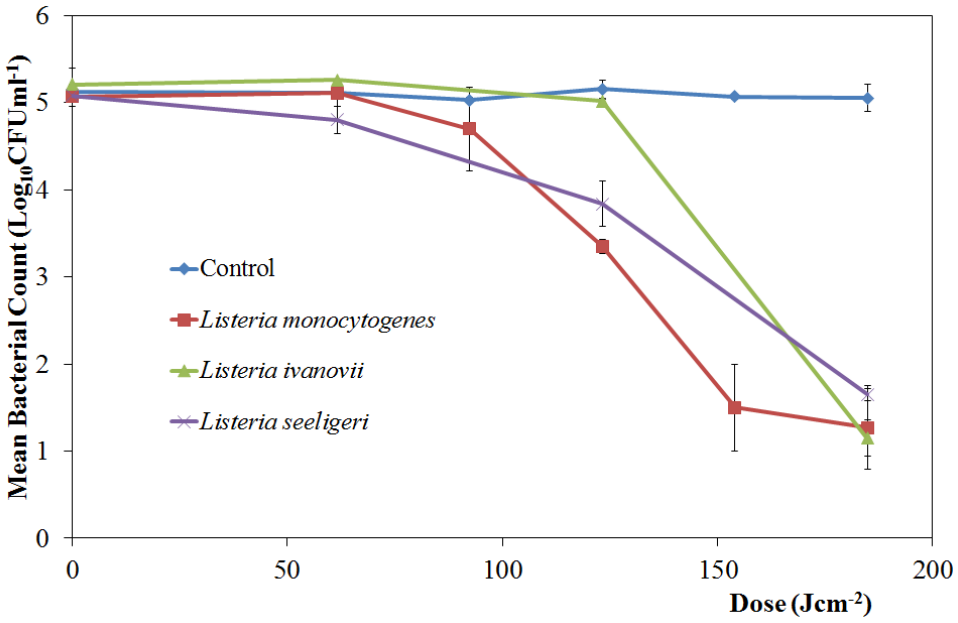

Fig. 6.9. *Inactivation curve of three species of Listeria after exposure to 405 nm high-intensity light from an LED array with an irradiance of 85.6 mWcm^{-2}.*

When three different doses (61.6, 123.3 and 185 Jcm^{-2}) were used for inactivation of the three species of *Listeria*, and surviving populations of *L. ivanovii* were compared to *L. monocytogenes*, results demonstrated that a significant difference was achieved after exposure to a dose of 123.3 Jcm^{-2}. However no significant difference resulted when the surviving population of *L. seeligeri* was compared to *L. monocytogenes* for these doses. A significant difference was also observed after an applied dose of 123.3 Jcm^{-2} when the surviving population of *L. ivanovii* was compared to *L. seeligeri*. However although some such differences were recorded, overall the pattern of results indicated that the use of 405 nm light from the LED array for inactivation of the three species of *Listeria* resulted in similar inactivation kinetics for bacteria within the same genus.

Fig. 6.10 is an inactivation curve for inactivation of *S. enteritidis* using the 405 nm LED array treatment. It can be observed from Fig. 6.10 that *S. enteritidis* proved

more resistant to inactivation, with a 1.3-$\log_{10}$ reduction achieved after 740 Jcm^{-2} of exposure.

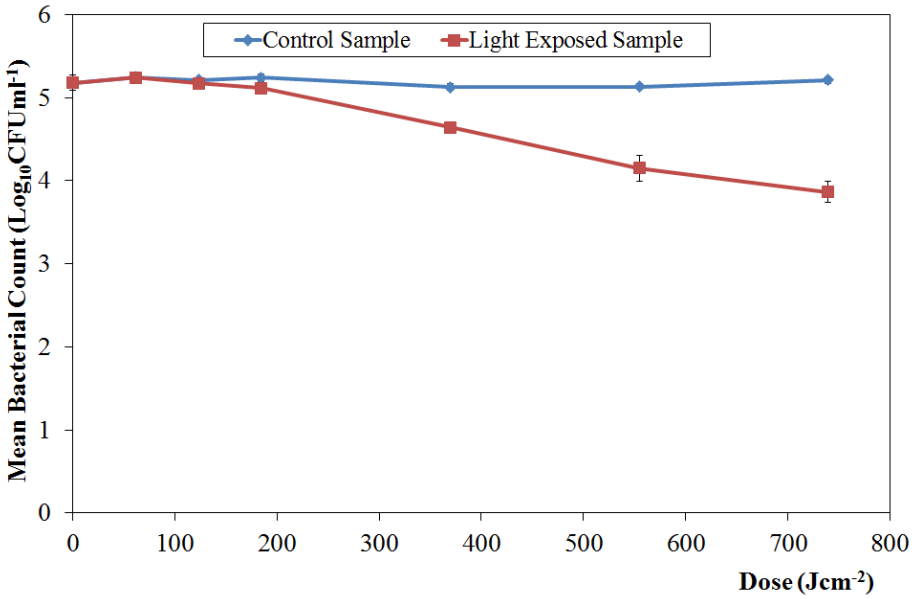

Fig. 6.10. *Inactivation curve for Salmonella enteritidis after exposure to the 405 nm high-intensity light from an LED array with an irradiance of 85.6 $mWcm^{-2}$.*

Fig. 6.11 shows the effect of the 405 nm LED array treatment for *Sh. sonnei*, with a 3.9-$\log_{10}$ reduction in bacterial population achieved after exposure to a dose of 555 Jcm^{-2}. When *Sh. sonnei* suspensions were exposed to the 405 nm LED array with a dose of 740 Jcm^{-2}, the total surviving population was less than 10^1 $CFUml^{-1}$ (4.7-$\log_{10}$ reduction).

Significant $\log_{10}$ reduction of *E. coli* 0157:H7 was achieved after exposure to a dose more than 370 Jcm^{-2}, as shown in Fig. 6.12. It can be observed from Fig. 6.12 that with an applied dose of 555 Jcm^{-2}, *E. coli* 0157:H7 suspensions could be inactivated with a 4.2-$\log_{10}$ reduction in bacterial population.

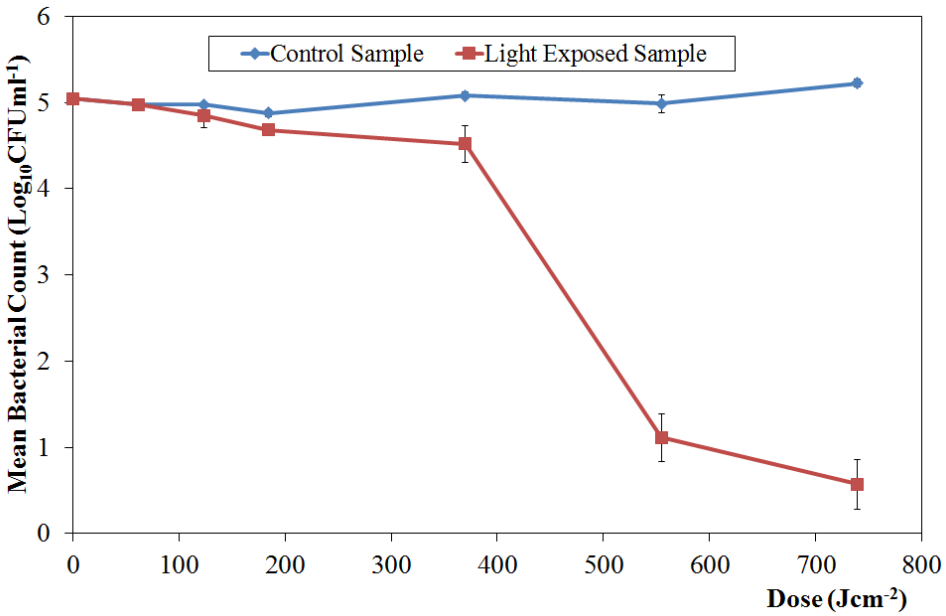

Fig. 6.11. *Inactivation curve for Shigella sonnei after exposure to the 405 nm high-intensity light from an LED array with an irradiance of 85.6 mWcm^{-2}.*

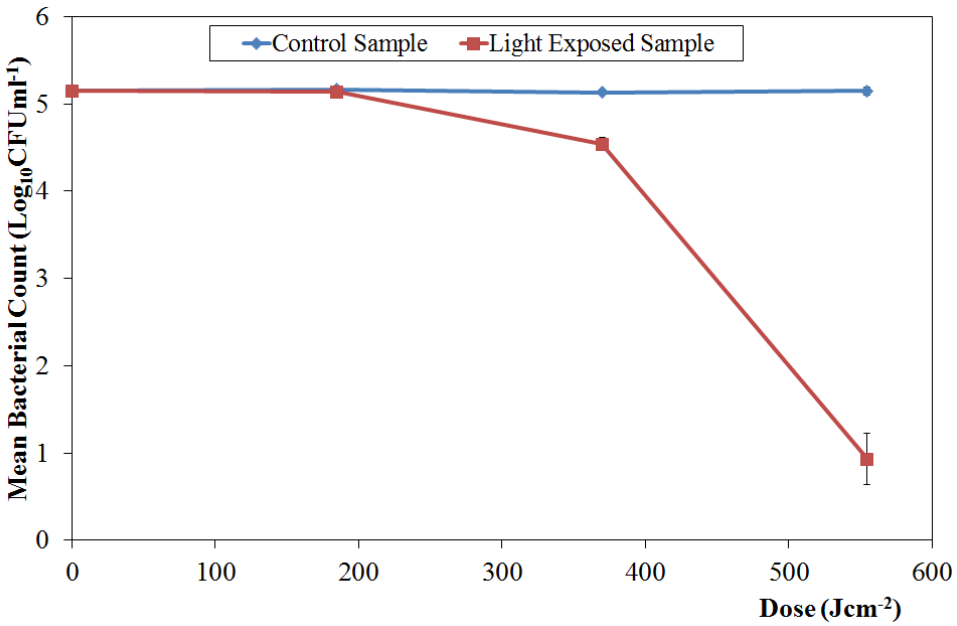

Fig. 6.12. *Inactivation curve for Escherichia coli 0157:H7 after exposure to the 405 nm high-intensity light from an LED array with an irradiance of 85.6 mWcm^{-2}.*

When the inactivation curve for *L. monocytogenes* is compared to those for *S. enteritidis*, *Sh. Sonnei* and *E. coli* O157:H7, the results show that *L. monocytogenes* is more susceptible than the three other bacteria, whereas *S. enteritidis* is the most resistant.

To ensure bacterial samples were not affected by heat during light exposure, control samples and light exposed samples had their temperature monitored during each independent experiment. Temperatures were found to only rise to around 30 °C after light exposure, and around 29 °C for control samples.

6.4 405 nm dose-dependence experiments

In this Section, the aim of the study was to investigate whether inactivation of bacterial suspensions using 405 nm high-intensity light was a dose-dependent effect. In order to investigate the dependence of the applied dose of 405-nm light on the inactivation of suspensions of *L. monocytogenes*, samples were exposed to four different doses: 61.6, 92.5, 123.3 and 154.1 Jcm^{-2}. For these four different doses, samples were exposed to four different irradiances levels (8.6, 44.7, 66.1 and 85.6 $mWcm^{-2}$), with the exposure time being adjusted in order to maintain the same dose exposure for each experiment. This was done by adjusting the exposure time according to the equation:

$$H = E\,t, \tag{6.1}$$

where, H = radiant exposure (dose) in Jcm^{-2}, E = irradiance in Wcm^{-2}, and t = exposure time in seconds [170].

Table 6.1 shows the inactivation parameters for dose-dependence experiments for *L. monocytogenes* exposure to the 405 nm high-intensity LED array.

Table 6.1 *Summary inactivation parameters for dose-dependence experiments*

Dose (Jcm^{-2})	Irradiance ($mWcm^{-2}$)	Exposure Time (Min)	Voltage (± 0.1 V)	Current (± 0.1 A)
61.6	8.6	120	8.9	0.1
	44.7	23	9.7	0.4
	66.1	16	10.1	0.6
	85.6	12	10.5	0.7
92.5	8.6	180	8.9	0.1
	44.7	34	9.7	0.4
	66.1	23	10.1	0.6
	85.6	18	10.5	0.7
123.26	8.6	240	8.9	0.1
	44.7	46	9.7	0.4
	66.1	31	10.1	0.6
	85.6	24	10.5	0.7
154.1	8.6	300	8.9	0.1
	44.7	57	9.7	0.4
	66.1	39	10.1	0.6
	85.6	30	10.5	0.7

6.4.1 Experimental method for inactivation of *L. monocytogenes* in liquid suspension with differing irradiance levels

The experimental set-up used in this set of experiments is described in Section 6.2.3 (Fig. 6.3). Two ml volumes of bacterial suspension were continuously agitated and exposed to increasing durations of 405 nm light, using four different irradiance levels: 8.6, 44.7, 66.1 and 85.6 $mWcm^{-2}$ at the surface of suspension, before being plated onto agar and incubated at 37 °C for 24 hours. Control samples were set-up using the same procedure but exposed to normal laboratory lighting.

6.4.2 Experimental results

Table 6.2 and Fig. 6.13 show inactivation data for *L. monocytogenes* exposed to 405 nm light using four different irradiances.

When *L. monocytogenes* was exposed to 405 nm light with irradiance of 8.6 $mWcm^{-2}$, significant log_{10} reductions were achieved after exposure to a dose of more than 92.5 Jcm^{-2}. Around 2.4-log_{10} reduction was achieved after exposure to a dose of 154.1 Jcm^{-2}. When an irradiance of 44.70 $mWcm^{-2}$ was used for inactivation of *L. monocytogenes*, it can be seen that a 3.59-log_{10} reduction in bacterial population was achieved after exposure to a dose of 154.1 Jcm^{-2}.

As stated in Table 6.2, an irradiance of 66.1 $mWcm^{-2}$ was also used for inactivation of *L. monocytogenes.* The results demonstrate that around 0.01-log_{10} reduction in bacterial population was achieved after exposure to a dose of 61.6 Jcm^{-2}. Increasing the dose up to 154.1 Jcm^{-2} causes a significant 3.82-log_{10} reduction of *L. monocytogenes*. Results following exposure to 405 nm light with an irradiance of 85.6 $mWcm^{-2}$ show that significant log_{10} reductions were achieved after applied doses of 123.3 and 154.1 Jcm^{-2}, with 1.79, and 3.57-log_{10} reduction in bacterial population, respectively.

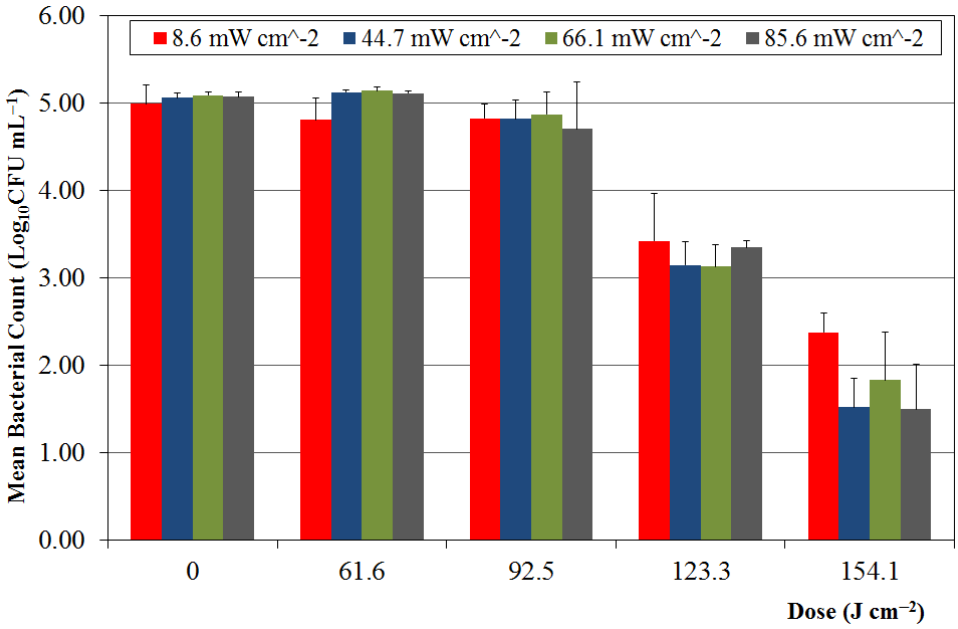

Fig. 6.13. *Dose-dependence experiments investigating the inactivation rate of L. monocytogenes following exposure to a 405 nm high-intensity LED array with differing irradiance levels.*

Table 6.2 *Summary results for dose-dependence experiments*

Dose (Jcm^{-2})	Irradinace ($mWcm^{-2}$)	Exposure Time (Min)	Initial Population, N_0 ($Log_{10}CFUml^{-1}$)	Final Population, N ($Log_{10}CFUml^{-1}$)	$Log_{10}(N/N_0)$ Reduction	Germicidal Efficiency η ($Log_{10}(N/N_0)/Jcm^{-2}$)	Statistical significance
0	8.60	0	4.99 (± 0.22)	4.99 (± 0.22)	0.00		
	44.70	0	5.06 (± 0.05)	5.06 (± 0.05)	0.00		
	66.10	0	5.09 (± 0.04)	5.09 (± 0.04)	0.00		
	85.60	0	5.07 (± 0.05)	5.07 (± 0.05)	0.00		
61.60	8.60	120	4.91 (± 0.07)	4.73 (± 0.27)	0.18	0.0029	0.23
	44.70	23	5.18 (± 0.03)	5.12 (± 0.03)	0.06*	0.0010	0.05
	66.10	16	5.15 (± 0.02)	5.14 (± 0.05)	0.01	0.0002	0.77
	85.60	12	5.15 (± 0.02)	5.11 (± 0.02)	0.04	0.0006	0.06
92.50	8.60	180	5.02 (± 0.11)	4.82 (± 0.13)	0.20*	0.0022	0.05
	44.70	34	5.05 (± 0.04)	4.82 (± 0.22)	0.23	0.0024	0.11
	66.10	23	5.15 (± 0.04)	4.87 (± 0.25)	0.26	0.0028	0.07
	85.60	18	5.03 (± 0.03)	4.70 (± 0.54)	0.33	0.0036	0.32
123.30	8.60	240	4.96 (± 0.30)	3.42 (± 0.47)	1.54*	0.0125	0.00
	44.70	46	5.04 (± 0.03)	3.14 (± 0.27)	1.90*	0.0154	0.00
	66.10	31	5.11 (± 0.01)	3.13 (± 0.25)	1.98*	0.0161	0.00
	85.60	24	5.14 (± 0.02)	3.35 (± 0.08)	1.79*	0.0145	0.00
154.10	8.60	300	4.79 (± 0.15)	2.37 (± 0.22)	2.42*	0.0157	0.00
	44.70	57	5.07 (± 0.03)	1.48 (± 0.30)	3.59*	0.0233	0.00
	66.10	39	5.07 (± 0.04)	1.84 (± 0.48)	3.23*	0.0210	0.00
	85.60	30	5.07 (± 0.03)	1.50 (± 0.51)	3.57*	0.0232	0.00

*Significant bacterial log_{10} reductions, calculated at a 95% confidence interval (p value ≤ 0.05). (Light-exposed sample value was significantly different from control value).

The overall results demonstrate that when *L. monocytogenes* is exposed to 405 nm light using four different irradiances similar patterns of inactivation curves and inactivation kinetics are achieved. The results clearly indicate that inactivation of *L. monocytogenes* in liquid suspension using 405 nm LED array is a dose-dependent reaction.

6.5 Discussion and Conclusions

In Part I, the study has compared data for inactivation of *S. aureus*, MRSA, *S. epidermidis* and *L. monocytogenes* using the 405 nm filtered light and 405 nm LED array. When the inactivation kinetics of bacteria were compared using the 405 nm HINS-light generated from a light emitting diode (LED) array and using the 405 nm filtered light from a Xenon lamp, similar results were found for each strain of bacteria, indicating that the applied dose of 405 nm light was the important factor, not the light source.

Fig. 6.5 shows the $\log_{10}$ reduction curve of *S. aureus* suspension through exposure to the 405 nm LED array. It can be observed from Fig 6.5 that the complete inactivation of *S. aureus* was achieved after exposure to a dose of 154.1 Jcm^{-2} with a 4.6-$\log_{10}$ reduction in bacterial population. From the data, shown in Fig. 6.6, it can be seen that significant $\log_{10}$ reduction in bacterial population were achieved after light exposure to a dose above 60 Jcm^{-2} and the complete inactivation (5-$\log_{10}$ reduction in bacterial population) of 10^5 $CFUml^{-1}$ MRSA was achieved after light exposure to a dose of 123.3 Jcm^{-2}.

A previous study by Maclean *et al.* which utilized a similar treatment system, achieved 5-$\log_{10}$ reductions of the bacteria *S. aureus* and MRSA after exposure to a dose of 36 Jcm^{-2} and 45 Jcm^{-2} of 405 nm HINS-light, respectively [117]. Meanwhile, a study by Murdoch demonstrated that 5-$\log_{10}$ reduction of *S. aureus* and MRSA were achieved with exposure to a dose of 144 and 108 Jcm^{-2}, respectively, of 405 nm HINS-light [159]. The results shown in the present study are similar to those achieved in the study by Murdoch. When the results of inactivation of *S. aureus* and MRSA in the present study are compared to a study by Maclean *et al.*, several times

the applied doses were required to achieve the same level of bacterial $\log_{10}$ reduction, respectively. The possible reason for these differences in results could be due to differences in the experimental protocols used for preparation of the bacterial cultures and differences in the light treatments applied.

The effectiveness of visible light for photodynamic inactivation of *S. aureus* in conjunction with exogenous photosensitiser is also compared to that found in the present study. Zaeina *et al*. has demonstrated the use of standard light (white light) in combination with methlyne blue (100 $\mu g.ml^{-1}$) for inactivation of *S. aureus* [171]. They found that a 5-$\log_{10}$ reduction in bacterial population was achieved after an applied dose of 25.2 Jcm^{-2} [171]. A study by Lambrechts *et al.* reported that *S. aureus* can be inactivated by a white light source from a 500 W halogen lamp in conjunction with TriP[4], an approximately 5-$\log_{10}$ reduction was achieved after exposure to a dose of 27 Jcm^{-2} [172]. Other studies by Bertoloni *et al.* [173] and Nitzan *et al.* [174] have also demonstrated the effectiveness of white light in combination with hematoporphyrin (10 $\mu g.ml^{-1}$) and δ-ALA induced porphyrins for inactivation of *S. aureus*, respectively. They found that 4.5 and 2.5-$\log_{10}$ reductions in bacterial population were achieved after applied doses of 3.6 and 75 Jcm^{-2}, respectively [173, 174]. Studies which used dyes as the photosensitising molecules (the use of exogenous photosensitisers) have demonstrated that applied doses of approximately 2 – 6 times less than in the present study resulted in similar $\log_{10}$ reduction in bacterial population [171-174]. However, the present study has shown that photodynamic inactivation of *S. aureus* can be achieved without the addition of exogenous photosensitisers.

As stated in Table 5.4, *L. monocytogenes* can be inactivated by exposure to wavelengths of 400-500 nm and >400 nm filtered light, with a 5.1 and 4.7-$\log_{10}$ reduction in bacterial population, after light exposure to a dose of 907 and 1360.8 Jcm^{-2}, respectively. These data are valuable to compare to inactivation data gained using both the 405 nm filtered light and 405 nm LED array (the results are compared in Table 6.3). Germicidal efficiency data demonstrates that the use of the 405 nm high-intensity LED array and 405 nm filtered light for inactivation of

L. monocytogenes had much higher germicidal efficiency when compared to that for the use of >400 nm and 400-500 nm filtered light from the Xenon lamp.

This result is readily explained when the emission spectra of the 405 nm light sources (filtered light from Xenon lamp and LED array) as shown in Fig. 6.1 and the emission spectrum of >400 nm and 400-500 nm filtered light from Xenon lamp as shown in Fig. 5.2 are compared. The main reason why the 405 nm light sources are much more efficient is because all the energy emitted is used for inactivation. However with the >400 nm and 400-500 nm light sources the energy emitted is broadband and only a small fraction of the energy is useful for inactivation. This result explains the low value of germicidal efficiency achieved for >400 nm and 400-500 nm filtered light from the Xenon lamp after exposure to a dose of 1360.8 and 907 Jcm^{-2}, respectively.

The germicidal efficiency of the 405 nm LED array and the 405 nm filtered light was similar, although the LED array was slightly more efficient. No significant difference was observed between the germicidal efficiency data from the 405 nm filtered light and the 405 nm high-intensity LED array. The reason is the fact that the 405 nm filtered light from the Xenon lamp and the 405 nm HINS-light generated from an LED had nearly the same the peak wavelength, 401.51 nm for the 405 nm filtered light and 400.46 nm for the 405 nm high-intensity LED array, as well as a similar bandwidth (Fig. 6.1). As shown in Table 6.3, the germicidal efficiency for inactivation of *L. monocytogenes* was 0.025 $\log_{10}(N/N_0)$ per Jcm^{-2} after exposure to a dose of 185 Jcm^{-2} (with an irradiance of 8.6 $mWcm^{-2}$). When *L. monocytogenes* was exposed to the 405 nm high-intensity LED array at a dose of 185 Jcm^{-2} (with an irradiance of 85.6 $mWcm^{-2}$), this resulted in a similar rate of inactivation, 0.02 $\log_{10}(N/N_0)$ per Jcm^{-2}. This result clearly indicates that the applied dose for bacterial inactivation was the important factor, not the light source.

Table 6.3 *Summary parameters for inactivation of 10^5 CFUml^{-1} Listeria monocytogenes suspensions following exposure to >400 nm, 400-500 nm, 405 nm filtered light from the Xenon lamp and from the 405 nm high-intensity LED array.*

Type of Inactivation	**Dose (Jcm^{-2})**	**Exposure time (min)**	**Log_{10} (N/N_0) Reduction**	**Germicidal Efficiency (Log_{10} (N/N_0) per Jcm^{-2}**
>400 nm filtered light	1360.8	180	4.7	0.003
400-500 nm filtered light	907	120	5.1	0.006
405 nm filtered light	185	360	4.4	0.024
405 nm LED array	185	360	4.6	0.025

In Part II, the study investigated the use of a 405 nm LED array for inactivation of various foodborne pathogens. Comparative data for inactivation of three species of *Listeria* (*Listeria monocytogenes*, *Listeria ivanovii* and *Listeria seeligeri*), and also the significant Gram-negative food-borne pathogens *Salmonella enteritidis*, *Shigella sonnei* and *Escherichia coli* 0157:H7 following exposure to the 405 nm high-intensity LED array are summarised in Table 6.4.

When *Sh. sonnei* and *E. coli* 0157:H7 were exposed to the 405 nm LED array at a doses of 370 and 555 Jcm^{-2}, the result shows quite similar the germicidal efficiency values, with 0.001 $\log_{10}(N/N_0)$ per Jcm^{-2} for a dose of 370 Jcm^{-2}. Germicidal efficiency values of 0.007 $\log_{10}(N/N_0)$ per Jcm^{-2} for *Sh. sonnei* and 0.008 $\log_{10}(N/N_0)$ per Jcm^{-2} for *E. coli* 0157:H7 were achieved at a dose of 555 Jcm^{-2}.

Treatment of *L. monocytogenes* and the other *Listeria* species using the 405 nm LED array (Fig. 6.9) resulted in similar inactivation kinetics, indicating that bacteria within the same genus may undergo very similar inactivation reactions. This result obtained with different *Listeria* species shows a similar effect to that reported with different Staphylococcus species in by Maclean *et al.* [117].

Fig. 6.9 shows the inactivation curve for *L. monocytogenes* after exposure to the 405 nm LED array with an irradiance of 85.6 $mWcm^{-2}$. It can be observed from Fig. 6.9 that significant $\log_{10}$ reductions in bacterial populations were achieved after exposure to doses of 123.3, 154.1 and 185 Jcm^{-2}, with 1.79, 3.57 and 3.72-$\log_{10}$ reductions, respectively. When *L. ivanovii* was exposed to the 405 nm LED array with an irradiance of 85.6 $mWcm^{-2}$, significant $\log_{10}$ reductions in bacterial populations were also achieved after an applied dose of 185 Jcm^{-2} (4.2-$\log_{10}$ reduction), as shown in Fig. 6.9. The results, shown in Fig. 6.9, also demonstrate that significant $\log_{10}$ reductions of *L. seeligeri* were achieved after applied doses of 123.3 and 185 Jcm^{-2}, with 1.2 and 3.3-$\log_{10}$ reductions in bacterial population, respectively.

Table 6.4 *Summary parameters for inactivation of Gram-positive and Gram-negative bacteria associated with foodborne diseases following exposure to the 405 nm high-intensity LED array*

Organism	**Irradiance ($mWcm^{-2}$)**	**Exposure Time (min)**	**Dose Jcm^{-2}**	**Log_{10} (N/N_0) Reduction**	**Jcm^{-2} per Log_{10} (N/N_0)**	**Germicidal Efficiency (Log_{10} (N/N_0) per Jcm^{-2})**
Listeria monocytogenes	85.6	36	185	3.7	50.0	0.020
Listeria ivanovii	85.6	36	185	4.1	45.1	0.022
Listeria seeligeri	85.6	36	185	3.3	56.0	0.018
Salmonella enteritidis	85.6	144	740	1.3	569.2	0.002
Escherichia coli 0157:H7	85.6	108	555	4.2	132.1	0.008
Shigella sonnei	85.6	144	740	4.7	157.3	0.006

Maclean *et al.* [117] and Murdoch *et al.* [118] have demonstrated *E. coli* inactivation using a 405 nm LED array light exposure. They found that *E. coli* could be inactivated with around 3.1 and 5.3-$\log_{10}$ reductions in bacterial populations after exposure to a dose of 180 and 288 Jcm^{-2}, respectively. In the present study, with an application dose of around two times that used in the study by Murdoch *et al.*, around 4.2- $\log_{10}$ reduction of *E. coli* was achieved after application of a dose of 555 Jcm^{-2}. Murdoch *et al.* also reported that *S. enteritidis* in liquid suspension can be inactivated by 405 nm light exposure, with a 3-$\log_{10}$ reduction achieved after exposure to a dose of 288 Jcm^{-2} [118].

In the present study suspensions of *E. coli* and *Sh. sonnei* required 3 – 4 times the dose for log reductions similar to those achieved with *Listeria*. *S. enteritidis* was found to be the least susceptible of the organisms tested, with a reduction of approximately 1.3-$\log_{10}$ after exposure to 4-times the dose (740 Jcm^{-2}). This is similar to the trend found in the study by Maclean *et al.* [117] which showed that, in general, Gram-positive organisms required lower doses of 405-nm light exposure for inactivation to be initiated.

The inactivation kinetics of all the organisms (Fig. 6.9 – Fig.6.12) investigated in this study show a sigmoidal shape, similar to those from previous studies [116-118]. The mechanism of action of the 405 nm light is hypothesised to be the result of the photoexcitation of endogenous porphyrin molecules, the levels and types of which may vary from genus to genus, and species to species. A build-up of oxidative damage, which occurs as a result of the generation of singlet oxygen and other reactive oxygen species, must occur before any damaging effects become evident through viable colony-forming unit counts – evident through the initial lag phase of the inactivation curve. Once oxidative damage becomes physically detrimental, cell death appears to occur at a relatively rapid rate. The focus of the present study was to investigate the wavelength sensitivity and inactivation kinetics of *L. monocytogenes*, and did not investigate the oxidative damage to the bacterial cells, however expansion of knowledge on the mechanism of action would be extremely advantageous in order to further understand and exploit this inactivation method for novel decontamination processes.

There is only limited data in the literature investigating the photodynamic inactivation of *Listeria* through visible-light exposure without the addition of exogenous photosensitisers. The present study presents for the first time the inactivation of *Listeria* species through exposure to 405 nm light without the addition of photosensitiser molecules or other pre-treatments.

Much of the literature focuses on photodynamic inactivation processes that use *Listeria* populations that have been pre-incubated with molecules which either increase synthesis of endogenous porphyrin levels prior to light exposure, or act as photosensitizing agents themselves. Buchovec *et al.* [175] reported that (7.5 mM) 5-aminolevulinic acid (ALA) used in conjunction with a 400 nm LED-based light source could be used to inactivate of *L. monocytogenes*. They achieved a 3.7-$\log_{10}$ reduction on packaging material, a 3.1-$\log_{10}$ reduction in bacterial biofilms and a 4-$\log_{10}$ reduction in *L. monocytogenes* cell suspensions after exposure to a dose of 20 Jcm^{-2}. A study by Luksiene *et al.* utilized a 405 nm LED with an intensity of 20 $mWcm^{-2}$, in conjunction with Na-Chlorophyllin (Na-Chl)-based photosensitization for inactivation of *Listeria monocytogenes* in PBS suspension and on packaging surfaces [176]. They found that with a dose of 36 Jcm^{-2} *Listeria* in suspension could be inactivated by 7-$\log_{10}$, and for packaging surfaces, results demonstrated that Na-Chl-based photosensitization, was much more effective against *Listeria* than washing with water or 200 ppm sodium-hypochlorite, with respective $\log_{10}$ reductions in bacterial population of 4.5, 1.7 and <1 being achieved [176].

A further study by Paskeviciute *et al.* employed a 400nm LED-based light source and Na-Chl for decontamination of the surface of strawberries seeded with *L. monocytogenes*, and after 30 minutes exposure to an irradiance of 20 $mWcm^{-2}$, pathogen levels were reduced by up to 98% [177]. These results highlight the accelerated inactivation rates which can be achieved when exogenous photosensitiser molecules are incorporated into the system. Although the inactivation of *L. monocytogenes* in the present study required much higher doses, this inactivation was achieved solely through exposure to 405-nm light. There can be significant advantages, particularly in practical decontamination applications, in attaining microbial inactivation without relying on the addition of exogenous chemicals.

With regards to light-based decontamination technologies, the application of UV-light for inactivation of the foodborne pathogen *Listeria* has been studied widely [178-183]. Rapid inactivation rates are achievable through the use of UV-light however, in some practical situations, there can be disadvantages such as its low penetrability, degradation of materials and human safety. Considering safety, the use of high intensity 405 nm light is significantly safer due to these wavelengths being part of the visible-light spectrum, and this coupled with the fact that inactivation occurs through exposure to light alone and does not require additional chemical pretreatments or molecules, this makes the use of this inactivation mechanism very attractive for a range of potential decontamination applications.

In Part III of this study results have demonstrated dose-dependence effects for inactivation of *L. monocytogenes* in liquid suspension.

Table 6.2 contains a summary of parameters applied during dose-dependence experiments for inactivation of *L. monocytogenes* in liquid suspension as well as including all results that were achieved during the experiments.

When the inactivation rates of *L. monocytogenes* following exposure to the 405 nm high-intensity LED array, using differing irradiance levels (dose of 61.6 Jcm^{-2}) are compared, it can be seen that the highest log_{10} reduction (0.18-log_{10}) was achieved after application of 8.6 $mWcm^{-2}$ for 120 min exposure while the significant log_{10} reduction in bacterial population being achieved through exposure to an irradiance of 44.7 $mWcm^{-2}$. As stated in Table 6.2, no significant log_{10} reductions in bacterial populations were observed when *L. monocytogenes* was exposed to a dose of 92.5 Jcm^{-2} at the three irradiance levels tested (44.7, 66.1 and 85.6 $mWcm^{-2}$). The inactivation rates for all four irradiance levels are quite similar, with an irradiance of 85.6 $mWcm^{-2}$ exposure displaying the highest rate of inactivation, and consequently it has the highest germicidal efficiency with a value of 0.0036 log_{10} (N/N_0) per Jcm^{-2}.

Fig. 6.13 shows the results of dose-dependence experiments for the inactivation of *L. monocytogenes* in liquid suspension through exposure to the 405-nm LED array. It can be observed from Fig. 6.13 that over the range of applied doses, of

approximately 62 – 152 Jcm^{-2}, the inactivation rate of *L. monocytogenes* is relatively similar when the same dose is applied using the four different light intensities.

Table 6.5 also allows comparison of the bacterial reductions achieved with the different combinations of irradiance and dose applied in the dose-dependence experiments. Four different inactivation doses were investigated and for each of these doses, four irradiance levels were utilized. Statistical analysis showed no significant differences in inactivation rates when irradiances of 44.7, 66.1 and 85.6 $mWcm^{-2}$ are compared for the same applied dose. Although inactivation kinetics were similar, statistically significant differences in inactivation rate were however found when using an irradiance of 8.56 $mWcm^{-2}$ for bacterial inactivation at doses of 61.6 and 154.1 Jcm^{-2} (indicated by the asterisk in Table 6.5). Overall however, the results show that, over the range tested, the dose required for bacterial inactivation – regardless of how it is applied – yields similar final populations.

Overall, this study has demonstrated the sensitivity of *L. monocytogenes* to 405 nm light. Results have also proven that *L. monocytogenes* and other *Listeria* species, as well as other important foodborne pathogens including, *E. coli* 0157:H7, *S. enteritidis* and *Sh. sonnei*, can be successfully inactivated by exposure to high intensity 405 nm light. The results from this study, coupled with other recent literature, demonstrate the wide bactericidal activity of 405 nm light, providing justification for further investigation and development of 405 nm light for decontamination applications. It has also been shown that 405 nm LED arrays offer a compact and reliable light source that could be easily incorporated and used in practical decontamination systems.

Table 6.5 *Statistical analysis of the comparative 405 nm light doses required for inactivation when applied using four different power densities: analysis of data graphically displayed in Fig.6.13*

Comparative irradiance levels for inactivation	**Statistical significance (*p* value)**			
	Dose of 61.6 Jcm^{-2}	**Dose of 92.5 Jcm^{-2}**	**Dose of 123.3 Jcm^{-2}**	**Dose of 154.1 Jcm^{-2}**
8.6 mWcm^{-2} vs 44.7 mWcm^{-2}	0.036*	0.939	0.282	0.01*
8.6 mWcm^{-2} vs 66.1 mWcm^{-2}	0.032*	0.666	0.268	0.231
8.6 mWcm^{-2} vs 85.6 mWcm^{-2}	0.039*	0.926	0.424	0.028*
44.7 mWcm^{-2} vs 66.1 mWcm^{-2}	0.527	0.735	0.906	0.346
44.7 mWcm^{-2} vs 85.6 mWcm^{-2}	0.763	0.971	0.237	0.698
66.1 mWcm^{-2} vs 85.6 mWcm^{-2}	0.412	0.822	0.18	0.486

* Light-exposed sample value was significantly different to the light-exposed sample at the same level of inactivation dose for each applied irradiance level. (Significant differences in experiments are calculated using ANOVA (one way) with 95% confidence interval and $p \leq 0.05$ using MINITAB Release 16).

CHAPTER 7

INVESTIGATION INTO IRRADIANCE DISTRIBUTION OF LIGHT FROM AN LED LIGHT ENGINE

7.1 General

The work of the previous chapters has demonstrated the effectiveness of 405 nm high-intensity light for bacterial inactivation. For large-area environmental decontamination applications, work at the ROLEST facility has led to the development of a large-scale HINS-light prototype system [1]. This large-scale HINS-light Environmental Decontamination System (HINS-light EDS) has been developed for continuous decontamination of air and contact surfaces in occupied environments, and has been installed and successfully evaluated in a hospital environment, as shown in Fig. 7.1. The HINS-light EDS initial prototype design is a ceiling-mounted light source made up of light-emitting diodes (LEDs), covered by a Fresnel lens and diffuser, which emit a narrow band of high intensity visible light with peak output at 405 nm wavelength, blended with white light. HINS-light wavelengths cause photodynamic inactivation of bacteria without the use of exogenous photosensitizer molecules [1, 184]. This HINS-light EDS technology has many potential applications, for instances disinfection of air and surfaces in clinical environments, and disinfection of food contact surfaces. Despite the successful deployment of the initial prototype in the clinical environment, the system has some limitations, such as having power supplies which are not fully integrated, thermal management, and the light emission is more dominant in violet/blue than is desirable.

Because the main components of the HINS-light EDS are LED light sources, the work of this chapter will concentrate on a study of Lambert's cosine law to examine the irradiance distribution of a LED source for the design and development of an improved HINS-light EDS prototype. The study focuses on experimental work for

analysis of the irradiance distribution of a single LED array light source for both angular and linear distribution. To investigate the light distribution of the LED source used in the study the most important factor is the Lambertian mode number (m). Commonly, the Lambertian mode number (m) for each individual LED source is either provided by the manufacturer or can be determined by experimental methods. In practice, the Lambertian mode number (m) for each individual model of a LED is not identical, even though they are the same type and are from the same manufacturer. This fact justified an investigation of the Lambertian mode number (m) emitted from the LED source to be used in the new prototype HINS-light EDS to be developed later in this study.

Fig. 7.1. *HINS-light Environmental Decontamination System (HINS-light EDS) in a hospital isolation room (Glasgow Royal Infirmary, Scotland, UK).*

7.2 A study of the Lambertian mode number (*m*)

The main aspects of this study have involved analytical studies of the Lambertian mode number (m) and investigation into the effect of space distance between a LED source and lens system (Fresnel lens and diffuser combination).

7.2.1 Light source

The 405 nm light source used in the study was the ENFIS Uno Air Cooled Light Engine obtained from ENFIS Ltd, UK, pictured in Fig. 7.2.

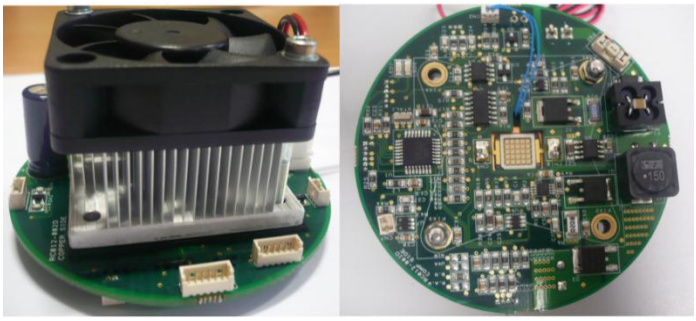

Fig. 7.2. *The 405 nm LED array light engine.*

The 405 nm LED light engine in Fig. 7.2 is a light engine in the form of a close-packed rectangular array with 25 individual LEDs, and had a manufacture's stated a typical power output of 4.9 mW. It is a spot source with high electrical power of up to 38W, and a small emitting area (0.5 cm^2). The light engine also has embedded thermistors to enable accurate feedback on LED chip temperature [Appendix C] [185]. The emission spectrum of the 405 nm high-intensity LED light engine is shown in Fig. 7.3. It can be seen that the peak wavelength was 405.72 nm with a bandwidth of 14 nm FWHM.

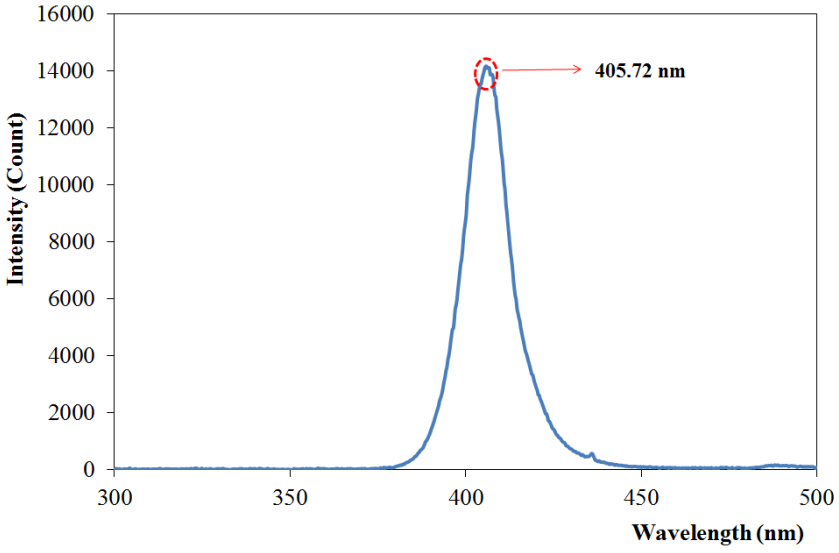

Fig. 7.3. *Emission spectrum of 405 nm LED light engine source.*

7.2.2 Fresnel lens and diffuser

The optical components used in this study were Fresnel lenses, one with a 2.54 cm focal length (LFQ2561) and another with a 4 cm focal length (LFQ40100) obtained from Knight Optical Ltd., UK and a holographic Light Shaping Diffuser (LSD; L20P1-12) with a 20°(FWHM) light shaping diffuser angle, sourced from LUMINIT LLC, USA. According to Knight Optical Ltd., UK "Fresnel lenses replace conventional lenses that have a curved surface with a series of concentric grooves, which are moulded into the surface of lightweight plastic sheets" [186].

The Fresnel lens is used to distribute the light in the required manner, and a diffuser to help spread out or scatter light in some manner, in order to achieve a more uniform distribution of light. LSDs have 85 – 92% transmission across a wide wavelength range of 400 – 1600 nm [187]. This diffuser has two sides, one rough and one smooth. When light falls perpendicular to the surface of the diffuser, both of the sides result in different patterns of light distribution. In the present study, only one configuration of lens system was used: the Fresnel lens and diffuser are arranged with rough-to-rough configuration, as shown in Fig 7.4. The complete configuration of the Fresnel lens and diffuser combination to be used in the HINS-light EDS is further discussed in Chapter 8.

Fig. 7.4. *The Fresnel lens and diffuser are arranged with rough-to-rough configuration.*

7.2.3 Radiant power meter

All data measurements of irradiance from the light source were measured using a radiant power meter (model 70260, L.O.T.-Oriel Ltd., UK) in conjunction with a photodiode detector (model PD300-UV, OPHIR, UK). To ensure the accuracy of light measurement for irradiance distribution as a function of linear displacement, the detector was calibrated by cosine correction. The experimental setup for calibration of the meter is shown in Fig. 7.5. The head of the detector was positioned in either a flattened or tilted position at a distance of 50 cm below the LED array light engine,

and then irradiance data was measured starting at *O* until reaching 45° from position *O*; all measurements were repeated three times to get accurate data.

Results, shown in Fig. 7.6, demonstrate that the head of the detector is angle dependent, meaning that all data measurements need cosine correction to ensure accurate measurement. The data measured with the detector both flattened and tilted correlates well with the data using cosine correction. When data is measured using the detector in the flattened position, to get the real data, these data measurements are divided by cosine correction. Meanwhile, if data measurements were taken using the detector in the tilted position, the real data is the data measurements multiplied by cosine correction.

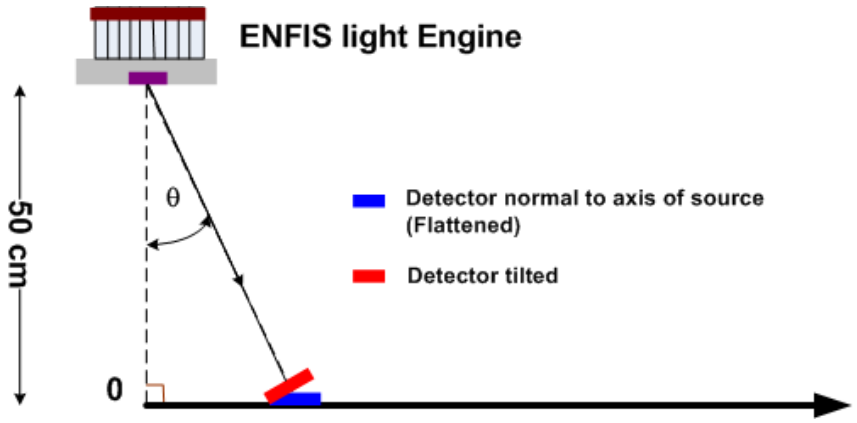

Fig. 7.5. *Experimental setup for calibration of the radiant power meter.*

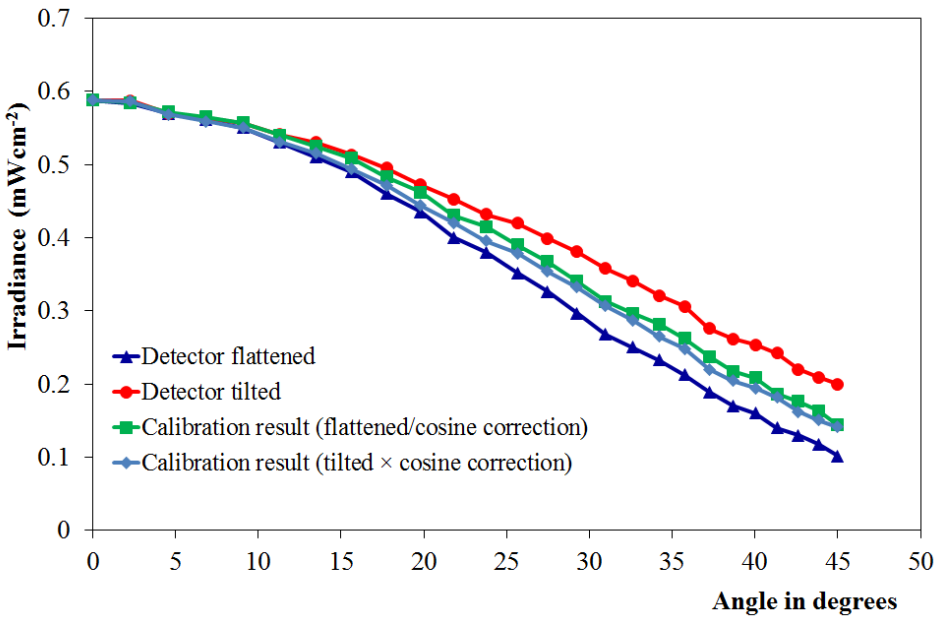

Fig. 7.6. *Calibration data for radiant power meter.*

7.2.4 Experiment methods for angular distribution

Fig. 7.7 was used to examine the irradiance distribution as a function of the angular displacement. The 405 nm LED light engine is rotated about an axis directly through the head of detector (-90° to 90°) and the irradiance distributions were measured at 10, 15, 20 and 30 cm from that axis, as shown in Fig. 7.7a (Method A).

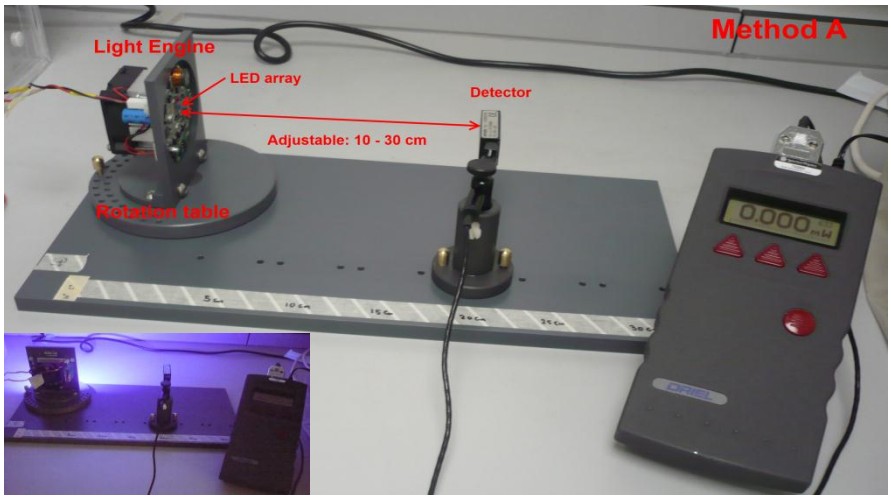

(a)

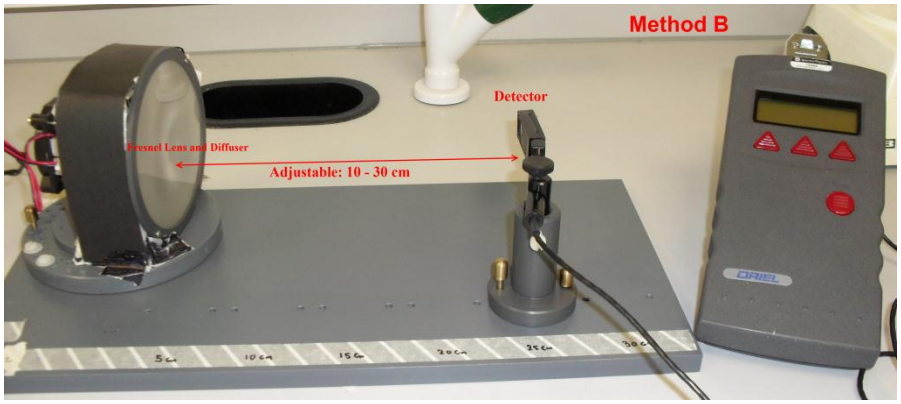

(b)

Fig. 7.7. *Photograph of equipment for analysis of the irradiance distribution as a function of the angular displacement for the LED light source: a) without a Fresnel lens and diffuser (Method A), b) with a Fresnel lens and diffuser (Method B).*

For analysis of the irradiance distribution when the light is passing through the lens system, as shown in Fig. 7.7b, the space distance between the 405 nm LED array and the lens system (Fresnel lens and diffuser) was fixed at 4 cm. The space distance (4 cm) has been selected for examination of the relationship between focal length and Fresnel lens. As with method A, the light source is rotated about an axis directly through the head of the detector (-90° to 90°) and the irradiance distributions were measured at 10, 15, 20 and 30 cm from that axis (Method B). For all experiments the voltage was set to 11.25 ± 0.1 V with a current of 0.25 ± 0.01 A.

7.2.4.1 Results for angular distribution without lens system (Method A)

Fig. 7.8 shows the results of the irradiance distribution as a function of angular displacement without the lens system. It can be seen that the irradiance distribution of the 405 nm LED array has a bell-shaped pattern with peak irradiance when the light from the LED array falls on the detector surface at 0°.

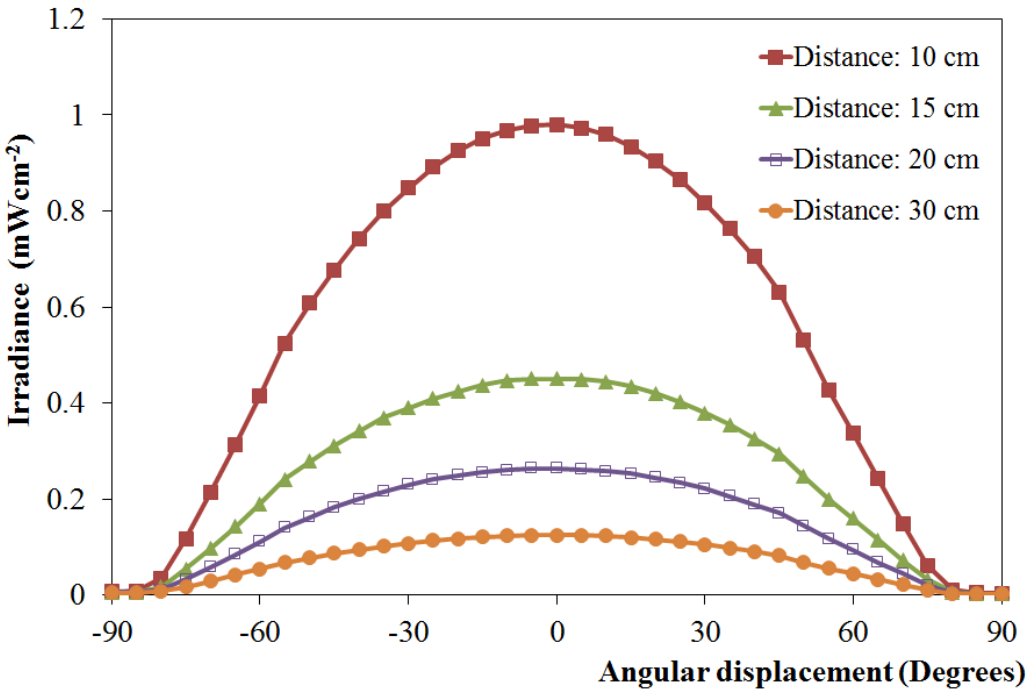

Fig. 7.8. *Irradiance distribution as a function of the angular displacement for the LED light source without a Fresnel lens and diffuser.*

In order to compare the angular distribution pattern of the LED array with the Lambertian pattern (m = 1, defined as "the luminous intensity in any direction from an element of a perfectly diffusing surface varies as the cosine of the angle between that direction and the perpendicular to the surface element" [2]). From Eq. (2.8), the angular distribution of the irradiance can be expressed as follows:

$$\frac{E(\theta)}{E_0} = \cos^m \theta. \tag{7.1}$$

With data from Fig. 7.8, the angular distribution could be redrawn to polar plot, replacing irradiance ($mWcm^{-2}$) with the relative intensity of irradiance (a.u.), as shown in Fig. 7.9. The relative intensity is the normalised power density from experimental data, $\frac{E(\theta)}{E_0}$. It can be observed from Fig. 7.9 that the irradiation pattern is nearly a Lambertian in pattern.

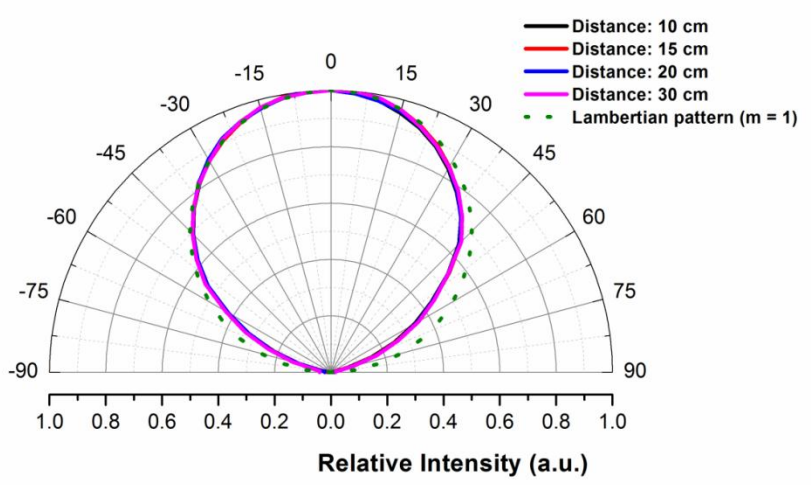

Fig. 7.9. *Angular distribution in the form of polar plot: the normalised irradiance as a function of angular displacement for the LED light source without a Fresnel lens and diffuser.*

Eq. (7.1) was used to provide a curve fit method to determine the Lambetian mode number (m) from the irradiance distribution. The normalised irradiances from experimental data as a function of angular displacement were analysed using QtiPlot 0.9.8.5 svn 2126 to get the best fit curve, and this is plotted in Fig. 7.10. The curve

fitting method used in the study was the Scaled Levenberg-Marquardt (LM) algorithm with tolerance = 0.0001 and no weighting method. Levmar reported that the LM algorithm is a standard technique for non-linear least-squares problems, and can be considered as a combination of steepest descent and the Gauss-Newton method [188]. This algorithm is suitable for determining the Lambertian mode number (*m*) during the study due to the advantages in the fitting process. The fitting process depends on the starting parameter values are close to the minimum (optimum value), this algorithm acts as a steepest descent method (slow but guaranteed to converge), if solution is outlying from the correct solution, and the algorithm turn into a Gauss-Newton method, if the solution is nearly the correct solution [188].

The results, shown in Fig. 7.10, demonstrate that the best curve fitting the experimental data for the Lambertian mode number (*m*) is with a value of 1.3. The results showed that the distance between the head of detector and the LED array did not give a significant effect.

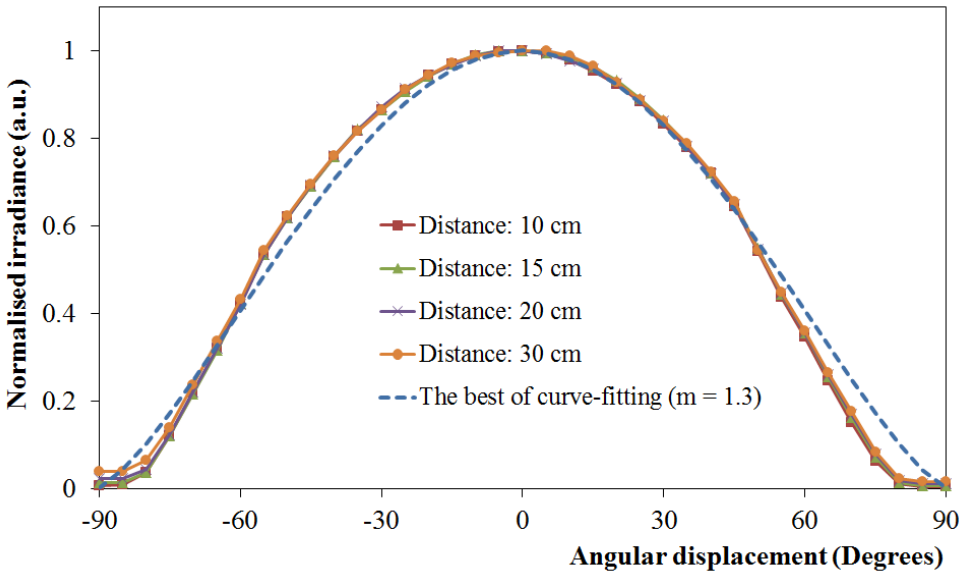

Fig. 7.10. *The normalised irradiances from experimental data with the best curve-fitting value.*

7.2.4.2 Results for angular distribution with the lens system (Method B)

Fig. 7.11 and Fig. 7.12 are the irradiance distribution of the 405 nm LED array as a function of the angular displacement with a diffuser and each of the Fresnel lenses, with focal lengths of 2.54 cm and 4 cm, respectively. Similarly, to the results in

Section 7.2.4.1, it can be seen that the irradiance distribution pattern is a bell-shaped curve. In comparison with the previous results, the angular distribution with a Fresnel lens and diffuser has a narrow distribution compared to the angular distribution without a Fresnel lens and diffuser.

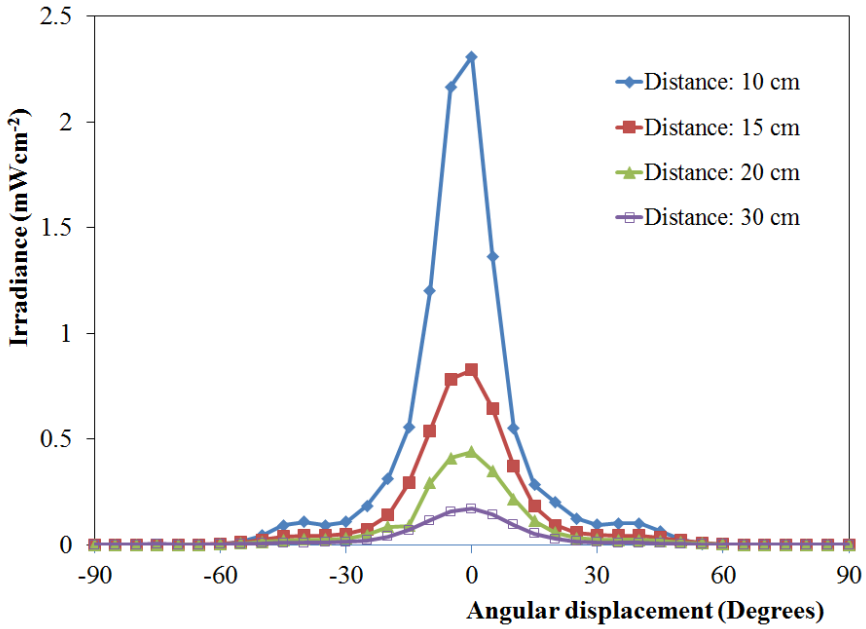

Fig. 7.11. *Irradiance distribution as a function of the angular displacement for the LED light source with a Fresnel lens with a focal length of 2.54 cm and diffuser.*

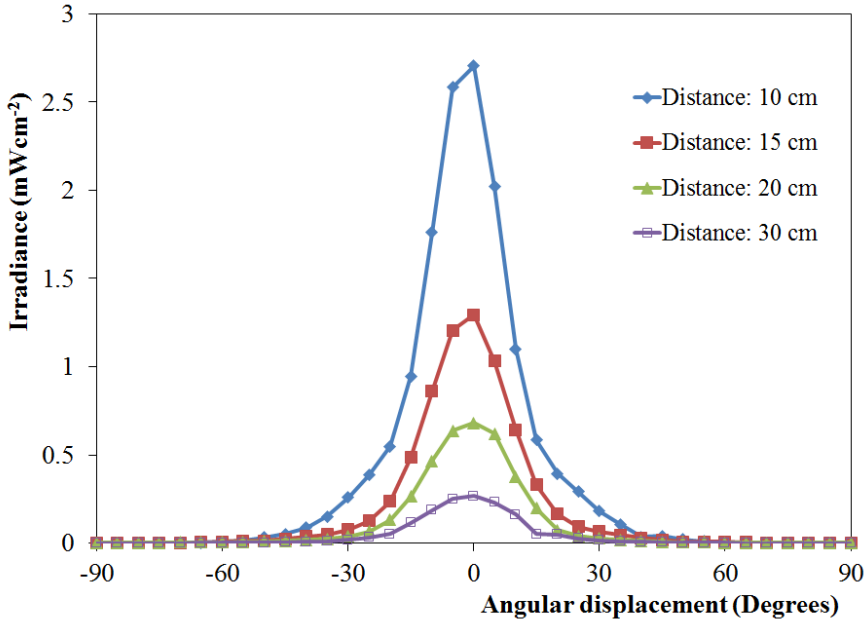

Fig. 7.12. *Irradiance distribution as a function of the angular displacement for the LED light source with a Fresnel lens with a focal length of 4 cm and diffuser.*

Comparative data of relative intensity of irradiance as a function of angular displacement for the configurations of the diffuser with the Fresnel lens with a 2.54 cm focal length, and the diffuser with the Fresnel lens with a 4 cm focal length, are plotted in Fig. 7.13 and Fig. 7.14, respectively. The results show that the irradiance pattern for the two types of Fresnel lens configurations have a light distribution of narrow spread with a value of $< 30^0$ (FWHM). A study of the Lambertian mode number (m) for both are summarised in Table 7.1. The best curve fitting of the Lambertian mode number (m) for experimental data was analysed using Eq. (7.1) by QtiPlot 0.9.8.5 svn 2126. As stated in Table 7.1, the Lambetian mode number (m) shows quite similar results when the study of Lambert's cosine law uses the combination of the diffuser and Fresnel lens with focal length 4 cm, with a value in the range of 32 – 40. Whereas, the Lambertian mode number (m) for the combination of a diffuser and Fresnel lens with focal length 2.54 cm has a varying value ranging from 31 – 60. The results indicate that both the Fresnel lens with the 2.54 cm focal length and the Fresnel lens with the 4 cm focal length have a pattern of irradiance distribution much narrow than the Lambertian pattern (m = 1) (see Fig. 7.13 and Fig. 7.14).

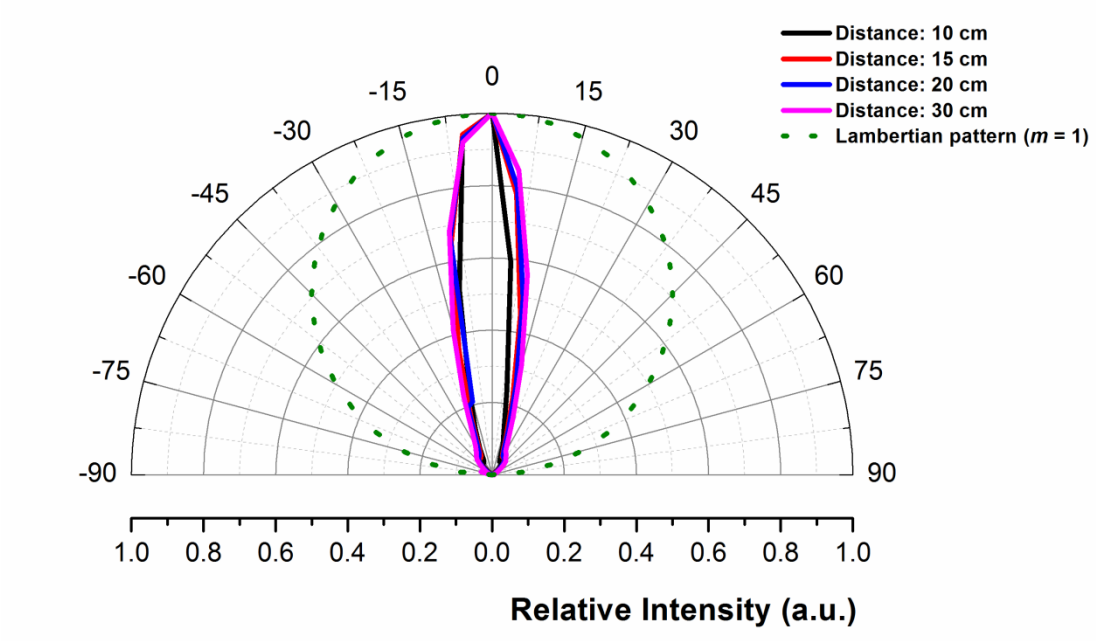

Fig. 7.13. *Angular distribution in polar plot: the normalised irradiances as a function of angular displacement for the LED light source with a Fresnel lens with a 2.54 cm focal length and diffuser.*

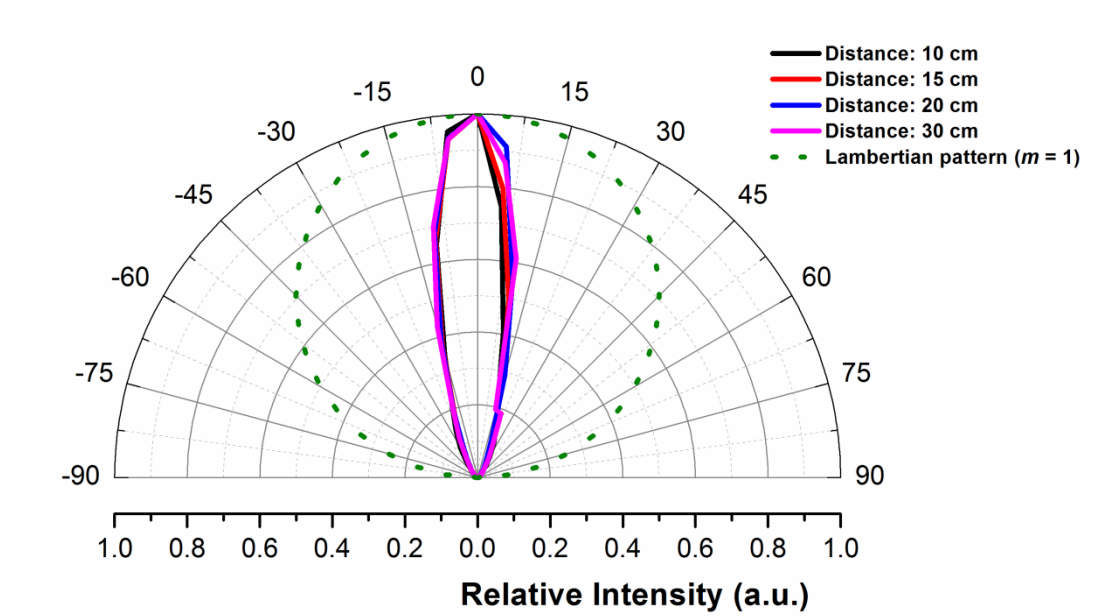

Fig. 7.14. *Angular distribution in polar plot: the normalised irradiances as a function of angular displacement for the LED light source with a Fresnel lens with a 4 cm focal length and diffuser.*

Table 7.1 *Summaries of the Lambertian mode number (m)*

Fresnel Lens	Space distance between LED array and Detector (cm)	Lambertian mode number (*m*)
Focal length = 2.54 cm	10	60.2 ± 0.6
	15	35.6 ± 0.6
	20	41.2 ± 0.6
	30	30.3 ± 0.6
Focal length = 4 cm	10	40.2 ± 0.6
	15	35.2 ± 0.6
	20	35.0 ± 0.6
	30	32.2 ± 0.6

7.2.5 Experimental methods for linear distribution analysis

An illustration of the experimental arrangement used to assess the irradiance distribution as a function of linear displacement is pictured in Fig. 7.15. For light measurement without a Fresnel lens and diffuser (Method A), the detector head was shifted away from the centre every 10 cm until 200 cm, for instance at a distance of

30 cm below the LED array. Space distances between the detector head and the LED array used in the study were 30, 40, 50, 60, 70, 80, 90, 100, 120, 120, 140 and 150 cm in the centre. A similar method was used for the linear distribution analysis for light measurements with the diffuser and the Fresnel lenses with focal lengths of 2.54 cm and 4 cm (Method B).

An additional factor for Lambert's cosine law study in this study was the space distance between the LED array and the lens system (Fresnel lens and diffuser). Three space distances were used in the study, and these were 2.5, 4, and 10 cm. As described in Section 7.2.2, the Fresnel lens and diffuser were arranged with rough-to-rough configuration. For example, light measurement for linear distribution using the combination of the diffuser and the Fresnel lens with a focal length of 2.54 cm, used a value of 2.5 cm for the space distance between LED array and lens system (u) and 30 cm for the space distance between the LED array and detector head (z).

Irradiance data was obtained from light measurements taken with the detector starting from the centre, at distance of 30 cm below the LED array, and then shifted away every 5 cm until 200 cm, and then repeat with different space distances between the LED array and lens system (u). The light source was driven using a power supply with fixed voltage and current (11.3 ± 0.1 V and 0.26 ± 0.01 A).

7.2.5.1 Results for linear distribution without lens system (Method A)

Fig. 7.16 shows the results of the irradiance distribution as a function of linear displacement. As with the pattern for angular distribution, the graph had has bell-shaped curve with peak irradiance at a distance of 30 cm below the LED array.

(a) (b)

Fig. 7.15. *Experimental arrangement for analysis of linear distribution: a) experimental setup of the LED light source without/with a lens system (Fresnel lens and diffuser) b) dimension of light engine holder.*

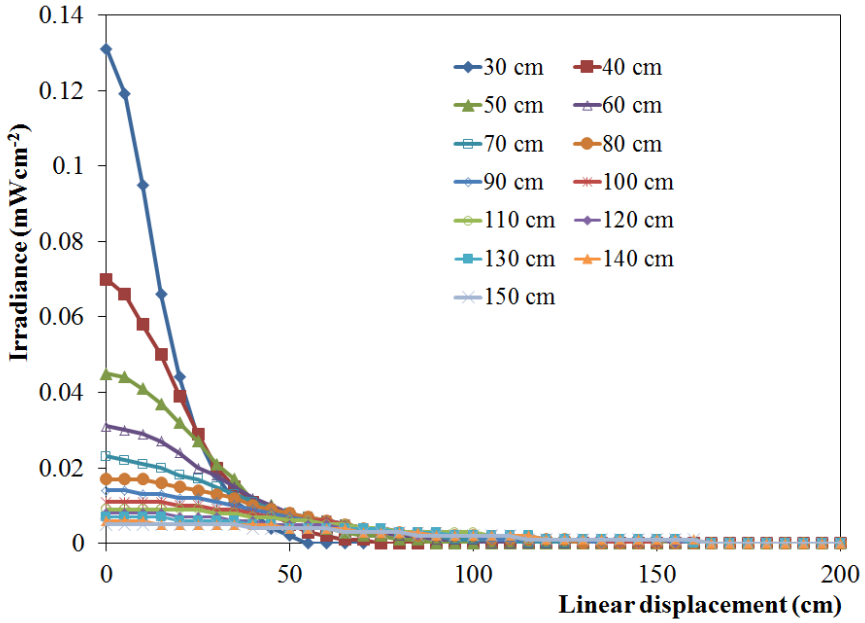

Fig. 7.16. *Irradiance distribution as a function of linear displacement of the LED light source without the lens system.*

The normalised irradiances from the experimental data as a function of linear displacement were analysed using QtiPlot 0.9.8.5 svn 2126 to determine the best fit curve of the Lambetian mode number (*m*). Analytical studies of the Lambertian mode number (*m*) in the study used Eq. (2.15).

Table 7.2 allows comparison of the Lambertian mode number (*m*) for all experimental data. The results show that the space distance between the LED array

and the detector head at E_0 (when the detector head was perpendicular with the light source), *z*, did not significantly affect the Lambertian mode number (*m*).

7.2.5.2 Results for linear distribution with lens system (Method B)

Fig. 7.17, Fig. 7.18 and Fig. 7.19 show the irradiance distribution as a function of linear displacement with the Fresnel lens with 2.54 cm focal length and diffuser. For light measurement at the central position, E_0 (with the detector head perpendicular to the light source), it can be observed that when the space distance between the LED array and the lens system (*u*) is equal to the focal length (*u* = 2.54 cm), the value of irradiance ($mWcm^{-2}$) is bigger than found with the other space distances (*u* = 4 and 10 cm). As described in Section 7.2.5.1, the results shows that the graph has a bell-shaped curve.

Table 7.2 *The Lambertian mode number (m) for linear distribution of the LED light source without the lens system*

Space distance between LED array and detector at E_0 (cm) (*z*)	Lambertian mode number (*m*)
30	2.93 ± 0.06
40	2.45 ± 0.07
50	2.11 ± 0.09
60	2.16 ± 0.06
70	2.19 ± 0.08
80	2.16 ± 0.09
90	2.10 ± 0.09
100	2.20 ± 0.11
110	2.09 ± 0.14
120	2.41 ± 0.17
130	2.27 ± 0.18
140	2.33 ± 0.19
150	2.15 ± 0.20

As described in Section 7.2.5.1, the Lambertian mode number (*m*) can be analysed by a curve fitting method using Eq. (2.15). Summary of the Lambertian mode number (*m*) for the light source with the Fresnel lens with a 2.54 cm focal length and

diffuser are presented in Table 7.3. It can be seen that when u = 2.5 and 4 cm, the Lambertian mode numbers (m) are similar regardless of how z is applied. As stated in Table 7.3, the Lambertian mode number (m) for u = 2.5 and 4 cm is in the range 20 – 30.

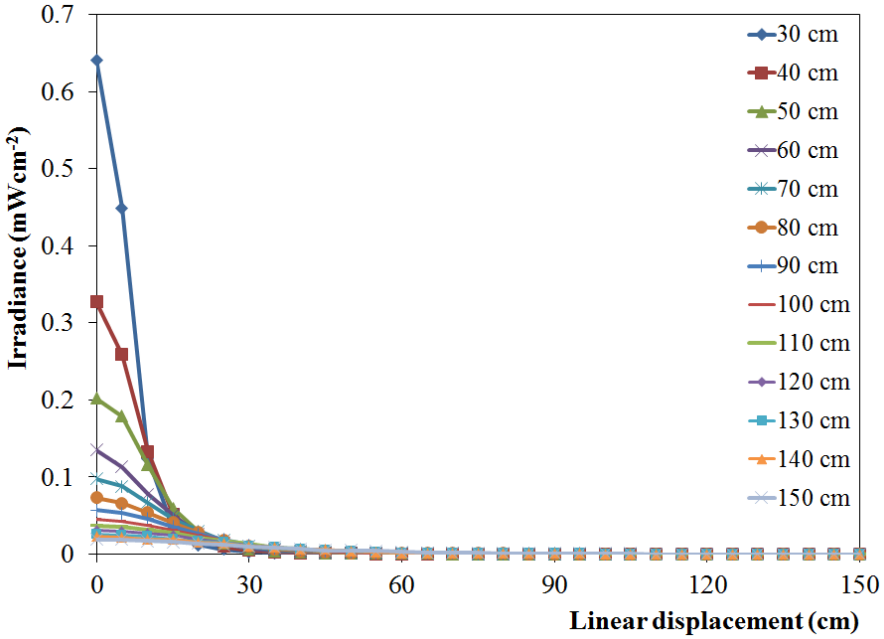

Fig. 7.17. *Irradiance distribution as a function of linear displacement for the LED light source with a Fresnel lens with a 2.54 cm focal length and diffuser at a distance of 2.5 cm between the LED array and the lens system.*

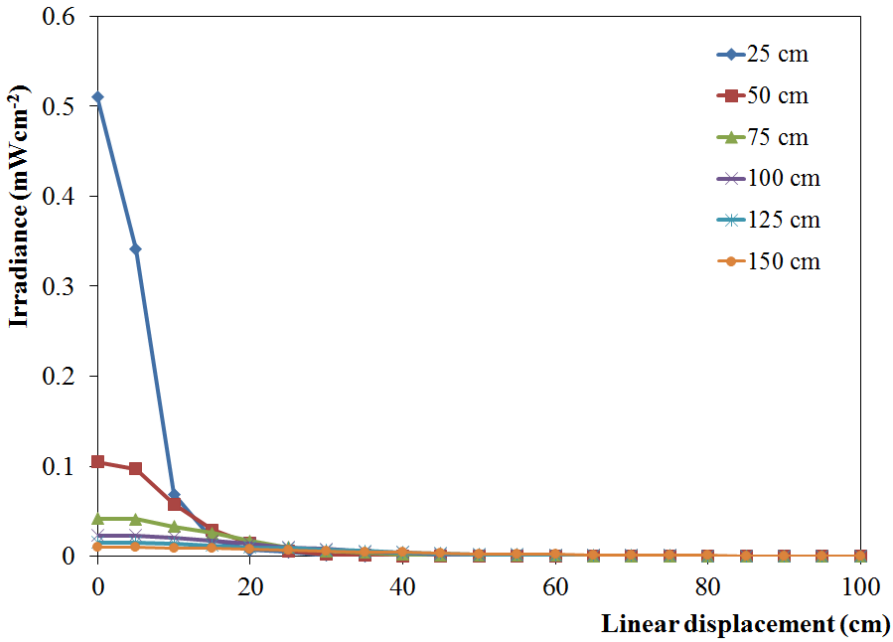

Fig. 7.18. *Irradiance distribution as a function of linear displacement for the LED light source with a Fresnel lens with a focal length of 2.54 cm and diffuser at a distance of 4 cm between the LED array and the lens system.*

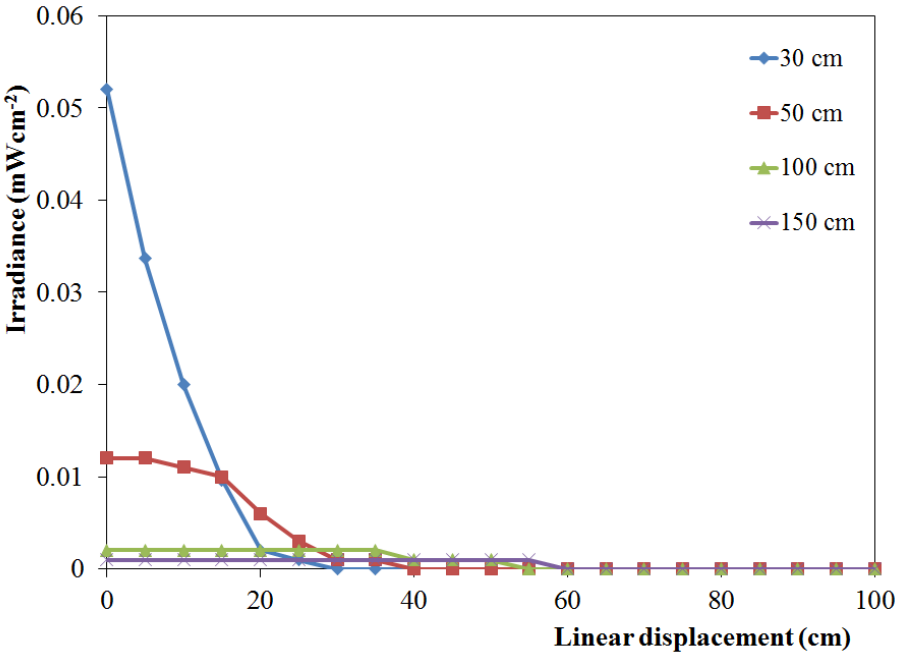

Fig. 7.19. *Irradiance distribution as a function of linear displacement for the LED light source with a Fresnel lens with a focal length of 2.54 cm and diffuser at a distance of 10 cm between the LED array and the lens system.*

Table 7.3 *The Lambertian mode number (m) for linear distribution of the LED light source with lens system (Fresnel lens with a focal length of 2.54 cm and diffuser)*

***z* (cm)**	**Lambertian mode number (*m*)**		
	***u* = 2.5 cm**	***u* = 4 cm**	***u* = 10 cm**
25		20.5 ± 1.2	
30	25.7 ± 0.8		16.0 ± 2.2
40	25.7 ± 0.6		
50	24.1 ± 0.6	25.5 ± 1.1	7.4 ± 1.3
60	30.4 ± 1.4		
70	28.0 ± 1.1		
75		22.8 ± 0.6	
80	28.1 ± 1.0		
90	27.0 ± 0.8		
100	26.7 ± 0.9	22.4 ± 0.7	3.7 ± 1.6
110	25.9 ± 1.0		
120	27.2 ± 1.0		
125		23.2 ± 0.7	
130	27.2 ± 1.0		
140	27.5 ± 0.9		
150	25.0 ± 1.0	23.0 ± 0.8	4.4 ± 2.9

z = space distance between LED array and head of detector at E_0
u = space distance between LED array and lens system

Fig. 7.20, Fig. 7.21, and Fig. 7.22 show the irradiance distributions as a function of linear displacement with a Fresnel lens with a focal length of 4 cm and diffuser. As for the results of linear distribution for the light source with the Fresnel lens with a focal length of 2.54 cm, when the space distance between the LED array and the lens (u) system equals the focal length (u = 4 cm), the value of irradiance ($mWcm^{-2}$) is bigger than found with the other space distances (u = 2.5 and 10 cm).

The Lambertian mode numbers (m) for this study are summarised in Table 7.4. The results shows that the Lambertian mode number (m) for u = 2.5 cm has a value quite similar, in the range 19 – 23, whilst for u = 4 and 10 cm, the Lambertian mode number has varying values. The smallest Lambertian mode number (m) was 10.8, when the light measurement data was taken at u = 10 cm and z = 100 cm.

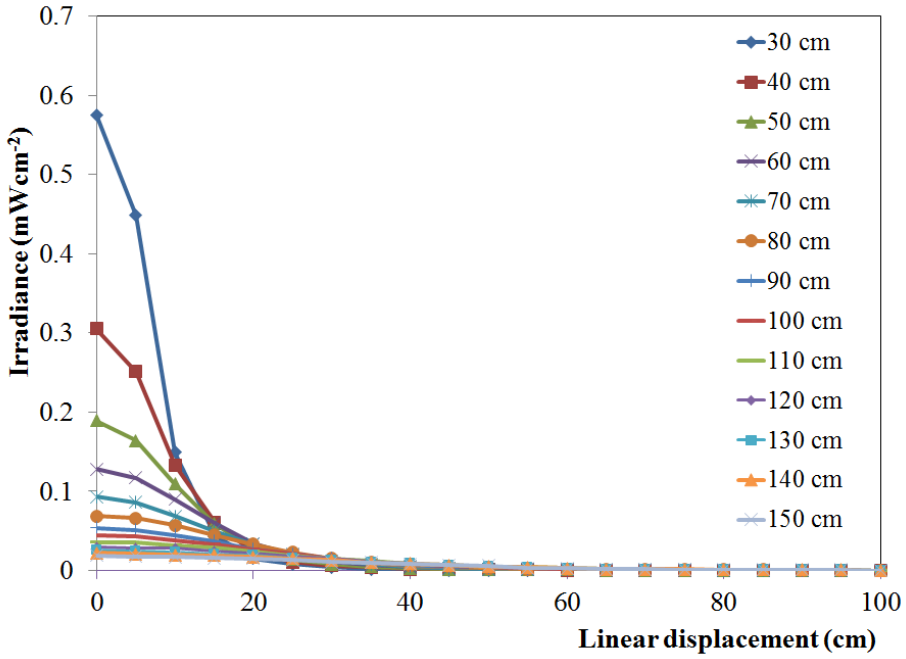

Fig. 7.20. *Irradiance distribution as a function of linear displacement for the LED light source with a Fresnel lens with a 4 cm focal length and diffuser at a distance of 2.5 cm between the LED array and the lens system.*

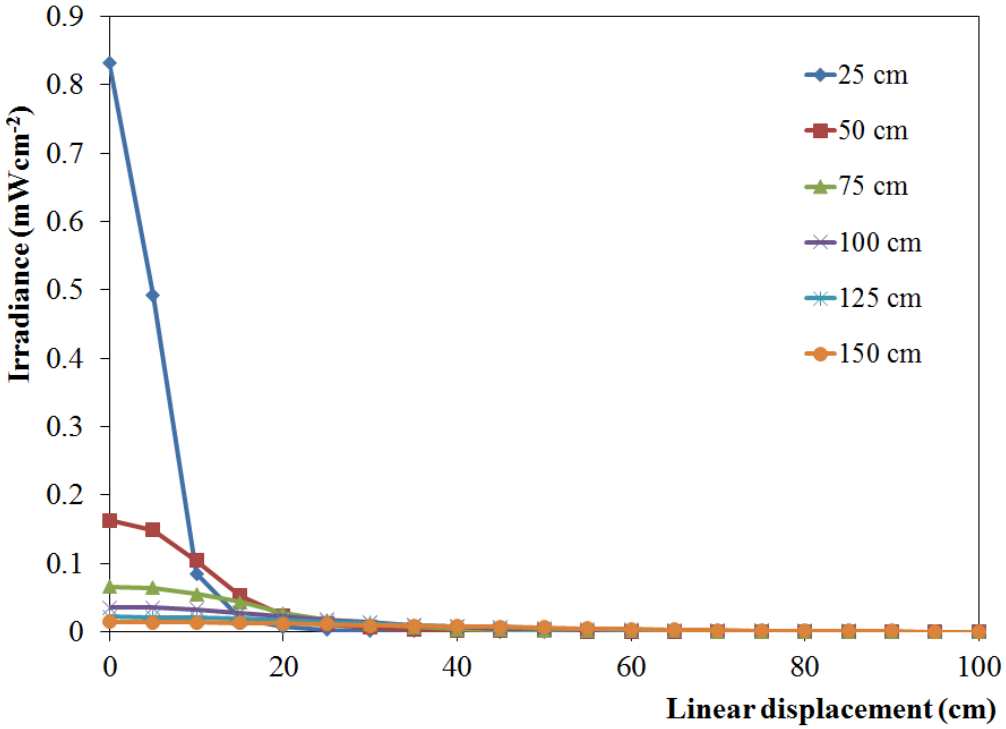

Fig. 7.21. *Irradiance distribution as a function of linear displacement for the LED light source with a Fresnel lens with a 4 cm focal length and diffuser at a distance of 4 cm between the LED array and the lens system.*

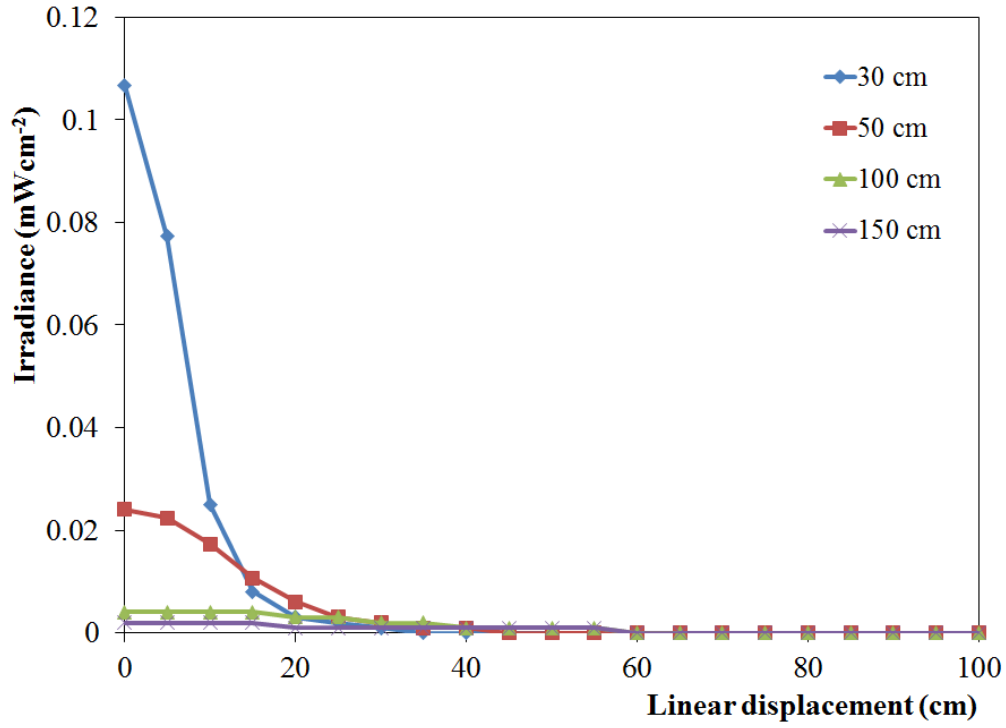

Fig. 7.22. *Irradiance distribution as a function of linear displacement for the LED light source with a Fresnel lens with a 4 cm focal length and diffuser at a distance of 10 cm between the LED array and the lens system.*

Table 7.4 *The Lambertian mode number (m) for linear distribution of the LED light source with the lens system (Fresnel lens with a 4 cm focal length and diffuser)*

***z* (cm)**	**Lambertian mode number (*m*)**		
	***u* = 2.5 cm**	***u* = 4 cm**	***u* = 10 cm**
25		25.2 ± 0.7	
30	20.1 ± 1.1		22.6 ± 1.0
40	22.5 ± 0.6		
50	23.5 ± 0.6	21.6 ± 0.6	15.0 ± 0.5
60	21.3 ± 0.5		
70	22.8 ± 0.7		
75		20.8 ± 0.6	
80	20.2 ± 0.5		
90	22.0 ± 0.8		
100	20.7 ± 0.5	17.9 ± 0.4	10.8 ± 1.1
110	19.6 ± 0.6		
120	19.3 ± 0.4		
125		17.2 ± 0.4	
130	21.2 ± 0.7		
140	20.7 ± 0.5		
150	22.1 ± 0.7	16.5 ± 0.6	19.3 ± 4.0

z = space distance between LED array and head of detector at E_0
u = space distance between LED array and lens system

7.3 Discussion and Conclusions

As described in Section 2.9, in order to examine the accuracy of reconstruction, the difference between the pattern of the mathematical model and the experimental data must be compared by calculation of both the normalized cross correlation (NCC) (Eq. (2.19) and the root mean square (RMS) error (Eq. (2.20)).

Fig. 7.23, Fig. 7.24, Fig. 7.25 and Fig. 7.26 show the results of the normalized cross correlation (NCC) for angular distribution for a system without the Fresnel lens and diffuser. It can be observed from graphs that the NCC between the experimental data and mathematical model is greater than 99%. From the literature it is known that NCC greater than 99% gives enough accuracy for most applications [16]. This confirms that the experimental data and mathematical model give similar results.

Results of the RMS error between the experimental data and the mathematical model (Eq. (7.1)) show that all data is less than the standard limit of 5%, meaning that the experimental data give accurate data compared to the mathematical model (Eq. (7.1)).

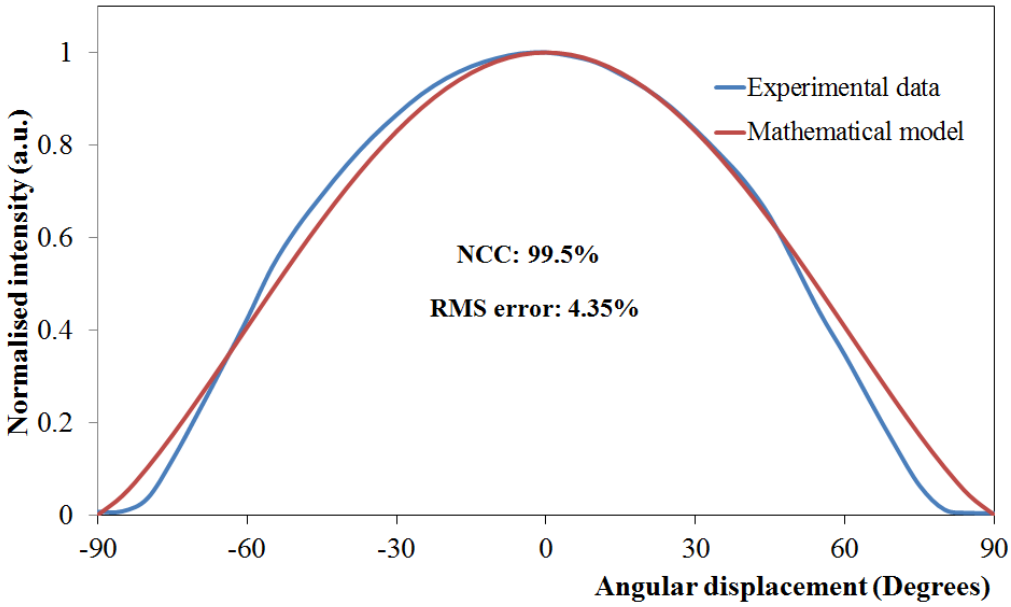

Fig. 7.23. *Comparative data for irradiance distribution as a function of angular displacement for the LED light source without the lens system at a distance of 10 cm (E_0).*

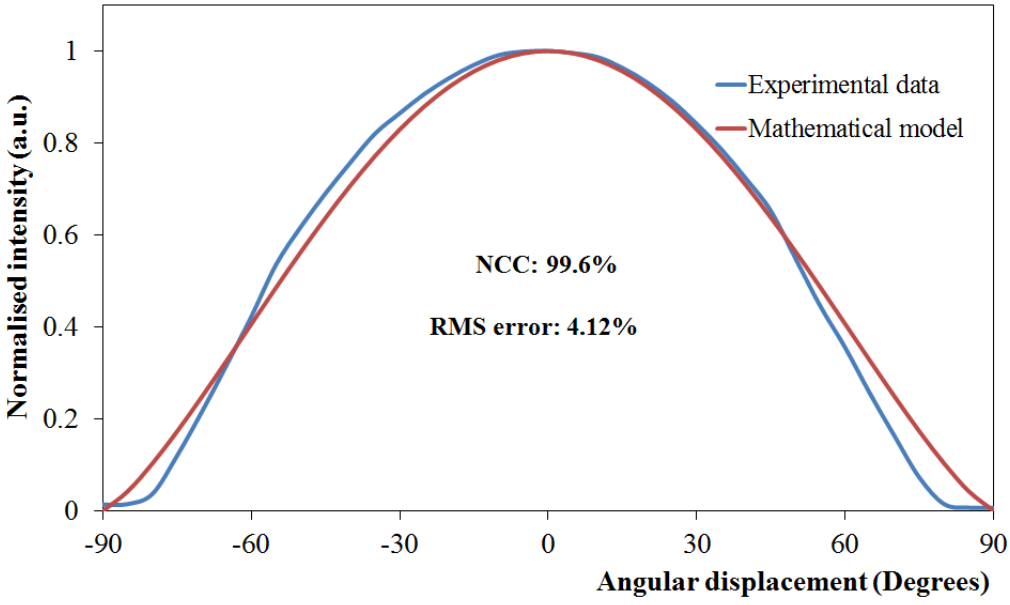

Fig. 7.24. *Comparative data for irradiance distribution as a function of angular displacement for the light source without the lens system at a distance of 15 cm (E_0).*

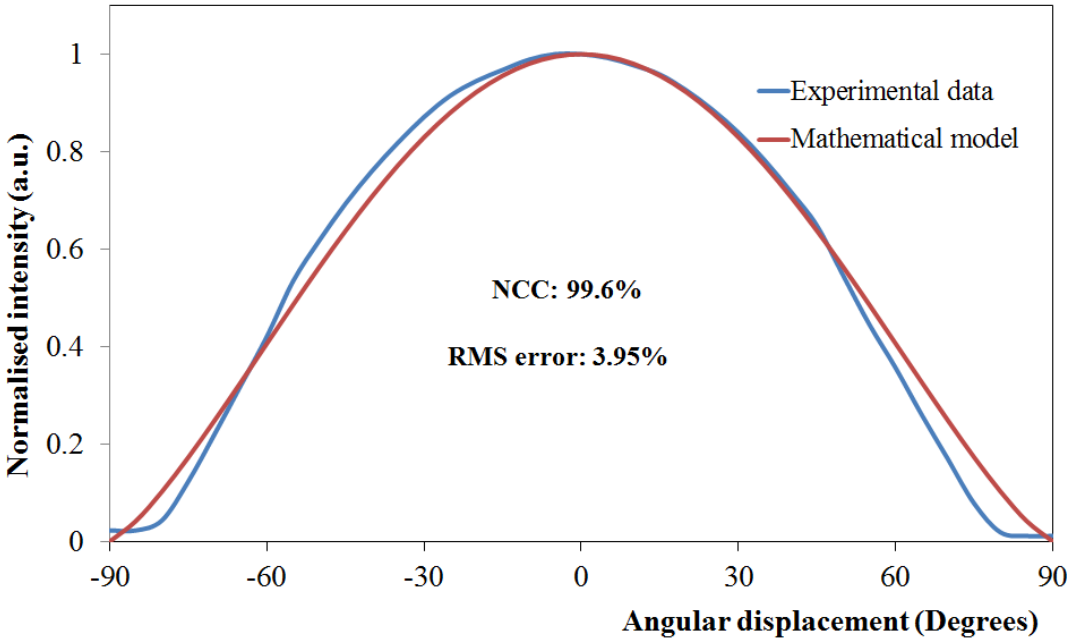

Fig. 7.25. *Comparative data for irradiance distribution as a function of angular displacement for the LED light source without the lens system at a distance of 20 cm (E_0).*

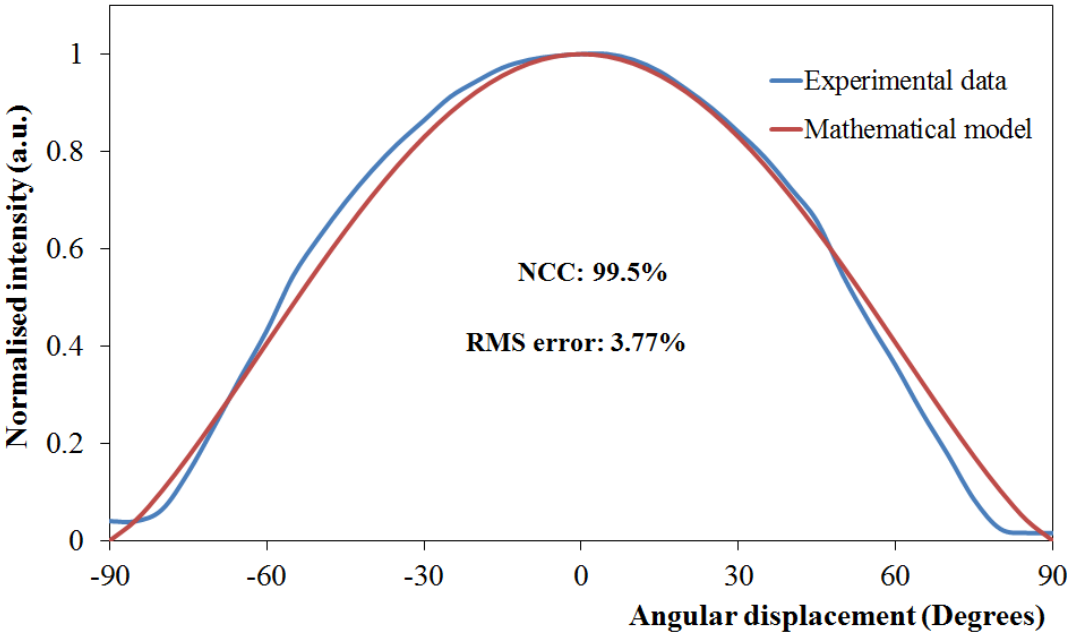

Fig. 7.26. *Comparative data for irradiance distribution as a function of angular displacement for the LED light source without the lens system at a distance of 30 cm (E_0).*

Table 7.5 allows comparison of the data of the angular distribution for the LED light source with the lens system. When the light source with a Fresnel lens with a 2.54 cm focal length and diffuser was used, it was only when z = 30 cm that the NCC was greater than 99% and RMS error less than 5%. Meanwhile, when the LED light source with a Fresnel lens with 4 cm focal length and diffuser was used, it was only z = 10 cm which had NCC of less than 99% and RMS error greater than 5%. The results indicate that the minimum distance between the LED array and the head of the detector at E_0 for the light source with lens systems should be 20 cm for a Fresnel lens with a focal length of 2.54 cm, and 10 cm for a Fresnel lens with a 4 cm focal length.

Table 7.5 *Summary data of the angular distribution for the LED light source with the lens system*

Fresnel Lens	z (cm)	Lambertian mode number (m)	NCC (%)	RMS error (%)
Focal length = 2.54 cm	10	60.2 ± 0.6	96.8	6.49
	15	35.6 ± 0.6	98.8	4.60
	20	41.2 ± 0.6	98.9	4.91
	30	30.3 ± 0.6	99.3	4.46
Focal length = 4 cm	10	40.2 ± 0.6	98.0	5.78
	15	35.2 ± 0.6	99.2	3.77
	20	35.0 ± 0.6	99.6	3.38
	30	32.2 ± 0.6	99.1	4.19

z = space distance between LED array and head of detector at E_0
NCC = normalized cross correlation
RMS = root mean square

As with the angular distribution, to ensure the accuracy of the difference between the experimental data and the mathematical model for the linear distribution, the data from the experimental measurement and the mathematical model must be compared by the NCC and RMS error. The result of calculations should give a value of more than 99% for the NCC and less than 5% for the RMS error.

The mathematical model used in the study was Eq. (2.16), with modification parameters $r = x$ and $h = z$ ($E(x) = E_o\left(1+\frac{x^2}{z^2}\right)^{-\frac{(3+m)}{2}}$, where $E(x)$ is the irradiance over every point (x) on the horizontal surface at distance of z from the LED, E_0 is the irradiance (Wm^{-2}) at the viewing angle $\theta = 0°$ and m is the Lambertian mode number, $m > 0$).

The NCC and RMS error for a linear distribution of the LED light source with the diffuser and both the Fresnel lens with a 2.54 cm focal length and a 4 cm focal length are presented in Table 7.6 and Table 7.7, respectively.

As stated in Table 7.6 and Table 7.7, when the space distance between the LED array and the lens system was 10 cm, there was a significant difference between the experimental data and the mathematical model, and the data shows that the system is not suitable for general lighting application.

Table 7.6 *Summary data of the linear distribution for the LED light source with a Fresnel lens with a 2.54 cm focal length*

z (cm)	***u* = 2.5 cm**		***u* = 4 cm**		***u* = 10 cm**	
	NCC (%)	**RMS error (%)**	**NCC (%)**	**RMS error (%)**	**NCC (%)**	**RMS error (%)**
25			99.87	1.59		
30	99.93	1.19			99.35	3.93
40	99.97	1.07				
50	99.96	1.13	99.88	1.81	98.80	7.89
60	98.83	2.46				
70	99.88	2.25				
75			99.93	1.44		
80	99.92	2.10				
90	99.91	2.17				
100	99.93	2.06	99.83	2.27	85.17	20.26
110	99.85	2.66				
120	99.85	2.81				
125			99.77	2.55		
130	99.86	2.81				
140	99.46	2.54				
150	99.71	3.58	99.65	2.97	45.88	24.28

z = space distance between LED array and head of detector at E_0
u = space distance between LED array and lens system
NCC = normalized cross correlation
RMS = root mean square

Table 7.7 *Summary data of the linear distribution for the LED light source with a Fresnel lens with a 4 cm focal length*

z (cm)	*u* = 2.5 cm		*u* = 4 cm		*u* = 10 cm	
	NCC (%)	RMS error (%)	NCC (%)	RMS error (%)	NCC (%)	RMS error (%)
25			99.96	0.82		
30	99.86	1.81			99.93	1.28
40	99.95	1.26				
50	99.96	1.28	99.94	1.37	99.93	1.44
60	99.96	1.28				
70	99.95	1.74				
75			99.88	1.89		
80	99.96	1.50				
90	99.89	2.20				
100	99.93	1.65	99.91	1.68	97.94	7.59
110	99.91	2.15				
120	99.95	1.48				
125			99.84	2.06		
130	99.89	2.54				
140	99.54	1.98				
150	99.79	2.67	99.55	3.55	83.49	16.41

z = space distance between LED array and head of detector at E_0
u = space distance between LED array and lens system
NCC = normalized cross correlation
RMS = root mean square

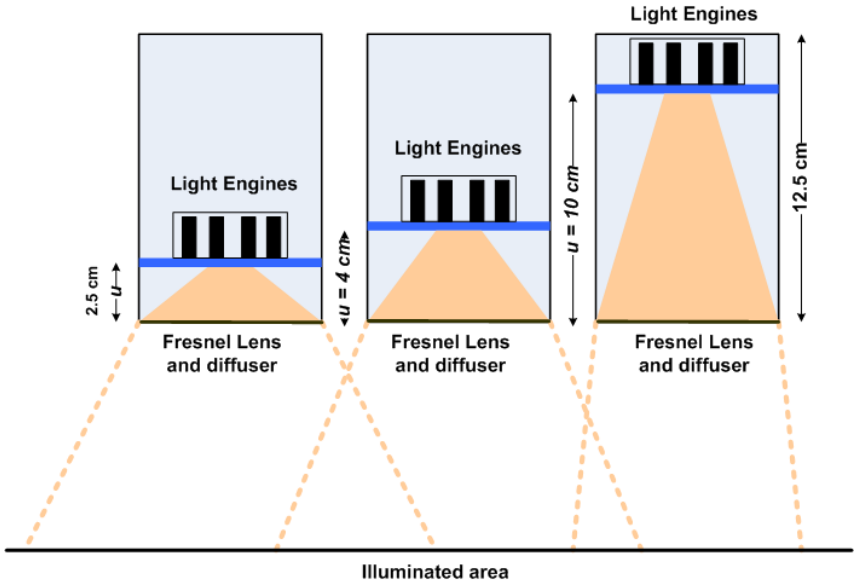

Fig. 7.27. *Illustration of the irradiance distribution as a function of linear displacement for the LED light source with a lens system.*

The light source with the lens system is illustrated in Fig. 7.27, and it can be observed that when the light source used in the experimental work has u = 10 cm, only a small part of the light can be spread in a wide area because some light is blocked by the PVC tube.

Results in Fig. 7.28 show the evidence that the system does not give enough irradiance distribution on the illuminated area, and the graph appears as a 'saw-curve' rather than a 'bell-shaped' curve.

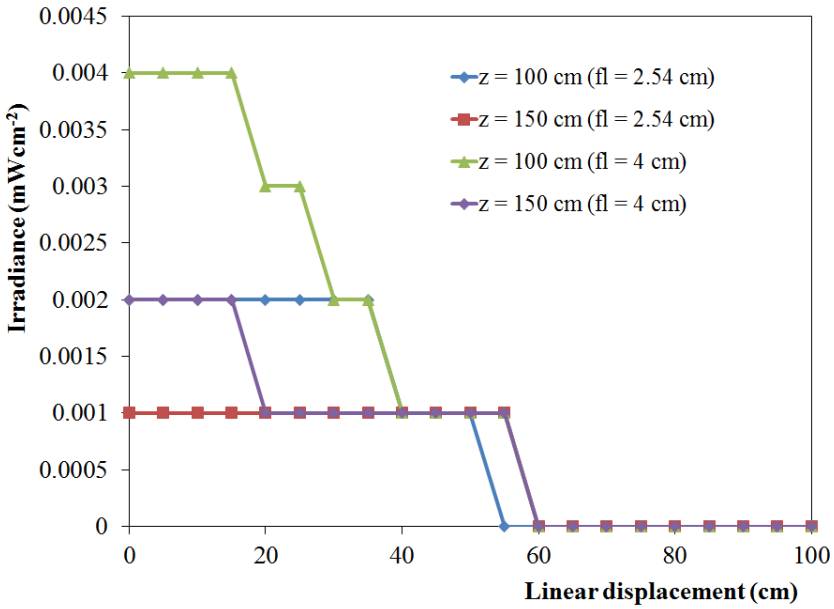

Fig. 7.28. *Irradiance distribution as a function of linear displacement for the LED light source with a lens system where experimental data were taken at u = 10 cm and a space distance between the LED array and the detector head at E_0 at 100 and 150 cm.*

Overall, this study has demonstrated the accuracy of the experimental method for a study of Lambert's cosine law. The results show that the similarity and the accuracy between the experimental data and the mathematical model gives values of more than 99% for the normalised cross correlation (NCC) and less than 5% for the root mean square (RMS) error. The importance of this is that these experimental data and the mathematical model can now be reliably used for accurate design of the optical properties of the new prototype HINS-light EDS, for which uniform distribution and wider spread of light are key design requirements, and will be further discussed in Chapter 8.

CHAPTER 8

OPTIMISATION OF THE HIGH-INTENSITY NARROW-SPECTRUM-LIGHT ENVIRONMENTAL DECONTAMINATION SYSTEM (HINS-LIGHT EDS)

8.1 General

As described in Chapter 7, the high intensity narrow spectrum (HINS)-light environmental decontamination systems (EDS) technology has many potential applications such as disinfection of air and surfaces in clinical environments, and disinfection of food contact surfaces. However, the initial prototype system that had been developed prior to this project had limitations such as a power supply which was not fully integrated, limited thermal management options and only generated dominant violet/blue light.

The aim of the study described in this Chapter is the optimisation, testing and modelling of an improved fully-integrated large-scale HINS-light EDS (ceiling mounted light source). The main aspects of this study have involved:

1. Design and development of an improved, fully-integrated and controllable HINS-light EDS unit
2. Development of a mathematical model to enable simulations of the light intensity distribution
3. Studies of thermal management options.

8.2 A new prototype HINS-light EDS

To develop a new HINS-light EDS, there were 4 main factors that had to be investigated before the system could be developed:

1. Configuration of a Fresnel lens and diffuser
2. The Lambertian mode number (m)
3. Space distance between the LED and lens system (Fresnel lens and diffuser), hereinafter referred to u
4. The optimum LED-to-LED array spacing, hereinafter referred to d.

8.3 Investigation into the optimal configuration of a Fresnel lens and diffuser

The Fresnel lens used in this study was LFQ100200 obtained from the Knight Optical (UK) Ltd. This lens was made from Acrylic material with 100 mm focal length, 2 mm thickness, 200 mm (diameter) effective aperture and 0.5 mm facet width [186]. The Fresnel lens LFQ100200 is pictured and illustrated in Fig. 8.1 and Fig. 8.2, respectively. The overall size of this lens is 210 × 210 mm and transmits parallel light on grooved side.

Fig. 8.1. *The Fresnel lens LFQ100200 sourced from Knight Optical, Ltd., UK.*

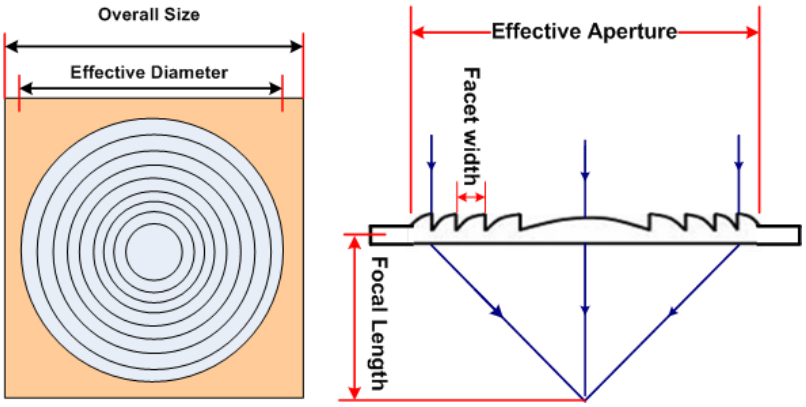

Fig. 8.2. *Illustration for the Fresnel lens LFQ100200 sourced from Knight Optical, Ltd., UK (Adapted from [186]).*

The diffuser used in this study was a type L20P1-12 Light Shaping Diffusers (LSD). This is a holographic diffuser with light shaping diffuser angle 20° (FWHM) and made up from Polyester material with 3 mm thickness sourced from the LUMINIT LLC, USA [187]. As described in Section 7.2.2, the diffuser LSD has 85 – 92% transmission performance in a wide wavelength range of 400 – 1600 nm [187]. This diffuser has two sides one of which is rough and the other smooth. When light falls perpendicular on the surface of diffuser both sides produce different patterns of light distribution. The light source used in the experimental work was at 405 nm LED array ENFIS Uno Air Cooled Light Engine obtained from the ENFIS Ltd, UK (see Section 7.2.1). The pattern of light distribution through the surface of the diffuser is illustrated in Fig. 8.3, also shown in Fig. 8.3 is the light distribution pattern obtained from the light source without diffuser.

Analysis of the RGB histogram from Fig. 8.4a and Fig. 8.4c used in this study found that a similar result (RGB level) were achieved after light exposure through the diffuser when the smooth side faced the LED array as was achieved without a diffuser (Fig. 8.3a and Fig. 8.3c). Meanwhile, when light exposure occurred through the diffuser with the rough side facing the LED array (Fig. 8.3b) this yielded a different result, as shown in Fig. 8.4b. It can be observed from Fig. 8.3b, that when light passed through using this configuration it resulted in a more smooth and uniform light distribution. For this reason it was decided to use the diffuser with the rough side facing the LED array.

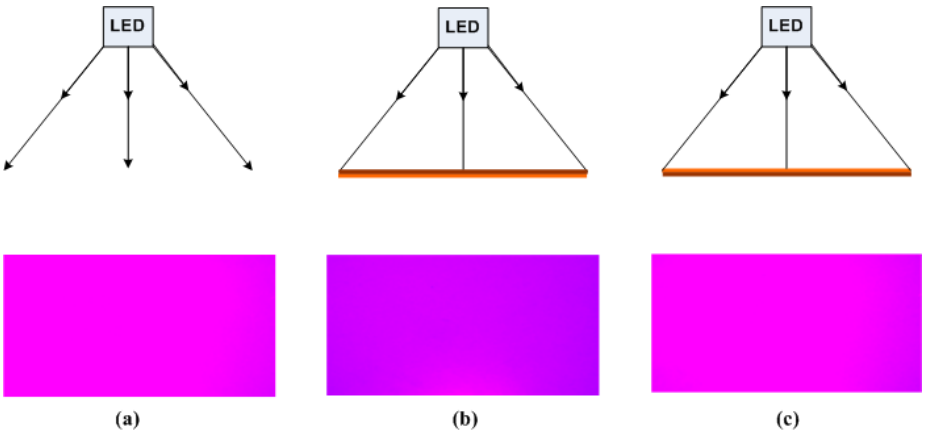

Fig. 8.3. *The light source falling perpendicular on the surface: a) without diffuser, b) with diffuser when the rough side faced the LED array and c) with diffuser when the smooth side faced the LED array.*

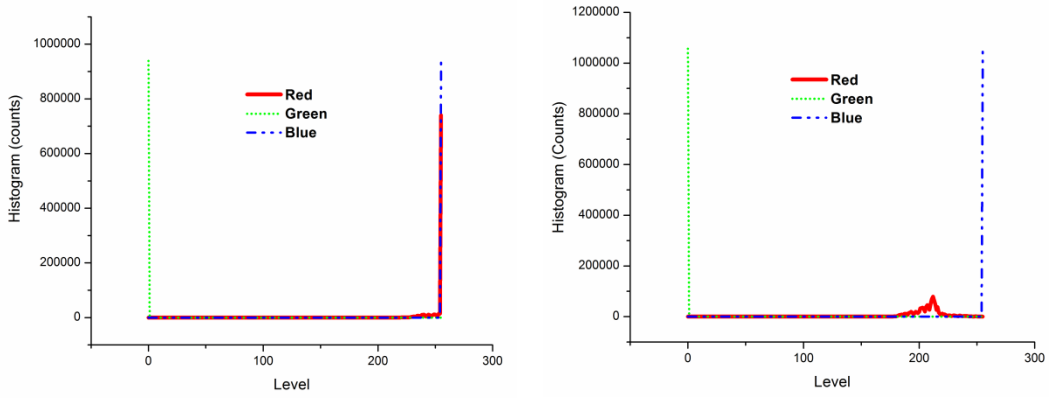

(a) (b)

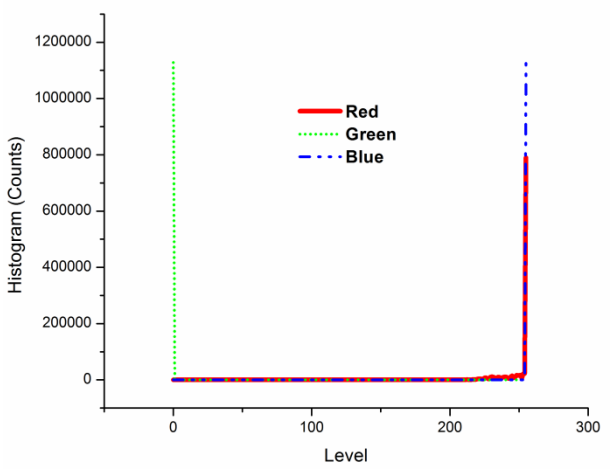

(c)

Fig. 8.4. *Visual assessment of the light source falling perpendicular on the surface: a) without diffuser, b) with diffuser when the rough side faced the LED array and c) with diffuser when the smooth side faced the LED array.*

8.3.1 Experimental method

The configuration of a Fresnel lens and diffuser (lens system) used in the study involved four variations, as shown in Fig. 8.5. To determine the best configuration to be used in the practical design, all four types of configuration was evaluated using the Lambert's cosine law. The experimental setup used in the study is illustrated in Fig. 8.6. As described in Section 8.2.1, the diffuser used in the study was orientated with its rough side faced to the LED array. The space distances between the LED array and the lens system (u) used in the study were 5 and 7.5 cm, while the space distance between the LED array and the illuminated area (z) was 100 cm. For all experiments the voltage was set to 14.1 ± 0.1 V with a current of 0.11 ± 0.01 A. The irradiance distribution of light over an illuminated area parallel to the light source was measured using a radiant power meter (model 70260, L.O.T.-Oriel Ltd., UK) and all point data were taken with three replicates for each independent experiment to ensure accuracy.

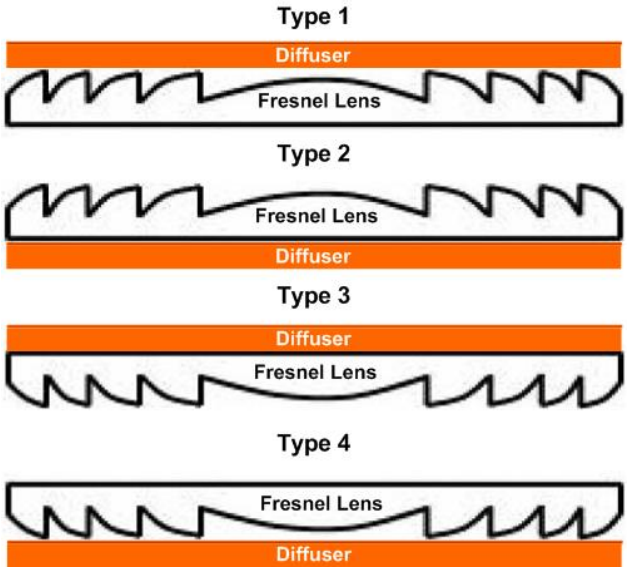

Fig. 8.5. *Four type of configuration for the Fresnel lens and diffuser.*

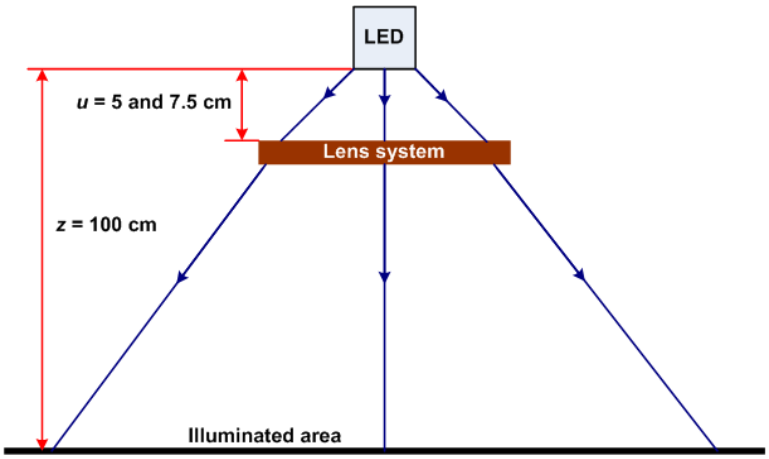

Fig. 8.6. *Experimental setup to determine the best configuration for the Fresnel lens and diffuser.*

8.3.2 Results

Fig. 8.7 and Fig. 8.8 show the results of the irradiance distributions over an illuminated area parallel to the LED array using a distance of 5 and 7.5 cm between the LED array and a lens system (*u*), respectively.

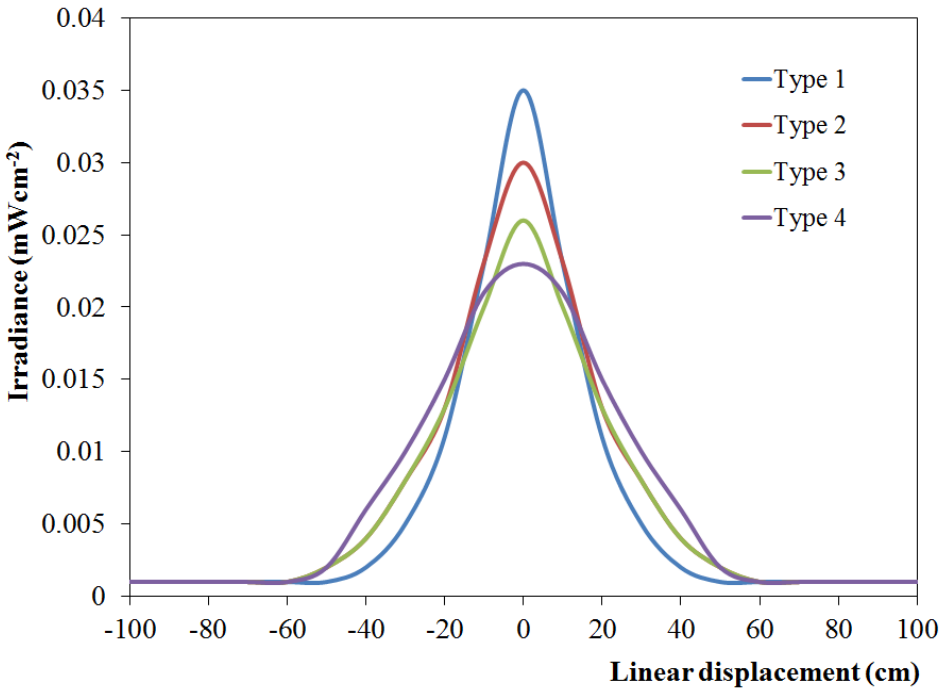

Fig. 8.7. *Irradiance distribution as a function of linear displacement when the space between the LED array and the Fresnel lens and diffuser was 5 cm for the different configurations of the Fresnel lens and diffuser (Types 1,2,3,and 4).*

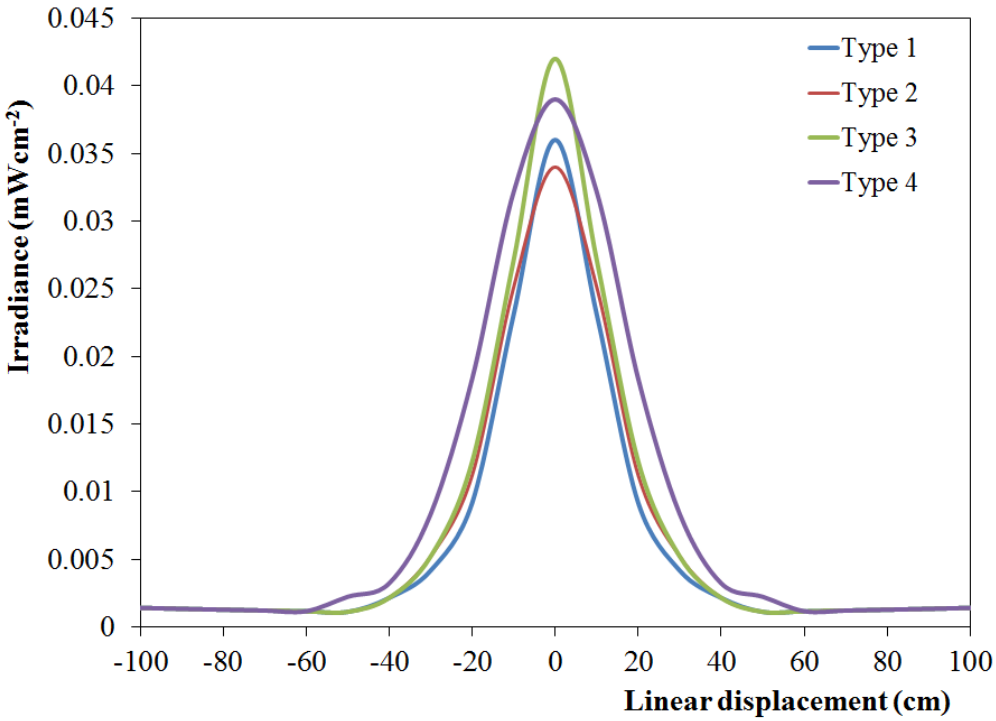

Fig. 8.8. *Irradiance distribution as a function of linear displacement when the space between the LED array and the Fresnel lens and diffuser was 7.5 cm.*

The best configuration of a lens system can be established by calculating the maximum volume restricted by a bell shape distribution curve, *V*. This volume will give the value of total light power delivered by the optical system. This method is illustrated in Fig. 8.9. When a function of y = E(x) is rotated at y-axis, the volumes of solids of revolution can be calculated on interval (y_0, y_1) as follows [189]:

$$V = \int_{y_0}^{y_1} dV = \pi \int_{y_0}^{y_1} f(y)^2 dy, \tag{8.1}$$

where,

y_0 and y_1 = the lower and upper limits of the area being rotated,

E(x) = function of Eq. (2.16) in term of y,

dV = the part of total volumes of solids of revolution.

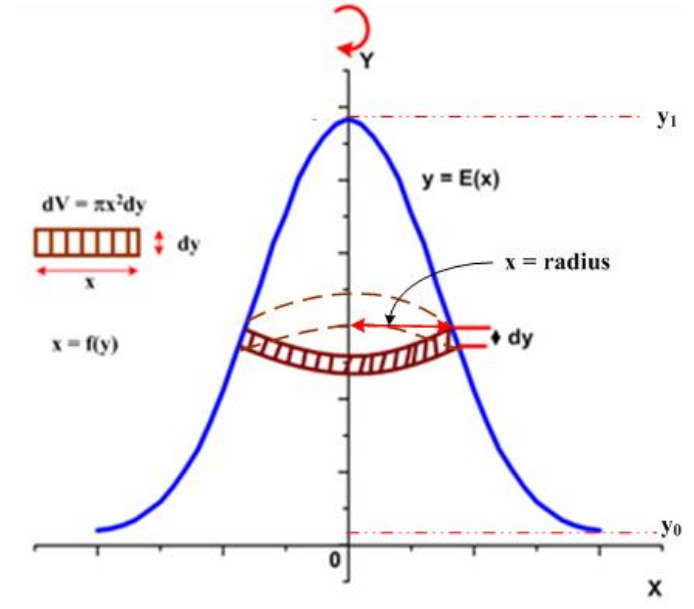

Fig. 8.9. *Volumes of solids of revolution.*

Function of f(y) can be expressed from Eq. (2.16) in term of y ($r = x$ and $h = z$),

$$y = E(x) = E_0\left(1+\frac{x^2}{z^2}\right)^{-\frac{(3+m)}{2}}, \tag{8.2}$$

where m is the Lambertian mode number (m > 0), E_0 is the irradiance at centre measurement with a distance of z cm below the LED array and z is space distance between the LED and the perpendicular to the illuminated area.

Let's assume, $q = -\frac{(3+m)}{2}$, and then Eq. (8.2) can be written into,

$$y = E_0\left(1+\frac{x^2}{z^2}\right)^{q}, \tag{8.3}$$

Eq. (8.3) can be re-expressed in the form,

$$\left(\frac{y}{E_0}\right)^{\frac{1}{q}} = 1+\frac{x^2}{z^2}, \tag{8.4}$$

then,

$$x^2 = z^2\left[\left(\frac{y}{E_0}\right)^{\frac{1}{q}} - 1\right], \tag{8.5}$$

so,

$$x = z\sqrt{\left(\frac{y}{E_0}\right)^{\frac{1}{q}} - 1}, \tag{8.6}$$

and finally,

$$f(y) = x = z\sqrt{\left(\frac{E_0}{y}\right)^{\frac{2}{3+m}} - 1}, \tag{8.7}$$

In combining Eq. (8.1) and Eq. (8.7), volumes of solids of revolution can be calculated by Eq. (8.8).

$$V = \pi z^2 \int_{y_0}^{y_1}\left[\left(\frac{E_0}{y}\right)^{\frac{2}{3+m}} - 1\right]dy, \tag{8.8}$$

where V is the total volumes of solids of revolution, the units in standard international (SI) can be expressed in Watt (W). In order to avoid divergence in Eq. (8.8), value of the lower limit of the area being rotated (y_0) should be more than 0, because at $y_0 = 0$ there is a singularity point and the integral diverges.

As described in Section 2.5, the accuracy of the experimental method used in this study was also investigated. The similarity and accuracy between the experimental data and the mathematical model can be compared by calculation of both the normalised cross correlation (NCC) and the root mean square (RMS) error, respectively. As stated in Table 8.1 and Table 8.2, the best configuration of the Fresnel lens and diffuser used in this study was type 4. This indicates that the light distribution from this configuration is optimal for general applications, especially when used as an environmental decontamination system.

Table 8.1 *Summary data for the four configurations of the Fresnel lens and diffuser when the space between the LED array and the Fresnel lens and diffuser experimental (u) = 5 cm*

Configuration	u = 5 cm			
	m	**NCC (%)**	**RMS error (%)**	**Total Power (W)**
Type 1	57.29	99.58	4.22	0.04
Type 2	32.48	99.56	4.64	0.06
Type 3	27.01	99.66	4.68	0.06
Type 4	16.55	99.79	2.68	0.08

Table 8.2 *Summary data for the four configurations of the Fresnel lens and diffuser when the space between the LED array and the Fresnel lens and diffuser experimental (u) = 7.5 cm*

Configuration	u = 7.5 cm			
	m	**NCC (%)**	**RMS error (%)**	**Total Power (W)**
Type 1	68.54	99.70	4.22	0.03
Type 2	49.66	99.83	3.66	0.04
Type 3	62.50	99.64	4.08	0.04
Type 4	33.38	99.93	2.68	0.07

It can be observed from Table 8.1 and Table 8.2, that type 4 configuration provides not only a larger total power but also more accurate data than type 1, 2 and 3. When data from the type 4 configuration are compared with regard to the experimental and mathematical models this resulted in 2.68% (RMS error) both for u = 5 and 7.5 cm, and 99.79% and 99.93% (NCC) for u = 5 and 7.5 cm, respectively.

8.4 Analytical studies of the Lambertian mode number (*m*)

As described in Section 7.2.5.1, the Lambertian mode number (m) can be analysed by the curve fitting method using Eq. (2.16). The aim of this study was to investigate the effects of the position of the single LED array (Fig. 7.2) relative to the lens system and the illuminated area in order to determine the Lambertian mode number (m) and the irradiance distribution pattern. The normalised cross correlation (NCC) and RMS error were also investigated.

8.4.1 Influence of *u* and *z* with regard to the Lambertian mode number (*m*)

8.4.1.1 Experimental method

Fig. 8.10 illustrates the experimental method used to determine whether the values of *u* and *z* have a significant effect on the Lambertian mode number (*m*). The space distances between the LED array (Fig. 7.2) and the lens system (type 4) (*u*) used in the study were 5 and 7.5 cm, while the space distances between the LED array and the illuminated area (*z*) were 100 and 150 cm. For all experiments the voltage were set to 14.1 ± 0.1 V with a current of 0.11 ± 0.01 A. The irradiance distribution of light over an illuminated area parallel to the light source was measured using a radiant power meter. All point data were taken in the direction of the x- axis and y-axis for the positive values with three replicates taken for each independent experiment to ensure data accuracy.

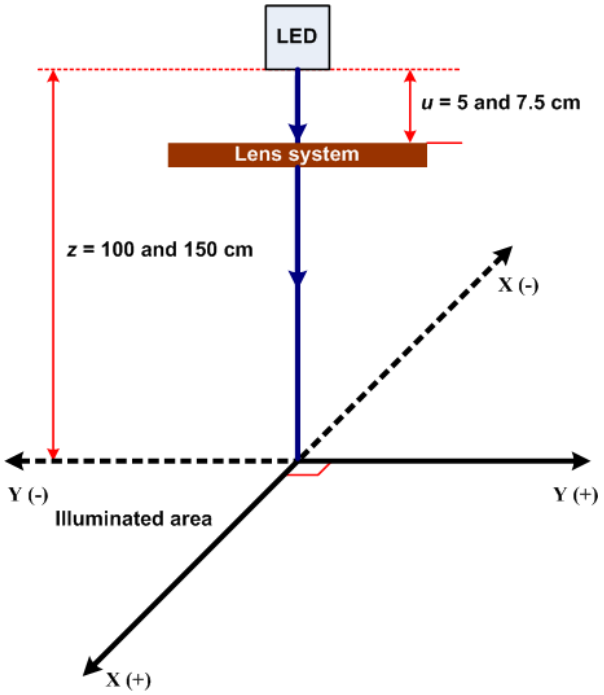

Fig. 8.10. *Experimental method for analysis of the influence of u and z on the Lambertian mode number (m).*

8.4.1.2 Results

Results of irradiance distribution as a function of linear displacement for the system with *u* = 5 and 7.5 cm and with *z* = 100 and 150 cm is shown in Fig. 8.11 and Fig. 8.12, respectively. It can be seen that the irradiance distribution of the light

source along the x-axis and y-axis are similar indicating that the irradiance distribution of the light source is uniform.

Results for the Lambertian mode number (*m*) for this study are displayed in Fig. 8.13, Fig. 8.14, Fig. 8.15 and Fig. 8.16 and values of NCC and RMS are also shown in the graphs. Because the irradiance distribution for the x-axis and y-axis have similar values, analysis of the Lambertian mode number (*m*) can be calculated using the irradiation distribution data from either the x-axis or y-axis.

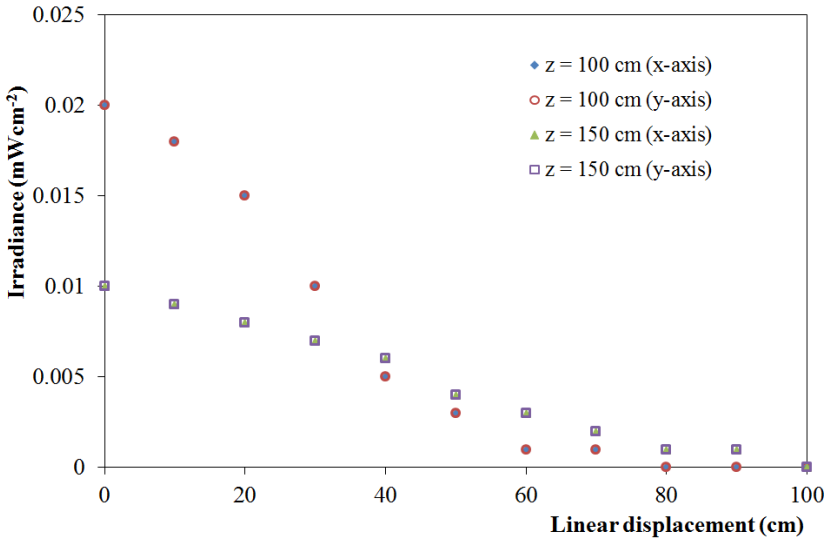

Fig. 8.11. *The irradiance distribution as a function of linear displacement for the light system with u = 5 cm.*

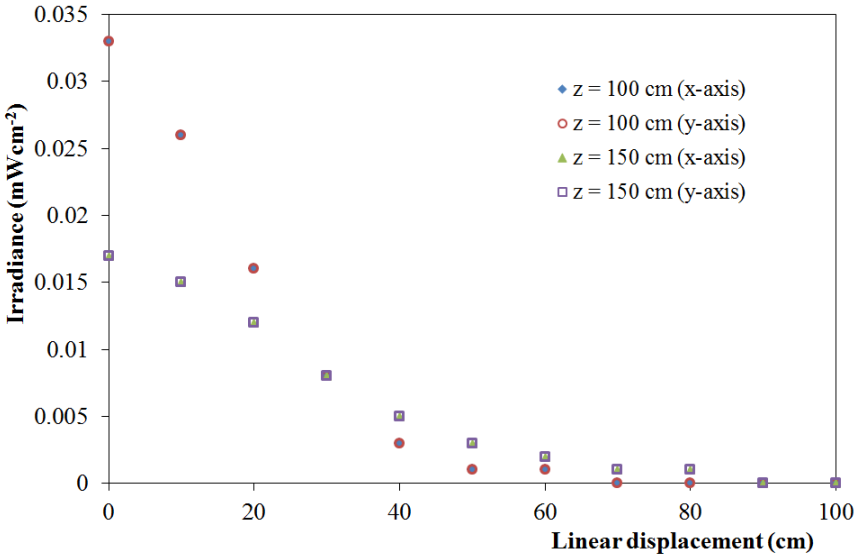

Fig. 8.12. *The irradiance distribution as a function of linear displacement for the light system with u = 7.5 cm.*

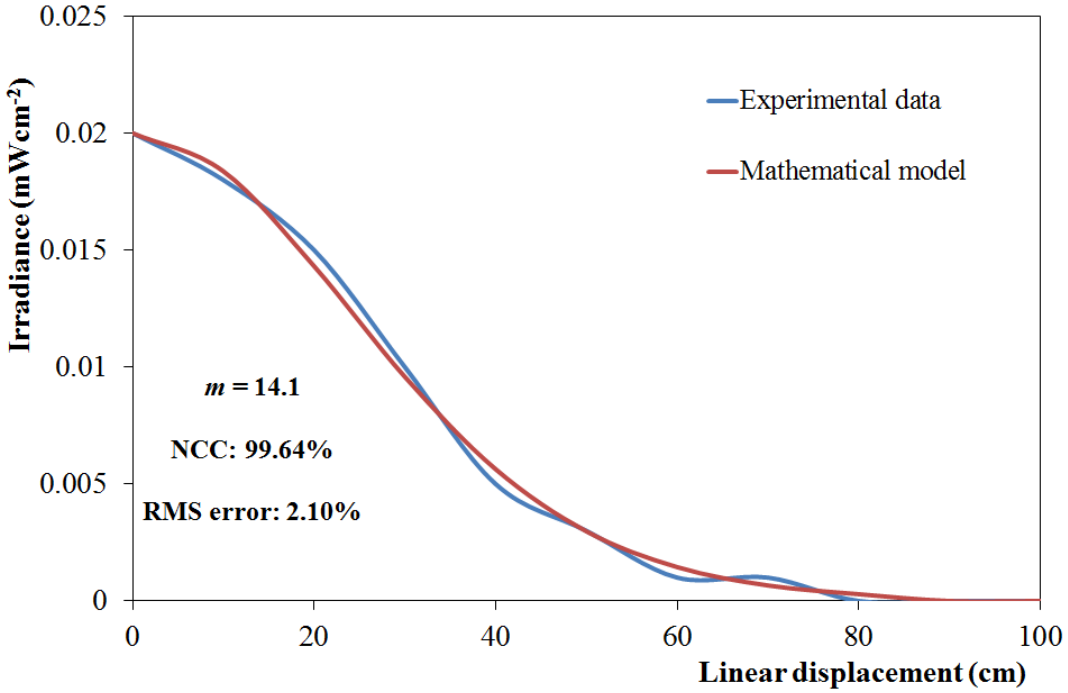

Fig. 8.13. *Irradiance distribution as a function of linear displacement for a specific Lambertian mode number (m = 14.1) and the NCC and RMS error for the light system with u = 5 cm and z = 100 cm.*

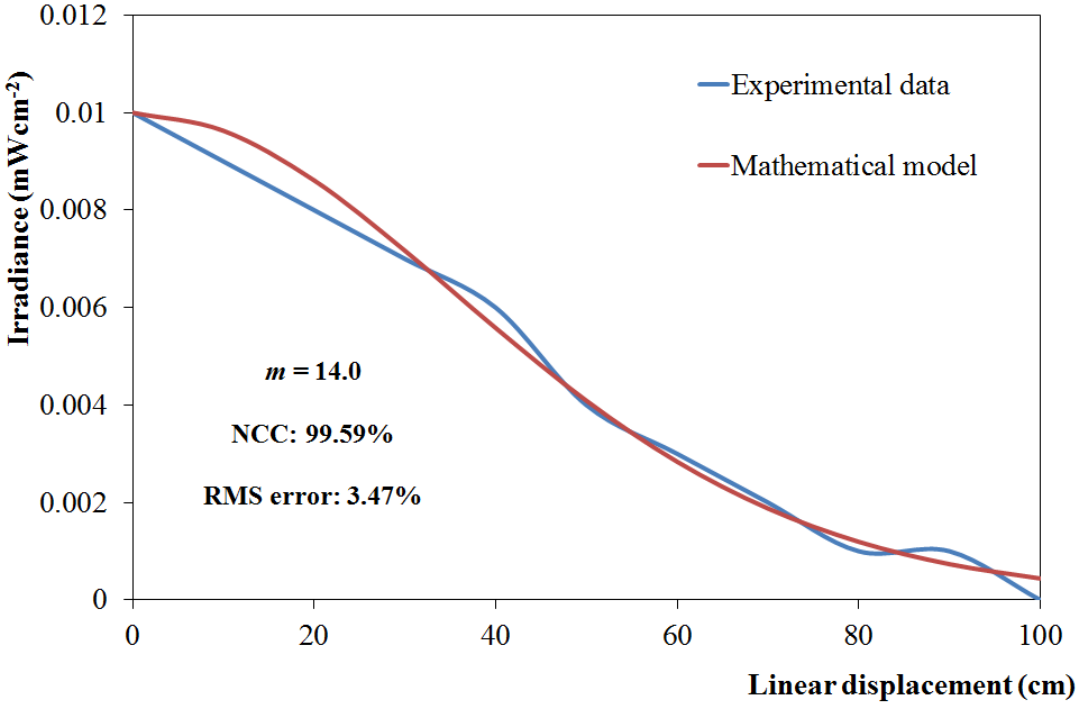

Fig. 8.14. *Irradiance distribution as a function of linear displacement for a specific Lambertian mode number (m = 14.0) and the NCC and RMS error for the light system with u = 5 cm and z = 150 cm.*

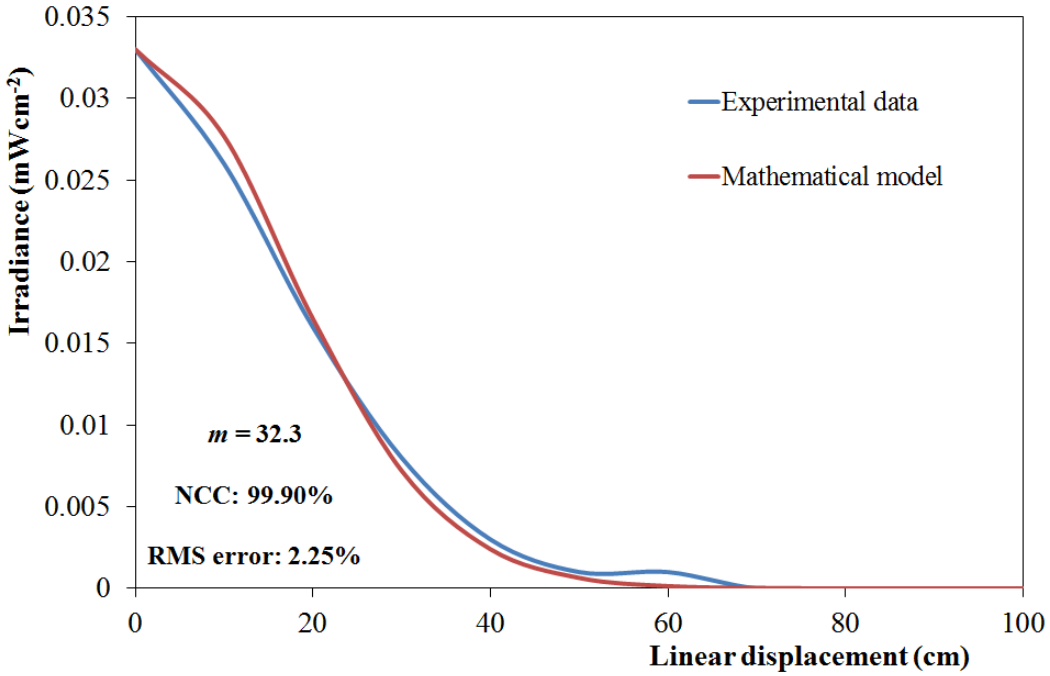

Fig. 8.15. *Irradiance distribution as a function of linear displacement for a specific Lambertian mode number (m = 32.3) and the NCC and RMS error for the light system with u = 7.5 cm and z = 100 cm.*

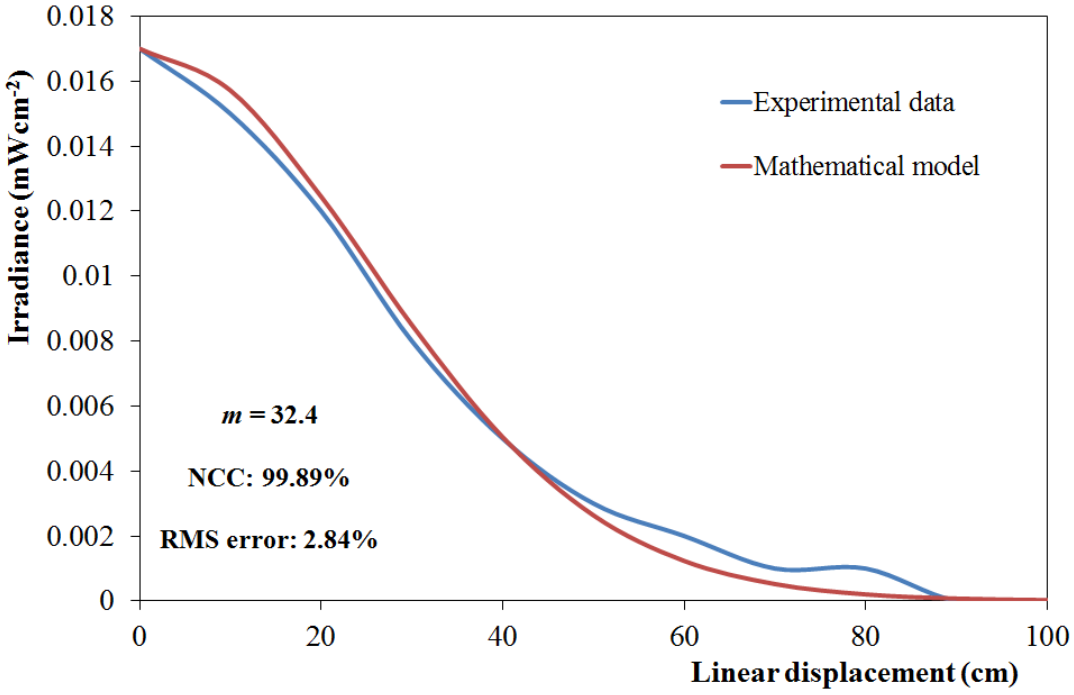

Fig. 8.16. *Irradiance distribution as a function of linear displacement for a specific Lambertian mode number (m = 32.4) and the NCC and RMS error for the light system with u = 7.5 cm and z = 150 cm.*

It can be observed from Fig. 8.13, Fig. 8.14, Fig. 8.15 and Fig. 8.16 that when the light system is set up with u = 5 and 7.5 cm, regardless of how z = 100 and 150 cm are applied, this results in a quite similar Lambertian mode number (m). The Lambertian mode number (m) for the light system with u = 5 cm was m =14.1 for z = 100 cm and 14.0 for z = 150 cm while the light system with u = 5 cm resulted in m = 32.3 for z = 100 cm and m = 32.4 for z = 150 cm. These results correlate well with the results in the previous study in Section 7.2.5.2, when the light system used a Fresnel lens of both type LFQ2561 (focal length = 2.52 cm) and LFQ40100 (focal length = 4 cm) with u = 2.5 and 5 cm. By calculating the normalised cross correlation (NCC), the similarity between the experimental data and mathematical model for all data analysis gives values greater than 99%. This result indicates that the irradiance distribution from the experimental data and the mathematical model are quite similar when both of them are compared.

When the experimental data and mathematical model are compared by calculation of the root mean square (RMS) error, the results shows that all data analysis gives values less than 5%. This confirms that the experimental method and mathematical model used in the study gave consistent results.

Fig. 8.17 and Fig. 8.18 shows the comparative data of relative irradiance (E/E_0) as a function of linear displacement according to the irradiance distribution as a function of linear displacement for the light system with u = 5 and 7.5 cm and z = 100 and 150 cm from Fig. 8.11 and Fig. 8.12, respectively. The results demonstrate that when the light system has a small value of m this causes the irradiance distribution produced by the light system to be wide spread on the illuminated area compared to when the light system has a large value of m, regardless of how u and z are applied.

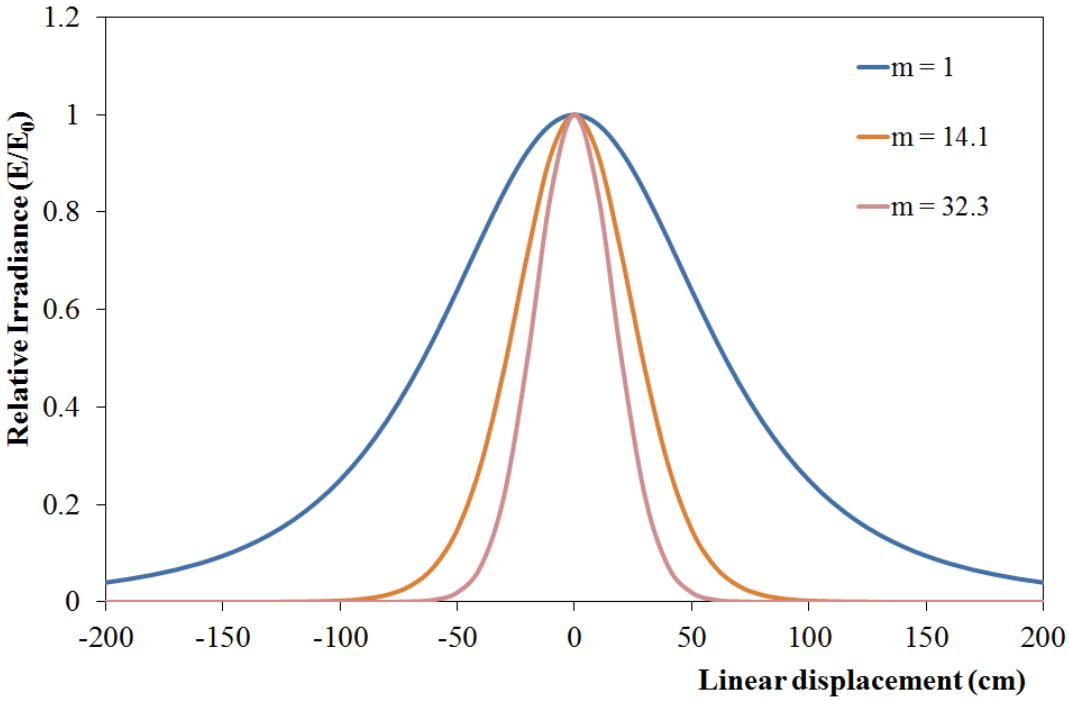

Fig. 8.17. *The comparative data of relative irradiance (E/E_0) as a function of linear displacement for the light system with z =100 cm from Fig. 8.11 and Fig. 8.12.*

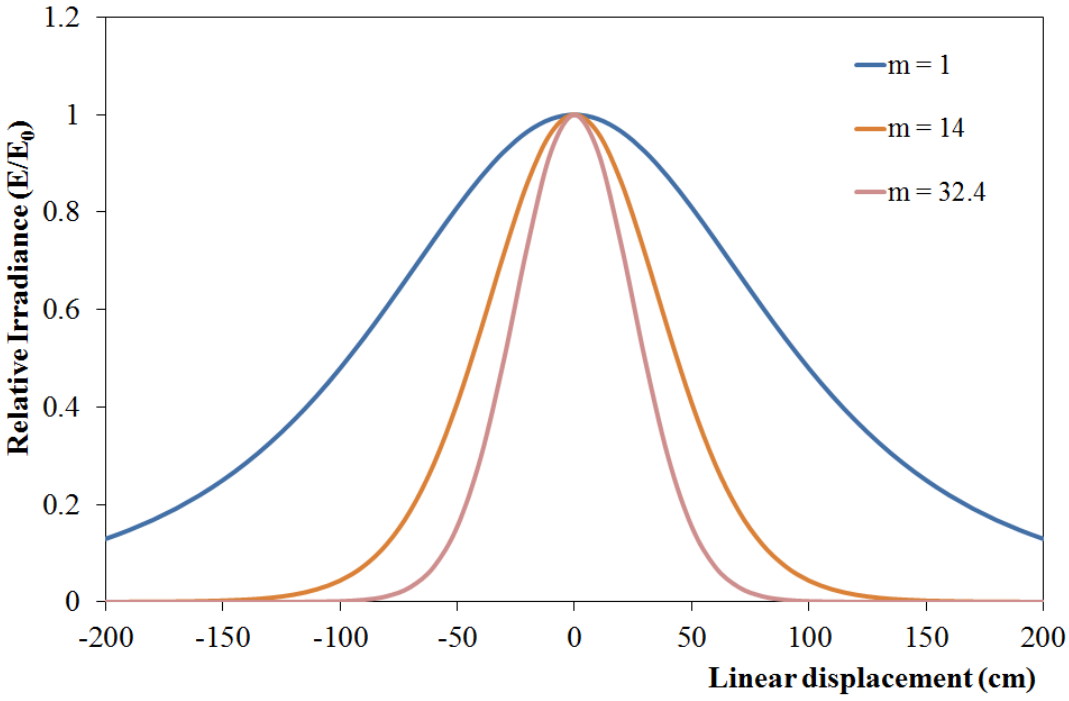

Fig. 8.18. *The comparative data of relative irradiance (E/E_0) as a function of linear displacement for the light system with z = 150 cm from Fig. 8.11 and Fig, 8.12.*

8.4.2 Investigation of the effect of the position of the LED array relative to the lens system

The previous study demonstrated the Lambertian mode number (m) for the light system when the LED array was aligned with the centre of the Fresnel lens and diffuser with varying space distances between the LED array and the lens system, u. The study will now investigate the effect of off-setting the position of the LED array relative to the lens system and illuminated area to determine the Lambertian mode number (m) and the irradiance distribution pattern on the illuminated area.

8.4.2.1 Experimental method

Fig. 8.19 shows the experimental set up used in the study. Three locations of the position of the LED array were examined: p = 0 cm, the LED array placed at the centre, p = 1 and 3 cm indicates the LED array placed at 1 and 3 cm off centre in direction of the negative y-axis. The space distances between the LED array and lens system (type 4) (u) were 5 and 7.5 cm, while the space distance between the LED array and the illuminated area (z) was 100 cm.

For all experiments the voltage was set to 14.1 ± 0.1 V with a current of 0.11 ± 0.01 A. The irradiance distribution of light over an illuminated area parallel to the light source was measured using a radiant power meter and all point data was taken in all direction of x- axis and y-axis with three replicates for each independent experiment to ensure accurate data.

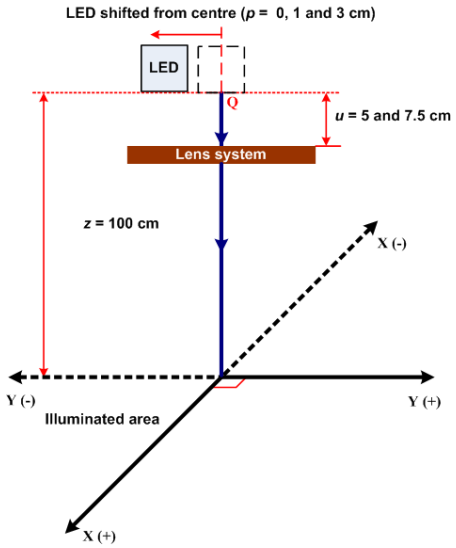

Fig. 8.19. *Experimental setup for determining the effect of the position of the LED array relative to the lens system.*

8.4.2.2 Results

The irradiance distribution as a function of linear displacement for the light system with u = 5 cm for differing distances of the position of the LED array with reference to the centre of the light system at position Q (Fig. 8.19) are shown in Fig. 8.20 and Fig. 8.21. When the LED array was shifted 3 cm off centre in the direction of the negative y-axis, the irradiance pattern on the illuminated area had a change in the peak irradiance at position 0 and shifted 20 cm in the direction of the positive y-axis, whereas in x-axis, the peak irradiance dropped 15.8% compare to p = 0 cm.

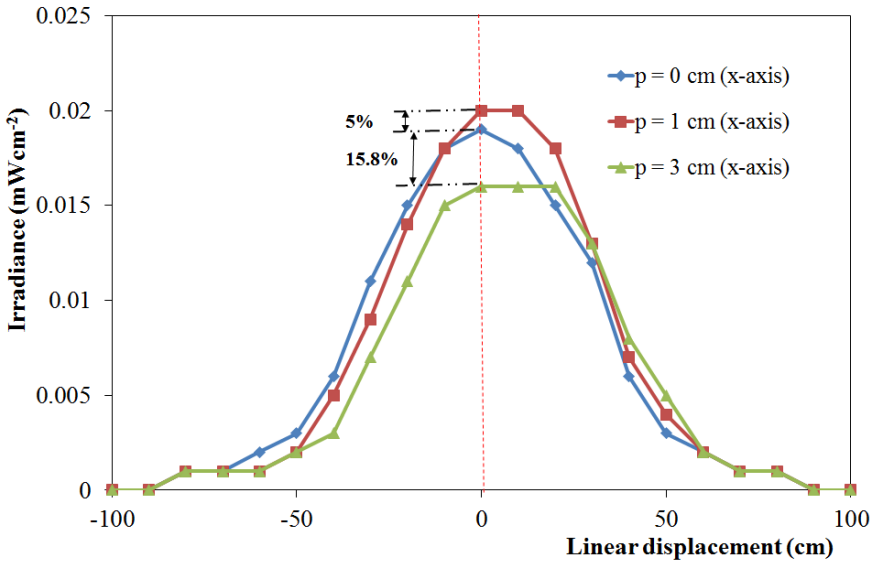

Fig. 8.20. *Irradiance distribution as a function of linear displacement for the light system with u = 5 cm and z = 100 cm in direction x-axis.*

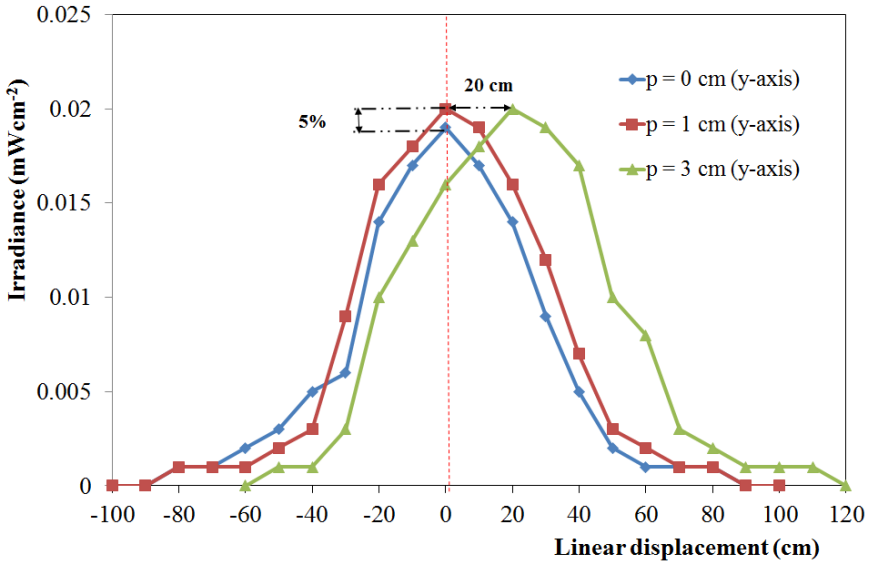

Fig. 8.21. *Irradiance distribution as a function of linear displacement for the light system with u = 5 cm and z = 100 cm in direction y-axis.*

The irradiance pattern for the light system when the LED array was shifted 1 cm (p = 1 cm) off centre had a similar pattern (Gaussian distribution) with the irradiance pattern for the LED array on centre (p = 0 cm) (both in x-axis and y-axis). It not only had a change in the peak irradiance at position 0 but also in the irradiance distribution. The peak irradiance with the LED array with p = 1 cm was 5% greater than p = 0 cm for both in x-axis and y-axis.

To determine the similarity and accuracy between the experimental data and the mathematical model both the NCC and the RMS error were calculated. The mathematical model used in the study was Eq. (2.16), with modification parameters $r = x$ and $h = z$ = 100 cm ($E(x) = E_o\left(1+\frac{x^2}{(100)^2}\right)^{-\frac{(3+m)}{2}}$). The Lambertian mode number (m) for the experimental data was also investigated. The NCC, the RMS error and the Lambertian mode number (m) for this study are summarised in Table 8.3.

Table 8.3 *The NCC, RMS error and the Lambertian mode number (m) for the light system with u = 5 cm and z = 100 cm when applied using p = 0, 1 and 3 cm*

***p* (cm)**	**x-axis**			**y-axis**		
	m	**NCC (%)**	**RMS error (%)**	***m***	**NCC (%)**	**RMS error (%)**
0	11.2	99.65	3.26	14.2	99.23	4.34
1	12.1	98.65	6.15	13.3	98.87	5.51
3	NA	NA	NA	NA	NA	NA

NA = not applicable

Fig. 8.22 and Fig. 8.23 show the results of the irradiance distribution as a function of linear displacement for the light system with u = 7.5 cm and z = 100 cm for differing positions of the LED array with reference to the centre of the light system at position Q (Fig. 8.19).

As in the previous results with the light system with u = 5 cm, the irradiance patterns for p = 1 cm and p = 0 cm give a similar irradiance distribution (Gaussian distribution) for both in x-axis and y-axis, with the peak irradiance p = 1 cm was 5%

greater than p = 0 cm. Results of the irradiance measurements on the illuminated area when the LED array was shifted 3 cm off centre in the direction of the negative y-axis, shown in Fig. 8.22 and Fig. 8.23, respectively, demonstrate that the irradiance pattern on the illuminated area in the direction of the y-axis had a change in the peak irradiance at position 0 and was shifted 20 cm in the direction of the positive y-axis, whereas in x-axis, the peak irradiance dropped 36.8% compare to p = 0 cm.

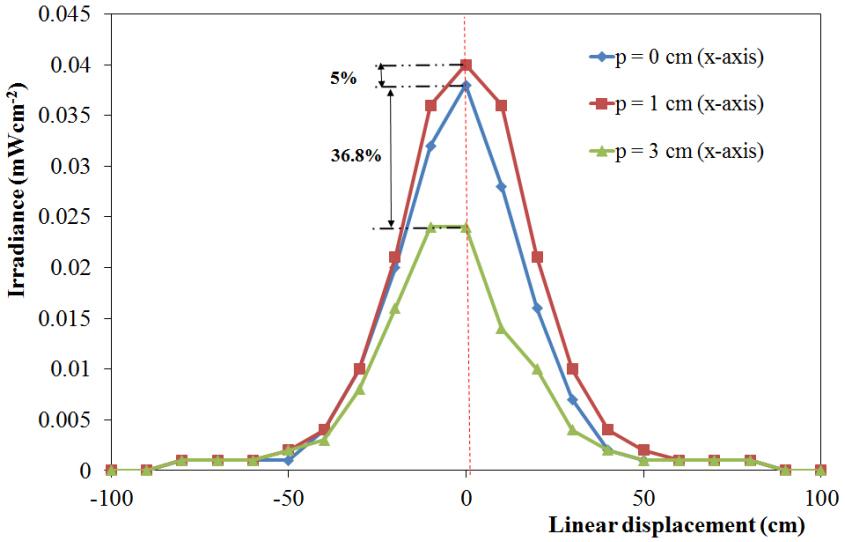

Fig. 8.22. *Irradiance distribution as a function of linear displacement for the light system with u = 7.5 cm and z = 100 cm in direction x-axis.*

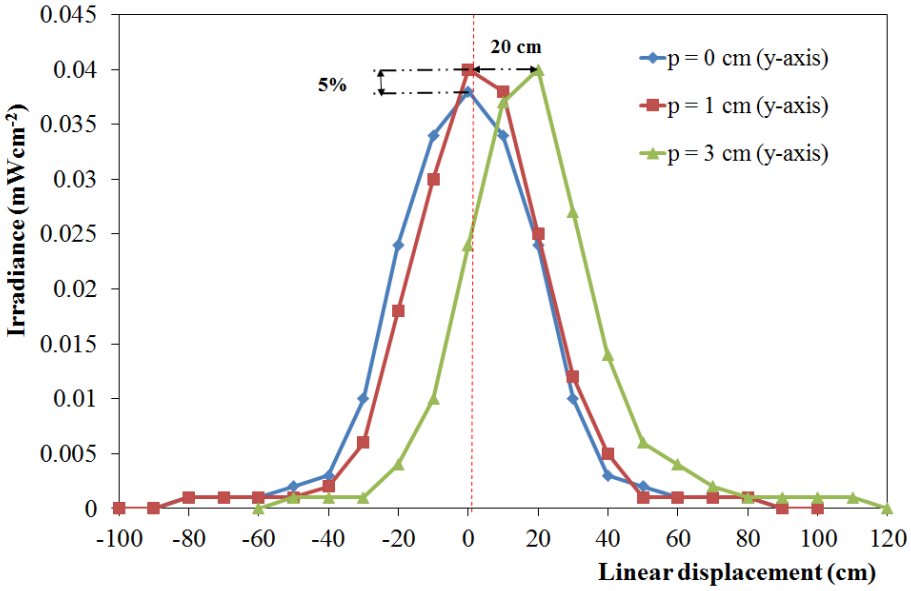

Fig. 8.23. *Irradiance distribution as a function of linear displacement for the light system with u = 7.5 cm and z = 100 cm in direction y-axis.*

Parameters of the NCC, RMS error and the Lambertian mode number (*m*) for this study are presented in Table 8.4. Results, presented in Table 8.3 and Table 8.4, demonstrate that the best position for the LED array is when the LED array is placed at the centre of the light system.

Table 8.4 *The NCC, RMS error and the Lambertian mode number (m) for the light system with u = 7.5 cm and z = 100 cm when applied using p = 0, 1 and 3 cm*

***p* (cm)**	**x-axis**			**y-axis**		
	m	**NCC (%)**	**RMS error (%)**	***m***	**NCC (%)**	**RMS error (%)**
0	33.9	99.49	3.6	25.2	99.67	2.97
1	28.2	99.86	2.08	29.9	98.74	5.3
3	NA	NA	NA	NA	NA	NA

NA = not applicable

8.5 Determination of the optimal distance between the LED array and the lens system

The aim of this study was to determine the optimal distance between the LED array and lens system (type 4) (*u*). Nine different values of *u* were used in the study is 2.5, 4, 5, 6, 7, 7.5, 8, 9 and 10 cm. The space distance between the LED array and the illuminated area (*z*) was 100 cm. The experimental setup for this study is illustrated in Fig. 8.24.

For all experiments the voltage was set at 20.1 ± 0.1 V with a current of 1.67 ± 0.01 A. The irradiance distribution of light over an illuminated area parallel to the light source was measured using a radiant power meter and all data points were taken in all direction of x-axis with three replicates for each independent experiment to ensure accurate data.

Fig. 8.25 shows the irradiance distribution as a function of linear displacement for determining the best value of *u*. The irradiance distribution for the system without a lens system is also shown. The result shows that the peak irradiance at the centre (*O*) of the illuminated area will be increased when the value of *u* increases.

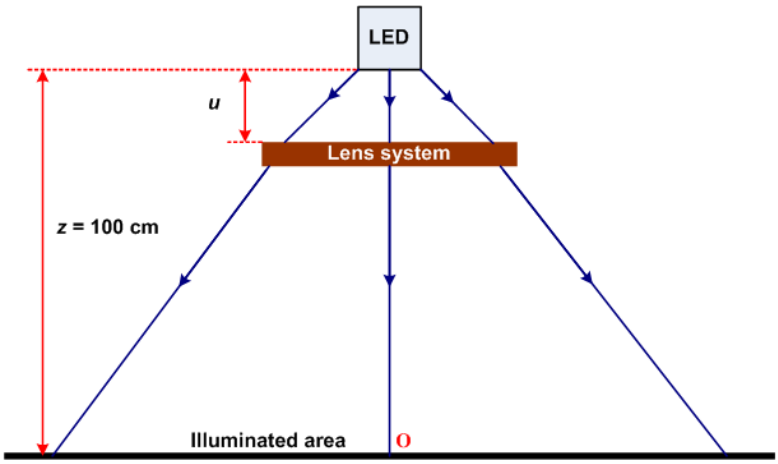

Fig. 8.24. *Experimental setup for determining the best value of u.*

As described in Section 8.3.2, the best value of *u* can also be calculated from the total power by volumes of solids of revolution, Eq. (8.8). To ensure similarity and accuracy the normalised cross correlation (NCC) and the RMS error for comparison of data between the experimental method and the mathematical model have been calculated. The NCC, RMS error, the Lambertian mode number (*m*) and volumes of solids of revolution (hereafter refer to as total power expressed in W) for this study are summarised in Table 8.4.

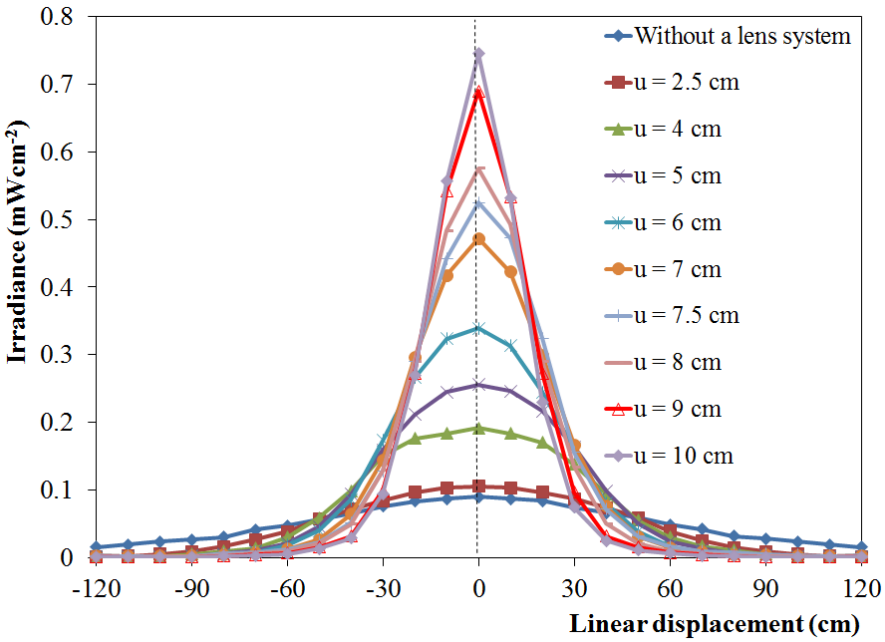

Fig. 8.25. *Irradiance distribution as a function of linear displacement for the light system with differing values of u. The data for the light system without a lens system is also shown.*

All data presented in Table 8.5 for the NCC and RMS error show that when the experimental data and mathematical model are compared, the similarity and accuracy were achieved with the NCC greater than 99% and the RMS error less than 5%, respectively. This confirms that the experimental method used in the study is accurate.

According to the results in Table 8.5, the best value of *u* is achieved when the space distance between the LED array and lens system is at 4 cm with a total power of 1.5 W.

Table 8.5 *The NCC, RMS error and the Lambertian mode number (m) and total power (W) for this study*

***u* (cm)**	**Irradiance (Wm^{-2}) at centre (E_0)**	***m***	**NCC (%)**	**RMS (%)**	**Total Power (W)**
2.5	1.06	3.58	99.50	4.61	1.45
4	1.92	7.06	99.44	4.61	1.50
5	2.56	10.09	99.69	3.26	1.45
6	3.39	14.50	99.81	2.19	1.37
7	4.72	21.88	99.92	1.15	1.30
7.5	5.25	25.78	99.81	1.89	1.23
8	5.76	31.02	99.96	0.76	1.13
9	6.9	43.62	99.96	0.90	0.97
10	7.45	52.71	99.86	1.59	0.87

As described in Section 8.4.2.1, when the light system has a small Lambertian mode, the light distribution produced by the light system becomes widespread on the illuminated area compared to when the mode number is larger, regardless of how *u* and *z* are applied. The total power for the system with $u = 4$ cm is higher than for topology with $u = 2.5$ cm. Therefore, this configuration is ideal for application of the light system for environmental decontamination as not only has it the biggest total power (W) but also the light system has a wide spread distribution on the illuminated area.

8.6 Investigation into the optimum LED-to-LED array spacing

The high-intensity narrow spectrum-light environmental decontamination system (HINS-light EDS) is a ceiling-mounted light source. This has to be retro-fitted into the space normally occupied by a ceiling tile. This requires a square shape with dimension 59.2 × 59.2 cm. The Fresnel lens has a 20 cm diameter and the optimum LED-to-LED spacing (d) in the study is 30 cm (see Appendix D). The initial layout design for the four light engine light source is shown in Fig. 8.26.

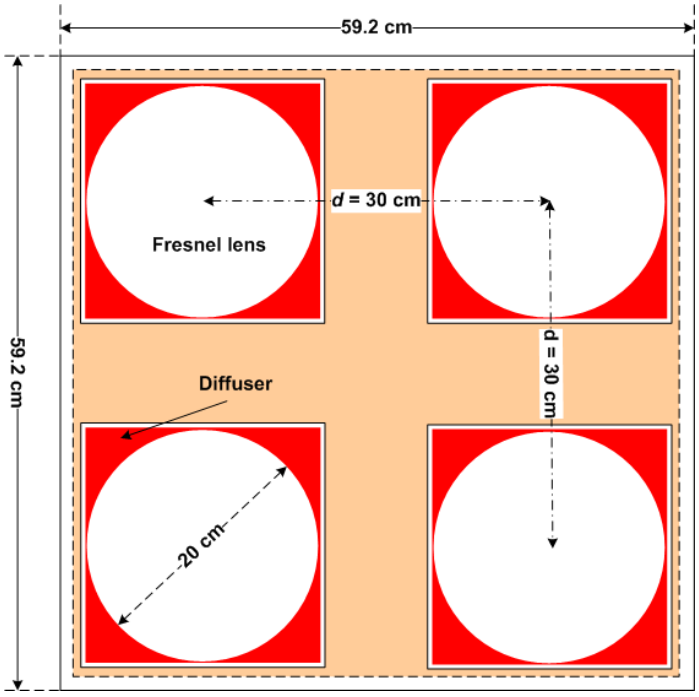

Fig. 8.26. *The optimum LED-to-LED spacing for an initial design.*

The Fresnel lens LFQ100200 (focal length = 10 cm) with diameter 20 cm has been chosen for the final design rather than type LFQ2561 (focal length = 2.54 cm) and LFQ40100 (focal length = 4 cm) because LFQ100200 has a wider spread of the irradiance distribution than LFQ2561 and LFQ40100, as shown in Fig. 8.27. Fig. 8.27 demonstrates the irradiance distribution as a function of linear displacement when the space distance between the LED array and the illuminated area (z) was 100 cm. The space between the LED array and lens system (u) used in the study was 4 cm.

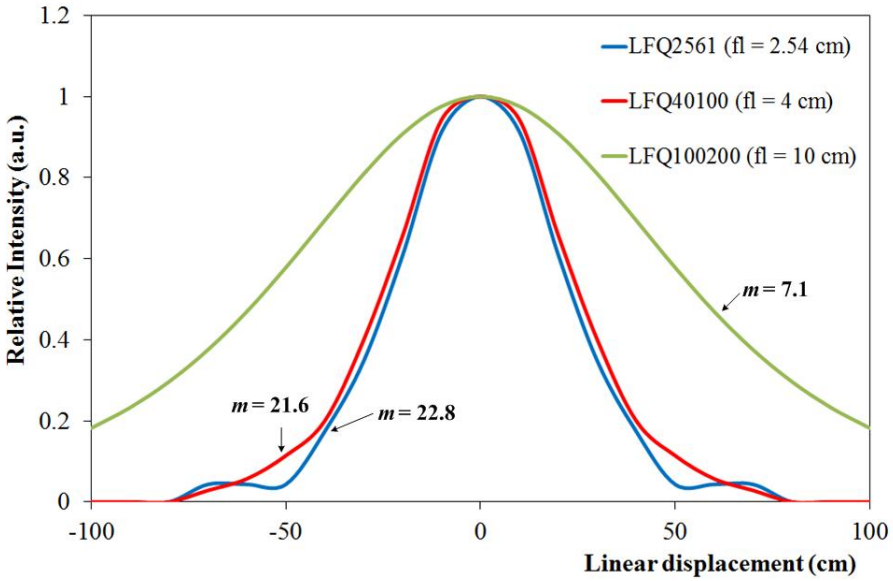

Fig. 8.27. *Comparative Lambertian mode numbers (m) for three different Fresnel lens.*

8.7 Design and development of a new prototype HINS-light EDS

As shown by results in Part I, four main factors were identified for designing and developing a new HINS-light EDS. The main factors involved: (i) Type 4 – configuration of a Fresnel lens and diffuser, (ii) the Lambertian mode number (m) – which depends on the light system used, (iii) u = 4 cm – space distance between the LED array and lens system and (iv) d = 30 cm – the optimum LED-to-LED array spacing. The aim of this part was the development, testing and modelling of a fully-integrated large-scale HINS-light EDS.

8.7.1 Designing the light source

The active components of the new prototype HINS-light EDS are 405-nm LEDs and white LEDs covered by a Fresnel and diffuser. Fig. 8.28 provides a diagram of the new HINS-light EDS developed for bacterial inactivation. The Fresnel lens and diffuser positioned below the LED source allows a widespread and more uniform distribution of the light over the illuminated area.

The topology diagram of the make up the new prototype HINS-light EDS system is shown in Fig. 8.29. The purple boxes represent 405 nm LED arrays and the blue circles are single white-light LEDs. As described in Section 7.2.1, the 405 nm LED

light engine in Fig. 7.2 is an array made up of 25 individual LEDs with typical light output 4.9 mW and embedded thermistors give accurate feedback on LED chip temperature [185]. The new prototype HINS-light EDS is made up of 4 individual 405 nm LED light engines, as shown in Fig. 8.29.

To ensure that the system did not generate dominant violet illumination but would also produce comfortable room lighting, 12 high power white-light LEDs with typical light output of 3 W for each white LED, with 90^0 viewing angle and a warm-white emitting colour were used in the design of the new HINS-light EDS. The photograph of a white LED is shown in Fig. 8.30. The white LEDs used in the study were obtained from the Ledman Optoelectronic Co., Ltd., China [190]. It is known that blue or violet light may cause dizziness, headaches or nausea [184] and for this reason the white LEDs have been incorporated into the HINS-light EDS system.

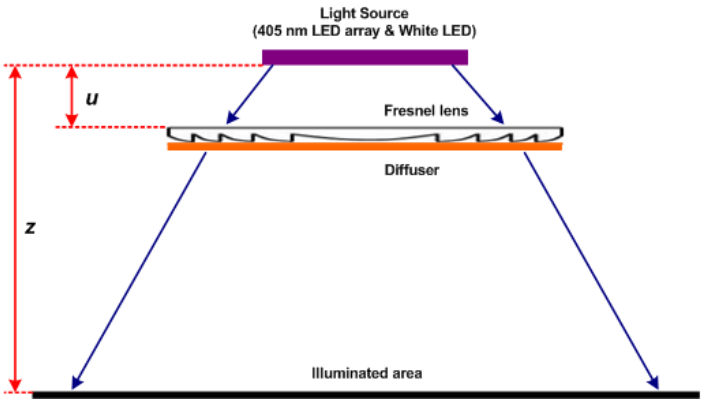

Fig. 8.28. *General layout of the new HINS-light EDS illumination system developed for bacterial inactivation.*

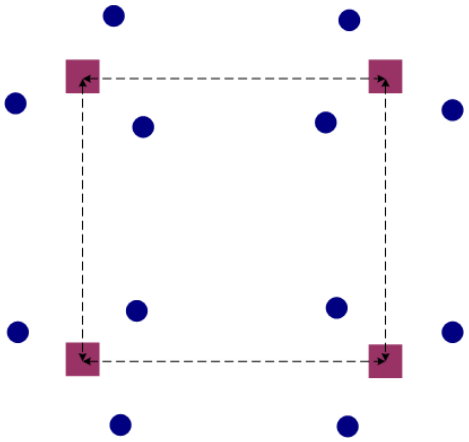

Fig. 8.29. *Topology of the new HINS-light EDS light source (The purple boxes = 405 nm LED arrays and the blue circles = single white-light LEDs).*

Fig. 8.30. *Photograph of a 3 W white LED.*

8.7.2 Development equation (mathematical model) of the irradiance distribution pattern for the new prototype HINS-light EDS

The topology of the light source for the equation (mathematical model) used in the study was square incorporating four LED arrays, as shown in Fig. 8.31. It was only irradiance data from the 405 nm LED arrays that was used for modelling and testing of the irradiance distribution pattern of the new HINS-light EDS. The irradiance $E_O(x_O, y_O, z_O)$ in Fig. 8.31 is given by the sum of the irradiance from the LED_1, LED_2, LED_3, and LED_4 in a square with a side length d and where the LEDs are placed in each corner,

$$E_O(x_O, y_O, z_O) = E_1(x_1, y_1, z_1) + E_2(x_2, y_2, z_2) + E_3(x_3, y_3, z_3) + E_4(x_4, y_4, z_4). \quad (8.9)$$

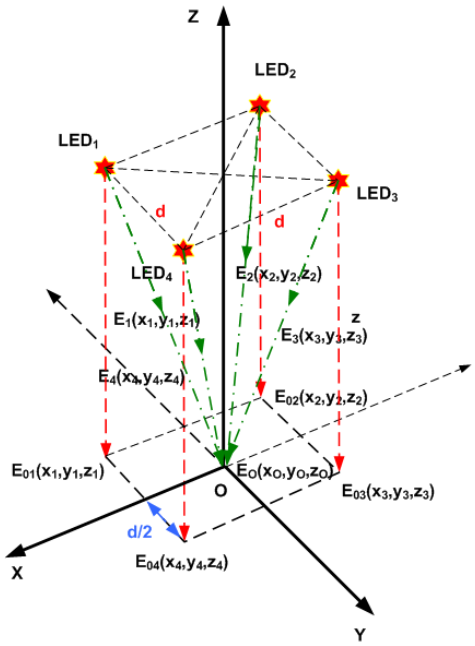

Fig. 8.31. *Square LED array topology for modelling and testing of the new HINS-light EDS.*

As described in Section 2.4, the irradiance distribution across a horizontal surface in the terms of a Cartesian coordinates (x, y, z) for a single LED can be expressed by Eq. (2.18), so that Eq. (8.9) can be written as,

$$E_O(x_O, y_O, z_O) = \left\{ \begin{array}{l} E_{01}(x_1, y_1, z_1) \bullet z_1^{(3+m_2)} \bullet \left[z_1^{\,2} + (x_1 - d/2)^2 + (y_1 + d/2)^2 \right]^{-\frac{(3+m_1)}{2}} \\ + E_{02}(x_2, y_2, z_2) \bullet z_2^{(3+m_2)} \bullet \left[z_2^{\,2} + (x_2 + d/2)^2 + (y_2 + d/2)^2 \right]^{-\frac{(3+m_2)}{2}} \\ + E_{03}(x_3, y_3, z_3) \bullet z_3^{(3+m_3)} \bullet \left[z_3^{\,2} + (x_3 + d/2)^2 + (y_3 - d/2)^2 \right]^{-\frac{(3+m_3)}{2}} \\ + E_{04}(x_4, y_4, z_4) \bullet z_4^{(3+m_4)} \bullet \left[z_4^{\,2} + (x_4 - d/2)^2 + (y_4 - d/2)^2 \right]^{-\frac{(3+m_4)}{2}} \end{array} \right\}, \quad (8.10)$$

where,

$z_1 \ldots z_4$ = space distance between the light sources ($LED_1 \ldots LED_4$) and illuminated area,

d = LED-to-LED array spacing,

$m_1 \ldots m_4$ = the Lambertian mode number of light sources ($LED_1 \ldots LED_4$),

$E_{01}(x_1, y_1, z_1) \ldots E_{04}(x_4, y_4, z_4)$ = the irradiance measurement at a distance of *z* cm below the $LED_1 \ldots LED_4$ on the illuminated area.

Let assume,

$$1.\ m = m_1 = m_2 = m_3 = m_4 \ (m > 0),$$
$$2.\ z = z_1 = z_2 = z_3 = z_4,$$

and then Eq. (8.10) can be expressed as follows,

$$E_O(x_O, y_O, z_O) = z^{(3+m)} \left\{ \begin{array}{l} E_{01}(x_1, y_1, z) \left[z^2 + (x_1 - d/2)^2 + (y_1 + d/2)^2 \right]^{-\frac{(3+m)}{2}} \\ + E_{02}(x_2, y_2, z) \left[z^2 + (x_2 + d/2)^2 + (y_2 + d/2)^2 \right]^{-\frac{(3+m)}{2}} \\ + E_{03}(x_3, y_3, z) \left[z^2 + (x_3 + d/2)^2 + (y_3 - d/2)^2 \right]^{-\frac{(3+m)}{2}} \\ + E_{04}(x_4, y_4, z) \left[z^2 + (x_4 - d/2)^2 + (y_4 - d/2)^2 \right]^{-\frac{(3+m)}{2}} \end{array} \right\}. \quad (8.11)$$

For the condition,

$E_0(x,y,z) = E_{01}(x_1,y_1,z_1) = E_{02}(x_2,y_2,z_2) = E_{03}(x_3,y_3,z_3) = E_{04}(x_4,y_4,z_4)$, Eq. (8.11) can be re-expressed as follows:

$$E_O(x_O,y_O,z_O) = z^{(3+m)}E_0(x,y,z)\sum_{i=1}^{2}\sum_{j=1}^{2}\left[\begin{matrix}\left(x-(3-2i)(d/2)\right)^2 \\ +\left(y-(3-2j)(d/2)\right)^2+z^2\end{matrix}\right]^{-\frac{(3+m)}{2}} . \quad (8.12)$$

8.7.3 A study of the irradiance distribution pattern for the new prototype HINS-light EDS

8.7.3.1 Experimental method

In order to get accurate data for the light distribution pattern in three dimensions, 400 data readings of irradiance (20 × 20) were taken from the illuminated area at a distance of *z* cm below the light source. Fig. 8.32 shows that to measure irradiance ($mWcm^{-2}$) of the light distribution in the illuminated area, the light source was placed at a distance of *z* cm above the level of the illuminated area. The main studies have involved two methods. Method 1, the space distances between the light source and illuminated area (*z*) used in the study were 100 and 200 cm. The space distance between the light source and lens system (*u*) was 7.5 cm. For all experiments the voltage was set to 16.3 ± 0.1 V with a current of 0.8 ± 0.1 A (the intensity level for each individual 405 nm LED array was set to 0% by computer). In Method 2, values of *u* used in the study were *u* = 4 and 5 cm at *z* = 200 cm. For all experiments the voltage was set to 12.0 ± 0.1 V with a current of 14.6 ± 0.1 A (the intensity level for each individual 405 nm LED array was set to 100% by computer).

A photograph of the experimental setup is shown in Fig. 8.32a. The illuminated area was divided into 4 quadrants and each quadrant gave 100 values of irradiance ($mWcm^{-2}$) from the light source. Overall, the data measurements were taken starting from the centre of the illuminated area (*O*) and then the radiant power detector was shifted every 10 cm along the x-axis and y-axis (Fig. 8.32b). This method was used to investigate whether the mathematical model (Eq. (8.11)) could be used to predict and estimate the light distribution from the light source.

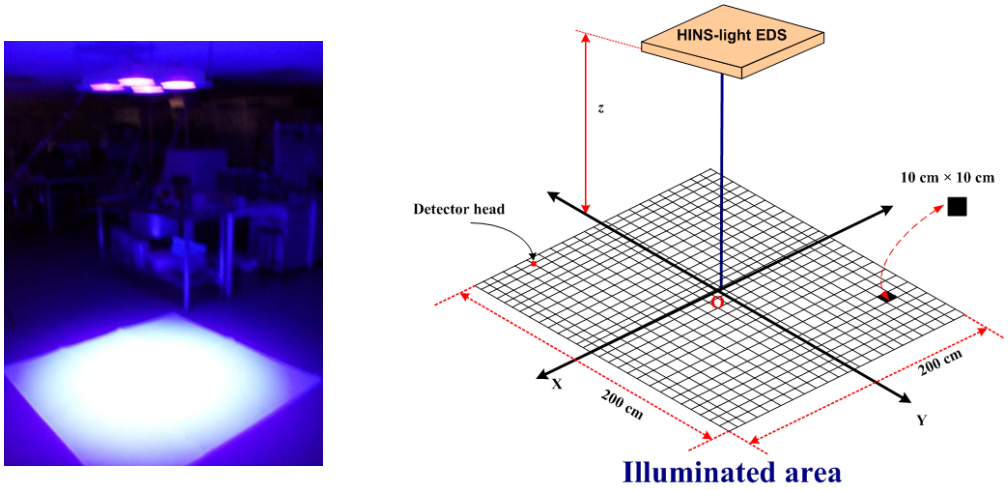

(a) (b)

Fig. 8.32. *Experimental setup for measuring the irradiance distribution pattern of the new prototype HINS-EDS, a) photograph of the irradiance pattern sourced from the system and b) the experimental method used.*

8.7.3.2 Results

Method 1

All data measurements were plotted by OriginPro 8.1 to generate the irradiance distribution pattern in terms of Cartesian coordinates (x, y, z) [191], as shown in Fig. 8.33 and Fig. 8.34. The measurements show that the irradiance distribution follows a Gaussian distribution curve (see in Section 8.75). When the space distance between the light source and illuminated area was increased, this caused the peak irradiance at the centre of the illuminated area (*O*) to decrease and the light distribution produced became more widespread.

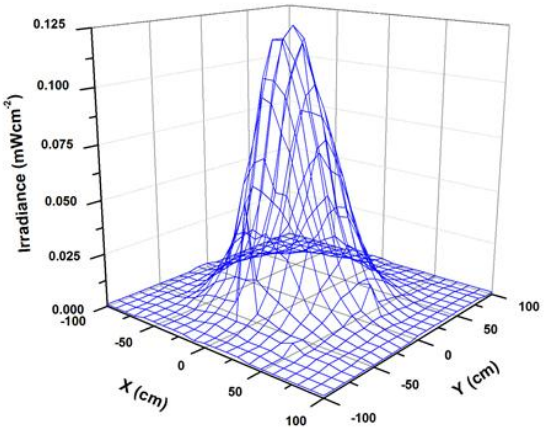

Fig. 8.33. *Irradiance distribution pattern in terms of Cartesian coordinates (x, y, z) for light (4 LED engines) source with u = 7.5 cm and z = 100 cm.*

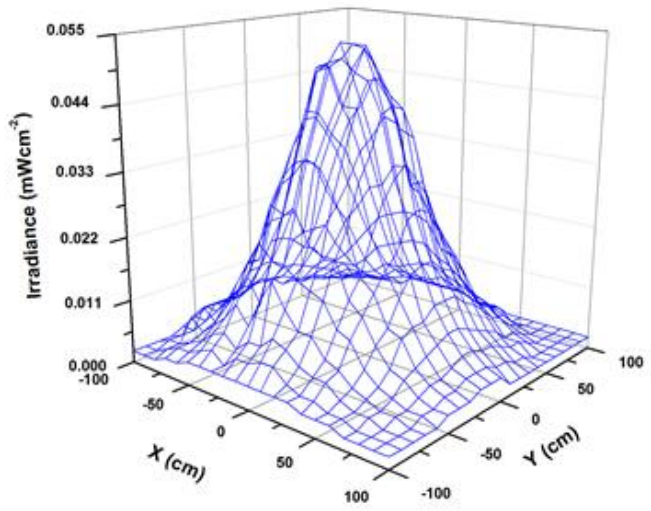

Fig. 8.34. *Irradiance distribution pattern in terms of Cartesian coordinates (x, y, z) for light source (4 LED engines) with u = 7.5 cm and z = 200 cm.*

Method 2

Fig. 8.35 and Fig. 8.36 show the irradiance distribution pattern in term Cartesian coordinate (x, y, z) for u = 4 and 5 cm at z = 200 cm, respectively. As shown in the results in method 1, the results demonstrate that the irradiance distribution profile follows a Gaussian distribution curve (see in Section 8.75).

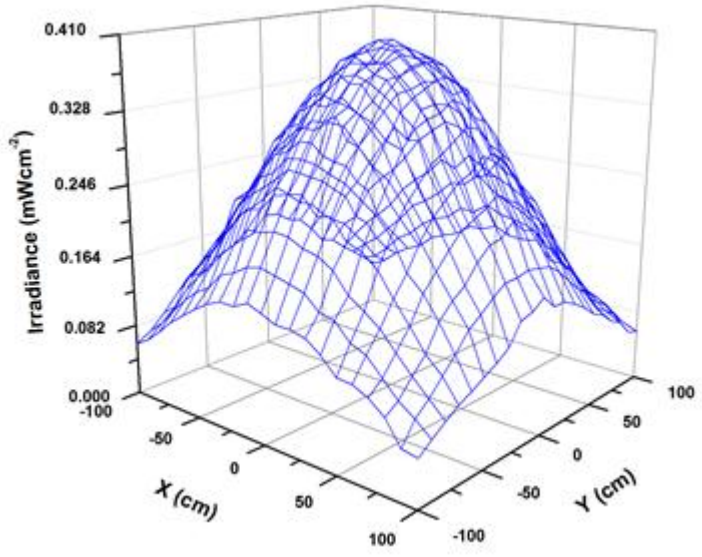

Fig. 8.35. *Irradiance distribution pattern in terms of Cartesian coordinates (x, y, z) for light source (4 LED engines) with u = 4 cm and z = 200 cm.*

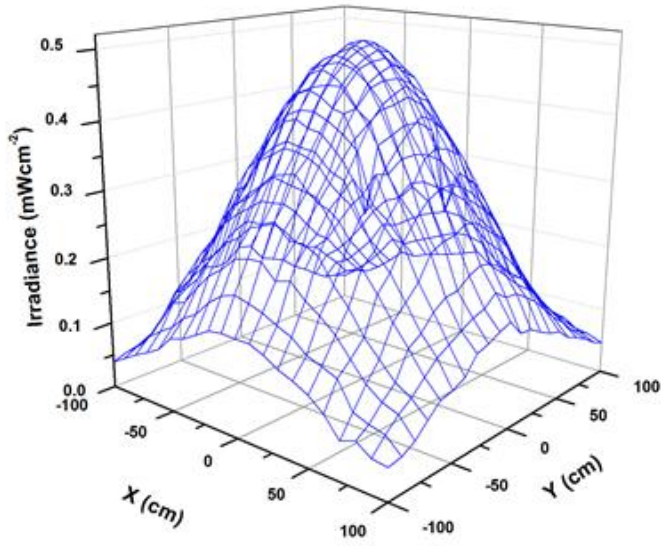

Fig. 8.36. *Irradiance distribution pattern in terms of Cartesian coordinates (x, y, z) for light source (4 LED engines) with u = 5 cm and z = 200 cm.*

8.7.4 Study of a mathematical model for modelling the irradiance distribution pattern of the New HINS-light EDS

The aim of this study was to investigate whether the mathematical model (Eq. (8.11)) could be used to predict and estimate irradiance distribution pattern from the new HINS-light EDS. To investigate the irradiance distribution pattern of the new HINS-light EDS, three main steps should be done and will be discussed in this section as follows:

1. Measurements of E_0 and m for single array
2. Mathematical model (Eq. (8.11)) uses experimental E_0 and m to obtain distribution for 4 superimposed sources
3. Analytical distribution for 4 light sources has been compared with practical distribution produced by the EDS system with 4 light engines.

8.7.4.1 Experimental method: the influence of voltage input to the LED array driver on measured irradiance

As described in Section 8.7.2, the irradiance distribution in terms of Cartesian coordinates (x, y, z) for the square LED array topology can be modelled by Eq. (8.11). For modelling the irradiance distribution pattern, it is assumed that only the irradiances on the illuminated area parallel to the light source are measured and that the Lambertian mode number (m) for the four light engines used as the light source have same number. Values of E_{01}, E_{02}, E_{03} and E_{04} were measured at a distance of z cm below LED_1, LED_2, LED_3 and LED_4 with two methods, respectively. The aim of this experiment was to investigate the relationship between the measured irradiance and voltage input to the driver of the LED array. In the first (method A_1), the light source was driven by 16.3 ± 0.1 V for all four LEDs but only one of four LEDs gave data measurement, as illustrated in Fig. 8.37a. Although all four LEDs were in the ON condition, the output from the three other LEDs was blocked. In the second method (method A_2), only one LED gave data measurement and the three other LEDs were in the condition OFF, as illustrated in Fig. 8.37b. Similarly, in the second method, input to the driver was 16.3 ± 0.1 V. Parameters for modelling used in the study are summarised in Table 8.6. All three-dimensional profiles of the irradiance distribution were modelled by SigmaPlot 9 [192].

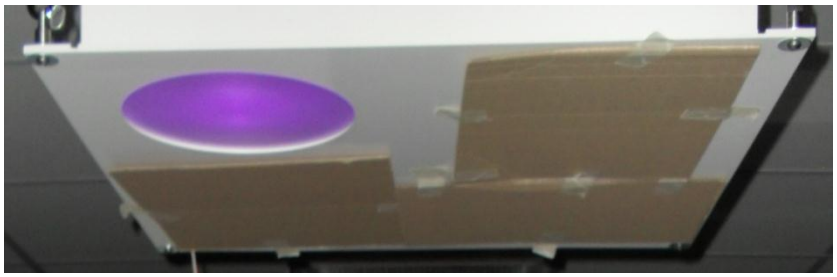

(a)

(b)

Fig. 8.37. *Methods used to measure E_{01}, E_{02}, E_{03} and E_{04}, a) Method A_1 and b) Method A_2.*

Table 8.6 *Parameters for modelling of the light source with u = 7.5 cm*

Light source	z = 100 cm, d = 30 cm, m = 12.56		z = 200 cm, d = 30 cm, m = 24.52	
	E_0 (mWcm^{-2})	E_0 (mWcm^{-2})	E_0 (mWcm^{-2})	E_0 (mWcm^{-2})
	Method A_1	**Method A_2**	**Method A_1**	**Method A_2**
LED_1	0.036	0.054	0.012	0.018
LED_2	0.040	0.050	0.011	0.020
LED_3	0.050	0.074	0.015	0.023
LED_4	0.036	0.053	0.015	0.020

8.7.4.2 Results

Results, shown in Fig. 8.38 and Fig. 8.39, demonstrate the three-dimensional profile for modelling of the light source when the space distance between the light source and the illuminated area (z) equals to 100 cm.

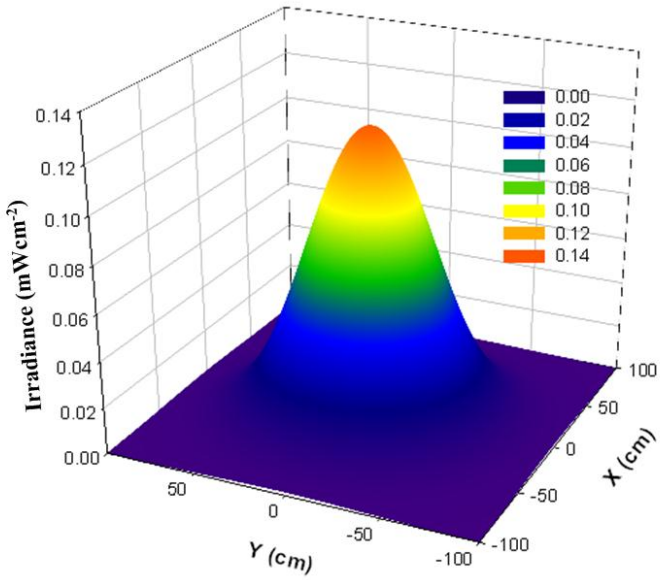

Fig. 8.38. *Irradiance distribution pattern in terms of Cartesian coordinates (x, y, z) for light source (4 LED engines) with z = 100 cm (Method A_1).*

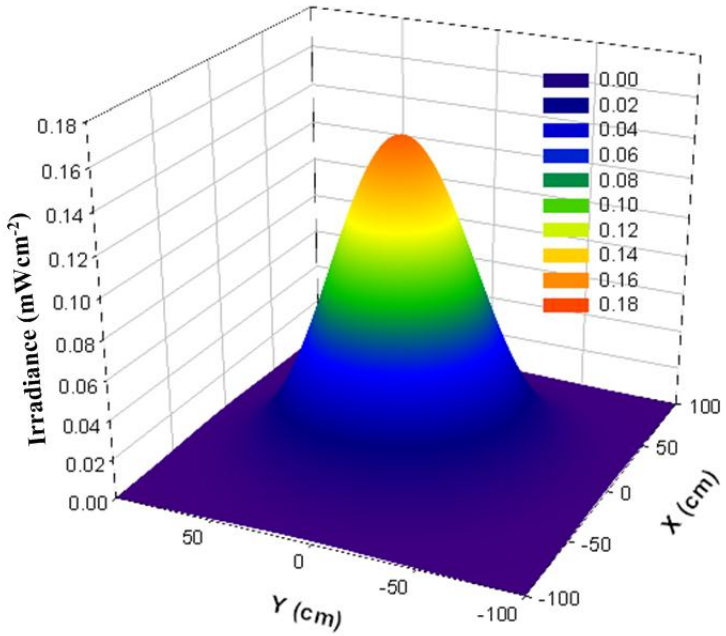

Fig. 8.39. *Irradiance distribution pattern in terms of Cartesian coordinates (x, y, z) for light source (4 LED engines) with z = 100 cm (Method A_2).*

The irradiance distributions as a function of linear displacement in three-dimensions with z = 200 cm using methods A_1 and A_2 are displayed in Fig. 8.40 and Fig. 8.41.

.

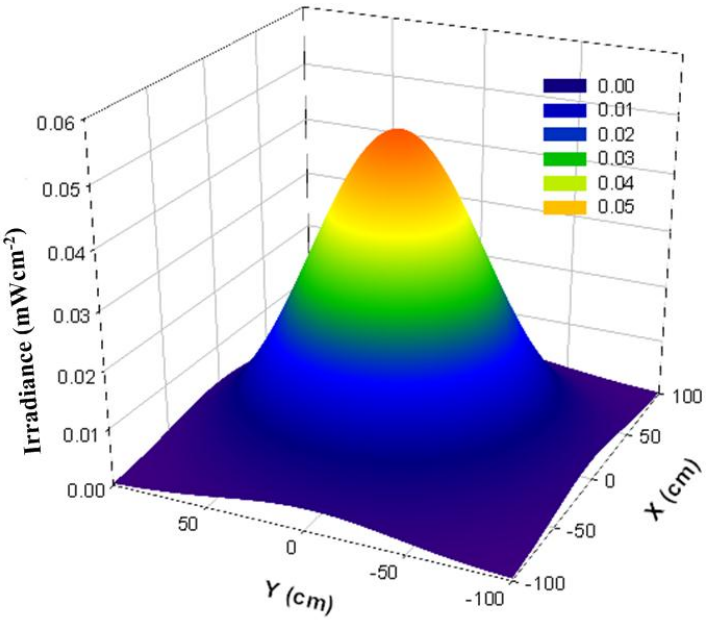

Fig. 8.40. *Irradiance distribution pattern in terms of Cartesian coordinates (x, y, z) for light source (4 LED engines) with z = 200 cm (Method A_1).*

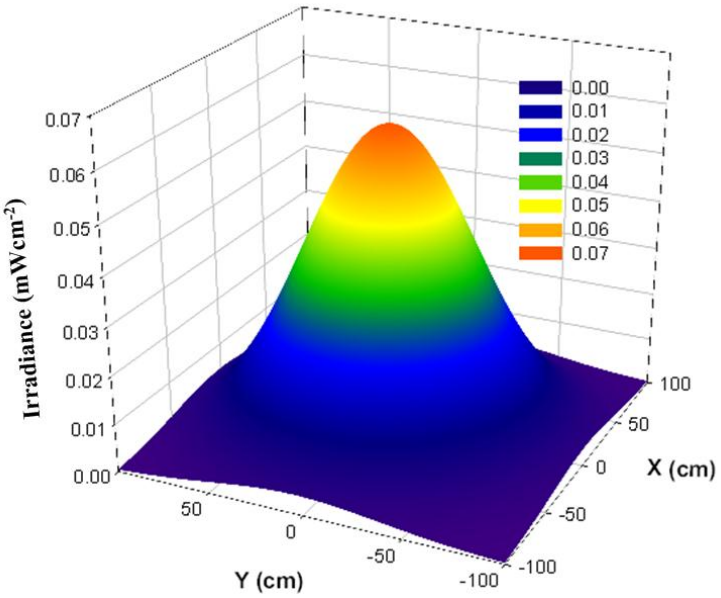

Fig. 8.41. *Irradiance distribution pattern in terms of Cartesian coordinates (x, y, z) for light source (4 LED engines) with z = 200 cm (Method A_2).*

When the three-dimensional profiles using method A_1 and method A_2 are compared, they were not only different in peak irradiance but also different with regard to the irradiance distribution pattern across a horizontal surface in the illuminated area. This result is readily clarified when the measured irradiance for each individual LED are compared. Method A_1 produced an irradiance less than method A_2, due to differences in the voltage input to the LED array driver. However in method A_1 current was split between all 4 LED engines (with light output blocked from 3 of these) whereas with method A_2 all of the current was flowing to one engine (as the other 3 were turned off) and this resulted in the higher output irradiances observed with method A_2.

To analysis which mathematical model (Eq. (8.11)) using either method A_1 or method A_2 can be used to predict and estimate the irradiance distribution profile from the light source in terms of Cartesian coordinates (x, y, z), two-dimensional cross-sections for all three-irradiance profiles are compared for both the experimental data and the mathematical model. Comparative data of the irradiance distributions in two-dimensional profiles for all data are displayed in Fig. 8.42 and

Fig. 8.43. Fig. 8.42 and Fig. 8.43 show comparative data of the irradiance distribution when the space distance between the light source and illuminated area (z) were 100 and 200 cm, respectively. The results demonstrate that the curve of the irradiance distribution model using method A_1 was similar to the curve obtained from the experimental data.

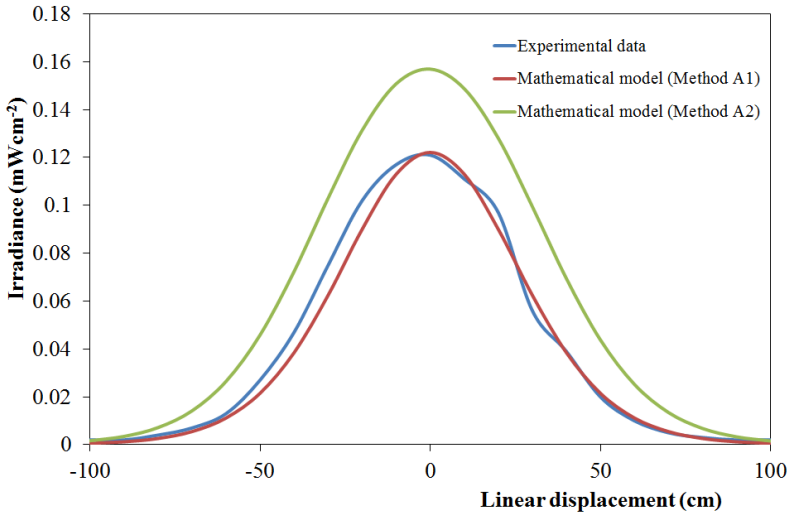

Fig. 8.42. *Comparative data on the irradiance distribution using either the experimental data or the mathematical model when z = 100 cm.*

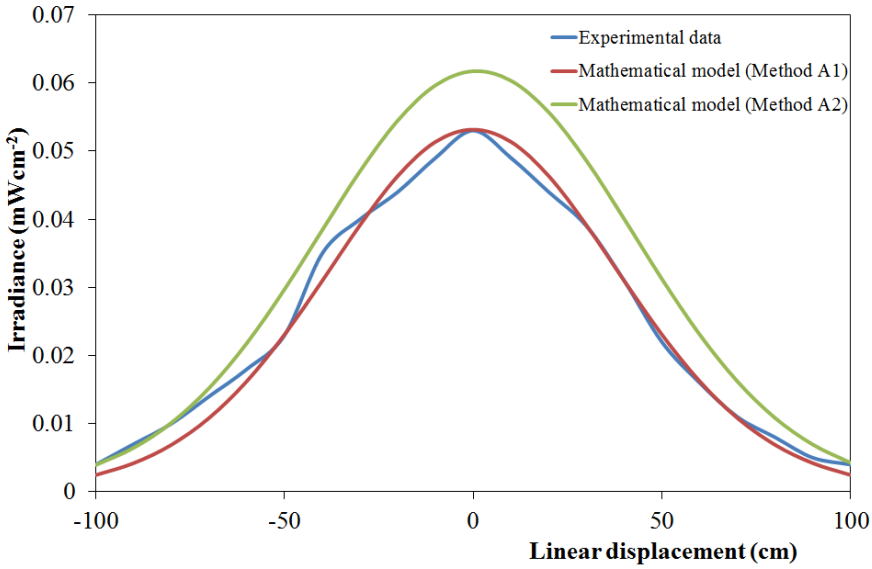

Fig. 8.43. *Comparative data on the irradiance distribution using either the experimental data or the mathematical model when z = 200 cm.*

Having identified that method A_1 gave good performance, the study then investigated the irradiance distribution from the light source with u = 4 and 5 cm and z = 200 cm. Parameters for modelling of irradiance distribution are summarised in Table 8.7.

Table 8.7 *Parameters for modelling of the light source with z = 200 cm*

Light source	***u* = 4 cm, *d* = 30 cm, *m* = 7.4**	***u* = 5 cm, *d* = 30 cm, *m* = 9.91**
	E_0 (mWcm^{-2})	**E_0 (mWcm^{-2})**
LED_1	0.111	0.142
LED_2	0.096	0.141
LED_3	0.109	0.139
LED_4	0.105	0.125

The irradiance distribution as a function of linear displacement for the mathematical model are displayed in Fig. 8.44 and Fig. 8.45. Results demonstrate that the irradiance distribution profile in terms of Cartesian coordinates (x, y, z) for the light system with u = 4 cm or u = 5 cm gave similar results to the profile that resulted from the experimental data.

The Two-dimensional cross section of the curve was used to analysis the similarity between the experimental data and the mathematical model (Eq. 8.11) from the irradiance distribution profile in terms of Cartesian coordinates (x, y, z). The two-dimensional cross sections of the irradiance distribution curves, as shown in Fig. 8.46 and Fig. 8.47, indicate the similarity between the experimental data and the mathematical model. The mathematical model (Eq. 8.11) produced a distribution of light irradiance which fits the experimental data.

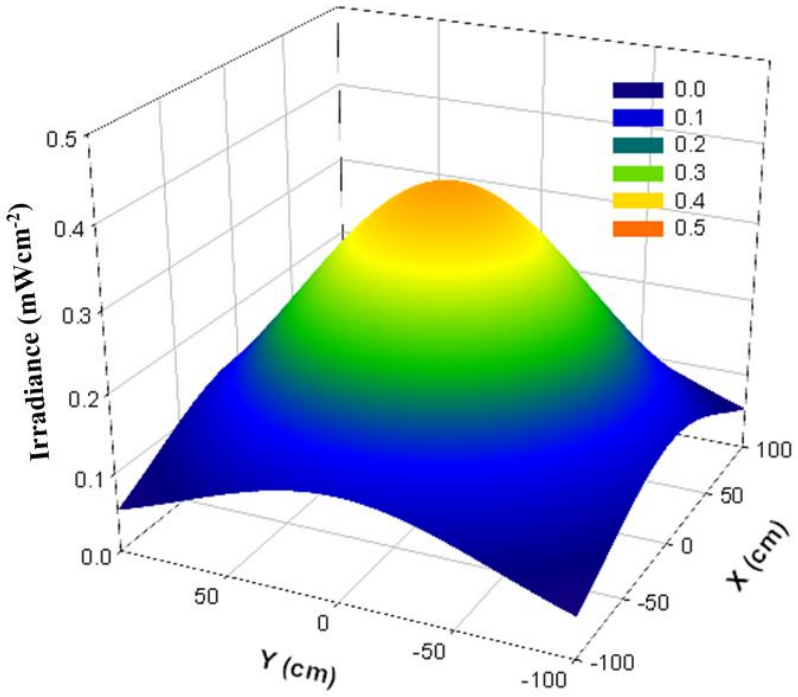

Fig. 8.44. *Irradiance distribution pattern in terms of Cartesian coordinates (x, y, z) for light source (4 LED engines) with u = 4 cm and z = 200 cm (Method A_1).*

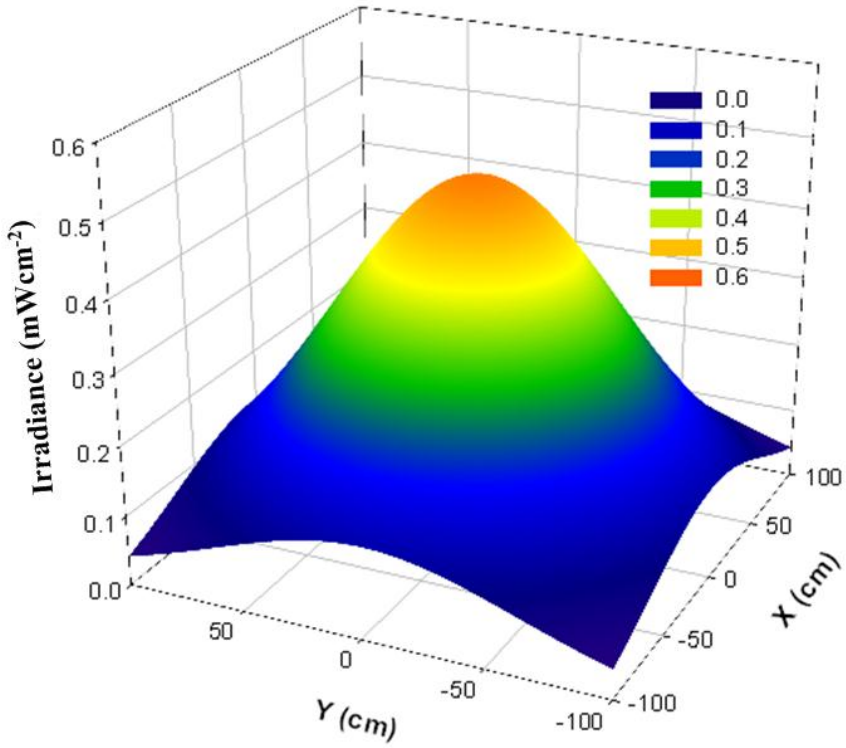

Fig. 8.45. *Irradiance distribution pattern in terms of Cartesian coordinates (x, y, z) for light source (4 LED engines) with u = 5 cm and z = 200 cm (Method A_1).*

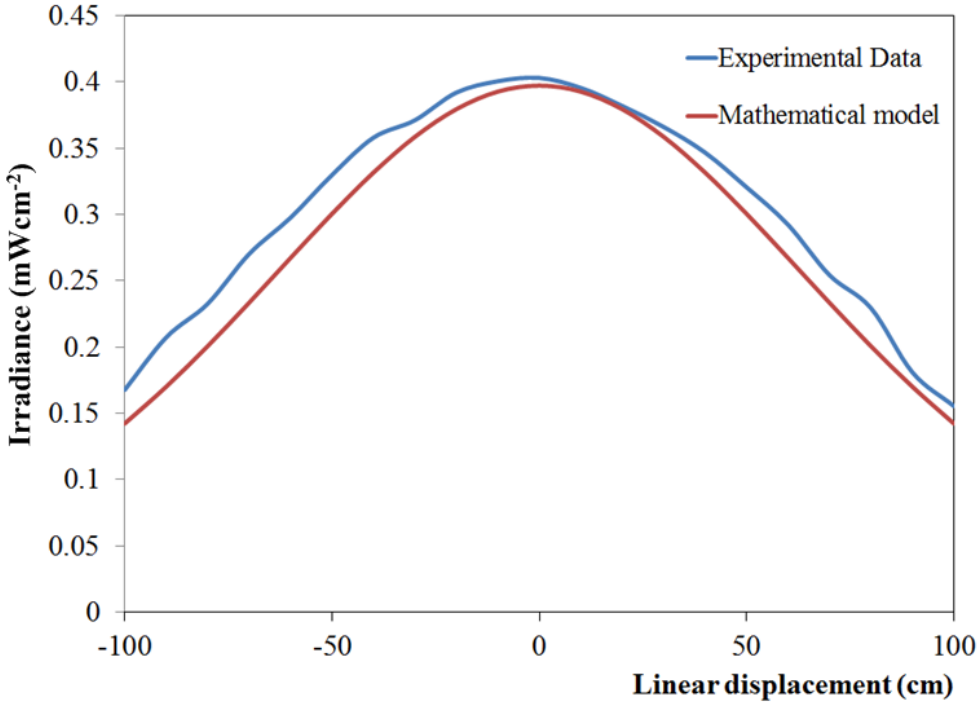

Fig. 8.46. *Comparative data for the irradiance distribution using either the experimental data or the mathematical model when u = 4 cm.*

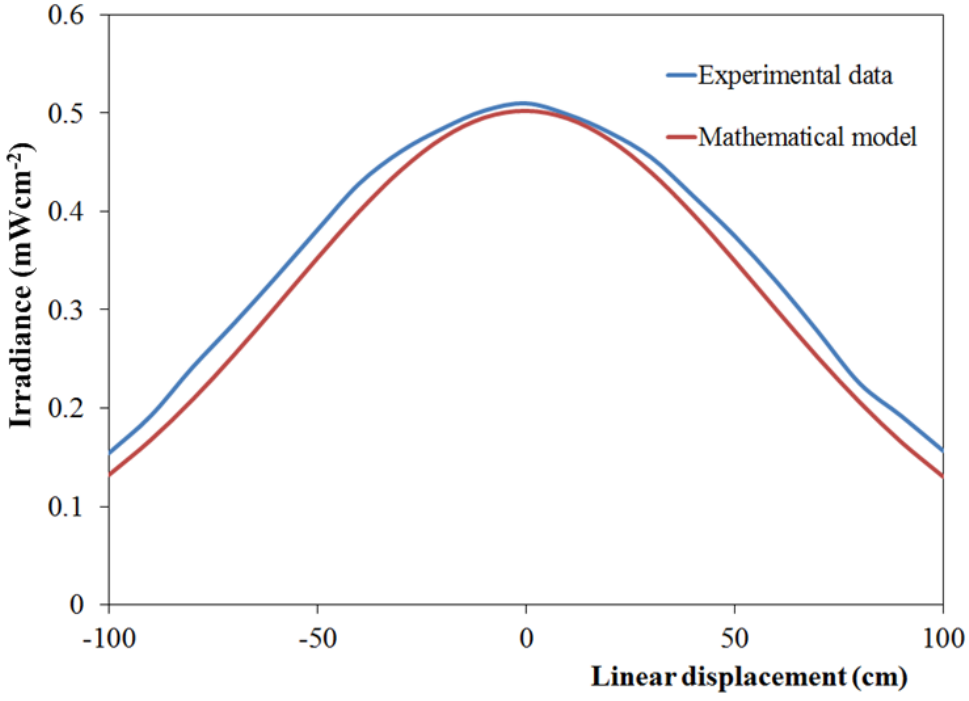

Fig. 8.47. *Comparative data for the irradiance distribution using either the experimental data or the mathematical model when u = 5 cm.*

The normalised cross correlation (NCC) and the RMS error have been used to determine the similarity and accuracy between the experimental data and the mathematical model (Eq. (8.11)) when both of them are compared. Data obtained from calculation of the NCC and the RMS error using either method A (u = 7.5 cm) or method B (z = 200 cm), as presented in Table 8.8 and Table 8.9, gives enough evidence that the mathematical model could be used to quickly predict and estimate the irradiance distribution pattern from the light source with values > 99% for the NCC and < 5% for the RMS error.

Table 8.8 *Summary data obtained from calculation of the NCC and RMS error for method A (When the experimental data and mathematical model 1 are compared)*

***z* (cm)**	**NCC (%)**	**RMS error (%)**
100	99.47	4.37
200	99.65	3.60

Table 8.9 *Summary data obtained from calculation of the NCC and RMS error for method B*

***u* (cm)**	**NCC (%)**	**RMS error (%)**
4	99.44	4.71
5	99.88	3.72

8.7.5 A study of three-dimensional surface fitting using Gauss2D model

8.7.5.1 Method

As described in Section 8.7.3.2, irradiance distribution profiles that obtained from experimental data follow a Gaussian distribution curve. In order to determine whether the profile of the experimental data obtained in this study has a Gaussian distribution pattern, three-dimensional surface fitting using the Levenberg-Marquardt iterative algorithm with Gauss2D model was used, as illustrated in Fig. 8.48 [188,

193]. Calculation of the similarity between the experimental and the mathematical model (Eq. (8.13)) has been calculated by the Gaussian surface [194]:

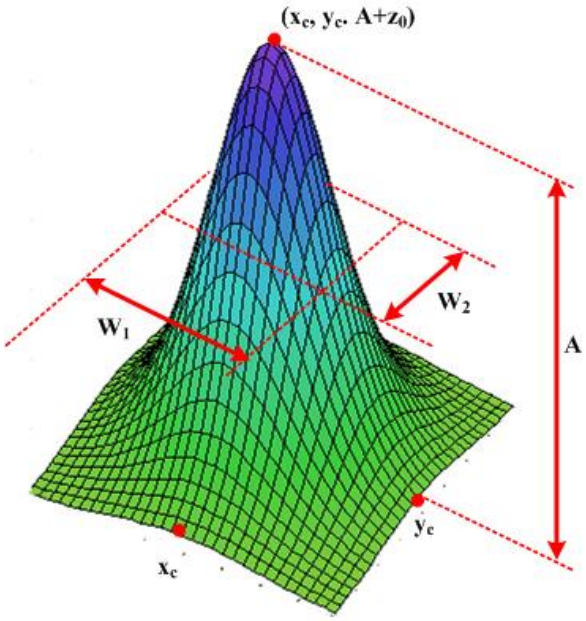

Fig. 8.48. *Sample curve for 3D surface fitting using Gauss2D model (Adapted from [194]).*

$$z = z_0 + A\exp\left\{-\frac{1}{2}\left(\frac{x-x_c}{w_1}\right)^2 - \frac{1}{2}\left(\frac{y-y_c}{w_2}\right)^2\right\}, \tag{8.13}$$

where,

z_0 = z offset ($mWcm^{-2}$),

A = height ($mWcm^{-2}$),

x_c = x centre (cm),

y_c = y centre (cm),

w_1 = x width (cm),

w_2 = y width (cm).

8.7.5.2 Results

Parameters and statistical analysis of three-dimensional surface fitting for the experimental data from Section 8.3.2 using method 1 with z = 100 and 200 cm are

presented in Table 8.10. Meanwhile, three-dimensional surface fitting for the experimental data using method 2 with u = 4 and 5 cm are summarised in Table 8.11.

As shown in Table 8.10 and Table 8.11, overall the study has demonstrated that the three-dimensional curve of the experimental data could be analysed using the three-dimensional surface fitting using the Gauss2D model, with a value of R^2 close to 1 and a small value of Residual Sum of Square (RSS). The irradiance distribution of the light source was uniform in all directions, with a value of w_1 near to w_2.

Table 8.10 *Parameters and statistical analysis resulting from three-dimensional surface fitting using Gauss2D model for method 1*

Parameter	z = 100 cm		z = 200 cm	
	Value[$]	Standard error	Value[$]	Standard error
z_0	0.0017	1.46E-04	0.002	1.05E-04
A	0.1238	7.23E-04	0.052	2.23E-04
x_c	-6.0203	0.15336	-7.955	0.16959
w_1	26.2617	0.16527	39.416	0.22168
y_c	-1.1939	0.15376	-2.457	0.16654
w_2	26.3305	0.16572	38.745	0.21859
Statistical analysis	**Value**		**Value**	
[+]Degrees of freedom	435		435	
[++]Reduced Chi-square	5.67E-06		1.17E-06	
[+++]RSS	2.47E-03		5.11E-04	
[*]R-Square	0.99085		0.99311	
[**]Adjusted R-Square	0.99074		0.99303	
[***]Root-MSE	0.00238		0.00108	

[+]Degree of freedom (*df*) = the number of values in the final calculation of a statistic that are free to vary [195].

[++] Reduced Chi-square (χ^2_{red}) value, which equals to the residual sum of square divided by the degree of freedom [194].

[+++]Residual Sum of Square (RSS) = calculation of the difference between the experimental data and mathematical model. A small value of RSS demonstrates that the experimental data close to the mathematical model.

[*]R-square (R^2) close to 1 indicates that the fit is a good. Value of R^2 should in the range 0 – 1.

**Adjusted R-square $= 1 - \frac{RSS/df_{error}}{TSS/df_{error}}$, where TSS = the total sum of square. The number should be near 1, indicates that the fit is a good.

***Root-Mean Square error or Standard deviation = $\sqrt{\text{Reduced Chi-square}}$.

[$] Units, see Eq. (8.13).

Table 8.11 *Parameters and statistical analysis resulting from three-dimensional surface fitting using Gauss2D model for method 2*

Parameter	u = 4 cm		u = 5 cm	
	Value[$]	Standard error	Value[$]	Standard error
z_0	-0.01862	0.00371	-0.00723	0.00314
A	0.42085	0.00325	0.5157	0.00266
x_c	-2.20319	0.14751	-1.06269	0.15496
w_1	75.45048	0.63973	64.20585	0.45845
y_c	-1.50944	0.14134	-1.85279	0.15133
w_2	73.33274	0.62583	63.04784	0.45288
Statistical analysis	**Value**		**Value**	
Degrees of Freedom	435		435	
Reduced Chi-Square	4.07E-05		8.24E-05	
RSS	0.01772		3.59E-02	
R-Square	0.99514		0.99473	
Adjusted R-Square	0.99509		0.99467	
Root-MSE	0.00638		0.00908	

[+]Degree of freedom (*df*) = the number of values in the final calculation of a statistic that are free to vary [195].

[++] Reduced Chi-square (χ^2_{red}) value, which equals to the residual sum of square divided by the degree of freedom [194].

[+++]Residual Sum of Square (RSS) = calculation of the difference between the experimental data and mathematical model. A small value of RSS demonstrates that the experimental data close to the mathematical model.

[*]R-square (R^2) close to 1 indicates that the fit is a good. Value of R^2 should in the range 0 – 1.

**Adjusted R-square $= 1 - \frac{RSS/df_{error}}{TSS/df_{error}}$, where TSS = the total sum of square. The number should be near 1, indicates that the fit is a good.

***Root-Mean Square error or Standard deviation = $\sqrt{\text{Reduced Chi-square}}$.

[$] Units, see Eq. (8.13).

8.7.6 A study of angular distribution pattern for the new prototype HINS-light EDS

Fig. 8.49 shows the experimental setup for determining angular distribution and all data were measured using a radiant power meter. As an initial position the detector (radiant power meter) was placed at *r* (cm) and 0° below the system where *r* can be adjusted in the range 30 – 200 cm. Furthermore, the detector was moved every 10 ±

2° for each independent experiment until 90°. The experiment was then repeated for angular displacement in the range 0° to -90°.

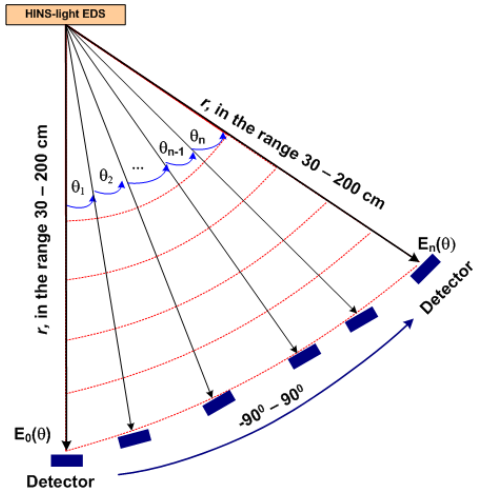

Fig. 8.49. *Experimental setup for determining angular distribution of the new HINS-light EDS*

The angular distributions of the HINS-light EDS system developed in the present study are displayed in Fig. 8.50 and Fig. 8.51. Fig. 8.50 is the angular distribution in the form of a polar plot while Fig. 8.51 represents irradiance distribution as a function of angular displacement.

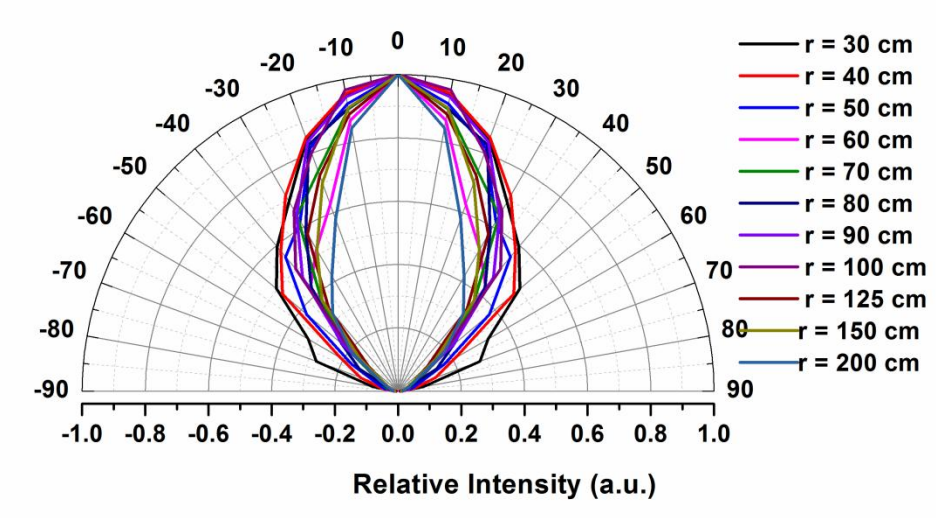

Fig. 8.50. *Angular distribution of the new prototype HINS-light EDS in the form of a polar plot.*

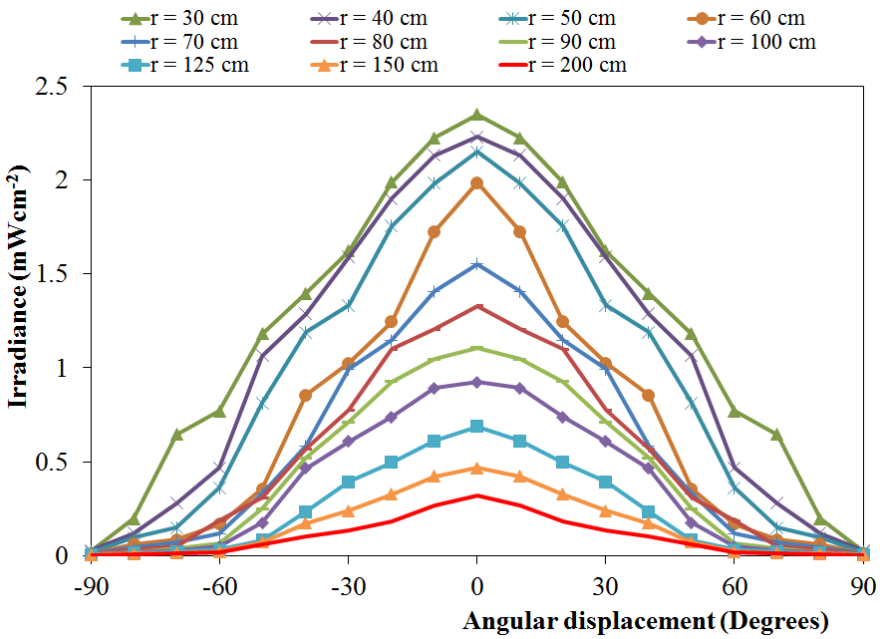

Fig. 8.51. *Irradiance distribution as a function of angular displacement for the new prototype HINS-light EDS.*

All light distribution patterns radiated from the HINS-light EDS spreading above 40° on the illuminated area (Fig. 8.50), provides information that the light distribution is spread widely enough to cover an illuminated area of 200 cm radius. This confirmed that the new HINS-light EDS had a wide spread of light distribution; this is an important factor for practical applications of the environmental decontamination system.

8.8 An analytical study of thermal management options

As described in Section 8.3.1, to ensure that the system did not generate dominant violet illumination but produced more normal room lighting, 12 high power white-light LEDs, with typical light output of 3 W for each individual white LEDs, were incorporated into the design of HINS-light EDS. When the white LEDs were added to the light source to produce more conventional room lighting this also resulted in more heat production. The aim of this section focuses on an analytical study of

thermal management options for the white LEDs used in the light source. The main aspect involved determining the heat sink requirements for the white LEDs.

8.8.1 Basic theory of thermal resistance for determining heat sink usage

"Heat sinks are devices that enhance heat dissipation from a hot surface, usually the case of a heat generating component, to a cooler ambient, usually air" [196]. The fundamental calculation of heat transfer is illustrated in Fig. 8.52, with T_c and T_s being the case temperature (°C) and sink temperature (°C), respectively. According to ALTERA, "Thermal resistance is the measure of a substance's ability to dissipate heat, or the efficiency of heat transfer across the boundary between different media" [197]. Thermal resistance has been calculated using Eq. (8.14) for determining heat sink usage [196-198].

$$R_{sa} = \frac{T_j - T_a}{Q} - \left(R_{jc} + R_{cs}\right), \tag{8.14}$$

where,

Q = total power or rate of heat dissipation in W,

T_j = maximum junction temperature of the device in °C,

T_a = ambient air temperature in °C,

R_{jc} = thermal resistance, junction to case in °CW^{-1},

R_{cs} = thermal resistance, case to heat sink in °CW^{-1},

R_{sa} = thermal resistance, heat sink to ambient in °CW^{-1}.

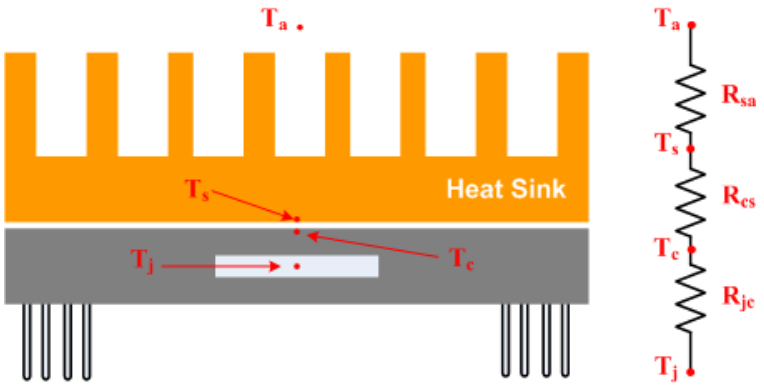

Fig. 8.52. *Thermal resistance circuit model (Adapted from [196]).*

8.8.2 Calculation of thermal resistance for determining heat sink usage

Parameters used for the calculation of thermal resistance were obtained from the datasheet of the White LED and adhesive thermal pad (Fig. 8.53) and these are summarised in Table 8.12 [190, 199].

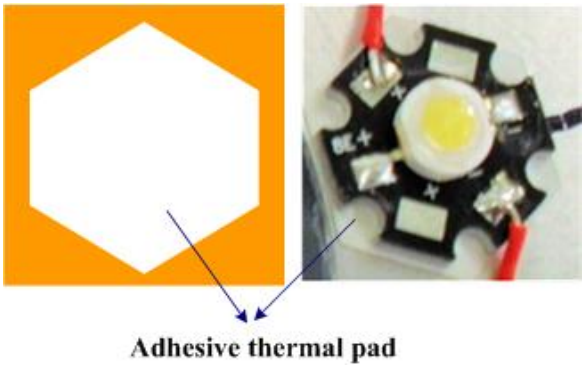

Fig. 8.53. *Adhesive thermal pad used.*

Table 8.12 *Parameters for calculation of thermal resistance to determine heat sink requirements*

Parameter	Value	Reference
T_j	125 °C	[190]
T_a	25 °C	[190]
R_{jc}	8 °CW^{-1}	[190]
R_{cs}	0.49 °CW^{-1}	[199]
Forward Voltage	3.8 V	[190]
Forward Current	700 mA	[190]

For 12 white LEDs, thermal resistance junction to case (R_{jc}) can be calculated:

$$R'_{jc} = \frac{R_{jc}}{Number\ of\ \ white\ LED} = \frac{8\ °CW^{-1}}{12} = 0.67\ °CW^{-1}, \tag{8.15}$$

and total power or rate of heat dissipation (Q):

$$Q = 12 \times 3.8V \times 0.7\,A = 31.92W \tag{8.16}$$

Using data obtained from Table 8.12 and combining Eq. (8.14), (8.15) and (8.16), thermal resistance for heat sink to ambient can be calculated as follows:

$$\begin{aligned} R_{sa} &= \frac{T_j - T_a}{Q} - \left(R'_{jc} + R_{cs} \right) \\ &= \frac{125\,°C - 25\,°C}{31.92\,W} - \left(0.67\,°CW^{-1} + 0.49\,°CW^{-1} \right) \\ &= 1.97\,°CW^{-1}, \end{aligned} \tag{8.17}$$

To determine the best heat sink for designing the HINS-light EDS especially for the white LEDs, it was considered that the heat sink will work most effectively when the thermal resistance R_{sa} is less than the required 1.97 °CW^{-1}.

The heat sink used in the study was aluminium plate with a dimension 53 × 53 cm and 2 mm of thickness (Fig. 8.54). The thermal conductivity of the aluminium plate was 237 $Wm^{-1}K^{-1}$ [200]. For aluminium plate with thermal conductivity k ($Wm^{-1}K^{-1}$), area of plate A (m^2) and thickness L (m), thermal conductance in WK^{-1} (equivalent to: W°C^{-1}) can be calculated with Eq. (8.18).

$$\begin{aligned} \text{Thermal conductance} &= \frac{kA}{L} = \frac{237\ \text{Wm}^{-1}\text{K}^{-1} \times 0.2809\ \text{m}^2}{2\times10^{-3}\text{m}} \\ &= 33287.7\ \text{WK}^{-1} = 33287.7\,W°C^{-1}. \end{aligned} \tag{8.18}$$

The thermal resistance is defined as 1/Thermal conductance; therefore, Eq. (8.18) can be rewritten,

$$\text{Thermal resistance} = \frac{1}{\text{Thermal conductance}} = 3.0\times10^{-5}\,°CW^{-1}. \tag{8.19}$$

If the results obtained from Eq. (8.19) and Eq. (8.17) are compared, the thermal resistance obtained by Eq. (8.19) is less than by Eq. (8.17). This confirms that the heat sink which has been selected satisfies the criteria of a heat sink for the HINS-light EDS system.

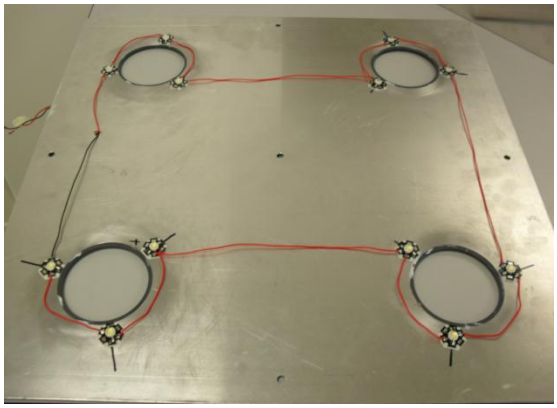

Fig. 8.54. *Heat sink used for thermal management of the white LEDs.*

Monitoring of the surface temperature when all twelve white LEDs were switched ON for 3 x 24 hours, showed that the temperature was in the range 37 – 40 °C. According to an operational time for the HINS-light EDS in the hospital environment (switched on for 10 hours/day) the results show that the heat produced by the white LEDs is controlled by the heat sink and will therefore not generate detrimental effects on the HINS-light EDS system.

8.9 Conclusions

A new design for the HINS-light EDS has been developed and its irradiance distribution has been studied. Optimal parameters for designing and developing have been established including: the Lambertian mode number (m), configuration of the Fresnel lens and diffuser, space distance between the light engines (LEDs), Fresnel lens and diffusers, and topology of the light engines.

A mathematical model (Eq. (8.11)) which allows analysis of the light distribution from a square LED array topology has been successfully developed, with results proving that intensity distribution of the system is in good agreement with experimental data. The comparison between the mathematical model and the experimental data show that the NCC is greater than 99% and the RMS error is less than 5%. Analysis of thermal management options showed that the heat sink chosen has the ability to keep the white LEDs working in ideal thermal conditions. Comparison of the initial HINS-light EDS prototype with the new upgraded prototype will be discussed in Chapter 9.

CHAPTER 9

DESIGN OF THE HINS-LIGHT ENVIRONMENTAL DECONTAMINATION SYSTEM

9.1 General

Following establishment of the optimal parameters for the HINS-light EDS – which included configuration of the Fresnel lens and diffuser (type 4), the distance between the light source and the lens system, and the optimal LED-to-LED array spacing – the practical design of the new HINS-light EDS prototype has been completed. The present chapter describes the work on the design and construction of this new prototype and consists of two main parts. Part I describes the electrical and mechanical design and construction, as well as the controllability features of the new HINS-light EDS. A comparison of the initial ROLEST HINS-light EDS prototype and the prototype designed and developed in this study is also presented. In Part II, the study was focused on providing a full safety analysis and risk assessment of the new HINS-light EDS prototype.

9.2 Mechanical Design and Configuration

The final design of the new HINS-light EDS prototype is pictured in Fig. 9.1. As described in Chapter 8, the main components of the HINS-light EDS are 405 nm LED light engines and white LEDs covered with a Fresnel lens and diffuser combination. The total irradiance of the HINS-light EDS source is 0.32 $mWcm^{-2}$ at a distance of 200 cm below the system. The total illuminance for the four 405 nm LED engines is 107 lux. By adding white light with an illuminance of 102 lux, the total illuminance of the HINS-light EDS becomes 209 lux. This illuminance is close to illuminance of a typical room lighting source which is between 300 and 500 lux. To

ensure the HINS-light EDS produces white-dominant light and does not generate any disturbing effects; the Fresnel lens and diffuser were used, as shown in Fig. 9.1a. Visual inspection of the light emitted from the new light system (Fig. 9.1a) confirms that the new HINS-light EDS produces light similar with a typical laboratory lighting source. Dimensions of the new HINS-light EDS are shown in Fig. 9.2, Fig. 9.3 and Fig. 9.4.

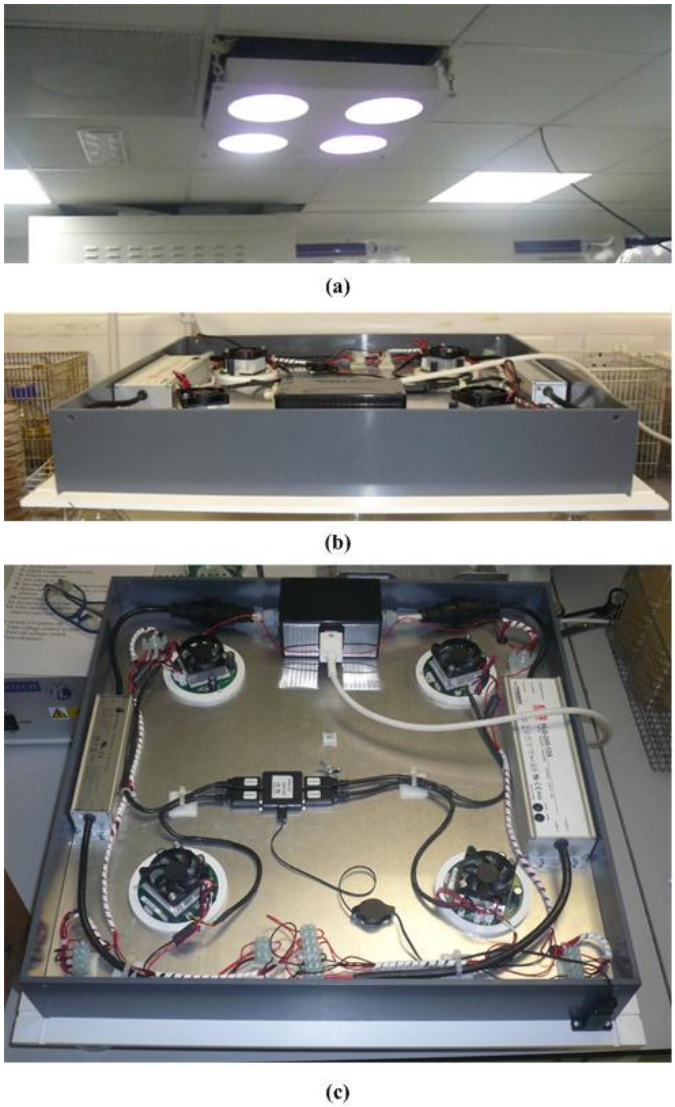

Fig. 9.1. *Photographs of the final design of the new HINS-light EDS prototype, a) suspended from the ceiling, b) side view and c) top view.*

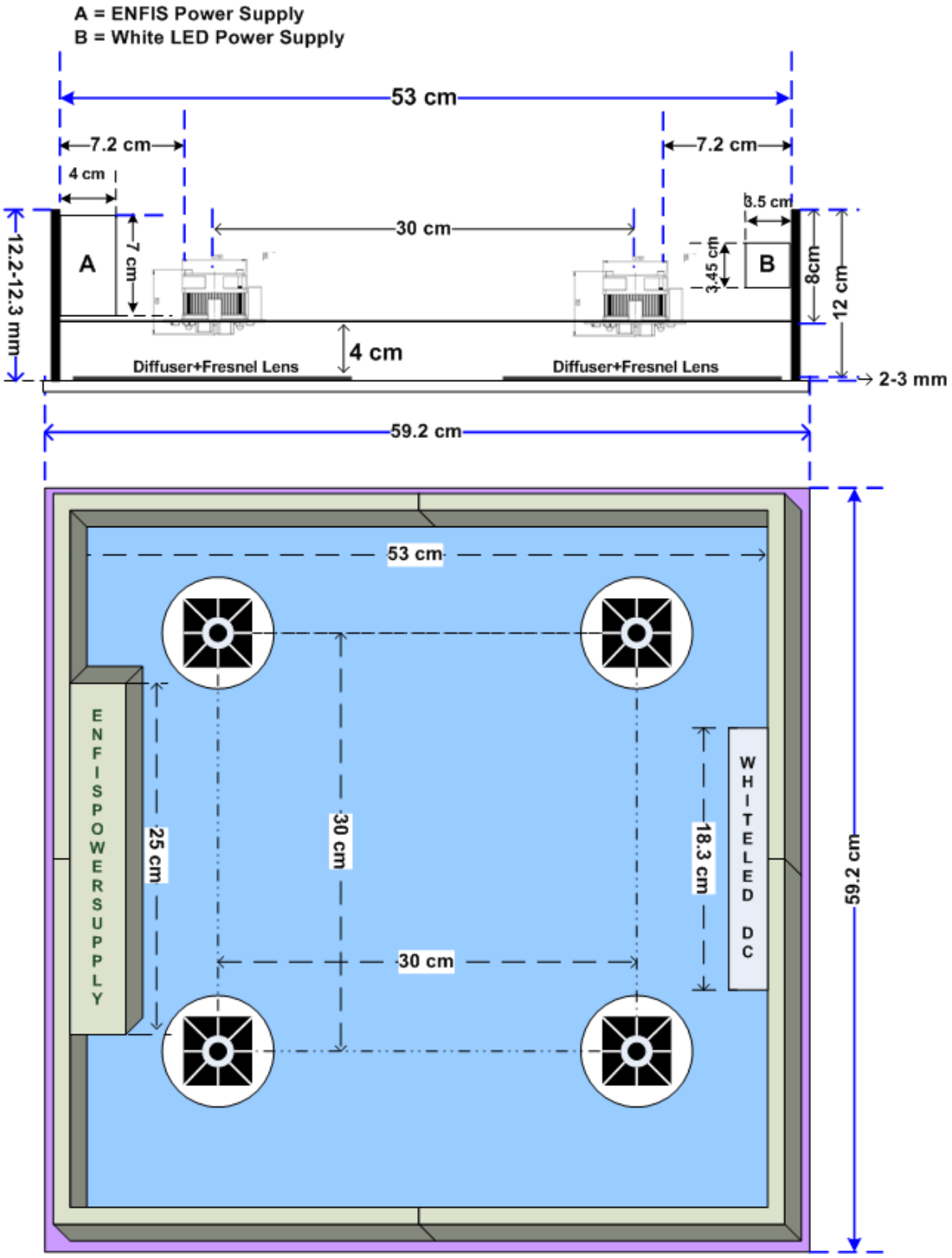

Fig. 9.2. *Schematic diagram of the HINS-light EDS.*

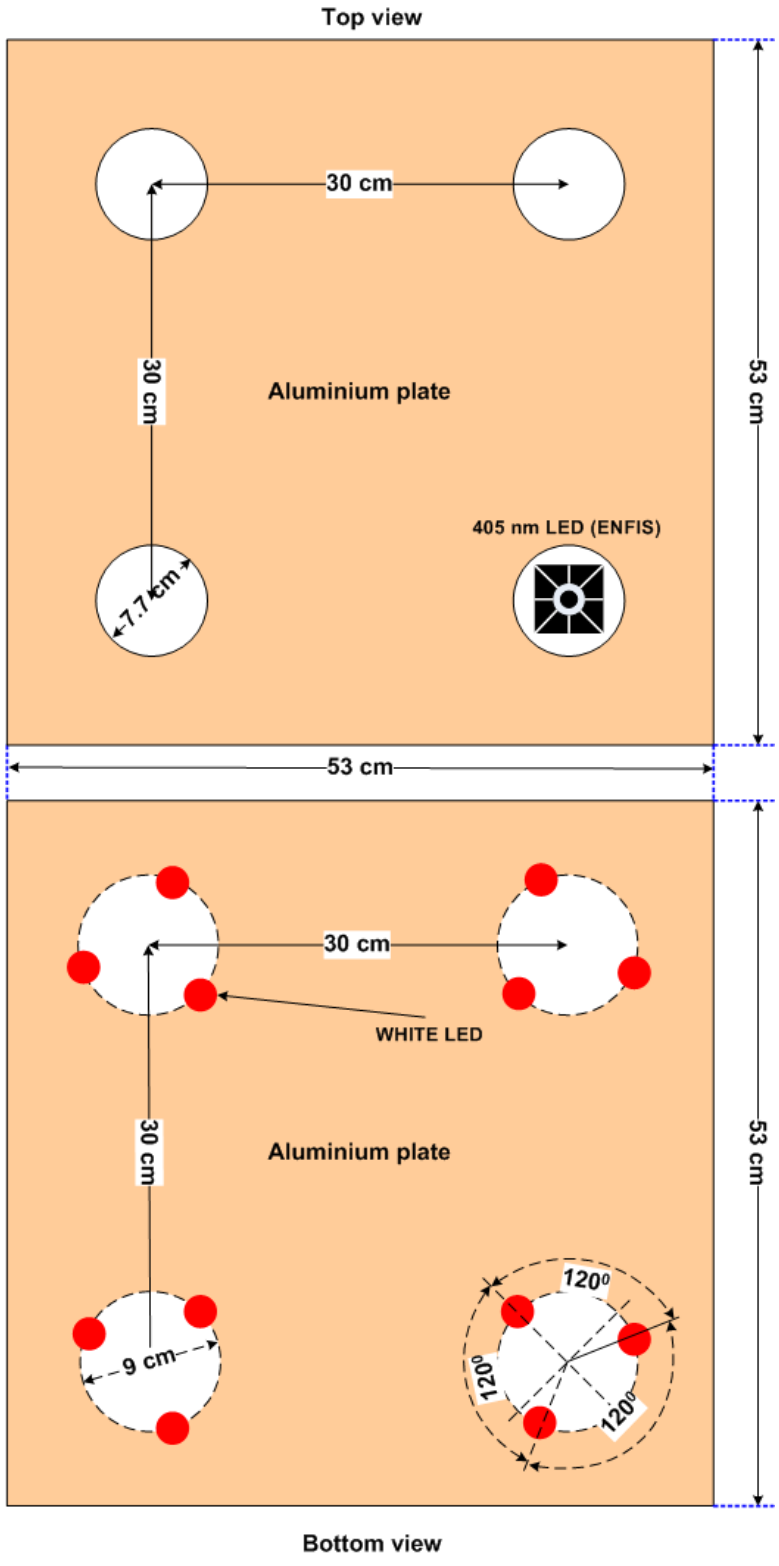

Fig. 9.3. *Dimensions for the 405 nm LED light engines and the white LEDs.*

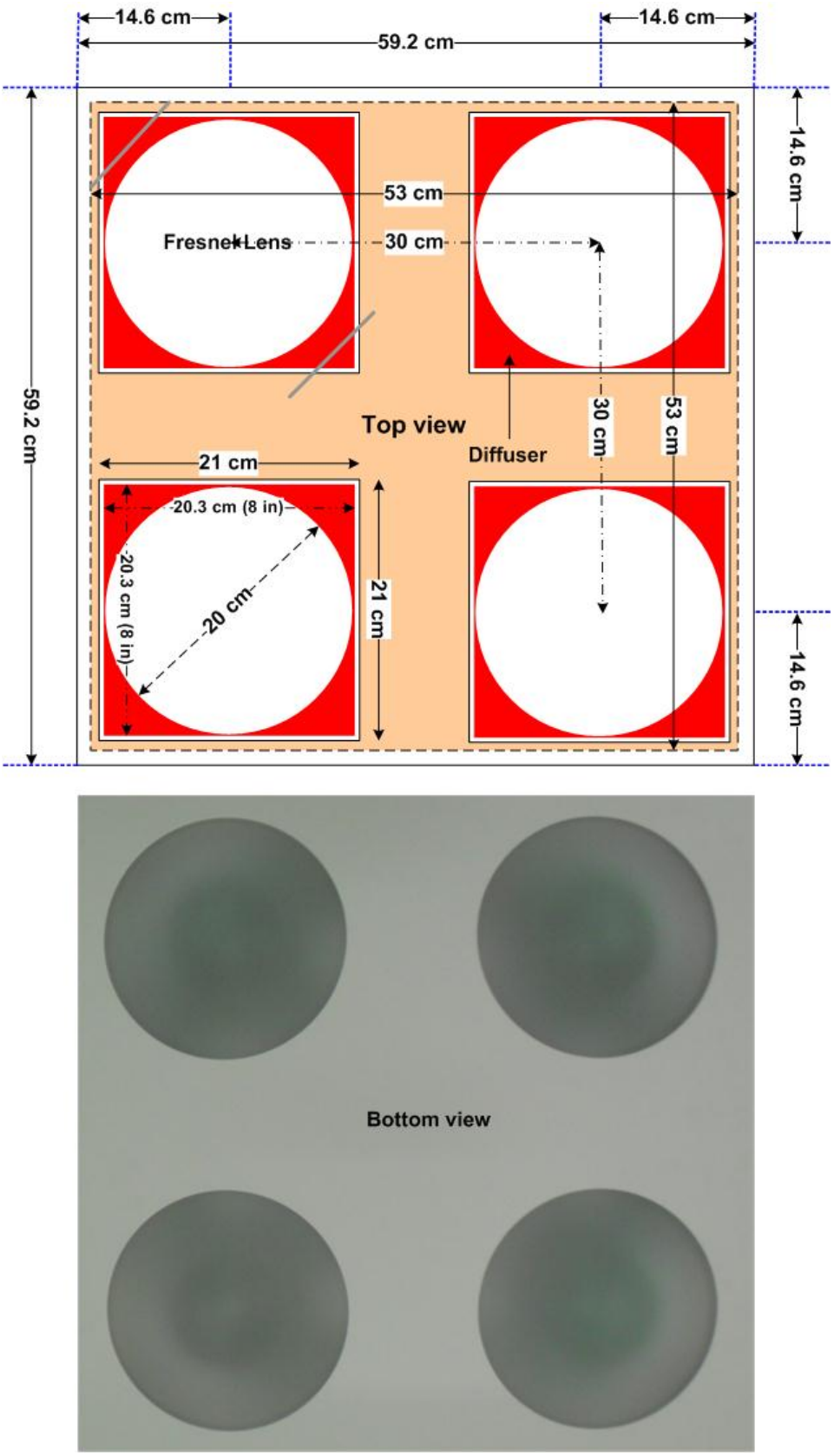

Fig. 9.4. *Dimensions for the Fresnel lens and diffuser.*

9.3 Electrical Design and Configuration

The power supply used to drive the HINS-light EDS was a 240W single output Switching Power Supply (HLG-240-12A) obtained from the Mean Well Direct, UK (Fig. 9.5) [201]. The power supply had an IP65 rated design suitable for LED lighting and moving sign applications [201]. IP65 as defined in the international standard, IEC 60529, indicates that the power supply has a dust proof and water proof design protection to ensure that "water projected by a nozzle against the enclosure from any direction shall have no harmful effects" [201, 202]. The constant voltage output from the power supply was 12 V with a rated power of 192 W and rated current of 16 A [201].

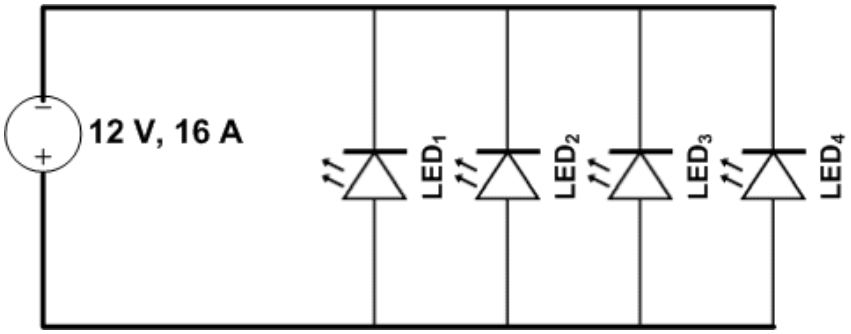

Fig. 9.5. *Circuit diagram to drive the 405 nm LED light engines connected in parallel.*

Fig. 9.6 shows the circuit diagram to driver the white LEDs, the power supply used in the circuit was an LED Power Supply with a constant current of 450 mA, output voltage in the range 33 – 66 V, an IP67 rated design and efficiency of 86% (LXC30-0450S, Excelsys Technologies Ltd., Ireland) [203].

According to IEC 60529, IP67 rated design indicates that the power supply has a dust proof and water proof design to ensure that "ingress of water in harmful quantity shall not be possible when the enclosure is immersed in water under defined conditions of pressure and time (up to 1 m of submersion)" [202].

The total power consumption of the EDS light source including power consumption of the 405 nm LED light engines (set as 100 % intensity output) and the white LEDs is 194 W. The level of intensity of the 405 nm LEDs will be discussed in Section 9.4.

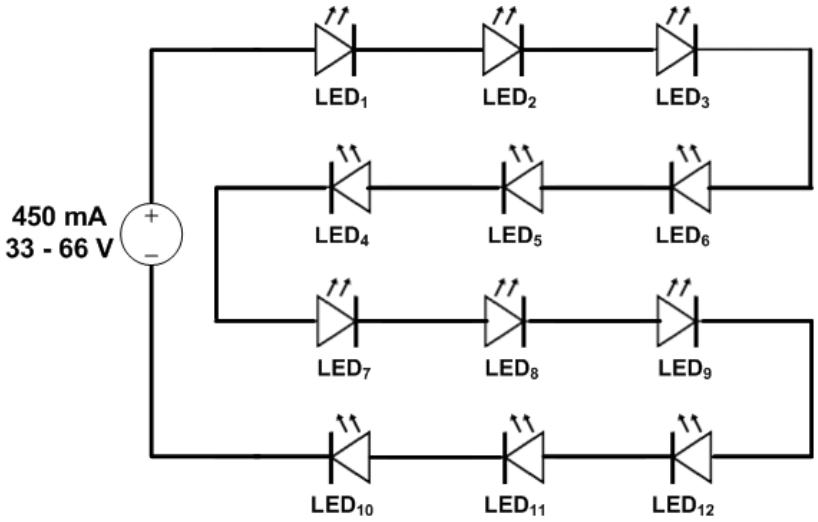

Fig. 9.6. *Circuit diagram to drive the white LEDs in series.*

9.4 System Control

The new HINS-light EDS prototype is equipped with a control system which allows adjustment of each individual 405 nm LED light engine using a PC connected to the 405 nm light engines via a USB cable. The software also allows monitoring of input and output voltage and current, temperature and fan status, as shown in Fig. 9.7 and Fig. 9.8.

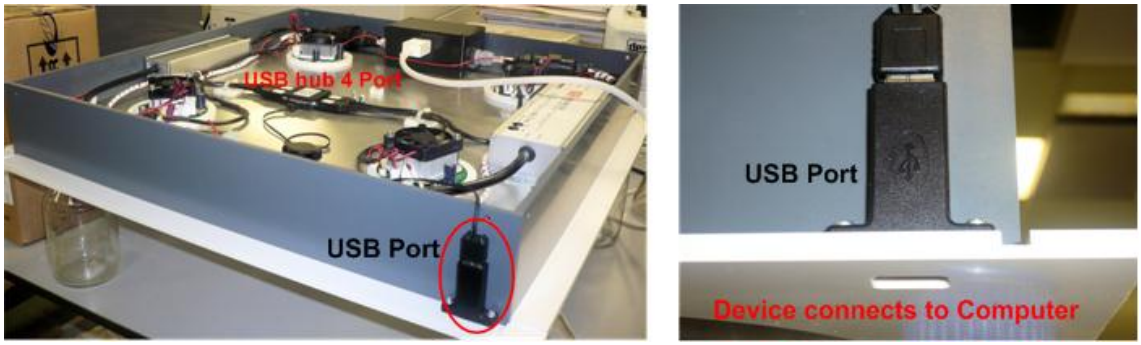

Fig. 9.7. *Photograph of the USB port for controlling and monitoring the 405 nm LEDs.*

Fig. 9.8. *Display of the LE sentinel (V2.2) software on a computer screen. This software is supplied by ENFIS Ltd., UK, for controlling and monitoring the 405 nm LED light engines.*

As displayed in Fig. 9.8, the intensity level for each individual 405 nm LED light engine can be adjusted in the range 0 – 100%. Examples of irradiance ($mWcm^{-2}$) as a function of level (%) for the light source with a value of u = 4, 5 and 7.5 cm are displayed in Fig. 9.9, Fig. 9.10 and Fig. 9.11, respectively. All measured data were taken at a distance of 200 cm below each individual 405 nm LED light engine at a central position (Fig. 8.31). Results demonstrate that when the 405 nm LED light engines are set at the same level (%) they do not provide the same level of irradiance. To ensure that each individual light engine produces irradiance at same level, for example 0.2 $mWcm^{-2}$ (Fig. 9.11), LED_1, LED_2, LED_3 and LED_4 should be adjusted at to give output levels of ~86, ~88, ~95 and ~78%, respectively.

Temperature for each individual 405 nm LED light engine can be monitored. When the temperature reaches a value above 35 °C (Fig. 9.12), the fan attached to the heat sink will start to operate to provide thermal protection. The fan will stop when the temperature decreases to ~32°C. Input voltage, LED current, LED voltage, temperature, light level and fan status can be saved into a file that in the future can be used to analyse what has happened in the system, as shown in Fig. 9.12. Establishing the relationship between the irradiance ($mWcm^{-2}$) and output level (%) for each individual 405 nm LED light engine (Fig. 9.9, Fig. 9.10 and Fig. 9.11),

means that the 405 nm light engine can be set in order to achieve the same irradiance level on the illuminated area to ensure the light distribution is uniform for all directions.

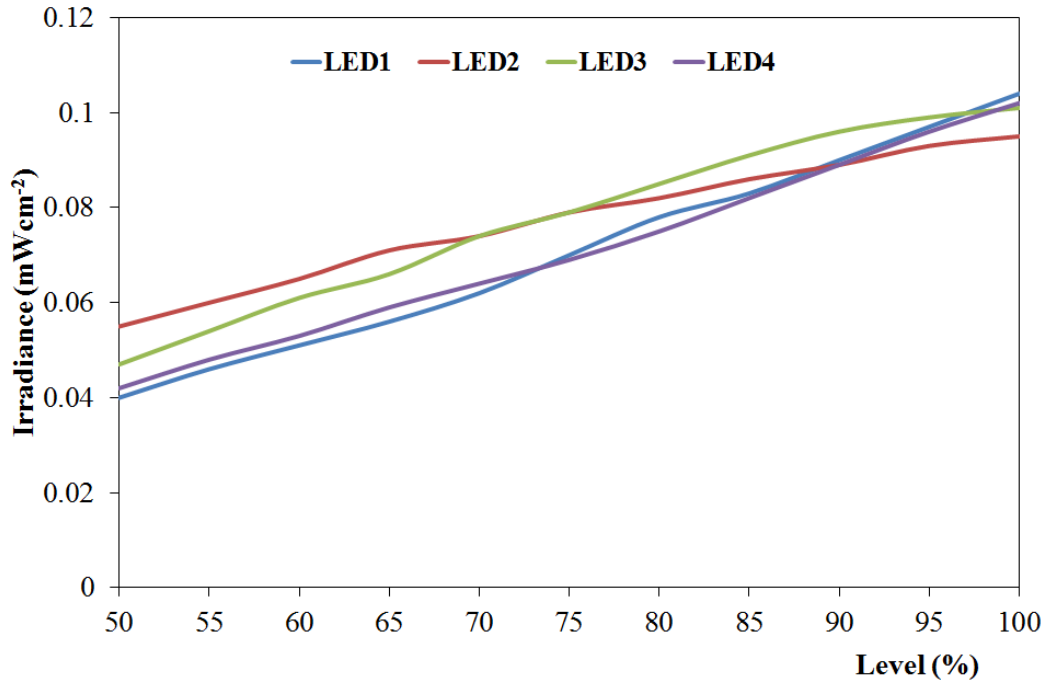

Fig. 9.9. *Irradiance ($mWcm^{-2}$) as a function of level (%) for each individual 405 nm LED light engine when the light system had a value of u = 4 cm.*

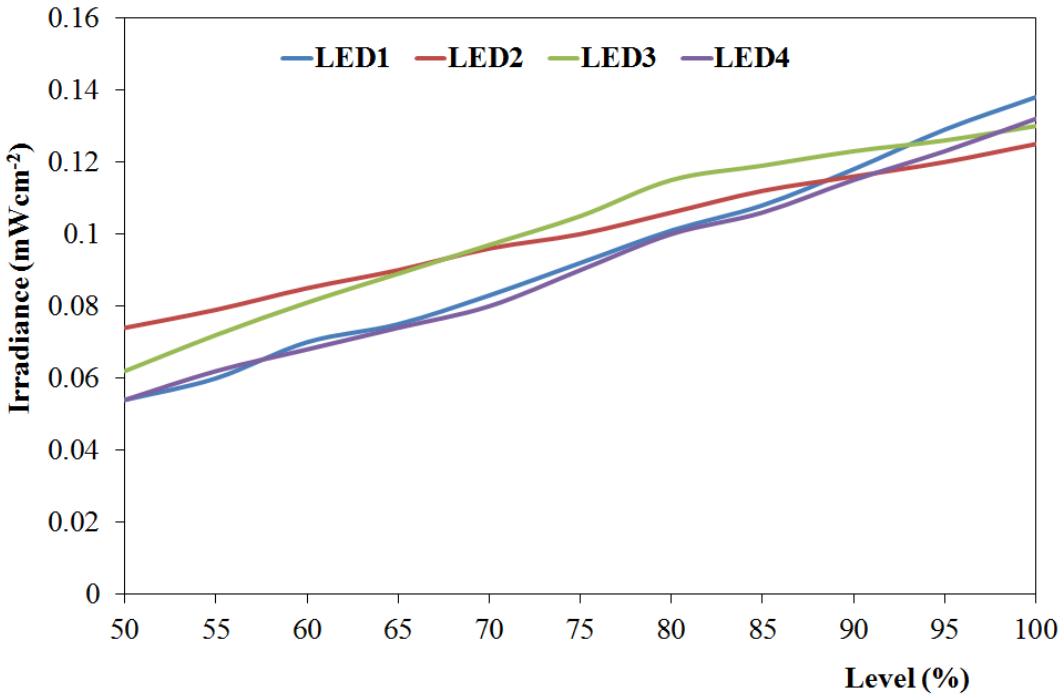

Fig. 9.10. *Irradiance ($mWcm^{-2}$) as a function of level (%) for each individual 405 nm LED light engine when the light system had a value of u = 5 cm.*

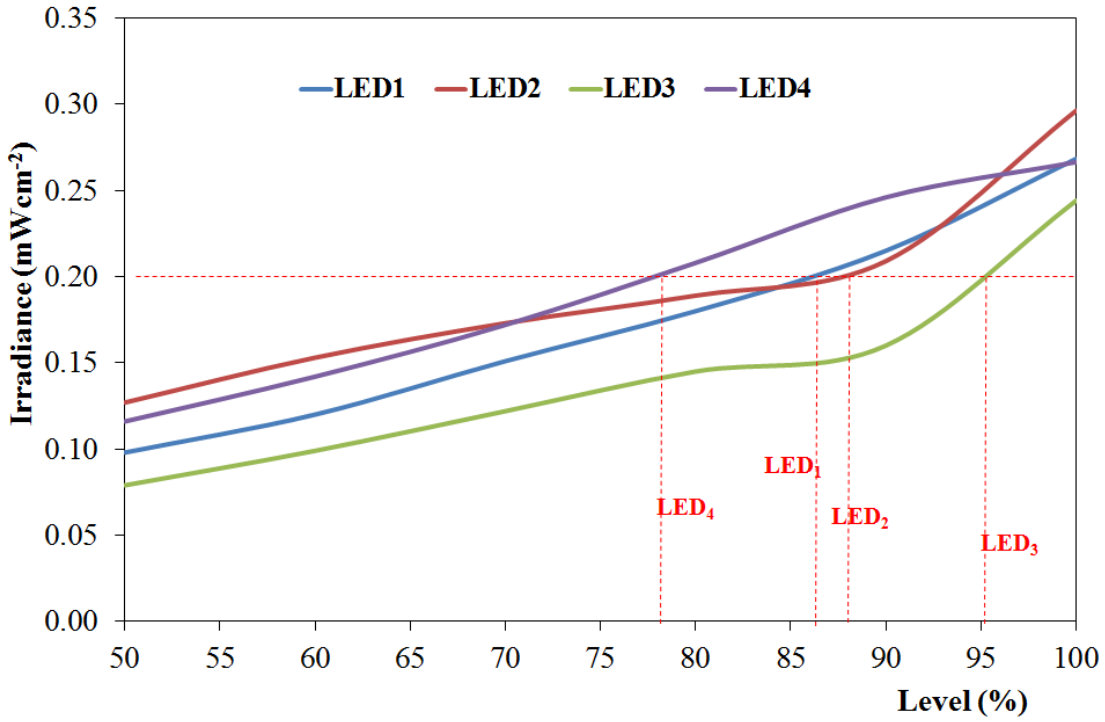

Fig. 9.11. *Irradiance ($mWcm^{-2}$) as a function of level (%) for each individual 405 nm LED light engine when the light system had a value of u = 7.5 cm.*

UAV148R160									
Date/Time	Array Voltage	Array Current	Input Voltage	Temperature	Error	Fan Status	Light Level (mW)	Aux0	Aux1
14/01/2010 09:17	16.19	342	11.87	32.5	None	Off	600.7	N/A	N/A
14/01/2010 09:17	15.78	226	11.98	32.7	None	Off	369.4	N/A	N/A
14/01/2010 09:17	15.78	228	11.98	32.9	None	Off	373.3	N/A	N/A
14/01/2010 09:19	14.34	66	11.87	31.9	None	Off	325	N/A	N/A
14/01/2010 09:19	14.43	198	11.84	32	None	Off	325	N/A	N/A
14/01/2010 09:19	14.79	93	11.39	32.6	None	Off	325	N/A	N/A
14/01/2010 09:20	15.83	237	11.95	34	None	Off	390	N/A	N/A
14/01/2010 09:20	15.74	218	11.92	34.2	None	Off	353.3	N/A	N/A
14/01/2010 09:20	15.74	222	11.81	34.7	None	Off	360.5	N/A	N/A
14/01/2010 09:20	15.74	222	11.95	35.2	None	Off	361.6	N/A	N/A
14/01/2010 09:20	15.74	222	11.9	35.1	None	On	361.1	N/A	N/A
14/01/2010 09:20	15.74	214	11.9	33.9	None	On	344.4	N/A	N/A
14/01/2010 09:21	15.74	209	11.95	32.8	None	On	334.4	N/A	N/A
14/01/2010 09:21	15.74	205	11.78	32.2	None	Off	326.6	N/A	N/A
14/01/2010 09:21	15.74	207	12.01	32	None	Off	330	N/A	N/A
14/01/2010 09:21	15.74	209	11.9	32.8	None	Off	333.8	N/A	N/A
14/01/2010 09:21	15.74	211	11.92	33.2	None	Off	338.8	N/A	N/A
14/01/2010 09:21	15.74	214	12.01	33.4	None	Off	345	N/A	N/A
14/01/2010 09:21	15.74	215	11.9	33.6	None	Off	347.7	N/A	N/A
14/01/2010 09:21	15.74	218	11.98	33.6	None	Off	352.7	N/A	N/A
14/01/2010 09:21	15.74	219	12.06	34.4	None	Off	355.5	N/A	N/A
14/01/2010 09:22	15.74	222	11.9	34.5	None	Off	360.5	N/A	N/A
14/01/2010 09:22	15.74	223	11.98	34.5	None	Off	363.3	N/A	N/A
14/01/2010 09:22	15.74	226	12.01	35.2	None	Off	369.4	N/A	N/A
14/01/2010 09:22	15.74	227	11.95	35.2	None	Off	370.5	N/A	N/A
14/01/2010 09:22	15.74	218	11.95	34.7	None	On	352.2	N/A	N/A
14/01/2010 09:22	15.74	213	11.92	33.4	None	On	342.2	N/A	N/A
14/01/2010 09:22	15.74	204	11.87	32.2	None	On	325	N/A	N/A
14/01/2010 09:22	15.74	205	11.92	32.1	None	Off	326.1	N/A	N/A
14/01/2010 09:23	15.74	209	11.87	32.9	None	Off	334.4	N/A	N/A
14/01/2010 09:23	15.74	208	11.92	32.6	None	Off	333.3	N/A	N/A

Fig. 9.12. *Example of the monitoring data which is recorded for the 405 nm LED light engines. The fan attached to heat sink will start and stop to provide thermal protection when the temperature reaches values of ~35 and ~32 ℃, respectively.*

9.5 A study of light distribution for the new prototype HINS-light EDS

Fig. 9.13, Fig. 9.14, Fig. 9.15 and Fig. 9.16 demonstrate irradiance ($mWcm^{-2}$) as a function of linear displacement (cm) for each individual 405 nm LED light engine with u = 4, 5 and 7.5 cm, respectively. The irradiance was measured at a distance of 1.5 m below the 405 nm light engine (Fig. 8.59), and the power supply to drive the 405 nm light engine was set at 12.0 ± 0.1 V and 3.4 ± 0.1 A. The output intensity level for each of the light sources was 100%.

Overall, these results for all four light engines show that the light distribution had a similar irradiance pattern (Gaussian distribution), with the largest peak irradiance value ($mWcm^{-2}$) registered for u = 7.5 cm and the lowest of the Lambertian mode number (m) registered for u = 4 cm. All parameters obtained in this study are summarised in Table 9.1. As stated in Table 9.1, results show that the highest total power (W) was generated in the system with a value of u = 4 cm. This confirms that the optimal distance between the light source and the lens system (u) is 4 cm.

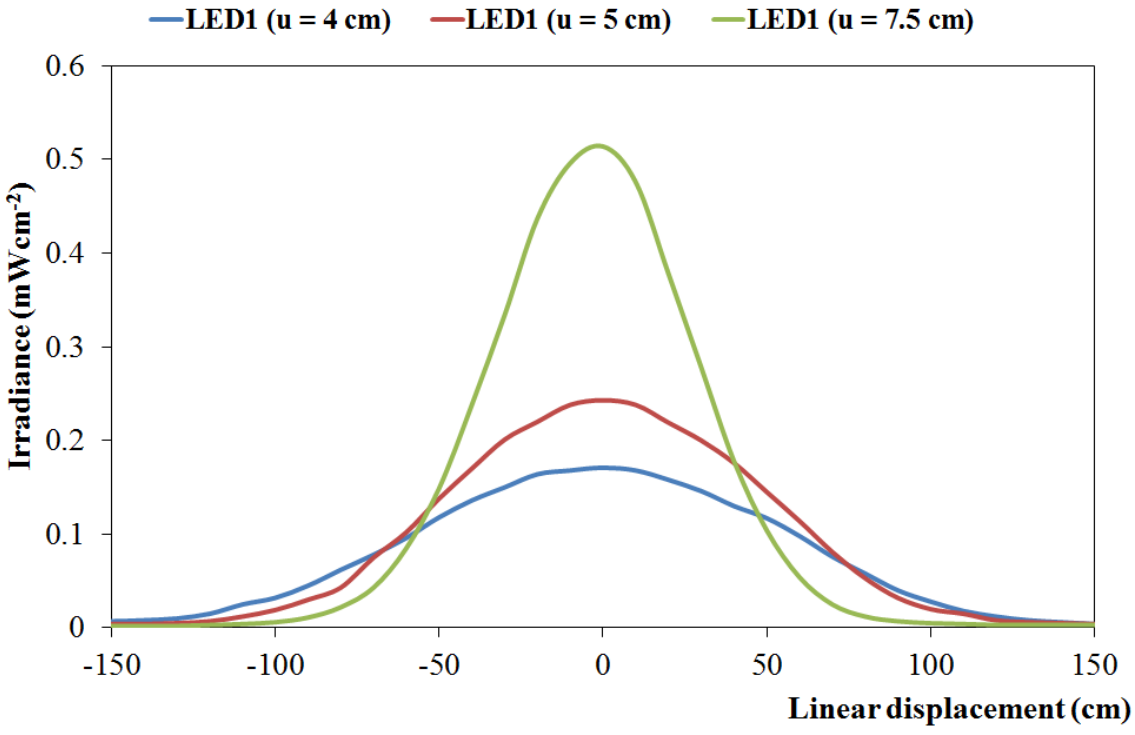

Fig. 9.13. *Irradiance distribution as a function of linear displacement for LED_1 with z = 150 cm.*

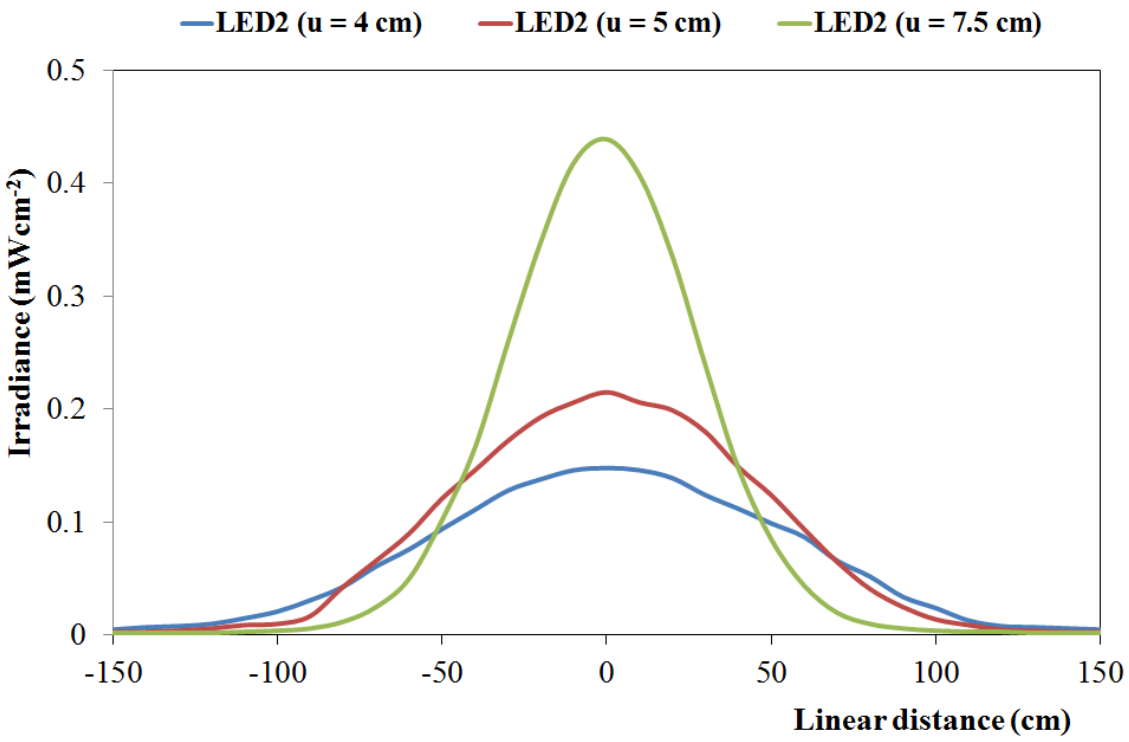

Fig. 9.14. *Irradiance distribution as a function of linear displacement for LED_2 with z = 150 cm.*

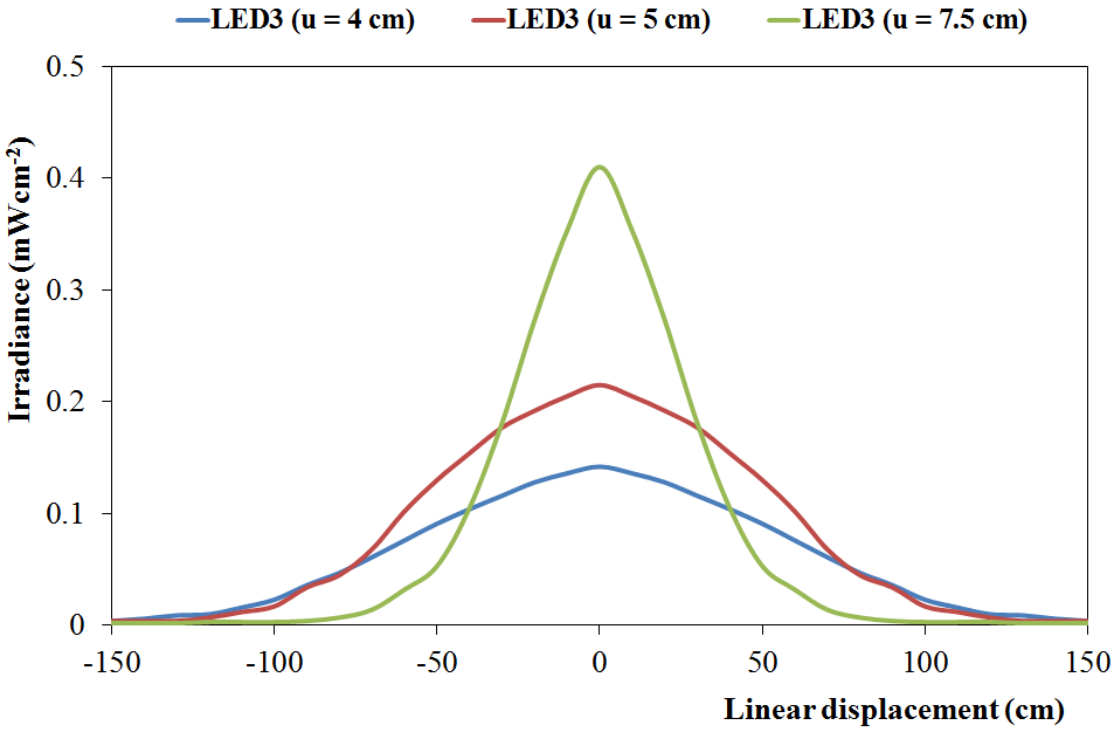

Fig. 9.15. *Irradiance distribution as a function of linear displacement for LED_3 with z = 150 cm.*

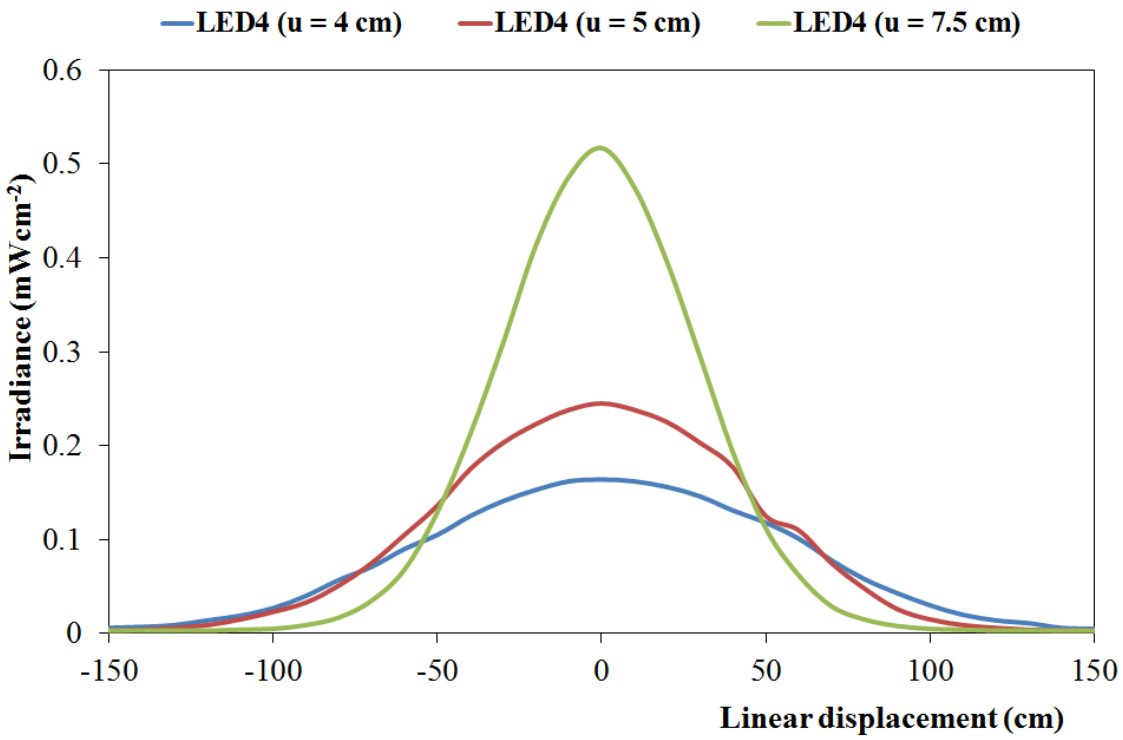

Fig. 9.16. *Irradiance distribution as a function of linear displacement for LED_4 with z = 150 cm.*

Table 9.1 *Calculation of the Lambertian mode number (m), irradiance at a distance of 1.5 m below the LED (E_0) and total light power delivered by the optical system (W)*

Light source	u = 4 cm			u = 5 cm			u = 7.5 cm		
	m^+	E_0 (Wm^{-2})	Total light power (W)*	m^+	E_0 (Wm^{-2})	Total light power (W)*	m^+	E_0 (Wm^{-2})	Total light power (W)*
LED_1	5.61	1.71	3.65727	8.72	2.43	3.53429	24.12	5.14	2.89272
LED_2	5.90	1.48	3.03232	9.30	2.15	2.95096	26.53	4.39	2.25435
LED_3	4.45	1.42	3.68345	8.36	2.15	3.24732	38.09	4.1	1.48279
LED_4	5.55	1.64	3.53969	9.03	2.45	3.45325	24.67	5.17	2.84726

$^+$Calculated with Eq. (2.16), *Calculated with Eq. (8.8),

9.6 Comparison of an initial prototype and the new prototype HINS-light EDS

9.6.1 Design of light source

As described in Section 8.1, the purpose of this study was the development, testing and modelling of a fully-integrated large-scale HINS-light EDS based on the initial prototype. The initial prototype was a ceiling mounted light source made up of a matrix of sixteen 405 nm LED arrays and 5 white LEDs covered by a Fresnel and diffuser, to control the irradiance distribution of the LEDs, as shown in Fig. 8.28. The matrix of 405 nm LEDs and white LEDs are mounted on a heat sink with a configuration as illustrated in Fig. 9.17. The system used two power supplies to drive the LEDs (one for the 405nm arrays and one for the white LEDs) [184].

Each of the 405 nm LED arrays was made up of 99 individual LEDs (OD-405-99-070) with power output of 1.7 W and radiation beam angle of 70° obtained from the Opto Diode Corp, USA [204]. 3.6 W white LEDs (GE-VHD-1A3B8 obtained from the General Electric (GE), USA) were used in the design to achieve the appropriate level of room lighting [205]. The initial prototype had a total illuminance of between 6 lux and 24 lux and total irradiance of 0.33 $mWcm^{-2}$ at a distance of 200 cm below the light source [184].

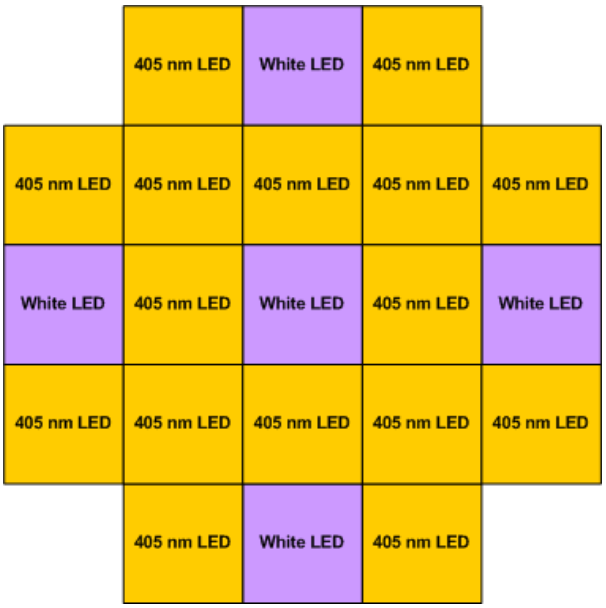

Fig. 9.17. *Diagram of the matrix design of the initial prototype HINS-light EDS.*

A comparison of the design of the initial prototype and the newly designed prototype HNS-light EDS, including specifications such as dimension, power consumption, weight and thermal management options, are summarised in Table 9.2 and shown in Fig. 9.18.

Fig. 9.18. *Comparative design of aspects of the initial prototype and the new prototype HINS-light EDS: a) light emitted from initial prototype still produced dominant violet illumination whilst the new prototype emits light close in appearance to laboratory lighting. b) dimensional comparison between the initial prototype and the new prototype, and c) power supply to drive the EDS: detached and bulky for the initial prototype whilst small and integrated into the system for the new prototype.*

Table 9.2 *Comparative design specifications for the initial prototype and the new prototype HINS-light EDS*

Item	Initial Prototype	New Prototype
Heat Sink	Large and Heavy	Embedded in system, Small and light
Power Supply	Detached and Bulky	Small and integrated
Controllable	By power supply	By computer
Integrated	No	Yes
Dimension	59.2 cm × 59.2 cm × 24 cm	59.2 cm × 59.2 cm × 8 cm
Power	293.45 W	193.87 W
I/O	No	USB port
Weight	13 Kg	7 Kg
Cost	"Confidential"	50% lower than the initial prototype

9.6.2 A study of light distribution as a function of linear displacement

9.6.2.1 Experimental method

Having demonstrated that the level of intensity of 405 nm light engines can be controlled by computer, a study then investigated the comparative light distribution pattern between the initial prototype and the new prototype, and used this data to ensure that the irradiance pattern of the new prototype was of a similar pattern to the initial prototype. This section examines and discusses a study of light distribution as a function of linear displacement and involves two methods. In Method I, the study focuses on a comparison of the light distribution produced by the new prototype and the initial prototype. Levels of intensity (controlled by computer) used in the study were 50, 60, 70, 80, 90 and 100%. The space distances between the light source and the lens system (u) were set at 4, 5 and 7.5 cm, and the space distance between the light source and the illuminated area was 200 cm. All 405 nm light engines were set at 12.0 ± 0.1 V. The relationship between current (A) and levels of software intensity (%) for each individual 405 light engine is shown in Fig. 9.19.

In Method II, the experiment focuses on a comparison between the light distribution produced by the new prototype and the initial prototype when the level of irradiances of the new prototype were set at 0.092 $mWcm^{-2}$ for each individual LED. These data were measured by a radiant power meter (Model 70260, L.O.T.-Oreiel Ltd., UK). Similar to Method I, the space distances between the light source and the lens system (u) were set at 4, 5 and 7.5 cm, and the space distance between the light source and the illuminated area is 200 cm.

9.6.2.2 Experimental results

Method I

Current as a function of software intensity level (%) for each individual light engine used in the experiment is shown in Fig. 9.19. Voltage input for all light engines was set at 12.0 ± 0.1 V, and all light engines were connected in parallel (Fig. 9.5). It can be observed from Fig. 9.19 that all four light engines have different levels of power consumption. For example, when the software intensity level was set at 50%, it shows that the current (A) generated from each individual light engine is different: 0.84 A for LED_1,1.95 A for LED_2, 1.03 A for LED_3 and 0.91 A for LED_4.

Fig. 9.20, Fig. 9.21 and Fig. 9.22 show light distribution as a function of linear displacement for u = 4, 5 and 7.5 cm, respectively. Graphs also shown the light distribution for the initial prototype as a comparison. The light distribution pattern for the initial prototype, shown Fig. 9.20, demonstrate that the pattern was closed to the new prototype at a level of intensity of 80% and 90%. The Lambertian mode number (m) and total power (W) obtained in these tests are summarised in Table 9.3. Total power for the initial prototype has a value of between 80% and 90% of intensity level for the new prototype.

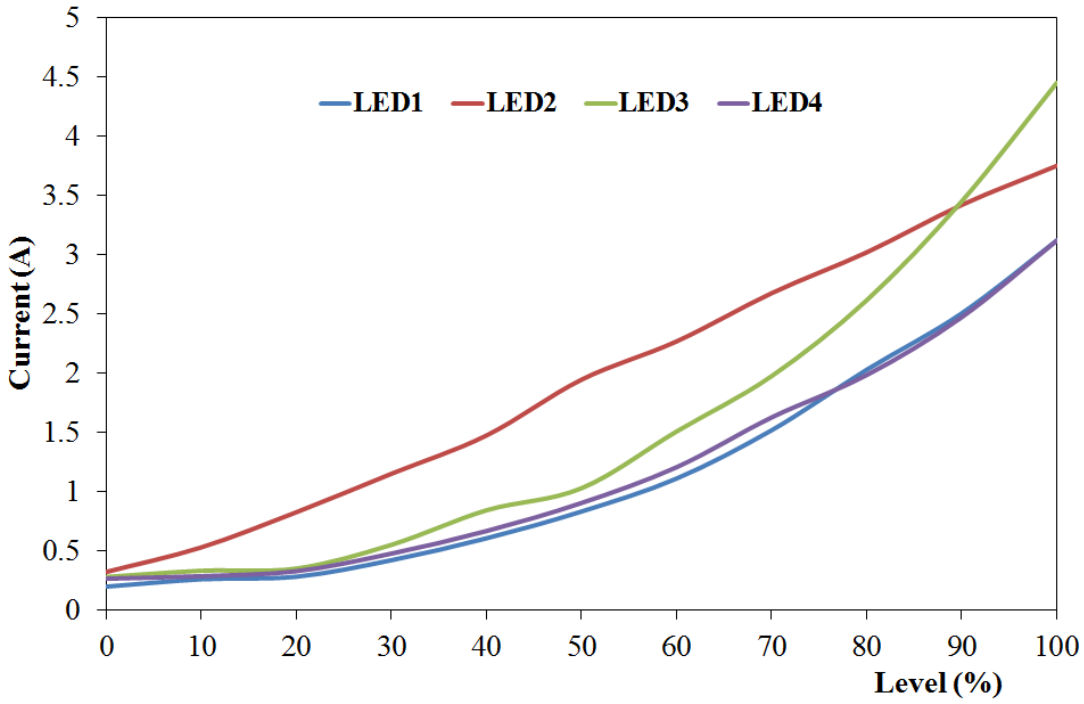

Fig. 9.19. *Current as a function of software level (%) for each individual 405 nm light engine.*

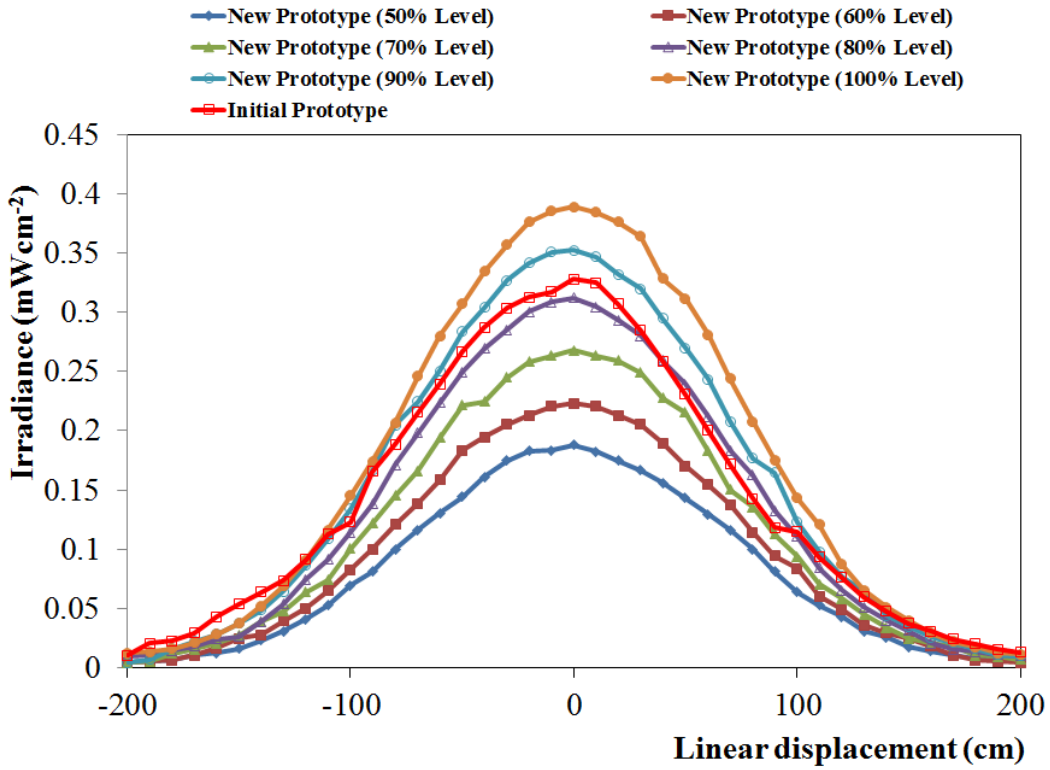

Fig. 9.20. *Comparative data the light distribution between the initial prototype and the new prototype with differing levels of intensity, with a value of u = 4 cm and z = 200 cm.*

Table 9.3 *Comparative data for the Lambetian mode number (m), E_0 ($mWcm^{-2}$) and total power (W) between the new prototype (u = 4 cm) and the initial prototype*

Light source	m^+	E_0 (Wm^{-2})	Total Power (W)*
New prototype (50% Level)	6.45	1.88	6.34
New prototype (60% Level)	6.30	2.23	7.68
New prototype (70% Level)	6.35	2.68	9.16
New prototype (80% Level)	6.38	3.12	10.63
New prototype (90% Level)	6.14	3.52	12.39
New prototype (100% Level)	6.09	3.89	13.79
Initial prototype	6.18	3.28	11.48

*Calculated with Eq. (8.8), $^+$Calculated with Eq. (2.16)

Results, shown in Fig. 9.21, demonstrate that all patterns of light distribution emitted by the light source with u = 5 cm are different from the pattern of the initial prototype. Summary calculation of the Lambartian mode number (m) and total power (W) for both the initial and the new prototype are summarised in Table 9.4.

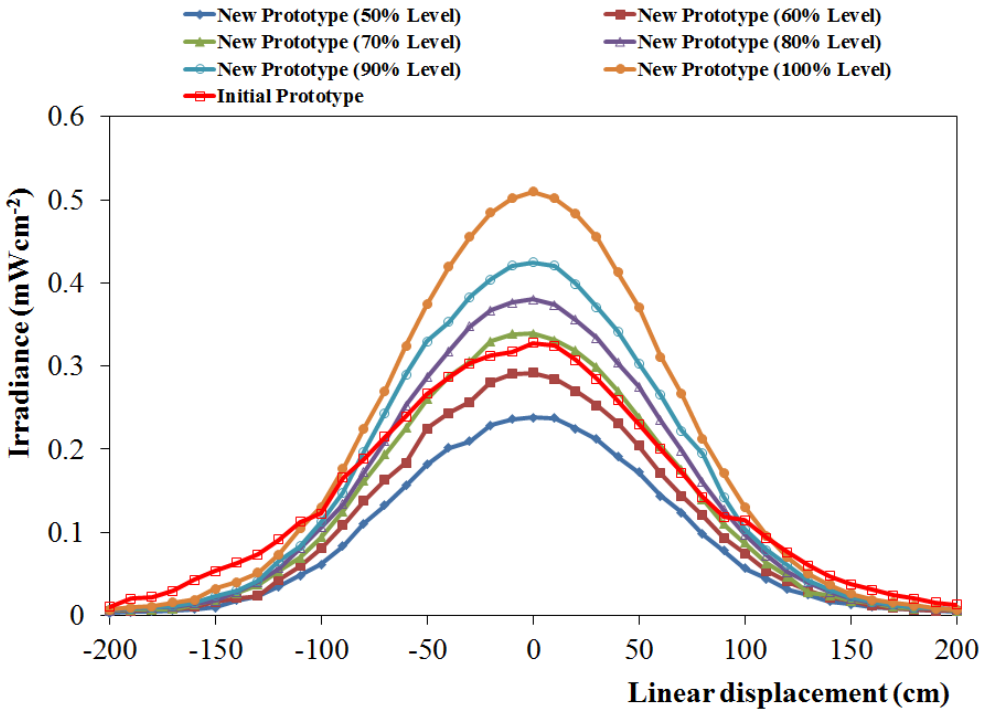

Fig. 9.21. *Comparative data for the light distribution between the initial prototype and the new prototype with differing levels of intensity, with a value of u = 5 cm and z = 200 cm.*

Table 9.4 *Comparative data for the Lambetian mode number (m), E_0 ($mWcm^{-2}$) and total power (W) between the new prototype (u = 5 cm) and the initial prototype*

Light source	m^+	E_0 (Wm^{-2})	Total Power (W)*
New prototype (50% Level)	8.72	2.38	6.15
New prototype (60% Level)	8.83	2.92	7.47
New prototype (70% Level)	8.62	3.39	8.86
New prototype (80% Level)	8.59	3.80	9.96
New prototype (90% Level)	8.52	4.25	11.22
New prototype (100% Level)	8.80	5.10	13.08
Initial prototype	6.18	3.28	11.48

*Calculated with Eq. (8.8), $^+$Calculated with Eq. (2.16)

Fig. 9.22 shows the results of measurement of light distribution as a function of linear displacement for the light source with u = 7.5 cm and z = 200 cm. Total power (W) irradiated and the Lambertian mode number (m) for both the new prototype and the initial prototype have been calculated with Eq. (8.8) and Eq. (7.16), respectively and are presented in Table 9.5.

Table 9.5 *Comparative data for the Lambertian mode number (m), E_0 ($mWcm^{-2}$) and total power (W) between the new prototype (u = 7.5 cm) and the initial prototype*

Light source	m^+	E_0 (Wm^{-2})	Total Power (W)*
New prototype (50% Level)	18.25	3.66	4.78
New prototype (60% Level)	20.19	4.50	5.34
New prototype (70% Level)	20.34	5.36	6.31
New prototype (80% Level)	20.21	6.23	7.38
New prototype (90% Level)	20.40	7.17	8.42
New prototype (100% Level)	21.90	8.60	9.44
Initial prototype	6.18	3.28	11.48

*Calculated with Eq. (8.8), $^+$Calculated with Eq. (2.16)

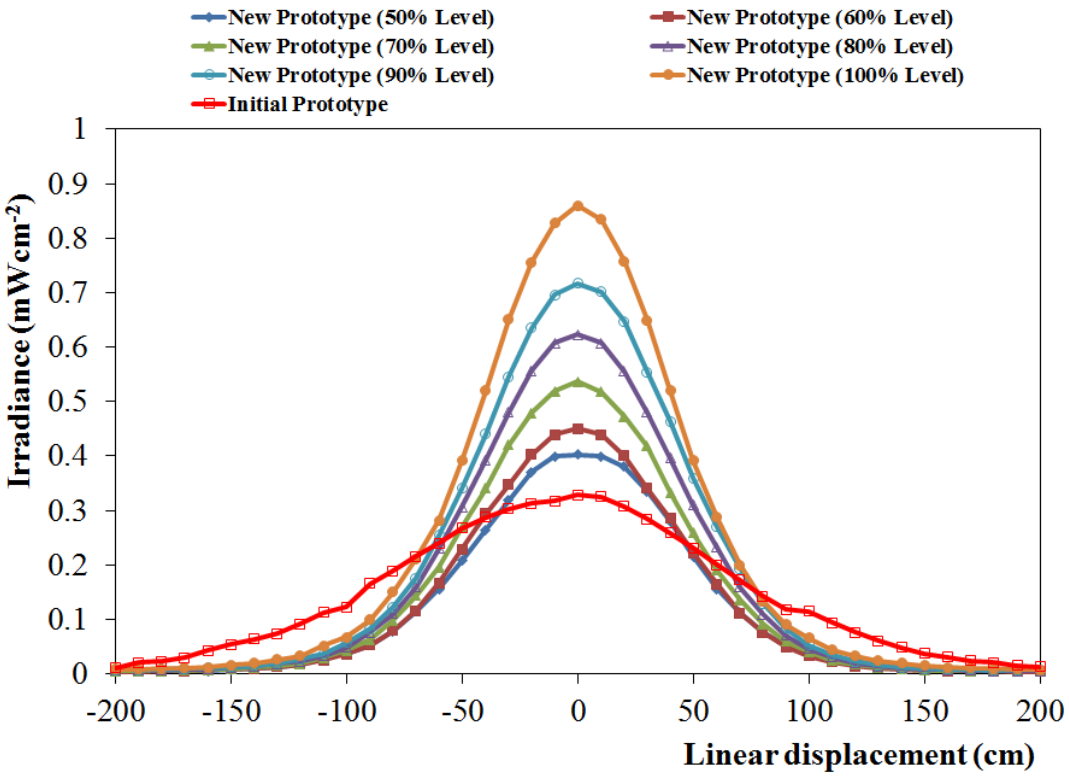

Fig. 9.22. *Comparative data for the light distribution between the initial prototype and the new prototype with differing levels of intensity, with a value of u = 7.5 cm and z = 200 cm.*

Method II

The light distribution as a function of linear displacement for the new prototype HINS-light EDS, with irradiance levels for each individual light engines set at 0.092 mWcm^{-2}, is shown in Fig. 9.23. For reference, the light distribution for the initial prototype is also given in Fig. 9.23. Calculation of the total power (W) demonstrates that the highest power was achieved when the new prototype has u = 4 cm, as stated in Table 9.6.

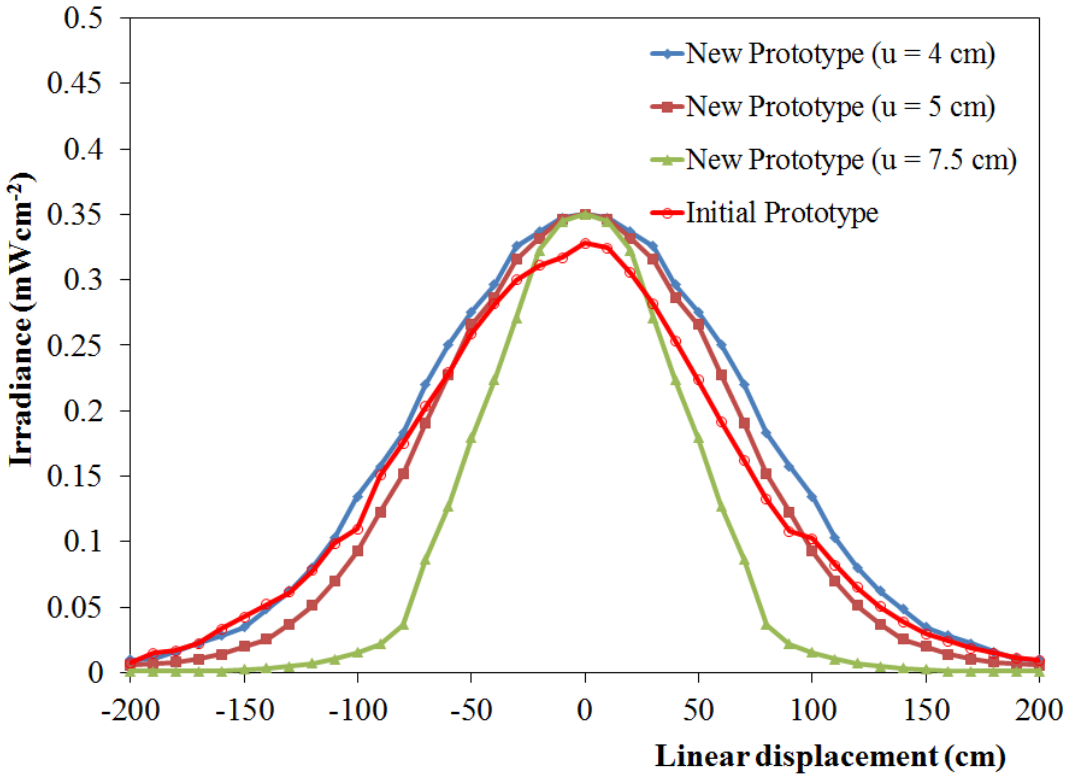

Fig. 9.23. *Comparative data of the light distribution between the initial prototype and the new prototype with the power density of each light engine set at 0.092 mWcm^{-2}.*

Table 9.6 *Comparative data of the Lambertian mode number (m), E_0 (mWcm^{-2}) and total power (W) between the initial and the new prototype with power densities set at 0.092 mWcm^{-2} for each individual 405 nm light engine*

Light source	m^+	E_0 (Wm^{-2})	**Total power (W)***
New prototype (u = 4 cm)	6.08	3.50	12.4
New prototype (u = 5 cm)	8.45	3.50	9.3
New prototype (u = 7.5 cm)	21.44	3.50	3.9
Initial prototype	6.18	3.28	11.5

*Calculated with Eq. (8.8), $^+$Calculated with Eq. (2.16)

Upon identification that the topology of the new prototype with u = 4 cm and the irradiance level for each individual LED set at 0.092 mWcm^{-2} provides a light distribution close to the light distribution of the initial prototype, the study then focused on investigating this topology for two levels of irradiance for each individual LED light engine. These levels were set at 0.076 and 0.080 mWcm^{-2}. All data of

light distribution from the new prototype were then compared to the data of the light distribution from the initial prototype.

The light distribution as a function of linear displacement between the initial prototype and the new prototype, with same level of power densities for each individual 405 nm light engine, is shown in Fig. 9.24. The results demonstrate that when the 405 nm LED light engines are set at a level of 0.08 mWcm^{-2}, the light distribution pattern is a similar to the light distribution pattern of the initial prototype.

Total power (W) and the Lambertian mode number (*m*) for both the new prototype and the initial prototype are presented in Table 9.7. As stated in Table 9.7, the total power (W) of the new prototype HINS-light EDS has a value less than the initial prototype when the light sources are set at 0.076 mWcm^{-2}.

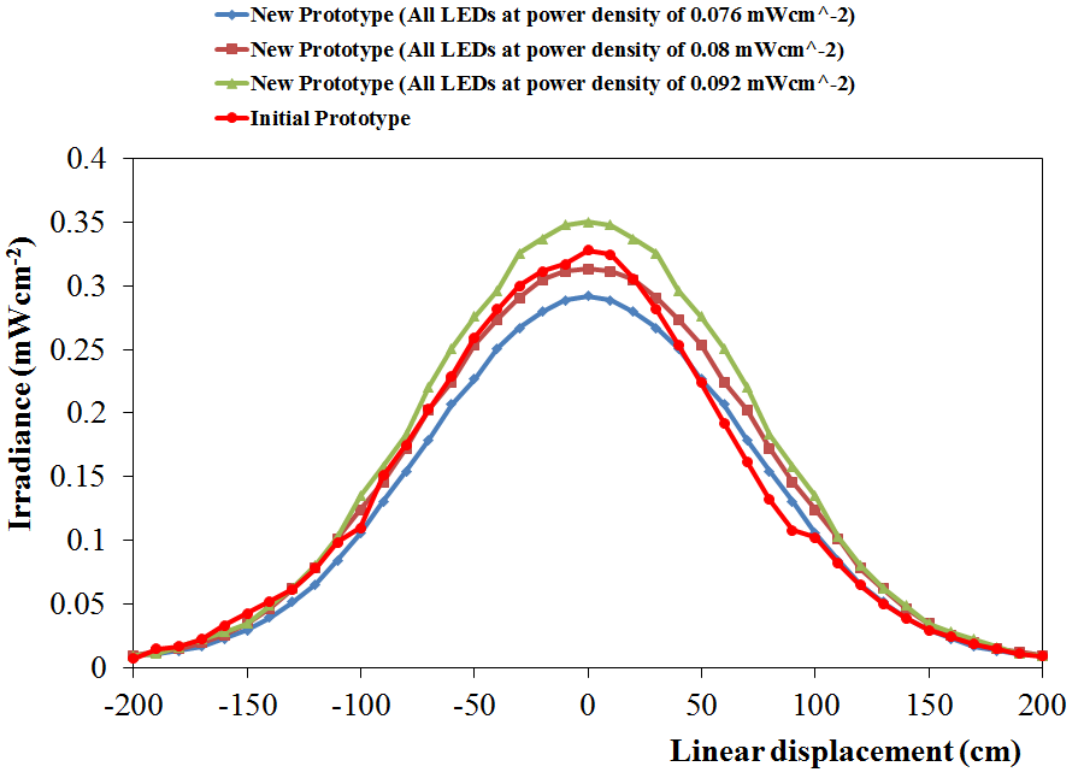

Fig. 9.24. *Comparative data for the light distribution between the initial prototype and the new prototype, the three identical levels of intensity for each individual 405 nm light engine (new prototype) used in the study were 0.076, 0.08 and 0.092 mWcm^{-2}.*

Table 9.7 *Comparative data of the Lambertian mode number (m), E_0 ($mWcm^{-2}$) and total power (W) between the new prototype (u = 4 cm) and the initial prototype*

Light source	Irradiance (Wm^{-2})				m^+	E_0 (Wm^{-2})	Total Power (W)*
	LED_1	LED_2	LED_3	LED_4			
New prototype	0.76	0.76	0.76	0.76	6.23	2.92	10.15
New prototype	0.80	0.80	0.80	0.80	5.67	3.13	11.79
New prototype	0.92	0.92	0.92	0.92	6.08	2.92	12.42
Initial prototype					6.18	3.28	11.48

[+]Calculated with Eq. (2.16), *Calculated with Eq. (8.8)

9.7 Analytical studies involving safety calculations of HINS-light EDS

As described in Section 8.7.1, the active components of an HINS-light EDS are four 405 nm LED light engines. The emission spectrum for each individual 405 nm LED light engine used is shown in Fig. 9.25, with the peak wavelength for all four 405 nm LED engine in the range 405 ± 7 nm. Analysis of the emission spectrum found that no part of the HINS- light EDS falls within the UV-B/UV-C regions. It is UV light in the UV-B and UV-C wavelength regions that causes the majority of cases of UV damage to skin and eyes. However approximately 20% of the HINS-light falls within the UV-A region in the wavelength region 380 nm to 400 nm (Fig. 9.26), where potential damaging effects are small [184], but this issue will be considered in further discussions.

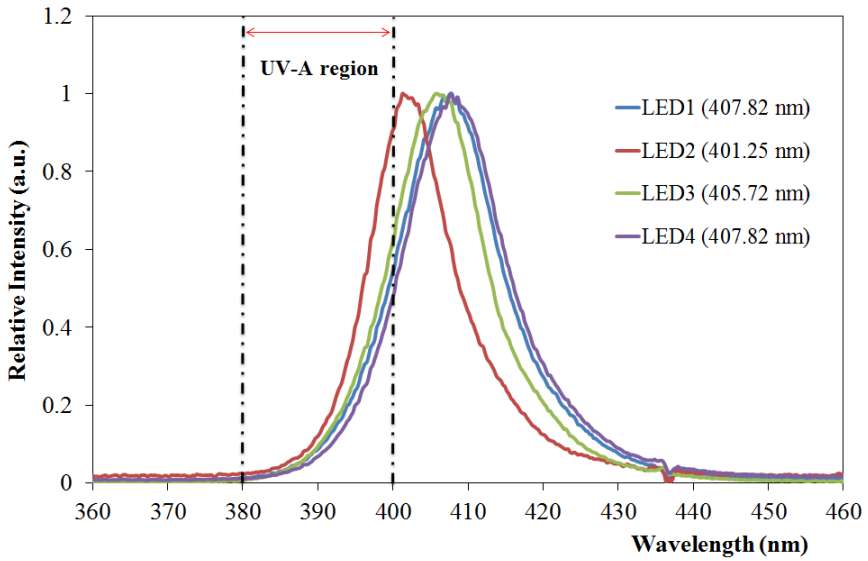

Fig. 9.25. *Emission spectra of the four 405 nm LED light engines.*

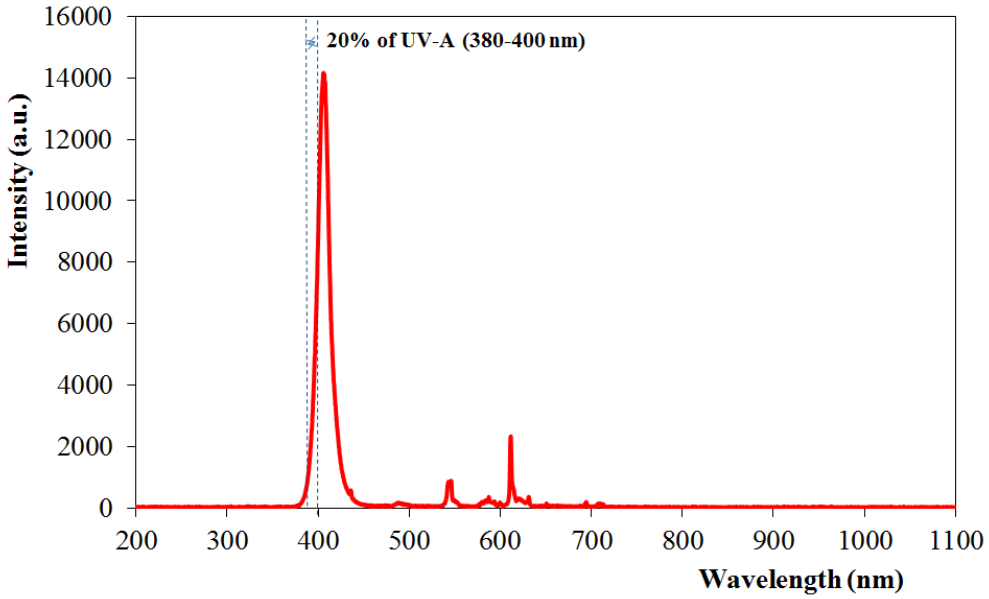

Fig. 9.26. *Portion of the new HINS-light EDS (4 LED light engines) emission spectrum (380 – 400 nm) that falls within the UV-A wavelength region.*

9.7.1 Safety calculations

9.7.1.1 Luminous flux and luminance

To analysis exposure limits for the new HINS-light EDS and ensure that it is safe for eye and skin exposure with regard to the guidelines on limits of exposure to optical radiation such as ultraviolet, visible light and infrared (IR), photometric and radiometric values for each individual LED were measured.

The peak wavelength for all individual LED light engines used in the new HINS-light EDS were between 401 and 408 nm (Fig. 9.25). The luminous flux (lm) for each individual LED can be calculated with reference to the photopic curve as shown in Fig. 9.27 which is the photopic curve for the wavelength region 400 – 410 nm.

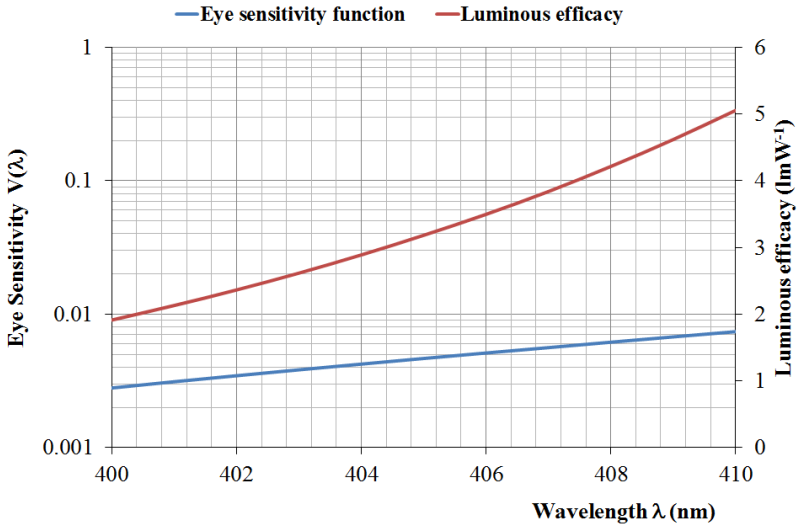

Fig. 9.27. *Eye sensitivity function, V(λ) and luminous efficacy in the wavelength region 400 – 410 nm.*

Luminous flux is defined as follows: "a monochromatic light source emitting an optical power of (1/683) watt at 555 nm has a luminous flux of 1 lumen (lm)" [29]. The luminous flux values for each individual LED light engine used in the new HINS-light EDS are summarised in Table 9.8.

Values of luminous flux contained in Table 9.8 were obtained using the luminous efficacy (lmW^{-1}) and radiant flux (W) values. Results demonstrate that the luminous flux for each individual 405 nm LED light engines varies within the range 10 – 19 lm, with a total luminous flux of 63.65 lm for ~ 20 W light source of the new HINS-light EDS.

Table 9.8 *The peak wavelength (nm), luminous efficacy (lmW^{-1}), radiant flux (W) and luminous flux (lm) for all four the 405 nm LED light engines used in the new HINS-light EDS*

Light source	Peak wavelength (nm)	Luminous efficacy (lmW^{-1})	Radiant flux* (W)	Luminous flux (lm)
LED_1	407.82	3.84	4.90	18.82
LED_2	405.72	3.18	4.90	15.58
LED_3	407.82	3.84	4.90	18.82
LED_4	401.25	2.13	4.90	10.44

*Values of radiant flux obtained from the datasheet of ENFIS Uno Air Cooled Light Engine [185].

Measurement of the illuminance (lux) using a LUTRON LX-101 Digital Lux Meter (LUTRON Electronic Enterprise Co., Ltd, Taiwan) resulted in a value of 29 lux for LED_1, 26 lux for LED_2, 25 lux for LED_3 and 30 lux for LED_4. All measurement data were taken at a distance of 200 cm below the 405 nm LED light engine at the centre position for each light source. When all four of the 405 nm LED light engines were used for measuring illuminance, the total illuminance was 107 lux at a distance of 200 cm below the light source at the centre position of the system (E_{v0}), as illustrated in Fig. 9.28.

As described in Section 8.7.1, in addition to the four 405 nm LED light engines, the new HINS-EDS also includes 12 white light-emitting diodes (LEDs) in order to produce a more normal room lighting effect. According to the datasheet provided the luminous flux for each white LED was 90 lm, thus the total luminous flux for 12 white LEDs is 90 lm × 12 equals to 1080 lm. Similarly, the measured illuminance (lux) for the 12 white LEDs was 102 lux.

By adding the illuminance from the 405 nm LED light engines and white LEDs, the total illuminance was 209 lux at a distance of 200 cm below the light source. This value is a relatively low-light level compared to home lighting of between 30 lux and 300 lux, office desk lighting of between 100 lux and 1,000 lux and surgery lighting of 10,000 lux [29].

Luminance can be calculated using Eq. (2.29), and a value of solid angle can be determined as follows:

$$\Omega = \pi\left(\frac{r}{d}\right)^2, \tag{9.1}$$

where r is the radius of the source and d is the perpendicular distance from the source to the point where the irradiance is E_v. In the case, r and d were 10 cm (radius of a Fresnel lens) and 200 cm, respectively. Thus, a value of solid angle (Ω) for each individual 405 nm LED light engines equals to 0.00785 sr. Since E_{v1} (LED_1) = 29 lux, E_{v2} (LED_2) = 26 lux, E_{v3} (LED_3) = 25 lux, E_{v4} (LED_4) = 30 lux and Ω = 0.00785 sr, the luminances are 3694.3 $cd.m^{-2}$, 3312.1 $cd.m^{-2}$, 3184.7 $cd.m^{-2}$, and 3821.7 $cd.m^{-2}$, respectively.

For radiometric quantities, irradiance ($mWcm^{-2}$) for each individual 405 nm LED light engine was 0.08 $mWcm^{-2}$ as measured by a radiant power meter. The total irradiance of the active components of a HINS-light EDS source was 0.32 $mWcm^{-2}$ at a distance of 200 cm below the light system (E_0), as illustrated in Fig. 9.28.

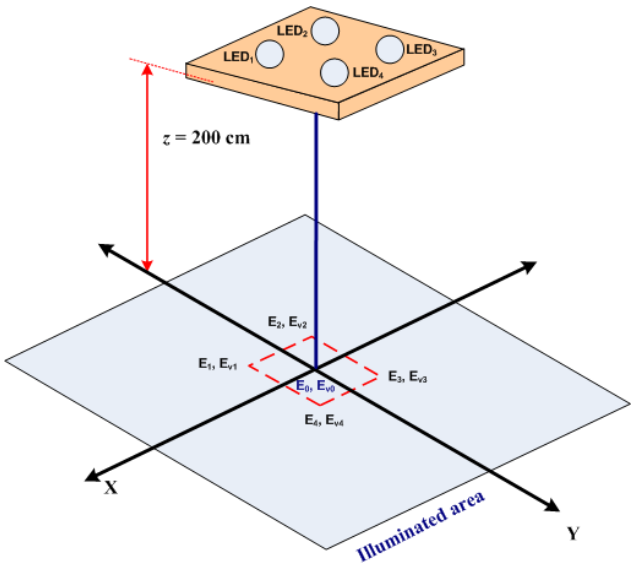

Fig. 9.28. *Measurement method for obtaining photometric and radiometric quantities.*

9.7.1.2 Blue light hazard

A radiance (L) for each individual LED light engine can be calculated as follows:

$$L = \frac{E}{\Omega}, \tag{9.2}$$

where E is irradiance from measurement (0.08 $mWcm^{-2}$) and $\Omega = 0.00785$ sr for each individual 405 nm LED light engine and therefore radiance is 10 $mW.cm^{-2}.sr^{-1}$. According to ICNIRP guidelines regarding exposure limits for blue light in the range 300 – 700 nm, long-term exposure to a particular source is permissible when the effective blue-light radiance is $\leq$ 10 $mWcm^{-2}sr^{-1}$ [25]. The results calculated above show that the radiance of each individual 405 nm LED light engine is equal to the safe exposure limit, therefore further assessment of the blue light hazard is necessary.

In order to calculate effective radiance for each individual 405 nm LED light engine array, the effective blue light radiance (L_B) can be calculated using Eq. (2.23), where

L_λ is obtained using data given in Fig. 9.29 and B(λ) is given in Fig. 2.11. This analysis is valid for normal healthy eyes. In order to evaluate the safety exposure for eyes with removed lens (after a cataract operation), the effective blue light radiance (L_A) can be calculated using Eq. (2.25), where A(λ) is the aphakic hazard function (unitless) obtained from Fig. 2.11. Values of the blue light radiance both for normal healthy eyes and for eyes which have had the normal lens removed, as well as exposure time maximum and percentage threshold limit value (TLV) for this study are summarised in Table 9.9.

These analyses show that all four LED light engines have a value of effective blue light radiance (L_B) that is less than 10 $mWcm^{-2}sr^{-1}$ for both normal healthy eyes and for eyes which have had the normal lens removed (with %TLV in the range 4 – 8% and ranging from 32 to 36%, respectively). The maximum of exposure time in direct viewing at a perpendicular distance from the source of 200 cm for all four LED light engines result in a value in the range 33 – 57 hours for normal healthy eyes and 7.8 – 8.6 hours for eyes with the normal lens removed.

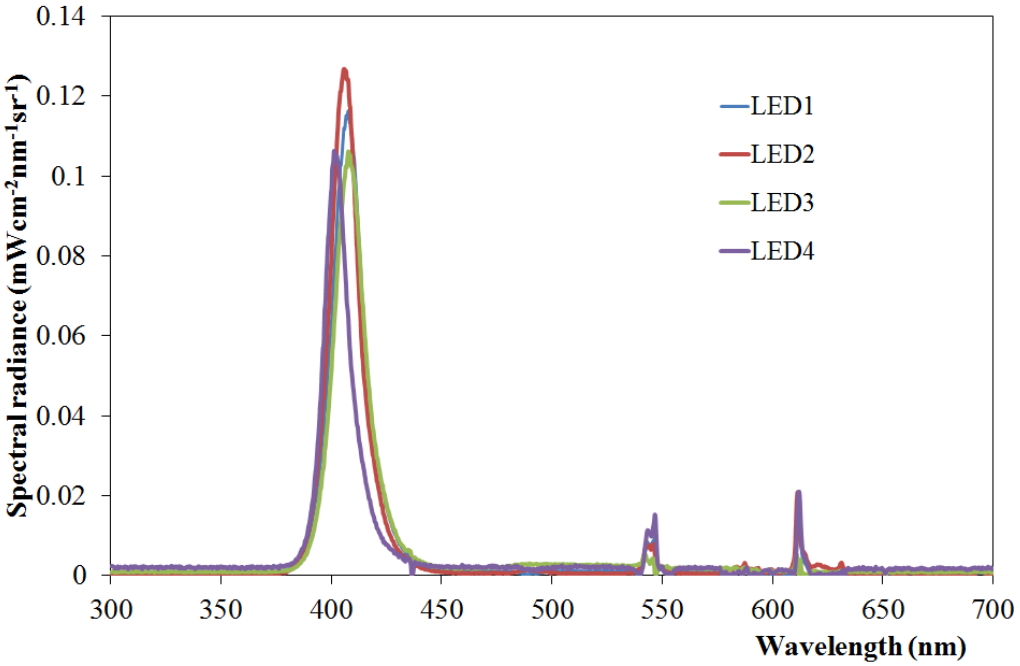

Fig. 9.29. *Spectral radiance for a HINS-light EDS source.*

Table 9.9 *The blue light radiance (L_B) and exposure time maximum calculations of the new HINS-light EDS*

Parameter	**Normal healthy eyes**				**Eyes with the normal lens removed**			
	LED_1	**LED_2**	**LED_3**	**LED_4**	**LED_1**	**LED_2**	**LED_3**	**LED_4**
Blue light radiance, L_B ($Wm^{-2}sr^{-1}$)	7.9	6.9	8.2	4.9	34.6	33.4	32.3	35.5
Exposure time (hours)	35.2	40.3	33.9	56.7	8.0	8.3	8.6	7.8
% TLV	7.9	6.9	8.2	4.9	34.6	33.4	32.3	35.5

Table 9.10 *Safety calculations in relation to UV interaction with skin and eyes, exposure time maximum and % TLV for the new HINS-light EDS*

Parameter	LED_1	LED_2	LED_3	LED_4
$E_{eff\ UV}$ (Wm^{-2})	1.9×10^{-4}	1.3×10^{-4}	2.0×10^{-4}	3.3×10^{-4}
Exposure Limit (Hours) to reach 30 Jm^{-2} (UV)	45	65	42	25
Portion of HINS-light source in the UV-A region ($mWcm^{-2}$)	3.1×10^{-4}	3.4×10^{-4}	2.5×10^{-4}	4.9×10^{-4}
Exposure limit (%) to reach 1 $mWcm^{-2}$ (UV-A)	0.31	0.34	0.25	0.49

9.7.1.3 UV-light and Thermal hazard

It has been demonstrated that HINS light at the irradiance level of 0.08 $mWcm^{-2}$ for each individual 405 nm LED light engine is safe in relation to blue light radiation, especially for protection of the retina against photorentinitis in the wavelength region 300 – 700 nm. The study then conducted a safety analysis in relation to both thermal and UV interaction with skin and eyes.

Fig. 9.26 shows that the new HINS-light EDS emits a light spectrum which has no infrared component, and according to the ICNIRP (regarding retinal thermal hazard in the wavelength region 380 – 1400 nm) the light source needs to be analysed if the luminance of the source is more than 1 candela per cm^2 (10^4 $cd.m^{-2}$) of the surface area of the source [25]. Previous results in Section 9.7.1.1, regarding calculation of luminance for each individual LED light engine, demonstrate that all LED light engines have a value less than 10^4 $cd.m^{-2}$, with actual values of between 3100 $cd.m^{-2}$ and 3850 $cd.m^{-2}$. This clearly demonstrates that the new HINS-light EDS is safe in relation to retinal thermal hazard.

As shown in Section 9.7, approximately 20% of HINS-light falls within the the wavelength region 380 nm to 400 nm (Fig. 9.26) which is within the UV-A region. Fig. 9.30 demonstrates that a small portion of the emission spectrum for all four LED light engines overlaps with the ultraviolet damage function or relative spectral effectiveness, S(λ). According to the ICNIRP, limits of exposure to UV radiation incident upon unprotected skin and eyes should be calculated by dividing 3 $mJcm^{-2}$ by the effective irradiance (E_{eff}) of the UV source in $mWcm^{-2}$ [26]. To determine whether the new HINS-light EDS satisfy these safety limits, E_{eff} has been calculated using Eq. (2.26). For these calculations the relative spectral effectiveness, $S(\lambda)$ (Fig. 2.13) and spectral irradiance , E_λ (Fig. 9.31) have been used.

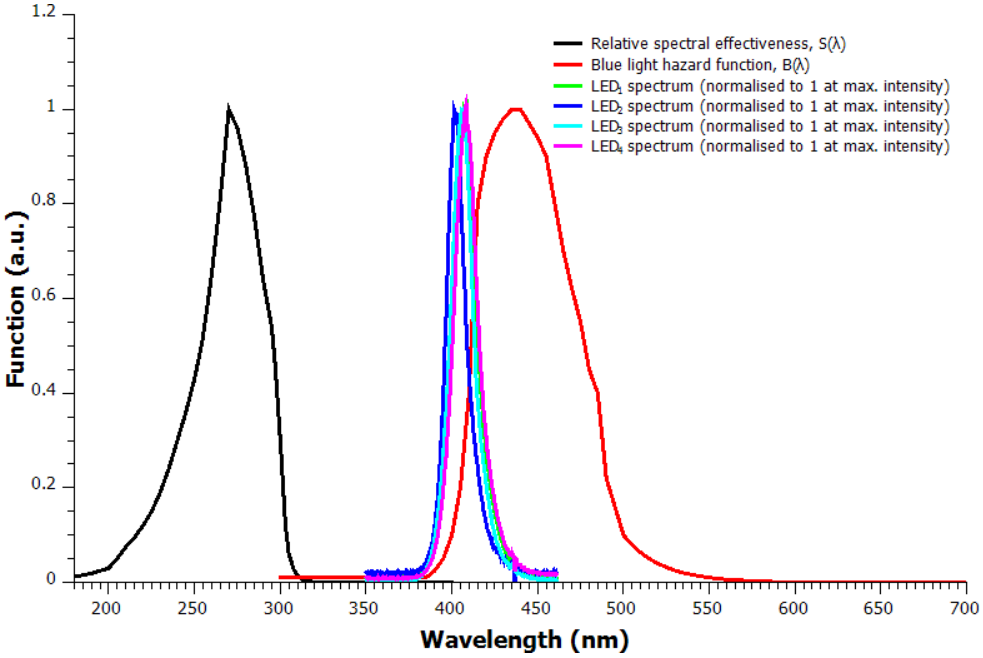

Fig. 9.30. *Correlation between the relative spectral effectiveness, S(λ), blue light hazard function B(λ) and emission spectrum of the new HINS-light EDS .*

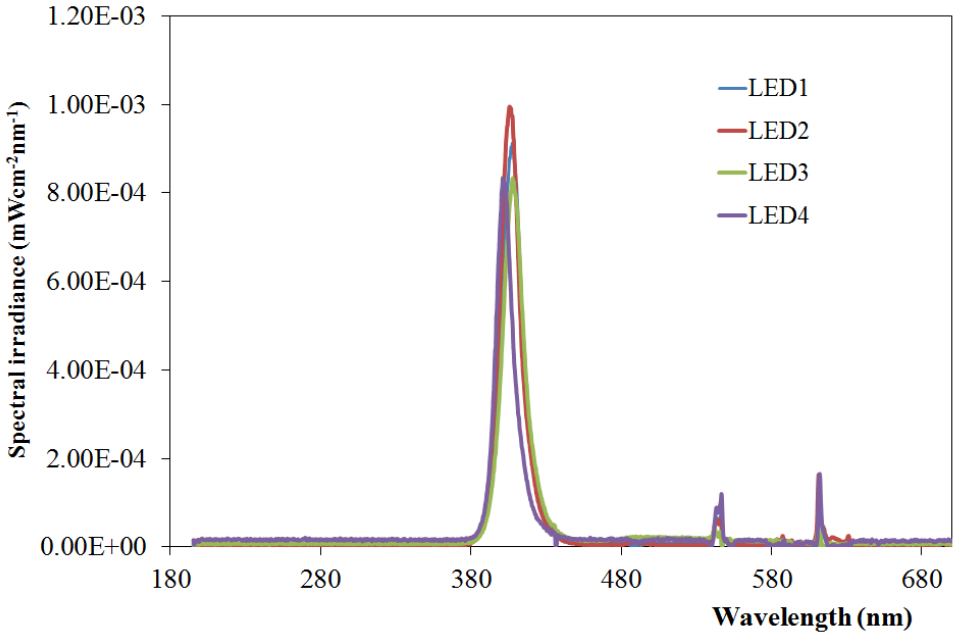

Fig. 9.31. *Spectral irradiance for the four HINS-light EDS sources with a total irradiance of 0.08 mWcm^{-2}.*

According to the ICNIRP, the total ultraviolet radiant exposure in the wavelength region 315 – 400 nm (UV-A) should not exceed 10^4 Jm^{-2} or 1 Jcm^{-2} and a maximum irradiance should be 1 $mWcm^{-2}$ [26, 206]. The following equation has been used to calculate the radiant exposure of the HINS light EDS in the UV-A wavelength region,

$$\frac{\sum_{315}^{400} E_{\lambda}.\Delta\lambda}{\sum_{0}^{\infty} E_{\lambda}.\Delta\lambda}, \tag{9.3}$$

where E_{λ} is spectral irradiance from measurement in $mWcm^{-2}nm^{-1}$ (Fig. 9.35) and $\Delta\lambda$ is wavelength intervals (nm). Results of the safety analysis in relation to UV interaction with skin and eyes are summarised in Table 9.11.

As stated in Table 9.10, regarding the UV-A wavelength region ranging from 315 nm to 400 nm, the new prototype HINS-light EDS source has values at in the range 2.5×10^{-4} $mWcm^{-2}$ to 4.9×10^{-4} $mWcm^{-2}$. This is 0.25% – 0.49% of the exposure limit established by the ICNIRP [26, 206], which indicates that the HINS-light EDS at an irradiance level of 0.08 $mWcm^{-2}$ is safe in relation to UV interaction with skin and eyes.

9.7.2 Risk assessment

In the previous section, it has been demonstrated that each individual 405 nm LED light engine satisfies the safety requirements in relation to UV radiation, UV-A, Blue light and retinal thermal hazards. The study then investigated whether the fully constructed new HINS-light EDS, which contains four LED light engines, and when installed as a ceiling mounted light source with diffuser and Fresnel lens is safe in relation to UV radiation, UV-A, Blue light and retinal thermal hazards.

The Health Protection Agency (HPA), provides information on exposure limits that are appropriate if someone stares into the light sources for 8 hours. According to these criteria Table 9.11 shows maximum permissible exposure (MPE) limits for UV, UV-A, Blue-light and retinal thermal hazards [207].

Table 9.11 *Maximum permissible exposure (MPE) for UV radiation, UV-A, Blue-light and retinal thermal hazards (Adapted from [207])*

Limit	Wavelength (nm)	The exposure limit	Maximum permissible exposure (MPE)	Comment
a	180 - 400	$H_{eff} = 30\ Jm^{-2}$	Time = $30\ Jm^{-2}/E_{eff\ UV}$, in seconds	If this is > 8 hours, there is no risk that the exposure limit will be exceeded at distance r
b	315 - 400	$H_{eff} = 10^4\ Jm^{-2}$	Time = $10^4\ Jm^{-2}/E_{eff\ UV\text{-}A}$, in seconds	If this is > 8 hours, there is no risk that the exposure limit will be exceeded at distance r
d	300 - 700	$L_B = 100\ Wm^{-2}sr^{-1}$		If the effective radiance, L_B, is less than the exposure limit, there is no risk that the exposure limit will be exceeded. This applies to all distances, so long as θ remains the same
g	380 - 1400	$L_R = 280\ KWm^{-2}sr^{-1}$ or $10^4\ cdm^{-2}$		If the effective radiance, L_R, is less than the exposure limit, there is no risk that the exposure limit will be exceeded. This applies to all distances, so long as θ remains the same

To assess the risk from the new HINS-light EDS as a single light source for all emission directions, irradiance data which radiated from the new HINS-light EDS has been measured directly below the light source for distances 30 – 200 cm is shown in Fig. 9.33.

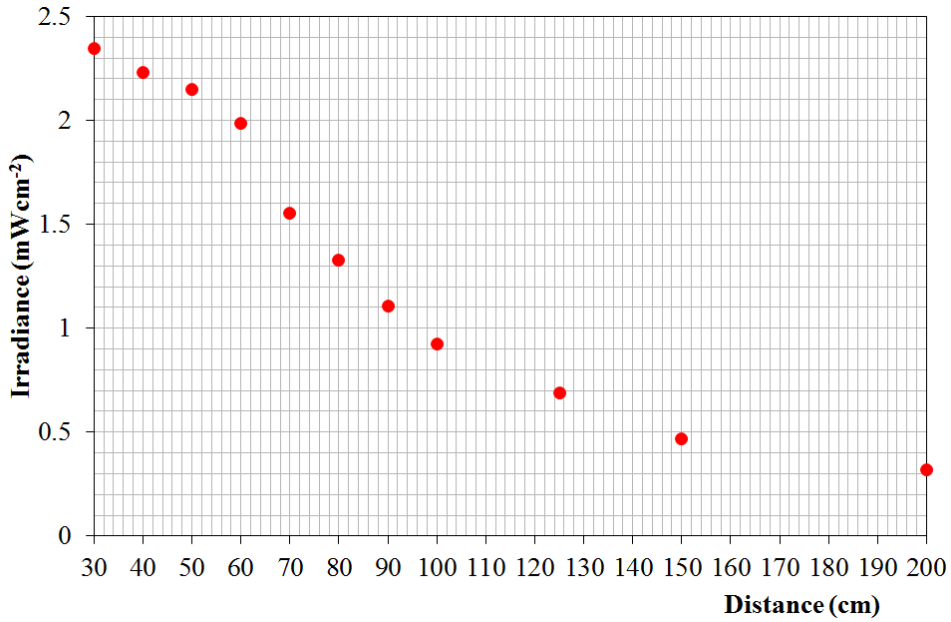

Fig. 9.32. *Irradiance measured directly below the new HINS-light EDS source for distances 30 – 200 cm.*

9.7.2.1 UV and UV-A hazards

Analysis of the safe distance from the HINS-light EDS for unprotected eyes with regard to the UV-A hazard is given in Fig. 9.32. Irradiance at any eye level (E_{eff}) can be calculated using the inverse square law method (Eq. (2.6)) as described in Section 2.3.2.6.

$$E_{eff} = E_z \frac{z^2}{z_{eff}^2} = E_z \left(\frac{1}{1+\tan^2 \theta} \right), \qquad (9.4)$$

where E_z is irradiance measured at θ degrees and distance z cm from the HINS-light EDS and z_{eff} is the eye level position (cm). The space distance between an eye level and the centre line of the HINS-light EDS in horizontal level can be calculated with $d = z \tan \theta$ (Fig. 9.33).

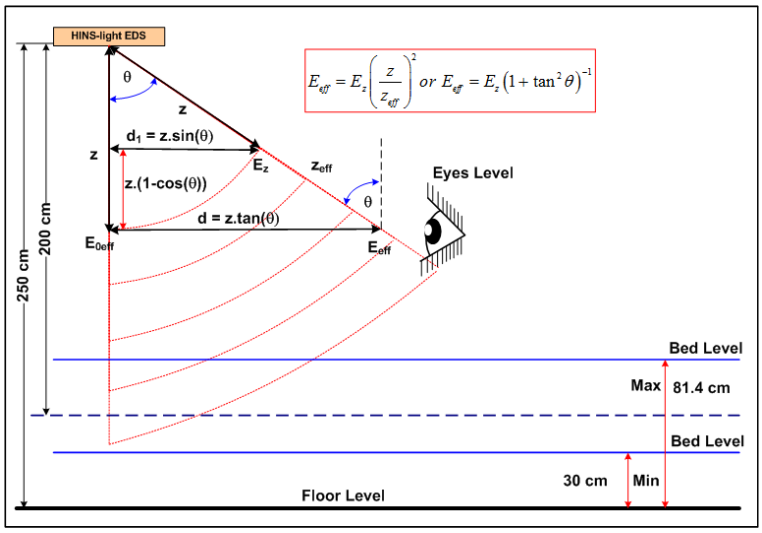

Fig. 9.33. *Illustration of safety level according to angular distribution of irradiance from the new HINS-light EDS.*

To assess the risk from the new HINS-light EDS as a single light source in relation to UV radiation (180 – 400 nm) and UV-A radiation (315 – 400 nm), effective irradiance (E_{eff}) has been calculated and evaluated using Eq. 2.26 and Eq. 9.3. Irradiance measured directly below the light source for distances 30 – 200 cm and the spectral irradiance at a distance of 100 cm are shown Fig 9.32 and Fig. 9.34, respectively. Detailed spectral irradiance data for distances 30 – 200 cm are shown in Appendix E.

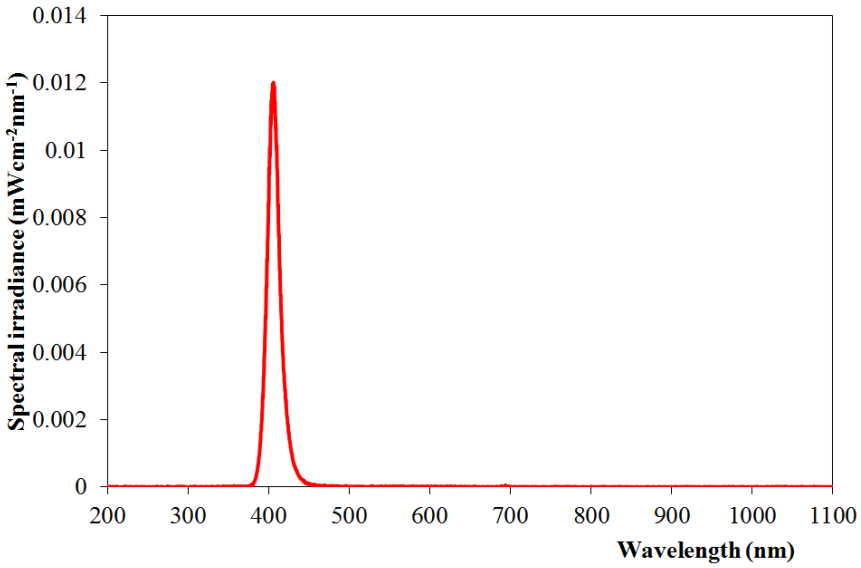

Fig. 9.34. *Spectral irradiance for the new HINS-light EDS source at a distance of 100 cm.*

Fig. 9.35 and Fig. 9.36 show maximum permissible exposure (MPE) and E_{eff} for UV and UV-A radiation ranges for distance in the range 30 – 200 cm below the HINS-light EDS source.

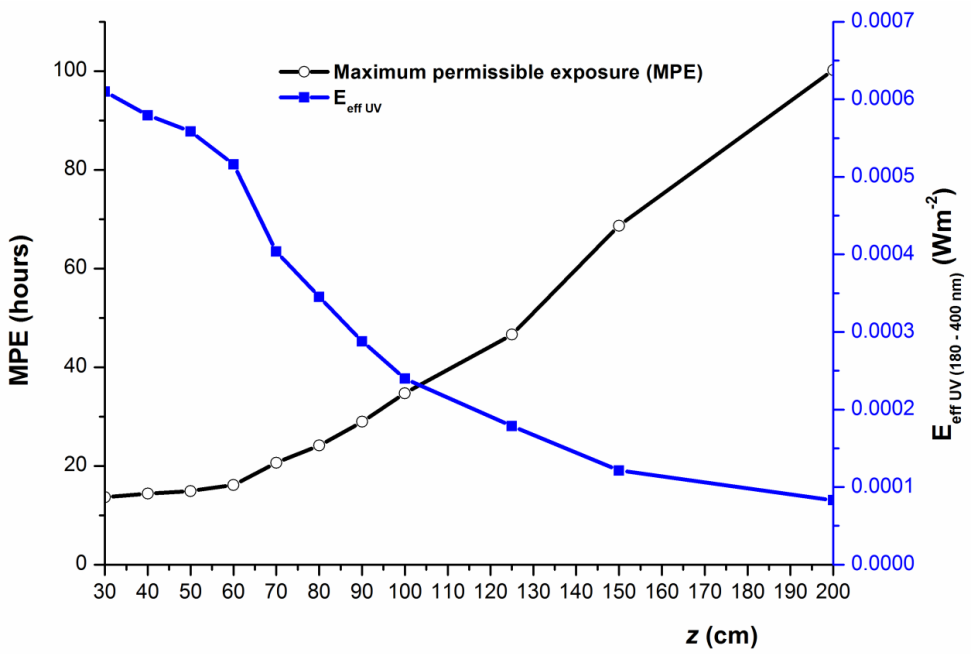

Fig. 9.35. *UV radiation (180 – 400 nm) assessment for the new HINS-light EDS. Data has been measured at a distance of 30 – 200 cm perpendicular into the light source.*

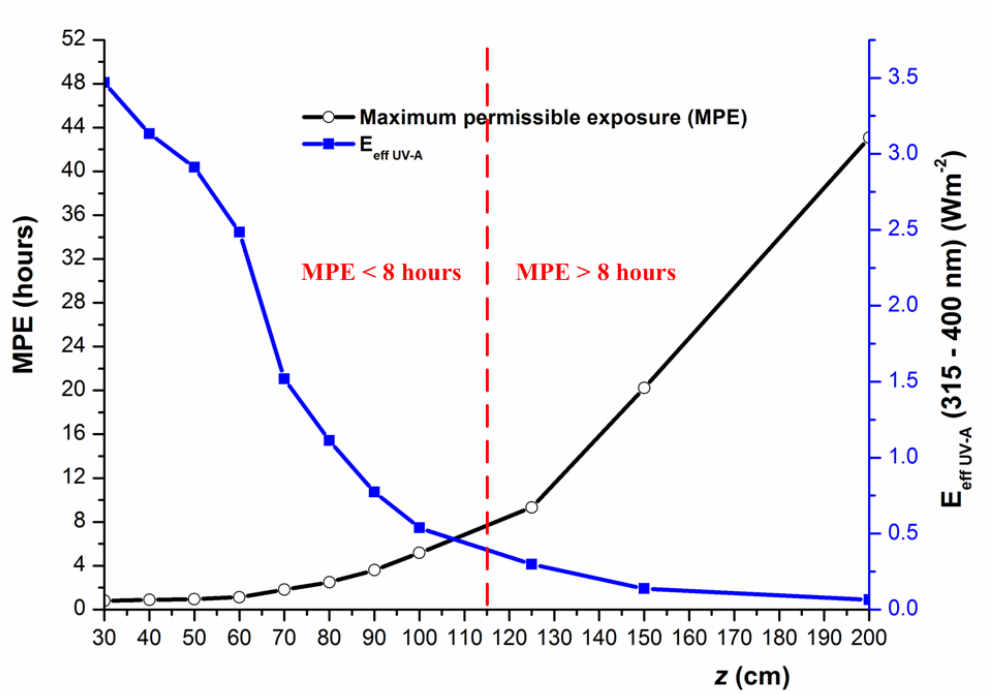

Fig. 9.36. *UV-A radiation (315 – 400 nm) assessment for the new HINS-light EDS. Data has been measured at a distance of 30 – 200 cm perpendicular into the light source.*

It can be observed from Fig. 9.35 that the MPE for the HINS-light EDS is larger than 8 hours (E_{eff} equals to 0.001 Wm^{-2}) for the UV spectral range at a distance range from 30 – 200 cm. According to HPA, "*If the MPE time is > 8 hours, there is no risk that the exposure limit will be exceeded at distance r*" [207].

Fig. 9.36 shows the MPE for the HINS-light EDS for the spectral range UV-A. It can be seen that the MPE at distances smaller than < 115 cm is shorter than 8 hours (E_{eff} equals to 0.35 Wm^{-2}), but for distance greater than 115 cm the MPE is longer than 8 hours. According to HPA, *"If the MPE time is < 8 hours, it will be necessary to demonstrate that actual personal occupancy at r is less than the MPE time. In this case, occupancy can exclude any time spent with the face oriented away from the source" and "If the MPE time is > 8 hours, there is no risk that the exposure limit will be exceeded at distance r"* [207].

From Fig. 9.34, Fig. 9.35 and Fig. 9.36 the safe distances and maximum permissible exposure can be determined. For a quick assessment, of the HINS-light EDS it can be assumed that "the luminous intensity in any direction from an element of a perfectly diffusing surface varies as the cosine of the angle between that direction and the perpendicular to the surface element" [2], therefore the effective irradiance (E_{eff}) can be calculated as follows :

$$E_{eff} = E_{0eff} \cos(\theta) \tag{9.5}$$

The maximum permissible exposure (MPE) and E_{eff} (Wm^{-2}) for both $E_{eff\,UV}$ and $E_{eff\,UV\text{-}A}$ are presented in Fig. 9.37 and Fig. 9.38, respectively. Dash lines in Fig. 9.37 and Fig. 9.38 show the MPE levels at 8 hours (the exposure limit). Using the data shown in Fig. 9.37 and Fig. 9.38 safe distances can be determined for the HINS-light EDS when it is located on the ceiling.

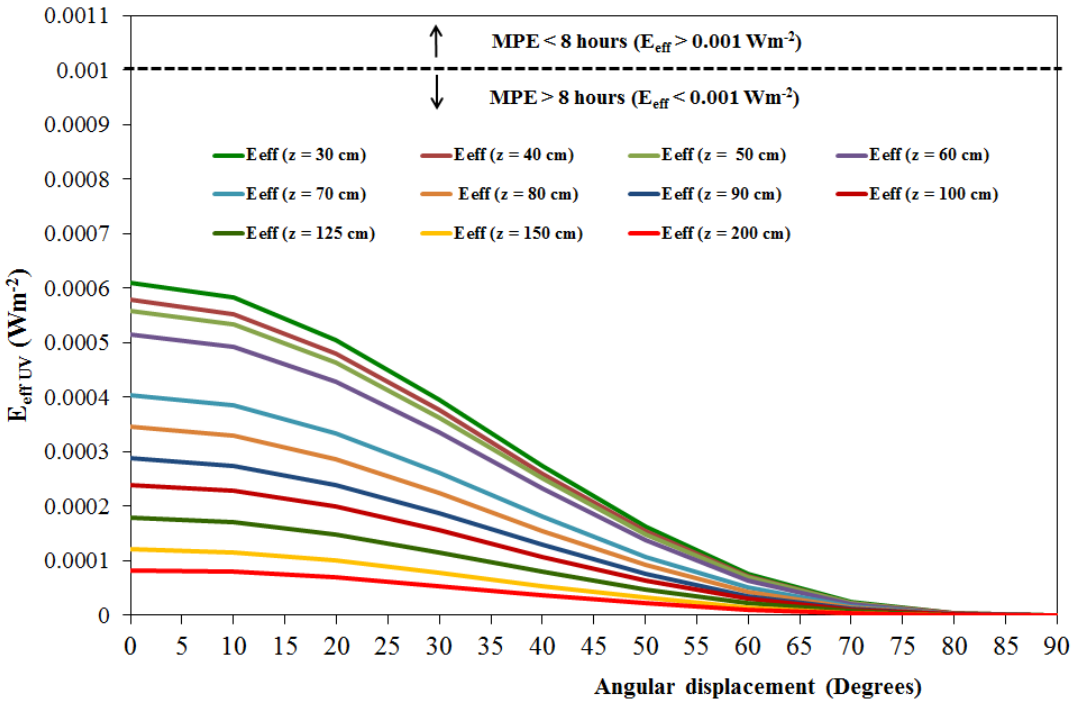

Fig. 9.37. *Relationship between angular displacement (degrees) and effective irradiance (E_{eff}) for UV radiation (180 – 400 nm).*

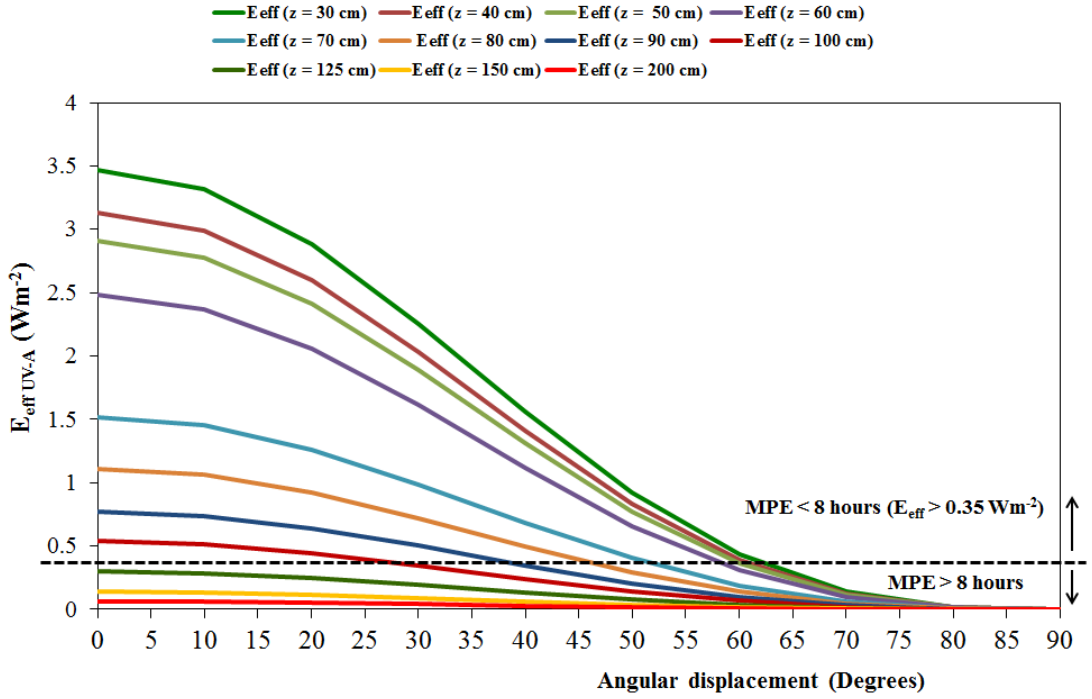

Fig. 9.38. *Relationship between angular displacement (degrees) and effective irradiance (E_{eff}) for UV-A radiation (315 – 400 nm).*

Fig. 9.39 demonstrates safe distances for UV-A radiation if someone stares directly into HINS-light EDS. Overall, Fig. 9.37 – Fig. 9.39 provide the necessary information on safe distances and MPE that can be used for assessment of the new HINS-light EDS.

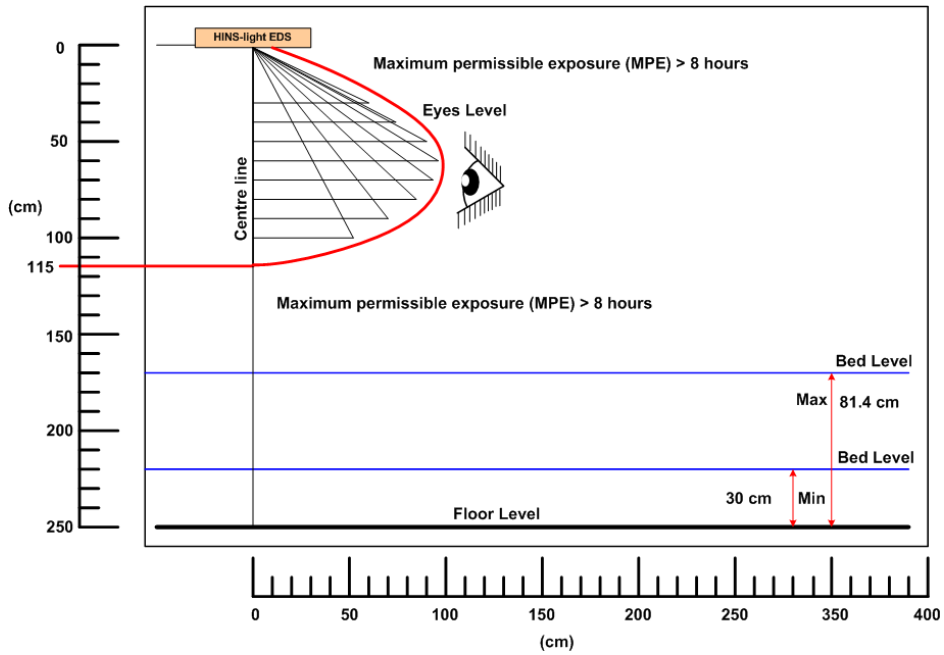

Fig. 9.39. *Safety guide for UV-A radiation if someone stares into the HINS-light EDS.*

9.7.2.2 Blue light and Retinal thermal hazards

In order to assess the risk from the light source regarding the blue-light hazard, the effective radiance (L_B) of the HINS-light EDS should be determined. Fig. 9.40 shows a photograph of the HINS-light EDS as a four LED light engine ceiling mounted light source with diffusers and Fresnel lenses. Each of the four individual light sources has a surface area of 3504.64 cm^{-2}, therefore the solid angle (Ω) subtended by the source at the eye level (at a distance of 200 cm below the HINS-light EDS) is 0.087616 sr.

First, the irradiance of the complete HINS-light EDS source (four 405 nm LED light engines) was measured at a distance of 200 cm and found to be 0.32 $mWcm^{-2}$. Each 405 nm LED light engine contributes 0.08 $mWcm^{-2}$ to the total irradiance (Section 9.7.1.1). The measured spectral radiance is shown in Fig. 9.41. Then, effective radiance (L_B) can be determined using Eq. (2.23).

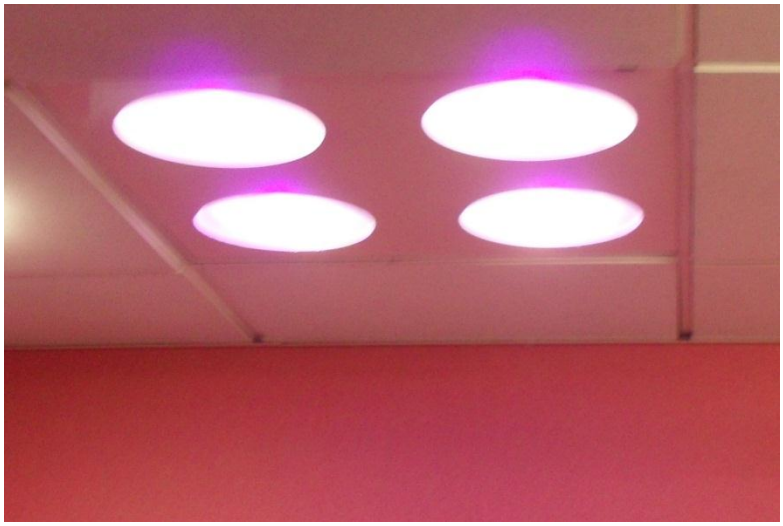

Fig. 9.40. *Photograph of the new HINS-light EDS as a bank of four ceiling mounted light sources each with a diffuser and Fresnel lens.*

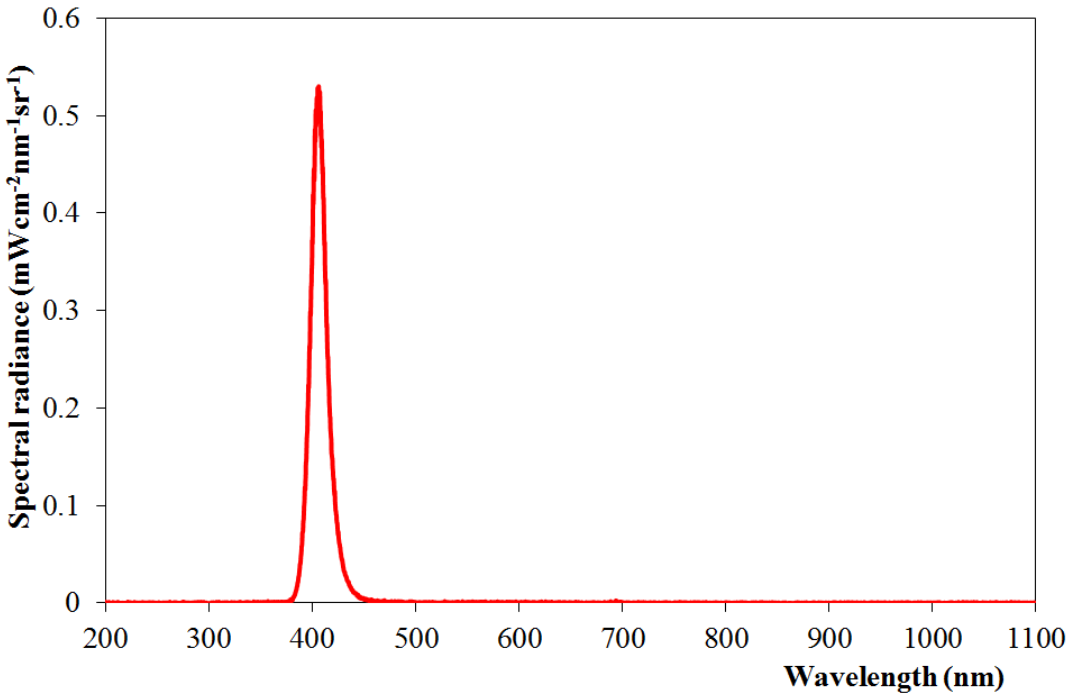

Fig. 9.41. *Spectral radiance measured at a distance of 200 cm for the new HINS-light EDS as a bank of four ceiling mounted light sources each with a diffuser and Fresnel lens.*

The calculated effective radiance (L_B) of the complete HINS-light EDS is 0.26 Wm^{-2}/0.87616 sr = 2.97 $Wm^{-2}sr^{-1}$ for normal eyes. Using the same method, the

effective radiance for eyes with the lens removed (L_A) has been calculated to be 1.16 Wm^{-2}/0.087616 sr = 13.24 $Wm^{-2}sr^{-1}$.

According to the HPA, the exposure limit for blue-light hazard is 100 $Wm^{-2}sr^{-1}$. Therefore, the effective radiance (L_B) of the new HINS-light EDS, 2.97 $Wm^{-2}sr^{-1}$, is less than the exposure limit. The HPA has mentioned that *"if the effective radiance, LB, is less than the exposure limit, there is no risk that the exposure limit will be exceeded. This applies to all distances, so long as θ remains the same"* [207].

The last hazard which is necessary to assess is the potential for retinal thermal injury. It has been shown in Section 9.7.1.1, that the new HINS-light EDS has an illuminance of 209 lux. This value was measured at a distance of 200 cm perpendicular to the HINS-light source and included all LEDs (405 nm LEDs and white LEDs). With solid angle of 0.087616 sr, the luminance of the complete HINS-light EDS is therefore 209 lux/0.087616 sr = 2385 $cd.m^{-2}$.

According to the ICNIRP and the HPA, the exposure limit for retinal thermal injury is 10^4 $cd.m^{-2}$ [25, 207]. This mean that the luminance of the new HINS-light EDS is less than the exposure limit. The HPA has mentioned that *"if the effective radiance, LR, is less than the exposure limit, there is no risk that the exposure limit will be exceeded. This applies to all distances, so long as θ remains the same"* [207].

In this section, the complete safety analysis of the new HINS-light EDS has been carried out. The results demonstrate that the new HINS-light EDS operated with an irradiance level of 0.08 $mWcm^{-2}$ for each individual 405 nm LED light engine (giving a total irradiance level of 0.32 $mWcm^{-2}$ and total illuminance of 209 lux) at a distance of 200 cm below the system is safe in relation to UV, UV-A, Blue light and retinal thermal hazards. Table 9.12 contains a summary of the risk assessment of new HINS-light EDS. Also to provide a comparison of the HINS light EDS with normal lighting, the MPE for typical laboratory lighting has been obtained using the same method. The results show, as expected, that typical laboratory lighting as provided in the ROLEST research facility satisfies the required safety limits in relation to UV, UV-A, blue light and retinal thermal hazards [see Appendix F].

Table 9.12 *Risk assessment summary of the new HINS-light EDS as a ceiling mounted light source*

The exposure limit	Hazard	Comparison with exposure limit	Limit	Comment
30 Jm^{-2}	photokeratitis	6. 1×10^{-4} –	a	**MPE > 8 hours , z = 30 - 200 cm**
	Photoconjunctivitis, cataractogensis,erythema, elastosis, skin cancer	8.3×10^{-5} Wm^{-2}		If the MPE time is > 8 hours, there is no risk that the exposure limit will be exceeded at distance r [207]
10^4 Jm^{-2}	cataractogenesis	3.47 – 0.06 Wm^{-2}	b	**MPE < 8 hours (z < 115 cm)**
				If the MPE time is < 8 hours, it will be necessary to demonstrate that actual personal occupancy at r is less than the MPE time. In this case, occupancy can exclude any time spent with the face oriented away from the source [207]
				MPE > 8 hours (z ≥ 115 cm)
				If the MPE time is > 8 hours, there is no risk that the exposure limit will be exceeded at distance r [207]
100 $Wm^{-2}sr^{-1}$	photoretinitis	L_B = 2.97 $Wm^{-2}sr^{-1}$	d	**L_B < the exposure limit, L_A < the exposure limit**
		L_A = 13.24 $Wm^{-2}sr^{-1}$		If the effective radiance, L_B/L_A, is less than the exposure limit, there is no risk that the exposure limit will be exceeded. This applies to all distances, so long as θ remains the same [207]
10^4 cdm^{-2}	retinal burn	2385 cdm^{-2}	g	**Luminance < the exposure limit**
				The exposure limit is not exceeded [207]

9.8 Conclusions

The new improved HINS-light EDS has been successfully developed and built. It has been demonstrated that the new HINS-light EDS has significant advantages over the initial prototype HINS-light EDS (Table 9.2). Safety analysis conducted for the new HINS-light EDS has demonstrated that this new system satisfies required safety limits.

According to an evaluation of safety limits for the initial prototype HINS-light EDS conducted by Professor Gerry Woosley (internal report), "placed at a height of 200 cm above the level of operation, and providing an irradiance of 0.33 $mWcm^{-2}$, is safe in relation to both thermal and UV interaction with skin and eyes" [184]. The initial prototype system was also judge to be safe in relation to blue light hazards. Calculation of the safety levels by Prof Woolsey for this system are summarised in Table 9.13 [184]. When the calculations of safety factors for the initial prototype and the new system are compared (at a distance of 200 cm below the light source), the results demonstrate that for the UV-A hazard to unprotected eyes, the new HINS-light EDS is safer than the initial prototype, with a value of 0.64% of the threshold limit value (TLV) (Table 9.12). For the blue light hazard to unprotected eyes, the new HINS-light EDS is also safer than the initial prototype, with a value of 2.97 % of the TLV (Table 9.12). For both the thermal hazard and the UV hazard to unprotected skin and eyes both the initial prototype and new HINS-light EDS have been assessed to be safe.

Table 9.13 *The safety factors for different interaction processes for the initial HINS- light EDS as percentages of the TLVs specified by the ACGIH (Adapted from [184])*

Process of interaction	% Threshold Limit Values (TLV)
Thermal to unprotected skin and eyes	Negligible
UV to unprotected skin	Negligible
UV to unprotected eyes	4
Blue light to unprotected eyes	23

It has been shown that the HINS-light EDS can be used for the environmental decontamination of air and all exposed surfaces without the need for skin and eye protection against UV, thermal and blue light hazards. The HINS-light EDS can be employed in rooms occupied by workers (as shown in Fig. 9.42) or by patients and hospital staff in wards or isolation rooms.

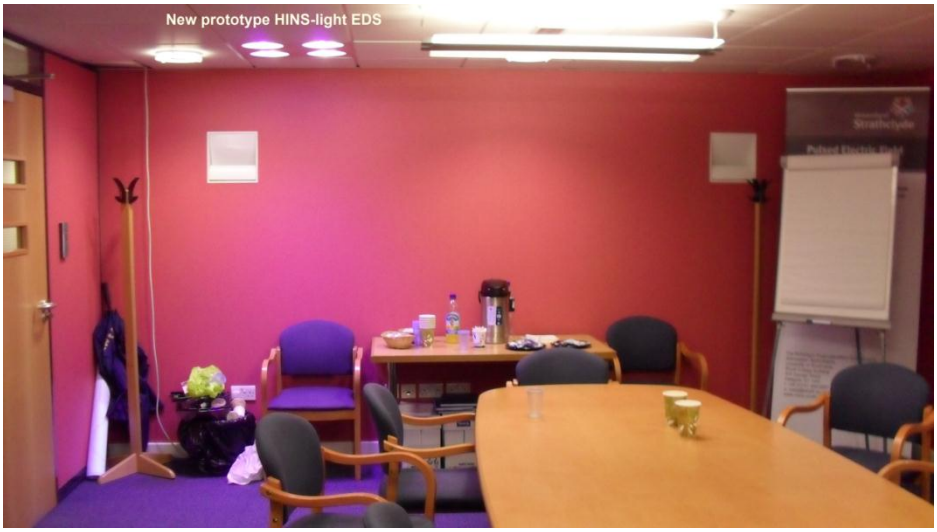

Fig. 9.42. *New prototype HINS-light EDS installed in the ROLEST conference room.*

The ability to operate the HINS-light EDS in the presence of people is a clear advantage over exiting light decontamination system. For example, Nerandzic *et al.* [120] and Rutala *et al.* [121], utilised UV-C light radiated by the Tru-D™ Rapid Room Disinfection device (Lumalier, Memphis, TN) in order to kill pathogens in a contaminated hospital room [120, 121]. The decontamination process had to be carried out in an empty hospital room with the Tru-D™ system located in the room, with all doors closed and the system operated using a wireless remote control [120, 121].

The unique features of the new HINS-light EDS opens up many potential applications for the continuous disinfection of air and surfaces in hospital wards, clinics, the food industry and within public buildings. Further discussion on applications of the new HINS-light EDS for bacterial inactivation will be given in Chapter 10.

CHAPTER 10

APPLICATION OF THE NEW PROTOTYPE HINS-LIGHT ENVIRONMENTAL DECONTAMINATION SYSTEM FOR INACTIVATION OF PATHOGENIC BACTERIA

10.1 General

This chapter investigates the effectiveness of the new prototype HINS-light EDS for the inactivation of clinical and foodborne pathogens such as *Staphylococcus aureus*, *Escherichia coli* and *Listeria monocytogenes*.

In Part I, the study investigates the effectiveness of individual 405 nm LED light engine components of the HINS-light EDS for inactivation of *Staphylococcus aureus* in liquid suspensions. In Part II, the study focuses on an investigation into the effectiveness of the new prototype HINS-light EDS for bacterial inactivation on agar surfaces. A comparison of the inactivation efficacy of the new prototype HINS-light EDS with the previous HINS-light EDS prototype is also included.

10.2 Inactivation of *Staphylococcus aureus* in liquid suspension using individual 405 nm LED light engines

10.2.1 Microorganism and Sample preparation

The microorganism used in the study was *Staphylococcus aureus* and this was cultured and prepared for experimental use, as described in Section 3.2.2. Two ml volumes of bacterial suspension with a population density of 10^5 CFUml^{-1} were used in the experiments.

10.2.2 Experimental Method

The new prototype HINS-light EDS contains four light engines which emit the 405nm radiation. These 405 nm light sources were ENFIS Uno Air Cooled Light Engines obtained from the ENFIS Ltd, UK [185]. It was considered important to investigate the variability of the emission spectra from individual light engines and to

determine if this would affect their bactericidal properties. To investigate variability, three individual 405 nm LED light engines with slightly different peak wavelength were used for comparison. The actual peak wavelength of these light engines were 400.46, 405.72 and 407.82 nm.

As in Section 6.2.3, for bacterial exposure to the 405 nm LED light engines, 2 ml volumes of bacterial suspension (7 mm depth) were held in one well of a 12-well plate with the light engine placed above the sample at a distance of 3 cm. The sample was mechanically agitated during light exposure.

Control samples were set-up using the same procedure but not exposed to the 405 nm light engines. For all experiments the voltage was set to 11.8 ± 0.1 V with a current of 0.30 ± 0.01 A, giving an intensity of 14.5 $mWcm^{-2}$ at the surface of the suspension. Bacterial samples were then plated and enumerated as described in Section 3.4.2.

10.2.3 Results

Fig. 10.1 shows log_{10} reductions as a function of dose for inactivation of *S. aureus* in liquid suspension with an initial population of approximately 10^5 $CFUml^{-1}$. Results demonstrate that the complete inactivation of *S. aureus* was achieved after exposure to a dose of 208.8 Jcm^{-2} with a 4.96, 4.96 and 5.14-log_{10} reduction in bacterial population for the three light sources with peak wavelengths at 400.46, 405.72 and 407.82 nm, respectively.

When the three different 405 nm light engines with peak wavelengths of 400.46, 405.72 and 407.82 nm are used for inactivation of *S. aureus,* the results demonstrate that the same pattern of log_{10} reductions in bacterial population were achieved and all data points demonstrate no significant difference when the three 405 nm light engines of 405 nm LED are compared, except with a dose of 156.6 Jcm^{-2} (Table 10.1).

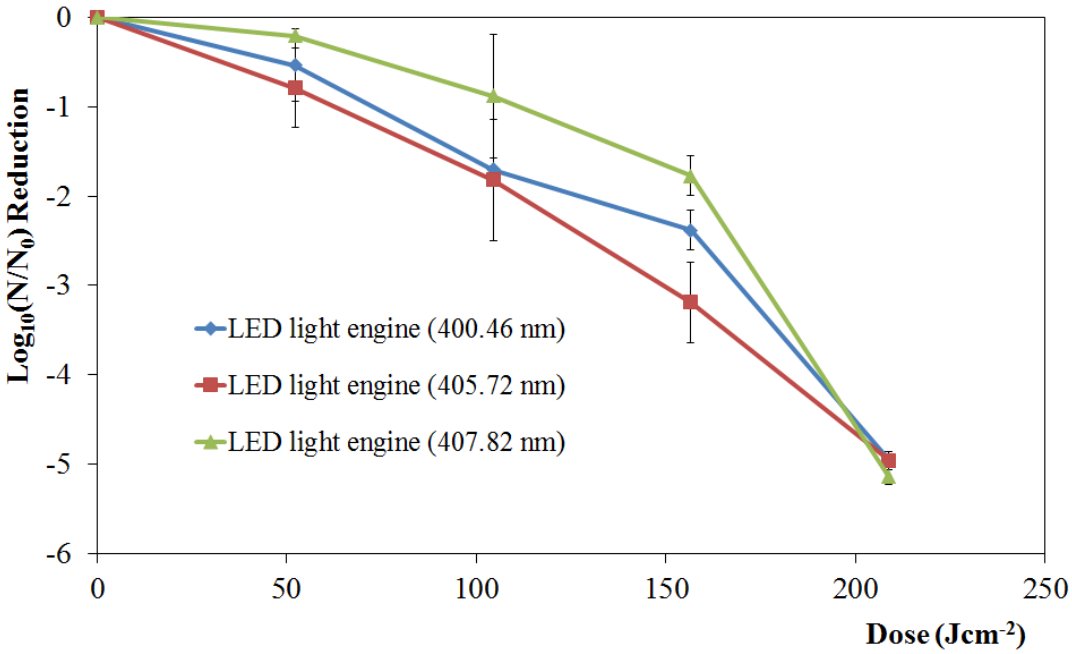

Fig. 10.1. *Log_{10} (N/N_0) reduction as a function of dose for inactivation of 10^5 $CFUml^{-1}$ S. aureus suspension using three 405 nm LED light engines with differing peak wavelengths.*

Table 10.1 *Statistical significance (*) when log_{10} reductions are compared with log_{10} reductions for different peak wavelengths of light engine, p value ≤ 0.05 calculated at the 95% confidence interval using one-way ANOVA MINITAB Release 16.*

Dose (Jcm^{-2})	***p* value for comparison of data log_{10} reductions for different peak wavelengths of light engine**		
	400.46 nm vs 405.72 nm	**400.46 nm vs 407.82 nm**	**405.72 nm vs 407.82 nm**
52.2	0.248	0.247	0.168
104.4	0.767	0.065	0.127
156.6	0.003*	0.003*	0.001*
208.8	1.000	0.053	0.052

A summary of $\log_{10}$ reduction and germicidal efficiency for inactivation of *S. aureus* using the three LED light engines with slightly different peak wavelengths are presented in Table 10.2, Table 10.3 and Table 10.4.

Table 10.2 *Log_{10} reduction, germicidal efficiency and statistical significance for bacterial inactivation of S. aureus using light engine with peak wavelength at 400.46 nm*

Dose (Jcm^{-2})	N_0	N	$Log_{10}(N/N_0)$ Reduction	η ($Log_{10}(N/N_0)/Jcm^{-2}$)	*p* value
0	5.14 (± 0.02)	5.14 (± 0.02)	0.00	0.000	-
52.2	5.11 (± 0.04)	4.57 (± 0.33)	0.54*	0.010	0.001
104.4	5.09 (± 0.04)	3.38 (± 0.60)	1.71*	0.016	0.000
156.6	5.08 (± 0.07)	2.70 (± 0.23)	2.38*	0.015	0.000
208.8	4.96 (± 0.07)	0.00 (± 0.00)	4.96*	0.024	0.000

Table 10.3 *Log_{10} reduction, germicidal efficiency and statistical significance for bacterial inactivation of S. aureus using light engine with peak wavelength at 405.72 nm*

Dose (Jcm^{-2})	N_0	N	$Log_{10}(N/N_0)$ Reduction	η ($Log_{10}(N/N_0)/Jcm^{-2}$)	*p* value
0	5.14 (± 0.02)	5.14 (± 0.02)	0.00	0.000	-
52.2	5.11 (± 0.04)	4.32 (± 0.35)	0.79*	0.015	0.000
104.4	5.09 (± 0.04)	3.27 (± 0.51)	1.82*	0.017	0.000
156.6	5.08 (± 0.07)	1.89 (± 0.38)	3.19*	0.020	0.000
208.8	4.96 (± 0.07)	0.00 (± 0.00)	4.96*	0.024	0.000

Table 10.4 *Log_{10} reduction, germicidal efficiency and statistical significance for bacterial inactivation of S. aureus using light engine with peak wavelength at 407.82 nm*

Dose (Jcm^{-2})	N_0	N	$Log_{10}(N/N_0)$ Reduction	η ($Log_{10}(N/N_0)/Jcm^{-2}$)	*p* value
0	5.15 (± 0.05)	5.15 (± 0.05)	0.00	0.000	-
52.2	5.11 (± 0.03)	4.90 (± 0.03)	0.21*	0.004	0.007
104.4	5.06 (± 0.05)	4.18 (± 0.54)	0.88*	0.008	0.000
156.6	5.10 (± 0.02)	3.32 (± 0.38)	1.78*	0.011	0.000
208.8	5.14 (± 0.06)	0.00 (± 0.00)	5.14*	0.025	0.000

N_0 is initial population ($Log_{10}CFUml^{-1}$)
N is final population ($Log_{10}CFUml^{-1}$)
η is germicidal efficiency
* Significant bacterial $\log_{10}$ reductions, calculated at a 95% confidence interval (*p* value ≤ 0.05). (Light-exposed sample value was significantly different from control value).

Overall, this study has demonstrated that a sample selection of three of the 405 nm LED light engines used in the design of the new prototype HINS-light EDS are effective for inactivation of *S. aureus* in liquid suspension, and therefore have good bactericidal activity. This confirms that these 405 nm LED light engines, although somewhat variable in their peak wavelength emission are nevertheless suitable components for the HINS-light EDS.

10.3 Bacterial inactivation on surfaces using the new prototype HINS-light EDS

10.3.1 Microorganism, Sample preparation and Enumeration

The microorganisms used in this part of the study were *Staphylococcus aureus*, *Listeria monocytogenes* and *Escherichia coli*. Microorganisms were cultivated for 18 – 24 h in 100 ml Nutrient Broth at 37 °C under rotary conditions (120 rpm).

Cultures were centrifuged and re-suspended in PBS and then serially diluted in PBS to provide the appropriate population densities for experimental use (Section 3.4.1). 100 µl volumes of bacterial suspension with population density of 10^3 CFUml^{-1} were pipetted onto an agar plate (63.59 cm^2) and spread over the agar surface using a sterile L-shaped spreader. This gave approximately 200 CFUplate^{-1} for *S. aureus* and *E. coli*, and 100 CFUplate^{-1} for *L. monocytogenes*. These seeded agar plates were then exposed to the HINS-light EDS with the plate lid off.

After light treatment, all samples were incubated at 37 °C for 24 hours before manual enumeration (Section 3.4.2).

10.3.2 Is this new prototype effective for bacterial inactivation?

10.3.2.1 Experimental method

For the light treatment using the HINS-light EDS only the 405 nm LED light engines were switched on. The white LED components that are incorporated only for visual aesthetic effect were left off. To assess bactericidal effectiveness 12 sample agar plates were prepared (as in Section 10.3.1) and placed at a distance of 120 cm below the light source, as shown in Fig. 10.2. The average irradiance used in the study was

0.17 ± 0.03 mWcm^{-2} using 405 nm LEDs only, with exposure times set at 1, 3, 6 and 9 hours for each independent experiment. Control samples were set-up using the same procedure but not exposed to 405 nm light sources but left in normal laboratory lighting conditions. In this study, all data were taken a minimum of three times for each independent experiment, and the results are documented as mean values with standard deviation (SD) being included.

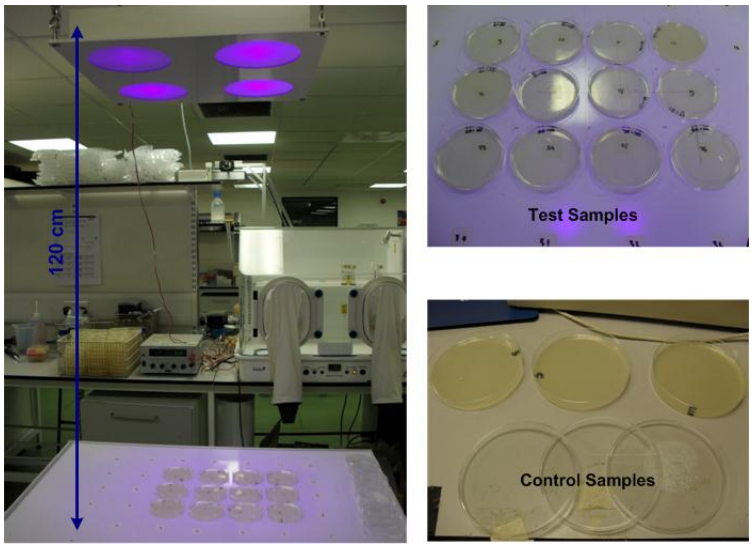

Fig. 10.2. *Experimental setup for inactivation of S. aureus on agar surfaces using the new prototype HINS-light EDS.*

10.3.2.2 Results

Results from this study are displayed in Fig. 10.3, and it can be seen that the new prototype HINS-light EDS is effective for inactivation of *S. aureus* on agar surfaces with an average of around 62 CFUplate^{-1} surviving after exposure to 3 hours (66.7 % kill). When sample plates were light exposed for 6 and 9 hours, an average of 17 and 19 CFUplate^{-1} (88.5 and 90 % kill) of *S. aureus* survived, respectively. Comparison of the inactivation rate for each individual test sample are summarised in Table 10.5. As stated in Table 10.5, all data tests demonstrate significant differences in bacterial inactivation (test samples compared with test samples for different times of exposure) except when light exposed samples for 6 and 9 hours are compared. The possible reason for these results is due to a slow rate of inactivation after exposure time of 6 hours.

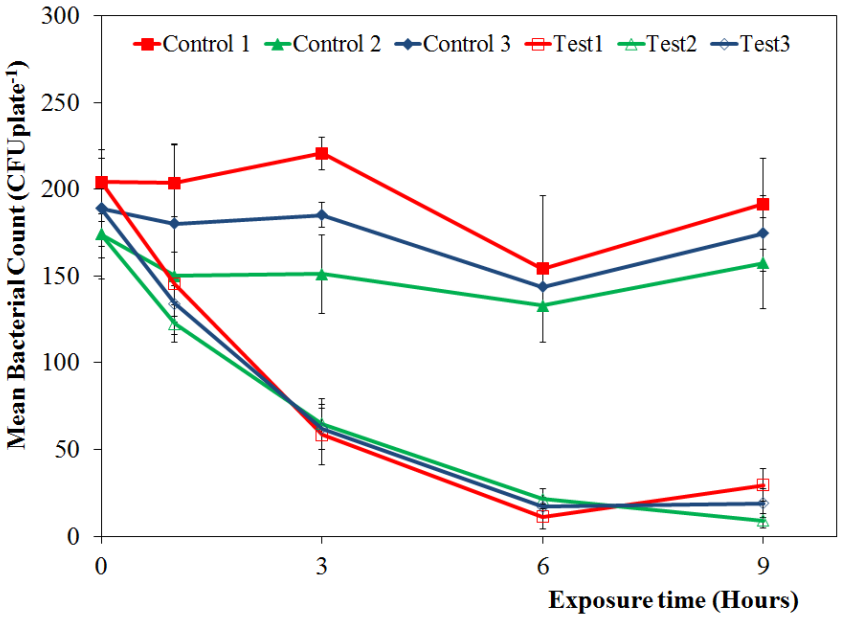

Fig. 10.3. *Inactivation of S. aureus on agar surfaces using the new prototype HINS-light EDS.*

Table 10.5 *Statistical significance (*) when test samples are compared with test samples for different times of exposure, p value ≤ 0.05 calculated at the 95% confidence interval using one-way ANOVA MINITAB Release 16*

Comparison of data inactivation rates for different times of light exposure	***p* value**
0 Hour *vs* 1 Hour	0.002*
0 Hours *vs* 3 Hours	0.000*
0 Hour *vs* 6 Hours	0.000*
0 Hour *vs* 9 Hours	0.000*
1 Hour *vs* 3 Hours	0.000*
1 Hour *vs* 6 Hours	0.000*
1 Hour *vs* 9 Hours	0.000*
3 Hours *vs* 6 Hours	0.000*
3 Hours *vs* 9 Hours	0.000*
6 Hours *vs* 9 Hours	0.178

10.3.3 How does inactivation rate vary with irradiance?

10.3.3.1 Experimental method

The aim of this study was to determine how the effectiveness of the new prototype HINS-light EDS for bacterial inactivation varies with irradiance. This was done for a radius of 200 cm measured from centre at a distance of 200 cm below the light source. For the light treatment, 21 seeded agar plates were prepared (as in Section 10.3.1) and placed at a distance of 200 cm below the light source as illustrated in Fig. 10.4. Exposure times used in the study were set at 1, 3, 6 and 9 hours for each independent experiment. Control samples were set-up using the same procedure but not exposed to 405 nm light sources but left in laboratory lighting conditions.

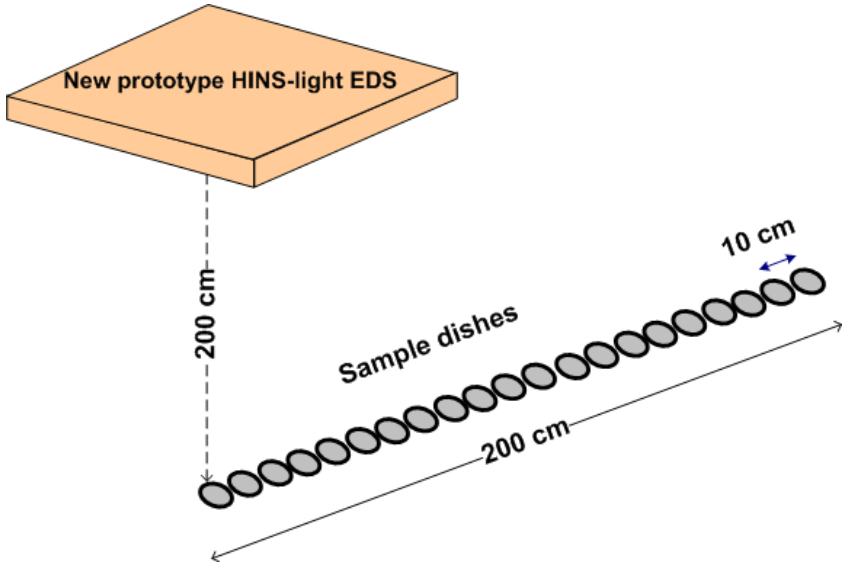

Fig. 10.4. *Experimental method for investigation of how inactivation of S. aureus on agar surfaces varies with irradiance using the new prototype HINS-light EDS.*

10.3.3.2 Results

Fig. 10.5 shows an inactivation curve for light treatment of *S. aureus* on agar surfaces and how inactivation varies with irradiance along a 200 cm distance from the centre at a distance of 200 cm below the new prototype HINS-light EDS. Irradiance measurement as a function of distance is also shown in Fig. 10.5. The results, shown in Fig. 10.5, demonstrate inactivation rates of *S. aureus* on agar

surfaces at a distance of 200 cm below the HINS-light source, and 51.6, 82.1 and 83.7% reductions in bacterial population after 3, 6 and 9 hours exposure were achieved, respectively. When the agar plates placed at 200 cm off centre (at a distance of 200 cm below the HINS-light EDS) had exposures of 3, 6, and 9 hours, approximately 18, 10, and 30% reductions in bacterial population were achieved, respectively.

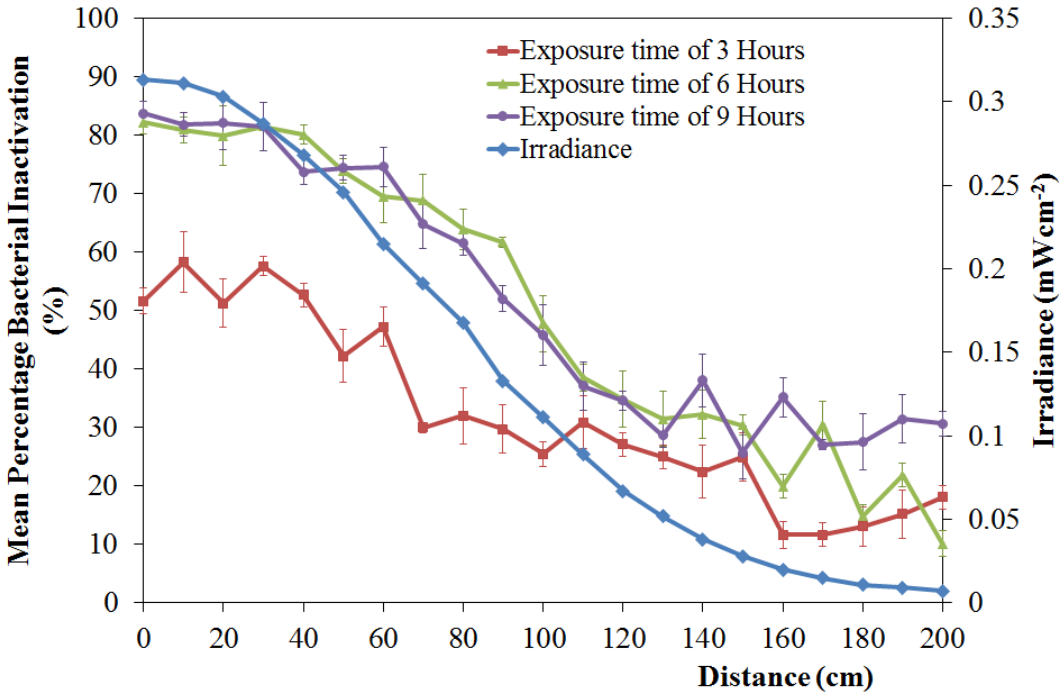

Fig. 10.5. *Investigation of how inactivation of S. aureus on agar surfaces varies with irradiance using the new prototype HINS-light EDS.*

10.3.4 How uniform is the inactivation effect?

10.3.4.1 Irradiance measurements

Measurement of irradiance distributions were taken every 20 cm from the centre along five directions, as illustrated in Fig. 10.6. Space distance between the new prototype HINS-light EDS and illuminated area was set at 200 cm. The data of irradiance used in the study is shown in Fig. 10.7, and it can be seen that all data show a similar value along each of the 5 directions, indicating that the irradiance distribution is uniform along the five directions.

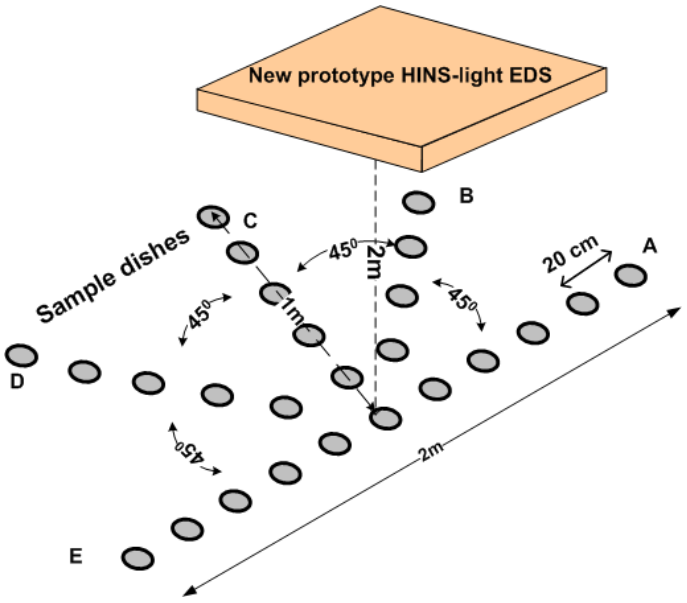

Fig. 10.6. *Experimental arrangement for irradiance measurements for all five directions.*

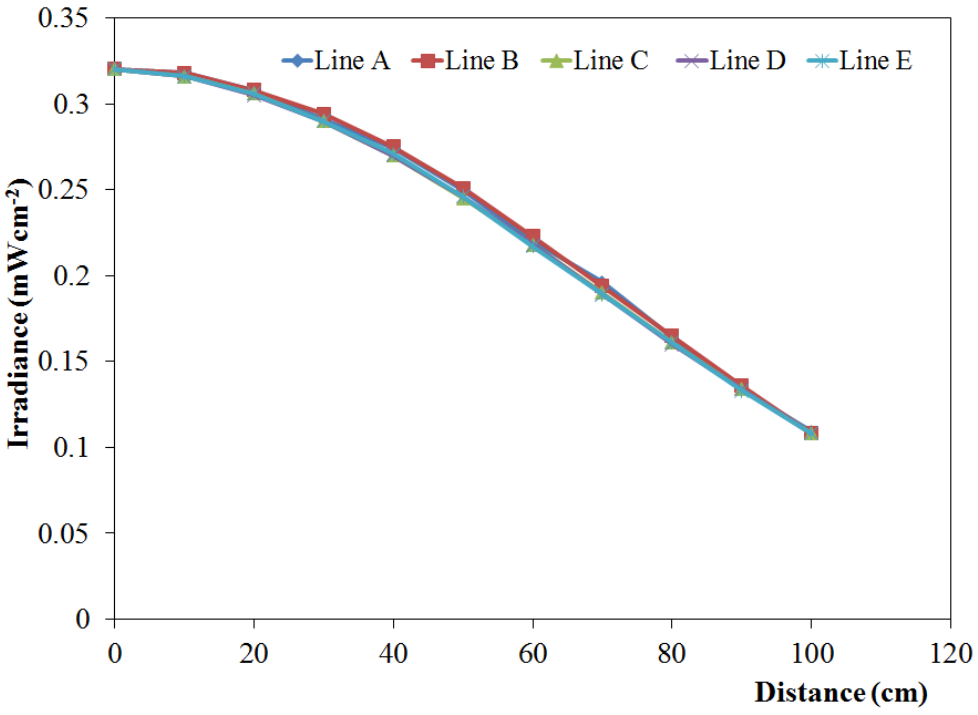

Fig. 10.7. *Irradiance as a function of distance for all five directions.*

10.3.4.2 Experimental method

For light treatment, 26 sample plates were prepared (as in Section 10.3.1) and placed at a distance of 200 cm below the light source along five directions as illustrated in Fig. 10.8. Exposure times used in the study were set at 6 hours for each independent experiment. Control samples were set-up using the same procedure but not exposed to 405 nm light sources and left in laboratory lighting conditions.

In this study, all data were taken a minimum of three times for each independent experiment, and the results are documented as mean values with standard deviation (SD) being included. Significant differences in experiments are resulted from data analysis one-way ANOVA with 95% confidence interval and p value ≤ 0.05 using MINITAB Release 16.

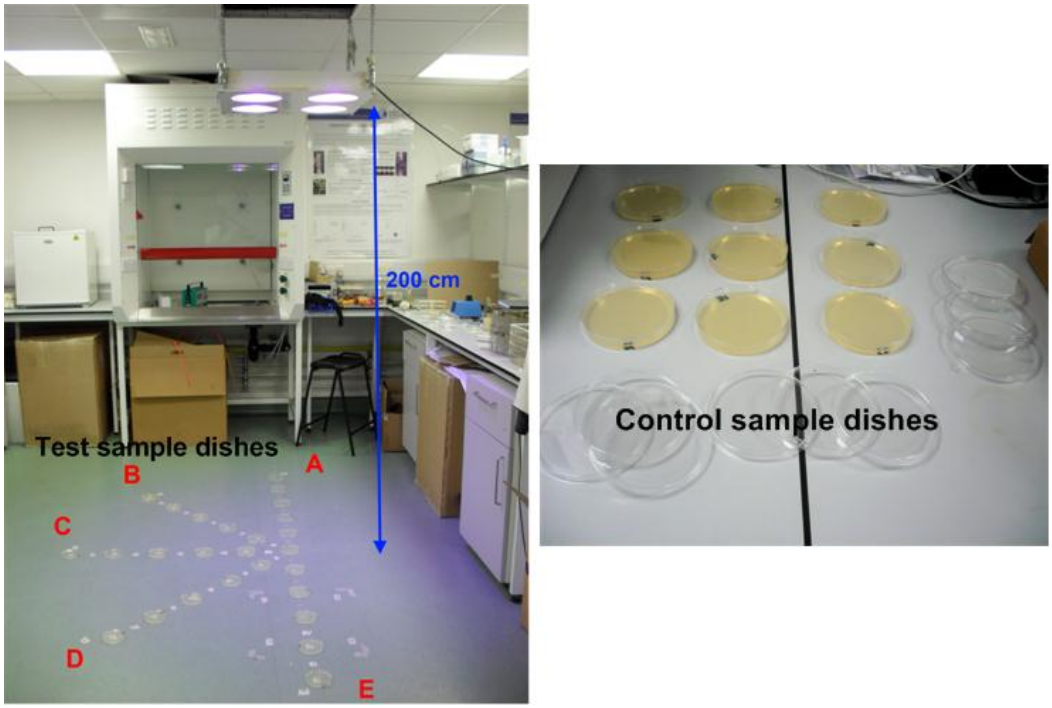

Fig. 10.8. *Experimental method for inactivation of S. aureus on agar surfaces to determine whether the new prototype HINS-light EDS produces a uniform inactivation effect.*

10.3.4.3 Results

Results, shown in Fig. 10.9, demonstrate that similar inactivation rates were achieved along all five directions, with around 73% bacterial inactivation at a distance of 200 cm directly below the new HINS-light EDS. Table 10.6 contains comparison data for test sample plates for each independent experiment at the same position (all five directions). Statistical analysis showed that there was no significant differences in the inactivation rate for all five directions, except with three tests (line A and E at 20 cm, line B and E at 20 cm and line B and C at 40 cm), as stated in Table 10.6. Significant differences for the three tests are only less than 5% bacterial inactivation (as shown in Fig. 10.9), and, the general trendlines clearly indicate that the inactivation rate is uniform along all five directions.

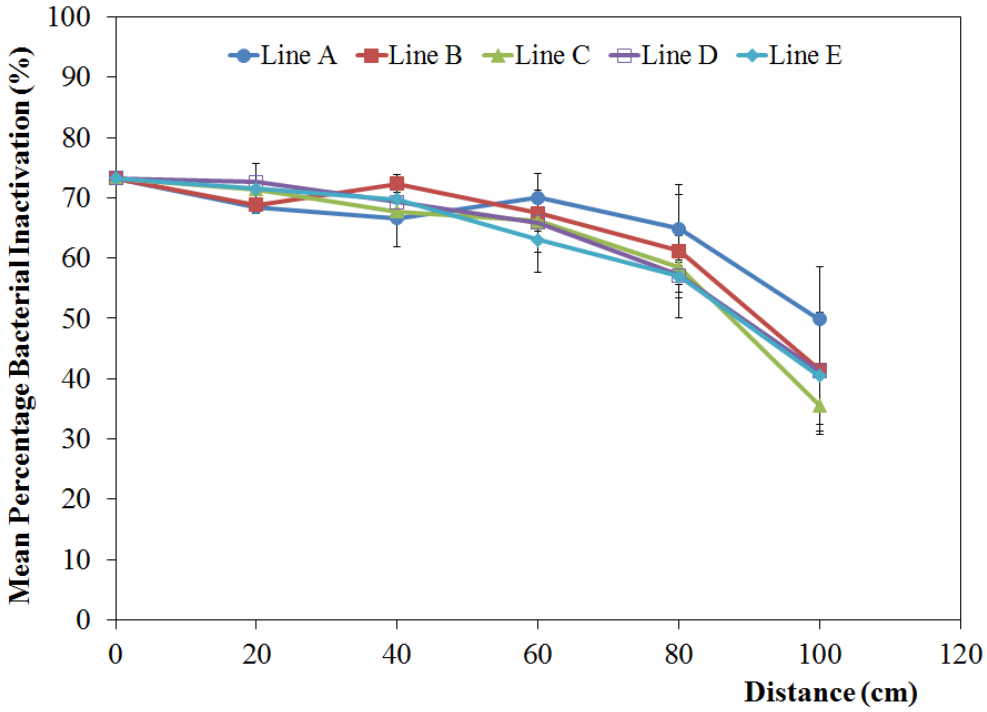

Fig. 10.9. *Inactivation rate of S. aureus for all five directions below the HINS-light EDS.*

Table 10.6 *Statistical significance (*) when test samples compared with test samples at same position for all five directions, p value ≤ 0.05 calculated at the 95% confidence interval using one-way ANOVA MINITAB Release 16*

Comparative data inactivation rates along line	at 20 cm *(p value)*	at 40 cm *(p value)*	at 60 cm *(p value)*	at 80 cm *(p value)*	at 100 cm *(p value)*
A *vs* B	0.635	0.113	0.362	0.627	0.319
A *vs* C	0.093	0.713	0.36	0.218	0.069
A *vs* D	0.081	0.428	0.168	0.082	0.32
A *vs* E	0.001*	0.363	0.147	0.091	0.271
B *vs* C	0.186	0.017*	0.696	0.725	0.369
B *vs* D	0.133	0.142	0.271	0.569	0.965
B *vs* E	0.042*	0.183	0.248	0.558	0.893
C *vs* D	0.623	0.389	0.938	0.689	0.425
C *vs* E	0.938	0.279	0.511	0.67	0.457
D *vs* E	0.585	0.842	0.427	0.917	0.932

10.3.5 Inactivation of *Escherichia coli* and *Listeria monocytogenes* on agar surfaces

10.3.5.1 Experimental method

As described in Section 10.3.1, 100 µl volumes of bacterial suspension of 10^3 CFUml^{-1} were spread onto 63.59 cm^2 Petri dish plates of Nutrient Agar (NA). These samples (with the Petri lid off) were placed underneath the HINS-light EDS at a distance of 200 cm below the centre, with plates at 20 cm intervals moving outwards from the centre (as in Fig. 10.8). The populations of around 200 CFUplate^{-1} of *E. coli* and 100 CFUplate^{-1} of *L. monocytogenes* were exposed for 3, 6 and 9 hours.

Control samples were also set-up; 100 µl volumes of bacterial suspension of 10^3 CFUml^{-1} were spread onto NA plates and left in laboratory lighting condition. In this study, all data were taken a minimum of three times for each independent experiment, and the results are documented as mean values with standard deviation (SD) being included.

10.3.5.2 Results

Fig. 10.10 and Fig. 10.11 show bacterial inactivation curves for *E. coli* and *L. monocytogenes* on agar surfaces, and how inactivation varies with distance from the centre of the light source. The results of *E. coli* inactivation, shown in Fig. 10.10, demonstrate that at a distance of 200 cm below the HINS-light EDS, 29.7%, 57.1%, and 61.9% reductions were achieved after 3, 6 and 9 hours exposure, respectively. After light exposure to 3, 6 and 9 hours at 100 cm off centre (at a distance of 200 cm below the HINS-light EDS), 18.1%, 33.6% and 42.1% reductions in bacterial population were achieved, respectively.

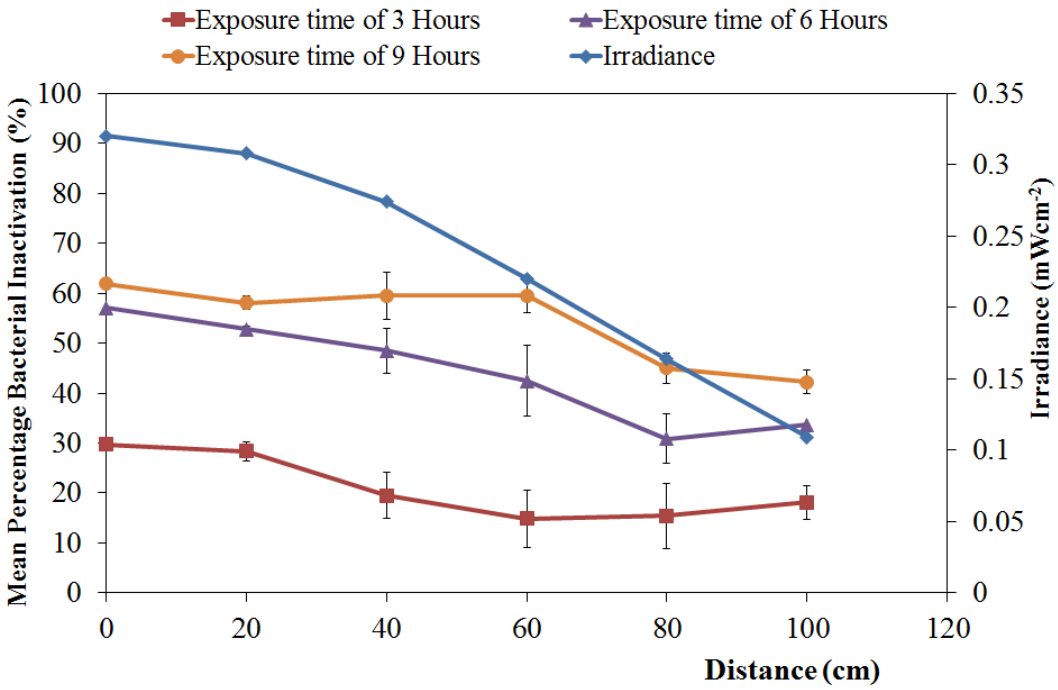

Fig. 10.10. *Inactivation rates of E. coli on agar surfaces using the HINS-light EDS.*

When *L. monocytogenes* was light-exposed for 9 hours, the results show that the mean percentage bacterial inactivation was around 77 – 74% reduction in bacterial population for plates placed at 20 – 100 cm from the centre below the light source at a distance of 200 cm, as shown in Fig. 10.11.

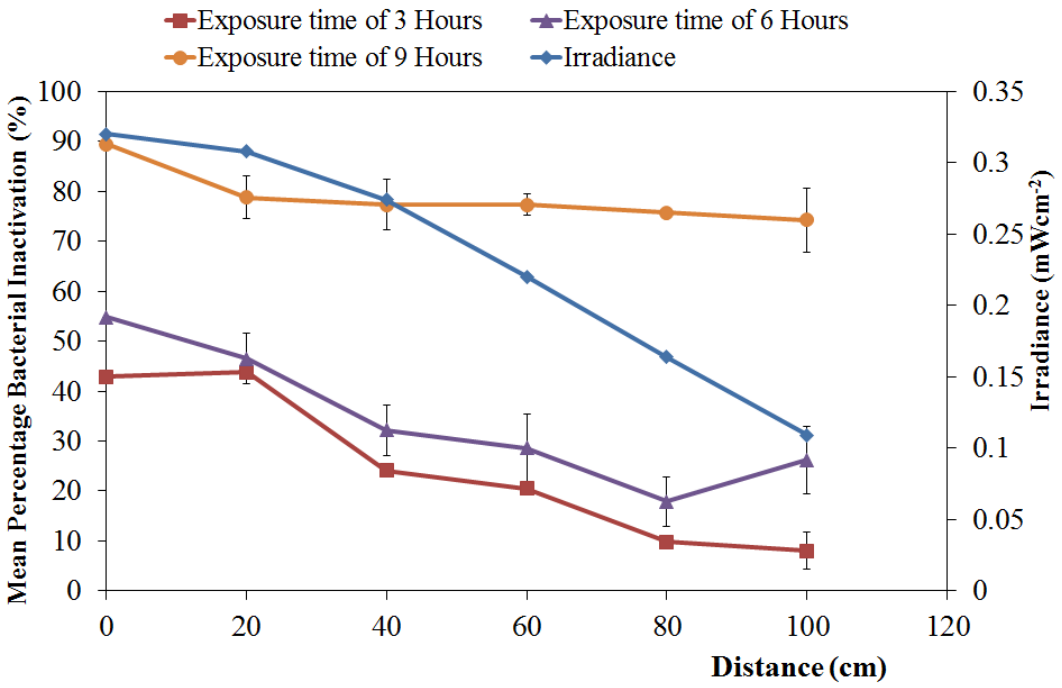

Fig. 10.11. *Inactivation rates of L. monocytogenes on agar surfaces using the HINS-light EDS.*

10.3.6 Comparison of the inactivation efficacy of the HINS-light EDS previous prototype versus the new developed prototype

10.3.6.1 Experimental method

For this experiment, agar plates seeded with *S. aureus* were exposed to light treatment from the previous (initial) HINS-light EDS prototype, with the aim of comparing these inactivation kinetics with those achieved using the newly-developed prototype. A description of the initial prototype can be found in Chapter 9, Section 9.6. As described in Section 10.3.2.1, 12 sample agar plates were prepared (as in Section 10.3.1) and placed at a distance of 156 cm below the HINS-light EDS unit, as shown in Fig. 10.12. The average irradiance used in the study was 0.18 ± 0.01 $mWcm^{-2}$ using the 405 nm LEDs only, with exposure times set at 1, 3, 6 and 9 hours for each independent experiment. Control samples were set-up using the same

procedure but not exposed to 405 nm light sources but left in normal laboratory lighting conditions. In this study, all data were taken in triplicate for each independent experiment, and the results are documented as mean values with standard deviation (SD) being included.

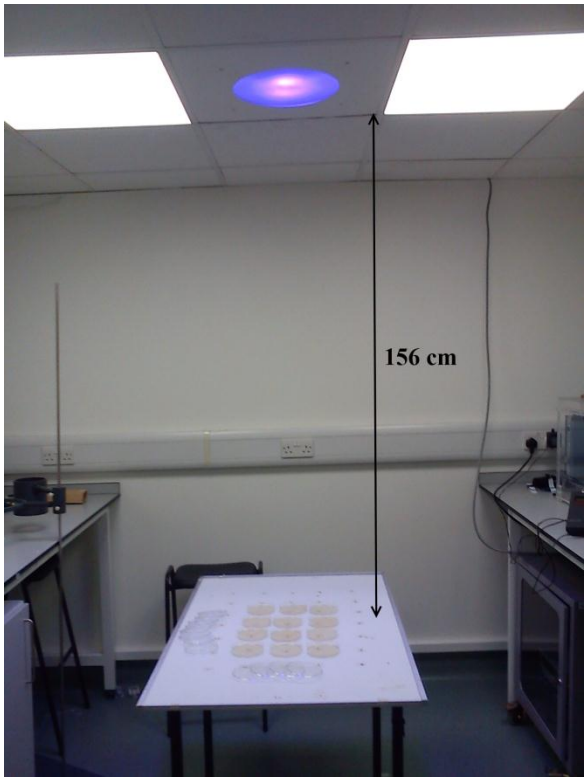

Fig. 10.12. *Experimental setup for inactivation of S. aureus on agar surfaces using the initial HINS-light EDS prototype.*

10.3.6.2 Results

The results, shown in Fig. 10.13, demonstrate the inactivation curve for *S. aureus* on agar surfaces using the initial prototype, with 8.0, 9.0, 54.2 and 93.2 % reductions in bacterial population after 1, 3, 6, and 9 hours exposure, respectively.

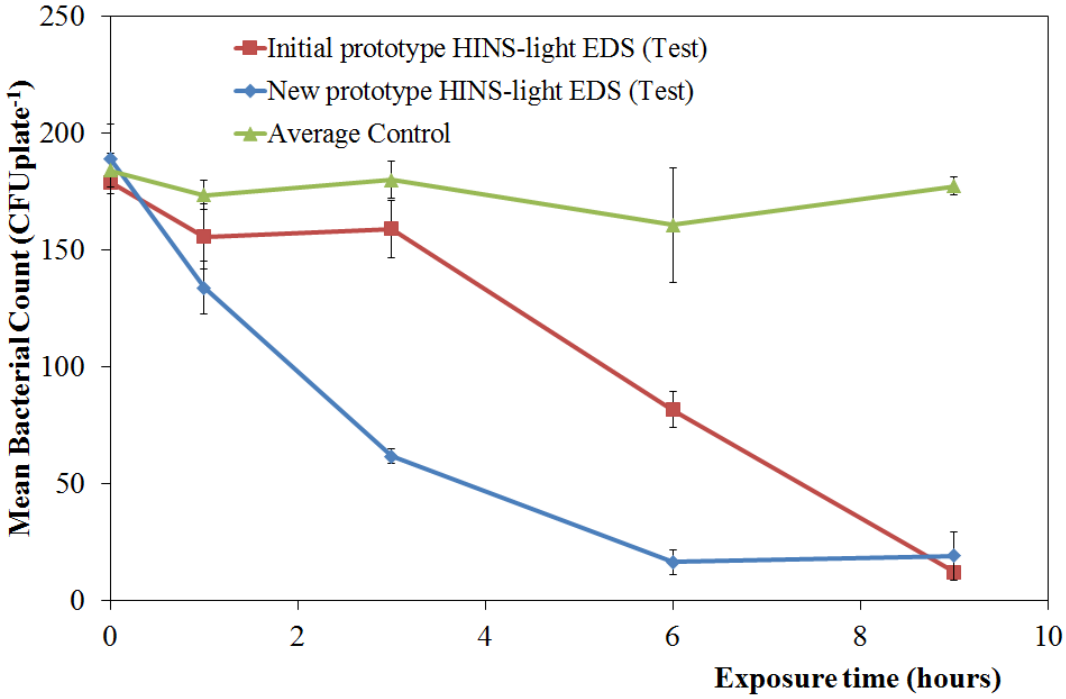

Fig. 10.13. *Inactivation rates of S. aureus on agar surfaces using both the initial and new prototype HINS-light EDS.*

It can be observed from Fig. 10.13 that statistically significant differences were obtained when test samples were compared after 1, 3, and 6 hours exposure for inactivation of *S. aureus* on agar surfaces using both the initial and new prototype HINS-light EDS, p value ≤ 0.05 calculated at the 95% confidence interval using one-way ANOVA MINITAB Release 16.

Table 10.7 contains a comparison of the inactivation rate for each individual test sample using the initial prototype EDS. It can be observed from Table 10.7 that all data demonstrate a significant difference in bacterial inactivation (test samples compared with test samples for different times of exposure) except when the light exposed samples for 1 and 3 hours are compared.

Table 10.7 *Statistical significance (*) when test samples are compared with test samples for different times of exposure using the initial EDS prototype, p value ≤ 0.05 calculated at the 95% confidence interval using one-way ANOVA MINITAB Release 16.*

Comparison of data inactivation rates for different times of light exposure to initial EDS	***p* value**
0 Hour *vs* 1 Hour	0.045*
0 Hours *vs* 3 Hours	0.047*
0 Hour *vs* 6 Hours	0.000*
0 Hour *vs* 9 Hours	0.000*
1 Hour *vs* 3 Hours	0.771
1 Hour *vs* 6 Hours	0.001*
1 Hour *vs* 9 Hours	0.000*
3 Hours *vs* 6 Hours	0.001*
3 Hours *vs* 9 Hours	0.000*
6 Hours *vs* 9 Hours	0.000*

10.4 Discussion and Conclusions

In Part I, the study has demonstrated the effectiveness of the individual 405 nm LED light engine components of the HINS-light EDS for inactivation of *Staphylococcus aureus* in liquid suspensions. When three of the light engines were compared for inactivation of *S. aureus* suspensions, similar the inactivation curves were found for each individual light engine although they had slightly different peak wavelengths. This result provided reassurance that the new HINS-light prototype units that would each contain four different light engines would provide effective bactericidal light even though there would be some variability in the emission spectra of the individual light engines.

As shown in Fig. 6.5, *S. aureus* suspensions can be inactivated by exposure to both 405 nm filtered light and a 405 nm LED array, with a 4.7 and 4.6-$\log_{10}$ reduction in bacterial population, respectively, after light exposure to a dose of 154.1 Jcm^{-2}. These data can be compared to the inactivation data generated using the three 405 nm light engines (peaks at 400.46, 405.72 and 407.82 nm), and this comparison is shown in Table 10.8. Germicidal efficiency data demonstrates that the use of 405

nm LED array and the 405 nm filtered light for inactivation of *S. aureus* (in Chapter 6) had somewhat higher germicidal efficiency when compared to that for the use of the three different 405 nm light engines. All three of the 405 nm light engines had similar germicidal efficiency, with 0.024 and 0.025 $\log_{10}(N/N_0)$ per Jcm^{-2}, as stated in Table 10.8. The possible reason for these differences in results is most probably due to the different protocols used in these experiments. Regardless of these differences, the results obtained clearly show that the 405 nm light engines can be used for bacterial inactivation.

Table 10.8 *Summary parameters for inactivation of 10^5 CFUml^{-1} suspensions of S. aureus following exposure to 405 nm filtered light from Xenon lamp, 405 nm high-intensity LED array and 405 nm light engines.*

Light source	Peak Wavelength (nm)	Dose (Jcm^{-2})	Log$_{10}$ (N/N$_0$) reduction	Germicidal efficiency (Log$_{10}$ (N/N$_0$) per Jcm^{-2})
405 nm filtered light	401.51	154.1	4.71	0.031
405 nm LED array	400.46	154.1	4.62	0.030
405 nm light engine	400.46	208.8	4.96	0.024
405 nm light engine	405.72	208.8	4.96	0.024
405 nm light engine	407.82	208.8	5.14	0.025

In Part II, this study has demonstrated the effectiveness of the new prototype HINS-light EDS design for inactivation of *Staphylococcus aureus, Escherichia coli* and *Listeria monocytogenes* on agar surfaces.

As shown in Fig. 10.3, the new prototype HINS-light EDS is effective for inactivation of *S. aureus* on agar surfaces. The new prototype has been shown to provide reductions on agar surface of up to 90% following 9 hours exposure. These data are valuable to compare to inactivation data gained using the initial prototype HINS-light EDS, and the results are compared in Fig. 10.14.

The results, shown in Fig 10.14, demonstrate that the new prototype is more effective than the initial prototype when mean percentage bacterial inactivations are compared for exposure times 1, 3 and 6 hours. Similar mean percentage bacterial inactivation was achieved after 9 hours exposure for both the new prototype and the initial prototype HINS-light EDS, with approximately 90% reductions in bacterial population.

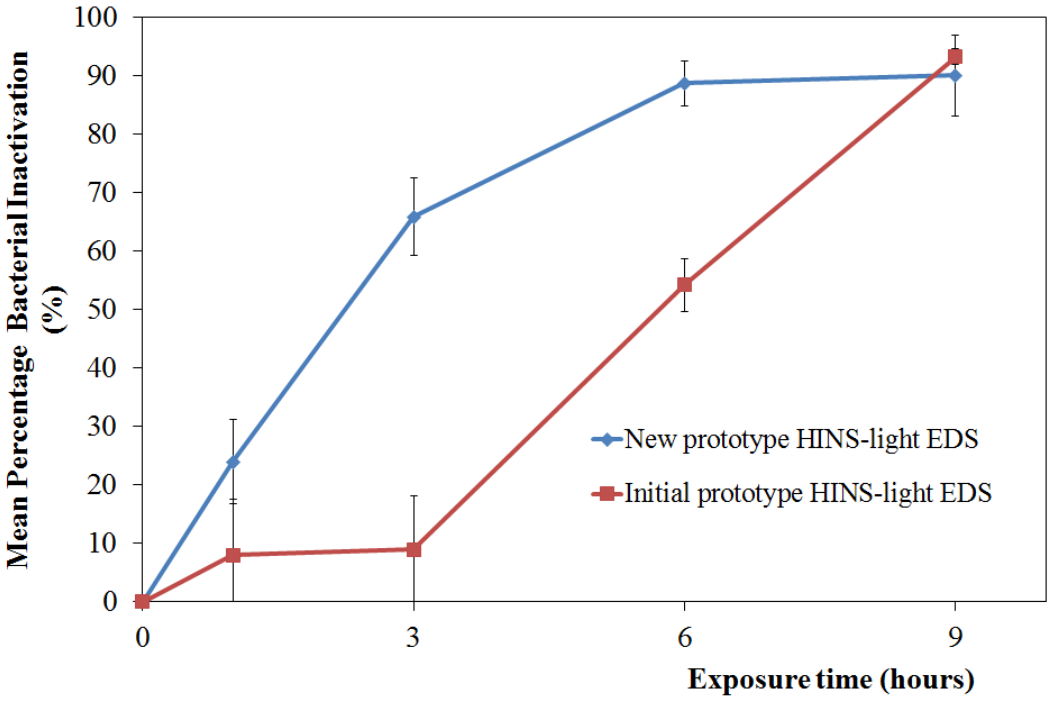

Fig. 10.14. *Inactivation rates of S. aureus on agar surfaces using the new prototype and initial prototype HINS-light EDS.*

When inactivation data for both the new prototype and the initial prototype are compared, all data points demonstrate significant differences except when light exposed samples for 9 hours are compared. The inactivation achieved after 9 hours exposure is not significantly different between the two units. This indicates that the two systems have a similar efficiency over longer time periods, but the new prototype appears to be more efficient over the shorter exposure times.

As stated in Table 10.8, the use of the 405 nm LED array (the main component of the initial prototype HINS-light EDS) for inactivation of *S. aureus* suspensions had higher germicidal efficiency when compared to that of the three different 405 nm light engines (the main component of the new prototype HINS-light EDS). However when the light engines are incorporated into the new prototype HINS-light EDS units, they appear to achieve similar results. Both the initial and new prototypes achieved 90% reduction in bacterial populations after 9 hours exposure.

The difference in the experimental germicidal efficiency value results is readily explained when the area of the 405 nm LED array (320 mm^2) as shown in Fig. 6.2a and the 405 nm light engine (50 mm^2) as shown in Fig. 7.2 are compared to the area of one well of a 12-well plate (380 mm^2) as shown in Fig. 6.4. The main reason why the 405 nm LED array is more efficient in this experimental set up is due to the fact that the whole well can be exposed. Whereas with the 405 light engine is not all regions in the well can be irradiated (Fig. 10. 15). This difference does not apply with the full scale HINS-light EDS prototypes as these were compared for bacterial inactivation of *S. aureus* on agar surfaces. In these full scale tests it has been demonstrated that a similar inactivation rate was achieved after 9 hours exposure. This was not surprising since the new prototype HINS-light EDS was designed to have an output wavelength emission and irradiance pattern similar to the initial prototype.

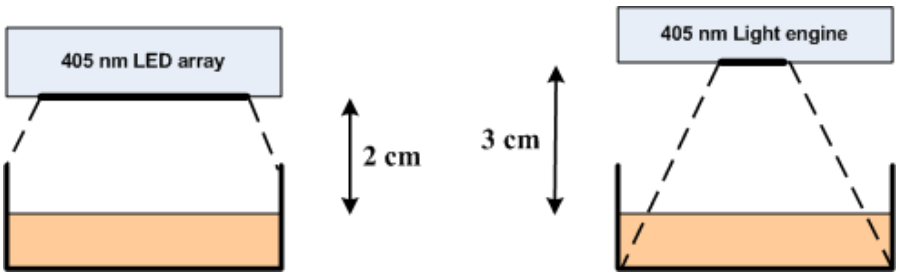

Fig. 10.15. *Comparison of the use of the 405 nm LED array and 405 nm light engine for bacterial-suspension exposure.*

The results from Fig. 10.5, Fig. 10.9, Fig. 10.10, and Fig. 10.11 demonstrate bacterial inactivation on agar surfaces using the new prototype HINS-light EDS, and can be summarized as follows:

- The new prototype HINS-light EDS is effective for bacterial inactivation and that the extent of inactivation varies with irradiance.
- The new prototype HINS-light EDS produces a uniform level of irradiation (Fig. 10.7) and bacterial inactivation along all directions below the source.
- Bacterial inactivation data using this new prototype HINS-light EDS showed that reductions of 83.7% for *S. aureus*, 61.9% for *E. coli* and 83.7% for *L. monocytogenes* were achieved after 9 hours exposure at a distance of 200 cm below the system.

As described in Section 8.7.1, the HINS-light EDS is a ceiling-mounted High Intensity Narrow Spectrum (HINS) light source and it incorporates 405 nm and white light-emitting diodes (LEDs) covered by a Fresnel lens and a diffuser.

Current work in the ROLEST laboratory has demonstrated that light of 405 nm wavelength can be used to inactivate pathogenic bacteria in the air and on surfaces [116-118], without the use of exogenous photosensitiser molecules, and that a ceiling-mounted source of light at this wavelength can be used to substantially reduce the bacterial levels in a clinical environment [1].

A study by Maclean *et al.*, which employed a continuous xenon broadband white-light source in combination with bandpass filters (10 nm Full-width Half-Maximum) ranging from 400 – 420 nm for inactivation of *S. aureus* in liquid suspension, reported that 405 (± 5) nm was the most effective wavelength for inactivation of *S. aureus* [116].

Maclean *et al.* utilised the initial prototype HINS-light EDS for bacterial inactivation on environmental surfaces, where the system had been installed in a hospital isolation room (Glasgow Royal Infirmary, Scotland, UK) used to treat burns patients. They reported that around 90% and in the range 58 to 86% reductions of surface bacterial levels were achieved when the room was unoccupied and when the room was occupied by an MRSA-infected burns patient, respectively[1].

Using an alternative technology a study by Nerandzic *et al.* [120] and Rutala *et al.* [121] employed UV-C radiation (with peak wavelength at 254 nm) as a light based technology for room decontamination. This system demonstrated it's effectiveness to reduce clinically important nosocomial pathogens in a contaminated hospital room. Another study by Boyce *et al.* utilised Hydrogen Peroxide Vapor (HPV) to eliminate *Clostridium difficile* as a source of environmental contamination [122]. These and similar studies reported that these systems could only be used in areas that are unoccupied and sealed for the period of the disinfection process. However the HINS-light EDS, which utilises visible light wavelengths is harmless to patients and staff when applied as a room decontamination system.

Overall, the findings of the present study confirm that the new prototype HINS-light EDs has an output wavelength emission and irradiance pattern similar to the initial prototype and can be effectively used for environmental decontamination. Morover the new prototype incorporates substantial improvements in operational and functional design.

CHAPTER 11

GENERAL CONCLUSIONS AND RECOMMENDATIONS FOR FUTURE WORK

11.1 General

This study has demonstrated the use of light based technologies for microbial inactivation. Two main aspects that have been investigated during this study are the microbiological effects of the light technologies investigated and the engineering systems used for the light-based microbial inactivation. Regarding the microbiology aspects, pulsed ultra violet (PUV) light for microbial inactivation was investigated using both broadband spectrum light and 260 (± 10) nm light pulses. The study then utilised the use of visible-light wavelengths for microbial inactivation. These experiments were carried out using a continuous xenon white-light source in conjunction with a range of short-wave pass (SWP), long-wave pass (LWP) and band pass (BP) filters. Investigations were then carried out into the bactericidal effects of 405 nm filtered light generated from a 150W continuous xenon broadband white-light source in conjunction with a 405 (± 5) nm optical filter and 405 nm high intensity narrow spectrum (HINS) light generated from light-emitting diodes (LEDs).

For the engineering aspects, the study has investigated the use of Lambert's cosine law for determining irradiance distributions for both angular and linear distribution. Modelling optimisation of the High-Intensity Narrow-Spectrum light Environmental Decontamination System (HINS-light EDS) has been examined including design and development of an improved, fully-integrated and controllable HINS-light EDS unit. A mathematical model has been developed to enable simulations of the light intensity distribution. Studies of thermal management options, safety calculations and risk assessment of optical radiation and studies of bacterial inactivation using the new prototype HINS-light EDS are also investigated.

11.2 Conclusions

11.2.1 Investigation into the use of Pulsed UV-light for microbial inactivation

The ultraviolet light source used in the study was a low-pressure (450 torr) xenon-filled flashlamp (Heraeus Noblelight XAP series, Germany), constructed from a clear fused quartz tube filled with xenon. This light source produced a broadband light spectrum with high ultraviolet emission. Ultraviolet light, which is a non-thermal high-peak power technology, is capable of achieving rapid inactivation of microorganisms. The rapid inactivation effect of broadband spectrum PUV-light was demonstrated in this study for *Staphylococcus epidermidis* and *Saccharomyces cerevisiae*, with 7-$\log_{10}$ and 5-$\log_{10}$ reductions in microbial population being achieved after exposure to 10 pulses, respectively. Moreover, the performance of sample agitation proved to significantly improve treatment efficacy when exposing densely populated suspensions. When the $\log_{10}$ reductions of *Staphylococcus aureus* suspension exposed to pulsed UV-light treatment using both broadband spectrum and 260 (± 10) nm light pulses are compared, the results show that ten times the number of pulses of 260 nm light were required to achieve the equivalent 5-$\log_{10}$ reduction achieved with broadband light pulses. The main reason was due to the much greater total energy received by the bacterial suspension from the broadband source even though the wavelength of 260 nm is highly germicidal against microorganisms [159, 160, 208].

11.2.2 Investigation into the visible light wavelength sensitivity of pathogenic bacteria

The wavelength sensitivity of *Listeria monocytogenes* was investigated with a 150W continuous xenon broadband white-light source (Lightningcure LC5, Hamamatsu Photonics UK, Ltd), in conjunction with short-wave pass (SWP) and long-wave pass (LWP) filters (>400 nm, >450 nm, <500 nm and 400-450 nm). The most rapid inactivation rate was found upon exposure to wavelengths of 500 nm and less. The result is readily explained as when the *L. monocytogenes* suspension was exposed to <500 nm light, that included both visible light wavelengths (400-500nm) and UV light wavelengths (<400nm), to which much of its bactericidal action could be accredited. Within the visible-wavelength regions tested, *L. monocytogenes* was most susceptible

to light of wavelength 400-500 nm, with an approximately 50% faster inactivation rate than that found when exposed to wavelengths of 400 nm and above. Upon exposure to 450 nm and above, results demonstrated a much less notable effect on the bacterium *L. monocytogenes*, with only an approximate ~0.1-$\log_{10}$ reduction in bacteria cell population being achieved. This confirmed that the visible wavelengths inducing inactivation of *L. monocytogenes* were within the visible wavelength region in the range between 400 nm and 450 nm.

The causative bandwidth inducing inactivation of *L. monocytogenes*, *S. aureus* and meticillin-resistant *Staphylococcus aureus* (MRSA) was investigated using a continuous xenon broadband white-light source (Lightningcure LC5, Hamamatsu Photonics UK, Ltd), in conjunction with bandpass filters ranging from 400 nm to 450 nm at bandwidths of 10 nm (Full width half maximum, FWHM). Significant $\log_{10}$ reductions in bacterial population were achieved through exposure to 400 – 440 nm bandwidths for *L. monocytogenes*, and wavelength in the range 400 – 430 nm for *S. aureus* and MRSA, with the peak $\log_{10}$ reduction for all three bacteria resulting from exposure to 405 (± 5) nm.

11.2.3 Investigation into the use of 405 nm HINS-light for bacterial inactivation

Following identification of 405 (± 5) nm as the most bactericidal wavelength using 405 nm filtered light from the continuous white-light source in conjunction with a 405 (± 5) nm filter, the study then investigated the use of high-intensity 405 nm light, generated from light-emitting diodes (LEDs). This 405nm LED light source was in the form of a close-packed rectangular array with 99 individual LEDs in an 11 by 9 matrix (0D-405-99-070, OptoDiode Corp, USA), with a power output and radiation beam angle of 1.3 W and 70°, respectively. Results demonstrated that when the inactivation kinetics of *S. aureus*, *S. epidermidis*, *L. monocytogenes* and MRSA were compared using the 405 nm LED array and using the 405 nm filtered light, similar results were found for each strain of bacteria, indicating that the applied dose of 405 nm light was the important factor, not the light source.

The study then has investigated the use of the 405 nm light from the LED array for inactivation of various foodborne pathogens, such as *Listeria monocytogenes* and the significant Gram-negative food-borne pathogens *Salmonella enteritidis*, *Shigella*

sonnei and *Escherichia coli* 0157:H7. Inactivation of three species of *Listeria* (*Listeria monocytogenes*, *Listeria ivanovii* and *Listeria seeligeri*) was also investigated. When *L. monocytogenes* was exposed to the 405 nm LED array, results demonstrated that the 405 nm LED array could be used for inactivation of *L. monocytogenes* in liquid suspension without relying on the addition of exogenous chemicals.

Exposure of other *Listeria* species and the foodborne pathogens *Escherichia coli*, *Salmonella enteritidis* and *Shigella sonnei* to the 405 nm light from the LED array also demonstrated significant bacterial inactivation. Treatment of *L. monocytogenes* and the other *Listeria* species using the 405 nm LED array resulted in similar inactivation kinetics, suggesting that bacteria within the same Genus may undergo very similar inactivation reactions. When compared to the other foodborne pathogens, *Listeria* had higher susceptibility to inactivation through 405 nm light exposure.

In order to investigate the dependence of the applied dose on the inactivation of suspensions of *L. monocytogenes*, FOUR different doses for inactivation were investigated (61.6, 92.5, 123.3 and 154.1 Jcm^{-2}), and for each of these doses four irradiance levels were utilized (8.6, 44.7, 66.1 and 85.6 $mWcm^{-2}$). When *L. monocytogenes* is exposed to 405 nm light using four different irradiances and doses the results show that similar patterns of inactivation kinetics were achieved. The results indicate that inactivation of *L. monocytogenes* in liquid suspension using the 405 nm LED array is a dose-dependent reaction. Overall, the results show that the dose required for bacterial inactivation - regardless of how it is applied - yields similar final populations.

11.2.4 Investigation into irradiance distribution of light from an LED light engine

The irradiance pattern both for linear and angular distribution have been studied and mathematical model (Eq. (2.18)), which allows for analysis of the light distribution for single LED light source has been successfully developed.

A mathematical model (Eq. (2.18)) was developed to enable simulations of the light intensity distribution, with results proving that the intensity distribution of the system is in good agreement with experimental data. When the differences between the mathematical model and the experimental data are compared, it resulted in normalised cross correlation (NCC) greater than 99% and the root mean square (RMS) error less than 5%. This confirms that the similarity and the accuracy between the mathematical model and the experimental data were achieved.

The study has demonstrated influence of Fresnel lens and diffuser regard to the Lambertian mode number (m). The results show that the addition of lens system both the Fresnel lens with the 2.54 cm focal length and the Fresnel lens with the 4 cm focal length caused a pattern of irradiance distribution much narrow than the Lambertian pattern system without lens system.

The key results in the study has demonstrated that the space distance between the LED source and the Fresnel lens and diffuser (u) can influence to the irradiance distribution pattern from the LED source and the peak irradiance, E_0 ($mWcm^{-2}$) regard to the focal length of Fresnel lens.

11.2.5 Optimisation of the HINS-light Environmental Decontamination System

A new prototype for the High-Intensity Narrow-Spectrum light Environmental Decontamination System (HINS-light EDS) has been developed and its light distribution has been studied. The four main factors which had to be investigated for the design and development of the new HINS-light EDS were follows:

1. The configuration of the Fresnel lens and the diffuser
2. The Lambertian mode number (m)
3. The space distance between the LED light engines and the lens system (Fresnel lens and diffuser)
4. The optimum LED-to-LED array spacing.

The significant area of this study was the development mathematical model for a square LED array topology (Eq. (8.11)), which allows to predict and estimate light distribution from the new prototype HINS-light EDS.

To optimise emission pattern of new prototype HINS-light EDS (4 light source), the four main steps which had to be done were follows:

1. The model was used application of the generalized Lambert's cosine law at any point on the horizontal surface as a function of (x, y) (Eq. (2.18))

2. Maximum irradiance E_0 and the Lambertian mode number (m) have been obtained from experiment.

3. Advanced model for multiple light sources based on superposition method has been developed (Eq. (8.11)).

4. E_0 and m parameters have been used in advanced analytical model in order to obtain light distribution from multiple (4) light sources.

Results demonstrated that the model is in good agreement with experimental data with the normalised cross correlation (NCC) greater than 99% and the root mean square (RMS) error less than 5%.

Due to improvement in the thermal management, the new prototype HINS-light EDS is much lighter and easier to retrofit into hospital ceilings. The heat sink can be used to control the heat produced by the white LEDs, results demonstrate that for the typical operation time (10 hours/day) of the HINS-light EDS in the hospital environment, the heat sink will not generate detrimental effects on the HINS-light EDS system.

11.2.6 Design of the HINS-light Environmental Decontamination System

A new improved HINS-light EDS prototype has been successfully developed and built which has significant advantages over the initial prototype:

1. Compact

2. Light-weight

3. Fully-integrated

4. Good thermal management
5. Improved colour blending
6. Controllability through USB and software.

The active component of the new prototype HINS-light EDS is made up of 405 nm LED light engines and white light-emitting diodes covered by a Fresnel lens and diffuser. The position of the Fresnel lens and diffuser below the LED sources allows a wide and more uniform distribution of light over the illuminated area. The new prototype HINS-light EDS uses four individual 405 nm LED light engines. To ensure that the system does not generate dominant violet illumination and produces normal room lighting, 12 high power white-light LEDs were incorporated into the design of the new prototype HINS-light EDS

Analytical study of safety calculations has been evaluated and calculated. The results confirm that the HINS-light EDS, at the irradiance level of 0.08 $mWcm^{-2}$ for each individual 405 nm LED light engine, and a total irradiance level of 0.32 $mWcm^{-2}$ (and total illuminance of 209 lux) at a distance of 200 cm below the system, is safe in relation to UV and thermal interaction with unprotected skin and eyes and blue light retinal hazard. All four LED light engines had a value of blue light radiance (L_B) less than 10 $mWcm^{-2}sr^{-1}$ both for normal healthy eyes and eyes with the normal lens removed, with %TLV (Threshold Limit Values) in the range 4 – 8% for normal healthy eyes and ranging from 32 to 36% for eyes with the normal lens removed, respectively. The maximum exposure time in direct viewing at a perpendicular distance from the source of 200 cm for all four LEDs resulted in a value in the range 34 – 57 hours for normal healthy eyes and 7.8 – 8.6 hours for eyes with the normal lens removed. In the UV-A wavelength region ranging from 315 nm to 400 nm, the new prototype HINS-light EDS source has a value in the range 2.5×10^{-4} $mWcm^{-2}$ to 4.9×10^{-4} $mWcm^{-2}$. Approximately between 0.25% and 0.5% of the exposure limit as established by the International Commission on Non-ionizing Radiation Protection (ICNIRP).

Risk assessment of the new HINS-light EDS as a ceiling mounted light source with diffuser and Fresnel lens shows that for UV radiation, when someone stares into the

light source at a distance of 30 to 200 cm, this represents as safe level position with maximum permissible exposure (MPE) > 8 hours. For UV-A radiation, more consideration is required as when the face is oriented directly towards the source at a distance of less than 115 cm the MPE is less than 8 hours. According to HPA, *"If the MPE time is < 8 hours, it will be necessary to demonstrate that actual personal occupancy at r is less than the MPE time. In this case, occupancy can exclude any time spent with the face oriented away from the source" and "If the MPE time is > 8 hours, there is no risk that the exposure limit will be exceeded at distance r"* [207].

For both blue light and retinal thermal hazard, the new HINS-light EDS has a value (2.97 $Wm^{-2}sr^{-1}$ and 2385 $cd.m^{-2}$) less than the maximum exposure limit of 100 $Wm^{-2}sr^{-1}$ for blue light hazards and 10^4 $cd.m^{-2}$ for retinal thermal hazards, respectively. These results give guarantee that HINS-light EDS is safe in relation to blue light and retinal thermal hazards at a distance of 30 – 200 cm underneath the light source. This safety data helps to determine the best position of the lights in a room/ward. As with normal room lighting, HINS-light EDS would never be positioned directly above a patient or a worker and therefore people would never be <115cm directly below the source. Consequently although UV-A safety is the most important consideration, people would never realistically be exposed to hazardous levels of this. The overall conclusion from these safety consideration is that the HINS-light EDS prototype is harmless to patient and staff when applied as room decontamination system [1].

11.2.7 Application of the new prototype HINS-light Environmental Decontamination System for inactivation of pathogenic bacteria

The new prototype system has good bactericidal efficacy, and inactivation studies show that decontamination occurred faster with the new prototype system.

Bacterial inactivation data using this new prototype HINS-light EDS has been shown to provide reductions in bacteria on agar surfaces of up to 73% reduction for *Staphylococcus aureus,* 57% reduction for *Escherichia coli* and 55% reduction for *Listeria monocytogenes,* with these achieved after 6 hours exposure at a distance of 200 cm below the system. The results demonstrate that the improved prototype system is effective for inactivation of pathogenic bacteria in exposed environments.

Finally, potential applications of the HINS-light EDS technology could be for disinfection of air and surfaces in areas such as hospital wards (as already demonstrated [1]), clinics, food industry, and public buildings.

11.3Future work

11.3.1 Microbiological aspects

11.3.1.1 Pulsed ultraviolet (PUV)-light for microbial inactivation

This study focused only on the effectiveness of PUV-light treatment for the inactivation of the yeast *Saccharomyces cerevisiae* and the bacterium *Staphylococcus epidermidis* in liquid suspension. Investigation into the effects of PUV-light on bacteria associated with healthcare associated infections (HAIs) and foodborne and/or waterborne pathogens are needed in further work.

PUV exposure was performed using a broadband xenon flashlamp, and complete inactivation of 10^7 $CFUml^{-1}$ *S. epidermidis* was achieved within 10 pulses, and 10^7 $CFUml^{-1}$ and 10^5 $CFUml^{-1}$ populations of *S. cerevisiae* showed complete inactivation within 75 and 10 pulses, respectively. In addition, the performance of sample agitation proved to significantly increase treatment efficacy when exposing densely populated suspensions. Further work into the development of PUV systems which incorporate methods of mechanical agitation could greatly improve the efficacy of PUV-light for industrial disinfection and sterilization applications.

11.3.1.2 Mechanism of HINS-light inactivation

The current study has examined the effectiveness of 405 nm HINS-light inactivation of microorganisms in liquid suspension. An important addition to further work would be the investigation into the effects of 405 nm HINS-light for inactivation of microorganisms on both material surfaces and in air samples.

As described in Chapter 5, the 405 (± 5) nm wavelength is an effective wavelength for photodynamic inactivation without the use of exogenous photosensitizers and this visible-light inactivation through exposure to 400 – 420 nm is thought to be the result of the photo-stimulation of intracellular porphyrins, thereby producing singlet oxygen ($^1O_2$) which reacts with intracellular components, and causes, bacterial cell death. It would be interesting to expand the study to determine the type and levels of

porphyrins involved in the 405 nm HINS-light inactivation mechanism. A study by Ashkenazi *et al.* successfully determined and quantified endogenous porphyrins produced in *Propionibacterium acnes* after illumination with intense blue light at 407 – 420 nm. They found the types of porphyrin produced by *P. acnes* are coproporphyrin and δ-aminolevulinic acid (ALA) through analysis using high-performance liquid chromatography (HPLC) [111].

As stated in the experimental method for the 405 nm HINS-light inactivation, 2 ml volumes of bacterial suspension were held in one well of a 12-well plate which contained a small magnetic follower, which when positioned on a magnetic stirrer, permitted continuous agitation of the sample when being exposed to different durations of light. Further investigation will be important to determine possible effects of the 405 nm HINS-light inactivation on bacterial suspensions without using both magnetic follower and magnetic stirrer to eliminate the agitation effect.

11.3.2 Engineering aspects

11.3.2.1 Optimisation of HINS-light EDS

As discussed in Chapter 8 and 9, for modelling the irradiance distribution pattern, only the irradiances on the illuminated area parallel to the light source were measured. Results showed similarity and accuracy between the mathematical model and the experimental data when both of them are compared. According to Moreno *et al.* that "the perceived homogeneity depends on several factors, including distance of the observer from the target field, incidence angle of illuminating beam, background luminance, target reflectance, target pattern, and target colour" [18]. Further work should be carried out to investigate and analyse global illumination. A local illumination method has been defined as "method which calculates and analyses the light energy transfer from direct lighting while global illumination methods take into account the light energy transfer to all surfaces in an environment (direct and indirect lighting)" [209]. Irradiance distribution for all directions can be calculated with the irradiance volume, it refers to volumetric approximation of the irradiance distribution at every point in space [209].

The present work has successfully developed and designed this new prototype HINS-light EDS which has proved effective for inactivation of a range of significant bacterial species (*Staphylococcus aureus*, *Escherichia coli* and *Listeria monocytogenes*) on agar surfaces. Results have demonstrated the effectiveness of the new prototype HINS-light EDS to eliminate both Gram-negative and Gram-positive bacteria on test agar surfaces. The new prototype HINS-light EDS system has been shown to provide reductions in surface levels of pathogenic bacteria of up to 73%, following 6 hours exposure at a distance of 200 cm below the system source. Further work should be carried out to investigate the effectiveness of the new prototype HINS-light EDS for inactivation of bacteria associated with healthcare associated infections (HAIs) and foodborne pathogens on both inanimate surfaces and air. Generation of this data would support implementation of the new prototype HINS-light EDS for disinfection of air and surfaces in areas such as hospital wards, clinics, the food industry and public buildings.

11.3.2.2 New model and configuration for future HINS-light EDS

Potential ideas for future alternative designs/configurations of the HINS-light are displayed in Fig. 11.1, and Fig. 11.2. Future development could potentially see the HINS-light EDS not only being used to kill pathogenic bacteria in the room environment, but also used for lighting in general applications. People may feel comfortable to receive HINS-light EDS as a room lighting in the home and public building, whilst providing a level of background decontamination.

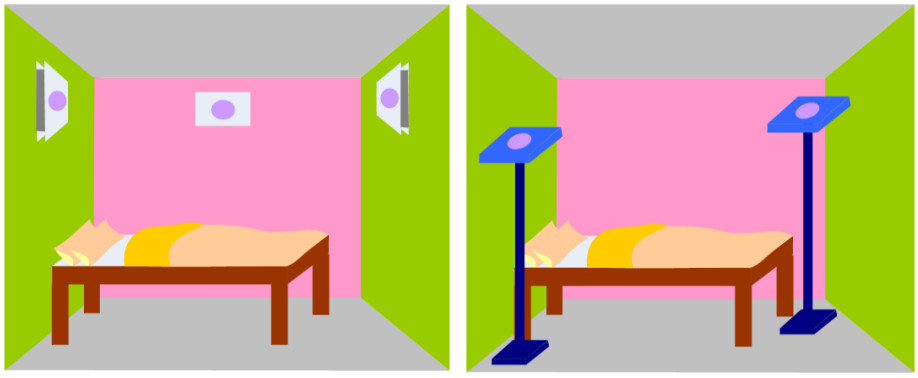

(a) (b)

Fig. 11.1. *New design for HINS-light EDS, a) model 1 and b) model II .*

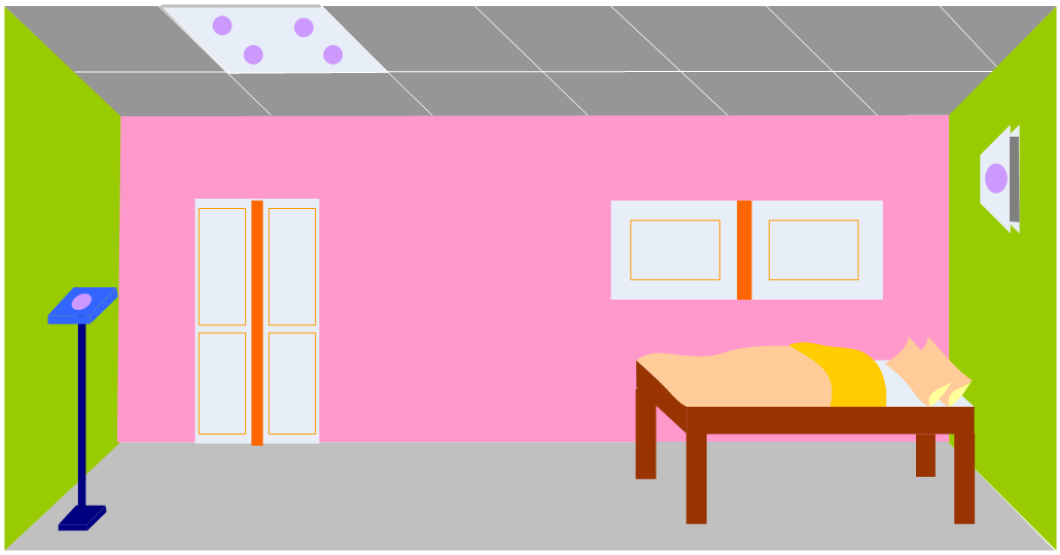

Fig. 11.2. *New design for HINS-light EDS III.*

A C K N O W L E D G E M E N T S

Firstly, I would like to say thank you to my main supervisor Professor Scott J. MacGregor who has given the opportunity to conduct research in ROLEST during this PhD study, and second supervisor Dr Igor Timoshkin for their support, hospitality, sharing knowledge, constructive criticism, suggestion and encouragement throughout the course of this study.

Special thanks are also to Professor John G. Anderson and Professor Gerry Woolsey for the discussion and invaluable input regarding the microbiological aspect and engineering aspect especially in modelling, design and development of the new prototype HINS-light EDS.

Many thanks to Dr Michelle Maclean for her assistance, support, time for discussion, invaluable input, friendliness and encouragement during this PhD study, without her it is impossible to finish this thesis and PhD study.

Thanks to all technicians of the Electrical Engineering Workshop who have helped in making experimental equipment for analytical study of light distribution and final design of new prototype HINS-light EDS. Thanks are also to Mr Dave Currie for his assistance, friendliness and encouragement during this PhD study.

Thanks to my friends all over friendship during this study, Dr Mark Wilson, Dr Sarah Griffiths, Dr Sharon Smith, Dr Melissa Webster, Dr Lynne Murdoch, Karen McKenzie, Richard McDonald, Guangming Huang, Athanasios Mermigkas, Sarah Bache and Angela Coyle.

I would like to thank the Indonesian Government, the Ministry of National Education, Directorate General of Higher Education (DIKTI) and Physics Department, Institut Teknologi Sepuluh Nopember (ITS) Surabaya, Indonesia for providing the scholarship and also to The Robertson Trust for the funding support.

And finally, I would like to dedicate this work to my beloved wife “Dinni Indraswari”, my daughter “Faustina Elita Rahmah” and my son “Faiq Ikram Anwar”.

REFERENCES

[1] M. Maclean, S.J. MacGregor, J.G. Anderson, G.A. Woolsey, J.E. Coia, K. Hamilton, I. Taggart, S.B. Watson, B. Thakker, and G. Gettinby, "Environmental decontamination of a hospital isolation room using high-intensity narrow-spectrum light," *J Hosp Infect.*, Vol. 76, No. 3, pp. 247-251, 2010.

[2] IESNA, *IESNA lighting handbook: Reference & Application*, 9th ed., 2000.

[3] A. Ryer. Light measurement handbook, 1998 [Online] (Accessed on 17th August 2010). Available from: http://optdesign.narod.ru/book/light_measurement_handbook_1997.pdf

[4] J.R. Bolton, *Ultraviolet application handbook*, 3rd ed.: Bolton Photosciences, Inc. Ayr, ON, CA N0B 1E0., 2010.

[5] A. Acher, E. Fischer, R. Turnheim, and Y. Manor, "Ecologically friendly wastewater disinfection techniques," *Water Res*, Vol. 31, No. 6, pp. 1398-1404, 1997.

[6] NAS. The Ozone layer, 2001 [Online] (Accessed on 25th February 2011). Available from: http://www.nas.nasa.gov/About/Education/Ozone/ozonelayer.html

[7] NTP. Broad-band spectrum Ultraviolet (UV) radiation, and UVA, and UVB, and UVC, 2000 [Online] (Accessed on 25th February 2011). Available from: http://ntp.niehs.nih.gov/ntp/newhomeroc/roc10/UV.pdf

[8] WHO. Water sanitation and health (WSH), Managing water in the home: accelerated health gains from improved water supply, 2011 [Online] (Accessed on 25th February 2011). Available from: http://www.who.int/water_sanitation_health/dwq/wsh0207/en/index4.html

[9] J.L. Zimmer and R.M. Slawson, "Potential repair of *Escherichia coli* DNA following Exposure to UV radiation from both Medium- and Low-Pressure UV sources used in drinking water treatment," *Appl Environ Microbiol*, Vol. 68, No. 7, pp. 3293-3299, July 1, 2002 2002.

[10] IUPAC. Excimer lamp, 2007 [Online] (Accessed on 25th February 2011). Available from: http://old.iupac.org/goldbook/ET07372.pdf

[11] S.S. Block, *Disinfection, sterilization, and preservation* 4th ed.: Lea & Febiger, Philadelpia, 1991.

[12] N. Elmnasser, S. Guilou, F. Leroi, N. Orange, A. Bakhrouf, and M. Federighi, "Pulsed-light system as a new novel food decontamination technology: a review," *Can. J. Microbiol.*, Vol. 53, pp. 813 - 821, 2007.

[13] Y. Lamont, A. Rzezutka, J.G. Anderson, S.J. MacGregor, M.J. Given, C. Deppe, and N. Cook, "Pulsed UV-light inactivation of poliovirus and adenovirus," *Lett Appl Microbiol*, Vol. 45, pp. 564 – 567, 2007.

[14] J.G. Anderson, N.J. Rowan, S.J. MacGregor, R.A. Fouracre, and O. Farish, "Inactivation of food-borne enteropathogenic bacteria and spoilage fungi using pulsed-light," *IEEE Trans. Plasma Sci.*, Vol. 28, No. 1, pp. 83-88, 2000.

[15] M. Calin and S. Parasca, "Light sources for photodynamic inactivation of bacteria," *Lasers Med Sci*, Vol. 24, No. 3, pp. 453-460, 2009.

[16] W.T. Chien, C.C. Sun, and I. Moreno, "Precise optical model of multi-chip white LEDs," *Opt. Express*, Vol. 15, No. 12, pp. 7572-7577, 2007.

[17] A.E.F. Taylor. Illumination fundamentals, 2000 [Online] (Accessed on 9th August 2010). Available from: www.opticalres.com/lt/illuminationfund.pdf

[18] I. Moreno, M. Avendaño-Alejo, and R.I. Tzonchev, "Designing light-emitting diode arrays for uniform near-field irradiance," *Appl. Opt.*, Vol. 45, No. 10, pp. 2265-2272, 2006.

[19] I. Moreno and C.C. Sun, "Modeling the radiation pattern of LEDs," *Opt. Express*, Vol. 16, No. 3, pp. 1808-1819, 2008.

[20] I. Moreno, "LED intensity distribution," in *The International Optical Design Conference*, 2006.

[21] P. Manninen, J. Hovila, P.Karha, and E. Ikonen, "Method for analysing luminous intensity of light-emitting diodes," *Meas Sci Technol*, Vol. 18, No. 1, p. 223, 2007.

[22] C.C. Sun, T.X. Lee, S.H. Ma, Y.L. Lee, and S.M. Huang, "Precise optical modeling for LED lighting verified by cross correlation in the midfield region," *Opt. Lett.*, Vol. 31, No. 14, pp. 2193-2195, 2006.

[23] C.C. Sun, C.Y. Chen, H.Y. He, C.C. Chen, W.T. Chien, T.X. Lee, and T.H. Yang, "Precise optical modeling for silicate-based white LEDs," *Opt. Express*, Vol. 16, No. 24, pp. 20060-20066, 2008.

[24] D.H. Sliney, "Optical radiation safety of medical light sources," *Phys Med Biol*, Vol. 42, No. 5, pp. 981-996, 1997.

[25] ICNIRP, "Guidelines on limits of exposure to broad-band incoherent optical radiation (0.38 to 3 μm)," *Health Physics Society*, pp. 539-554, 1997.

[26] ICNIRP, "Guidelines on limits of exposure to ultraviolet radiation of wavelengths between 180 nm and 400 nm (incoherent optical radiation)," *Health Physics Society*, Vol. 87, No. 2, pp. 171-86, 2004.

[27] S. Miller, R. James, R. Landry, and J. Pfefer, "Optical characterization of cutaneous transilluminators for eye safety," *Biomed. Opt. Express*, Vol. 1, No. 3, pp. 771-779, 2010.

[28] H. Jin. 1988 CIE photopic luminous efficiency function, [Online] (Accessed on 20th August 2010). Available from: http://note.j-i-n.name/2005/06/photopic-luminous-efficiency-function.html

[29] E.F. Schubert, *Light emitting diodes, Second edition*, 2nd ed.: Cambridge University Press, 2006.

[30] 1988 C.I.E. photopic luminous efficiency function, [Online] (Accessed on 20th August 2010). Available from: http://members.misty.com/don/photopic.html

[31] POST. Infections control in healthcare settings, 2005 [Online] (Accessed on 4th February 2011). Available from: http://www.parliament.uk/documents/post/postpn247.pdf

[32] WHO. Prevention of hospital-acquired infections - A pratical guide, 2002 [Online] (Accessed on 1st February 2011). Available from: http://www.who.int/csr/resources/publications/whocdscsreph200212.pdf

[33] WHO. Global patient safety challenge: 2005-2006, 2005 [Online] (Accessed on 4th February 2011). Available from: http://www.who.int/patientsafety/events/05/GPSC_Launch_ENGLISH_FINAL.pdf

[34] NAO. Improving patient care by reducing the risk of hospital acquired infection: A progress report, 2004 [Online] (Accessed on 6th February 2011). Available from: http://www.nao.org.uk/publications/0304/improving_patient_care.aspx?alreadysearchfor=yes

[35] J. Sarma and G. Ahmed, "Infection control with limited resources: Why and how to make it possible?," *Indian J Med Microbiol,* Vol. 28, No. 1, pp. 11-16, 2010.

[36] WHO. WHO Global Strategy for Containment of Antimicrobial Resistance, 2001 [Online] (Accessed on 1st February 2011). Available from: http://www.who.int/drugresistance/WHO_Global_Strategy_English.pdf

[37] Eurobarometer. Antimicrobial Resistance, 2010 [Online] (Accessed on 1st February 2011). Available from: http://ec.europa.eu/public_opinion/archives/ebs/ebs_338_en.pdf

[38] EFSA. European food safety authority: Antimicrobial resistance, 2010 [Online] (Accessed on 17th November 1974). Available from: http://www.efsa.europa.eu/en/topics/topic/amr.htm

[39] P.S. Mead, L. Slutsker, V. Dietz, L.F. McCaig, J.S. Bresee, C. Shapiro, P.M. Griffin, and R.V. Tauxe, "Food-related illness and death in the United States," *Emerg Infect Diseases,* Vol. 5, No. 5, pp. 607-625, 1999.

[40] WHO. Food safety and foodborne illness, [Online] (Accessed on 18th August 2010). Available from: http://www.who.int/mediacentre/factsheets/fs237/en/

[41] WHO/FAO. (2004, 10th March 2011). Risk assessment of *Listeria monocytogenes* in ready-to-eat foods : interpretative summary. Available: http://www.who.int/foodsafety/publications/micro/en/mra4.pdf

[42] FDA. Quantitative assessment of relative risk to public health from foodborne *Listeria monocytogenes* among selected categories of ready-to-eat foods, 2003 [Online] (Accessed on 10th March 2011). Available from: http://www.fda.gov/downloads/food/scienceresearch/researchareas/riskassessmentsafetyassessment/ucm197330.pdf

[43] CDC. Outbreak of listeriosis-Northeastern United States, 2002, 2002 [Online] (Accessed on 18th August 2010). Available from: http://www.cdc.gov/mmwr/preview/mmwrhtml/mm5142a3.htm

[44] J. McLauchlin, R.T. Mitchell, W.J. Smerdon, and K. Jewell, "*Listeria monocytogenes* and listeriosis: a review of hazard characterisation for use in microbiological risk assessment of foods," *Int J Food Microbiol* Vol. 92, pp. 15 - 33, 2004.

[45] C.W. Donnelly, "*Listeria monocytogenes*: A continuing challenge," *Nutr Rev,* Vol. 59, No. 6, pp. 183-194, 2001.

[46] W.F. Schlech and D. Acheson, "Foodborne Listeriosis," *Clin Infect Dis,* Vol. 31, No. 3, pp. 770-775, September 1, 2000 2000.

[47] WHO. Safer Water, Better Health: Costs, benefits, and sustainability of interventions to protect and promote health., 2008 [Online] (Accessed on 9th February 2011). Available from: http://whqlibdoc.who.int/publications/2008/9789241596435_eng.pdf

[48] A. Smith, M. Reacher, W. Smerdon, G.K. Adak, G. Nichols, and R.M. Chalmers, "Outbreaks of waterborne infectious intestinal disease in England and Wales, 1992–2003," *Epidemiol Infect* Vol. 134, No. 6, pp. 1141–1149, 2006.

[49] S.H. Lee, D.A. Levy, G.F. Craun, M.J. Beach, and R.L. Calderon. Surveillance for Waterborne-Disease Outbreaks --- United States, 1999--2000, 2002 [Online] (Accessed on 9th February 2011). Available from: http://www.cdc.gov/mmwr/preview/mmwrhtml/ss5108a1.htm

[50] J.S. Yoder, M.C. Hlavsa, G.F. Craun, V. Hill, V. Roberts, P. A. Yu, L. A. Hicks, N.T. Alexander, R. L. Calderon, S.L. Roy, and M.J. Beach. Surveillance for Waterborne Disease and Outbreaks Associated with Recreational Water Use and Other Aquatic Facility-Associated Health Events --- United States, 2005--2006, 2008 [Online] (Accessed on 9th Feebruary 2011). Available from: http://www.cdc.gov/mmwr/preview/mmwrhtml/ss5709a1.htm

[51] CDC. Waterborne Diseases Could Cost over $500 Million Annually in U.S., 2010 [Online] (Accessed on 9th February 2011). Available from: http://www.cdc.gov/media/pressrel/2010/r100714.htm

[52] I. Caminiti, I. Palgan, A. Muñoz, F. Noci, P. Whyte, D. Morgan, D. Cronin, and J. Lyng, "The effect of Ultraviolet light on microbial inactivation and quality attributes of apple juice," *Food and Bioprocess Tech,* pp. 1-7, 2010.

[53] J.A. Guerrero-Beltran and G.V. Barbosa-Canovas, "Advantages and limitations on processing foods by UV light," *Food Sci Tech Int,* Vol. 10, No. 3, pp. 137-147, June 1, 2004 2004.

[54] J.C.H. Chang, S.F. Ossoff, D.C. Lobe, M.H. Dorfman, C.M. Dumais, R.G. Qualls, and J.D. Johnson, "UV inactivation of pathogenic and indicator microorganisms," *Appl Environ Microbiol,* Vol. 49, No. 6, pp. 1361-1365, 1985.

[55] R. Sommer, T. Haider, A. Cabaj, E. Heidenreich, and M. Kundi, "Increased Inactivation of *Saccharomyces cerevisiae* by protraction of UV irradiation," *Appl Environ Microbiol,* 1996.

[56] D.E. Huffman, A. Gennaccaro, J.B. Rose, and B.W. Dussert, "Low- and medium-pressure UV inactivation of microsporidia *Encephalitozoon intestinalis*," *Water Res*, Vol. 36, No. 12, pp. 3161-3164, 2002.

[57] S.A. Craik, D. Weldon, G.R. Finch, J.R. Bolton, and M. Belosevic, "Inactivation of *Cryptosporidium parvum* oocysts using medium- and low-pressure ultraviolet radiation," *Water Res*, Vol. 35, No. 6, pp. 1387-1398, 2001.

[58] W.L. Nicholson and B. Galeano, "UV resistance of *Bacillus anthracis* spores revisited: Validation of *Bacillus subtilis* spores as UV surrogates for spores of *B. anthracis* sterne," *Appl Environ Microbiol*, Vol. 69, No. 2, pp. 1327–1330, 2003.

[59] M.M. Guivan, T. Kamikozawa, H. Kurokawa, H. Motomura, K. Kadowaki, and M. Jinno, "Comparative inactivation of *Bacillus subtilis* spores Using a DBD-Driven Xenon Iodide Excilamp and a conventional Mercury lamp," *IEEE Trans. Plasma Sci.*, Vol. 38, No. 8, pp. 1972-1977, 2010.

[60] H. Guo, X. Chu, and J. Hu, "Effect of host cells on low- and medium-pressure UV inactivation of adenoviruses," *Appl Environ Microbiol*, Vol. 76, No. 21, pp. 7068-75, 2010.

[61] S.J. MacGregor, N.J. Rowan, L. McIlvaney, J.G. Anderson, R.A. Fouracre, and O. Farish, "Light inactivation of food-related pathogenic bacteria using a pulsed power source," *Lett Appl Microbiol*, Vol. 27, pp. 67 - 70, 1998.

[62] T. Wang, S.J. MacGregor, J.G. Anderson, N.J. Rowan, and Y. Lamont, "Inactivation of pathogenic microorganisms using pulsed UV ilumination and its application in water disinfection," in *The XIV International Conference on Gas Discharges and their Applications*, Liverpool, pp. 116-119, 2002.

[63] M.N. Lani, J.G. Anderson, S.J. MacGregor, and G.A. Woolsey, "Use of a pulsed xenon flashlamp for inactivation and photoreactivation of microorganisms," in *16th International Conference on Gas Discharges and their Applications (GD2006)*, Xi'an, China, 2006.

[64] N.J. Rowan, S.J. MacGregor, J.G. Anderson, R.A. Fouracre, L. Mcllvaney, and O. Farish, "Pulsed-light inactivation of food-related microoraginsms," *Appl Environ Microbiol*, Vol. 65, pp. 1312-1315, 1999.

[65] Endarko, M. Maclean, I.V. Timoshkin, S.J. MacGregor, and J.G. Anderson, "Pulsed light technology for microbial inactivation," in *Universities Power Engineering Conference (UPEC), 2009 Proceedings of the 44th International* pp. 1-4, 2009.

[66] A. Wekhof, "Pulsed UV Disintegration (PUVD): a new sterilisation mechanism for packaging and broad medical-hospital applications," presented at the The First International Conference on Ultraviolet Technologies, Washington D.C., USA, 2001.

[67] K.F. McDonald, R.D. Curry, T.E. Clevenger, K. Unklesbay, A. Eisenstark, and J. Golden, "A comparison of pulsed and continuous Ultraviolet light sources for the decontamination of surfaces," *IEEE Trans. Plasma Sci.*, Vol. 28, No. 5, pp. 1581-1587, October 2000.

[68] V.M. Gómez-López, F. Devlieghere, V. Bonduelle, and J. Debevere, "Factors affecting the inactivation of micro-organisms by intense light pulses," *J Appl Microbiol,* Vol. 99, No. 3, pp. 460-470, 2005.

[69] T. Bintsis, E. Litopoulou-Tzanetaki, and R.K. Robinson, "Existing and potential applications of ultraviolet light in the food industry – a critical review," *J Sci Food Agric,* Vol. 80, No. 6, pp. 637-645, 2000.

[70] J.A. Guerrero-Beltran and G.V. Barbosa-Canovas, "Reduction of *Saccharomyces cerevisiae, Escherichia coli* and *Listeria innocua* in apple juice by ultraviolet light," *J Food Process Eng,* Vol. 28, No. 5, pp. 437-452, 2005.

[71] C.H. Sommers, O.J. Scullen, and J.E. Sites, "Inactivation of foodborne pathogens on frankfurters using ultraviolet light and gras antimicrobials," *J. Food Safety,* Vol. 30, No. 3, pp. 666-678, 2010.

[72] M. Keyser, I.A. Muller, F.P. Cilliers, W. Nel, and P.A. Gouws, "Ultraviolet radiation as a non-thermal treatment for the inactivation of microorganisms in fruit juice," *Innovat Food Sci Emerg Tech,* Vol. 9, No. 3, pp. 348-354, 2008.

[73] K.M.D. Lima-Bessa, M.G. Armelini, V. Chiganças, J.F. Jacysyn, G.P. Amarante-Mendes, A. Sarasin, and C.F.M. Menck, "CPDs and 6-4PPs play different roles in UV-induced cell death in normal and NER-deficient human cells," *DNA Repair,* Vol. 7, No. 2, pp. 303-312, 2008.

[74] R.P. Sinha and D.P. Häder, "UV-induced DNA damage and repair: a review," *Photochem. Photobiol. Sci.,* Vol. 1, pp. 225 – 236, 2002.

[75] F. Thoma, "Light and dark in chromatin repair: repair of UV-induced DNA lesions by photolyase and nucleotide excision repair," *EMBO J,* Vol. 18, No. 23, pp. 6585-6598, 1999.

[76] D.B. Swartzlander, L.M. Griffiths, J. Lee, N.P. Degtyareva, P.W. Doetsch, and A.H. Corbett, "Regulation of base excision repair: Ntg1 nuclear and mitochondrial dynamic localization in response to genotoxic stress," *Nucleic Acids Res,* Vol. 38, No. 12, pp. 3963-3974, July 1, 2010 2010.

[77] R.P. Rastogi, Richa, A. Kumar, M.B. Tyagi, and R.P. Sinha, "Molecular mechanisms of ultraviolet radiation-induced DNA damage and repair," *Journal of Nucleic Acids,* Vol. 2010, p. 32, 2010.

[78] A.R. Lehmann, "Nucleotide excision repair and the link with transcription," *Trends in Biochemical Sciences,* Vol. 20, No. 10, pp. 402-405, 1995.

[79] A. Sancar, "Structure and function of DNA photolyase," *Biochemistry,* Vol. 33, No. 1, pp. 2-9, 1994.

[80] A. Sancar, "No "End of History" for Photolyases," *Science,* Vol. 272, No. 5258, pp. 48-49, April 5, 1996 1996.

[81] A. Yasui, A.P. Eker, S. Yasuhira, H. Yajima, T. Kobayashi, M. Takao, and A. Oikawa, "A new class of DNA photolyases present in various organisms including aplacental mammals.," *The EMBO Journal,* Vol. 13, No. 24, pp. 6143-6151, 1994.

[82] K.G. Lindenauer and J.L. Darby, "Ultraviolet disinfection of wastewater: Effect of dose on subsequent photoreactivation," *Water Res,* Vol. 28, No. 4, pp. 805-817, 1994.

[83] K. Oguma, H. Katayama, and S. Ohgaki, "Photoreactivation of Escherichia coli after Low- or Medium-Pressure UV Disinfection Determined by an Endonuclease Sensitive Site Assay," *Appl. Environ. Microbiol.*, Vol. 68, No. 12, pp. 6029-6035, December 1, 2002 2002.

[84] T. Maisch, S. Hackbarth, J. Regensburger, A. Felgenträger, W. Bäumler, M. Landthaler, and B. Röder, "Photodynamic inactivation of multi-resistant bacteria (PIB) – a new approach to treat superficial infections in the 21st century," *JDDG: J Dtsch Dermatol Ges*, 2010.

[85] M.R. Hamblin and T. Hasan, "Photodynamic therapy: a new antimicrobial approach to infectious disease?," *Photochem. Photobiol. Sci.*, Vol. 3, pp. 436 - 450, 2004.

[86] T. Maisch, J. Baier, B. Franz, M. Maier, M. Landthaler, R.M. Szeimies, and W. Bäumler, "The role of singlet oxygen and oxygen concentration in photodynamic inactivation of bacteria," *Proceedings of the National Academy of Sciences,* Vol. 104, No. 17, pp. 7223-7228, April 24, 2007 2007.

[87] T. Maisch, R.M. Szeimies, G. Jori, and C. Abels, "Antibacterial photodynamic therapy in dermatology," *Photochem. Photobiol. Sci.*, Vol. 3, No. 10, pp. 907-917, 2004.

[88] A. Goldoni, "Porphysrins: Fascinating molecules with biological significance," *Reseach Highlights 2001-2002; Anatomic, Molecular and Supramoleculer Studies,* 2002.

[89] G. Jori and S.B. Brown, "Photosensitized inactivation of microorganisms," *Photochem. Photobiol. Sci.,* Vol. 3, No. 5, pp. 403-405, 2004.

[90] M. Segado and M. Reguero, "Mechanism of the photochemical process of singlet oxygen production by phenalenone," *Phys. Chem. Chem. Phys.*, Vol. 13, No. 9, pp. 4138-4148, 2011.

[91] R.D. Watkin and R.M. Tyrrell, "Study of the relationship between endogenous protoporphyrin IX concentration in human Lymphoblastoid cells and inactivation by UVA radiation," *Radiat Protect Dosim,* Vol. 91, No. 1-3, pp. 85-88, September 1, 2000 2000.

[92] S. Karrer, R.M. Szeimies, S. Ernst, C. Abels, W. Bäumler, and M. Landthaler, "Photodynamic inactivation of Staphylococci with 5-Aminolaevulinic Acid or Photofrin," *Lasers Med Sci,* Vol. 14, No. 1, pp. 54-61, 1999.

[93] R. Sailer, W.S.L. Strauss, K. König, A. Rück, and R. Steiner, "Correlation between porphyrin biosynthesis and photodynamic inactivation of Pseudomonas aeruginosa after incubation with 5-aminolaevulinic amid," *J. Photochem. Photobiol. B: Biol.,* Vol. 39, No. 3, pp. 236-242, 1997.

[94] R.W. Tuveson and L.J. Sammartano, "Sensitivity of HemA mutant *Escherichia coli* cells to inactivation by Near-UV light depends on the level of supplementation with δ-aminolevulinic acid," *Photochem Photobiol,* Vol. 43, No. 6, pp. 621-626, 1986.

[95] J. Walther, M.J. Bröcker, D. Wätzlich, M. Nimtz, M. Rohde, D. Jahn, and J. Moser, "Protochlorophyllide: a new photosensitizer for the photodynamic inactivation of Gram-positive and Gram-negative bacteria," *FEMS Microbiol Lett,* Vol. 290, No. 2, pp. 156-163, 2009.

[96] G.P. Tegos and M.R. Hamblin, "Phenothiazinium antimicrobial photosensitizers are substrates of bacterial multidrug resistance pumps," *Antimicrob. Agents Chemother.,* Vol. 50, No. 1, pp. 196-203, January 1, 2006 2006.

[97] L. Peloi, R. Soares, C. Biondo, V. Souza, N. Hioka, and E. Kimura, "Photodynamic effect of light-emitting diode light on cell growth inhibition induced by methylene blue," *J Biosciences,* Vol. 33, No. 2, pp. 231-237, 2008.

[98] M.L. Embleton, S.P. Nair, B.D. Cookson, and M. Wilson, "Selective lethal photosensitization of methicillin-resistant Staphylococcus aureus using an IgG–tin (IV) chlorin e6 conjugate," *J. Antimicrob. Chemother.,* Vol. 50, No. 6, pp. 857-864, December 1, 2002 2002.

[99] M. Schäfer, C. Schmitz, R. Facius, G. Horneck, B. Milow, K.H. Funken, and J. Ortner, "Systematic study of parameters influencing the action of rose bengal with Visible Light on bacterial cells: Comparison between the biological effect and singlet-oxygen production," *Photochem Photobiol,* Vol. 71, No. 5, pp. 514-523, 2000.

[100] D.A. Caminos, M.B. Spesia, and E.N. Durantini, "Photodynamic inactivation of *Escherichia coli* by novel meso-substituted porphyrins by 4-(3-N,N,N-trimethylammoniumpropoxy)phenyl and 4-(trifluoromethyl)phenyl groups," *Photochem. Photobiol. Sci.,* Vol. 5, No. 1, pp. 56-65, 2006.

[101] N. Fotinos, M. Convert, J.-C. Piffaretti, R. Gurny, and N. Lange, "Effects on Gram-Negative and Gram-Positive Bacteria Mediated by 5-Aminolevulinic Acid and 5-Aminolevulinic Acid Derivatives," *Antimicrob. Agents Chemother.,* Vol. 52, No. 4, pp. 1366-1373, April 1, 2008 2008.

[102] D. Matevski, R. Weersink, H.C. Tenenbaum, B. Wilson, R.P. Ellen, and G. Lépine, "Lethal photosensitization of periodontal pathogens by a red-filtered Xenon lamp in vitro," *J Periodontal Res,* Vol. 38, No. 4, pp. 428-435, 2003.

[103] N.S. Soukos, L.A. Ximenez-Fyvie, M.R. Hamblin, S.S. Socransky, and T. Hasan, "Targeted antimicrobial photochemotherapy," *Antimicrob. Agents Chemother.,* Vol. 42, No. 10, pp. 2595-2601, October 1, 1998 1998.

[104] Y. Chan and C.H. Lai, "Bactericidal effects of different laser wavelengths on periodontopathic germs in photodynamic therapy," *Laser Med Sci,* Vol. 18, No. 1, pp. 51-55, 2003.

[105] L.N. Dovigo, A.C. Pavarina, D.G. Ribeiro, C.S. Adriano, and V.S. Bagnato, "Photodynamic inactivation of four Candida species induced by photogem®," *Braz J Microbiol,* Vol. 41, pp. 42-49, 2010.

[106] J.S. Friedberg, C. Skema, E.D. Baum, J. Burdick, S.A. Vinogradov, D.F. Wilson, A.D. Horan, and I. Nachamkin, "*In vitro* effects of photodynamic theraphy on *Aspergillus fumigatus*," *J Antimicrob Chemother,* Vol. 48, pp. 105 - 107, 2001.

[107] S. Wohllebe, R. Richter, P. Richter, and D.P. Häder, "Photodynamic control of human pathogenic parasites in aquatic ecosystems using chlorophyllin and pheophorbid as photodynamic substances," *J Parasitol Res,* Vol. 104, No. 3, pp. 593-600, 2009.

[108] O.E. Akilov, W. Yousaf, S.X. Lukjan, S. Verma, and T. Hasan, "Optimization of topical photodynamic therapy with 3,7-bis(di-n-butylamino)phenothiazin-5-ium bromide for cutaneous leishmaniasis," *Lasers Surg Med* Vol. 41, No. 5, pp. 358-365, 2009.

[109] S. Nobbe, R.M. Trüeb, L.E. French, and G.F.L. Hofbauer, "Herpes simplex virus reactivation as a complication of photodynamic therapy," *Photodermatol Photoimmunol Photomed,* Vol. 27, No. 1, pp. 51-52, 2011.

[110] B. Bachmann, J. Knüver-Hopf, B. Lambrecht, and H. Mohr, "Target structures for HIV-1 inactivation by methylene blue and light," *J Med Virol,* Vol. 47, No. 2, pp. 172-178, 1995.

[111] H. Ashkenazi, Z. Malik, Y. Harth, and Y. Nitzan, "Eradication of *Propionibacterium acnes* by its endogenic porphyrins after illumination with high intensity blue light," *FEMS Immunol Med Microbiol,* Vol. 35, No. 1, pp. 17-24, 2003.

[112] P. Papageorgiou, A. Katasambas, and A. Chu, "Phototherapy with blue (415 nm) and red (660 nm) light in the treatment of acne vulgaris," *British Journal of Dermatology,* Vol. 142, pp. 973 - 978, 2000.

[113] O. Feuerstein, N. Persman, and E.I. Weiss, "Phototoxic effect of visible light on *Porphyromonas gingivalis* and *Fusobacterium nucleatum*: An *in vitro* study," *Photochem Photobiol,* Vol. 80, No. 3, pp. 412-415, 2004.

[114] R.A. Ganz, J. Viveiros, A. Ahmad, A. Ahmadi, A. Khalil, M.J. Tolkoff, N.S. Nishioka, and M.R. Hamblin, "Helicobacter pylori in patients can be killed by visible light," *Lasers Surg Med,* Vol. 36, pp. 260 – 265, 2005.

[115] J.S. Guffey and J. Wilborn, "*In vitro* bactericidal effects of 405-nm and 470-nm Blue light," *Photomed Laser Surg,* Vol. 24, No. 6, pp. 648-688, 2006.

[116] M. Maclean, S.J. MacGregor, J.G. Anderson, and G. Woolsey, "High-intensity narrow-spectrum light inactivation and wavelength sensitivity of *Staphylococcus aureus*," *FEMS Microbiol Lett,* Vol. 285, No. 2, pp. 227-232, 2008.

[117] M. Maclean, S.J. MacGregor, J.G. Anderson, and G. Woolsey, "Inactivation of bacterial pathogens following exposure to light from a 405-Nanometer Light-Emitting Diode array," *Applied and Environmental Microbiology,* Vol. 75, No. 7, pp. 1932 – 1937, 2009.

[118] L.E. Murdoch, M. Maclean, S.J. MacGregor, and J.G. Anderson, "Inactivation of Campylobacter jejuni by exposure to high-intensity 405-nm visible light," *Foodborne Pathog Dis,* Vol. 7, No. 10, pp. 1211-6, 2010.

[119] S.J. MacGregor, J.G. Anderson, M. Maclean, G.A. Woolsey, and G. Gettinby, "Clinical evaluation of the HINS-light Environmental Decontamination System (HINS-LIGHT EDS) " University of Strathclyde, Glasgow, 2010.

[120] M.M. Nerandzic, J.L Cadnum, M.J. Pultz, and C.J. Donskey, "Evaluation of an automated ultraviolet radiation device for decontamination of Clostridium difficile and other healthcare-associated pathogens in hospital rooms," *BMC Infect Dis,* Vol. 10, No. 197, 2010.

[121] W.A. Rutala, M.F. Gergen, and D.J. Weber, "Room decontamination with UV radiation," *Infect Control Hosp Epidemiol,* Vol. 31, No. 10, pp. 1025-1029, 2010.

[122] J.M. Boyce, N.L. Havill, J.A. Otter, L.C. McDonald, N.M.T. Adams, T. Cooper, A. Thompson, L. Wiggs, G. Killgore, A.Tauman, and J. Noble-Wang, "Impact of Hydrogen Peroxide Vapor room decontamination on *Clostridium difficile* environmental contamination and transmission in a healthcare setting," *Infect Control Hosp Epidemiol* Vol. 29, pp. 723–729, 2008.

[123] C. Vuong and M. Otto, "*Staphylococcus epidermidis* infections," *Microb Infect,* Vol. 4, No. 4, pp. 481-489, 2002.

[124] CDC. National Nosocomial Infections Surveillance (NNIS) System Report, Data Summary from October 1986-April 1998, Issued June 1998, 1998 [Online] (Accessed on 8th March 2011). Available from: http://www.cdc.gov/NCIDOD/DHQP/pdf/nnis/sar98net.PDF

[125] HPA. Healthcare associated infections (HCAI), [Online] (Accessed on 5th January 2011). Available from: http://www.hpa.org.uk/Topics/InfectiousDiseases/InfectionsAZ/HCAI/

[126] R.W. Tolan Jr, E.P. Baorto, and D. Baorto. *Staphylococcus aureus* Infection 2011 [Online] (Accessed on 9th May 2011). Available from: http://emedicine.medscape.com/article/971358-overview#showall

[127] MedlinePlus. Staphylococcal Infections [Online] (Accessed on 9th March 2011). Available from: http://www.nlm.nih.gov/medlineplus/staphylococcalinfections.html

[128] P.S. Mead, L. Slutsker, V. Dietz, L.F. McCaig, J.S. Bresee, C. Shapiro, P.M. Griffin, and R.V. Tauxe, "Food-related illness and death in the United States," *Emerg Infect Diseases,* Vol. 5, No. 5, pp. 607-625, 1999

[129] M. Guzmán-Blanco, C. Mejía, R. Isturiz, C. Alvarez, L. Bavestrello, E. Gotuzzo, J. Labarca, C.M. Luna, E. Rodríguez-Noriega, M.J.C. Salles, J. Zurita, and C. Seas, "Epidemiology of meticillin-resistant *Staphylococcus aureus* (MRSA) in Latin America," *Int J Antimicro Ag,* Vol. 34, No. 4, pp. 304-308, 2009.

[130] NAO. Reducing healthcare associated infections in hospitals in England, 2009 [Online] (Accessed on 4th February 2011). Available from: http://www.official-documents.gov.uk/document/hc0809/hc05/0560/0560.pdf

[131] B.S. Cooper, S.P. Stone, C.C. Kibbler, B.D. Cookson, J.A. Roberts, G.F. Medley, G.J. Duckworth, R. Lai, and S. Ebrahim, "Systematic review of isolation policies in the hospital management of methicillin-resistant *Staphylococcus aureus*: a review of the literature with epidemiological and economic modelling," *Health Technol Assess,* Vol. 7, No. 39, pp. 1-194, 2003.

[132] J.M. Farber and P.I. Peterkin, "*Listeria monocytogenes*, a Food-Borne Pathogen," *Microbiol Rev*, Vol. 55, No. 3, pp. 476 - 511, 1991.

[133] V. Ramaswamy, V.M. Cresence, J.S. Rejitha, M.U. Lekshmi, K.S. Dharsana, S.P. Prasad, and H.M. Vijila, "Listeria -review of epidemiology and pathogenesis," *J Microbiol Immunol Infect*, Vol. 40, No. 1, pp. 4 - 13, 2007.

[134] M. Zhu, M. Du, J. Cordray, and D.U. Ahn, "Control of *Listeria monocytogenes* contamination in ready-to-eat meat products," *Compr. Rev. Food Sci. Food Safety*, Vol. 4, No. 2, pp. 34-42, 2005.

[135] J.C. Low and W. Donachie, "A review of *Listeria monocytogenes* and listeriosis," *Vet J*, Vol. 153, No. 1, pp. 9-29, 1997.

[136] C. Guillet, O. Join-Lambert, A. Le Monnier, A. Leclercq, F. Mechaï, Marie-France Mamzer-Bruneel, M. K. Bielecka, M. Scortti, O. Disson, P. Berche, J. Vazquez-Boland, O. Lortholary, and M. Lecuit, "Human listeriosis caused by *Listeria ivanovii*," *Emerg Infect Diseases*, Vol. 16, No. 1, pp. 136-138, 2010.

[137] Y.M. Snapir, E. Vaisbein, and F. Nassar, "Low virulence but potentially fatal outcome--*Listeria ivanovii*," *Eur J Intern Med*, Vol. 17, No. 4, pp. 286-287, 2006.

[138] J.A. Vazquez-Boland, M. Kuhn, P. Berche, T. Chakraborty, G. Dominguez-Bernal, W. Goebel, B. Gonzalez-Zorn, J. Wehland, and J. Kreft, "*Listeria* pathogenesis and molecular virulence determinants," *Clin. Microbiol. Rev.*, Vol. 14, No. 3, pp. 584-640, July 1, 2001 2001.

[139] C. Steinweg, C.T. Kuenne, A. Billion, M.A. Mraheil, E. Domann, R. Ghai, S.B. Barbuddhe, U. Ka¨rst, A. Goesmann, A. Pu¨hler, B. Weisshaar, J. Wehland, R. Lampidis, J. Kreft, W. Goebel, T. Chakraborty, and T. Hain, "Complete genome sequence of *Listeria seeligeri*, a nonpathogenic member of the genus *Listeria*," *J. Bacteriol.*, Vol. 192, No. 5, pp. 1473–1474 2010.

[140] J. Rocourt, H. Hof, A. Schrettenbrunner, R. Malinverni, and J. Bille, "Acute purulent *Listeria seelingeri* meningitis in an immunocompetent adult," *Schweiz Med Wochenschr*, Vol. 116, No. 8, pp. 248-251, 1986.

[141] WHO. Guidelines for drinking-water quality: Third edition, incorporating first and second addenda, 2006 [Online] (Accessed on 15th January 2011). Available from: http://www.who.int/water_sanitation_health/dwq/gdwq3rev/en/

[142] P.D. Frenzen, T. Lynn Riggs, J.C. Buzby, T. Breuer, T. Roberts, D. Voetsch, S. Reddy, and T.F.W. Group, "*Salmonella* cost estimate updated using FoodNet data," *Food Rev*, Vol. 22, No. 2, 1999.

[143] K.D. Dunkley, T.R. Callaway, V.I. Chalova, J.L. McReynolds, M.E. Hume, C.S. Dunkley, L.F. Kubena, D.J. Nisbet, and S.C. Ricke, "Foodborne *Salmonella* ecology in the avian gastrointestinal tract," *Anaerobe*, Vol. 15, No. 1-2, pp. 26-35, 2009.

[144] B.R. Warren, M.E. Parish, and K.R. Schneider, "*Shigella* as a foodborne pathogen and current methods for detection in food," *Crit Rev Food Sci Nutr*, Vol. 46, No. 7, pp. 551 - 567, 2006.

[145] S. Ashkenazi, "*Shigella* infections in children: New insights," *Seminars in pediatric infectious diseases,* Vol. 15, No. 4, pp. 246-252, 2004.

[146] K. Lemarchand, L. Masson, and R. Brousseau, "Molecular biology and DNA microarray technology for microbial quality monitoring of water," *Crit Rev Microbiol,* Vol. 30, No. 3, pp. 145-172, 2004.

[147] S.K. Niyogi, "Shigellosis," *The Journal of Microbiology,* Vol. 43, No. 2, pp. 133-143, 2005.

[148] FDA. The "Bad Bug Book": Foodborne pathogenic microorganisms and natural toxins handbook, 2006 [Online] (Accessed on 15th January 2011). Available from: http://www.fda.gov/food/foodsafety/foodborneillness/foodborneillnessfoodbornepathogensnaturaltoxins/badbugbook/default.htm

[149] R.L. Vogt and L. Dippold, "*Escherichia coli* O157:H7 outbreak associated with consumption of ground beef, June–July 2002," *Public Health Rep,* Vol. 120, 2005.

[150] A. Enache-Angoulvant and C. Hennequin, "Invasive *Saccharomyces* infection: A comprehensive review," *Clin Infect Dis,* Vol. 41, No. 11, pp. 1559-1568, December 1, 2005 2005.

[151] A. Murphy and K. Kavanagh, "Emergence of *Saccharomyces cerevisiae* as a human pathogen: Implications for biotechnology," *Enzyme Microb. Technol,* Vol. 25, No. 7, pp. 551-557, 1999.

[152] J.N. Aucott, J. Fayen, H. Grossnicklas, A. Morrissey, M.M. Lederman, and R.A. Salata, "Invasive Infection with *Saccharomyces cerevisiae*: Report of Three Cases and Review," *J Infect Dis,* Vol. 12, No. 3, pp. 406-411, May 1, 1990 1990.

[153] B. Donnelly, J.E. Gilchrist, J.T. Peeler, and J.E. Campbell, "Spiral plate count method for the examination of raw and pasteurized milk," *Appl Environ Microbiol,* Vol. 32, No. 1, pp. 21-27, 1976.

[154] J.E. Gilchrist, J.E. Campbell, C.B. Donnelly, J.T. Peeler, and J.M. Delaney, "Spiral plate method for bacterial determination," *Appl Microbiol,* Vol. 25, No. 2, pp. 244-252, 1973.

[155] J. Dunn, T. Ott, and W. Clark, "Pulsed light treatment of food and packaging," *Food Technologist,* Vol. 49, No. 9, pp. 95-98, 1995.

[156] E. Noura, G. Sandrine, L. Francoise, O. Nicole, B. Amina, and F. Michel, "Pulsed-light system as a novel food decontamination technology: a review," *Can J Microbiol,* Vol. 53, No. 7, pp. 813-821, 2007.

[157] T. Wang, S.J. MacGregor, J.G. Anderson, and G.A. Woolsey, "Pulsed Ultra-Violet inactivation spectrum of *Escherichia coli*," *Water Res,* Vol. 39, pp. 2921 – 2925, 2005.

[158] M. Maclean, L.E. Murdoch, M.N. Lani, S.J. MacGregor, J.G. Anderson, and G.A. Woolsey, "Photoinactivation and photoreactivation responses by bacterial pathogens after exposure to pulsed UV-light," in *IEEE International Power Modulators and High Voltage Conference, Proceedings of the 2008* pp. 326-329, 2008.

[159] L.E. Murdoch, "An investigation into the use of high-intesity narrow spectrum light as a decontamination technology," PhD, Department of Electronic and Electrical Engineering, University of Strathclyde, Glasgow, Scotland, UK, 2010.

[160] M.N. Lani, "Inactivation of *Listeria monocytogenes* pulsed UV illumination and photorepair recovery of UV-damged cells," PhD, Department of Electronic and Electrical Engineering, University of Strathclyde, Glasgow, Scotland, UK, 2007.

[161] Lambda. Long / Short Wave Pass Filters (LWP / SWP), 2009 [Online] (Accessed on 10th February 2011). Available from: http://www.lambda.cc/320.asp

[162] LOT-Oriel. Edge Filters, [Online] (Accessed on 10th Febreuary 2011). Available from: http://www.lot-oriel.com/files/downloads/andover/en/edgefilters.pdf

[163] LOT-Oriel. Light sources and optical filters: Standard bandpass filters, [Online] (Accessed on 10th February 2011). Available from: http://www.lot-oriel.com/files/downloads/lightsources/en/LQ_Standard_bandpass_filters_en.pdf

[164] A. Lipovsky, Y. Nitzan, H. Friedmann, and R. Lubart, "Sensitivity of *Staphylococcus aureus* strains to broadband visible light," *Photochem Photobiol*, Vol. 85, pp. 255 - 260, 2009.

[165] C.S. Enwemeka, D. Williams, S. Hollosi, and D. Yens, "Blue light photo-destroys methicillin resistant *Staphylococcus aureus* (MRSA) *in-vitro*," in *Light Activated Tissue Regeneration and Thereapy Conference* pp. 33 - 37, 2008.

[166] J.S. Guffey and J. Wilborn, "Effects of combined 405-nm and 880-nm light on *Staphylococcus aureus* and *Pseudomonas aeruginosa in vitro*," *Photomed Laser Surg*, Vol. 24, No. 6, pp. 680-683, 2006.

[167] C.S. Enwemeka, D. Williams, S. Hollosi, D. Yens, and S.K. Enwemeka, "Visible 405 nm SLD light photo-destroys methicillin-resistant *Staphylococcus aureus* (MRSA) *in vitro*," *Lasers Surg Med* Vol. 40, pp. 734 - 737, 2008.

[168] V.M. Griego and K.D. Spence, "Inactivation of *Bacillus thuringiensis* spores by ultraviolet and visible light," *Appl Environ Microbiol*, Vol. 35, No. 5, pp. 906-910, 1978.

[169] M. Elman, M. Slatkine, and Y. Harth, "The effective treatment of acne vulgaris by a high-intensity, narrow band 405–420 nm light source," *J Cosmet Laser Ther*, Vol. 5, 2003.

[170] D. Sliney, D. Aron-Rosa, F. DeLori, F. Fankhauser, R. Landry, M. Mainster, J. Marshall, B. Rassow, B. Stuck, S. Trokel, T.M. West, and M. Wolffe, "Adjustment of guidelines for exposure of the eye to optical radiation from ocular instruments: statement from a task group of the International Commission on Non-Ionizing Radiation Protection (ICNIRP)," *Appl. Opt.*, Vol. 44, No. 11, pp. 2162-2176, 2005.

[171] B. Zeina, J. Greenmab, W.M. Purcell, and B. Das, "Killing of cutaneous microbial species by photodynamic therapy," *Br J Dermatol*, Vol. 144, pp. 274 - 278, 2001.

[172] S.A.G. Lambrechts, M.C.G. Aalders, F.D. Verbraak, J.W.M. Lagerberg, J.B. Dankert, and J.J. Schuitmaker, "Effect of albumin on the photodynamic inactivation of microorganisms by a cationic porphyrin," *J Photochem Photobiol B*, Vol. 79, No. 1, pp. 51-57, 2005.

[173] G. Bertoloni, F.M. Lauro, G. Cortella, and M. Merchat, "Photosensitizing activity of hematoporphyrin on *Staphylococcus aureus* cells," *Biochimica et Biophysica Acta (BBA) - General Subjects*, Vol. 1475, No. 2, pp. 169-174, 2000.

[174] Y. Nitzan and M. Kauffman, "Endogenous porphyrin production in bacteria by δ-aminolaevulinic acid and subsequent bacterial photoeradication," *Lasers Med Sci*, Vol. 14, No. 4, pp. 269-277, 1999.

[175] I. Buchovec, E. Paskeviciute, and Z. Luksiene, "Photosensitization-based inactivation of food pathogen *Listeria monocytogenes* in vitro and on the surface of packaging material," *J. Photochem. Photobiol. B: Biol.*, Vol. 99, No. 1, pp. 9-14, 2010.

[176] Z. Luksiene, I. Buchovec, and E. Paskeviciute, "Inactivation of several strains of *Listeria monocytogenes* attached to the surface of packaging material by Na-Chlorophyllin-based photosensitization," *J. Photochem. Photobiol. B: Biol.*, Vol. 101, No. 3, pp. 326-331, 2010.

[177] E. Paskeviciute and Z. Luksiene, "Effective non-thermal photosensitization-based decontamination of strawberries from microorganisms," *Sodininkystė ir Daržininkystė,* Vol. 28, No. 4, pp. 89-97, 2009.

[178] H. Chun, J. Kim, K. Chung, M. Won, and K.B. Song, "Inactivation kinetics of *Listeria monocytogenes*, *Salmonella enterica serovar Typhimurium*, and *Campylobacter jejuni* in ready-to-eat sliced ham using UV-C irradiation," *Meat Sci*, Vol. 83, No. 4, pp. 599-603, 2009.

[179] C.H. Sommers, P.H. Cooke, X. Fan, and J.E. Sites, "Ultraviolet Light (254 nm) Inactivation of Listeria monocytogenes on Frankfurters That Contain Potassium Lactate and Sodium Diacetate," *Journal of Food Science*, Vol. 74, pp. M114-M119, 2009.

[180] N.M. Keklik, A. Demirci, and V.M. Puri, "Inactivation of*Listeria monocytogenes*on unpackaged and vacuum-packaged chicken frankfurters using Pulsed UV-Light," *J Food Sci*, Vol. 74, No. 8, pp. M431-M439, 2009.

[181] A.H.E. Yousef and E.L.H. Marth, "Inactivation of *Listeria monocytogenes* by Ultraviolet Energy," *J Food Sci*, Vol. 53, No. 2, pp. 571-573, 1988.

[182] J. McKinney, R.C. Williams, G.D. Boardman, J.D. Eifert, and S.S. Sumner, "Dose of UV light required to inactivate *Listeria monocytogenes* in distilled Water, fresh brine, and spent brine," *J. Food Prot.*, Vol. 72, No. 10, pp. 2144-2150, 2009.

[183] K.M. Gailunas, K.E. Matak, R.R. Boyer, C.Z. Alvarado, R.C. Williams, and S.S. Sumner, "Use of UV Light for the Inactivation of Listeria

monocytogenes and Lactic Acid Bacteria Species in Recirculated Chill Brines," *J. Food Prot,* Vol. 71, pp. 629-633, 2008.

[184] G. Woolsey, "HINS light safety - v.2," 2008.

[185] ENFIS. ENFIS Uno Air Cooled Light Engine, 2008 [Online] (Accessed on 9th September 2009). Available from: http://www.enfis.com/files/Uno%20Air%20Cooled%20Light%20Engine%20General.pdf

[186] Knightoptical. Fresnel lens, [Online] (Accessed on 17th June 2009). Available from: http://www.knightoptical.co.uk/acatalog/LensesFresnellensesPrecisionrange.htm

[187] Luminit. Light Shaping Diffuser (LSD), 2009 [Online] (Accessed on 17th June 2009). Available from: http://www.luminitco.com/files/u1/Technical_Data_Sheet_rev_9-28-10.pdf

[188] Levmar. A brief description of the Levenberg-Marquardt algorithm implemened, 2005 [Online] (Accessed on 7th March 2010). Available from: http://www.ics.forth.gr/~lourakis/levmar/levmar.pdf

[189] P. Dawkins. Paul's Online Math Notes: Calculus I - Notes, 2011 [Online] (Accessed on 10th January 2011). Available from: http://tutorial.math.lamar.edu/Classes/CalcI/VolumeWithRings.aspx

[190] LEDMAN. 3W High power LED - LPSH01RRWR3-L90, [Online] (Accessed on 10th August 2010). Available from: http://docs-europe.electrocomponents.com/webdocs/0d69/0900766b80d699f5.pdf

[191] OriginLab. OriginPro 8.1, [Online] (Accessed on 10th April 2010). Available from: http://www.originlab.com/

[192] Systat. *SigmaPlot 9, Systat Software Inc*. Available: www.systat.com

[193] J. Moré, "The Levenberg-Marquardt algorithm: Implementation and theory," in *Numerical Analysis*. vol. 630, G. Watson, Ed., ed: Springer Berlin / Heidelberg, 1978, pp. 105-116.

[194] OriginLab. 3D Surface Fitting - OriginPro 8.1 (Academic), [Online] (Accessed on 20th January 2011). Available from: http://www.originlab.com/index.aspx?go=Products/Origin/DataAnalysis/CurveFitting&pid=1082

[195] Degrees of freedom (df) - Internet Glossary of Statistical Terms, 2002 [Online] (Accessed on 1st April 2011). Available from: http://www.animatedsoftware.com/statglos/sgdegree.htm

[196] S. Lee. How to select a Heat Sink, [Online] (Accessed on 13rd July 2010). Available from: http://www.aavidthermalloy.com/technical/papers/pdfs/select.pdf

[197] ALTERA. Thermal Management, [Online] (Accessed on 13rd July 2010). Available from: http://www.altera.com/support/devices/power/thermal/pow-thermal.html

[198] W. Engineering. An introduction to Heatsinks and Cooling - Wakefield Engineering, 2004 [Online] (Accessed on 13rd July 2010). Available from: http://homepages.which.net/~paul.hills/Heatsinks/HeatsinksBody.html

[199] Adhesive thermal pad for STAR MCPCB, [Online] (Accessed on 10th August 2010). Available from: http://www.led-mounting-bases.com/product.php?id_product=130

[200] Thermal interface materials - Peltier device information directory, [Online] (Accessed on 13rd July 2010). Available from: http://www.peltier-info.com/tims.html

[201] Meanwell. 240W Single output switching power supply (HLG-240 series), 2009 [Online] (Accessed on 20th August 2010). Available from: http://www.meanwelldirect.co.uk/public/ranges/pdfs%5Cr1421%5Cr1421_3.pdf

[202] M. Rugged. IP65 Information, [Online] (Accessed on 20th April 2011). Available from: http://www.mruggedmobile.com/ip65-information.aspx

[203] Excelsys. LED Power supply - Constant current power supplies (LXC30 series), [Online] (Accessed on 20th August 2010). Available from: http://www.excelsys.com/industry_segment/documents/LXC30%2030W%20LED%20Power%20Supply.pdf

[204] Optodiode. 99 DIE LED array, [Online] (Accessed on 25th February 2010). Available from: www.digchip.com/data/626/OD40599070.pdf

[205] GE. Vio data sheet - High power white LED, [Online] (Accessed on 20th August 2010). Available from: http://www.gelighting.com/eu/resources/literature_library/prod_tech_pub/downloads/Vio_DataSheet_WEB_2009_03.pdf

[206] ICNIRP, "Proposed change to the IRPA 1985 guidelines on limits of exposure to Ultraviolet radiation," *Health Physics Society*, Vol. 56, No. 6, pp. 971-972, 1989.

[207] HPA. A Non-Binding Guide to the Artificial Optical radiation Directive 2006/25/EC, 2008 [Online] (Accessed on 17th March 2011). Available from: http://www.hse.gov.uk/radiation/nonionising/aor-guide.pdf

[208] T. Wang, "Waterborne microorganisms disinfection with pulsed UV light," PhD, Department of Electronic and Electrical Engineering, University of Strathclyde, Glasgow, Scotland UK, 2005.

[209] G. Greger, P. Shirley, P.M. Hubbard, and D.P. Greenberg, "The irradiance volume," *Computer Graphics and Applications, IEEE*, Vol. 18, No. 2, pp. 32-43, 1998.

A P P E N D I C E S

A p p e n d i x A

Irradiance values for microbial inactivation were taken directly under the Xenon flashlamp at fixed distance of 8 cm

No. of Pulses	Irradiance ($mWcm^{-2}$)	No. of Pulses	Irradiance ($mWcm^{-2}$)
1	3.5	**41**	8.8
2	1.8	**42**	1
3	9.7	**43**	5.3
4	8.8	**44**	8.9
5	2.2	**45**	1.7
6	9.1	**46**	2.7
7	3.3	**47**	7
8	5.8	**48**	8.2
9	4.2	**49**	9.8
10	9.7	**50**	2.6
11	6.6	**51**	9.8
12	9.4	**52**	1.3
13	4.6	**53**	9.6
14	4.9	**54**	9.1
15	1.9	**55**	6.9
16	6.3	**56**	8.9
17	7.1	**57**	9.4
18	8.2	**58**	9.8
19	9.8	**59**	9.4
20	8.9	**60**	9.5
21	2.1	**61**	3.4
22	3.5	**62**	8
23	1	**63**	1.6
24	7	**64**	9.9
25	1.9	**65**	9.3
26	8.7	**66**	8.7
27	7.8	**67**	4.7
28	9.2	**68**	9.8
29	8.7	**69**	5.2
30	8.7	**70**	1.6
31	9.6	**71**	7.6
32	8.6	**72**	1.4
33	6.2	**73**	9.8
34	6.1	**74**	6.8
35	6.4	**75**	9.9
36	6.1	**76**	4.3
37	7.3	**77**	2
38	2.6	**78**	3.2
39	1	**79**	1.5
40	6.5	**80**	9.4

No. of Pulses	Irradiance ($mWcm^{-2}$)	No. of Pulses	Irradiance ($mWcm^{-2}$)
81	5.3	**121**	3.5
82	2.9	**122**	1.8
83	5	**123**	9.7
84	5.2	**124**	8.8
85	4.2	**125**	2.2
86	8	**126**	9.1
87	7	**127**	3.3
88	9.8	**128**	5.8
89	7.8	**129**	4.2
90	1.1	**130**	9.7
91	9.7	**131**	6.6
92	1.1	**132**	9.4
93	9.7	**133**	4.6
94	8.1	**134**	4.9
95	8.7	**135**	1.9
96	6	**136**	6.3
97	7.5	**137**	7.1
98	9.6	**138**	8.2
99	8.4	**139**	9.8
100	9.8	**140**	8.9
101	9.7	**141**	2.1
102	1.5	**142**	3.5
103	9.6	**143**	1
104	1.1	**144**	7
105	4	**145**	1.9
106	9.1	**146**	8.7
107	9.7	**147**	7.8
108	9.1	**148**	9.2
109	6.8	**149**	8.7
110	9.7	**150**	8.7
111	1.3	**151**	9.6
112	9.7	**152**	8.6
113	2.7	**153**	6.2
114	8.7	**154**	6.1
115	1.1	**155**	6.4
116	7.6	**156**	6.1
117	6.5	**157**	7.3
118	8.9	**158**	2.6
119	9.5	**159**	1
120	7.7	**160**	6.5

No. of Pulses	Irradiance ($mWcm^{-2}$)	No. of Pulses	Irradiance ($mWcm^{-2}$)
161	8.8	**181**	3.4
162	1	**182**	8
163	5.3	**183**	1.6
164	8.9	**184**	9.9
165	1.7	**185**	9.3
166	2.7	**186**	8.7
167	7	**187**	4.7
168	8.2	**188**	9.8
169	9.8	**189**	5.2
170	2.6	**190**	1.6
171	9.8	**191**	7.6
172	1.3	**192**	1.4
173	9.6	**193**	9.8
174	9.1	**194**	6.8
175	6.9	**195**	9.9
176	8.9	**196**	4.3
177	9.4	**197**	1
178	9.8	**198**	3.2
179	9.4	**199**	1.5
180	9.5	**200**	9.4

Values in Appendix 1 were taken three times for each independent experiment using radiant Power Meter (Model 70260, L.O.T.-Oreiel Ltd.) to ensure accurate measurements. Total irradiance = 6.4 $mWcm^{-2}$ per pulse (1280.8 $mWcm^{-2}$/200 pulses).

A p p e n d i x B

Emission spectrum of bandpass filters used in the study

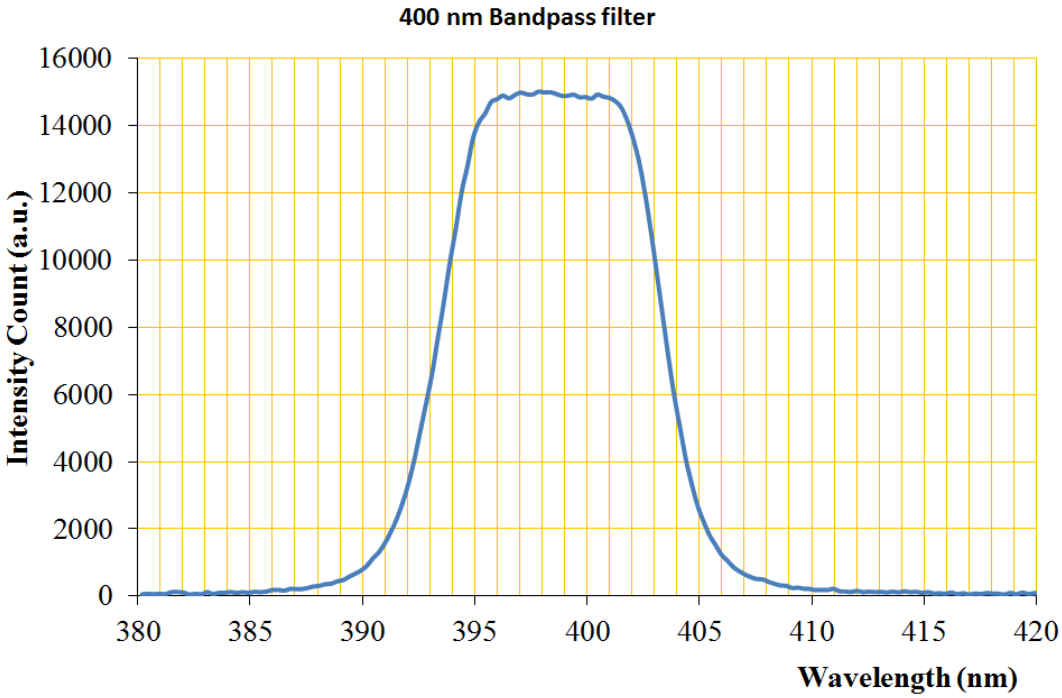

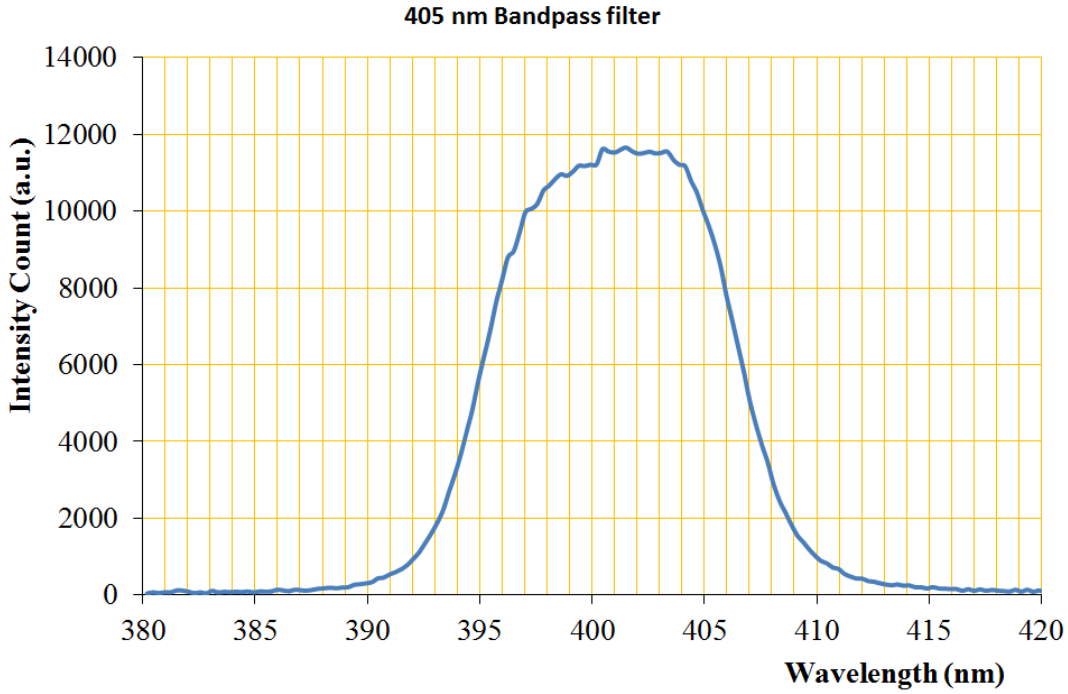

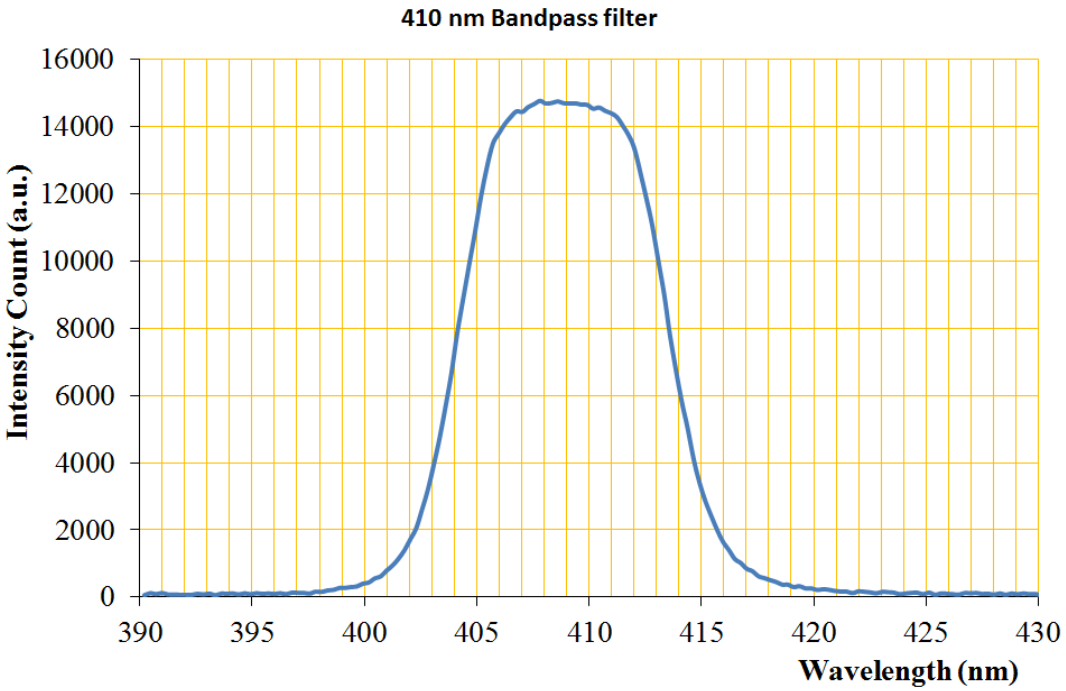
410 nm Bandpass filter
Intensity Count (a.u.)
16000
14000
12000
10000
8000
6000
4000
2000
0
390
395
400
405
410
415
420
425
430
Wavelength (nm)

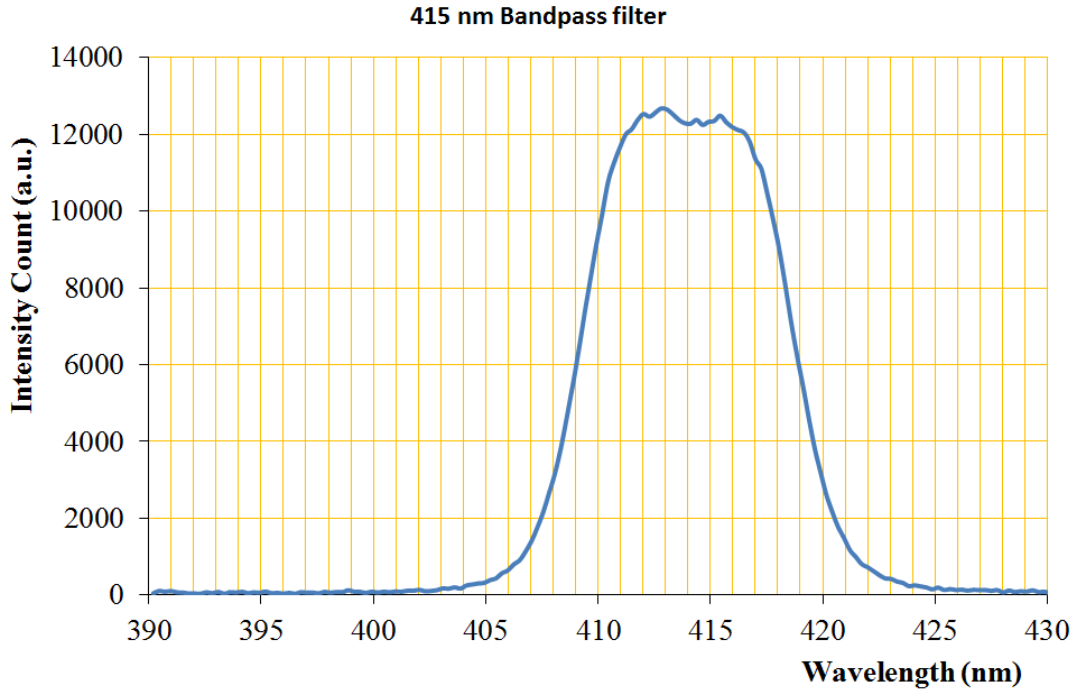
415 nm Bandpass filter
Intensity Count (a.u.)
14000
12000
10000
8000
6000
4000
2000
0
390
395
400
405
410
415
420
425
430
Wavelength (nm)

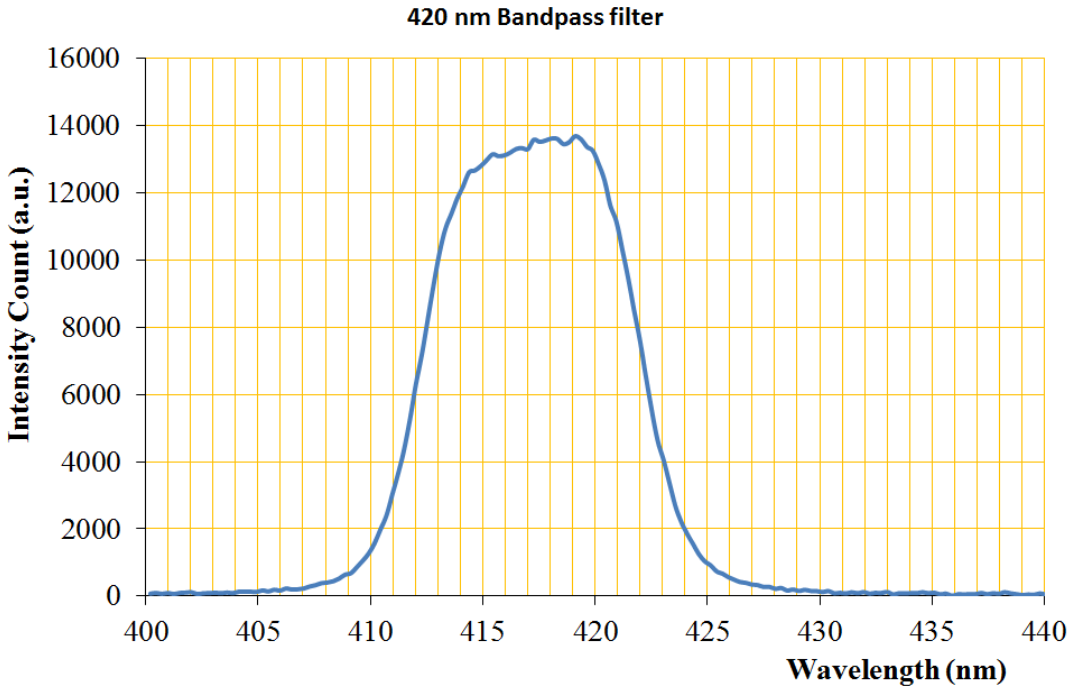
420 nm Bandpass filter
Intensity Count (a.u.)
16000
14000
12000
10000
8000
6000
4000
2000
0
400
405
410
415
420
425
430
435
440
Wavelength (nm)

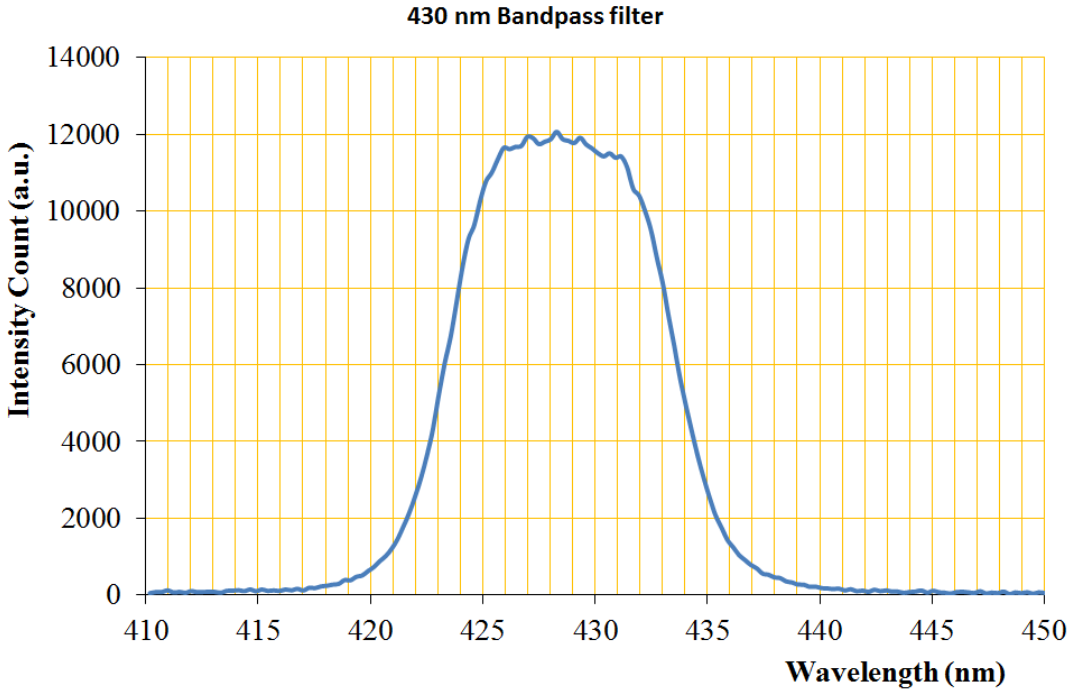
430 nm Bandpass filter
Intensity Count (a.u.)
14000
12000
10000
8000
6000
4000
2000
0
410
415
420
425
430
435
440
445
450
Wavelength (nm)

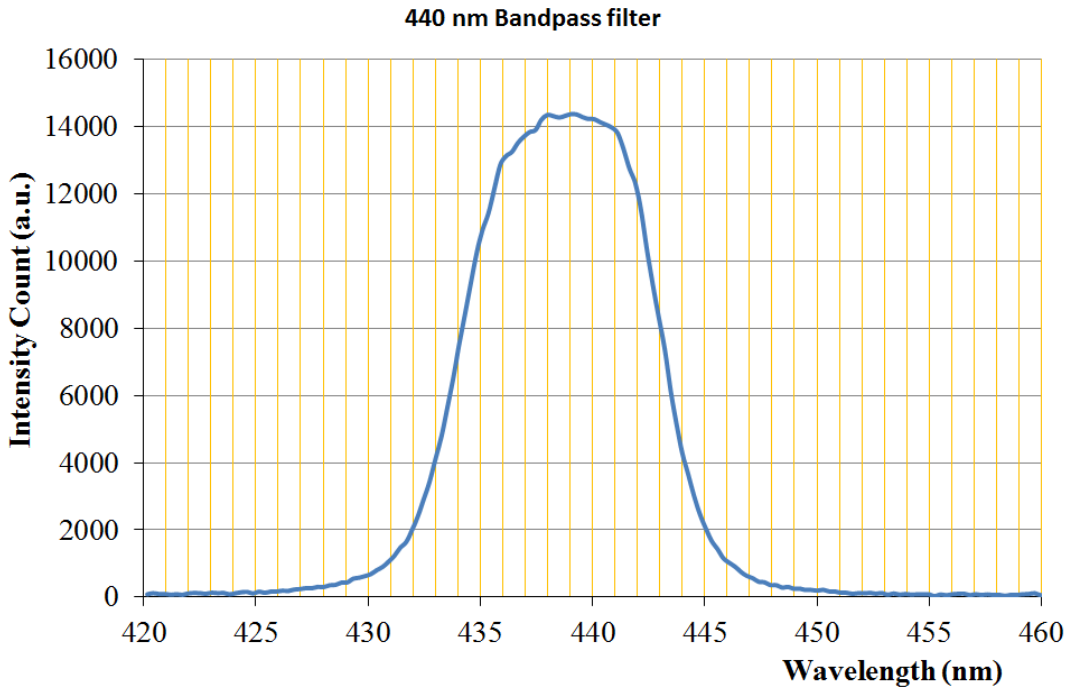
440 nm Bandpass filter
Intensity Count (a.u.)
16000
14000
12000
10000
8000
6000
4000
2000
0
420
425
430
435
440
445
450
455
460
Wavelength (nm)

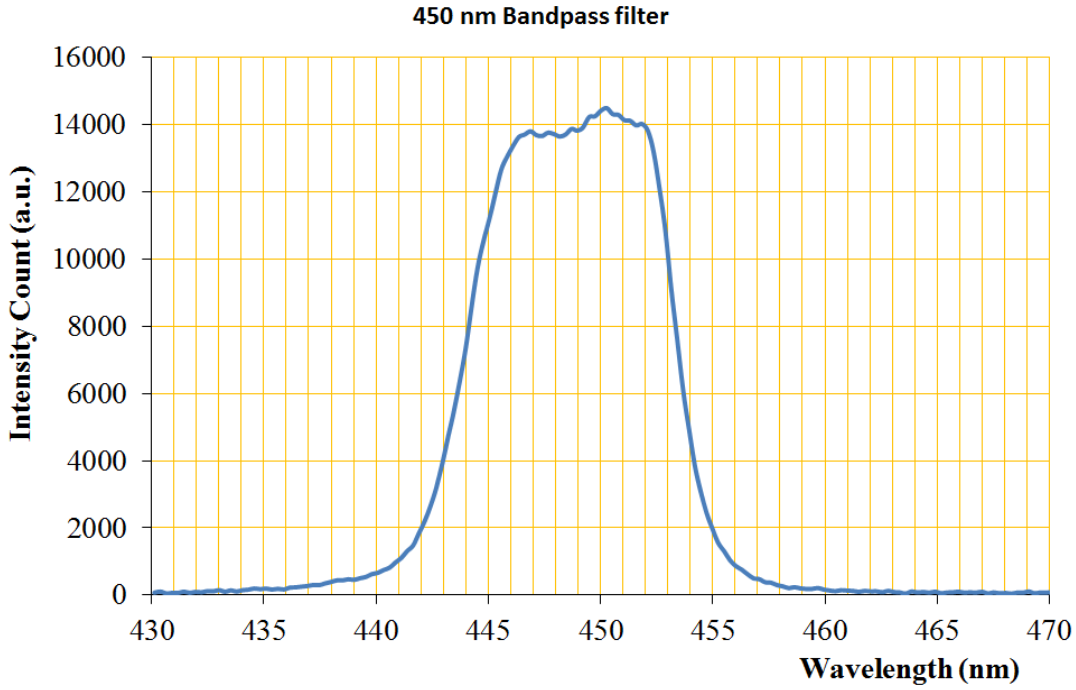
450 nm Bandpass filter
Intensity Count (a.u.)
16000
14000
12000
10000
8000
6000
4000
2000
0
430
435
440
445
450
455
460
465
470
Wavelength (nm)

A p p e n d i x C

ENFIS UNO Air Cooled Light Engine

ENFIS UNO Air Cooled Light Engine

Smart, compact, efficient, high power LED spot source - total solution

Features & Benefits

Plug & Play
- Just plug in and go straight from the box!
- Ideal for product development and volume
- Reduces integration time and risk

USB Connection for monitoring input, output and temperature

Neutral White (4250K)

Single colours 365nm to 870nm

Ultra high density array up to 100 LEDs within 0.5cm² aperture

Smart thermal protection system

Optional life-long 100% lumen maintenance

Up to 38W

Long life, low maintenance

System 3-year warranty

Applications & Markets

- Lighting
  - Entertainment
  - Retail
  - Task
- Medical
  - Skin treatment
  - Neo-natal
  - Dental applications
- Industrial
  - Forensics
  - Security and surveillance
  - Non-destructive testing
  - Epoxy/adhesive curing

Outline Specification

Wavelength	Typical Light Output
365nm	600mW
375nm	1150mW
405nm	4900mW
465nm	5750mW
520nm	1850mW
595nm	1150mW
630nm	3850mW
870nm	1750mW
4250°K	1000 lm

ENFIS LIMITED
Technium 2, Kings Road,
Swansea Waterfront,
Swansea, SA1 8PJ, UK
Tel +44 (0)1792 485660
Fax +44 (0)1792 485537
www.enfis.com
info@enfis.com

ENFIS

Uno Air Cooled Light Engine Rev 5 July 08

ENFIS UNO Air Cooled Light Engine

Technical Specification

Electro-Optical Characteristics

Colour	Peak Wavelength (nm)	Typ. Light Output (mW)	Typ. Light Output (lm)	Total Electrical Power (W)
SUVA	365	600	-	18
UVA	375	1150	-	18
Violet	405	4900	-	38
Blue	465	5750	330	38
Green	520	1850	860	38
Amber	595	1150	520	30
Red	630	3890	615	30
NIR	870	1750	-	16
Neutral White	3900-4600K	-	1000	38
Please contact Enfis Ltd for further information Amber, Red and NIR Power is limited by driver power supply				

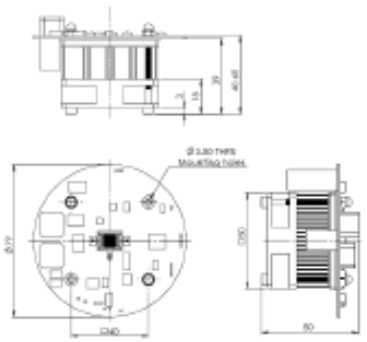

Ambient temperature = 25ºC

Electronics:

Technical Specification

Operating temperature	-10ºC to +45ºC
Storage temperature	-20ºC to +85ºC
Typical Driver Efficiency	> 90%

Input To Driver

Input voltage

Blue / Green / Violet / UVA / White	12V <5A DC
Red / Amber	9V <5A DC
NIR	5V <5A DC

LED Driver PCB

Efficient LED driver based on switch mode technology
Temperature monitoring and control
USB/Serial PC interface

Connectivity

TTL interface with USB convertor (USB connector head provided)

Thermal Management

Composite metal heatsink with integrated low noise DC fan
Low thermal resistance <1ºC/W

Handling LED Array

Contact with the encapsulation on the surface of the LED array must be avoided to prevent damage. Do not apply pressure to the encapsulation or allow it to come into contact with sharp objects. During operation the encapsulation will be hot and contact should be avoided.

Static Electricity

Care must be taken when handling, these products are sensitive to static electricity . Observe static handling precautions.

Cleaning

Avoid touching the LED array surface.
To clean—BLOW surface with either dry air or nitrogen gas

Eye Safety Precautions

The light output of the products may cause injuries to human eyes in circumstances where the products are viewed directly with unshielded eyes for more than a few seconds.

Please refer to IEC 60825-1:2001 for further information

ENFIS LIMITED
Technium 2, Kings Road,
Swansea Waterfront,
Swansea, SA1 8PJ, UK
Tel +44 (0)1792 485660
Fax +44 (0)1792 465537
www.enfis.com
info@enfis.com

ENFIS

A p p e n d i x D

Determination of the optimum LED-to-LED array spacing

Square LED array

The irradiance at O in Fig. 1 is given by the sum of the irradiance from the LED_1, LED_2, LED_3, and LED_4 with an equal sides has length ***d*** where LEDs is placed in each corner,

$$E_O(x,y,h) = E_1(x_1,y_1,h) + E_2(x_2,y_2,h) + E_3(x_3,y_3,h) + E_4(x_4,y_4,h), \quad (1)$$

With,

$$E_1(x_1,y_1,h) = h^{(3+m_1)} E_{01}(x_1,y_1,h)\left[h^2 + \left(x_1 - d/2\right)^2 + \left(y_1 + d/2\right)^2\right]^{-\frac{(3+m_1)}{2}}, \quad (2)$$

$$E_2(x_2,y_2,h) = h^{(3+m_2)} E_{02}(x_2,y_2,h)\left[h^2 + \left(x_2 - d/2\right)^2 + \left(y_2 + d/2\right)^2\right]^{-\frac{(3+m_2)}{2}}, \quad (3)$$

$$E_3(x_3,y_3,h) = h^{(3+m_3)} E_{03}(x_3,y_3,h)\left[h^2 + \left(x_3 - d/2\right)^2 + \left(y_3 + d/2\right)^2\right]^{-\frac{(3+m_3)}{2}}, \quad (4)$$

$$E_4(x_4,y_4,h) = h^{(3+m_4)} E_{04}(x_4,y_4,h)\left[h^2 + \left(x_4 - d/2\right)^2 + \left(y_4 + d/2\right)^2\right]^{-\frac{(3+m_4)}{2}}, \quad (5)$$

Let assume,

1. $E_{01}(x_1,y_1,h) = E_{02}(x_2,y_2,h) = E_{03}(x_3,y_3,h) = E_{04}(x_4,y_4,h) = E_0(x,y,h).$
2. $m = m_1 = m_2 = m_3 = m_4$

From Eq. (1) to Eq. (6), can be expressed as follows:

$$E_O(x,y,h) = h^{(3+m)} E_0(x,y,h) \sum_{i=1}^{2}\sum_{j=1}^{2}\left[\begin{matrix}\left(x - (3-2i)(d/2)\right)^2 \\ +\left(y - (3-2i)(d/2)\right)^2 + h^2\end{matrix}\right]^{-\frac{(3+m)}{2}}. \quad (6)$$

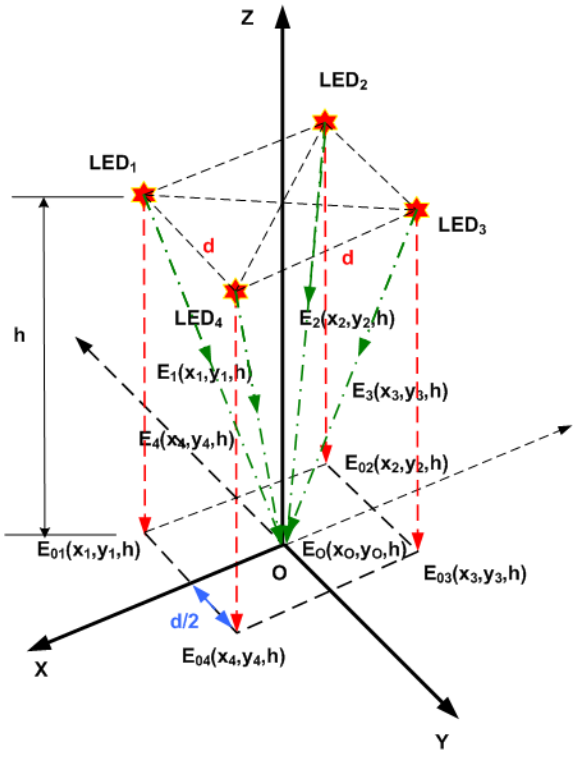

Fig. 1. *Square LED array topology.*

Based on Sparrow's criterion used in image resolution, which is given by a maximally flat condition [18]. A space distance d can be adjusted to eliminate the minimum between the maxima from irradiance pattern of two LEDs array. To achieve uniform irradiance pattern from two - LEDs array, the implicit second-order term (inverse square law) of Eq. (6) vanishes. Differentiating E twice and setting $\frac{\partial^2 E}{\partial x^2} = 0$ at $x = 0$ and $y = 0$, the maximally flat condition for d can be calculated as follows:

$$d = \frac{2h}{\sqrt{m+3}} \tag{7}$$

Table 1 *The NCC, RMS error and the Lambertian mode number (m) and total power (W) for this study (Data from Table 8.5)*

***u* (cm)**	**Irradiance (Wm^{-2}) at centre (E_0)**	***m***	**NCC (%)**	**RMS (%)**	**Total Power (W)**
2.5	1.06	3.58	99.50	4.61	1.45
4	1.92	7.06	99.44	4.61	1.50
5	2.56	10.09	99.69	3.26	1.45
6	3.39	14.50	99.81	2.19	1.37
7	4.72	21.88	99.92	1.15	1.30
7.5	5.25	25.78	99.81	1.89	1.23
8	5.76	31.02	99.96	0.76	1.13
9	6.9	43.62	99.96	0.90	0.97
10	7.45	52.71	99.86	1.59	0.87

Data: m = 7.06, u = 4 cm and E_0 (x, y, h) = 1.92 Wm^{-2}

$$d = h*0.6142951168$$

The maximally flat condition for *d*:

- h = 1 m→ d = 0.6142951168 m
- h = 1.5 m→ d = 0.9214426753 m
- h = 2 m → d = 1.228590234 m

Practical design:

d = 30 cm → Why?

(a) Dimension of ceiling (tile) → 59.2 cm x 59.2 cm(square LED array)

(b) Dimension of Fresnell lens ∅ 20 cm

(c) Compact design due to ensure that the system did not generate dominant violet illumination but would also produce comfortable room lighting, 12 high power white-light LEDs with typical light output of 3 W for each white

LED, with 90° viewing angle and a warm-white emitting colour were used in the design of the new HINS-light EDS.

(d) Due to point (a) and (b), the optimum LED-to-LED array spacing should be 20 cm < d < 35 cm

Analysis of light distribution pattern for a square LED array topology, using Eq. (6), with m = 7.06 and E0 (x, y, h) = 1.92 Wm^{-2}

***u* = 4 cm, *z* = 200 cm, *d* = 10 cm**

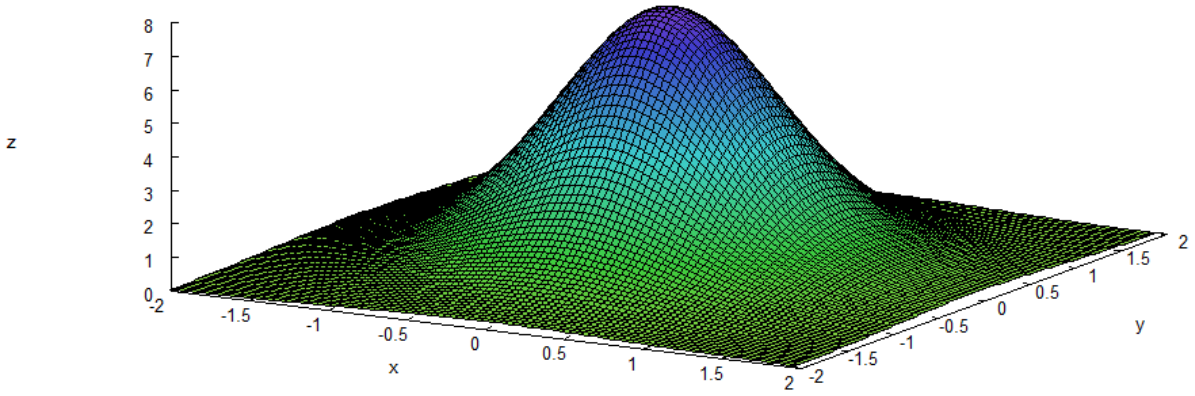

***u* = 4 cm, *z* = 200 cm, *d* = 20 cm**

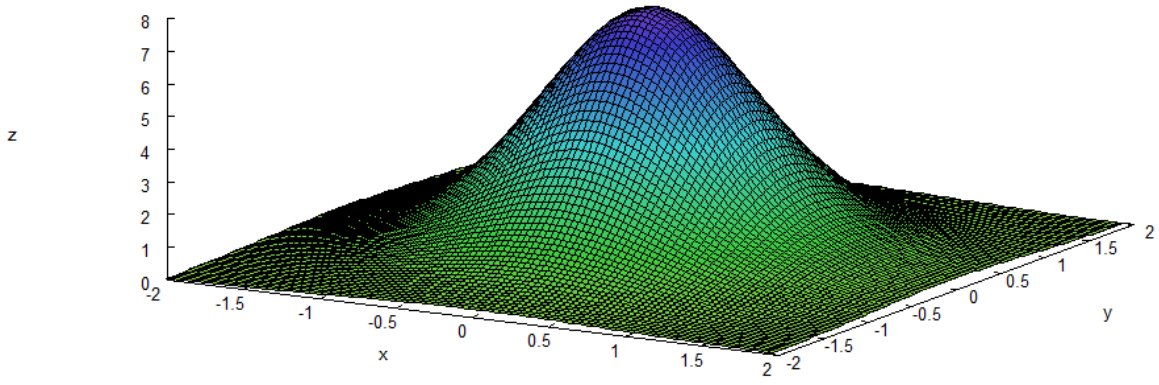

***u* = 4 cm, *z* = 200 cm, *d* = 30 cm**

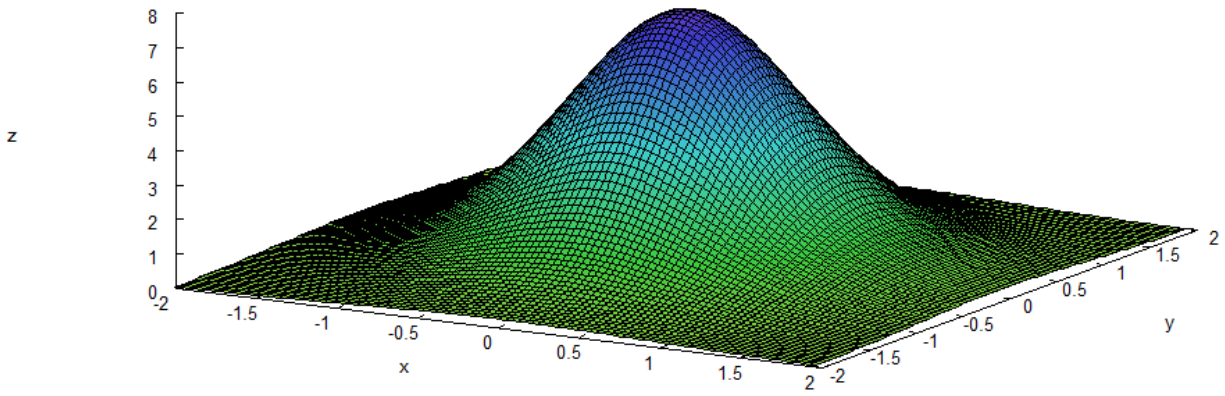

***u* = 4 cm, *z* = 200 cm, *d* = 40 cm**

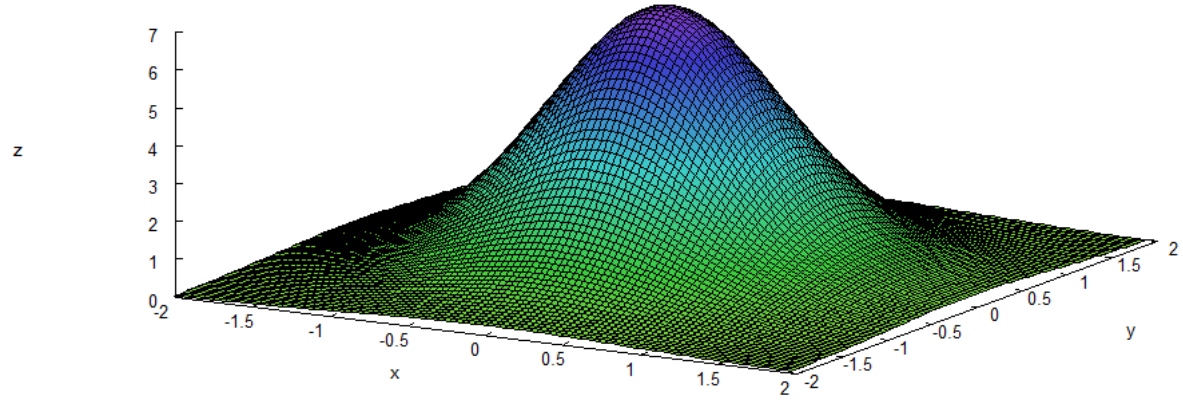

***u* = 4 cm, *z* = 200 cm, *d* = 50 cm**

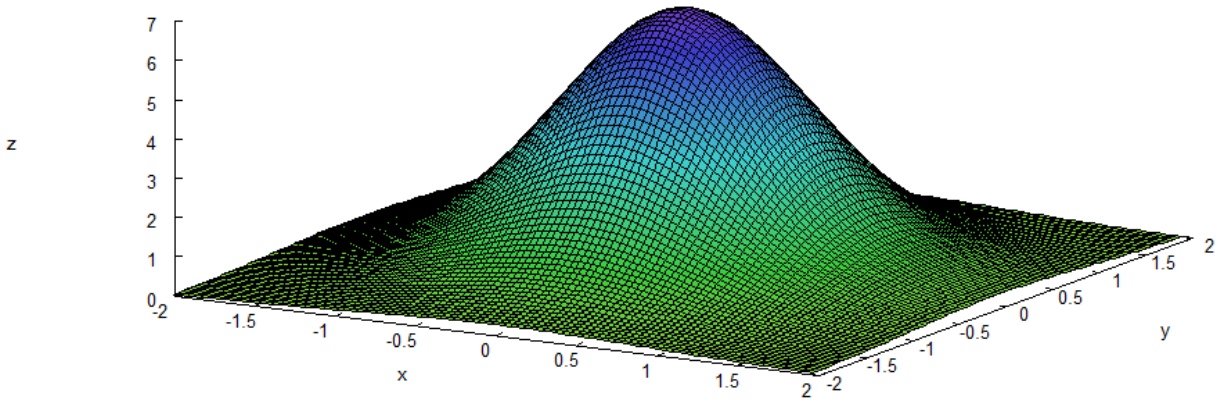

***u* = 4 cm, *z* = 200 cm, *d* = 60 cm**

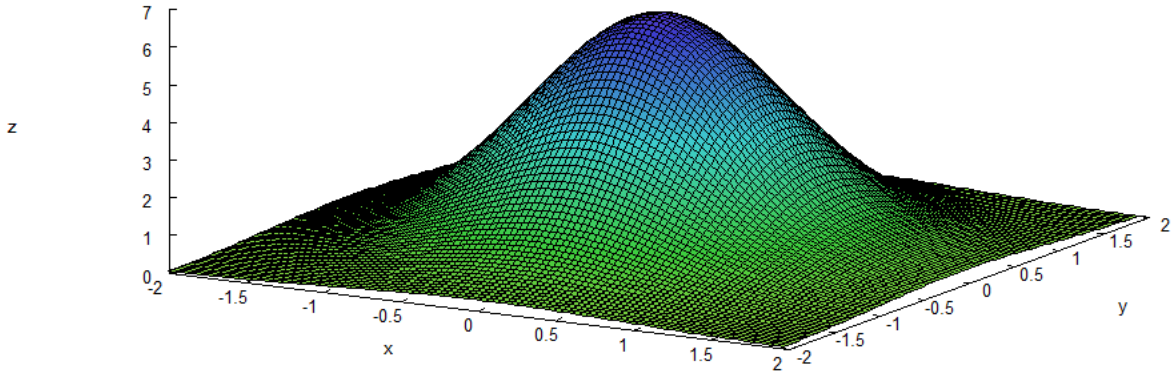

***u* = 4 cm, *z* = 200 cm, *d* = 100 cm**

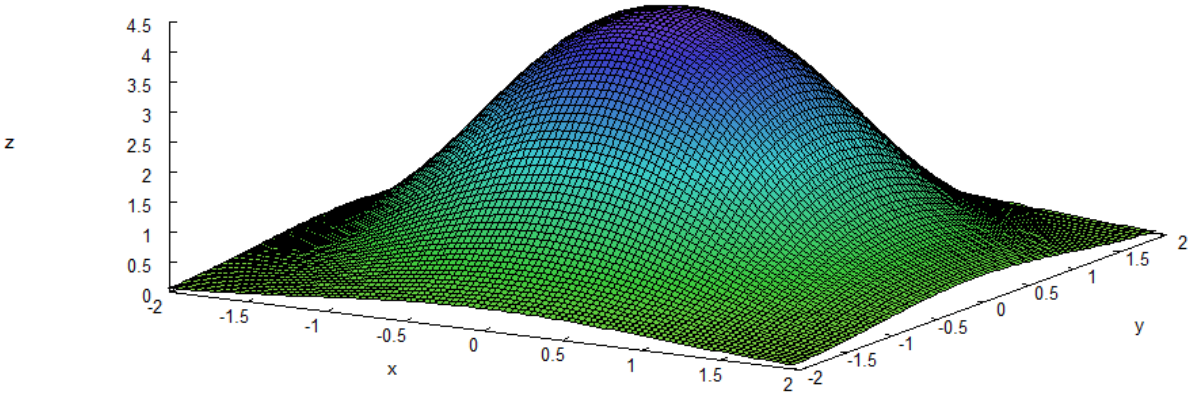

***u* = 4 cm, *z* = 200 cm, *d* = 1.228590234 m**

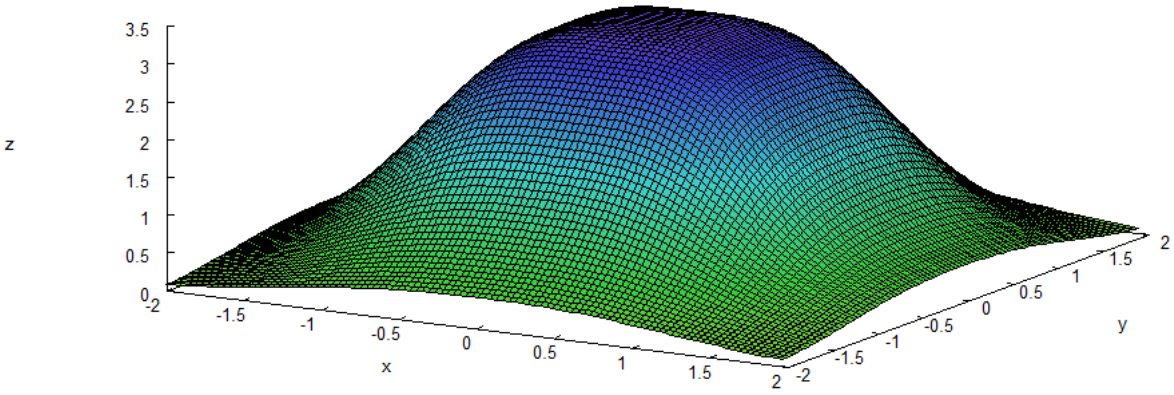

***u* = 4 cm, *z* = 200 cm, *d* = 1.5 m**

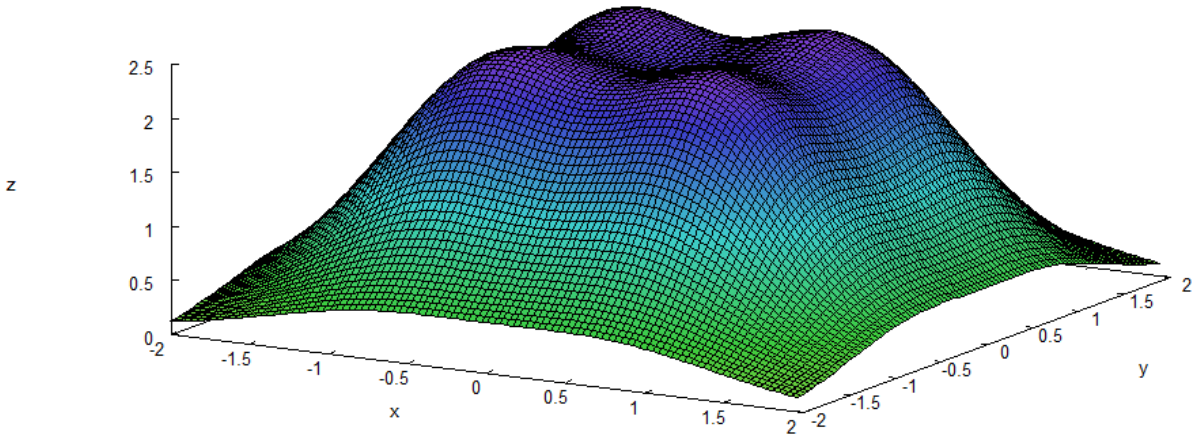

A p p e n d i x E

Spectral irradiance of HINS-light EDS with various distance measurements

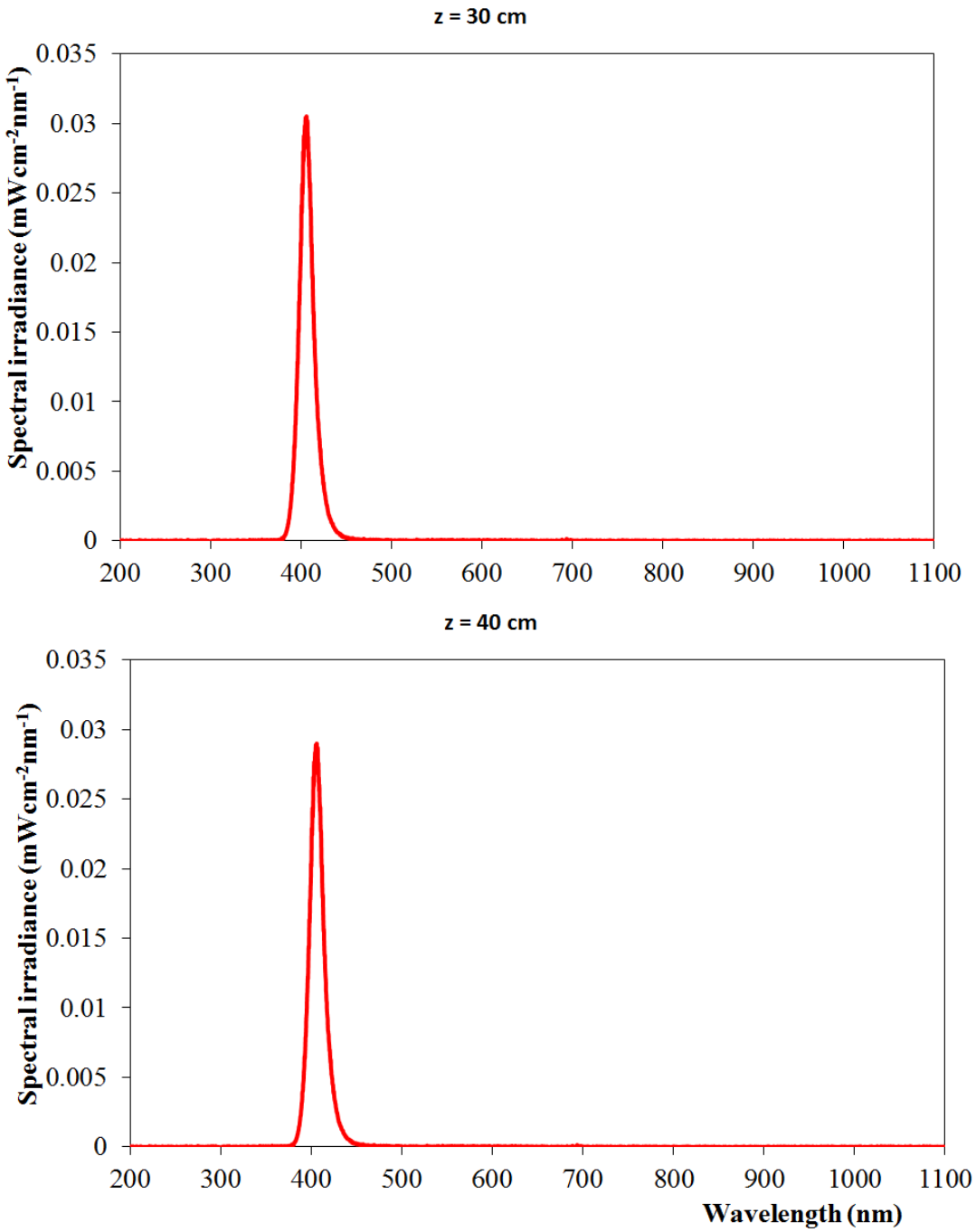

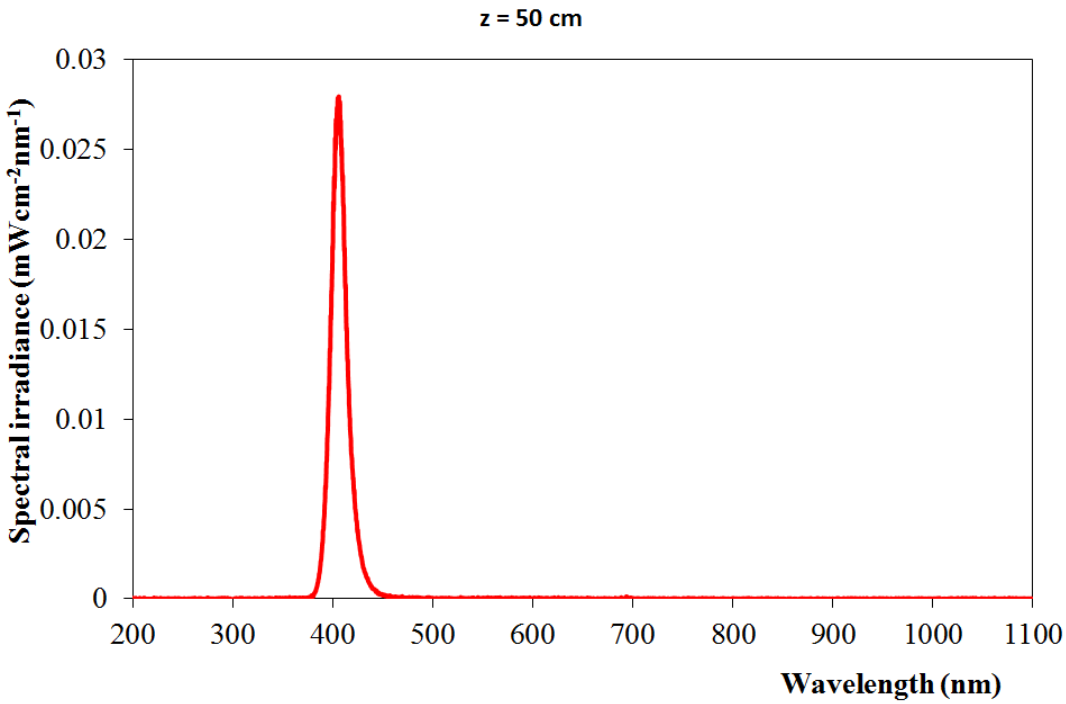
z = 50 cm
Spectral irradiance (mWcm-2nm-1)
0.03
0.025
0.02
0.015
0.01
0.005
0
200
300
400
500
600
700
800
900
1000
1100
Wavelength (nm)

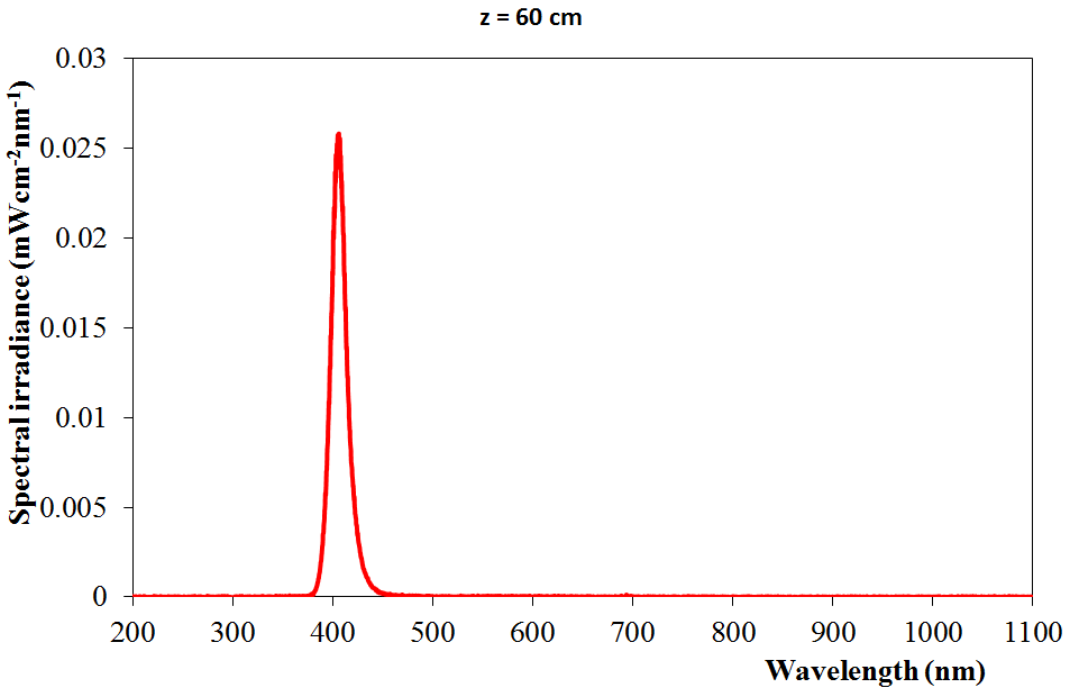
z = 60 cm
Spectral irradiance (mWcm-2nm-1)
0.03
0.025
0.02
0.015
0.01
0.005
0
200
300
400
500
600
700
800
900
1000
1100
Wavelength (nm)

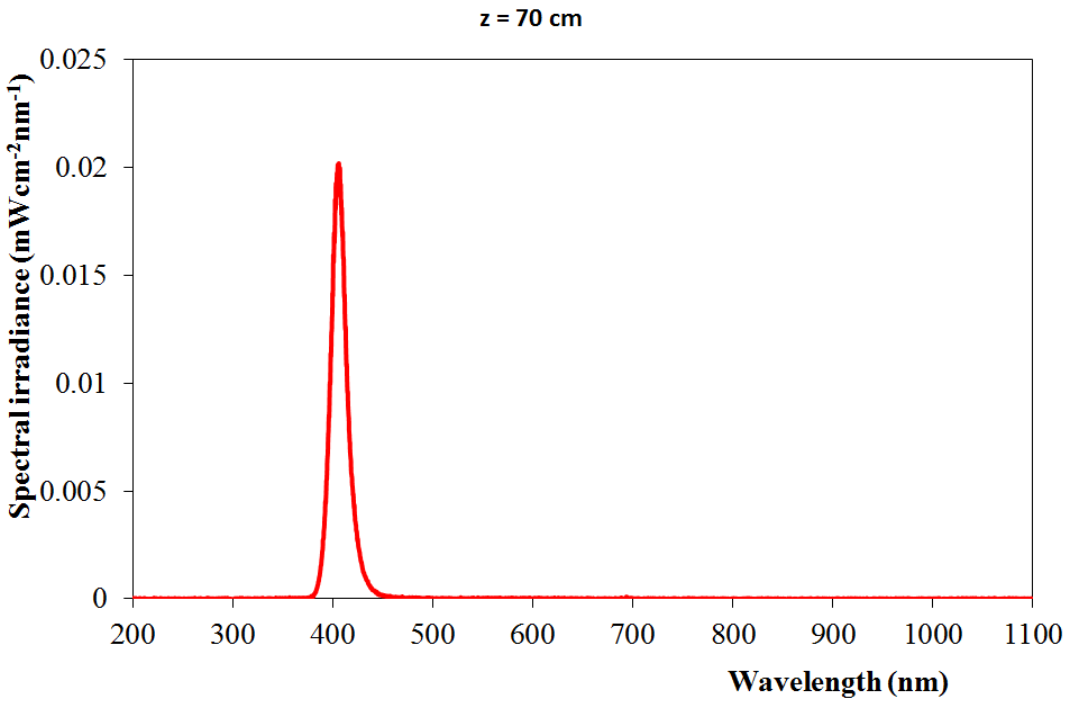
z = 70 cm
Spectral irradiance (mWcm-2nm-1)
0.025
0.02
0.015
0.01
0.005
0
200
300
400
500
600
700
800
900
1000
1100
Wavelength (nm)

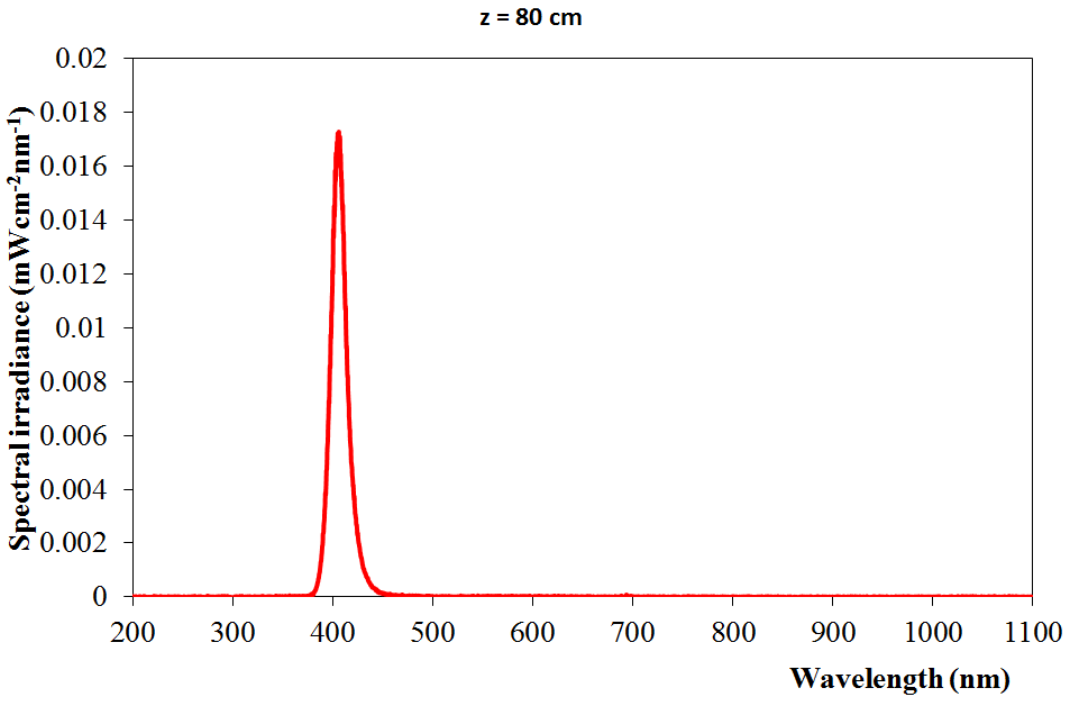
z = 80 cm
Spectral irradiance (mWcm-2nm-1)
0.02
0.018
0.016
0.014
0.012
0.01
0.008
0.006
0.004
0.002
0
200
300
400
500
600
700
800
900
1000
1100
Wavelength (nm)

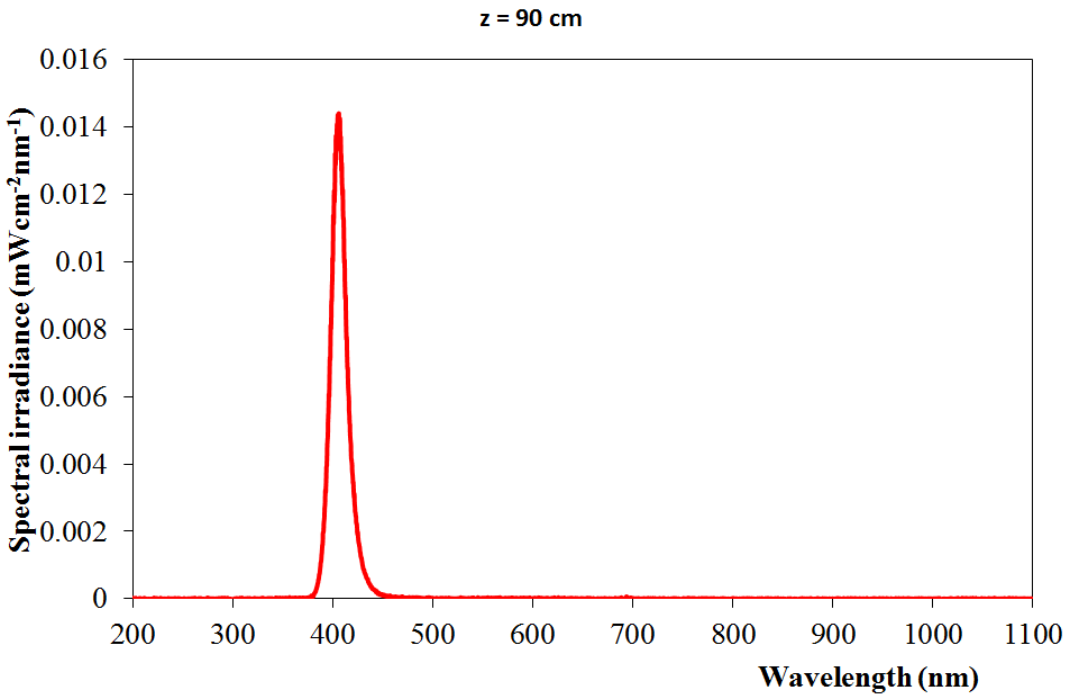
z = 90 cm
Spectral irradiance (mWcm-2nm-1)
0.016
0.014
0.012
0.01
0.008
0.006
0.004
0.002
0
200
300
400
500
600
700
800
900
1000
1100
Wavelength (nm)

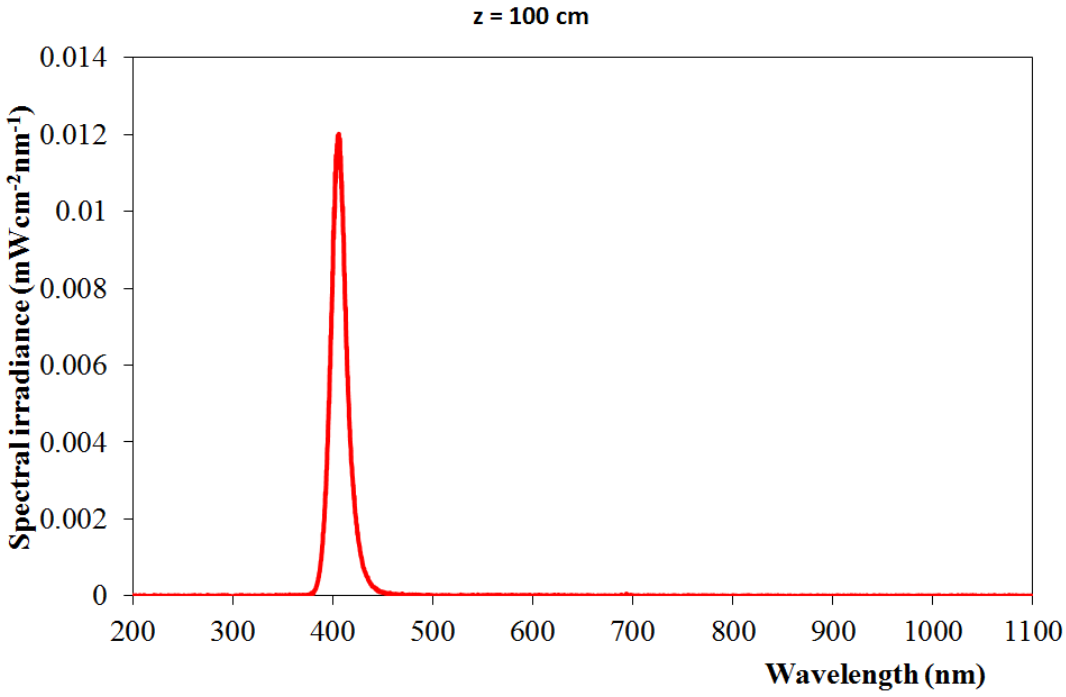
z = 100 cm
Spectral irradiance (mWcm-2nm-1)
0.014
0.012
0.01
0.008
0.006
0.004
0.002
0
200
300
400
500
600
700
800
900
1000
1100
Wavelength (nm)

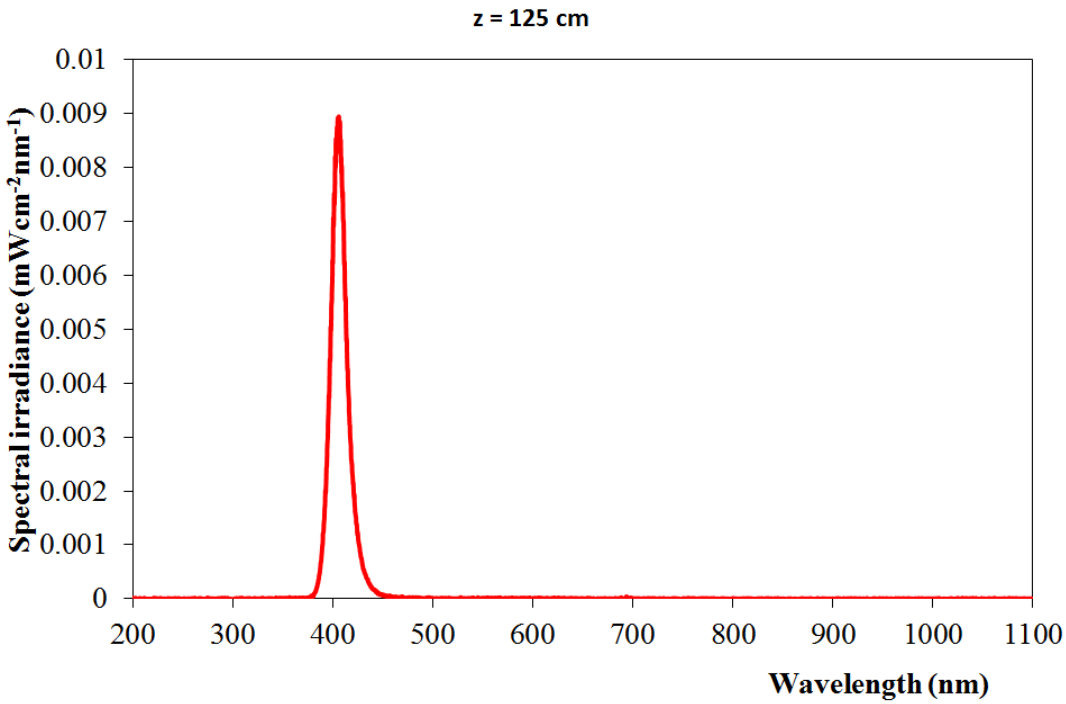
z = 125 cm
Spectral irradiance (mWcm-2nm-1)
0.01
0.009
0.008
0.007
0.006
0.005
0.004
0.003
0.002
0.001
0
200
300
400
500
600
700
800
900
1000
1100
Wavelength (nm)

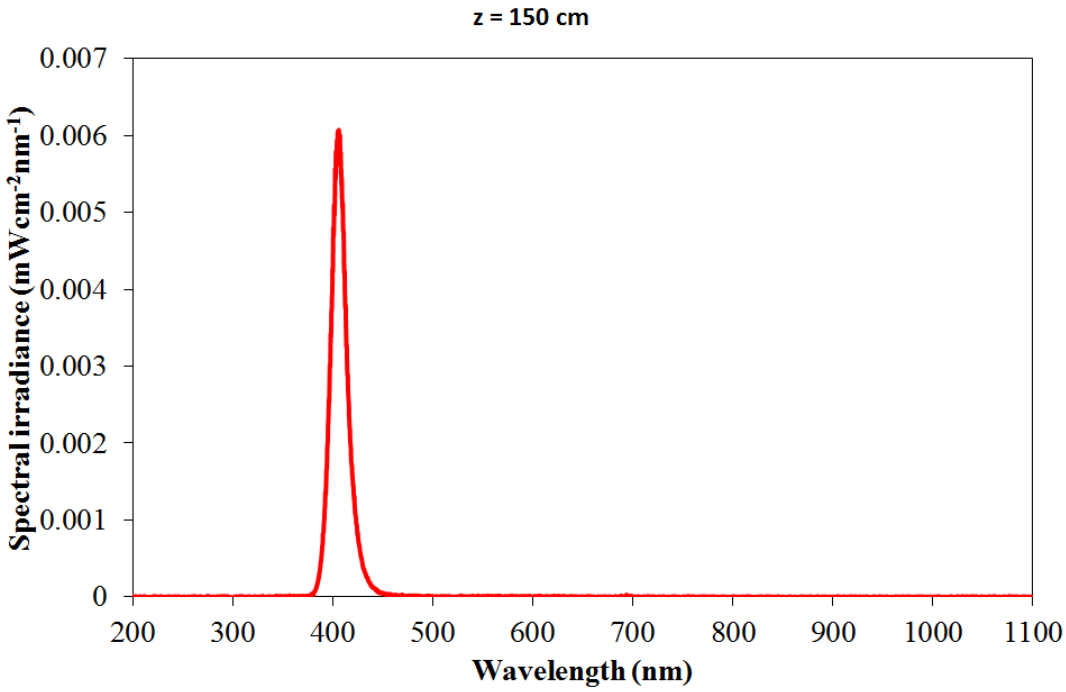
z = 150 cm
Spectral irradiance (mWcm-2nm-1)
0.007
0.006
0.005
0.004
0.003
0.002
0.001
0
200
300
400
500
600
700
800
900
1000
1100
Wavelength (nm)

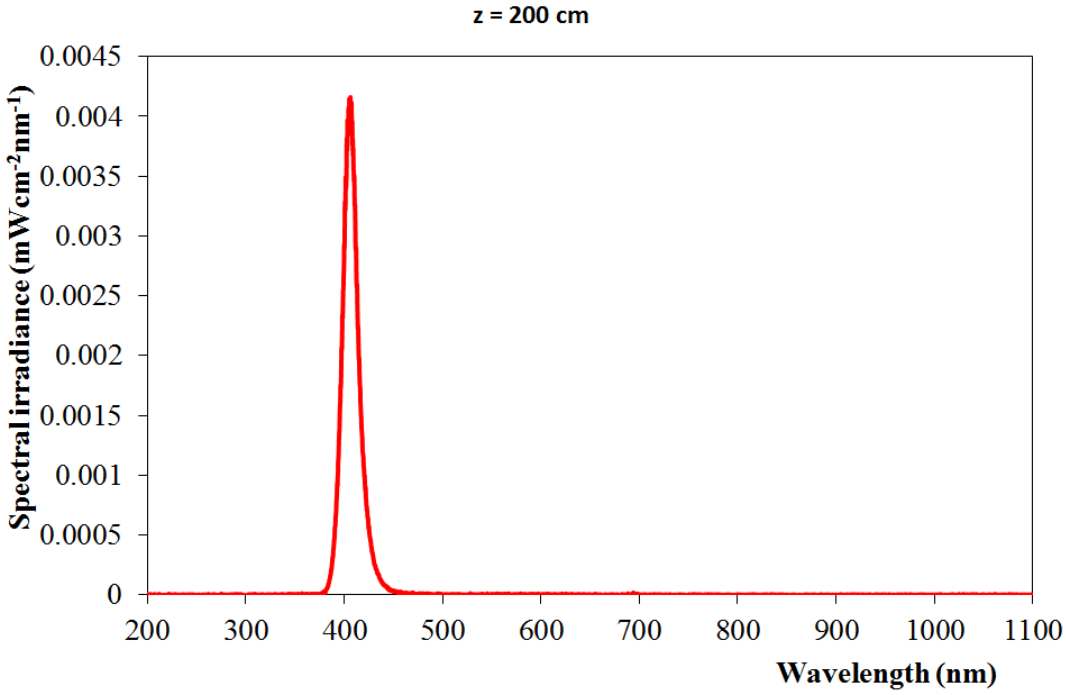
z = 200 cm
Spectral irradiance (mWcm-2nm-1)
0.0045
0.004
0.0035
0.003
0.0025
0.002
0.0015
0.001
0.0005
0
200
300
400
500
600
700
800
900
1000
1100
Wavelength (nm)

A p p e n d i x F

Risk assessment of the ROLEST laboratory lighting

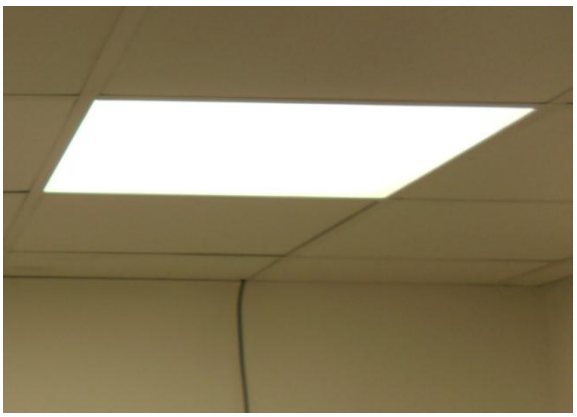

Geometric factors

- Spectral irradiance data will be measured at a distance of 30 – 200 cm from the lamp, looking directly at it
- For the ROLEST lighting has a surface area of 59.2 cm × 59.2 cm = 3504.64 cm^2
- Solid angle (Ω) = 0.087616 sr (h = 200 cm)

UV assessment (180 – 400 nm)

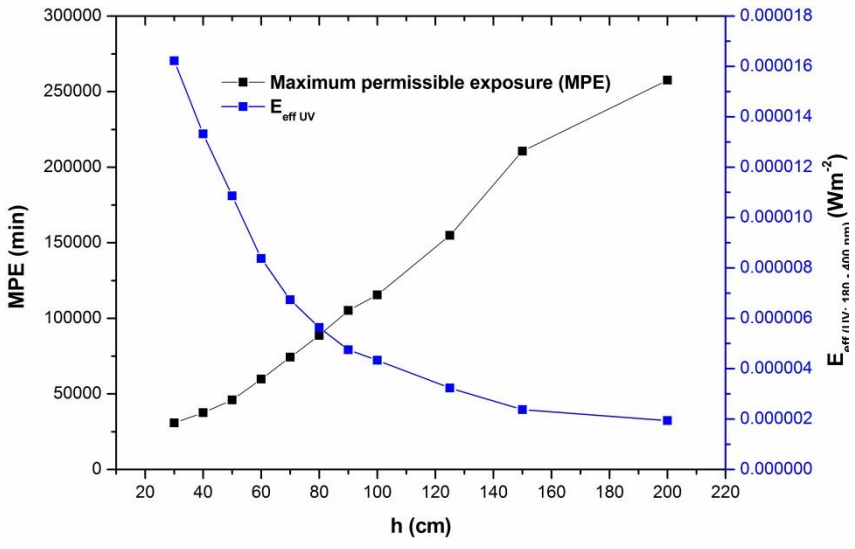

UV-A assessment (315 – 400 nm)

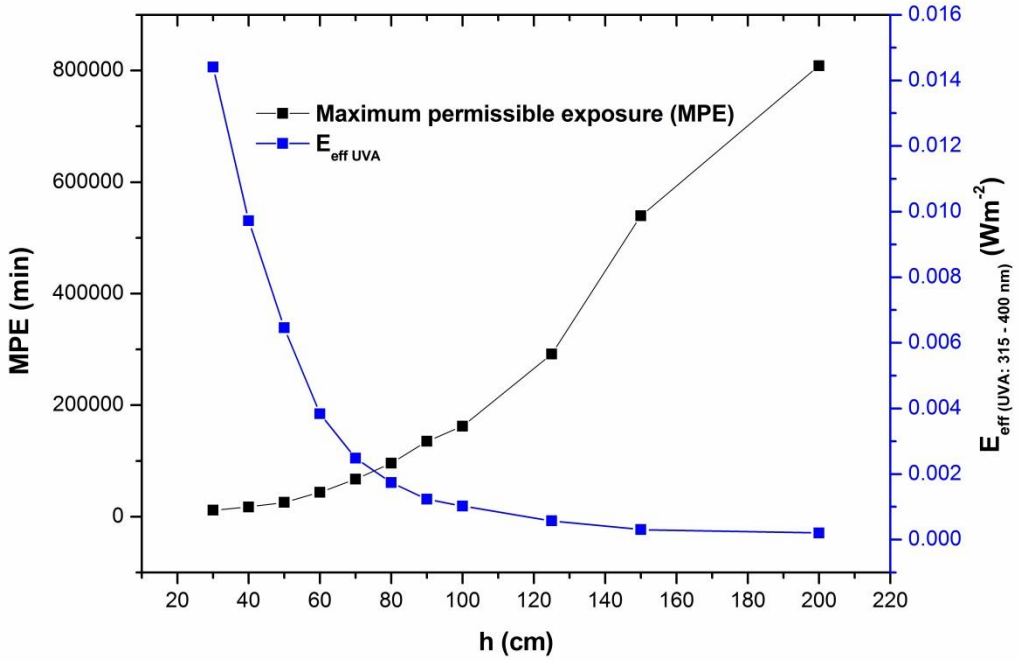

Risk Assessment: (*Comparison with exposure limits)*

1. **Limit a → The exposure limit is H_{eff} = 30 Jm^{-2} (UV: 180 – 400 nm)**

   MPE > 8 hours (h = 30 – 200 cm)

2. **Limit b → The exposure limit is H_{UVA} = 10^4 Jm^{-2} (UVA: 315 – 400 nm)**

   MPE > 8 hours (h = 30 – 200 cm)

3. **Limit d → The exposure limit is 100 $Wm^{-2}sr^{-1}$**

   LB = 0.47 $Wm^{-2}sr^{-1}$ and LA = 0.63 $Wm^{-2}sr^{-1}$

4. **Limit g → The exposure limit is 280 $kWm^{-2}sr^{-1}$ or 10^4 $cd.m^{-2}$**

h (cm)	lux
30	5000
100	1000
200	400

LR = 4556.4 < 10^4 $cd.m^{-2}$

A p p e n d i x G

Publications

1. "Pulsed Light Technology for Microbial Inactivation", Proceedings of the 44th International Universities Power Engineering Conference (UPEC 2009), Glasgow, Scotland, 1-4 September 2009. (**Oral Presentation**)

2. "High intensity 405 nm light inactivation of MSAA and MRSA strains of Staphylococcus aureus ", The Society for General Microbiology Conference, University of Nottingham, 6-9 September 2010 (**Poster Presentation**)

3. "High intensity 405nm light inactivation of *Listeria monocytogenes*", currently in preparation to submit into the journal of Photochemistry and Photobiology

4. "Ceiling-mounted light source for Bacterial Inactivation", currently in preparation to submit into the Journal of Biomedical Optics.

5. "Bactericidal effects of 405-nm light exposure demonstrated by inactivation of *Escherichia*, *Salmonella*, *Shigella*, *Listeria* and *Mycobacterium* species in liquid suspensions and on exposed surfaces", The Scientific World Journal. (co Author) [Submitted)

Society for General Microbiology Conference,

University of Nottingham, 6 – 9 September 2010

High intensity 405 nm light inactivation of MSSA and MRSA strains of Staphylococcus aureus

Endarko, M. Maclean, I.V. Timoshkin, S.J. MacGregor, & J.G. Anderson

The Robertson Trust Laboratory for Electronic Sterilisation Technologies (ROLEST), Dept. of Electronic and Electrical Engineering, University of Strathclyde, 204 George Street, Glasgow G1 1XW, UK

ABSTRACT

Photodynamic-inactivation of microorganisms is a research area gaining interest due to the emergence of resistance to control methods such as antibiotics and disinfectants. The present study demonstrates the visible-light wavelength sensitivity of methicillin-sensitive and methicillin-resistant Staphylococcus aureus (MSSA & MRSA) to 400-450nm light, and subsequently, bacterial inactivation using 405nm High Intensity Narrow Spectrum (HINS) light.

To determine the wavelength sensitivity of the test bacteria, this study utilized filtered light from a continuous xenon white-light source combined with a range of narrow-band optical filters (10nm FWHM) to expose bacterial suspensions. Results demonstrated that the bacteria showed sensitivity to wavelengths of light within the visible region, with the peak wavelength for inactivation being 405±5nm. Exposure to wavelengths longer than 430nm did not cause significant bacterial inactivation.

Following identification of 405±5nm as the most bactericidal wavelength band, the study then investigated the use of high-intensity 405-nm light, generated from light-emitting diodes (LEDs). Results demonstrate that when the inactivation kinetics of MSSA and MRSA were compared using the 405nm HINS-light LED array and using the 405nm filtered light, similar results were found for each strain of bacteria, indicating that the applied dose of 405nm light was the important factor, not the light source.

Pulsed Light Technology for Microbial Inactivation

Endarko, M. Maclean, I.V. Timoshkin, S.J. MacGregor, and J.G. Anderson

The Robertson Trust Laboratory for Electronic Sterilisation Technologies (ROLEST)
Department of Electronic and Electrical Engineering
University of Strathclyde, Royal College Building
204 George Street, Glasgow G1 1XW, UK

Abstract- **Pulsed ultraviolet-rich (PUV) light is a novel non-thermal high-peak power technology, which can achieve rapid inactivation of pathogenic and spoilage microorganisms. The aim of this study was to determine the effect of PUV-light for the inactivation of the bacterial species *Staphylococcus epidermidis* and the yeast species *Saccharomyces cerevisiae* whilst in liquid suspension. Results demonstrate that PUV-light exposure is highly microbicidal, with a 7-$\log_{10}$ reduction of *S. epidermidis* being achieved after application of less than 10 pulses. *S. cerevisiae* was also inactivated, with 5-$\log_{10}$ and 7-$\log_{10}$ reductions being achieved after exposure to 10 and 75 pulses, respectively. This study also demonstrates that agitation of the sample during PUV exposure significantly enhances the inactivation rate of densely populated microbial suspensions.**

Index Terms-- **Flashlamp; High-peak power; Pulsed ultraviolet; Pathogenic bacteria; Sterilization.**

I. Introduction

Sterilization technologies to destroy or eliminate microorganisms can be achieved by either physical or chemical process. Methods used widely for sterilization include the use of heat, chemicals, electroporation and ionizing radiation [1-7]. In addition, various methods of washing, filtering, purging, vacuuming and dehydration can be considered as mechanical approaches to sterilization [8, 9].

Ultraviolet (UV) light is well-established as being highly antimicrobial, and pulsed ultraviolet (PUV) light technology is becoming attractive for decontamination and sterilization applications due to its rapid energy delivery and inactivation rates [10-14].

Microbial inactivation through UV-light exposure is primarily induced through the absorption of UV-C photons by microbial DNA. This induces DNA-based damage in the form of mutagenic lesions, including cyclobutane pyrimidine dimers (CPD) and pyrimidine-pyrimidone 6-4 photoproducts (6-4PP), which block DNA replication and can ultimately render the microbial cell inactive [15].

In this study, pulses of UV-rich light, emitted from a broadband xenon flashlamp, were applied to liquid suspensions of test microorganisms, with results demonstrating the effectiveness of PUV-light for the inactivation of bacterial and yeast species. The effect of sample agitation during PUV-light exposure is also investigated.

II. Experimental Materials And Methods

A. *Pulsed UV System*

A pulse generator (Samtech Ltd, Glasgow, UK) and broadband xenon flashlamp, as shown in Fig. 1, was used for bacterial inactivation. The pulse generator contains a dual 15 kHz switch mode power supply (SMPS) which supplies 1.1 kV and 0.4 kV as follows: the SMPS energized to 1.1 kV charges an energy storage capacitor, and the 0.4 kV charges a primary trigger circuit and pulse repetition rate (PRR) control. The primary trigger circuit generates a 500 V pulse voltage when the system is switched on, which is stepped up to 25 kV by a pulsed transformer inside the flashlamp chamber. This causes the energy storage in the capacitor to discharge and transfer a stored energy of 20 J into the flashlamp, resulting in a peak power in the region of 1MW (Fig. 2).

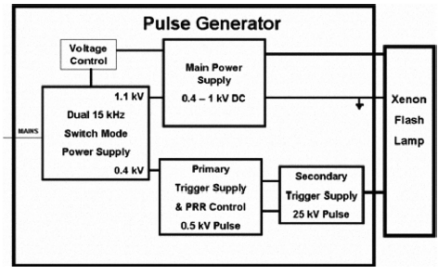

Fig. 1. Schematic diagram of the main components of pulse UV generator and flashlamp.

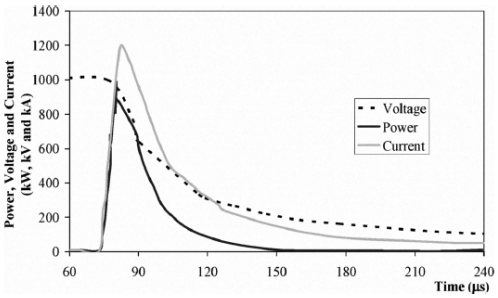

Fig. 2. Waveforms of the Xenon-filled flashlamp, recorded at an operating voltage of 1 kV.

978-0-947649-44-9/09/$26.00 ©2009 IEEE

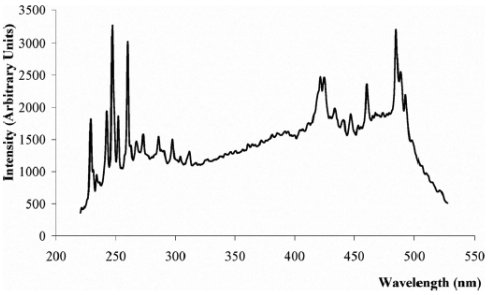

Fig. 3. Spectral output of xenon-filled flashlamp

The resulting very short duration pulses of UV-rich light are produced from an exponentially decaying waveform, as shown in Fig. 2, with the time to half value being approximately 40 µs. Each pulse has an approximate peak value lamp current of 1.2 kA and a 6.8 µs rise time, as shown in Fig. 2.

The light source used in the system is a low-pressure (450 torr) xenon-filled flashlamp (Heraus Noblelight XAP series), constructed from a clear fused quartz tube filled with xenon. The spectral emission of the flashlamp is broad, extending from ultraviolet to infrared, but as shown in Fig. 3, the emission is UV-rich, which is ideal for microbial inactivation.

B. Microorganisms and Sample Preparation

The test microorganisms *Staphylococcus epidermidis* and *Saccharomyces cerevisiae* were cultivated overnight in 100 ml Malt Extract Broth (MEB) and 100 ml Tryptone Soya Broth (TSB), respectively, at 37°C under rotary conditions (120 rpm). After an 18-24 hour incubation period, the cultures were centrifuged for 10 min at 4300 rpm and the cell pellet re-suspended in 100 ml of Phosphate Buffered Saline (PBS). The microbial suspensions were then serially diluted in PBS to provide the appropriate population densities for experimental use. Absorbance and transmission spectra of the microbial population densities were obtained using a Biomate 5 UV-Visible Spectrophotometer (Thermo Spectronic).

The unit of CFU/ml is the number of viable colony-forming units per millilitre of sample and is indicative of the population of living microorganisms in the sample. All culture media used throughout the study were sourced from Oxoid Ltd., UK.

C. Pulsed Ultraviolet (PUV) Light Exposure Experiments.

As described in Section II.A, a pulse generator and flashlamp were used in order to generate PUV-light. In the PUV microbial treatment system (as shown in Fig. 4) the flashlamp was enclosed within a PVC chamber, with a base platform on which microbial suspensions were held during PUV treatment. The suspensions were positioned directly under the flashlamp at a fixed distance of 8 cm, giving a total average power density of 6.4 mW/cm^2 per pulse.

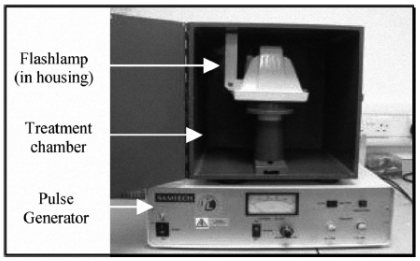

Fig.4. Photograph of PUV treatment system for microbial inactivation

For PUV-light treatment, 20 ml volumes of microbial suspension of known concentration were dispensed into 90 mm Petri dishes. These samples (with the Petri lid off) were then placed into the PVC treatment chamber and exposed to pulses of UV-rich light. Suspensions of *S. epidermidis* and *S. cerevisiae*, with population densities of 10^7 and 10^5 CFU/ml, respectively, were exposed to 2, 4, 6, 8 and 10 pulses. Further to this, *S. cerevisiae* suspensions with a population density of 10^7 CFU/ml, were exposed to 25, 50, 75, 100, 125 and 150 pulses. In this series of exposure experiments, the additional parameter of sample agitation was investigated. For this, the test suspension was manually agitated by rotating the Petri dish 10× clockwise and 10× anticlockwise after every 10 pulses.

After PUV treatment, test samples were immediately plated onto Malt Extract Agar (*S. cerevisiae*) and Tryptone Soya Agar (*S. epidermidis*) using standard microbiological plating methods, and incubated at 37°C for 24 hours before enumeration.

III. Experimental Results and Discussion

The results shown in Fig. 5 demonstrate the effect of PUV-light exposure on liquid suspensions of both *S. epidermidis* and *S. cerevisiae* with differing population densities. PUV-treatment showed that complete inactivation of 10^7 CFU/ml *S. epidermidis* and 10^5 CFU/ml *S. cerevisiae* was achieved within 10 pulses.

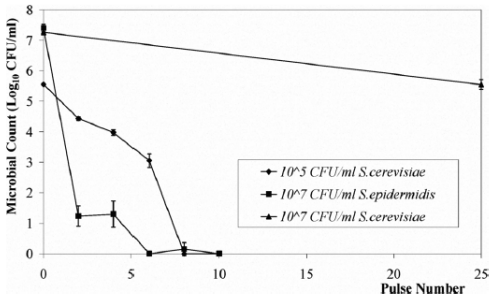

Fig. 5. PUV treatment of *S. cerevisiae* and *S. epidermidis* in liquid suspension, with differing population densities.

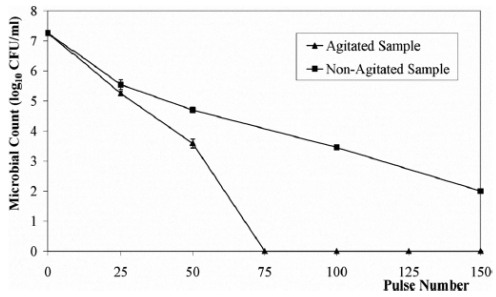

Fig. 6. PUV treatment of *S. cerevisiae* in liquid suspension with and without agitation.

The rapid inactivation effect observed for 10^7 CFU/ml *S. epidermidis* and 10^5 CFU/ml *S. cerevisiae* correlates well with data from a study by Maclean *et al*. [16]. This study, which utilized a similar treatment system, achieved 7-log_{10} reductions of the bacteria *Staphylococcus aureus* and *Listeria monocytogenes* within exposure to 10 pulses of UV-light.

It can be observed from Fig. 5 that 25 pulses of UV-rich light had a much less notable effect on the 10^7 CFU/ml population of *S. cerevisiae*, with only an approximate 1-log_{10} reduction in yeast cell population being achieved. As a consequence of this, samples were exposed to increased numbers of pulses. The results, shown in Fig. 6, demonstrate that approximately a 5-log_{10} reduction was achieved after application of 150 pulses.

When manual sample agitation was performed, it can be seen that this greatly enhanced the inactivation rate of the 10^7 CFU/ml yeast suspension, with a 7-log_{10} reduction achieved after exposure to 75 pulses.

The transmission and absorbance spectra of the 3 different microbial population densities used in this study are shown in Fig. 7. The scan of wavelengths utilized was 200 nm–400 nm in order to cover the ultraviolet region of the electromagnetic spectrum. With regards to microbial inactivation, the most efficient wavelengths for germicidal efficiency are within the UV-C region of approximately 240 nm–280 nm, due to the nucleotide base components of DNA having peak absorbancies in this region. This wavelength-dependent germicidal effect has been demonstrated for *Escherichia coli* [17]. UV-light of longer wavelength (280 nm-390 nm) can also cause microbial damage indirectly through the generation of reactive oxygen species which can cause protein-cross-linking [18].

Visual inspection of the population densities used in this study found that 10^7 CFU/ml liquid suspensions of *S. epidermidis* and 10^5 CFU/ml suspensions of *S. cerevisiae* suspensions are visibly clear, whereas 10^7 CFU/ml *S. cerevisiae* suspensions are opaque, with a cloudy white colour. Spectroscopic analysis of the microbial suspensions (Fig. 7) confirms that both the 10^7 CFU/ml *S. epidermidis* and 10^5 CFU/ml *S. cerevisiae* suspensions have low absorbance and high transmission of germicidal UV wavelengths. The 10^7 CFU/ml liquid suspension of *S. cerevisiae*, however, only permits low (<5%) transmission – and consequently a high absorbance – of germicidal UV wavelengths. This result is readily explained when the cell size of the two test microorganisms are compared. The bacterium *S. epidermidis* has a cell diameter of 0.5 – 1.5µm whereas the yeast *S. cerevisiae* has a much larger cell diameter of 5 – 10µm. Consequently *S. cerevisiae* will appear as a more opaque suspension than *S. epidermidis* at equivalent high cell density levels.

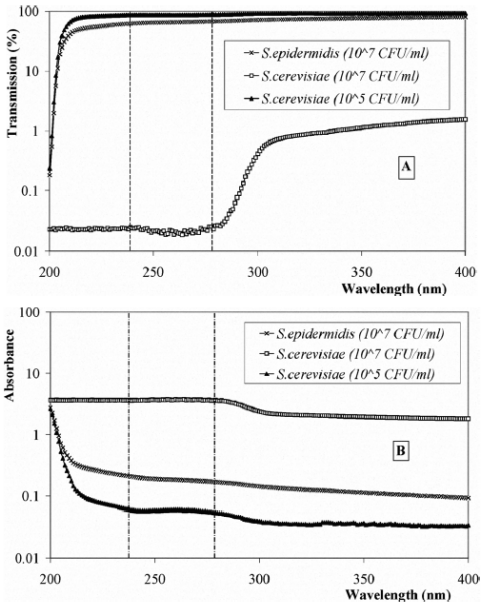

Fig. 7. Transmission (A) and absorbance (B) spectra of the microbial population densities used in the PUV-exposure experiments. The area between the dotted lines indicates the highly germicidal wavelength region of 240 - 280 nm.

This result gives reasoning to the low inactivation rate of the 10^7 CFU/ml population of *S. cerevisiae* observed after exposure to 25 pulses (Fig. 5). The low transmissibility of the suspension meant that the UV wavelengths were unable to completely penetrate through the suspension and affect the total yeast population. Instead, the observed inactivation (~1-log_{10} reduction) is likely to have been a result of inactivation of the yeast cells towards the top of the suspension. Cells below this top layer would have been, to some degree, shaded from the UV-wavelengths, and therefore a sufficient UV dose was not able to be applied to achieve complete inactivation

Upon exposure to a higher number of UV-rich light pulses, increased inactivation was achieved, and this is likely to be due to the higher applied dose, and possibly some degree of cellular protein damage from UV-B and UV-A wavelengths.

Agitation of the liquid suspension significantly enhanced the inactivation rate of the 10^7 CFU/ml *S. cerevisiae* population. This is thought to be due to the manual agitation permitting circulation of the yeast cells within the suspension, which as a consequence allows shaded cells to reach the surface of the suspension and become intermittently exposed to the pulses of UV-rich light.

IV. Conclusions

This study has demonstrated the effectiveness of PUV-light treatment for the inactivation of the yeast *Saccharomyces cerevisiae* and the bacterium *Staphylococcus epidermidis* in liquid suspension. PUV exposure was performed using a broadband xenon flashlamp, and complete inactivation of 10^7 CFU/ml *S. epidermidis* was achieved within 10 pulses, and 10^7 CFU/ml and 10^5 CFU/ml populations of *S. cerevisiae* showed complete inactivation within 75 and 10 pulses, respectively. In addition, the performance of sample agitation proved to significantly increase treatment efficacy when exposing densely populated suspensions.

Overall, this study has demonstrated that pulsed ultraviolet light, which is a non-thermal high-peak power technology, is capable of achieving rapid inactivation of microorganisms. Further work into the development of PUV systems which incorporate methods of mechanical agitation could greatly improve the efficacy of PUV-light for industrial disinfection and sterilization applications.

Acknowledgements

The first author would like to thank the Indonesian Government, Directorate General of Higher Education (DIKTI) and Physics Department, Institute of Technology Sepuluh Nopember (ITS) Surabaya, Indonesia for providing the scholarship. All authors would like to thank The Robertson Trust for their funding support.

References

[1] M. Okochi, T. Matsunaga, "Electrochemical sterilization of bacteria using a graphite electrode modified with adsorbed ferrocene", *Electrochimica Acta*, Vol. 42. Nos 20-22, pp. 3247-3250, 1997.

[2] L. Z. J. Toth, "The sterilizing effect of ethylene oxide vapor on different micro- organisms", *Archiv fur Mikrobiologie*, Bd.32, S.409-410, 1959.

[3] B.J. Park, D.H. Lee, J.-C. Park, I.-S. Lee, K.-Y. Lee, S.O. Hyun, M.-S. Chun and K.-H. Chung , "Sterilization using a microwave-induced argon plasma system at atmospheric pressure", *Physics of Plasmas*, Vol.10, No.11, pp.4539-4544, 2003.

[4] K.Lee, K.Y. Paek, W.T. Ju and Y. Lee, "Sterilization of bacteria, yeast, and bacterial endospores by atmospheric-pressure cold plasma using helium and oxygen", *The Journal of Microbiology*, Vol.44, No.3, pp.269-275, 2000.

[5] P. Muraca, J.E. Stout, and V.L. Yu, "Comparative assessment of chlorine, heat, ozone, and uv light for killing *Legionella pneumophila* within a model plumbing system", *Appl. Environ. Microbiol.*, Vol.53, No.2, pp. 447-453, 1987.

[6] E.M. Darmady, K.E.A. Hughes, J.D. Jones, D. Prince, and W. Tuke, "Sterilization by dry heat", *J. Clin. Path.*, Vol.14, No. 38, pp.38-44, 1961.

[7] N.J. Rowan, S.J. MacGregor, J.G. Anderson, R.A. Fouracre and O. Farish, "Pulsed electric field inactivation of diarrhoeagenic *Bacillus cereus* through irreversible electroporation", *Lett. Appl. Microbiol.*, Vol.31, pp. 110-114, 2000.

[8] S.T. Seet, J.R. Heil, S.J. Leonard, W.D. Brown, "High vacuum flame sterilization of canned diced tuna: preliminary process development and quality evaluation", *J. Food. Sci.*, Vol. 48, Issue 2, pp.364-369, 2006.

[9] S.G. Hong, H.M. Park, K.H. Cho, "Development of a washing, sterilization, dehydrating system for leaf vegetables", *Proceedings of the 4th International Symposium on Machinery and Mechatronics for Agriculture and Biosystems Engineering (ISMAB)*, pp.102-107, 27-29 May 2008, Taichung, Taiwan.

[10] J. Dunn, T.H. Ott and W. Clark, "Pulsed-light treatment of food and packaging",*Food Technology*, Vol. 49, No.9, pp. 95–99, 1995.

[11] K.F. McDonald, R.D. Curry, T.E. Clevenger, K. Unklesbay, A. Eisenstark, J. Golden, Senior Member, IEEE, and R.D. Morgan, "A comparison of pulsed and continuous ultraviolet light sources for the decontamination of surfaces", *IEEE Trans. Plasma Sci.*, Vol. 28, No. 5, 2000.

[12] S.J. MacGregor, N.J. Rowan, L. McIlvaney, J.G. Anderson, R.A. Fouracre and O. Farish, "Light inactivation of food-related pathogenic bacteria using a pulsed power source", *Lett. Appl. Microbiol.*, Vol.27, pp. 67–70, 1998.

[13] A. Wekhof, "Pulsed UV disintegration (PUVD): a new sterilisation mechanism for packaging and broad medical-hospital applications", *The First International Conference on Ultraviolet Technologies*, Washington D.C, USA, 2001.

[14] N. Elmnaser, S. Guillou, F. Leroi, N. Orange, A. Bakhrouf, and M. Federighi, "Pulsed-light systems as a novel food decontamination technology: a review", *Can. J. Microbiology*, Vol.53, pp.813-821, 2007.

[15] R.P. Sinha, D.P. Häder, "UV-induced DNA damage and repair: a review", *Photochem. Photobiol. Sci.*, Vol. 1, No.4, pp.225-36, 2002.

[16] M. Maclean, L.E. Murdoch, M.N. Lani, S.J. MacGregor, J.G. Anderson, and G.A. Woolsey, "Photoinactivation and photoreactivation responses by bacterial pathogens after exposure to pulsed UV-light", *In Proceeding of The IEEE International Power Modulator and High Voltage Conference*, pp.326-329, 2008.

[17] T. Wang, S.J. MacGregor, J.G. Andrson, and G.A Woolsey, "Pulsed ultra-violet inactivation spectrum of *Escherichia coli*", *Water Res.*, Vol.39, pp.2921-2925, 2005.

[18] S.S. Block, *Disinfection, sterilization, and preservation*, 4th edition, Published by Lea & Febiger, Philadelphia, USA, 1991.